

Edited by
Wolfgang H. Binder

Self-Healing Polymers

Related Titles

Thomas, S., Joseph, K., Malhotra, S.K.,
Goda, K., Sreekala, M.S.

Polymer Composites

Volume 2

2013

Print ISBN: 978-3-527-32979-3

Tsukruk, V.V., Singamaneni, S.

Scanning Probe Microscopy of Soft Matter

Fundamentals and Practices

2012

Print ISBN: 978-3-527-32743-0

Schlüter, D.A., Hawker, C., Sakamoto, J.

Synthesis of Polymers

New Structures and Methods

2012

Print ISBN: 978-3-527-32757-7

Lyon, L.A., Serpe, M.J.

Hydrogel Micro and Nanoparticles

2012

Print ISBN: 978-3-527-33033-1

Urban, M.W.

Handbook of Stimuli- Responsive Materials

2011

Print ISBN: 978-3-527-32700-3

Zhang, M., Rong, M.

Self-Healing Polymers and Polymer Composites

2011

Print ISBN: 978-0-470-49712-8

Thomas, S., Candau, Y.Y., Ibos, L.L.,
Boudenne, A.R.

Handbook of Multiphase Polymer Systems 2V Set

2011

Print ISBN: 978-0-470-71420-1

Edited by Wolfgang H. Binder

Self-Healing Polymers

From Principles to Applications

WILEY-VCH

Editor

Wolfgang H. Binder
MLU Halle-Wittenberg
Institut für Chemie
Von-Danckelmann-Platz 4
06120 Halle
Germany

All books published by **Wiley-VCH Verlag GmbH** are carefully produced. Nevertheless, authors, editors, and publisher do not warrant the information contained in these books, including this book, to be free of errors. Readers are advised to keep in mind that statements, data, illustrations, procedural details or other items may inadvertently be inaccurate.

Library of Congress Card No.: applied for

British Library Cataloguing-in-Publication Data

A catalogue record for this book is available from the British Library.

Bibliographic information published by the Deutsche Nationalbibliothek

The Deutsche Nationalbibliothek lists this publication in the Deutsche Nationalbibliografie; detailed bibliographic data are available on the Internet at <<http://dnb.d-nb.de>>.

© 2013 Wiley-VCH Verlag GmbH & Co. KGaA,
Boschstr. 12, 69469 Weinheim, Germany

All rights reserved (including those of translation into other languages). No part of this book may be reproduced in any form – by photoprinting, microfilm, or any other means – nor transmitted or translated into a machine language without written permission from the publishers. Registered names, trademarks, etc. used in this book, even when not specifically marked as such, are not to be considered unprotected by law.

Print ISBN: 978-3-527-33439-1

ePDF ISBN: 978-3-527-67021-5

ePub ISBN: 978-3-527-67020-8

Mobi ISBN: 978-3-527-67019-2

oBook ISBN: 978-3-527-67018-5

Cover Design Adam-Design, Weinheim

Typesetting Toppan Best-set Premedia Limited,
Hong Kong

Printing and Binding Markono Print Media Pte
Ltd, Singapore

Printed on acid-free paper

Contents

List of Contributors XIII

Introduction 1

Wolfgang Binder

Part One Design of Self-Healing Materials 5

- 1 Principles of Self-Healing Polymers 7**
Diana Döhler, Philipp Michael, and Wolfgang Binder
- 1.1 Introductory Remarks 7
- 1.2 General Concept for the Design and Classification of Self-Healing Materials 8
- 1.3 Physical Principles of Self-Healing 11
- 1.4 Chemical Principles of Self-Healing 15
- 1.4.1 Covalent Network Formation 16
- 1.4.1.1 Irreversible Covalent Network Formation Concepts 16
- 1.4.1.2 Reversible Covalent Network Formation Concepts 22
- 1.4.2 Supramolecular Network Formation 28
- 1.4.3 Mechanochemical Network Formation 38
- 1.4.3.1 Mechanochemical Generation of Reactive Species 38
- 1.4.3.2 Mechanochemical Activation of Catalysts 44
- 1.4.4 “Switchable” Network Formation 44
- 1.5 Multiple versus One-Time Self-Healing 49
- 1.6 Resume and Outlook 53
- Acknowledgments 53
- References 53
- 2 Self-Healing in Plants as Bio-Inspiration for Self-Repairing Polymers 61**
Thomas Speck, Rolf Mülhaupt, and Olga Speck
- 2.1 Self-Sealing and Self-Healing in Plants: A Short Overview 62

2.2	Selected Self-Sealing and Self-Healing Processes in Plants as Role Models for Bio-Inspired Materials with Self-Repairing Properties	63
2.2.1	Latex Plants as Concept Generators for Bio-Inspired Self-Healing Elastomers (Role Models: <i>Ficus benjamina</i> and <i>Hevea brasiliensis</i>)	63
2.2.2	Lianas as Concept Generators for Bio-Inspired Self-Sealing Membranes for Pneumatic Structures (Role Model: <i>Aristolochia macrophylla</i>)	69
2.2.3	Succulent Plants as Concept Generators for Bio-Inspired Self-Sealing Membranes for Pneumatic Structures (Role Model <i>Delosperma cooperi</i>)	72
2.3	Bio-Inspired Approaches for the Development of Self-Repairing Materials and Structures	75
2.3.1	Bio-Inspired Self-Healing Elastomers	77
2.3.1.1	Micro-encapsulation	77
2.3.1.2	Ionomeric Elastomers	78
2.3.1.3	Supramolecular Co-networks	79
2.3.1.4	Nitrile Butadiene Rubber (NBR) Blends	80
2.3.2	Self-Sealing Foam Coatings for Membranes of Pneumatic Structures	81
2.3.2.1	Self-Sealing Membranes of Pneumatic Structures: Bio-Inspired Physical Transfer	82
2.3.2.2	Self-Sealing Membranes of Pneumatic Structures: Bio-Inspired Chemical Transfer	84
2.4	Bio-Inspired Self-Healing Materials: Outlook	85
	Acknowledgments	85
	References	86
3	Modeling Self-Healing Processes in Polymers: From Nanogels to Nanoparticle-Filled Microcapsules	91
	<i>German V. Kolmakov, Isaac G. Salib, and Anna C. Balazs</i>	
3.1	Introduction	91
3.2	Designing Self-Healing Dual Cross-Linked Nanogel Networks	92
3.2.1	Methodology	94
3.2.2	Results and Discussion	97
3.2.2.1	Applying a Tensile Deformation at Constant Force	97
3.2.2.2	Applying a Tensile Deformation at Constant Velocity	97
3.2.2.3	Optimizing the Mechanical Response of the Material	101
3.3	Designing “Artificial Leukocytes” That Help Heal Damaged Surfaces via the Targeted Delivery of Nanoparticles to Cracks	101
3.3.1	Methodology	103
3.3.2	Results and Discussion	105
3.3.2.1	Effect of Imposing a Steady Shear Flow	105
3.3.2.2	Utility of Applying a Pulsatile Flow	108
3.4	Conclusions	110
	References	111

Part Two Polymer Dynamics 113

- 4 Structure and Dynamics of Polymer Chains 115**
Ana Rita Brás, Wim Pyckhout-Hintzen, Andreas Wischnewski, and Dieter Richter
- 4.1 Foreword 115
 - 4.2 Techniques 116
 - 4.3 Structure 117
 - 4.4 Dynamics 120
 - 4.4.1 The Rouse Model 123
 - 4.4.2 The Tube Model 124
 - 4.5 Application to Self-Healing 130
 - 4.6 Conclusions and Outlook 133
 - References 135
- 5 Physical Chemistry of Cross-Linking Processes in Self-Healing Materials 139**
Joerg Kressler and Hans-Werner Kammer
- 5.1 Introduction 139
 - 5.2 Thermodynamics of Gelation 141
 - 5.3 Viscoelastic Properties of the Sol–Gel Transition 143
 - 5.4 Phase Separation and Gelation 147
 - 5.5 Conclusions 150
 - References 150
- 6 Thermally Remendable Polymers 153**
Tom Engel and Guido Kickelbick
- 6.1 Principles of Thermal Healing 153
 - 6.1.1 Physical Methods 153
 - 6.1.1.1 Molecular Diffusion across a Crack Interface 153
 - 6.1.1.2 Interpenetrating Networks 154
 - 6.1.1.3 Shape Memory Assisted Self-Healing 155
 - 6.1.2 Chemical Methods 155
 - 6.1.2.1 Thermoreversible Mechanisms 156
 - 6.1.2.2 Alternative Mechanism 163
 - 6.1.2.3 Perfluorocyclobutanes 163
 - 6.2 Inorganic–Organic Systems 164
 - 6.3 Efficiency, Assessment of Healing Performance 165
 - 6.4 Conclusions 168
 - Acknowledgments 169
 - References 169
- 7 Photochemically Remendable Polymers 173**
Jun Ling, Ming Qiu Zhang, and Min Zhi Rong
- 7.1 Background 173

7.2	Molecular Design	178
7.2.1	Polyurethane Containing Monohydroxy Coumarin Derivatives	178
7.2.2	Polyurethane Containing Dihydroxy Coumarin Derivatives	179
7.3	Reversible Photo-Crosslinking Behaviors	182
7.4	Evaluation of Photo-Remendability	185
7.5	Concluding Remarks	188
	Acknowledgments	189
	References	189
8	Mechanophores for Self-Healing Applications	193
	<i>Charles E. Diesendruck and Jeffrey S. Moore</i>	
8.1	Introduction	193
8.2	Mechanochemical Damage	194
8.2.1	Deformation	194
8.2.2	Homolytic Bond Cleavage	196
8.2.3	Heterolytic Bond Cleavage	197
8.3	Activation of Mechanophores	198
8.3.1	Ultrasound	198
8.3.2	Tensile Testing	198
8.3.3	Torsional Shear Testing	200
8.3.4	Compression	200
8.3.5	Others	201
8.4	Mechanochemical Self-Healing Strategies	202
8.4.1	Production of Reactive Species	202
8.4.2	Activation of Catalytic Species	204
8.4.3	Disruption of Equilibrium	207
8.5	Conclusions and Outlook	210
	References	211
9	Chemistry of Crosslinking Processes for Self-Healing Polymers	215
	<i>Roberto F.A. Teixeira, Xander K.D. Hillewaere, Stijn Billiet, and Filip E. Du Prez</i>	
9.1	Introduction	215
9.2	Extrinsic Self-Healing Materials	215
9.2.1	Catalytic Systems	218
9.2.1.1	Dicyclopentadiene (DCPD) +Grubbs' Catalyst Healing System	218
9.2.1.2	DCPD/5-Ethylidene-2-Norbornene (ENB)+Grubbs' Catalyst Healing System	220
9.2.1.3	Siloxane-Based Healing System	221
9.2.1.4	Epoxy + Latent Hardener/Catalyst Healing System	222
9.2.1.5	Thiol-Epoxy Healing System	224
9.2.1.6	Thiol-Ene Healing System	224
9.2.1.7	Thiol-Maleimide Healing System	225
9.2.1.8	Azide-Alkyne Healing System	225
9.2.2	Non-Catalytic Systems	225

9.2.2.1	Amine-Epoxy Healing System	225
9.2.2.2	Epoxy-Based Healing System	227
9.2.2.3	Isocyanates-Based Healing System	228
9.2.2.4	Vinyl Ester Healing System	228
9.2.2.5	Molecular Interdiffusion	228
9.3	Intrinsic Self-Healing Materials	229
9.3.1	Molecular Interdiffusion	229
9.3.2	Reversible Bond Formation	231
9.3.2.1	Diels–Alder/Retro-Diels–Alder	231
9.3.2.2	Photochemical Trigger	232
9.3.2.3	Disulfide Bridges	234
9.3.2.4	Radical Fission/Recombination	234
9.3.2.5	Anionic Reactions	235
9.3.2.6	pH-Responsive Systems	236
9.3.3	Other Systems	236
9.4	Concluding Remarks and Future Outlook	237
	References	238
10	Preparation of Nanocapsules and Core–Shell Nanofibers for Extrinsic Self-Healing Materials	247
	<i>Daniel Crespy and Yi Zhao</i>	
10.1	Selected Preparation Methods for the Encapsulation of Self-Healing Agents	247
10.1.1	Emulsion Droplets as Templates	247
10.1.2	Electrospinning	250
10.2	Mechanically Induced Self-Healing	251
10.2.1	Nanocapsules	251
10.2.2	Nanofibers and Nanotubes	255
10.3	Stimuli-Responsive Self-Healing Materials	258
10.3.1	Light-Responsive Capsules	258
10.3.2	pH-Responsive Systems	260
10.3.3	Temperature-Responsive Systems	263
10.3.4	Redox-Responsive Systems	263
10.4	Novel Approaches and Perspectives	264
	Abbreviations	265
	References	266
	Part Three Supramolecular Systems	273
11	Self-Healing Polymers via Supramolecular, Hydrogen-Bonded Networks	275
	<i>Florian Herbst and Wolfgang H. Binder</i>	
11.1	Introduction	275
11.2	Dynamics of Hydrogen Bonds in Solution	279

11.3	Supramolecular Gels	280
11.4	Self-Healing Bulk Materials	284
11.5	Conclusions	297
	Acknowledgment	297
	References	298
12	Metal-Complex-Based Self-Healing Polymers	301
	<i>Stefan Bode, Benedict Sandmann, Martin D. Hager, and Ulrich S. Schubert</i>	
12.1	Stimuli-Responsive Metallopolymers	305
12.2	Self-Healing Metallopolymers	307
12.3	Summary and Outlook	310
	Acknowledgments	311
	References	311
13	Self-Healing Ionomers	315
	<i>Nico Hohlbein, Max von Tapavicza, Anke Nellesen, and Annette M. Schmidt</i>	
13.1	Introduction	315
13.2	Basic Principles of Ionomers	315
13.2.1	Properties	319
13.2.2	Applications and Availability	320
13.3	Ionomers in Self-Healing Systems	322
13.3.1	General Mechanism	323
13.4	Actual Developments and Future Trends in Ionomeric and Related Self-Healing Systems	327
	References	331
 Part Four Analysis and Friction Detection in Self-Healing Polymers: Macroscopic, Microscopic and Nanoscopic Techniques 335		
14	Methods to Monitor and Quantify (Self-) Healing in Polymers and Polymer Systems	337
	<i>Ranjita K. Bose, Ugo Lafont, Jesús M. Vega, Santiago J. Garcia, and Sybrand van der Zwaag</i>	
14.1	Introduction	337
14.2	Visualization Techniques	338
14.2.1	Optical Microscopy	338
14.2.2	Scanning (SEM) and Environmental Scanning Electron (E-SEM) Microscopy	340
14.2.3	Acoustical Microscopy	341
14.2.4	Computed Tomography and Micro- (Computed) Tomography	341
14.3	Healing of Mechanical Properties	343
14.3.1	Healing after Static Damage	343

14.3.2	Healing after Fatigue Damage	345
14.3.3	Healing of Impact Damage	346
14.3.3.1	Impact Damage of Composites	346
14.3.3.2	Healing of Ballistic Damage in Ionomers	346
14.4	Healing of Functional Integrity	347
14.4.1	Healing of Esthetic Damage	347
14.4.2	Healing of Thermal and Electrical Conduction	348
14.4.2.1	Electrical Conduction Recovery	348
14.4.2.2	Thermal Conduction Recovery	350
14.4.3	Healing of Hydrophobicity and Surface Friction	350
14.4.3.1	Healing of Hydrophobicity	350
14.4.3.2	Friction Recovery	351
14.4.4	Healing of Protection Against Corrosion	351
14.4.4.1	Potentiostatic Measurements	352
14.4.4.2	Electrochemical Impedance Spectroscopy	352
14.4.4.3	Scanning Vibrating Electrode Technique	352
14.4.4.4	Scanning Electrochemical Microscopy	353
14.5	Summary	356
	References	356
15	Self-Healing Epoxies and Their Composites	361
	<i>Henghua Jin, Kevin R. Hart, Anthony M. Coppola, Ryan C. Gergely, Jeffrey S. Moore, Nancy R. Sottos, and Scott R. White</i>	
15.1	Introduction	361
15.2	Capsule-Based Healing System	362
15.2.1	Self-Healing Epoxies	363
15.2.1.1	Capsule/Catalyst Healing System	363
15.2.1.2	Dual-Capsule Healing System	364
15.2.1.3	Single Capsule Healing System	365
15.2.2	Self-Healing Fiber-Reinforced Epoxies	365
15.2.2.1	Recovery of Mode I Fracture Toughness	366
15.2.2.2	Recovery from Impact Damage	366
15.2.2.3	Recovery of Macroscale Properties and Interfacial Bond Strength	367
15.2.2.4	Recovery of Barrier Properties	368
15.3	Vascular-Based Healing Systems	368
15.3.1	Recovery of Fracture Damage	369
15.3.2	Recovery of Impact Damage	370
15.3.3	Healing of Coatings	370
15.3.4	Self-Sensing, Self-Healing Vascularized Composites	371
15.4	Intrinsic Healing Systems	371
15.4.1	Resin Design for Reversibility	371
15.4.2	Dissolved Healing Agents	373
15.4.3	Phase Separated Healing Agents	373
15.4.4	Solid-Phase Healing Agents	373

15.5	Conclusions	375
	References	376
16	Self-Healing Coatings	381
	<i>Dmitry G. Shchukin, Dimitriya Borisova, and Helmuth Möhwald</i>	
16.1	Introduction into Self-Healing Coatings	381
16.2	Concept of Micro- and Nanocontainer-Based Self-Healing Coatings	382
16.3	Types of Nanocontainers	386
16.4	Characterization of Nanocontainer-Based Self-Healing Coatings	389
16.5	Conclusions and Current Trends	395
	References	396
17	Application of Self-Healing Materials in Aerospace Engineering	401
	<i>Liberata Guadagno, Marialuigia Raimondo, Carlo Naddeo, and Pasquale Longo</i>	
17.1	General Considerations	401
17.1.1	Stability and Reactivity of Catalysts for Self-Healing Formulations	404
17.1.2	Healing Efficiency at Low Temperatures	408
17.2	Conclusions	410
	References	411
	Index	413

List of Contributors

Anna C. Balazs

University of Pittsburgh
Chemical Engineering Department
Pittsburgh, PA 15261
USA

Stijn Billiet

Ghent University
Department of Organic Chemistry
Polymer Chemistry Research Group
Krijgslaan 281 S4-bis
9000 Ghent
Belgium

Wolfgang H. Binder

Martin-Luther-Universität
Halle-Wittenberg
Institut für Chemie
Von-Danckelmann-Platz 4
06120 Halle
Germany

and

MLU Halle Wittenberg
Faculty of Natural Sciences II
von Danckelmannplatz 4
06120 Halle (Saale)
Germany

Stefan Bode

Friedrich-Schiller-University Jena
Laboratory of Organic and
Macromolecular Chemistry (IOMC)
Humboldtstr. 10
07743 Jena
Germany

and

Friedrich-Schiller-University Jena
Jena Center for Soft Matter (JCSM)
Philosophenweg 7
07743 Jena
Germany

Dimitriya Borisova

Max Planck Institute of Colloids and
Interfaces
Am Mühlenberg 1
14476 Golm
Germany

Ranjita K. Bose

Delft University of Technology
Faculty of Aerospace Engineering,
Novel Aerospace Materials
Kluyverweg 1
2629HS Delft
The Netherlands

Ana Rita Brás

Forschungszentrum Jülich
Jülich Centre for Neutron Science
JCNS-1
52425 Jülich
Germany

Diana Döhler

Martin-Luther-Universität
Halle-Wittenberg
Institut für Chemie
Von-Danckelmann-Platz 4
06120 Halle
Germany

Anthony M. Coppola

University of Illinois at
Urbana-Champaign
Beckman Institute for Advanced
Science and Technology
405 N. Mathews Ave.
Urbana, IL 61801
USA

Daniel Crespy

Max Planck Institute for Polymer
Research
Ackermannweg 10
55128 Mainz
Germany

Charles E. Diesendruck

University of Illinois at
Urbana-Champaign
Department of Chemistry and
Beckman Institute for Advanced
Science and Technology
405 N. Mathews Ave.,
Urbana, IL 61801
USA

Filip E. Du Prez

Ghent University
Department of Organic Chemistry
Polymer Chemistry Research Group
Krijgslaan 281 S4-bis
9000 Ghent
Belgium

and

SIM
Technologiepark Zwijnaarde 904
9052 Ghent
Belgium

Tom Engel

Saarland University
Inorganic Solid-State Chemistry
Am Markt, Zeile 3
66125 Saarbrücken
Germany

Santiago J. Garcia

Delft University of Technology
Faculty of Aerospace Engineering,
Novel Aerospace Materials,
Kluyverweg 1
2629HS Delft
The Netherlands

Ryan C. Gergely

University of Illinois at
Urbana-Champaign
Beckman Institute for Advanced
Science and Technology
405 N. Mathews Ave.
Urbana, IL 61801
USA

Liberata Guadagno

Università di Salerno
Dipartimento di Ingegneria
Industriale
Via Ponte Don Melillo
84084 Fisciano (SA)
Italy

and

Università di Salerno
Nano-Mates – Research Centre for
NANOMaterials and nanoTEchnology
Via Ponte don Melillo
84084 Fisciano (SA)
Italy

Martin D. Hager

Friedrich-Schiller-University Jena
 Laboratory of Organic and
 Macromolecular Chemistry (IOMC)
 Humboldtstr. 10
 07743 Jena
 Germany

and

Friedrich-Schiller-University Jena
 Jena Center for Soft Matter (JCSM)
 Philosophenweg 7
 07743 Jena
 Germany

Kevin R. Hart

University of Illinois at
 Urbana-Champaign
 Beckman Institute for Advanced
 Science and Technology
 405 N. Mathews Ave.
 Urbana, IL 61801
 USA

Florian Herbst

Martin-Luther-Universität
 Halle-Wittenberg
 Institut für Chemie
 Von-Danckelmann-Platz 4
 06120 Halle
 Germany

Xander K.D. Hillewaere

Ghent University
 Department of Organic Chemistry
 Polymer Chemistry Research Group
 Krijgslaan 281 S4-bis
 9000 Ghent
 Belgium

and

SIM
 Technologiepark Zwijnaarde 904
 9052 Ghent
 Belgium

Nico Hohlbein

Universität zu Köln
 Institut für Physikalische Chemie,
 Department Chemie
 Luxemburger Str. 116
 50733 Köln
 Germany

and

Fraunhofer Institut für Umwelt-,
 Sicherheits- und Energietechnik
 UMSICHT
 Osterfelder Str. 3
 46047 Oberhausen
 Germany

and

Institut für Zukunftorientierte
 Kompetenzentwicklung
 Hochschule Bochum
 Lennershofstr. 140
 44801 Bochum
 Germany

Henghua Jin

University of Illinois at
 Urbana-Champaign
 Beckman Institute for Advanced
 Science and Technology
 405 N. Mathews Ave.
 Urbana, IL 61801
 USA

Hans-Werner Kammer

Martin Luther University
 Halle-Wittenberg,
 Department of Chemistry
 06099 Halle (Saale)
 Germany

Guido Kickelbick

Saarland University
 Inorganic Solid-State Chemistry
 Am Markt, Zeile 3
 66125 Saarbrücken
 Germany

German V. Kolmakov

New York City College of Technology
Physics Department
300 Jay Street
Brooklyn, NY 11201
USA

Joerg Kressler

Martin Luther University
Halle-Wittenberg
Department of Chemistry
06099 Halle (Saale)
Germany

Ugo Lafont

Delft University of Technology
Faculty of Aerospace Engineering,
Novel Aerospace Materials
Kluyverweg 1
2629HS Delft
The Netherlands

Jun Ling

Sun Yat-sen (Zhongshan) University
Key Laboratory for Polymeric
Composite and Functional Materials
of Ministry of Education
DSAPM Lab
School of Chemistry and Chemical
Engineering
Guangzhou 510275
China

Pasquale Longo

Università di Salerno
Nano-Mates – Research Centre for
NANOMaterials and nanoTEchnology
Via Ponte don Melillo
84084 Fisciano (SA)
Italy

and

Università di Salerno
Dipartimento di Chimica e Biologia
Via Ponte Don Melillo
84084 Fisciano (Salerno)
Italy

Philipp Michael

Martin-Luther-Universität
Halle-Wittenberg
Institut für Chemie
Von-Danckelmann-Platz 4
06120 Halle
Germany

Helmuth Möhwald

Max Planck Institute of Colloids and
Interfaces
Am Mühlenberg 1
14476 Golm
Germany

Jeffrey S. Moore

University of Illinois at
Urbana-Champaign
Department of Chemistry and
Beckman Institute
405 N. Mathews Ave.
Urbana, IL 61801
USA

and

University of Illinois at
Urbana-Champaign
Beckman Institute for Advanced
Science and Technology
405 N. Mathews Ave.
Urbana, IL 61801
USA

Rolf Mülhaupt

Freiburg Materials Research Center
(FMF) and Freiburg Center for
Interactive Materials and Bio-Inspired
Technologies (FIT)
Stefan-Meier-Straße 21
79104 Freiburg
Germany

and

University of Freiburg
 Institute for Macromolecular
 Chemistry
 Stefan-Meier-Str. 31
 79104 Freiburg
 Germany

Carlo Naddeo

Università di Salerno
 Dipartimento di Ingegneria
 Industriale
 Via Ponte Don Melillo
 84084 Fisciano (SA)
 Italy

Anke Nelleßen

Universität zu Köln
 Institut für Physikalische Chemie,
 Department Chemie
 Luxemburger Str. 116
 50939 Köln
 Germany

and

Fraunhofer Institut für Umwelt-
 Sicherheits- und Energietechnik
 UMSICHT
 Osterfelder Str. 3
 46047 Oberhausen
 Germany

and

Institut für Zukunftsorientierte
 Kompetenzentwicklung
 Lennerhofstr. 140
 44801 Bochum
 Germany

Wim Pyckhout-Hintzen

Forschungszentrum Jülich
 Jülich Centre for Neutron Science
 JCNS-1
 52425 Jülich
 Germany

Marialuigia Raimondo

Università di Salerno
 Dipartimento di Ingegneria
 Industriale
 Via Ponte Don Melillo
 84084 Fisciano (SA)
 Italy

Dieter Richter

Forschungszentrum Jülich
 Jülich Centre for Neutron Science
 JCNS-1
 52425 Jülich
 Germany

Min Zhi Rong

Sun Yat-sen (Zhongshan) University
 Key Laboratory for Polymeric
 Composite and Functional Materials
 of Ministry of Education
 DSAPM Lab
 School of Chemistry and Chemical
 Engineering
 Guangzhou 510275
 China

Isaac G. Salib

University of Pittsburgh
 Chemical Engineering Department
 Pittsburgh, PA 15261
 USA

Benedict Sandmann

Friedrich-Schiller-University Jena
 Laboratory of Organic and
 Macromolecular Chemistry (IOMC)
 Humboldtstr. 10
 07743 Jena
 Germany

and

Friedrich-Schiller-University Jena
 Jena Center for Soft Matter (JCSM)
 Philosophenweg 7
 07743 Jena
 Germany

Annette M. Schmidt

Universität zu Köln
Institut für Physikalische Chemie,
Department Chemie
Luxemburger Str. 116
50733 Köln
Germany

and

Fraunhofer Institut für Umwelt-
Sicherheits- und Energietechnik
UMSICHT
Osterfelder Str. 3
46047 Oberhausen
Germany

and

Institut für Zukunftsorientierte
Kompetenzentwicklung
Hochschule Bochum
Lennershofstr. 140
44801 Bochum
Germany

Ulrich S. Schubert

Friedrich-Schiller-University Jena,
Laboratory of Organic and
Macromolecular Chemistry (IOMC)
Humboldtstr. 10
07743 Jena
Germany

and

Friedrich-Schiller-University Jena
Jena Center for Soft Matter (JCSM)
Philosophenweg 7
07743 Jena
Germany

Dmitry G. Shchukin

Max Planck Institute of Colloids and
Interfaces
Am Mühlentberg 1
14476 Golm
Germany

Nancy R. Sottos

University of Illinois at
Urbana-Champaign
Beckman Institute for Advanced
Science and Technology
405 N. Mathews Ave.
Urbana, IL 61801
USA

Olga Speck

University of Freiburg
Plant Biomechanics Group and
Botanic Garden
Schänzlestr. 1
79104 Freiburg
Germany

and

Competence Networks Biomimetics
and BIODON
Stefan-Meier-Straße 21
79104 Freiburg
Germany

Thomas Speck

University of Freiburg
Plant Biomechanics Group and
Botanic Garden
Schänzlestr. 1
79104 Freiburg
Germany

and

Competence Networks Biomimetics
and BIODON
Schänzlestr. 1
79104 Freiburg
Germany

and

Freiburg Materials Research Center
(FMF) and Freiburg Center for
Interactive Materials and Bio-Inspired
Technologies (FIT)
Stefan-Meier-Straße 21
79104 Freiburg
Germany

Max von Tapavicza

Universität zu Köln,
Institut für Physikalische Chemie,
Department Chemie
Luxemburger Str. 116
50939 Köln
Germany

and

Fraunhofer Institut für Umwelt-
Sicherheits- und Energietechnik
UMSICHT
Osterfelder Str. 3
46047 Oberhausen
Germany

and

Institut für Zukunftsorientierte
Kompetenzentwicklung
Hochschule Bochum
Lennershofstr. 140
44801 Bochum
Germany

Roberto F.A. Teixeira

Ghent University,
Department of Organic Chemistry
Polymer Chemistry Research Group
Krijgslaan 281 S4-bis
9000 Ghent
Belgium

and

SIM
Technologiepark Zwijnaarde 904
9052 Ghent
Belgium

Jesús M. Vega

Delft University of Technology
Faculty of Aerospace Engineering,
Novel Aerospace Materials
Kluyverweg 1
2629HS Delft
The Netherlands

Scott R. White

University of Illinois at
Urbana-Champaign
Beckman Institute for Advanced
Science and Technology
405 N. Mathews Ave.
Urbana, IL 61801
USA

Andreas Wischnewski

Forschungszentrum Jülich
Jülich Centre for Neutron Science
JCNS-1
52425 Jülich
Germany

Ming Qiu Zhang

Sun Yat-sen (Zhongshan) University
Key Laboratory for Polymeric
Composite and Functional Materials
of Ministry of Education
DSAPM Lab
School of Chemistry and Chemical
Engineering
Guangzhou 510275
China

Yi Zhao

Max Planck Institute for Polymer
Research
Ackermannweg 10
55128 Mainz
Germany

Sybrand van der Zwaag

Delft University of Technology
Faculty of Aerospace Engineering,
Novel Aerospace Materials
Kluyverweg 1
2629HS Delft
The Netherlands

Introduction

Wolfgang Binder

When the *Romans* invented concrete as a construction material more than 2000 years ago for erecting arches, water-pipes and monuments such as the *Pantheon*, it can be assumed that they did not know about any of the molecular mechanisms of self-healing. However, they surely knew and realized by observation of, for example, old Egyptian pyramids, that the construction of a many-century-lasting empire needs even longer lasting materials, remaining unchanged over many thousands of years, even into our modern times. As all modern materials, fabricated with a usually huge amount of intellectual and also hand- or machine-driven force, are subject to thermal or mechanical destruction as well as chemical degradation during their active lifetime, their use is therefore limited. Despite the inevitable fact that the renewing and destructive force has allowed new civilizations to emerge during the past (historical) times, a short look at nature makes the possibilities of repair and restoration of properties obvious—why would modern man not be able to achieve the same, similar, or even better?

As polymers and polymeric materials are “the” smart invention and technological driving force of the twentieth century, the quest for implementing self-healing-properties into polymers [1] is strong. Not only the practical demand of maximum usage-times of each fabricated thing, but also the everlasting limitation on natural resources and costs inevitably leads to the quest for generating self-repairing polymer materials. Similar to repair-mechanisms active in living nature, regeneration of material properties should be reachable without external action [2]. In such materials, stress of a certain magnitude (either chemical, physical, or thermal) induces a mechanical deformation in the polymer, which in turn activates a response [3] within the material, leading to “healing” of the generated (physical) damage.

Looking at even superficial injuries in mammal organisms shows that a vascular (e.g., bloodstream-supported) supply-system helps to restore and heal mechanical damage via the blood-clotting cascade and subsequent tissue regeneration. This very simple principle demonstrates that biomimicry might help in the design of self-healing polymers by applying similar capsule- or vascular-based logics. If one looks further, the principles of DNA-repair based on the radical scission of DNA-chains can induce a DNA-repair system, which in its complexity cannot be copied

into simple bulk polymeric materials. Thus, an important aspect of self-healing is the presence of a structure which is able to dynamically respond to an external stimulus [3], enabling the restoration of the initial material properties. Due to their highly complex chain structure, polymers, in particular, are ideally suited to serve as molecules for dynamic and thus self-healing properties, given that they are coupled to fast and efficient crosslinking reactions [4].

In self-healing polymers, many complex issues of chemical and physical-principles are interlinked, only then providing the necessary understanding of the underlying processes (see Chapter 1 by Binder *et al.* on the principles of self-healing polymers). Only a material able to recognize the damage-event can be able to heal autonomously, thus repairing without external action, similar to what is known in nature (see Chapter 2 by Speck *et al.* on biomimicry related to plants in self-healing polymers). Thus an inherent “sensing” ability of the polymer is required (see Chapter 8 by Moore *et al.* on mechanochemistry), which then shows a dynamic response to induce a repair mechanism and thus healing, usually via crosslinking processes. As the complexity of the “clotting-cascade” in living organisms cannot be reached in technical polymers, network-formation is among the central aspects of the healing mechanism, often related to permanent chemical crosslinking processes (see Chapter 9 by Du Prez *et al.*), reversible (covalent) crosslinking (see Chapter 6 by Kickelbick *et al.*) and via photochemical crosslinking (see Chapter 7 by Zhang *et al.*), requiring knowledge on the physicochemical principles of network formation (see Chapter 5 by Kressler *et al.*). Spatial separation of highly reactive intermediates by encapsulation (see Chapter 10 by Crespy *et al.*) is thus important.

Chain dynamics and principles of polymer physics are an important aspect for the design of self-healing polymers (see Chapter 3 by Balazs *et al.* and Chapter 4 by Pyckhout-Hintzen *et al.*). In order to design materials with dynamic properties, a reversible bonding system is required to enable a self-healing material, including aspects of supramolecular polymer chemistry. Thus noncovalent bonds such as hydrogen bonds and π - π -stacking (see Chapter 11 of Binder *et al.*); metal-metal-complexes (see Chapter 12 by Schubert *et al.*) and ionomers (see Chapter 13 by Schmidt *et al.*) are crucial elements, demonstrating the possibility of multiple healing cycles in contrast to covalently linked networks.

Self-healing polymers are already used in industrial engineering, fabricating material parts with self-healing properties. Thus reliably testing and understanding the mechanical properties of self-healing polymers is a crucial aspect, including modern micro- and nanoscaled testing methods, besides the classical mechanical testing-methods (see Chapter 14 by van der Zwaag *et al.*). Chapters on the applications of epoxy resins as the largest class of self-healing polymers (see Chapter 15 by White *et al.*), on self-healing polymers in the aerospace industry (see Chapter 17 by Guadagno *et al.*) and the use of layer-by-layer deposition for self-healing anticorrosion-surfaces (see Chapter 16 by Möhwald *et al.*) provide insight into the technological features of this fascinating class of materials.

The self-healing polymers are there on the market, they have become reality in material science. All in all, despite the different aspects of many research activities

and fields, spanning the range from molecular chemistry to polymer physics, as well as mechanical testing and industrial engineering aspects, there are still many open fields to discover. In the future, it will not be the versatility of chemists and physicists that will decide about self-healing polymers, but the markets and the needs of engineers, where self-healing polymers will be used—it is thus just a question of market and history that will decide if new emerging cultures of the future will find our current technical achievements after 2000 years or more still present in everyday life . . . self-healing principles surely will play a role in this.

References

- 1 (a) White, S.R., and Blaiszik, B.J. (2012) Selbstheilende Materialien. *Spektrum Wissenschaft*, **3**, 82–90; (b) Fischer, H. (2010) Self-repairing material systems—a dream or a reality? *Nat. Sci.*, **2** (8), 873–901; (c) Davis, D.A., Hamilton, A., Yang, J., Cremar, L.D., Van Gough, D., Potisek, S.L., Ong, M.T., Braun, P.V., Martinez, T.J., White, S.R., Moore, J.S., and Sottos, N.R. (2009) Force-induced activation of covalent bonds in mechanoresponsive polymeric materials. *Nature*, **459** (7243), 68–72; (d) White, S.R., Sottos, N.R., Geubelle, P.H., Moore, J.S., Kessler, M.R., Sriram, S.R., Brown, E.N., and Viswanathan, S. (2001) Autonomic healing of polymer composites. *Nature*, **409**, 794–817; (e) Cordier, P., Tournilhac, F., Soulie-Ziakovic, C., and Leibler, L. (2008) Self-healing and thermoreversible rubber from supramolecular assembly. *Nature*, **451**, 977–980; (f) Herbst, F., Dohler, D., Michael, P., and Binder, W.H. (2013) Self-healing polymers via supramolecular forces. *Macromol. Rapid Commun.*, **34** (3), 203–220.
- 2 (a) Caruso, M.M., Davis, D.A., Shen, Q., Odom, S.A., Sottos, N.R., White, S.R., and Moore, J.S. (2009) Mechanically-induced chemical changes in polymeric materials. *Chem. Rev.*, **109** (11), 5755–5798; (b) Murphy, E.B., and Wudl, F. (2010) The world of smart healable materials. *Prog. Polym. Sci.*, **35** (1–2), 223–251.
- 3 (a) Xia, F., and Jiang, L. (2008) Bio-inspired, smart, multiscale interfacial materials. *Adv. Mater.*, **20** (15), 2842–2858; (b) Youngblood, J.P., and Sottos, N.R. (2008) Bioinspired materials for self-cleaning and self-healing. *MRS Bull.*, **33**, 732–741; (c) Binder, W.H., Pulamagatta, B., Schunack, M., and Herbst, F. (2012) Biomimetic polymers, in *Bioinspiration and Biomimicry in Chemistry* (ed. G. Swiegers), John Wiley and Sons, Hoboken, NJ, pp. 323–366. ISBN 0470566671 and 9780470566671.
- 4 (a) Gragert, M., Schunack, M., and Binder, W.H. (2011) Azide/alkyne-“click”-reactions of encapsulated reagents: toward self-healing materials. *Macromol. Rapid Commun.*, **32** (5), 419–425; (b) Binder, W.H., and Herbst, F. (2011) Click chemistry in polymer science, in *McGraw-Hill Yearbook of Science & Technology* (ed. D. Blumel), McGraw-Hill, New York, pp. 46–49; (c) Binder, W.H., and Sachsenhofer, R. (2008) “Click”-chemistry in polymer and material science: an update. *Macromol. Rapid Commun.*, **29** (12–13), 952–981.

Part One
Design of Self-Healing Materials

1

Principles of Self-Healing Polymers^{*)}

Diana Döhler¹⁾, Philipp Michael¹⁾, and Wolfgang Binder

1.1 Introductory Remarks

All matter is subject to thermal or mechanical destruction as well as chemical degradation during its active lifetime – thus restricting the use of each crafted piece of matter which has been fabricated with a usually huge amount of intellectual and also hand- or machine-driven force. When the *Romans* invented concrete as a construction material more than 2000 years ago for erecting arches, water-pipes and building of monuments, such as the *Pantheon*, it might be assumed that they did not know about any of the molecular mechanisms of self-healing in this material. However, they surely knew and realized by observation of, for example, old Egyptian pyramids, that the construction of an empire to last for many centuries needs even longer lasting materials. Indeed, a useful construction material does not only need to be strong and stiff, it also needs to be flexible in shape and application, thus self-hardening concrete definitely is advantageous over handcrafted stone. The self-healing properties of concrete have provided us with testimony of this technically advanced (*Roman*) culture, whose achievements can be seen even in our modern times.

Polymers and polymeric materials are “the” smart invention and technological driving force of the twentieth century, hence the quest for self-healing or self-repairing polymers [1, 2] is strong. Not only the practical demand for maximum usage-times of each fabricated thing, but also the everlasting limitation of natural resources and costs leads to the search for self-repairing polymeric materials needing no direct human action for repair. Therefore, as new polymers and polymeric materials are designed, the quest for materials with self-healing properties (i.e., those which can regenerate similarly to living matter, especially after mechanical deformation and crack-formation) is increasing, culminating in the need for self-healing polymers after mechano-deformation [3–10]. In such

*) This chapter is partially based on thoughts published in *Macromol. Rapid Commun.* (2013), 34 (3), 203–220, written and designed by the very same authors.

1) Diana Döhler and Philipp Michael contributed with equal share to this article.

materials, stress of a certain magnitude (either chemical, physical, or thermal) induces a mechanical deformation in the polymer, which in turn activates a response within the material, leading to “healing” of the generated (physical) damage. Despite the inevitable fact that the destructive and renewing force has allowed new civilizations to emerge during the past (historical) times, a short look at nature makes the possibilities of repair and restoration of properties obvious—why would man not be able to achieve the same, similar, or even better? Naturally, mankind is taking steps to increase the lifetimes of all materials, in particular those of polymeric materials and composites, thus reducing the need for repair and replacement of such materials. Looking at superficial injuries in mammal organisms we see that a vascular (e.g., bloodstream-supported) supply-system helps to restore and heal mechanical damage via the blood-clotting cascade and subsequent tissue regeneration. This very simple principle demonstrates that biomimicry might help in the design of self-healing polymers by applying similar capsule- or vascular-based logics (see also Chapter 2). Looking further, principles of DNA-repair based on the radical scission of DNA-chains can induce a DNA-repair cascade, which in its complexity cannot be copied in simple bulk polymeric materials, but shows that a dynamic system is required to enable a self-healing material. Thus, an important aspect of self-healing is the presence of a structure which is able to respond dynamically to an external stimulus, enabling the restoration of the initial material properties. Due to their highly complex chain structure, polymers are ideally suited to serve as molecules for dynamic and thus self-healing properties.

1.2

General Concept for the Design and Classification of Self-Healing Materials

A polymer displaying self-healing properties needs the ability to transform physical energy into a chemical and/or physical response able to heal the damage—a process which normally is not present in “conventional–non-self-healing” polymers. Thus, the polymer needs to “sense” the damaging force, transforming it autonomously (without further external stimulus) into a healing-event, ideally at the damaged site. The possible mechanistic designs of self-healing polymers are depicted in Figure 1.1. A *self-healing polymer*, therefore, is supposed to heal damage (see Figure 1.1a, imposed by *shear-force* or another *rupturing event*) by either *physical processes* alone (see Figure 1.1b) or via a combination of chemical and physical processes (see Figure 1.1c). The design of self-healing polymers, therefore, is a multidisciplinary process, requiring knowledge of their structure, their individual dynamics, as well as a deep knowledge of chemical processes. Thus, the design of self-healing polymers needs a thorough understanding of the polymer’s individual chain-dynamics (see also Chapters 3 and 4), and not only the dynamics of whole chains or molecules within the polymeric material, but also the dynamics of each segment interacting with a specific part of the new interface or other polymeric/monomeric molecules.

Similar to biochemical healing processes, the initial damage (see Figure 1.1a) generates a *free (usually fresh) interface* (shown as a crack), which in turn can act

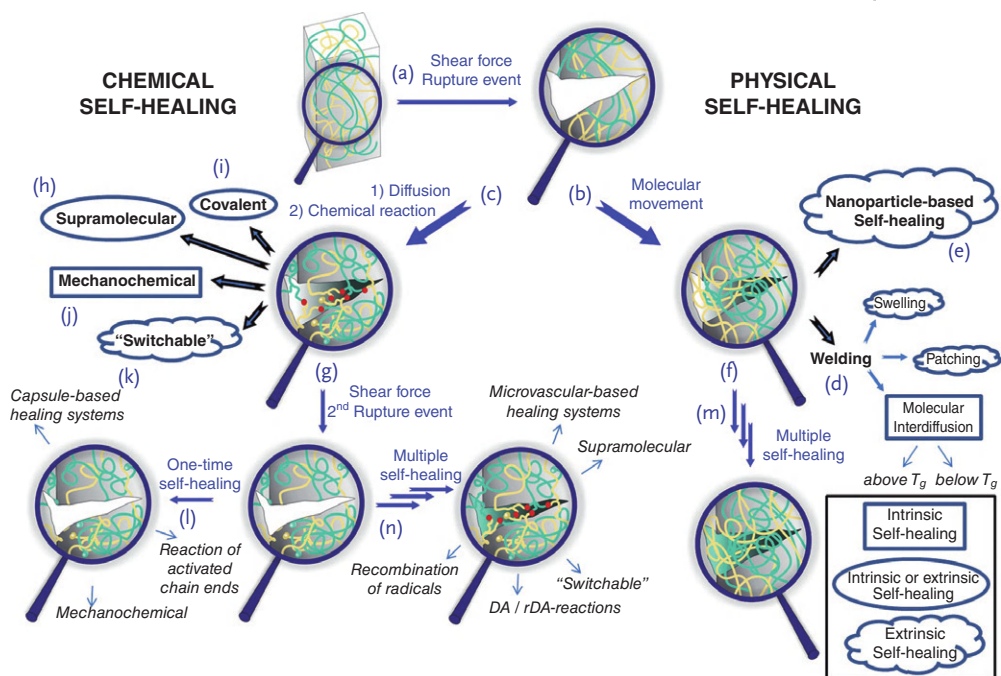


Figure 1.1 Design of self-healing polymers. (a) Shear-force or rupture is transformed into a crack, sensed by the polymer matrix. (b) Newly generated interfaces lead to concentration gradients, which allow enhanced diffusional processes (f), resulting in welding, swelling, patching, nanoparticle enrichment or simple molecular interdiffusion (physical entanglement) of polymer chains (d) and (e). (c) Molecular movements lead to contact

between functional groups and thus to a chemical healing process, resulting in crack closure by a newly formed network (g) Healing induced by a crosslinking reaction, either via supramolecular forces (h), covalent chemistry (i), mechanochemical (j) or "switchable" reactions (k). After a second rupture event at the same area the number of healing-cycles can vary, implying either a one-time healing process (l) or multiple healing (m) and (n).

as a site for molecular processes, such as *swelling*, *patching* or *simple molecular diffusion*, which can induce a *welding process* (see Figure 1.1d), subsequently leading to a closing of the crack and thus a "self-healing" process [11]. Nanoparticles (see Figure 1.1e), small, or even large molecules can diffuse to the interface, thus leading to changes in the local concentration, and also inducing changes in the individual local mobility of the molecules. This can in turn lead to the healing of the crack (see Figure 1.1f).

Chemical healing processes (see Figure 1.1c) always need a combination of physical and chemical healing principles, as a chemical reaction can only take place when contact between the reactants has been achieved. In general, after diffusion and reaction of the reactants, the crack is filled by a newly formed network (see Figure 1.1g [see also Chapter 5]), which results from the crosslinking reaction of individual polymer chains, either via purely physical ("supramolecular") forces [9, 12–14], or by action of truly chemical forces resulting in partially reversible [15–17] or stable [18, 19] covalent bonds (see Figure 1.1h and i). Purely *supramolecular*

interactions [9, 20–22] (see also Chapters 11–13), well known from molecular self-assembly, can reform, thus generating a network with dynamic properties by itself [23]; *covalent chemistry* (see Chapters 6–9, 15, and 17) is able to form a new network by a plethora of chemical crosslinks, often well known and well optimized by technical processes of resin-chemistry (“thermosets”). In particular Diels–Alder (DA) reactions [17, 24–28], epoxide chemistry [29–41], “click-based” chemistry [18, 42–54], isocyanate chemistry [55], olefin metathesis [19, 56–61], and thiol chemistry [62, 63] have gained significance in this respect. Choice of the chemical reactions to be used usually takes into account the efficiency (“free energy”) of the reactants as a major selection tool, besides the stability and selective incorporation of the respective functional groups into the final material, for example, via encapsulation strategies (see also Chapters 10 and 16).

Furthermore, so called *mechanochemical* reactions (see Figure 1.1j) (see also Chapter 8) can transform the physical energy of damage directly via a specially designed chemical group (“mechanophore”) [4, 64, 65] into an activated chemical state, which in turn allows self-healing. These specially designed reactions are intrinsically coupled to the existing polymeric chains, as the attached polymeric chains act as a “handle”, which by definition allows the conversion of applied mechanical energy into the actual chemical reaction [66]. Especially, ring-opening reactions [64, 65, 67–73] and carbene-based catalyst activation [74–78] have become prominent for realizing the concept of self-healing polymers.

Moreover, an *inherent “switch”* [79–82] (see Figure 1.1k) (see also Chapter 7) such as light or an electrochemical stimulus can be flipped, triggering a reversible network formation within the polymer and thus a self-healing response.

Additionally, the mentioned self-healing approaches can be divided into *intrinsic* and *extrinsic* concepts [7] (see Figure 1.1), where intrinsic self-healing polymers utilize an inherent material ability to self-heal, triggered either by a damage event or in combination with an external stimulus. In contrast, for extrinsic self-healing concepts the healing agents have to be pre-embedded into a (polymeric) matrix enabling their release during a rupture event and thus self-healing.

All these approaches display different features with respect to external conditions under which self-healing takes place (such as the required stress for activation, the temperature of healing as well as other external constraints imposed by the mechanism of the healing concept) the number of healing-cycles thus implying either a once-a-time-healing after one stress-event (see Figure 1.1g and k), or the possibility to repeatedly heal damage at the same position of the material (see Figure 1.1l and m) as well as the timescale on which the self-healing process is taking place. Hence, a large body of work has been dedicated to optimize the conditions of healing (temperature, additives, and optimization of catalysts) as well as the technical realization of the concept, thus being able to fabricate and produce a technically useful polymer at reasonable costs within a technical process (see Chapter 14).

The following sections will provide an overview of the chemical principles of the underlying concepts to fabricate self-healing polymers. The various possibilities of chemical and physicochemical approaches have, therefore, triggered a number

of strategies which will be discussed in separate chapters as their chemical and physical principles are totally different.

1.3

Physical Principles of Self-Healing

In general, all self-healing concepts have the aim to generate crosslinked networks, either by *covalent* or *supramolecular chemistry*, or by purely physical crosslinking via chain entanglements. Self-healing principles based on *physical interactions* constituted one of the first historically observed self-healing behaviors of manmade plastics and will be discussed in the following. Chemical self-healing concepts will be presented in Chapter 9. Physical principles implementable in self-healing approaches are based on *molecular diffusion*, induced either by Brownian motion, chain segment motion or entropy driven movement of molecules or particles with or without external stimulus. Several self-healing mechanisms, such as *molecular interdiffusion*, *welding*, *swelling*, or *self-healing via nanoparticles* can be assigned to this category. Additionally phase-separation phenomena in polymers can be an enhancing factor for self-healing [83–95] (e.g., see Chapter 13).

In order to understand the phenomena of self-healing based on physical interactions it is necessary to get fundamental knowledge of molecular mechanisms. The elementary steps of all physical self-healing principles are interdiffusion and entanglement of polymer chains [11, 96]. Both properties depend on intermolecular forces, which are closely linked to the chemical nature of the polymer and the length of the molecules, including the dependence on the average molecular weight. However, both factors often oppose each other. Accordingly, short chains enable fast molecular interdiffusion, while long chains generate materials with the ability for high strength recovery at the interface [11].

One of the best known and well understood self-healing approaches based on physical methods is the so-called *molecular interdiffusion*, which can be divided into thermoplastic and thermoset self-healing occurring above and also, at least theoretically, below the glass transition temperature (T_g). It has been shown that the polymer/polymer interface gradually vanishes and the mechanical strength at the initial interface increases by bringing two pieces of identical or even compatible polymers into contact. Thus, the polymer matrix is actually healed just due to molecular diffusion along the polymer/polymer interface [3, 11].

In order to understand this phenomenon, Wool and O'Connor [97] developed, in 1981, a five-stage mechanism to unscramble the complexity of strength recovery at ruptured polymer/polymer interfaces, and provide an explanation for the functioning principle of many self-healing concepts (see Figure 1.2), being strongly related to molecular interdiffusion at or above the glass transition (T_g). At this temperature polymer segments are mobile enough to enable an efficient self-healing process. This relatively simple model is, in its basic steps, applicable as a universal mechanism for nearly all self-healing concepts [98].

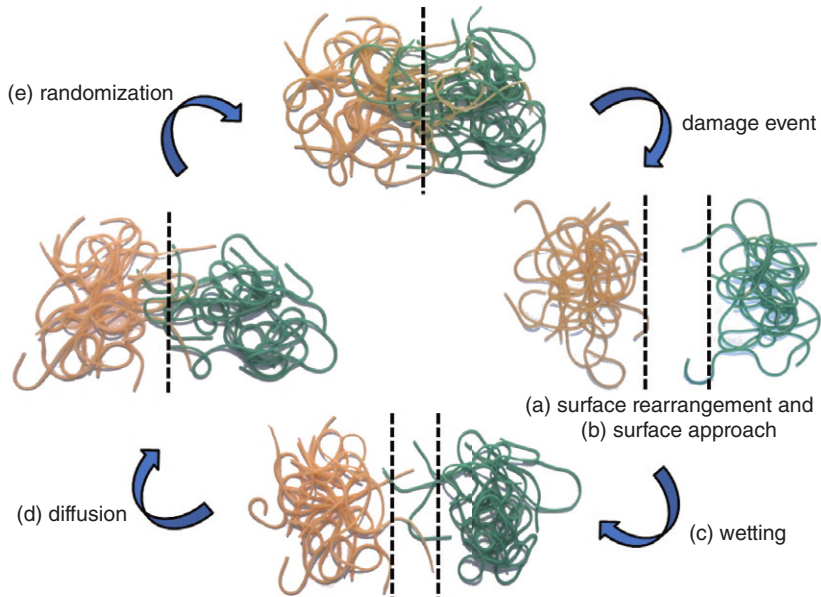


Figure 1.2 Stages of self-healing mechanism. (a) Surface rearrangement, (b) surface approach, (c) wetting, (d) diffusion and (e) randomization.

The principle stages of healing according to the mechanism of Wool and O'Connor [97] are illustrated in Figure 1.2 including the steps of surface rearrangement (a), surface approach (b), wetting (c), diffusion (d) and randomization (e). Surface rearrangement and surface approach are the first steps after a damage event has occurred. These steps are the most critical ones as healing can only take place if the ruptured interfaces can come into contact with each other. The surface rearrangement (a) influences the rate of crack healing significantly due to the discontinuity of the topography and the roughness of the created crack surface, which may change with time, temperature and the applied pressure [11, 97, 98]. Higher surface roughness leads to a higher contact area and, therefore, to higher rates of diffusion, and thus expectedly higher rates of self-healing. The surface approach (b) under controlled laboratory conditions appears to be the most trivial step. However, in practice, this is one of the most crucial steps regarding surfaces pulled apart by the damage event which might prevent the contact of the surface layers and thus terminate the self-healing process [98]. Moreover, the surface approach stage determines the mode of healing, for example, healing in point or line mode [97]. Before the healing process can start, the wetting of the cracked surfaces by each other or by healing agents has to be ensured. This is mostly achieved by ensuring sufficiently high chain mobility of the initial material, and also by increasing the temperature or adding solvents. The wetting stage (c) enables diffusion (d) which results in the entanglement of polymer chains and,

therefore, in the recovery of the mechanical properties of the healed material. Diffusion is a fractal random walk of polymer chains near to the surface which first results in the entanglement of the mobile chains and then in interpenetration into the unruptured matrix material. The diffusion stage is the most important step for restoring the mechanical properties during which the majority of these properties are recovered or healed [97–99]. During the randomization stage (e) the complete loss of initial crack interfaces can be observed.

As previously mentioned, it is possible to observe self-healing via *molecular interdiffusion*, not only above but also below the T_g , despite being a contradiction of the conventional knowledge of polymer movement suggesting no motion of polymer segments below their T_g . Nevertheless, wetting and diffusion can be observed at a certain healing temperature significantly below the T_g [96, 100–102]. Wool *et al.* [100, 102] observed crack healing processes in glassy polymers and related this to the interdiffusion of molecular chains and the subsequent reformation of molecular entanglements. It is claimed in literature, and highly controversially discussed in the scientific community, that this self-healing ability is caused by a potential reduction of the T_g at polymer surface layers compared to the T_g in the bulk [11, 96, 101, 103–105].

Four possible explanations for this behavior [106–115] are illustrated in Figure 1.3: (a) The accumulation of polymer end groups at the outer surface due to their higher space requirement compared to the corresponding chain segments leads to a lower density of chain segments at the inner surface, causing a higher chain mobility and thus a lower T_g . (b) The confinements for polymers with high molecular weight force them to alter their chain conformation (induced by a break in symmetry at the polymer surface—flattened chain conformation), resulting in decreasing interchain entanglements and a reduction in the chain segment density. (c) The collective motions along the chain (loop motions) dominating in thin film scenarios require a weaker free volume compared to the standard motion, leading to a decrease in the effective chain segment density and, therefore, to a reduction in the T_g at the interface. (d) The accumulation of low molecular weight polymers at the surface layer can cause, according to the Flory–Fox equation, a reduction in T_g . This effect can be explained by their lower surface tension and the reduction in free energy by a smaller change in conformational entropy. Following these assumptions, the final reduction in T_g at the surface layer will enhance the mobility of the chain segments and thus enable self-healing according to the basic steps of Wool and O’Connor [97–99].

A further self-healing concept based on physical interactions is *welding*. Beside the mentioned molecular interdiffusion it is one of the traditional self-healing methods. Welding relies on damage healing by forming chain entanglements between two contacting polymer surfaces in order to restore the original mechanical properties of the ruptured area [3]. Therefore, welding is, in a strict interpretation, a superordinated category of molecular interdiffusion. Nevertheless, it is often referred to separately due to its various manifestations. The welding process consists of the same healing stages mentioned above: surface rearrangement, surface approach, wetting, diffusion and final randomization (see Figure 1.2).

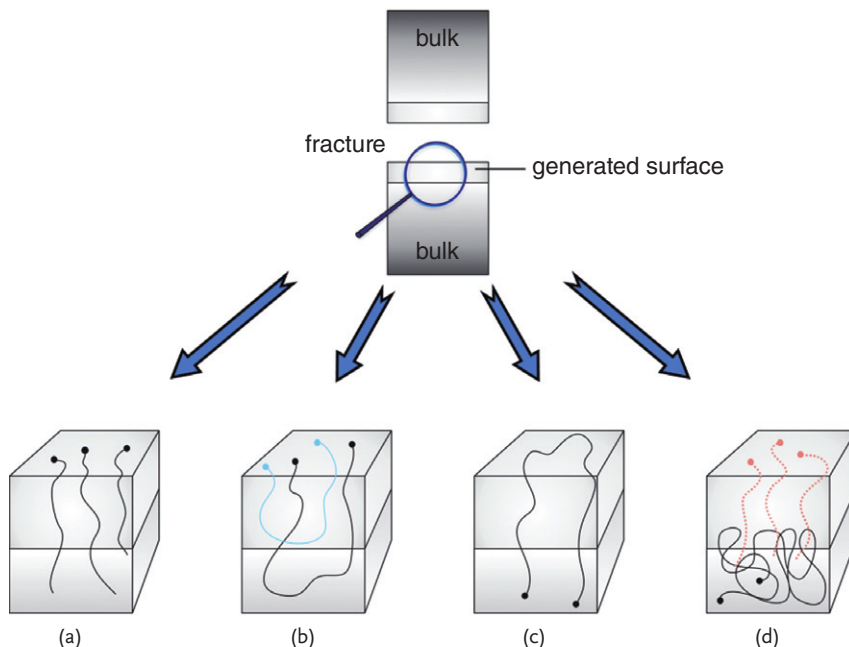


Figure 1.3 Reduction of T_g in polymer surface layers. The accumulation of polymer end groups at the outer surface (a), confinements for polymer chains due to high molecular weight (b), and collective motions along the chain (c) leading to a decrease in the effective chain segment density in all

three cases (a)–(c) and therefore to a reduction in the T_g at the interface. The enrichment of low molecular weight polymers at the surface (d) causes a reduction in T_g according to the Flory–Fox equation.

However, the rate of rearrangement and reorganization is influenced by various factors, such as the welding temperature, surface roughness, remaining chemical bonds between the surfaces, and the presence or absence of solvents [3]. In the case of covering or replacing damaged material by new externally added material the approach is also known as *patching*. If some solvents are involved to increase the mobility of the polymer chains the healing process is called *swelling*.

A completely different approach is the *nanoparticle-based* self-healing concept (see also Chapter 3) [3, 98, 116], inasmuch as it does not involve separation and rejoining of polymer chains like the previously discussed methods. This concept is based on the migration of nanoparticles to the damaged area. After cooling below a certain temperature a solid phase is formed recovering the mechanical strength and thus healing the damage. This method assumes a sufficiently high mobility of the nanoparticles in the polymer matrix. In order to enable this accumulation of particles at the crack surface the healing occurs commonly above T_g . Moreover, the modification of the nanoparticle surface is significant to ensure a sufficiently high driving force based on entropic and enthalpic interactions between the particles and the polymer matrix.

1.4 Chemical Principles of Self-Healing

All self-healing methods have the aim to generate crosslinks in networks, either by physical interactions, as discussed previously, or by chemical reactions of various kinds of functional groups, which will now be discussed in detail.

Chemical self-healing principles (see Chapters 2, 6–9, 11–13, 15 and 17) can be classified into two main categories, based either on covalent (see Figure 1.4a) or on supramolecular network formation (see Figure 1.4b). In the case of covalent network formation chemical bonds between functional groups are generated and thus a permanent, but sometimes even reversible, network is established. In contrast, supramolecular networks are commonly reversible associates of polymers linked via supramolecular interactions and show a higher dynamic behavior. Moreover, a subdivision into inherent “switchable” polymer systems (see Figure 1.4c) and concepts using mechanochemical activation of molecules by direct effect of a mechanical force (see Figure 1.4d) can be made. Concepts assigned to these two categories could also be classified into covalent or supramolecular network formation. The separations are, thereby, often blurred, enabling the assignment of several self-healing methods into more than one category.

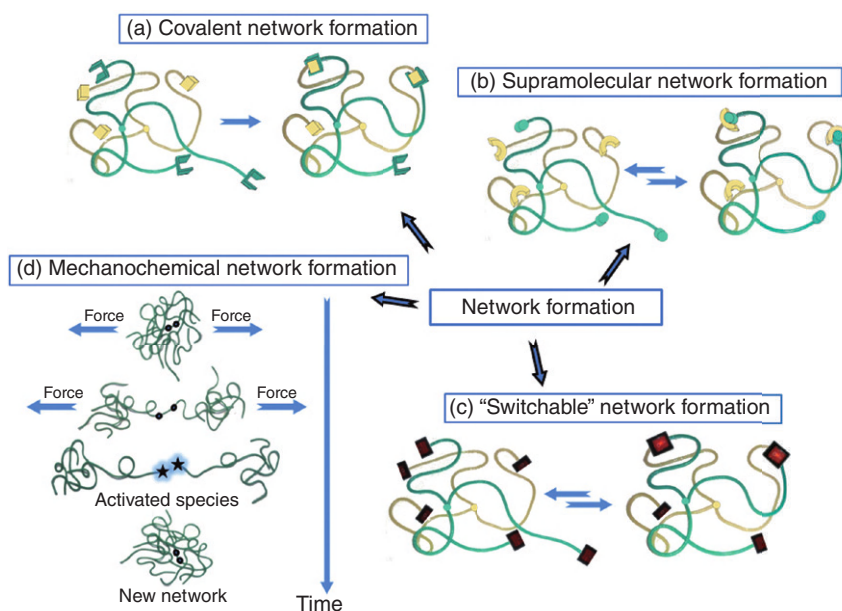


Figure 1.4 Different modes of chemical interactions resulting in crosslinked network formation. (a) Covalent network formation, (b) supramolecular network formation, (c) “switchable” network formation and (d) mechanochemical network formation.

1.4.1

Covalent Network Formation

A great challenge for chemists and material scientists involved in the evolution of self-healing polymers was the development of concepts that, in a fast and preferably simple way, form highly crosslinked networks. Therefore, they tuned the properties of the self-healing agents so that damage healing could occur under ambient conditions, like low temperatures, or humid and oxygen-containing environments. Furthermore, a large diversity of protection methods, such as encapsulation or *in situ* activation of catalysts, was developed. Moreover, some scientists explored various catalytic self-healing methods to accomplish a fast network formation at ambient temperatures, while others pursue higher temperature methods. Another challenging task was to guarantee a healing response only in direct response to a damage event. Therefore, reversible reactions shiftable to a “broken” stage and cured subsequently by re-shifting to the “healed” stage were used. Furthermore, different protection methods, preventing not only disturbing external influences but also undesired premature crosslinking reactions, found application. Accordingly, a large diversity of self-healing concepts has been developed up today.

In self-healing concepts based on covalently crosslinked networks, covalently linked network points are generated in a chemical reaction (see also Chapters 6–9 and 15). They exist in a large diversity and can be subdivided into *reversible and irreversible reactions*. Reversible methods, like DA/retro-DA reactions (DA/rDA) [17, 24–28, 117–123] or polycondensations [124, 125] provide the opportunity for multiple healing cycles, while irreversible methods, like the microcapsule-based ROMP concept [19, 59–61, 126], epoxides [127–130], or various click approaches [18, 42, 43, 48, 51], cannot heal a once ruptured area a second time. For more information see also Section 1.5.

1.4.1.1 Irreversible Covalent Network Formation Concepts

One of the most prominent self-healing methods based on *irreversible covalent network formation* was developed by White *et al.* [19] in 2001, who investigated the microencapsulation of dicyclopentadiene and subsequent embedding into an epoxy-matrix containing a Grubbs catalyst (see Figure 1.5a; Table 1.1a) (see also Chapters 9, 10, and 15). A damage event rips the microcapsules and releases the dicyclopentadiene monomer into the crack plane, where it comes into contact with a ruthenium-based Grubbs catalyst and triggers a ring opening metathesis polymerization (ROMP) [19, 56–58]. The subsequent generation of a dense network results in the recovery of the material properties, whereby self-healing efficiencies up to 99% can be achieved [126]. Further studies have resulted in the development of alternative monomers suitable for these ROMP systems, such as *endo*- [19] and *exo*-dicyclopentadiene [59], *endo*-1,2-dihydrodicyclopentadiene [59], norbornene [59], 5-ethylidene-2-norbornene [60], 5-(chloromethyl) norbornene [61], 5-(bromomethyl) norbornene [61] and norbornene carboxylic acid ethyl ester [61] (see Table 1.1b). Important, therefore, is a microencapsulation approach that can be applied now to nearly all kinds of polymers, such as thermosets, thermoplasts,

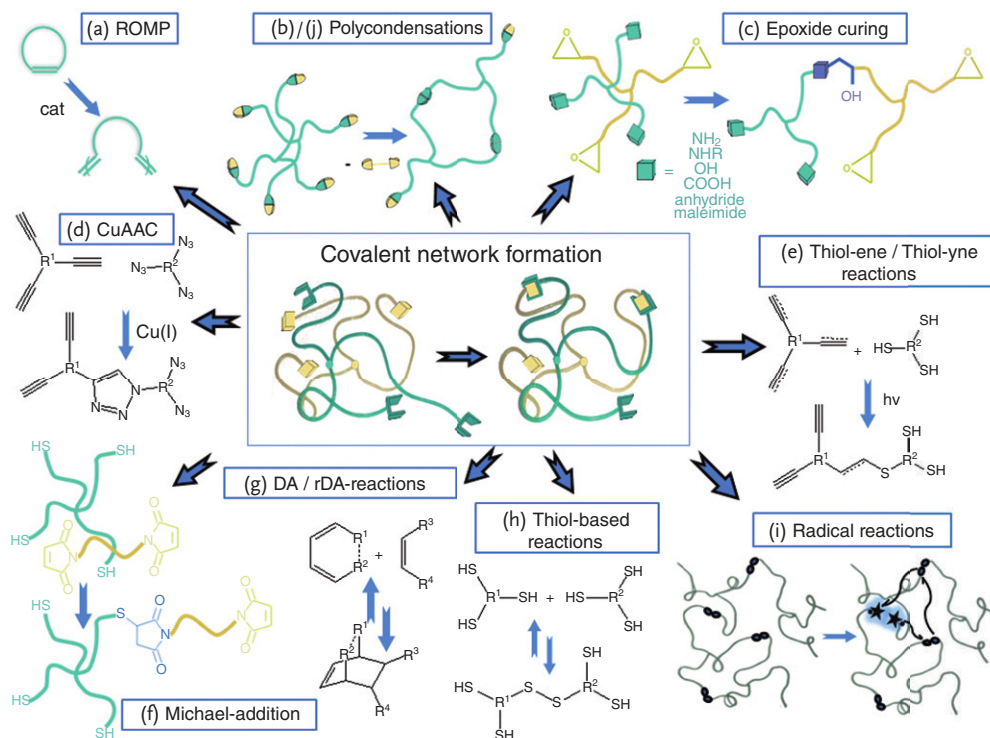


Figure 1.5 Self-healing methods based on covalently crosslinked networks, utilizing (a) ROMP, (b) irreversible polycondensations, (c) epoxide chemistry, (d) CuAAC or (e)

thiol-ene/thiol-yne click reactions, (f) Michael additions, (g) DA/rDA reactions, (h) thiol-based reactions, (i) radical reactions, or (j) reversible polycondensations as concept.

and elastomers [19, 37, 41, 133–139]. The advantage of applied encapsulation is the possibility to spatially separate the reactive compounds from each other, from the matrix and, therefore, from the environment, thus increasing the longtime stability of the healing system (see Chapter 9). However, the original material properties can be affected negatively by embedding microcapsules. Moreover, the high cost of the Grubbs catalyst may limit a wider technical implementation.

In order to overcome these shortcomings, in 2006 White *et al.* [131] studied a microcapsule-based self-healing systems using polycondensation reactions of technically available hydroxyl-terminated poly(dimethylsiloxane)s and poly-(diethoxysiloxane)s, efficiently catalyzed by cheaper organotin compounds (see Figure 1.5b; Table 1.1, entry 3). In order to prevent a premature reaction between the macromonomers, the tin compound was encapsulated in polyurethane microcapsules and embedded into the polymer matrix. In case of a rupture event the fluidity of the poly(dimethylsiloxane) enables flow into the crack, where a polycondensation reaction between the poly(dimethylsiloxane) and the poly(diethoxysiloxane), catalyzed by the tin compound, is triggered, forming a

Table 1.1 Irreversible covalent network formation concepts for self-healing applications.

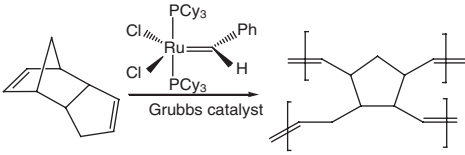
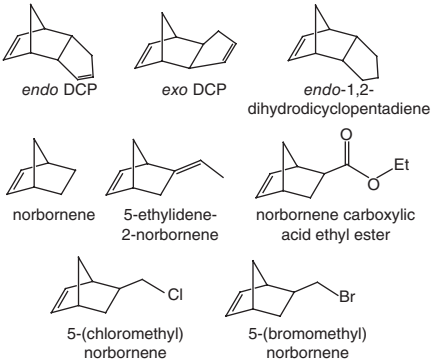
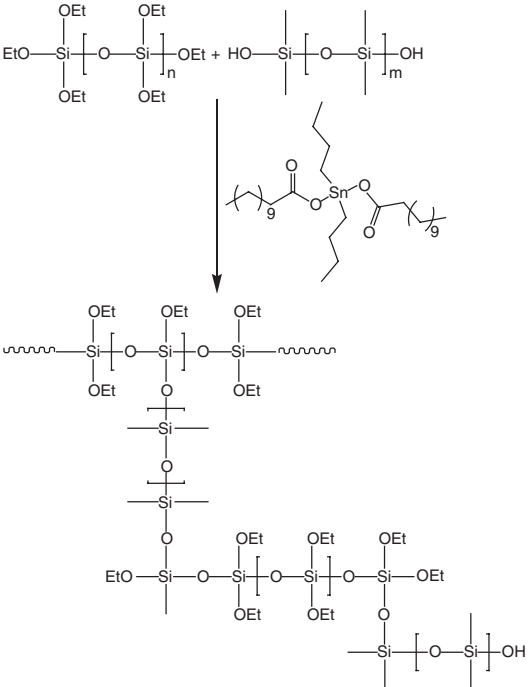
Entry	Example	Ref.
(a)	Ring-opening metathesis polymerization (ROMP)	
1	ROMP 	[19]
2	ROMP monomers applicable for self-healing 	[19, 59–61]
(b)	Polycondensation reactions	
3	Poly-siloxanes 	[131]

Table 1.1 (Continued)

Entry	Example	Ref.
(c)	Epoxy/hardener methods	
4	Epoxy/amine	[40]
5	Epoxy/mercaptane	[41]
(d) + (e)	Click reactions	
6	CuAAC	[18, 42, 43, 48, 51]
7	Thiol-ene/ thiol-yne click reaction	[52–54]
(f)	Michael addition	
8	Thiol/ maleimide	[132]

siloxane-crosslinked network within the damaged zone. Moreover, the healing system is applicable under aerobic and humid conditions due to the hydrophobic nature of both siloxane-based macromonomers and the stability of the released tin catalyst [131, 140]. This is of crucial importance for the practical realization of self-healing, and together with the lower cost of the catalyst was the prime motivation for developing such systems. However, it was not possible to achieve healing efficiencies of more than 24%, making a technical realization doubtful.

Another self-healing approach much closer to technical implementation utilized epoxides as matrix-embedded encapsulated healing agents [29–39] (see Figure 1.5c). Epoxides are highly strained three-membered rings which can undergo rapid coupling reactions with the second healing reagent, the so-called hardener, commonly substrates with activated hydrogen atoms, such as amines, alcohols, carboxylic acids, or mercaptans, as well as anhydrides and maleimides. In the course of the rupture event, the epoxide-containing capsules are cracked and release their content in order to react with the also embedded hardener via covalent bond formation. After treatment with these multifunctional and coreactive curing agents 100% conversion is usually reached, and insoluble thermosets are created composed of three-dimensional networks which fill the crack and restore the strength of the material. The crosslinking process can occur either at low temperatures (“cold curing”) or at elevated temperatures (“hot curing”), the latter being of minor interest for self-healing applications. Thus, primary and secondary aliphatic amines are most often used as hardeners because of their higher reactivity at low temperatures compared to other hardeners. Other important curing agents are acid anhydrides and formaldehyde resins which can react with the hydroxy groups of high molecular weight resins, resulting in further crosslinking reactions. While choosing the curing agent as well as the curing conditions the characteristics of the final resin, such as the crosslinking density and the morphology, can be freely tuned. Further, cationic curing can be induced photochemically [127–130]. Epoxy curing reveals some special advantages which make it to one of the most powerful self-healing concepts, especially for epoxy resin materials. While using epoxides as healing agents the same kind of material as the matrix is produced, thus ensuring a good adhesion between them and enabling full recovery of the initial material properties. Furthermore, together with the good healing efficiencies even at low temperatures, cold curing is the self-healing concept currently closest to commercial application. The sometimes lower longtime stability of the epoxy compounds can be partially compensated by the encapsulation, using specific wall materials or utilizing inherently more stable materials.

Recently, a self-healing system based on epoxy-amine resin formation [40] at ambient temperature was developed (see Table 1.1 entry 4). A modified aliphatic polyamine (EPIKURE 3274) and a diluted epoxy monomer (EPON 815C) were separately encapsulated and embedded into a thermoset epoxy matrix. The optimal mass ratio of amine to epoxy-containing capsules was determined to be 4:6 with an overall capsule content of 17.5% and an average healing efficiency up to 91%. However, a notable influence of the high capsule content within the polymer matrix on the material properties can be expected. A long term stability

of the healing system of at least 6 months was shown. Another example of cold curing epoxy systems consists of the conventional epoxy bisphenol-A-diglycidyl ether (EPON 828) and the mercaptane hardener pentaerythritol tetrakis(3-mercaptopropionate) (PETMP) acting as a two-compound healing system at room temperature [41] (see Table 1.1 entry 5). Both compounds were encapsulated into different types of microcapsules and incorporated into an epoxy resin matrix. An attractive healing efficiency of 104.5% with a low capsule content of 5% could be achieved after 24 h at 20 °C and also a sufficiently long term stability of the healing agents for at least 1 year could be demonstrated.

An approach of crosslinking concepts acting at ambient temperatures based on “click” reactions has been pursued by the groups of Binder [18, 42, 43] (see Figure 1.5d; Table 1.1 entry 6) and Kessler [48, 51], as well as by the thiol-ene/thiol-yne click concept [52–54] (see Figure 1.5e; Table 1.1 entry 7). However, they used a set of reactions called click chemistry [44–50], characterized by generating only one, mostly regiospecific pure product in high yields, working under simple reaction conditions and rapidly achieving complete conversion via a thermodynamic driving force greater than 20 kcal mol⁻¹. This definition was given by Sharpless *et al.* [141] and thus primed the capability of this reaction type for self-healing applications. Binder *et al.* [18, 42, 43] (see Table 1.1 entry 6) have developed a click-based self-healing system using the copper(I) catalyzed alkyne-azide cycloaddition (CuAAC) reaction. They investigated a system assembling fluid trivalent azido-telechelic poly(isobutylene)s (PIB) and various low molecular weight multivalent alkynes [18, 42]. Both reactants were encapsulated in urea-formaldehyde capsules and embedded into a polymer matrix containing Cu^I(PPh₃)₃Br and TBTA as catalytic system. After the rupture event the healing agents came into contact with each other and the catalyst, triggering the cycloaddition reaction, forming a crosslinked network, and thus healing the damage. In the present case, the crosslinked network formation proceeded at ambient temperatures and resulted in nearly full recovery of the tensile modulus of 91% at 25 °C or an increased value of 107% at 60 °C. Moreover, the network formation of two multivalent fluid polymers [43] was investigated and optimized using fluid trivalent star-shaped azido- and alkyne-telechelic PIBs or multivalent side-chain functionalized copolymers of poly(acrylate), respectively, with Cu^I(PPh₃)₃Br as catalyst. Thus, higher network strand densities and faster crosslinking could be observed, even at room temperature. Furthermore, autocatalytic behavior of the crosslinking reaction has been proven, increasing further the efficiency of the CuAAC toward self-healing polymers. Kessler *et al.* [48, 51] (see Table 1.1 entry 6) followed a very similar approach also based on the CuAAC which is potentially applicable for self-healing, using two low molecular weight reactants (bisphenol-A-based bisazide and bisphenol-E or tetraethylene glycol-based diynes), and thus ensuring flow of the components into the crack. After triggering the CuAAC by the copper(I) catalyst the network filled the crack and restored the material properties. However, due to the bivalent monomers, linear polymers were generated which formed networks only via physical chain entanglements, while the previously described polymers [18, 42, 43] were able to form three-dimensional networks by covalent chemical bonds. Other

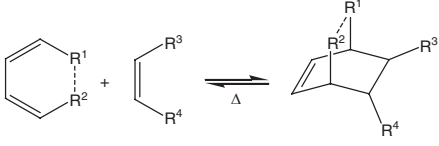
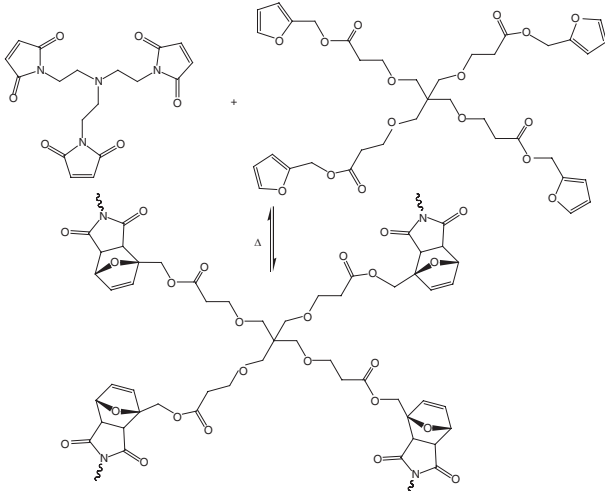
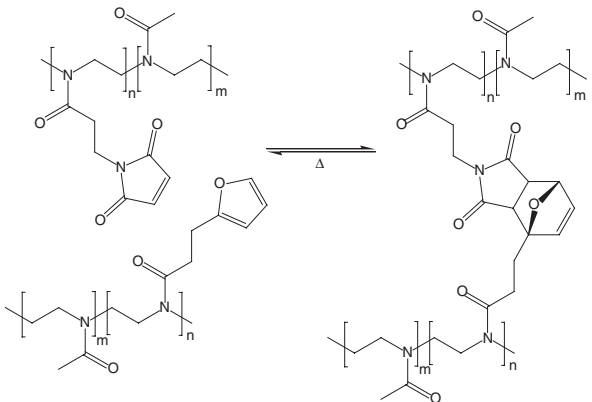
interesting potential self-healing approaches based on click chemistry might be strain-promoted azide-alkyne cycloaddition reaction or photochemically triggered thiol-ene or thiol-yne click reactions (see Table 1.1 entry 7). Thereby, the absence of biotoxic copper salts enables application in living systems. Moreover, thiol-ene and thiol-yne click reactions attract the attention of scientists due to their ability of combining the aforementioned advantages of click chemistry and the potential of light-triggered reactions, enabling a spatially and temporally controlled self-healing process. Further photochemically triggered reactions with similar advantages, like [2+2] or [4+4] cycloadditions, are discussed in Section 1.4.4 [6, 17, 142–144].

An alternative self-healing concept uses the Michael addition of tetravalent thiols and bivalent maleimides (see Figure 1.5f; Table 1.1 entry 8) and is thus an elegant method for damage healing of epoxy resin materials due to the ability of crosslinking between the residual amino groups at the crack surface and the maleimide moieties [132]. Therefore, a strong dependence of the healing efficiency on the used matrix resin can be observed, for example, using EPON 828 as matrix material reveals an average healing efficiency of 121% after curing for 5 days at 25 °C.

1.4.1.2 Reversible Covalent Network Formation Concepts

Prime examples of the class of *reversible covalent self-healing concepts* are versatile DA cycloaddition reactions [17, 24–28, 117–123] (see Figure 1.5f) (see Chapter 6). DA reactions are amongst the most important reactions in organic chemistry due to their ability for C–C bond formation in high yields and good stereochemistry. Therefore, a conjugated diene and a dienophile, both commonly electrochemically activated by substituents, react with each other via a [4+2] cycloaddition. Moreover, many DA products are able to undergo a thermally induced [4+2] cycloreversion, the so-called rDA reaction which is the basis of the self-healing ability of polymeric DA/rDA systems. Due to the weaker bond strength between diene and dienophile of the DA adduct compared to all the other covalent bonds, this bond will break preferentially during the damage event and the rDA reaction will take place [25]. If the damaged sample is heated again, the diene and dienophile will reconnect and the crack plane is healed. Heating is commonly necessary to enhance the mobility of the reactive groups at the crack plane and, therefore, to accelerate the DA reaction [17, 25]. Nevertheless, nowadays some DA/rDA systems are known which are able to mend a crack even at ambient temperatures [123]. Advantageous self-healing principles based on DA/rDA reactions do not need additional ingredients like microcapsules or microvascular networks, and allow multiple runs of self-healing processes in the same area. Nevertheless, the mentioned high mending temperatures, as well as oxidative side-reactions restrict the application area of the DA reaction. In principle, two different polymer architectures for DA/rDA systems are known: first the polymer backbone can either be functionalized along itself [27, 28, 120] (see Table 1.2 entries 11 and 13) or in the side chains [26, 121] (see Table 1.2 entry 12), and secondly, multivalent, often star-shaped systems with DA functionalities as end groups [24, 25, 27, 148] (see Table 1.2 entry 10) can be applied. Chemically, the utilizable functionalities for DA/rDA systems can be classified into three main categories: furan-maleimide-based polymers [17, 24–26, 117]

Table 1.2 Reversible covalent network formation concepts for self-healing applications.

Entry	Example	Ref.
(g)	Diels–Alder/retro Diels–Alder reaction (DA/rDA)	
9	DA/rDA 	
10	Furan-maleimide based DA/rDA 	[25]
11	Furan-maleimide based DA/rDA 	[17, 26]

(Continued)

Table 1.2 (Continued)

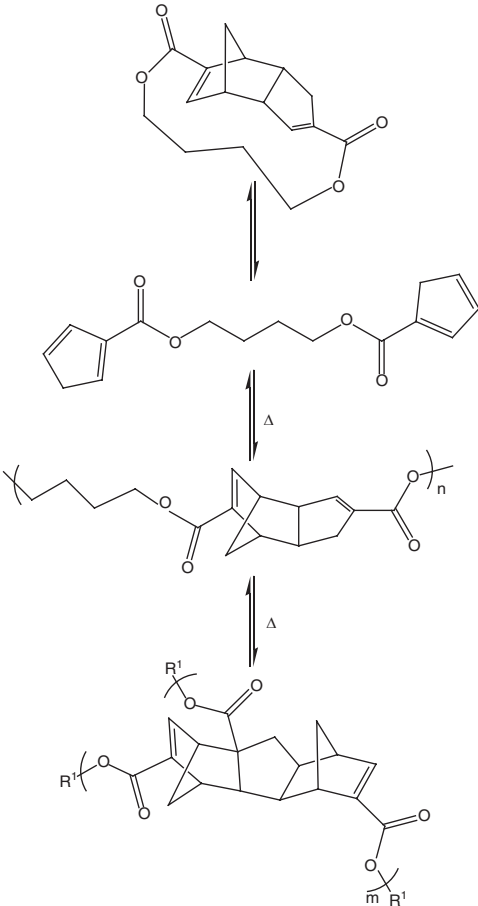
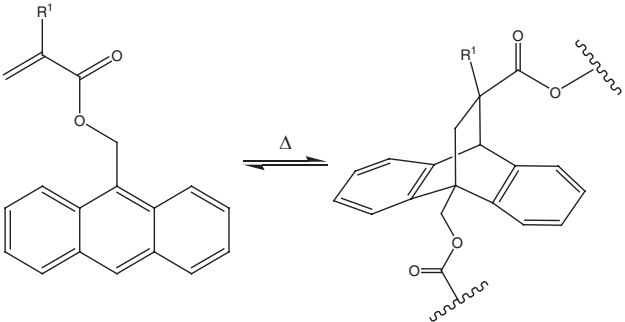
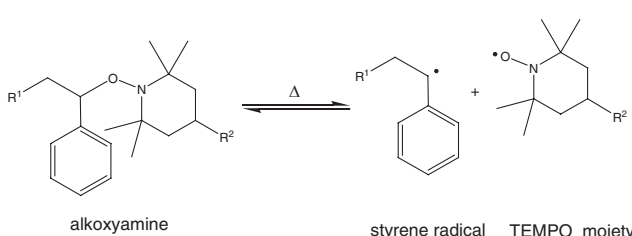
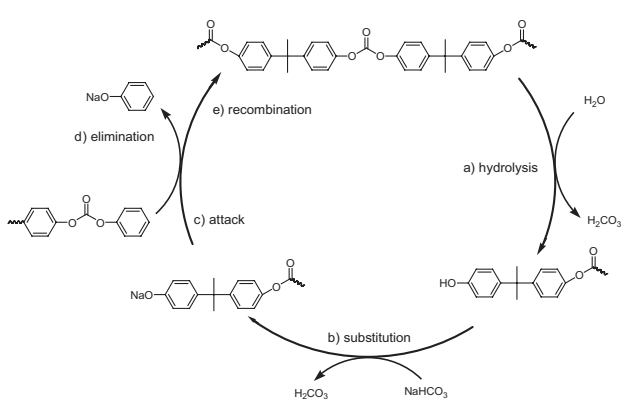
Entry	Example	Ref.
12 Cyclopentadiene- based DA/rDA	 <p>The diagram illustrates the synthesis and polymerization of a cyclopentadiene-based DA/rDA. It starts with a bicyclic dimer (top) in equilibrium with a linear dimer (middle). The linear dimer is then polymerized, as indicated by the Δ symbol, to form a polymer chain with a cyclopentadiene core (bottom). The polymer chain is shown with a repeating unit n and a terminal unit m with a substituent R^1.</p>	[27]
13 Anthracene-based DA/rDA	 <p>The diagram illustrates the synthesis of an anthracene-based DA/rDA. It shows a linear dimer (left) in equilibrium with a bicyclic dimer (right), as indicated by the Δ symbol. The linear dimer has a substituent R^1 and a terminal unit m with a substituent R^1. The bicyclic dimer has a substituent R^1 and a terminal unit n with a substituent R^1.</p>	[28]

Table 1.2 (Continued)

Entry	Example	Ref.
(h)	Thiol/disulfide linkages	
14	Side chain modified	[145]
15	Backbone modified	[62]
(i)	Radical-based methods	
16	RAFT-like systems	[146]

(Continued)

Table 1.2 (Continued)

Entry	Example	Ref.
17	Alkoxyamine-based systems 	[147]
(j)	Polycondensation reactions	
18	Polycarbonate 	[124, 125]

(see Table 1.2 entries 10 and 11), dicyclopentadiene-based polymers [17, 27] (see Table 1.2 entry 12), and anthracene-based polymers [17, 28, 118, 120, 148] (see Table 1.2 entry 13). Thus, Wudl *et al.* [24, 25] developed a self-healing concept using the thermally reversible DA/rDA reaction between star-shaped trivalent maleimides and tetravalent furans (see Table 1.2 entry 10), resulting in a highly dense network with thermoset properties via a polyaddition reaction. The damage event will break the DA-crosslinking points to form terminal maleimide and furan species, which in turn are able to react preferentially in a DA reaction, resulting in an average mending efficiency of about 50% at a temperature of 150 °C. Another thermally reversible DA method used modified poly(*N*-acetyleneimine)s bearing either maleimides or furans in the polymer side chain [26] (see Table 1.2 entry 11). Mixing of two suitable substituted polymers resulted in a dense network at a healing temperature of 80 °C. Further investigations of similar DA/rDA concepts consisting of polystyrene-bearing maleimides and several furan moieties indicate a limited thermal stability of furfuryl moieties with a therefore limited applicability for self-healing materials [121]. Furthermore, a single component self-healing polymer was developed using cyclic monomers containing dicyclopentadiene cores as reactive units [27] (see Table 1.2 entry 12),

which were utilized simultaneously as diene and dienophile in the DA cycloaddition reaction. Accordingly, a polymer consisting of thermally reversible DA adducts with further reactive sides could be synthesized. A second DA reaction can be started, resulting in the trimerization and thus a highly crosslinked polymer, showing the ability for self-healing achieving an average healing efficiency of 46% upon heating to 120 °C. Moreover, a further single-component system potentially applicable for self-healing using DA/rDA reactions was developed applying anthracene-substituted acrylates simultaneously as diene and dienophile [28] (see Table 1.2 entry 13). The polymerization of this monomer results in a network with thermally reversible crosslinkers and represents thus a probable healing concept for thermoset materials. Beside the aforementioned systems, some other classical DA/rDA reactions using acyclic dienes and dienophiles [123], as well as some hetero-DA reactions [122] are potentially applicable for self-healing.

Some other potential self-healing methods based on reversible bond formation are known, mostly disulfide bridges (SS) can be ruptured by reversible reduction into two thiol groups (SH) [62] (see Figure 1.5h). Thus, subsequent recrosslinking under re-formation of disulfide bridges via oxidative conditions enables the restoration of the initial material properties. For example, a redox-reversible hydrogel system based on thiol-modified poly(*N*-acetyleneimine) (see Table 1.2 entry 14) might use the interconversion between disulfide and thiol groups to heal the damaged area [145]. Another example can be a polystyrene-based block copolymer bridged by disulfides [62] (see Table 1.2 entry 15). The internal disulfide linkers could be cleaved under reducing conditions to thiols, separating the single blocks and thus releasing the accrued stress. Healing could occur after subsequent oxidation of the thiols re-forming the disulfide linkers.

Furthermore, another potential self-healing concept working in a similar, but slightly different way used the photoinduced reversible cleavage of allyl sulfide linkages in a polymer backbone under generation of thiyl radicals [146] (see Figure 1.5i; Table 1.2 entry 16) ($\text{RS}\cdot$) which increased the chain mobility. Rearrangement of polymer chains in crosslinked rubber-like materials was thus assumed, enabling rapid stress release at ambient conditions without degradation of mechanical properties. Stress application without light irradiation resulted in a strained sample as expected, but under irradiation stress relaxation was observed due to homolytic photolysis via addition–fragmentation chain transfer reaction forming radicals by the allyl sulfide functionalities.

Other self-healing concepts based on thermally reversible cleavage of alkoxyamine bonds use a similar stress relaxation mechanism (see Table 1.2 entry 17). For example, a poly(alkoxyamine ester) was developed which is able to undergo a reversible radical exchange reaction at 60 °C by homolytic cleavage of the C–O bond [147]. Thus, these systems reduced the destructive stress within the polymeric material and are potentially suitable for self-healing applications.

Another, totally different approach for self-healing uses polycondensation reactions in order to restore the initial material properties (see Figure 1.5j). In contrast to the previously discussed reversible self-healing concepts which are, at least theoretically, infinitely repeatable, polycondensations are limited in the number

of healing cycles due to the consumption of functional groups during the self-healing process. Nevertheless, they are commonly more than one-time healable and can be, therefore, attributed to the (partially) reversible concepts. However, the previously discussed example of White *et al.* [131] (*irreversible covalent network formation concepts*) based on a polycondensation reaction of two different poly(siloxane)s with tin catalysis cannot be attributed to the reversible self-healing systems due to the necessity of encapsulation of the catalyst (see Table 1.1 entry 3). Therefore, multiple healing of a once ruptured and subsequently healed area is not possible. However, as an example, a polycarbonate-based self-healing polymer for thermoplastic materials was developed [124, 125] (see Table 1.2 entry 18) as a reversible covalent self-healing polymer, splitting the carbonate bond by thermolysis or hydrolysis. Thus, phenoxy groups with terminal hydroxy moieties are generated, which are able to react with a phenyl end of an uncleaved chain, using sodium carbonate as healing agent in order to accelerate the reaction by exchanging protons of the hydroxy group with sodium ions. This healing mechanism is limited to certain types of thermoplastic materials which enable the recombination of chain ends via condensation reactions. This and the elevated temperatures restrict the range of polymers and applications to which this technology can be applied.

1.4.2

Supramolecular Network Formation

Supramolecular polymers use the “chemistry beyond the covalent bond” to combine reversible, secondary interactions with the attractiveness of conventional polymers [143]. Due to their highly dynamic properties, able to act in a reversible manner, their capability for designing self-healing polymers becomes evident. In special cases, networks can be formed solely by supramolecular bonds, thus opening the possibility for exploitation in self-healing materials. The relevant issues for utilizing supramolecular bonds in self-healing polymers are the timescale of the dynamics, relating dynamics of the bond to the timescale of healing, and their strength, resulting in stronger or weaker networks. Therefore we discuss here supramolecular network formation based on (a) *hydrogen bonding*, (b) *ionomers*, (c) *metal bonding* and (d) *π - π stacking* (for more information see Chapters 11–13). An overview of these interactions is given in Figure 1.6 and all examples discussed can be found in Table 1.3.

The design of self-healing polymers based on *hydrogen bonding* combines highly *dynamic properties* [156, 180–182] as bonds show a reversible “sticker-like” behavior enabling connection and reconnection, and thus *supramolecular network formation* [23, 182, 183] (see Figure 1.6a) as well as strength generated by the “stickiness” of the applied supramolecular bonds or by *cluster formation* [23, 184] between several hydrogen bonding motifs. Due to tunable and controllable dynamics, and thus the *reversibility* of network formation [153] via specific modes of association, *hydrogen bonded polymers* [156, 163, 182] can respond to an external damage event while emphasizing their attractiveness for self-healing purposes [6, 17].

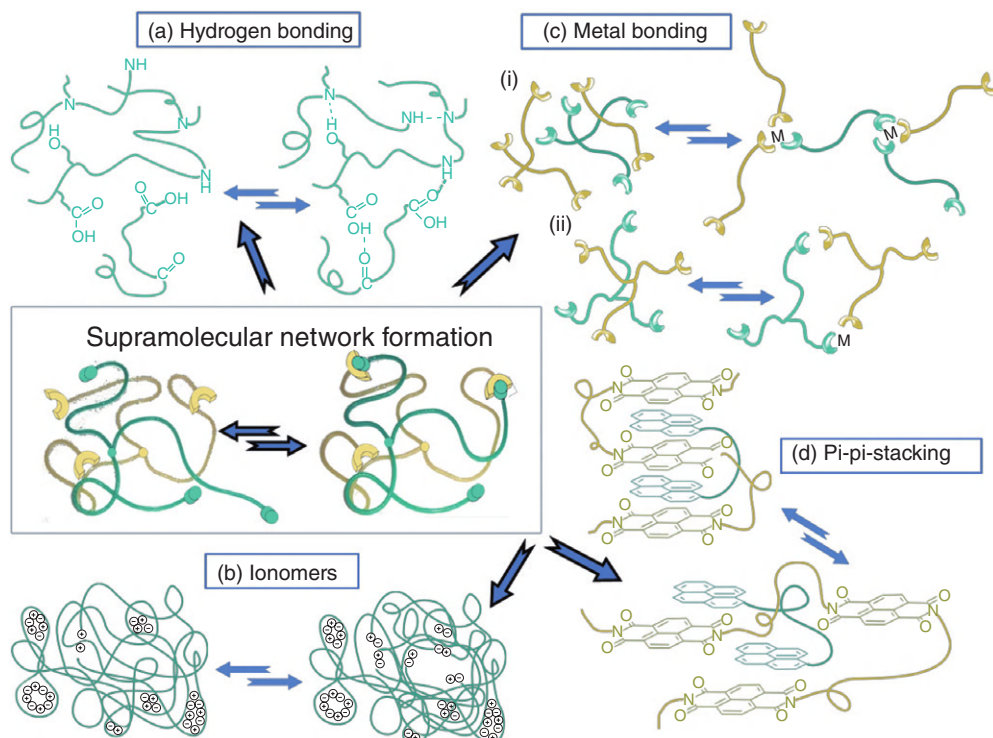
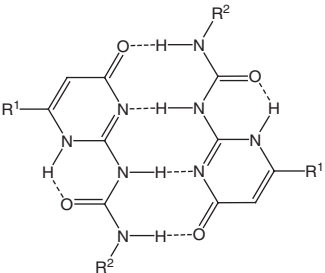
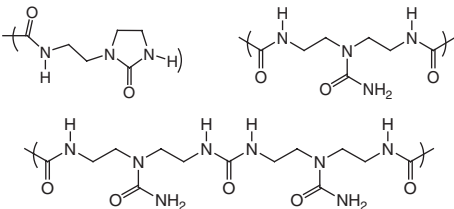


Figure 1.6 Supramolecular network formation via (a) hydrogen bonding, (b) ionomers, (c) metal bonding, or (d) π - π -stacking.

Table 1.3 Examples of supramolecular network formation.

Entry	Example	Ref.
(a)	Hydrogen bonding	
1	Ureido-pyrimidone bond–SupraPolix BV 	[143, 149]
2	Leibler bond 	[21]

(Continued)

Table 1.3 (Continued)

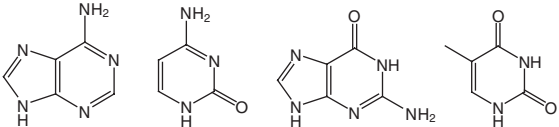
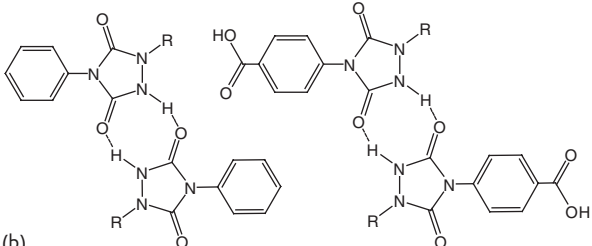
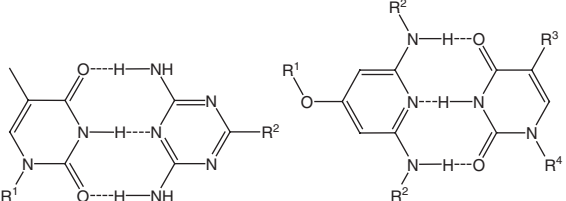
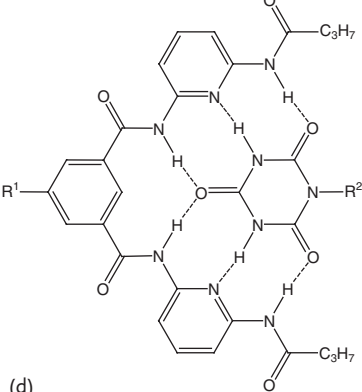
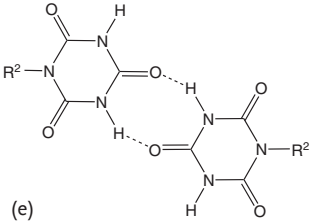
Entry	Example	Ref.
3 Nucleobases and similar systems	<p>(a) </p> <p>(b) </p> <p>(c) </p> <p>(d) </p> <p>(e) </p>	[6, 22, 23, 150–155]

Table 1.3 (Continued)

Entry	Example	Ref.
4	Butylurea of guanosine and 2,7-diamido-1,8-naphthyridine	[156, 157]
5	Poly(styrene) grafted with poly(acrylate amide)	[94]
6	(a) AAAA-DDDD quadruple hydrogen bond (b) double-closed loop topologies	[14, 83, 158]

(Continued)

Table 1.3 (Continued)

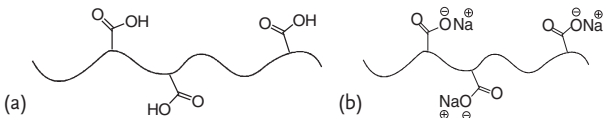
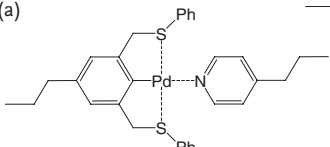
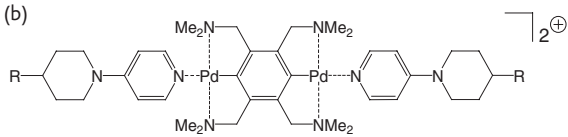
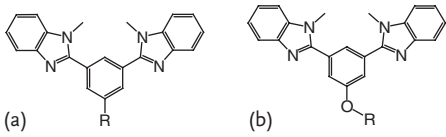
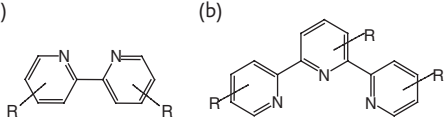
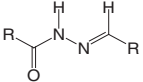
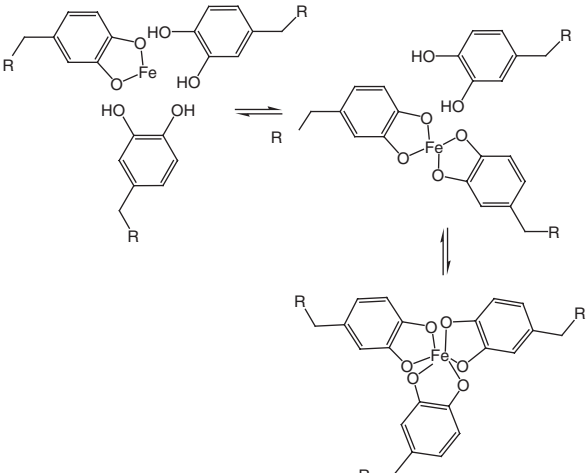
Entry	Example	Ref.
(b)	Ionomers	
7	(a) EMAA (b) partially neutralized EMAA	[3, 5, 11, 17, 87, 88, 159, 160]
		
(c)	Metal bonding	
8	Pincer complexes	[17, 161–168]
	(a) 	
	(b) 	
9	(a) Mebip (b) OMebip	[169–172]
		
10	(a) Bipyridines (b) Terpyridines	[17, 120, 130, 161, 164, 165]
		
11	Metallo-dynamers	[173–175]
		
12	Catechol-iron complex	[176]
		

Table 1.3 (Continued)

Entry	Example	Ref.
(d)	π - π -stacking	
13	Polydiimide + poly(siloxane) with pyrenyl endgroups	[177]
14	Copolyimide + poly(amide) with pyrenyl endgroups	[178]
15	Copolyimide + poly(amide) with pyrenyl endgroups	[20]
16	Copolyimide + polyurethane with pyrenyl endgroups	[179]

A strong change in materials properties is achieved with quadruple hydrogen bonds such as the ureido-pyrimidone bond [143, 149] (see Table 1.3 entry 1). Depending on the amount of binding sites, linear as well as crosslinked polymers were formed, whereas the absence of unspecific aggregation allowed excellent control over the formed network architecture. Thermal mending and thus dissociation of created thermoplastic elastomers could be observed at temperatures above 90 °C. Accordingly, this approach was adopted in industry by SupraPolix BV and found application in “real life” [143, 149].

A thermoreversible rubber was synthesized from multivalent fatty acids and urea with three different types of hydrogen bonding motifs, diamido tetraethyl triurea, di(amido ethyl) urea, and amidoethyl imidazolidone [21], respectively (see Table 1.3 entry 2). Samples plasticized with dodecane, showed a repeatable

self-healing response after cutting and bringing into contact again, with a shape recoverability up to several 100% due to hydrogen bonding.

The interaction behavior of supramolecular and thermosensitive polymers bearing different nucleobases (see Table 1.3 entry 3a) in solution as well as their capability to form films and fibers [151] were the first studied hydrogen bonding moieties applicable for self-healing concepts. Thus, already in the 1990s the investigation of urazole and 4-urazoylbenzoic acid as hydrogen bonding moieties [156] was started (see Table 1.3, entry 3b), revealing thermoplastic elastomeric behavior demonstrating different effects: urazole groups, when homogeneously distributed within the polymer, resulted in the formation of two hydrogen bonds and thus in the broadening of the rubbery plateau zone. In contrast, 4-urazoylbenzoic acid groups showed the formation of extended aggregates due to phase separation [156]. Similarly, thymine or uracil units were used for crosslinking complementary diaminotriazine functionalized copolymers, resulting in the formation of spherical aggregates due to thermally reversible three-point hydrogen bonding [154, 185] (see Table 1.3 entry 3c). In turn, to tune the properties of these materials by balancing intra- and intermolecular hydrogen bonding, diacyldiaminopyridine motifs have also been applied [154, 185]. In order to increase the secondary interaction the formation of supramolecular linear or crosslinked polymers based on a cyanuric wedge such as an ADA–ADA (A: hydrogen bond acceptor, D: hydrogen bond donor) array and a diaminopyridine-substituted isophthalamide receptor such as a DAD–DAD unit creating a well-defined sextuple hydrogen bond (see Table 1.3 entry 3d) were studied [152, 153]. While investigating the dynamics and the thermoreversible aggregation behavior [23] of poly(isobutylene)s functionalized with barbituric acid and Hamilton Wedge [22, 153] in the melt, a self-healing ability of samples functionalized with barbituric acid was found, showing self-healing at room temperature within 48 hours due to the formation of dynamic supramolecular clusters [22, 153].

Quadruple hydrogen bonds formed between the butylurea of guanosine and 2,7-diamido-1,8-naphthyridine [150, 157] show both, high fidelity as well as high stability (see Table 1.3 entry 4). Due to weak self-association and a high association constant this approach exceeds the fidelity of DNA base-pairing and is one of the strongest known neutral DNA base-pair analogs. Thus, supramolecular multi-block copolymers as well as thermoreversible supramolecular polymer blends with tunable properties can be created.

Another self-healing approach utilized a thermoplastic elastomer consisting of a poly(styrene) backbone grafted with poly(acrylate amide) as a self-healing concept [94] (see Table 1.3 entry 5). Due to immiscibility effects phase separation into a soft, supramolecular poly(acrylate amide) matrix and a hard poly(styrene) sphere could be observed. Accordingly, the approach combines elastomeric behavior, mechanical stiffness and molecular dynamics due to reversible hydrogen bonding within grafted brushes [94].

Due to the large number of hydrogen bonds, a number of promising but still unexploited hydrogen bonds as concepts for self-healing polymers exist. Examples are the AAAA-DDDD type [14] (see Table 1.3 entry 6a) with an association constant

up to 10^{12}M^{-1} as well as double-closed loop topologies [83, 158] (see Table 1.3 entries 6b and c) based on 2-ureido-4-pyrimidone or peptidomimetic-sheet modules.

Self-healing polymers based on supramolecular, dynamic networks can also be formed by *ionomers* [5]—supramolecular thermoplastic polymers with an ionic group content up to 15 mol%—while taking advantage of their characteristic *clustering* [85] (see Figure 1.6b and Table 1.3). Due to the ionic species within the polymer backbone, clusters can be formed acting as *physical crosslinking points*, and allowing reversible formation and re-formation of the network structure. Thus, the resulting complex microstructure and the order to disorder transition temperature emphasize a self-healing ability in response to *ballistic impact* [85]. Especially poly(ethylene-*co*-methacrylic acid) (EMAA)-based ionomers (see Table 1.3 entries 7a and b) were investigated to obtain information on the materials response and the underlying self-healing mechanism [3, 5, 11, 17, 85, 87, 88].

Although an increase in the ion content within the materials increases their fracture resistance and tensile strength, both pure EMAA and its ionomers showed the ability of fast self-healing upon ballistic puncture. Thus, it was hypothesized [159, 160] that the ionic content itself is not necessary for the healing response but that the existence of the polar acid groups within the material is mechanistically essential due to reversible hydrogen bonding. Furthermore, the self-healing ability is linked to the heat generated during the damage event and requires a high energy elastic response of the material. Thus, the localized molten polymer enables the viscoelastic recovery of the sample to snap back and close the hole. This stage is followed by an interdiffusion and sealing step, subsequently completed by the formation of crosslinking points. The strength regeneration within the material is based on continuing interdiffusion processes, crystallization as well as long-term relaxation of the polymer chains. Furthermore, the self-healing ability is affected by balanced elastic and viscous responses of the materials close to the impact region, wherein the elastic response provides the ability to rebound and the viscous response induces final sealing. Healing at low temperatures can occur if the material is locally sufficiently heated to the melted state. However, elevated temperatures do not promote healing if the energy within the material is dissipated faster, confirming the proposed elastic “snap back” step. Therefore, insufficient self-healing can be observed if not enough thermal energy is produced within the material during the ballistic impact. Therefore, healing efficiencies depend on the speed and the shape of the projectile [3, 5, 11, 17, 85, 87, 88, 159, 160].

Supramolecular network formation and thus a self-healing capability can also be achieved by *dynamic coordination bonds* [12, 167] with certain metal ions (see Figure 1.6c and Table 1.3). In contrast to ionomers, where clusters play the most crucial role for network formation, polymers with *multivalent metal–ligand interactions* [186] have to be carefully selected in order to construct reversibly cross-linkable networks with both sufficient stability and dynamics. Accordingly, the thermodynamic and kinetic parameters [12, 167, 168] of a coordination bond, indicated on the one hand by the equilibrium or association constant and by the formation or dissociation rate on the other hand, have to be taken into account to

control the materials responsiveness to environmental stimuli [170, 187] necessary for efficient self-healing. Thus, by controlling the dynamics, a *molecular toolbox* [12, 167] is obtained, which allows the design of structurally dynamic polymers suitable for self-healing approaches [188].

For the design of supramolecular networks based on metal–ligand interactions commonly *palladated or platinated pincer complexes* (see Table 1.3 entries 8a and b), *2,6-bis-(1'-methylbenzimidazolyl)pyridines and 4-oxy-2,6-bis(N-methylbenzimidazolyl)pyridines* (see Table 1.3 entries 9a and b) as well as *bi- and terpyridines* (see Table 1.3 entries 10a and b) are used as ligands [17, 161–165]. In order to create supramolecular networks the ligand requires at least two polydentate functionalities linked by a spacer group. Furthermore, the choice of the metal, ranging from main- to transition-group metals up to lanthanides, can influence the stability of the generated complex, and thus the dynamics as well as the reversibility of the metallosupramolecular interaction [17, 161–165].

Other promising candidates for self-healing materials are bifunctional Pt(II) or Pd(II) pincer complexes [17, 161–168] (see Table 1.3 entries 8a and b) forming a coordination complex with a side-chain pyridine ligand of a polymer backbone, most of all by controlling and understanding the dynamics of the network by selecting appropriate metal centers.

A tridentate ligand, namely, 2,6-bis-(1'-methylbenzimidazolyl)pyridine (Mebip) [170–172] (see Table 1.3 entry 9a) was investigated based on the work of Piguet and Buezli [169]. Linear metallosupramolecular polymers formed bidentate complexes with transition metal ions, whereas crosslinked samples were obtained from stable tridentate complexes with lanthanide ions. Thus, gels with a tunable crosslinking density could be obtained by adjusting the ratio of coordinating ions. In consequence, the complexation behavior of this ligand with metal ions like Fe(II), Co(II), Cd(II), Eu(III) or Zn(II), and the film formation due to phase separation were explored [17, 170]. Furthermore, supramolecular metallopolymerizations of ditopic poly(*p*-phenylene ethynylene) and poly(*p*-xylylene) end-capped with 2,6-bis(1'-methylbenzimidazolyl)pyridine (Mebip) (see Table 1.3 entry 9a) could be demonstrated [187]. Metallosupramolecular polymers with shape-memory properties based on 4-oxy-2,6-bis(*N*-methylbenzimidazolyl)pyridine (OMebip) (see Table 1.3 entry 9b) as ligand could be obtained [172] generating phase separated films with a temporary shape.

The group of Lehn [15, 173–175, 189] reported the synthesis of neutral metal-lodynamers of polyacylhydrazones (see Table 1.3 entry 11) with Zn(II) or Ni(II) ions showing a dynamic behavior in solution dependent on the coordination center. Furthermore, they proved the formation of films as well as reversible coordination in the bulk material and reversible formation of covalent imine bonds.

As last metal-based self-healing concept a catechol-iron complex [176] (see Table 1.3 entry 12) should be mentioned. The complex, used within a polymer chain inspired by mussel, resulted in pH-dependent gels with 100% self-healing ability. Accordingly, this approach can also be classed as “switchable” healing but is mentioned here due to its metal–ligand interaction.

Self-healing materials based on aromatic π - π stacking [6] (see Figure 1.6d and Table 1.3) interactions were first reported by Burattini *et al.* [190] who took advantage of combining π -electron-rich and π -electron-poor moieties [20, 179]. Therefore, *supramolecular complexes with chain-folded secondary structures*, and thus with a maximum amount of possible interactions, can be obtained [6]. As a result low-molecular-weight precursors can be converted into medium-molecular-weight species in a highly dynamic manner. Moreover, the so obtained stimuli-responsive products show great physical properties such as high tensile strength which is more commonly related to covalent bonds but tunable for various self-healing applications [179].

In Burattini's first approach, a siloxane polymer bearing π -electron rich pyrenyl endgroups at each side as well as a low-molecular-weight polydiimide containing multiple π -electron poor receptor moieties (see Table 1.3 entry 13) were synthesized. A reversible and rapid complexation behavior in solution, as well as the formation of homogeneous and thermodynamically stable films with an inherent healing capability at temperatures above 90 °C could be shown. Furthermore, it could be proven that the chain-folding of the polyimide [177] creates an optimal binding site for the pyrenyl endgroups forming a non-covalent, π - π -stacked supramolecular network [191] able to react with a self-healing response. Accordingly, healing can be initiated by the partial disruption of π - π -stacked crosslinking points at elevated temperatures. Due to the terminal flow of the polymer chains, the repair of a damaged region during cooling, and thus the restoration of the supramolecular interactions, was enabled, regenerating the initial materials properties.

An improved self-healing polymer based on π - π -stacking interactions was developed as the first concept lacked in stability [178]. Therefore, the polymer backbone was modified using a co-polyimide and a polyamide with two pyrenyl end-groups (see Table 1.3 entry 14). Healing could be achieved by bringing cut samples into contact, followed by subsequent heating, even after a separation time of up to 24 h. 80% recovery of the tensile modulus was achieved already after 5 min at 50 °C. Furthermore, full recovery of the tensile modulus could be shown for three times. Due to the increase in possible π - π -stacking interactions by increasing the amount of pyrene-endgroups per polymer chain from two to four [20] (see Table 1.3 entry 15) an increase in the binding constant in solution of nearly two orders of magnitude could be observed. The so prepared supramolecular blends featured increased toughness as well as an enhanced tensile strength but required longer times and higher temperatures for healing.

Beside these approaches, a healable polymeric blend based on the chain-folding of a polyimide and a pyrene-functionalized polyurethane was reported and proved the structural integrity in the bulk [179] (see Table 1.3 entry 16). Additionally to π - π -stacking, hydrogen bonds reinforced the formation of possible crosslinking points within the material. Due to the combination of π - π -stacking and hydrogen bonding a significant increase in the tensile modulus compared to the hydrogen bonding approach described by Leibler [21] was demonstrated. For further information regarding supramolecular network formation see also Part 3—*Supramolecular Systems*.

1.4.3

Mechanochemical Network Formation

Mechanochemistry [4, 64–78, 119, 192–206] is an elegant method for designing self-healing polymers due to the triggering of healing processes by the damage event itself. In its basics, mechanochemistry has been known since the middle of the last century, but only in the recent years it has become the focus of interest. Mechanochemical materials generate the reactive species as a consequence of applied mechanical stress via an *in situ* activation. This enables the direct embedding of the mechanophore into the matrix preventing further protection of the active species, like encapsulation. Mechanochemical induced self-healing is always an intrinsic self-healing method due to its inherent characteristics. In the following we consider self-healing methods which are able to generate a reactive species in the course of the rupture event. If a more general definition of mechanochemistry is applied, including all interactions and reactions caused directly or indirectly by mechanical force and thus by damage, almost all self-healing approaches could be assigned to this category. A detailed account of this topic is given in Chapter 8.

The mechanochemical concepts known to date can be classified into two main categories. The first class is able to generate reactive species, like radicals [4, 192–197, 206] (see Figure 1.7a, Table 1.4 entries 1–4) or strongly activated double bonds [4, 64, 66–68, 70–73, 119, 200, 201] (see Figure 1.7b; Table 1.4 entries 5–9), which can undergo various reactions in order to form a network, filling the crack and thus healing the damage. In the second class an active catalyst is generated under mechanical stress out of an inactive precursor [74, 75, 78, 202–205] (see Figure 1.7c; Table 1.4 entries 10–13), whereby a crosslinking reaction can take place, which heals the damage.

1.4.3.1 Mechanochemical Generation of Reactive Species

Some of the earliest concepts which generate reactive species due to the influence of mechanical force are based on natural and synthetic rubbers. These polymers create radicals by homolytic cleavage of carbon–carbon bonds as soon as they are cracked mechanically [192, 193] (see Figure 1.7a; Table 1.4 entry 1). Of course, it can be assumed that the main effect for self-healing can be attributed to the more probable molecular interdiffusion due to the low T_g of such polymers. Nevertheless, the involvement of radicals is proven [193, 206]. Moreover, these first analyses examined a molecular weight dependence with a minimum molecular weight required for cleavage [194], which was important for a deeper understanding and further developments of mechanical activatable systems. Pursuing this approach, new macromolecules with easier and more selective cleavable bonds were designed. Examples are peroxides in poly(vinylpyrrolidone) [195] (see Table 1.4 entry 2) or azo-linkers in linear poly(ethylene glycol) [4, 196], whereby the latter group cleaves off nitrogen under mechanical stress and thus generates two radicals which are able to recombine (see Table 1.4 entry 3). In a similar approach a poly(phenylene ether) (PPE) chain can be cut by an external force as well as by heat or light. The resulting radicals can react with a Cu(II) species while reforming the polymer in a redox

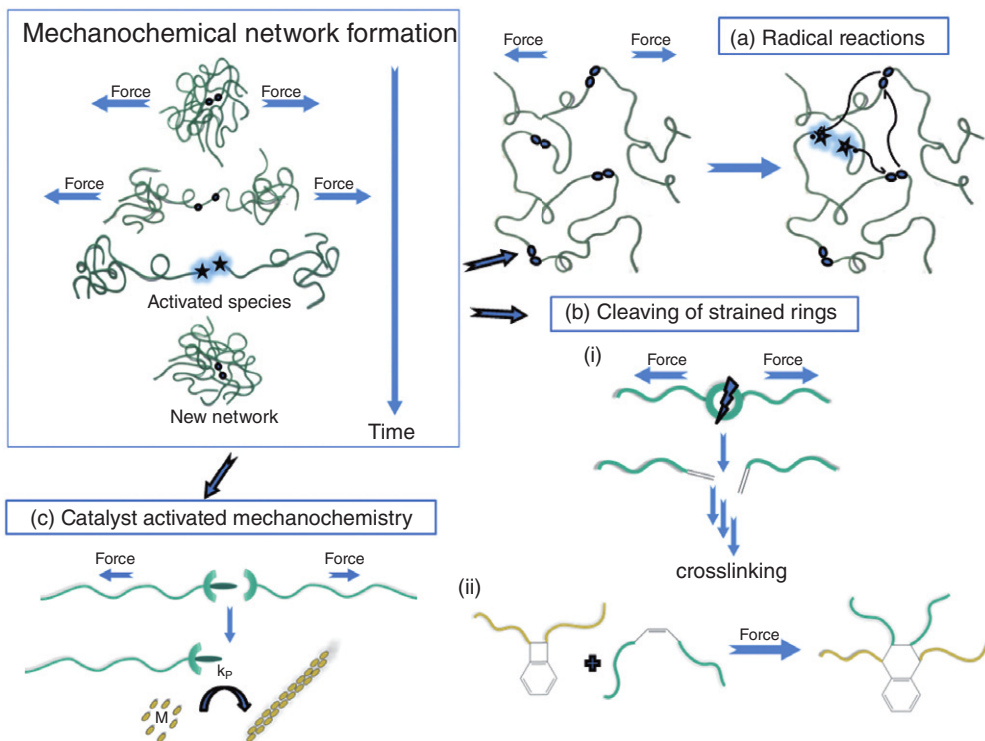


Figure 1.7 Overview of mechanochemically induced self-healing systems. (a) The generation of radicals by polymer chain scission and the subsequent recombination, (b) the generation of reactive species by cleaving of highly strained ring systems

under b(i) chain scission or b(ii) via subsequent pericyclic rearrangement, and (c) the mechanochemical activation of catalysts. All methods result in the formation of networks.

process [124, 197] (see Table 1.4 entry 4). Further considerations regarding these predetermined breaking points resulted in the development of completely new kinds of mechanochemically activatable polymers. These polymers consist basically of a mechanosensitive group and a polymer chain which “collects” and transmits the force to the commonly centered mechanosensitive group [4, 198, 199]. Similar to the rubber-based approaches, the mechanical force orientates the mechanophores (polymer chain and mechanosensitive group) in a preferred direction, whereby the polymer chains are stretched, resulting in a rupture of the weakest bond [4, 67, 198, 199] (see Figure 1.7). This approach only works if the polymer chains have a minimal length and therefore a minimal molecular weight depending on the kind of polymer. After cleavage the mechanosensitive group releases the reactive species, which can either react itself or is able to trigger further reactions. Mechanophores thus enable the transformation of energy from applied mechanical fields to productive chemical changes that can restore initial material properties,

Table 1.4 Examples of self-healing systems activated via mechanochemistry.


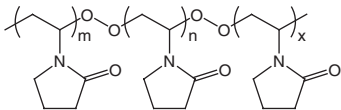
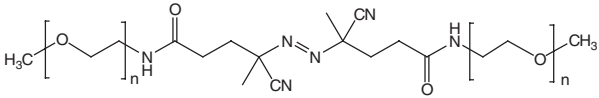
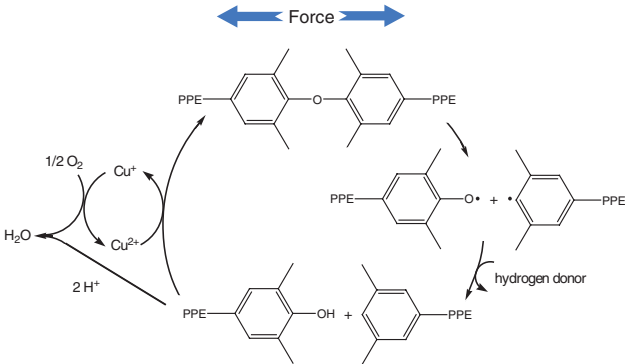
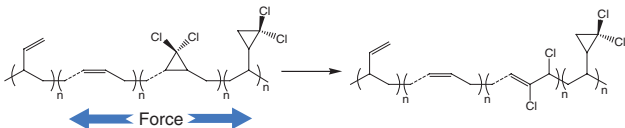
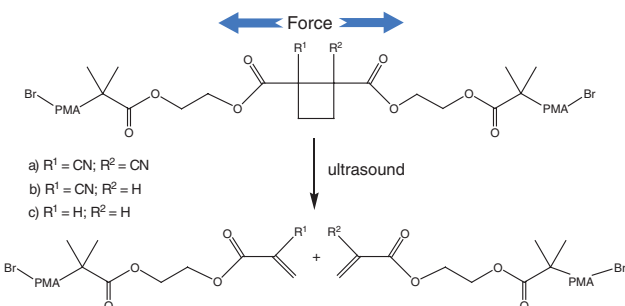
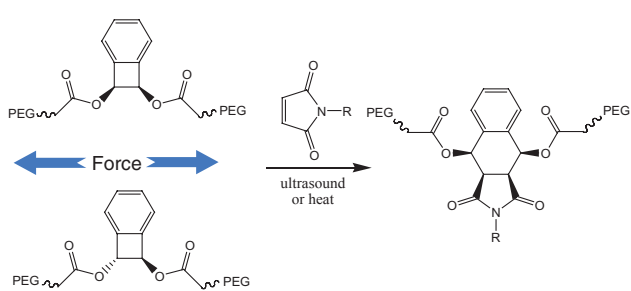
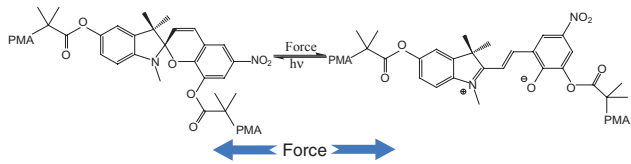
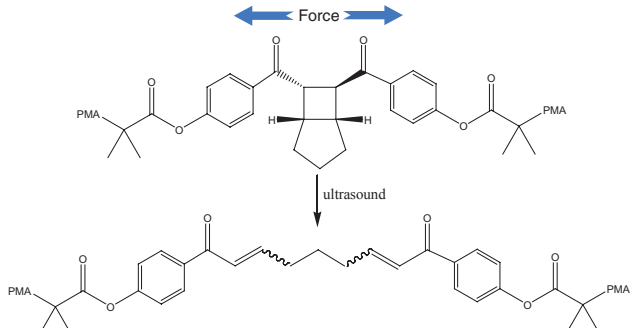
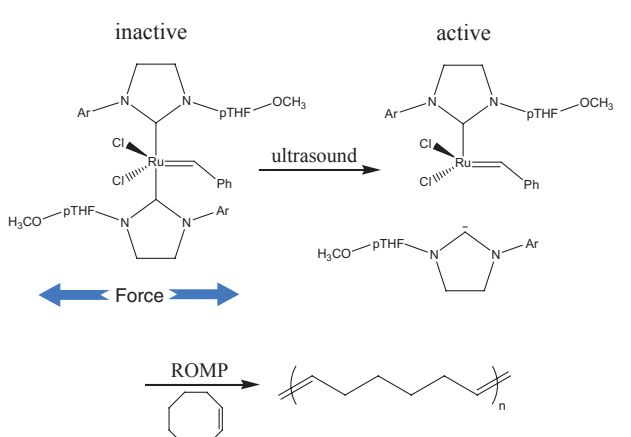
Entry	Example	Ref.
(a) + (b)	Mechanochemical generation of reactive species	
1	Homolysis of C–C bonds 	[192, 193]
2	Peroxide linked 	[195]
3	Azo-linked 	[4, 196]
4	Poly (phenylene ether) 	[124, 197]
5	Cyclic propanes 	[66, 71, 73]
6	Cyclic butanes  a) R ¹ = CN; R ² = CN b) R ¹ = CN; R ² = H c) R ¹ = H; R ² = H	[68, 200]

Table 1.4 (Continued)

Entry	Example	Ref.
7	<p>Cyclic butenes</p> 	[64, 70]
8	<p>Spiroprans</p> 	[70, 201]
9	<p>Bicyclic rings</p> 	[66]
(c)	<p>Mechanochemical activation of catalysts</p>	
10	<p>ROMP-based</p> 	[74, 75]

(Continued)

Table 1.4 (Continued)

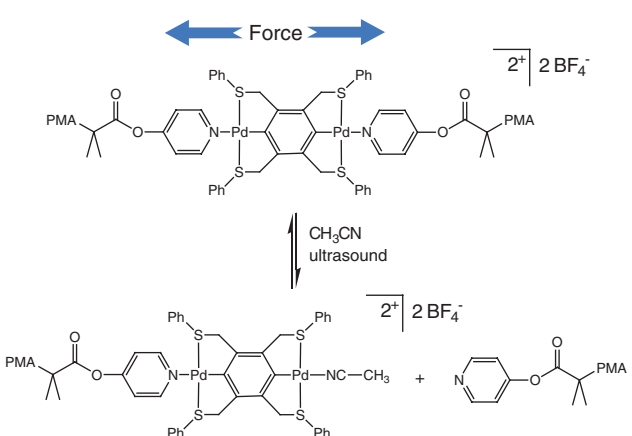
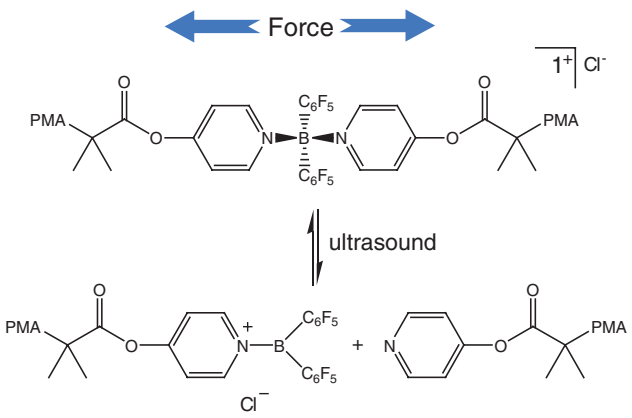
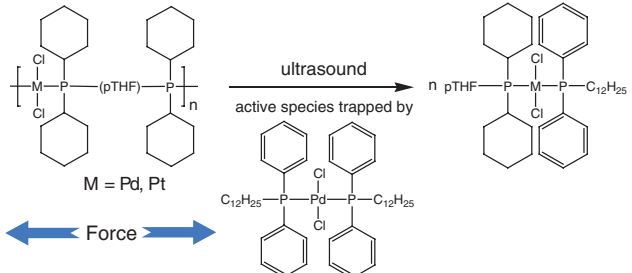
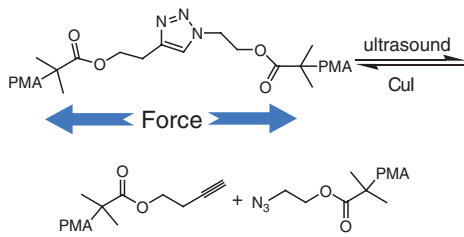
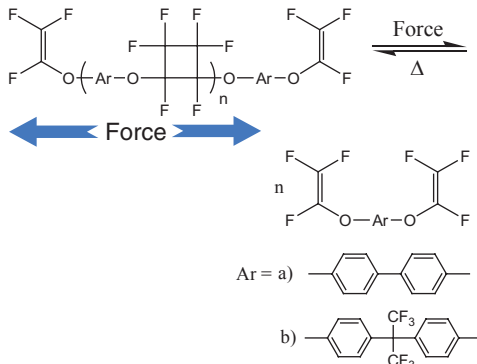
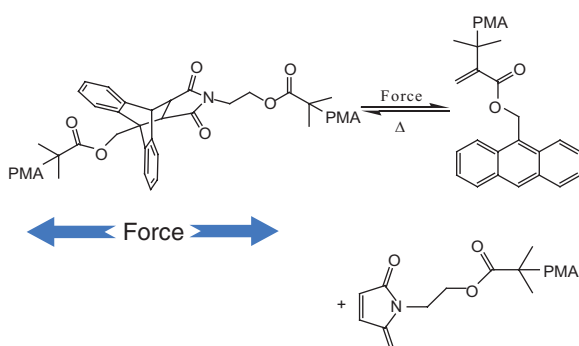
Entry	Example	Ref.
11	<p>Pincer complexes</p>  <p style="text-align: right;">[204]</p>	
12	<p>Boron complexes</p>  <p style="text-align: right;">[205]</p>	
13	<p>Phosphine-based complexes</p>  <p style="text-align: right;">[78, 202, 203]</p>	

Table 1.4 (Continued)

Entry	Example	Ref.
Alternative mechanochemical self-healing concepts		
14	Click-based 	[207]
15	Cyclic butanes 	[72]
16	Anthracene/ maleimide 	[118]

resulting finally in self-healing. Thus, mechanical stress causes on the one hand the damage, and on the other hand triggers the self-healing process by itself.

Examples for such self-healing concepts are cyclic, highly strained ring systems, like substituted cyclopropanes [66, 71, 73] (Table 1.4 entry 5), cyclobutanes [66, 68, 72, 200] (entry 6), cyclobutenes [4, 64, 72, 119] (entry 7), cyclopentanes [4, 67, 70, 201] (entry 8) (see Figure 1.7b) or bicyclic rings [66] (entry 9). A particularly illustrative mechanical activatable system was developed by Moore *et al.* [64, 70], who

harnessed the mechanical force to open a 1,2-poly(ethylene glycol) disubstituted benzocyclobutene. This is done in a pericyclic rearrangement including a 4 π electrocyclic ring-opening reaction, resulting in the formation of an *ortho*-quinodimethide diene, which can further react in the presence of a substituted maleimide in a fast DA reaction (see Figure 1.7b (ii); Table 1.4 entry 7).

1.4.3.2 Mechanochemical Activation of Catalysts

The mechanochemical activation of a previously inactive catalyst by force was shown by Sijbesma *et al.* [74, 75]. In contrast to the previously discussed polymers, the active catalyst triggered a chemical reaction instead of acting as a healing agent by itself (see Figure 1.7c; Table 1.4 entry 10). Their approach includes the mechanochemical dissociation of *N*-heterocyclic carbenes (NHC) (linked to poly-(tetrahydrofuran)s), coordinated silver- and ruthenium-based catalysts forming a free coordination site which enables the catalysis of transesterifications, ring-closing metathesis (RCM), or ring-opening metathesis polymerizations (ROMP), respectively. Especially, the ROMP of various derivatives of cyclooctene [75], norbornene [74], or dicyclopentadiene might be suitable as mechanically induced self-healing systems. Further mechanochemical concepts acting according to a similar mechanocatalytic mechanism are described in the literature [78, 202–205] and are partly shown in Table 1.4 entries 10–13. Bielawski *et al.* [205] has developed a potentially applicable self-healing concept based on the release of a pyridine moiety which can catalyze either an anionic polymerization, or can effect a Brønsted acid-base reaction (see Table 1.4 entry 12), both showing suitability for self-healing purposes. Therefore, an electron-deficient boron species, which is coordinated to two pyridine-capped poly(methyl acrylate)s, was used while cleaving one pyridine moiety under ultrasonication.

Of course, some other mechanical activatable systems for self-healing [4, 67, 70, 72, 118, 119, 198, 199, 201, 207–211] are known (some examples are shown in Table 1.4 entries 14–16), although they are not described here.

1.4.4

“Switchable” Network Formation

Self-healing concepts based on “switchable” network formation utilize materials with an inherent “switch”, as the word already implies. Thus, self-healing polymers using “switchable” concepts combine organic synthesis and polymer science in order to control functionalities on the molecular level while “turning the switch on and off” [79, 80] and thus changing material properties. Moreover, the reversibility and dynamics of the underlying chemistry can be controlled in a highly selective manner due to molecular “switching”, thus changing network properties on demand, which is a key point for a sufficient self-healing response [79, 81]. As “switch” a combination of (a) *light and external force*, (b) *light* of different wavelengths, (c) the *pH-value*, as well as an *electrochemical stimulus*, can be used to trigger a reversible reaction within the material applicable for self-healing [80, 82] (see Figure 1.8 and Table 1.5) (see also Chapter 7).

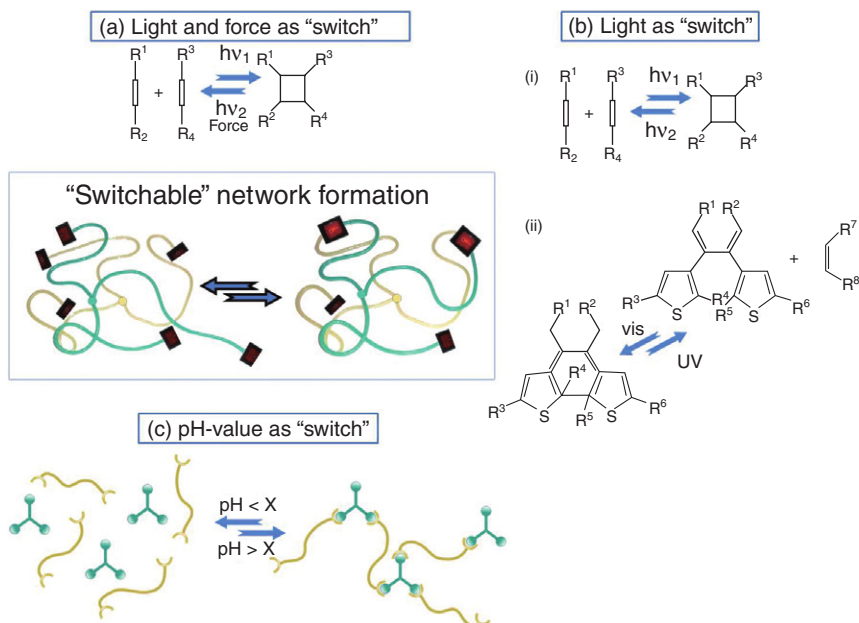


Figure 1.8 "Switchable" network formation, using (a) light in combination with force, (b) light, and (c) the pH-value as the inherent molecular "switch".

Davis *et al.* [65] used a mechanophore—a chemical group sensitive to mechanically induced force—to link glassy and elastomeric polymers. They selected the colorless spiroopyran moiety (see Table 1.5 entry 1) which can undergo a reversible, force-induced 6 π electrocyclic ring-opening reaction. Because of the rupture of the carbon–oxygen bond of the spiro-compound, the conjugation length of the formed planar merocyanine increased, resulting in an absorption shift to longer wavelengths, and thus a color change. Due to the visualization of the mechanochemical reaction they could demonstrate the selective breaking and reforming of covalent bonds by mechanical forces. Furthermore, the efficient transfer of the external energy to the mechanosensitive group indicated the damage event. The re-formation of the spiroopyran could be achieved via photocyclization using light as a "switch". The functional group is capable of translating crosslinking responses, serving as a concept for the development of regenerative self-healing polymeric materials [65]. Further examples of using light as a readily available, clean and cheap "switch" include reversible cycloaddition reactions, which allow the opening and closing of crosslinking ring structures within a polymer network. Especially, [2+2] cycloaddition reactions between cinnamoyl groups [6, 17, 142, 144] and coumarin groups [6, 17, 212–214], as well as [4+4] cycloaddition reactions of anthracene groups [6, 17, 215–222] (see Table 1.5 entries 2, 3a and 3b) attracted the interest of scientists. First, photochemical healing within a polymeric material was applied to poly(methacrylate)s with

Table 1.5 Examples of “switchable” network formation.

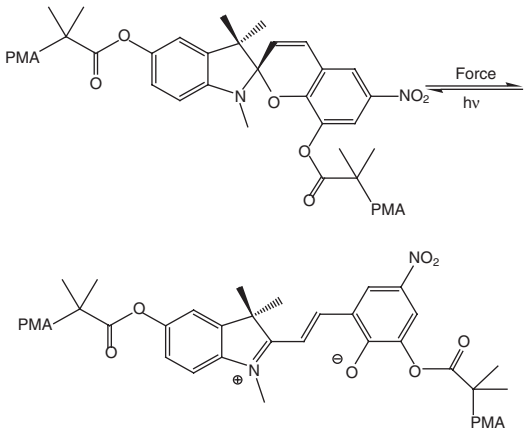
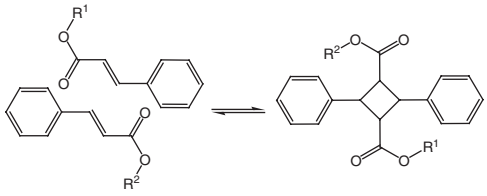
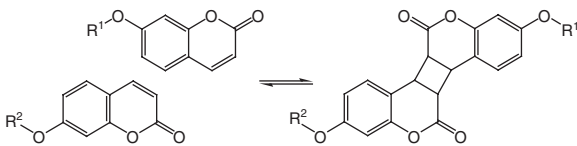
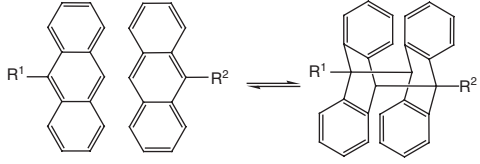
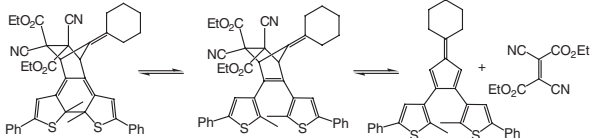
Entry	Example	Ref.
(a)	Light and force as “switch”	
1	Spiro-pyranes 	[65]
2	[2+2] cycloaddition reactions 	[6, 17, 142, 144]
(b)	Light as “switch”	
3	(a) [2+2] cycloaddition reactions 	[6, 17, 212–222]
	(b) [4+4] cycloaddition reactions 	
4	Photo-responsive DA-reactions 	[79, 81]

Table 1.5 (Continued)

Entry	Example	Ref.
5	<i>Cis-to-trans</i> isomerization of azobenzene units	[204, 223, 224]
(c)	pH-Value as "switch"	
6	(a) formation of hydrazones	[225, 226]
	(b) complexation of salicylhydroxamic acids and boronic acids	
(d)	Electrical "switch"	
7	Electrochemical redox reaction	[204, 227]

cyclobutanediyl crosslinks [6, 17, 144]. Upon a damage event the reversion of the strained cyclobutane ring occurred and a fast healing process could be initiated by photoirradiation with a wavelength above 280 nm, resulting in hard and insoluble films. If samples were additionally heated during irradiation, a higher recovery of flexural strength could be reached, whereas the flexural strength of the healed sample was always considerably reduced in comparison to the original sample [6, 17, 144] (see Table 1.5 entry 2). "Switchable" photo-induced crosslinking of

pendant coumarin groups has attracted the attention of several groups [17, 212, 213]. In acrylate-based copolymers, dimerization of coumarin moieties, and thus the formation of a polymeric network, was observed within the films after irradiation with 300 or 350 nm light. Photo-cleavage could be forced by irradiation of light with a wavelength of 254 nm. Furthermore, it was found that the photochemistry was determined by the copolymer composition. Thus, the rate of photocrosslinking for copolyacrylates with a T_g above room temperature depends on the chromophore content, whereas the rate for copolymers with a T_g below room temperature can be traced to chain segmental mobility [17, 212] (see Table 1.5 entry 3a). A great deal of effort was put in optimizing the [4+4] cycloaddition of anthracene-based polymers [6, 17, 215–222] (see Table 1.5 entry 3b) as this pericyclic reaction proceeds at longer wavelengths, which can be tolerated by a large variety of functional groups. Furthermore, the great proximity to the wavelength of sunlight makes it attractive for outdoor applications. Accordingly, the concept of photocrosslinking anthryl moieties has been applied to study aging processes in polymer backbones [215], for the preparation of molecularly imprinted polymers [220] and multifaceted porous and three-dimensional polymer films [217]. Moreover, “switchable” anthracene groups found application in dendritic macromonomers [219]. Network formation could also be observed in aqueous media with reversible change of the crosslinking density, as well as in the bulk showing full reversibility. The high density of functional groups and the low viscosity also emphasize the applicability for self-healing purposes [219].

Furthermore, light can also be used as a “switch” to turn on and off a photoreversible DA reaction of dithienylfuran dienes [79, 81] (see Figure 1.8b and Table 1.5 entry 4). This approach toward self-healing polymers is based on two reversible reactions. First, ultraviolet light can be used to introduce the ring-closed form of the dithienylfuran dienes, or visible light can be applied to force the ring-opened form. The second reversible reaction is the DA/rDA equilibrium, which can be established just by the ring-opened isomer, resulting in a “turned on” state applicable for self-healing polymers.

Due to the ability for molecular “switching” (see Table 1.5 entry 5) the light-induced *cis-trans* isomerization of azobenzene units [223] allows photochemically induced dynamics in the bulk [204, 224] which may be applied as a future self-healing concept.

Another “switch” used for dynamic self-healing polymers is the pH-value (see Figure 1.8c). One example of a pH-sensitive, reversible concept is based on condensation reactions of aldehydes with acylhydrazines, resulting in the formation of hydrazones as network points [225] (see Table 1.5 entry 6a). A similar approach utilizes complexation of salicylhydroxamic acid and boronic acid moieties within a polymer backbone to create a pH responsible polymer [226] (see Table 1.5 entry 6b).

Electrochemical processes can be used as “switchable” interactions (see Table 1.5 entry 7) for future self-healing polymers. For example, in a disulfide-aniline precursor, cleavage of crosslinking points could be forced by electrochemical reduction of disulfide moieties, whereas the oxidation of dithiolate groups resulted in the re-formation of the crosslinked structure [204, 227].

1.5 Multiple versus One-Time Self-Healing

The *encapsulation* of reactive components was one of the first and most prominent approaches toward self-healing polymers using dicyclopentadiene and a Grubb's catalyst as healing agents. While taking advantage of the mechanical performance of the polymeric composite a *one-time repair* after a localized rupture event could be triggered [19]. In contrast, embedded *vascular networks* allow a continuous delivery of the incorporated healing agents, affording the opportunity for *multiple self-healing* [228]. Accordingly, for the design of both one-time and multiple self-healing concepts, biomimetic approaches, like bleeding or the blood flow vascular system, inspired scientists. Thus, capsule-based and vascular (healant-loaded pipelines interconnected one-, two-, or three-dimensionally) self-healing principles (see Figure 1.9a,b) mimic nature [134] while using different microcontainers for healing agents. In the case of a propagating rupture event the active material—the healing agent—is released into the damaged area while wetting due to capillary action [7, 8]. After bonding to the interfaces of the matrix, either by physical or by chemical self-healing approaches, the crack can be healed due to the formation of a stable network. The recovery of the material properties is the consequence of network formation between the liquid and dynamic components, usually embedded separately into microcontainers within a matrix due to their high reactivity. The applied principle to sequester the healing agent determines, beside the repeatability of healing, also the healable damage volume and the recovery rate [7, 8].

Capsule-based one-time self-healing concepts reveal big advantages since they can be easily embedded and industrialized as the technique of microencapsulation

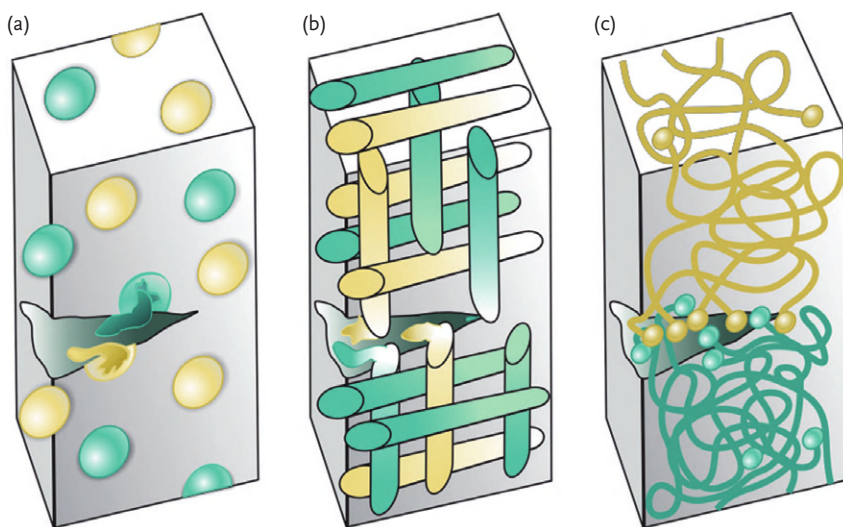


Figure 1.9 Multiple versus one-time self-healing. (a) Capsule-based, (b) vascular, and (c) intrinsic self-healing principles.

has been investigated since the 1950s [229, 230] (see also Chapter 10). Different encapsulation techniques involving *in situ* and interfacial encapsulation, as well as meltable dispersions and coacervation, are known, whereupon the first three mentioned are commonly used for self-healing materials. Beside these emulsion-based methods, microcapsules can also be prepared by spray drying, pan coating, and centrifugal extrusion [7, 8, 231].

In contrast to capsule-based healing concepts, vascular self-healing principles give the opportunity for multiple healing if the vascular network can be refilled from a connected but contemporaneously undamaged region of the vasculature [7]. A vascular approach using hollow glass tubes was first applied for healing of cracks in concrete materials [8] utilizing a three-component mixture based on methyl methacrylate [232]. Later the methodology was adopted for polymeric composite materials [233, 234] by using cyanoacrylate resins stored in glass pipette tubes.

Intrinsic self-healing materials (see Figure 1.9c) can always be healed multiple times as the self-healing process, and therefore the recovery of the material properties, are inherent material abilities [7]. These abilities largely rely on entanglement processes within the polymer matrix. Nevertheless, the need for an external trigger, like pressure, light or heat, might be necessary if the healing is not autonomously triggered by the damage event itself. Examples of intrinsic self-healing polymers are based on supramolecular network formation introduced by hydrogen bonding, ionomers, π - π -interactions or metal-bonding, thermally reversible reactions like DA/rDA reactions, and “switchable” functional groups [7] (see also Chapters 6 and 11–13). Of course, all physical self-healing approaches, like intermolecular diffusion or melting, are multiple time healing processes [7]. For further information about principles and methods of encapsulation and channel-based healing systems see also Chapters 10 and 15.

In order to highlight the contrast between a multiple versus a one-time healing approach two examples will be presented, both based on poly(isobutylene) (PIB) – a highly dynamic polymer due to its low T_g of about -70°C – while using different architectures as well as different endgroups, and thus two different self-healing principles [9, 18, 22, 23, 42, 43].

Based on PIBs bearing hydrogen bonding motifs a multiple time healing concept in the bulk was reported [22]. For this purpose bifunctional polymers endcapped with barbituric acid or Hamilton Wedge were synthesized and their dynamics and hence the self-healing behavior of these kinds of polymers in the melt state has been investigated (see Figure 1.10). Thus, pure polymers and equimolar mixtures of barbituric acid and Hamilton Wedge-bearing samples were studied via temperature-dependent rheology measurements. Surprisingly strong self-healing supramolecular rubbers with an increased thermal stability could be observed for samples with barbituric acid used as the hydrogen bonding motif. Rubber formation is based on the thermoreversible formation of larger aggregates [23] further enhanced by microphase separation between the nonpolar polymer backbone and the polar hydrogen bonding motifs (see Figure 1.10a).

The formation of dynamic junction points was additionally confirmed as the polymer with barbituric acid as endgroup showed terminal flow at low frequencies

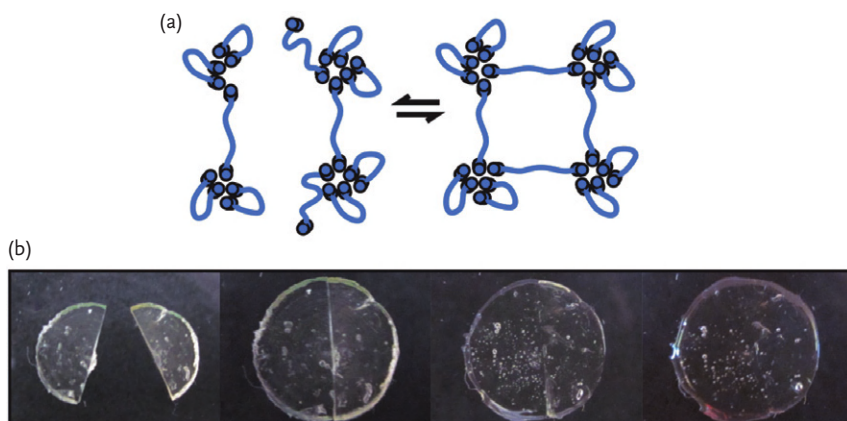


Figure 1.10 Multiple self-healing concept based on PIBs. (a) Thermoreversible formation of a supramolecular network via hydrogen bonding motifs. (b) Self-healing experiment of PIB functionalized with

barbituric acid, (i) cut parts, (ii) cut parts were just brought into contact, (iii) partially healed crack after 24 h, (iv) completely healed crack after 48 h (reprinted with permission of RSC Publishing) [22].

but a rubbery plateau at high frequencies [22]. This observation correlates with a semi-open or open state of the hydrogen bonding motif at low frequencies and hence long timescales, and with closed aggregates at higher frequencies, and hence short timescales, respectively. PIBs with barbituric acid groups could be healed completely after cutting into two pieces and bringing in contact again within 48 h proving possible application of this self-healing material at room temperature (see Figure 1.10b). In contrast, equimolar mixtures of PIBs bearing Hamilton Wedges and barbituric acid behaved like brittle rubbers at room temperature and terminal flow was only observed at temperatures above 100 °C [22] (for more information see also Chapter 11).

In contrast to this multiple time healing concept, a one-time healing concept based on the CuAAC of multivalent azide- and alkyne-functionalized PIBs and poly(acrylate)s was investigated [18, 42, 43]. Polymers with different molecular weights and different functional group densities were synthesized via living polymerization techniques. $\text{Cu}^{(I)}\text{Br}(\text{PPh}_3)_3$ was chosen as the best catalyst, achieving a crosslinking of equimolar polymer mixtures at room temperature and gelation times within the range of 2–15 h. The crosslinking behavior—investigated via *in situ* rheology—was studied in dependence on the molecular weight and on the concentration of functional groups, as well as on the starting viscosity of the samples. While analyzing the viscosity of the polymer mixtures, increasing reaction rates with increasing concentration of functional groups could be observed, and an autocatalytic effect [43] within the reaction up to a factor of 4.3 could be demonstrated (see Figure 1.11a).

The acceleration of further click reactions was traced back to clustering effects of the triazole rings, acting as internal ligands while preorientating the azide- and

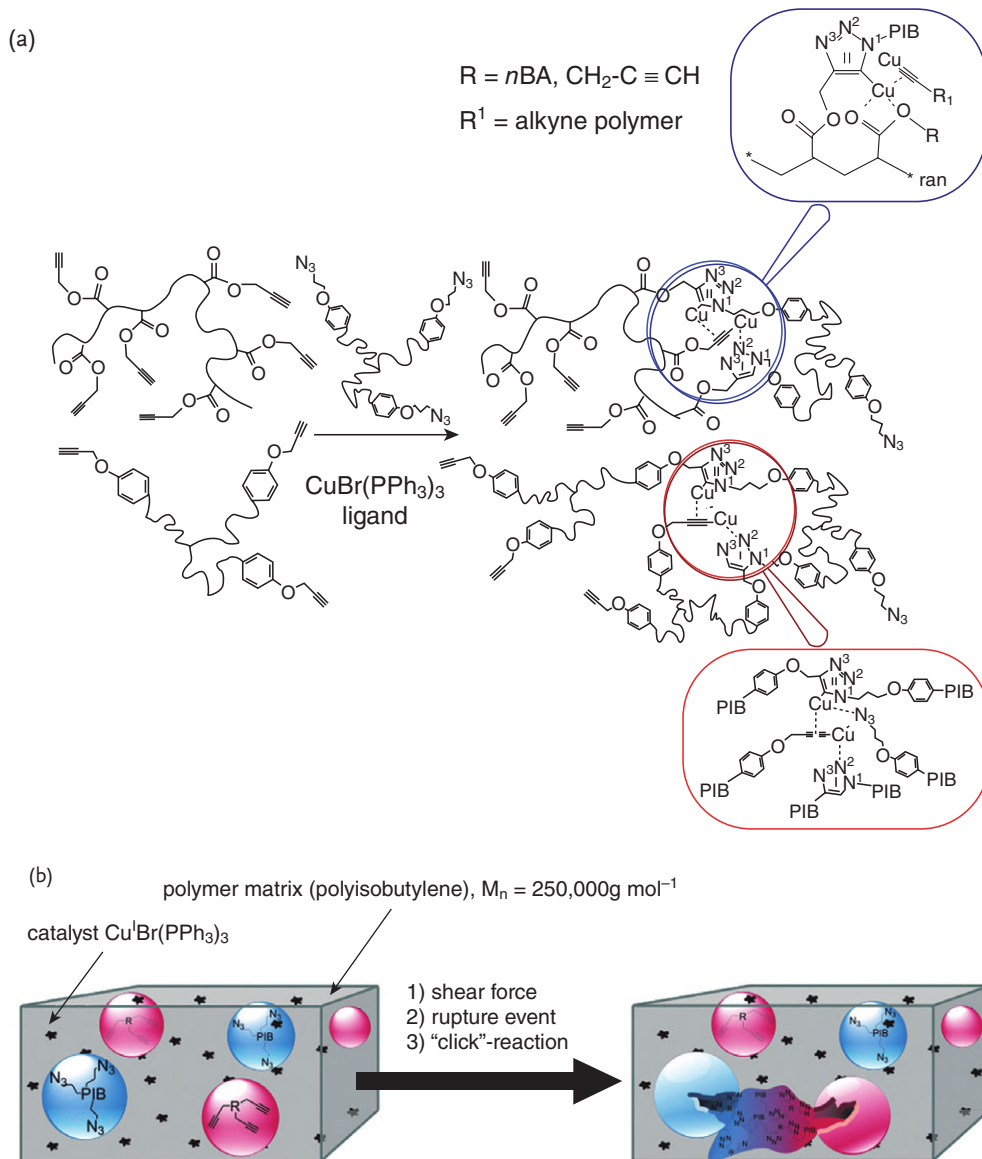


Figure 1.11 One-time self-healing concept based on PIBs and poly(acrylate)s. (a) Proposed mechanism of autocatalysis for crosslinking multivalent PIBs and poly(acrylate)s functionalized with azide- or alkyne-groups at room temperature using $Cu^0 Br(PPh_3)_3$ as catalyst (reprinted with permission of ACS Publications) [43]. (b) Concept for the design of shear sensitive

one-time self-healing materials based on the encapsulation of azide- and alkyne-functionalized polymers embedded in a high-molecular weight PIB matrix with finely dispersed $Cu^0 Br(PPh_3)_3$ as catalyst. Rupture of the capsules and thus release of reactive polymers is induced by shear force, resulting in network formation via CuAAC.

alkyne-groups near to the active copper(I) center. Thus, a polymeric self-healing approach suitable for room temperature application based on a deeper understanding of catalytic effects within the CuAAC was developed [43]. Previously, the successful encapsulation of highly reactive, multivalent azide-functionalized PIBs was shown using liquid polymers as reactive healing agents for the first time [18]. After embedding in a high-molecular weight PIB matrix together with finely dispersed $\text{Cu}^{\text{I}}\text{Br}(\text{PPh}_3)_3$, reactive polymers were released by shear force-induced rupture of capsules (see Figure 1.11). Due to the so-induced network formation via CuAAC, dynamic mechanical analyses showed 81% recovery of the tensile storage modulus at room temperature within five days, proving the concept of a capsule-based one-time self-healing approach [18, 42, 43].

1.6

Resume and Outlook

It can be imagined that the world of self-healing polymers is large, engulfing many different and complex physical and chemical principles. Materials scientists will approach the design of such materials entirely differently from chemists, physicists or biologists—this should be clear from the introductory remarks in this chapter. However, it also demonstrates that a vision of scientists has become reality, combining such different issues as chemical reactivity, polymeric design, supramolecular forces and catalytic action into one type of materials, whose technological applications can be already realized. As with many applications, price and the identification of technological areas of usefulness are now the next step for their application, together with their commercialization and consumer-adoption. The following chapters within this book will give a deeper insight into more chemical and physical principles, together with technological applications of these fascinating classes of self-healing materials.

Acknowledgments

We are grateful for the grant DFG BI 1337/8-1 (within the SPP 1568 “Design and Generic Principles of Self-Healing Materials”) and the EU-project IASS for financial support.

References

- 1 White, S.R., and Blaiszik, B.J. (2012) *Spektrum der Wissenschaft*, 3, 82–90.
- 2 Fischer, H. (2010) *Nat. Sci.*, 2 (8), 873–901.
- 3 Wu, D.Y., Meure, S., and Solomon, D. (2008) *Prog. Polym. Sci.*, 33, 479–522.
- 4 Caruso, M.M., Davis, D.A., Shen, Q., Odom, S.A., Sottos, N.R., White, S.R., and Moore, J.S. (2009) *Chem. Rev.*, 109 (11), 5755–5798.
- 5 Murphy, E.B., and Wudl, F. (2010) *Prog. Polym. Sci.*, 35 (1–2), 223–251.

- 6 Burattini, S., Greenland, B.W., Chappell, D., Colquhoun, H.M., and Hayes, W. (2010) *Chem. Soc. Rev.*, **39** (6), 1973–1985.
- 7 Blaiszik, B.J., Kramer, S.L.B., Olugebefola, S.C., Moore, J.S., Sottos, N.R., and White, S.R. (2010) *Annu. Rev. Mater. Res.*, **40**, 179–211.
- 8 Yuan, Y.C., Yin, T., Rong, M.Z., and Zhang, M.Q. (2008) *Express Polym. Lett.*, **2** (4), 238–250.
- 9 Herbst, F., Döhler, D., Michael, P., and Binder, W.H. (2013) *Macromol. Rapid Commun.*, **34**, 203–220, marc.201200675.
- 10 Zhang, M.Q., and Rong, M.Z. (2012) *Sci. China Chem.*, **55** (5), 648–676.
- 11 Zhang, M.Q., and Rong, M.Z. (2012) *J. Polym. Sci. Part B: Polym. Phys.*, **50** (4), 229–241.
- 12 Wojtecki, R.J., Meador, M.A., and Rowan, S.J. (2011) *Nat. Mater.*, **10** (1), 14–27.
- 13 Binder, W., and Zirbs, R. (2007) *Hydrogen Bonded Polymers*, Springer, Berlin, Heidelberg, p. 1.
- 14 Blight, B.A., Hunter, C.A., Leigh, D.A., McNab, H., and Thomson, P.I.T. (2011) *Nat. Chem.*, **3** (3), 244–248.
- 15 Lehn, J.-M. (2005) *Prog. Polym. Sci.*, **30**, 814–831.
- 16 Kolomiets, E., and Lehn, J.-M. (2005) *Chem. Commun.*, (12), 1519–1521.
- 17 Bergman, S.D., and Wudl, F. (2008) *J. Mater. Chem.*, **18** (1), 41–62.
- 18 Gragert, M., Schunack, M., and Binder, W.H. (2011) *Macromol. Rapid Commun.*, **32** (5), 419–425.
- 19 White, S.R., Sottos, N.R., Geubelle, P.H., Moore, J.S., Kessler, M.R., Sriram, S.R., Brown, E.N., and Viswanathan, S. (2001) *Nature*, **409**, 794–817.
- 20 Burattini, S., Greenland, B.W., Hayes, W., Mackay, M.E., Rowan, S.J., and Colquhoun, H.M. (2011) *Chem. Mater.*, **23** (1), 6–8.
- 21 Cordier, P., Tournilhac, F., Soulie-Ziakovic, C., and Leibler, L. (2008) *Nature*, **451**, 977–980.
- 22 Herbst, F., Seiffert, S., and Binder, W.H. (2012) *Polym. Chem.*, **3** (11), 3084–3092.
- 23 Herbst, F., Schröter, K., Gunkel, I., Gröger, S., Thurn-Albrecht, T., Balbach, J., and Binder, W.H. (2010) *Macromolecules*, **43** (23), 10006–10016.
- 24 Chen, X., Wudl, F., Mal, A.K., Shen, H., and Nutt, S.R. (2003) *Macromolecules*, **36**, 1802–1807.
- 25 Chen, X., Dam, M.A., Ono, K., Mal, A., Shen, H., Nutt, S.R., Sheran, K., and Wudl, F. (2002) *Science*, **295**, 1698–1702.
- 26 Chujo, Y., Sada, K., and Saegusa, T. (1990) *Macromolecules*, **23** (10), 2636–2641.
- 27 Murphy, E.B., Bolanos, E., Schaffner-Hamann, C., Wudl, F., Nutt, S.R., and Auad, M.L. (2008) *Macromolecules*, **41** (14), 5203–5209.
- 28 Dumitrescu, S., Grigoras, M., and Natansohn, A. (1979) *J. Polym. Sci. Polym. Lett.*, **17** (9), 553–559.
- 29 Yuan, Y.C., Rong, M.Z., Zhang, M.Q., and Yang, G.C. (2011) *Express Polym. Lett.*, **5** (1), 47–59.
- 30 Coope, T.S., Mayer, U.F.J., Wass, D.F., Trask, R.S., and Bond, I.P. (2011) *Adv. Funct. Mater.*, **21** (24), 4624–4631.
- 31 Guadagno, L., Longo, P., Raimondo, M., Naddeo, C., Mariconda, A., Sorrentino, A., Vittoria, V., Iannuzzo, G., and Russo, S. (2010) *J. Polym. Sci. Part B: Polym. Phys.*, **48** (23), 2413–2423.
- 32 Tian, Q., Yuan, Y.C., Rong, M.Z., and Zhang, M.Q. (2009) *J. Mater. Chem.*, **19** (9), 1289–1296.
- 33 Rahmathullah, M.A.M., and Palmese, G.R. (2009) *J. Appl. Polym. Sci.*, **113** (4), 2191–2201.
- 34 Wilson, G.O., Moore, J.S., White, S.R., Sottos, N.R., and Andersson, H.M. (2008) *Adv. Funct. Mater.*, **18** (1), 44–52.
- 35 Yin, T., Rong, M.Z., Zhang, M.Q., and Yang, G.C. (2007) *Compos. Sci. Technol.*, **67** (2), 201–212.
- 36 Rong, M.Z., Zhang, M.Q., and Zhang, W. (2007) *Adv. Compos. Lett.*, **16** (5), 167–172.
- 37 Caruso, M.M., Delafuente, D.A., Ho, V., Sottos, N.R., Moore, J.S., and White, S.R. (2007) *Macromolecules*, **40** (25), 8830–8832.
- 38 Brown, E.N., White, S.R., and Sottos, N.R. (2005) *Compos. Sci. Technol.*, **65** (15–16), 2466–2473.
- 39 Zako, M., and Takano, N. (1999) *J. Intel. Mater. Syst. Str.*, **10** (10), 836–841.

- 40 Jin, H., Mangun, C.L., Stradley, D.S., Moore, J.S., Sottos, N.R., and White, S.R. (2012) *Polymer*, **53**, 581.
- 41 Yuan, Y.C., Rong, M.Z., Zhang, M.Q., Chen, J., Yang, G.C., and Li, X.M. (2008) *Macromolecules*, **41** (14), 5197–5202.
- 42 Schunack, M., Gragert, M., Döhler, D., Michael, P., and Binder, W.H. (2012) *Macromol. Chem. Phys.*, **213** (2), 205–214.
- 43 Döhler, D., Michael, P., and Binder, W.H. (2012) *Macromolecules*, **45** (8), 3335–3345.
- 44 Binder, W.H., and Herbst, F. (2011) Click chemistry in polymer science, in: *McGraw-Hill Yearbook of Science and Technology*, McGraw-Hill Professional, New York.
- 45 Binder, W.H., and Sachsenhofer, R. (2007) *Macromol. Rapid Commun.*, **28** (1), 15–54.
- 46 Binder, W.H., and Sachsenhofer, R. (2008) *Macromol. Rapid Commun.*, **29** (12–13), 952–981.
- 47 Binder, W.H., and Kluger, C. (2007) *Curr. Org. Chem.*, **10**, 1791.
- 48 Sheng, X., Mauldin, T.C., and Kessler, M.R. (2010) *J. Polym. Sci. Part A Polym. Chem.*, **48** (18), 4093–4102.
- 49 Binder, W.H., and Zirbs, R. (2009) *Encyclopedia of Polymer Science and Technology*, John Wiley & Sons, Inc.
- 50 Binder, W.H., and Sachsenhofer, R. (2009) *Click Chemistry for Biotechnology and Materials Science* (ed. J. Lahann), Wiley-Blackwell, pp. 119–175.
- 51 Sheng, X., Rock, D.M., Mauldin, T.C., and Kessler, M.R. (2011) *Polymer*, **52** (20), 4435–4441.
- 52 Gokmen, M.T., Brassinne, J., Prasath, R.A., and Du Prez, F.E. (2011) *Chem. Commun.*, **47** (16), 4652–4654.
- 53 Espeel, P., Goethals, F., and Du Prez, F.E. (2011) *J. Am. Chem. Soc.*, **133** (6), 1678–1681.
- 54 Prasath, R.A., Gokmen, M.T., Espeel, P., and Du Prez, F.E. (2010) *Polym. Chem.*, **1** (5), 685–692.
- 55 Yang, J., Keller, M.W., Moore, J.S., White, S.R., and Sottos, N.R. (2008) *Macromolecules*, **41** (24), 9650–9655.
- 56 Sheng, X., Lee, J.K., and Kessler, M.R. (2009) *Polymer*, **50** (5), 1264–1269.
- 57 Lee, J.K., Liu, X., Yoon, S.H., and Kessler, M.R. (2007) *J. Polym. Sci. Part B: Polym. Phys.*, **45** (14), 1771–1780.
- 58 Larin, G.E., Bernklau, N., Kessler, M.R., and DiCesare, J.C. (2006) *Polym. Eng. Sci.*, **46** (12), 1804–1811.
- 59 Rule, J.D., and Moore, J.S. (2002) *Macromolecules*, **35** (21), 7878–7882.
- 60 Liu, X., Lee, J.K., Yoon, S.H., and Kessler, M.R. (2006) *J. Appl. Polym. Sci.*, **101** (3), 1266–1272.
- 61 Mauldin, T.C., Leonard, J., Earl, K., Lee, J.K., and Kessler, M.R. (2012) *ACS Appl. Mater. Interfaces*, **4** (3), 1831–1837.
- 62 Tsarevsky, N.V., and Matyjaszewski, K. (2002) *Macromolecules*, **35** (24), 9009–9014.
- 63 Amamoto, Y., Kamada, J., Otsuka, H., Takahara, A., and Matyjaszewski, K. (2011) *Angew. Chem. Int. Ed.*, **50** (7), 1660–1663.
- 64 Hickenboth, C.R., Moore, J.S., White, S.R., Sottos, N.R., Baudry, J., and Wilson, S.R. (2007) *Nature*, **446**, 423–427.
- 65 Davis, D.A., Hamilton, A., Yang, J., Cremar, L.D., Van Gough, D., Potisek, S.L., Ong, M.T., Braun, P.V., Martinez, T.J., White, S.R., Moore, J.S., and Sottos, N.R. (2009) *Nature*, **459** (7243), 68–72.
- 66 Kean, Z.S., and Craig, S.L. (2012) *Polymer*, **53** (5), 1035–1048.
- 67 Beiermann, B.A., Kramer, S.L.B., Moore, J.S., White, S.R., and Sottos, N.R. (2012) *ACS Macro Lett.*, **1** (1), 163–166.
- 68 Kryger, M.J., Munaretto, A.M., and Moore, J.S. (2011) *J. Am. Chem. Soc.*, **133** (46), 18992–18998.
- 69 Kingsbury, C.M., May, P.A., Davis, D.A., White, S.R., Moore, J.S., and Sottos, N.R. (2011) *J. Compos. Mater.*, **21** (23), 8381–8388.
- 70 Potisek, S.L., Davis, D.A., Sottos, N.R., White, S.R., and Moore, J.S. (2007) *J. Am. Chem. Soc.*, **129** (45), 13808–13809.
- 71 Lenhardt, J.M., Black, A.L., Beiermann, B.A., Steinberg, B.D., Rahman, F., Samborski, T., Elsagr, J., Moore, J.S., Sottos, N.R., and Craig, S.L. (2011) *J. Mater. Chem.*, **21** (23), 8454–8459.
- 72 Klukovich, H.M., Kean, Z.S., Iacono, S.T., and Craig, S.L. (2011) *J. Am. Chem. Soc.*, **133** (44), 17882–17888.

- 73 Lenhardt, J.M., Black, A.L., and Craig, S.L. (2009) *J. Am. Chem. Soc.*, **131** (31), 10818–10819.
- 74 Jakobs, R.T.M., and Sijbesma, R.P. (2012) *Organometallics*, **31** (6), 2476–2481.
- 75 Piermattei, A., Karthikeyan, S., and Sijbesma, R.P. (2009) *Nat. Chem.*, **1** (2), 133–137.
- 76 Karthikeyan, S., Potisek, S.L., Piermattei, A., and Sijbesma, R.P. (2008) *J. Am. Chem. Soc.*, **130** (45), 14968–14969.
- 77 Paulusse, J.M.J., Huijbers, J.P.J., and Sijbesma, R.P. (2006) *Chem. Eur. J.*, **12**, 4928–4934.
- 78 Paulusse, J.M.J., and Sijbesma, R.P. (2004) *Angew. Chem. Int. Ed.*, **43**, 4460–4462.
- 79 Erno, Z., Asadirad, A.M., Lemieux, V., and Branda, N.R. (2012) *Org. Biomol. Chem.*, **10** (14), 2787–2792.
- 80 Cardenas-Daw, C., Kroeger, A., Schaertl, W., Froimowicz, P., and Landfester, K. (2012) *Macromol. Chem. Phys.*, **213** (2), 144–156.
- 81 Lemieux, V., Gauthier, S., and Branda, N.R. (2006) *Angew. Chem. Int. Ed.*, **45** (41), 6820–6824.
- 82 Xia, F., and Jiang, L. (2008) *Adv. Mater.*, **20** (15), 2842–2858.
- 83 Guan, Z., Roland, J.T., Bai, J.Z., Ma, S.X., McIntire, T.M., and Nguyen, M. (2004) *J. Am. Chem. Soc.*, **126** (7), 2058–2065.
- 84 Rhaman, M.A., Penco, M., Spagnoli, G., Grande, A.M., and Di Landro, L. (2011) *Macromol. Mater. Eng.*, **296** (12), 1119–1127.
- 85 Varley, R.J., Shen, S., and van der Zwaag, S. (2010) *Polymer*, **51** (3), 679–686.
- 86 Aboudzadeh, M.A., Muñoz, M.E., Santamaría, A., Marcilla, R., and Mecerreyes, D. (2012) *Macromol. Rapid Commun.*, **33** (4), 314–318.
- 87 Varley, R.J., and van der Zwaag, S. (2008) *Polym. Test.*, **27** (1), 11–19.
- 88 Varley, R.J., and van der Zwaag, S. (2008) *Acta Mater.*, **56** (19), 5737–5750.
- 89 Tadano, K., Hirasawa, E., Yamamoto, H., and Yano, S. (1989) *Macromolecules*, **22** (1), 226–233.
- 90 Zare, P., Stojanovic, A., Herbst, F., Akbarzadeh, J., Peterlik, H., and Binder, W.H. (2012) *Macromolecules*, **45** (4), 2074–2084.
- 91 Zare, P., Mahrova, M., Tojo, E., Stojanovic, A., and Binder, W.H. (2013) *J. Polym. Sci. Part A: Polym. Chem.*, **51** (1), 190–202.
- 92 Schüssele, A.C., Nübling, F., Thomann, Y., Carstensen, O., Bauer, G., Speck, T., and Mülhaupt, R. (2012) *Macromol. Mater. Eng.*, **297** (5), 411–419.
- 93 Fischer, H.R., Tempelaars, K., Kerpershoek, A., Dingemans, T., Iqbal, M., Lonkhuyzen, H.V., Iwanowsky, B., and Semprimoschnig, C. (2010) *ACS Appl. Mater. Interfaces*, **2** (8), 2218–2225.
- 94 Chen, Y., Kushner, A.M., Williams, G.A., and Guan, Z. (2012) *Nat. Chem.*, **4**, 467–472.
- 95 Kushner, A.M., Vossler, J.D., Williams, G.A., and Guan, Z. (2009) *J. Am. Chem. Soc.*, **131** (25), 8766–8768.
- 96 Boiko, Y.M., and Prud'homme, R.E. (1998) *J. Polym. Sci. Part B: Polym. Phys.*, **36** (4), 567–572.
- 97 Wool, R.P., and O'Connor, K.M. (1981) *J. Appl. Phys.*, **52** (10), 5953–5963.
- 98 Wool, R.P. (2008) *Soft Matter*, **4** (3), 400–418.
- 99 Wool, R.P., and O'Connor, K.M. (1982) *J. Polym. Sci. Polym. Lett.*, **20** (1), 7–16.
- 100 Wool, R.P., and O'Connor, K.M. (1981) *Polym. Eng. Sci.*, **21** (14), 970–977.
- 101 Boiko, Y.M., and Prud'homme, R.E. (1997) *Macromolecules*, **30** (12), 3708–3710.
- 102 McGarel, O.J., and Wool, R.P. (1987) *J. Polym. Sci. Part B: Polym. Phys.*, **25** (12), 2541–2560.
- 103 Meyers, G.F., DeKoven, B.M., and Seitz, J.T. (1992) *Langmuir*, **8** (9), 2330–2335.
- 104 Kajiyama, T., Tanaka, K., and Takahara, A. (1995) *Macromolecules*, **28** (9), 3482–3484.
- 105 Mayes, A.M. (1994) *Macromolecules*, **27** (11), 3114–3115.
- 106 Fischer, H. (2005) *Macromolecules*, **38** (3), 844–850.
- 107 de Gennes, P.G. (2000) *Eur. Phys. J. E*, **2** (3), 201–205.
- 108 Jones, R.A.L. (2003) *Nat. Mater.*, **2** (10), 645–646.
- 109 Mattsson, J., Forrest, J.A., and Börjesson, L. (2000) *Phys. Rev. E*, **62** (4), 5187–5200.
- 110 van der Veen, J.F. (1999) *Surf. Sci.*, **433–435** (0), 1–11.

- 111 Wallace, W.E., Fischer, D.A., Efimenko, K., Wu, W.-L., and Genzer, J. (2001) *Macromolecules*, **34** (15), 5081–5082.
- 112 van der Gucht, J., Besseling, N.A.M., and Fleer, G.J. (2002) *Macromolecules*, **35** (17), 6732–6738.
- 113 Bliznyuk, V.N., Assender, H.E., and Briggs, G.A.D. (2002) *Macromolecules*, **35** (17), 6613–6622.
- 114 Pu, Y., Ge, S., Rafailovich, M., Sokolov, J., Duan, Y., Pearce, E., Zaitsev, V., and Schwarz, S. (2001) *Langmuir*, **17** (19), 5865–5871.
- 115 Tanaka, K., Kajiyama, T., Takahara, A., and Tasaki, S. (2002) *Macromolecules*, **35** (12), 4702–4706.
- 116 Lee, J.Y., Buxton, G.A., and Balazs, A.C. (2004) *J. Chem. Phys.*, **121** (11), 5531–5540.
- 117 Gandini, A. (2005) *Polím.: Ciênc. Tecnol.*, **15**, 95–101.
- 118 Wiggins, K.M., Syrett, J.A., Haddleton, D.M., and Bielawski, C.W. (2011) *J. Am. Chem. Soc.*, **133** (18), 7180–7189.
- 119 Wiggins, K.M., Brantley, J.N., and Bielawski, C.W. (2012) *ACS Macro Lett.*, **1** (5), 623–626.
- 120 Jones, J.R., Liotta, C.L., Collard, D.M., and Schiraldi, D.A. (1999) *Macromolecules*, **32** (18), 5786–5792.
- 121 Canary, S.A., and Stevens, M.P. (1992) *J. Polym. Sci. Part A Polym. Chem.*, **30** (8), 1755–1760.
- 122 Inglis, A.J., Nebhani, L., Altintas, O., Schmidt, F.G., and Barner-Kowollik, C. (2010) *Macromolecules*, **43** (13), 5515–5520.
- 123 Reutenauer, P., Buhler, E., Boul, P.J., Candau, S.J., and Lehn, J.-M. (2009) *Chem. Eur. J.*, **15** (8), 1893–1900.
- 124 Takeda, K., Tanahashi, M., and Unno, H. (2003) *Sci. Technol. Adv. Mat.*, **4** (5), 435–444.
- 125 Takeda, K., Unno, H., and Zhang, M. (2004) *J. Appl. Polym. Sci.*, **93** (2), 920–926.
- 126 Kessler, M.R., Sottos, N.R., and White, S.R. (2003) *Compos. Part A-Appl. S.*, **34** (8), 743–753.
- 127 Williams, K.A., Dreyer, D.R., and Bielawski, C.W. (2008) *MRS Bull.*, **33**, 759–765.
- 128 Yang, J.I., (1998) Part I: Synthesis of aromatic polyketones via soluble precursors derived from bis(A-amininitrile)s; Part II: Modifications of epoxy resins with functional hyperbranched poly(arylene ester), PhD Thesis, Virginia Tech (Roanoke).
- 129 Bhatnagar, M.S. (1996) *The Polymeric Materials Encyclopedia*, 1st edn, CRC Press, Inc.
- 130 Bourne, L.B., Milner, F.J.M., and Alberman, K.B. (1959) *Br. J. Ind. Med.*, **16**, 81–97.
- 131 Cho, S.H., Andersson, H.M., White, S.R., Sottos, N.R., and Braun, P.V. (2006) *Adv. Mater.*, **18**, 997–1000.
- 132 Billiet, S., Van Camp, W., Hillewaere, X.K.D., Rahier, H., and Du Prez, F.E. (2012) *Polymer*, **53** (12), 2320–2326.
- 133 Blaiszik, B.J., Caruso, M.M., McIlroy, D.A., Moore, J.S., White, S.R., and Sottos, N.R. (2009) *Polymer*, **50** (4), 990–997.
- 134 Brown, E.N., Sottos, N.R., and White, S.R. (2002) *Exp. Mech.*, **42** (4), 372–379.
- 135 Jones, A.S., Rule, J.D., Moore, J.S., White, S.R., and Sottos, N.R. (2006) *Chem. Mater.*, **18** (5), 1312–1317.
- 136 Keller, M.W., and Sottos, N.R. (2006) *Exp. Mech.*, **46**, 725–733.
- 137 Keller, M.W., White, S.R., and Sottos, N.R. (2007) *Adv. Funct. Mater.*, **17** (14), 2399–2404.
- 138 Keller, M.W., White, S.R., and Sottos, N.R. (2008) *Polymer*, **49** (13–14), 3136–3145.
- 139 Wang, H., Yuan, Y., Rong, M., and Zhang, M. (2009) *Colloid Polym. Sci.*, **287**, 1089–1097.
- 140 van Der Weij, F.W. (1980) *Makromol. Chem.*, **181** (12), 2541–2548.
- 141 Kolb, H.C., Finn, M.G., and Sharpless, K.B. (2001) *Angew. Chem. Int. Ed.*, **40** (11), 2004–2021.
- 142 Dilling, W.L. (1983) *Chem. Rev.*, **83** (1), 1–47.
- 143 Bosman, A.W., Sijbesma, R.P., and Meijer, E.W. (2004) *Mater. Today*, **7** (4), 34–39.
- 144 Chung, C.M., Roh, Y.S., Cho, S.Y., and Kim, J.G. (2004) *Chem. Mater.*, **16** (21), 3982–3984.
- 145 Chujo, Y., Sada, K., Naka, A., Nomura, R., and Saegusa, T. (1993) *Macromolecules*, **26** (5), 883–887.

- 146 Scott, T.F., Schneider, A.D., Cook, W.D., and Bowman, C.N. (2005) *Science*, **308** (5728), 1615–1617.
- 147 Ono, T., Nobori, T., and Lehn, J.-M. (2005) *Chem. Commun.*, (12), 1522–1524.
- 148 Yoshie, N., Saito, S., and Oya, N. (2011) *Polymer*, **52**, 6074–6079.
- 149 Sijbesma, R.P., Beijer, F.H., Brunsveld, L., Folmer, B.J.B., Hirschberg, J.H.K.K., Lange, R.F.M., Lowe, J.K.L., and Meijer, E.W. (1997) *Science*, **278** (5343), 1601–1604.
- 150 Park, T., Zimmerman, S.C., and Nakashima, S. (2005) *J. Am. Chem. Soc.*, **127** (18), 6520–6521.
- 151 Sivakova, S., Bohnsack, D.A., Mackay, M.E., Suwanmala, P., and Rowan, S.J. (2005) *J. Am. Chem. Soc.*, **127**, 18202–18211.
- 152 Berl, V., Schmutz, M., Krische, M.J., Khoury, R.G., and Lehn, J.-M. (2002) *Chem. Eur. J.*, **8** (5), 1227–1244.
- 153 Chang, S.K., and Hamilton, A.D. (1988) *J. Am. Chem. Soc.*, **110** (4), 1318–1319.
- 154 İlhan, F., Galow, T.H., Gray, M., Clavier, G., and Rotello, V.M. (2000) *J. Am. Chem. Soc.*, **122** (24), 5895–5896.
- 155 Cortese, J., Soulié-Ziakovic, C., Tencé-Girault, S., and Leibler, L. (2012) *J. Am. Chem. Soc.*, **134** (8), 3671–3674.
- 156 de Lucca Freitas, L.L., and Stadler, R. (1987) *Macromolecules*, **20** (10), 2478–2485.
- 157 Park, T., and Zimmerman, S.C. (2006) *J. Am. Chem. Soc.*, **128** (43), 13986–13987.
- 158 Roland, J.T., and Guan, Z. (2004) *J. Am. Chem. Soc.*, **126**, 14328–14329.
- 159 Kalista, S.J., Ward, T.C., and Oyetunji, Z. (2007) *Mech. Adv. Mater. Struct.*, **14**, 391–397.
- 160 Kalista, S.J., and Ward, T.C. (2007) *J. R. Soc. Interface*, **4**, 405–411.
- 161 Constable, E.C., and Thompson, A.M.W.C. (1992) *J. Chem. Soc. Dalton*, **24**, 3467–3475.
- 162 Kelch, S., and Rehahn, M. (1998) *Macromolecules*, **31** (13), 4102–4106.
- 163 Brunsveld, L., Folmer, B.J.B., Meijer, E.W., and Sijbesma, R.P. (2001) *Chem. Rev.*, **101** (12), 4071–4098.
- 164 Hofmeier, H., and Schubert, U.S. (2004) *Chem. Soc. Rev.*, **33** (6), 373–399.
- 165 Dobrawa, R., and Würthner, F. (2005) *J. Polym. Sci. Part A Polym. Chem.*, **43** (21), 4981–4995.
- 166 Kersey, F.R., Loveless, D.M., and Craig, S.L. (2007) *J. R. Soc. Interface*, **4** (13), 373–380.
- 167 Serpe, M.J., and Craig, S.L. (2006) *Langmuir*, **23** (4), 1626–1634.
- 168 Yount, W.C., Loveless, D.M., and Craig, S.L. (2005) *J. Am. Chem. Soc.*, **127** (41), 14488–14496.
- 169 Piguet, C., Williams, A.F., Bernardinelli, G., and Buenzli, J.C.G. (1993) *Inorg. Chem.*, **32** (19), 4139–4149.
- 170 Kumpfer, J.R., Jin, J., and Rowan, S.J. (2010) *J. Mater. Chem.*, **20** (1), 145–151.
- 171 Burnworth, M., Knapton, D., Rowan, S., and Weder, C. (2007) *J. Inorg. Organomet. P.*, **17** (1), 91–103.
- 172 Kumpfer, J.R., and Rowan, S.J. (2011) *J. Am. Chem. Soc.*, **133** (32), 12866–12874.
- 173 Lehn, J.-M. (2002) *Polym. Int.*, **51** (10), 825–839.
- 174 Chow, C.-F., Fujii, S., and Lehn, J.-M. (2007) *Angew. Chem. Int. Ed.*, **46** (26), 5007–5010.
- 175 Giuseppone, N., and Lehn, J.-M. (2004) *J. Am. Chem. Soc.*, **126** (37), 11448–11449.
- 176 Holten-Andersen, N., Harrington, M.J., Birkedal, H., Lee, B.P., Messersmith, P.B., Lee, K.Y.C., and Waite, J.H. (2011) *Proc. Natl. Acad. Sci. U. S. A.*, **108** (7), 2651–2655.
- 177 Scott Lokey, R., and Iverson, B.L. (1995) *Nature*, **375** (6529), 303–305.
- 178 Burattini, S., Colquhoun, H.M., Fox, J.D., Friedmann, D., Greenland, B.W., Harris, P.J.F., Hayes, W., Mackay, M.E., and Rowan, S.J. (2009) *Chem. Commun.*, (44), 6717–6719.
- 179 Burattini, S., Greenland, B.W., Merino, D.H., Weng, W., Seppala, J., Colquhoun, H.M., Hayes, W., Mackay, M.E., Hamley, I.W., and Rowan, S.J. (2010) *J. Am. Chem. Soc.*, **132** (34), 12051–12058.
- 180 Feldman, K.E., Kade, M.J., de Greef, T.F.A., Meijer, E.W., Kramer, E.J., and Hawker, C.J. (2008) *Macromolecules*, **41** (13), 4694–4700.
- 181 Müller, M., Dardin, A., Seidel, U., Balsamo, V., Iván, B., Spiess, H.W., and Stadler, R. (1996) *Macromolecules*, **29** (7), 2577–2583.
- 182 Binder, W.H., Enders, C., Herbst, F., and Hackethal, K. (2011) in *Complex Macromolecular Architectures: Synthesis, Characterization, and Self-Assembly* (eds. N. Hadjichristidis, A. Hirao, Y. Tezuka,

- F. Du Prez), John Wiley & Sons (Asia) Pte Ltd, pp. 53–95.
- 183 Desiraju, G.R. (2011) *Angew. Chem.*, **123**, 52.
- 184 Folmer, B.J.B., Sijbesma, R.P., Versteegen, R.M., van der Rijt, J.A.J., and Meijer, E.W. (2000) *Adv. Mater.*, **12** (12), 874–878.
- 185 Ilhan, F., Gray, M., and Rotello, V.M. (2001) *Macromolecules*, **34** (8), 2597–2601.
- 186 Liu, S.-J., Chen, Y., Xu, W.-J., Zhao, Q., and Huang, W. (2012) *Macromol. Rapid Commun.*, **33** (6–7), 461–480.
- 187 Knapton, D., Iyer, P.K., Rowan, S.J., and Weder, C. (2006) *Macromolecules*, **39** (12), 4069–4075.
- 188 Burnworth, M., Tang, L., Kumpfer, J.R., Duncan, A.J., Beyer, F.L., Fiore, G.L., Rowan, S.J., and Weder, C. (2011) *Nature*, **472**, 334–337.
- 189 Skene, W.G., and Lehn, J.-M.P. (2004) *Proc. Natl. Acad. Sci. U. S. A.*, **101** (22), 8270–8275.
- 190 Burattini, S., Colquhoun, H.M., Greenland, B.W., and Hayes, W. (2009) *Faraday Discuss.*, **143**, 251–264.
- 191 Greenland, B.W., Burattini, S., Hayes, W., and Colquhoun, H.M. (2008) *Tetrahedron*, **64** (36), 8346–8354.
- 192 Staudinger, H., and Heuer, W. (1934) *Ber. Dtsch. Chem. Ges. (A and B Series)*, **67** (7), 1159–1164.
- 193 Ayrey, G., Moore, C.G., and Watson, W.F. (1956) *J. Polym. Sci.*, **19** (91), 1–15.
- 194 Basedow, A., and Ebert, K. (1977) *Physical Chemistry*, vol. 22, Springer, Berlin/Heidelberg, p. 83.
- 195 Encina, M.V., Lissi, E., Sarasúa, M., Gargallo, L., and Radic, D. (1980) *J. Polym. Sci. Polym. Lett.*, **18** (12), 757–760.
- 196 Berkowski, K.L., Potisek, S.L., Hickenboth, C.R., and Moore, J.S. (2005) *Macromolecules*, **38** (22), 8975–8978.
- 197 Imaizumi, K., Ohba, T., Ikeda, S., and Takeda, K. (2001) *Mater. Sci. Res.*, **7** (4), 249–253.
- 198 Paulusse, J.M.J., and Sijbesma, R.P. (2006) *J. Polym. Sci. Part A Polym. Chem.*, **44**, 5445–5453.
- 199 Huang, Z., and Boulatov, R. (2011) *Chem. Soc. Rev.*, **40** (5), 2359–2384.
- 200 Kryger, M.J., Ong, M.T., Odom, S.A., Sottos, N.R., White, S.R., Martinez, T.J., and Moore, J.S. (2010) *J. Am. Chem. Soc.*, **132** (13), 4558–4559.
- 201 Beiermann, B.A., Davis, D.A., Kramer, S.L.B., Moore, J.S., Sottos, N.R., and White, S.R. (2011) *J. Mater. Chem.*, **21** (23), 8443–8447.
- 202 Paulusse, J.M.J., Huijbers, J.P.J., and Sijbesma, R.P. (2005) *Macromolecules*, **38** (15), 6290–6298.
- 203 Paulusse, J.M.J., and Sijbesma, R.P. (2008) *Chem. Commun.*, (37), 4416–4418.
- 204 Tennyson, A.G., Wiggins, K.M., and Bielawski, C.W. (2010) *J. Am. Chem. Soc.*, **132** (46), 16631–16636.
- 205 Wiggins, K.M., Hudnall, T.W., Tennyson, A.G., and Bielawski, C.W. (2011) *J. Mater. Chem.*, **21** (23), 8355–8359.
- 206 Sohma, J. (1989) *Prog. Polym. Sci.*, **14** (4), 451–596.
- 207 Brantley, J.N., Wiggins, K.M., and Bielawski, C.W. (2011) *Science*, **333** (6049), 1606–1609.
- 208 Beyer, M.K., and Clausen-Schaumann, H. (2005) *Chem. Rev.*, **105** (8), 2921–2948.
- 209 Black, A.L., Lenhardt, J.M., and Craig, S.L. (2011) *J. Mater. Chem.*, **21** (6), 1655–1663.
- 210 James, S.L., Adams, C.J., Bolm, C., Braga, D., Collier, P., Friscic, T., Grepioni, F., Harris, K.D.M., Hyett, G., Jones, W., Krebs, A., Mack, J., Maini, L., Orpen, A.G., Parkin, I.P., Shearouse, W.C., Steed, J.W., and Waddell, D.C. (2012) *Chem. Soc. Rev.*, **41** (1), 413–447.
- 211 Kaupp, G. (2009) *CrystEngComm*, **11** (3), 388–403.
- 212 Chen, Y., and Geh, J.-L. (1996) *Polymer*, **37** (20), 4481–4486.
- 213 Chujo, Y., Sada, K., and Saegusa, T. (1990) *Macromolecules*, **23** (10), 2693–2697.
- 214 Trenor, S.R., Shultz, A.R., Love, B.J., and Long, T.E. (2004) *Chem. Rev.*, **104** (6), 3059–3078.
- 215 Chang, J.-M., and Aklonis, J.J. (1983) *J. Polym. Sci. Polym. Lett.*, **21** (12), 999–1004.
- 216 Chujo, Y., Sada, K., Nomura, R., Naka, A., and Saegusa, T. (1993) *Macromolecules*, **26** (21), 5611–5614.
- 217 Connal, L.A., Vestberg, R., Hawker, C.J., and Qiao, G.G. (2008) *Adv. Funct. Mater.*, **18** (20), 3315–3322.

- 218 Coursan, M., Desvergne, J.P., and Deffieux, A. (1996) *Macromol. Chem. Phys.*, **197** (5), 1599–1608.
- 219 Froimowicz, P., Frey, H., and Landfester, K. (2011) *Macromol. Rapid Commun.*, **32** (5), 468–473.
- 220 Matsui, J., Ochi, Y., and Tamaki, K. (2006) *Chem. Lett.*, **35** (1), 80–81.
- 221 Torii, T., Ushiki, H., and Horie, K. (1993) *Polym. J.*, **25** (2), 173–183.
- 222 Zheng, Y., Micic, M., Mello, S.V., Mabrouki, M., Andreopoulos, F.M., Konka, V., Pham, S.M., and Leblanc, R.M. (2002) *Macromolecules*, **35** (13), 5228–5234.
- 223 Hartley, G.S. (1937) *Nature*, **140**, 281–281.
- 224 Izumi, A., Teraguchi, M., Nomura, R., and Masuda, T. (2000) *Macromolecules*, **33** (15), 5347–5352.
- 225 Deng, G., Tang, C., Li, F., Jiang, H., and Chen, Y. (2010) *Macromolecules*, **43** (3), 1191–1194.
- 226 Jay, J.I., Langheinrich, K., Hanson, M.C., Mahalingam, A., and Kiser, P.F. (2011) *Soft Matter*, **7** (12), 5826–5835.
- 227 Su, Y-Z., Niu, Y-P., Xiao, Y-Z., Xiao, M., Liang, Z-X., and Gong, K-C. (2004) *J. Polym. Sci. Part A Polym. Chem.*, **42** (10), 2329–2339.
- 228 Toohey, K.S., Sottos, N.R., Lewis, J.A., Moore, J.S., and White, S.R. (2007) *Nat. Mater.*, **6** (8), 581–585.
- 229 Fanger, G.O. (1974) *Chemtech*, **4**, 397–405.
- 230 Gardner, G.L. (1966) *Chem. Eng. Prog.*, **62**, 87–91.
- 231 Esser-Kahn, A.P., Odom, S.A., Sottos, N.R., White, S.R., and Moore, J.S. (2011) *Macromolecules*, **44**, 5539–5553.
- 232 Dry, C., and McMillan, W. (1996) *Smart Mater. Struct.*, **5** (3), 297–300.
- 233 Dry, C. (1992) *Int. J. Mod. Phys. B*, **6** (15–16), 2763–2771.
- 234 Dry, C. (1996) *Compos. Struct.*, **35**, 263–269.

2

Self-Healing in Plants as Bio-Inspiration for Self-Repairing Polymers¹⁾

Thomas Speck, Rolf Mülhaupt, and Olga Speck

Since the origin of life about 3.8 billion years ago, living beings have evolved fascinating properties, ensuring their survival in a huge variety of environments with tremendously differing environmental conditions and concomitant highly different selective pressures. Characteristic for all groups of living beings are the self-x-properties, including among others self-organization, self-adaptation and self-repair. These properties, and especially the ability for self-repair, are essential for life and allowed the successful colonization of different environments during earth history. These capacities distinguish living beings and their subsystems (organs, tissues, cells, macromolecules) from man-made structures and materials. Due to the importance of self-x-properties for the fitness of a given species of plants, animals, fungi, or bacteria a high selective pressure can be assumed to be acting on the evolution of efficient self-x-properties in nature. It has been proven for a multiplicity of functionally important traits, for example, the lianescent and the epiphytic growth habit in plants, that these traits have evolved independently in many lineages of living beings and that they are based on different structural adaptations [1, 2]. The same holds for the different self-x-properties for which also an autonomous evolution in different systematic groups and species can be assumed.

The development and the production of engineering materials with self-x-properties is one of the greatest challenges in modern materials sciences. Self-repair, and the other self-x-properties, may function on different hierarchical levels, ranging from the molecular, over the cellular and tissue level to the organ level. On the other hand self-organization, self-adaptation, and self-repair acting on a level of higher complexity (e.g., the organ or tissue level) may include variations on several lower hierarchical levels bringing about the final self-x-reactions. These self-x-reactions often appear very complicated but on closer inspection prove

1) This chapter is based in part on results and thoughts published in the review article:
Speck, T., Bauer, G., Flues, F., Oelker, K., Rampf, M., Schüssele, A.C., von Tapavicza, M., Bertling, J., Luchsinger, R., Nellesen, A., Schmidt, A.M., Mülhaupt, R., and Speck, O.

(2013) Bio-inspired self-healing materials, in *Materials Design Inspired by Nature: Function through Inner Architecture* (eds P. Fratzl, J.W.C. Dunlop, and R. Weinkamer). The Royal Society of Chemistry, London, pp. 359–389.

to be merely complex, that is, composed of several, often relatively simple, sub-steps acting on the different hierarchical levels. Analyzing this complexity found in the biological role models, breaking it down to the different sub-steps, abstracting the basic physical and chemical principles involved, and translating them technically offers a high potential for bio-inspired transfer from biological concept generators into novel biomimetic materials and structures. This biomimetic approach has been successfully applied over recent years to the development of bio-inspired self-repairing materials [3–6].

2.1

Self-Sealing and Self-Healing in Plants: A Short Overview

In plants, the topic of this chapter, morphological and anatomical studies of regenerative processes [7], and first results of a screening study on self-repair in plants [8] support the assumption of an independent multiple evolution of self-repair processes in different systematic plant groups [6, 9]. Manifold mechanisms involving different structures on various hierarchical levels have evolved that allow the repair of lesions. For analyses of self-repair processes in biology it is meaningful to discern lesions caused by internal growth processes, as for example, in the case of the Dutchman's pipe (*Aristolochia macrophylla*; see Section 2.2.2), from external injuries caused by environmental effects (e.g., wind, rain, hail) or by feeding or trampling animals, as for example, in the case of the weeping fig (*Ficus benjamina*, see Section 2.2.1) or of the pink carpet (*Delosperma cooperi*, see Section 2.2.3) [6, 7, 10].

The concept of self-repair is often used as an umbrella term. In plants—and many other living beings—the self-repair process typically can be subdivided into two phases: a first phase of rapid self-sealing and a subsequent (much) slower phase of self-healing. The first phase is characterized by fast self-sealing of the injury, preventing its further propagation. Fast self-sealing ensures reduction of water loss (especially important for plants from semi-arid and arid habitats, such as *Delosperma cooperi*) and protection from infection by bacteria and fungi spores (especially important for plants such as *Ficus benjamina*, originating from environments rich in germs as e.g., tropical rain forests). During the self-sealing phase typically fast mechanical deformations of plant organs or cells occur that are based mainly on physical and chemical processes and allow rapid sealing of the wound. During the self-sealing phase in intact cells neighboring the fissure a so-called oxidative burst often occurs. This oxidative burst evokes *inter alia* the formation of a so-called drought layer of dead cells, further impeding water loss from the fissure, and a plasticization of the cell wall. The plasticizing of the cell is (mainly) caused by non-enzymatic cleavage of stabilizing polysaccharides in the cell wall [11, 12]. By this process, improved sealing of the fissure by neighboring intact cells is facilitated due to plastic cell wall deformation. The self-sealing phase in plants typically lasts for several minutes to several hours, and is followed by a much slower phase of self-healing lasting for several days or

weeks and months. During the self-healing phase in plants typical “biological” processes take place, including pronounced bio-synthesis, cell division and/or lignification. This latter phase entails in plants the well know processes of callus formation and tissue regeneration. Finally, during this latter phase the functions and mechanical properties of the injured tissue or organ become increasingly restored [6].

Over recent years a variety of plants from different systematic groups were screened and selected according to different criteria in order to generate ideas for the development of bio-inspired self-healing technical materials and systems [6, 9].

2.2

Selected Self-Sealing and Self-Healing Processes in Plants as Role Models for Bio-Inspired Materials with Self-Repairing Properties

2.2.1

Latex Plants as Concept Generators for Bio-Inspired Self-Healing Elastomers (Role Models: *Ficus benjamina* and *Hevea brasiliensis*)

In the screening process we found several plant genera to be especially promising to analyze the latex-based self-sealing processes of external injuries in relation to their physical and chemical background. From the more than 20000 known latex-bearing plant species belonging to over 40 different families [13], we have chosen the three genera *Ficus*, *Euphorbia* and *Campanula* from three different families for detailed analysis. In the fig-family (Moraceae) we concentrated on the weeping fig (*Ficus benjamina*) for which the most complete analysis was performed [14–19]. For comparison we analyzed latex-based self-sealing also in the spurge-family (Euphorbiaceae) from which three species were analyzed (*Euphorbia amygdaloides*, *E. characias* and *E. myrsinites*), and in the bell-flower family (Campanulaceae) from which two species (*Campanula glomerata*, *C. latifolia*) were chosen [18].

Latex is a milky plant exudate, being typically white to yellow in color, which chemically represents an emulsion. Latex is stored in plant tissues in so-called “laticifers”, specialized elongated cellular micro-tubes. As the above examples show, latex production is widespread among plants and evolved independently in different lineages of the plant kingdom. Biochemically, latex is a complex mixture containing, among others, alkaloids, phenolics, proteases, and chitinases which are present in different concentrations in the latex of the various latex-bearing plant species ([20] and citations therein). Many possible functions of the sticky and often poisonous plant latices have been studied and discussed. One important function is their role as a plant defense system, other potential functions include their role as a transport system, or as a water reservoir, and the function of nutrition or a waste storage system [20, 21]. However, an additional function, the potential importance of latex as a self-sealing agent, was hardly mentioned [6]. This is surprising for at least two reasons: (i) From all biochemical components of plant latex, rubber (*cis*-1,4-polyisoprene) which is essential for the self-sealing process

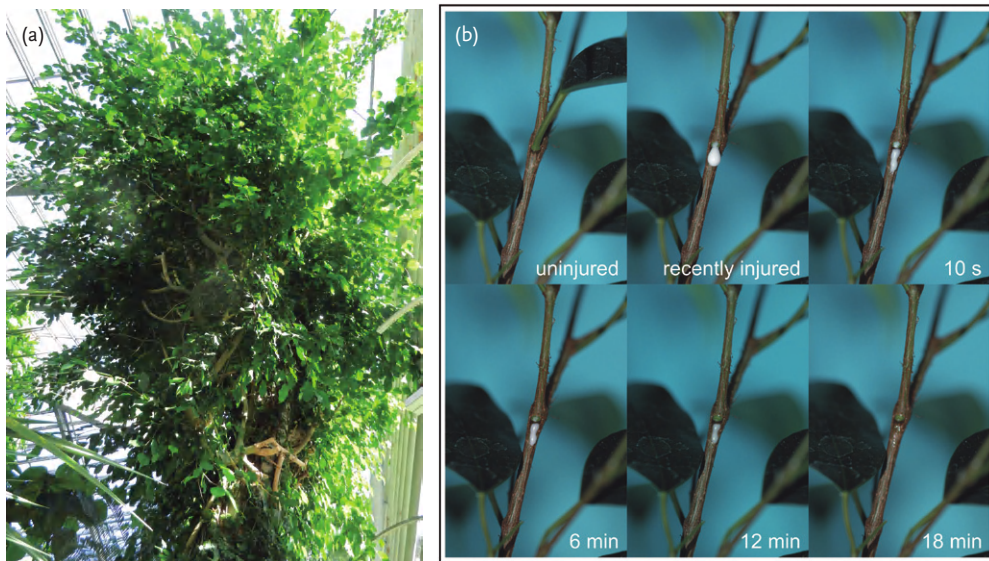


Figure 2.1 (a) Weeping fig tree in the greenhouse of the Botanic Garden Freiburg. (b) Macroscopic observation showing the process of latex coagulation after injuring the bark of a weeping fig (*Ficus benjamina*). Directly after injury the fresh latex droplet is

white due to total reflection of the fresh latex emulsion. During coagulation progress the latex droplet becomes increasingly translucent mirroring the chemical processes taking place in the latex during coagulation ((b) from [14]).

was most intensively studied over the last century due to its high economic importance. Rubber is known to be present in the latex of circa 300 different plant genera where it is often found in high concentration [22]. (ii) The rubber based self-sealing process is easily visible with the naked eye. When the different organs of a latex-bearing plant are injured latex oozes out and very efficiently seals the lesion by coagulating (cf. Figure 2.1b). Already, previous studies on the para rubber tree (*Hevea brasiliensis*), that represents, due to its economic importance, the best examined latex-bearing plant, show that the coagulation mechanism represents a smart autonomic self-healing system that functions without any external stimulus [23–25]. In this plant species latex is stored in the laticifer under high pressure in the range 7–15 bar. The latex of *Hevea brasiliensis* contains, among other substances, rubber particles and vacuolar structures, called “lutoids”, comprising the protein Hevein. Upon injury, due to the pressure drop from 7 bar or more in the intact laticifers to ambient pressure (ca. 1 bar) the lutoids burst and the protein Hevein is released. Then Hevein-dimers are formed under the influence of Ca^{2+} . They cross-link rubber particles which have binding sites for this protein on their surface, causing an autonomous latex coagulation [23, 24].

For analyzing the potential use of rubber-bearing plant latices as a role model for biomimetic self-repairing elastomers their self-sealing and self-healing capacities have to be analyzed. The self-healing ability of plants due to rubber particle-

based latex coagulation was tested in the weeping fig (*Ficus benjamina*) (Figure 2.1a). The weeping fig is native to South Asia and Australia. The plant grows either as a hemiepiphyte [1] or as a self-supporting tree. This species shows in many aspects a coagulation behavior of its latex which resembles that of the well studied para rubber tree [14, 15]. Similarly to *Hevea brasiliensis*, in the weeping fig macroscopic observations also reveal changes in latex viscosity and latex transparency as the milky-white fresh latex turns gradually transparent during coagulation. For *Ficus benjamina*, first changes in the latex transparency can be observed after about 6 min (Figure 2.1b), and after about 20 to 30 min no further macroscopically visible alterations occur [14, 16]. Changes in chemical bonds during coagulation of latex gathered from the stems of young weeping figs were analyzed qualitatively by infrared (IR) spectroscopy (Brukeroptics Vertex 70) with attenuated total reflection (ATR) in a common R&D project with Fraunhofer UMSICHT Oberhausen. In this type of test the measuring beam penetrates the sample up to a certain depth. During the penetration the beam is attenuated due to interactions with covalent bonds in the sample and then is reflected (ATR). The measurements were started immediately after the fresh latex samples were spread on the experimental set-up. The results of IR spectroscopic measurements of *Ficus benjamina* latex during coagulation fit well with the macroscopic observations, showing the most pronounced changes in the spectra in a time slot between six and ten min after injury (Figure 2.2a). The observed changes are mainly due to a decrease in water content caused by evaporation and to an increasing amount of amide bonds [14]. Further observations (data not shown) indicate that this increase is not related to effects like sedimentation of proteins but very probably to the formation of new covalent amide bonds. These data indicate that the theory of d'Auzac and coworkers [23], suggesting that the coagulation of *Hevea brasiliensis* latex is effected by the formation of new protein bonds between latex particles, can be assumed also for the latex of *Ficus benjamina*. This assumption is further corroborated by the finding that in *Ficus benjamina* the size distribution of latex particles analyzed by laser diffraction is bimodal, mirroring the existence of rubber particles and vesicular luteoids, and shows a similar pattern as described for *Hevea brasiliensis* latex [14, 15, 18].

The finding that latex was evolved many times independently in different groups of plants leads to the assumption that—in addition to the chemical coagulation mechanism described for *Hevea brasiliensis* latex and (very probably) also true for *Ficus benjamina*—there may exist other differing types of latex coagulation mechanisms. In order to test this hypothesis, an interspecific comparison of several parameters characterizing latex composition and latex coagulation was performed, including the three spurge and the two bell flower species [18]. We tested the “coagulation time”, that is, the time span between latex discharge upon injury and complete coagulation, the size distribution of latex particles in the latex and the wettability of the different latices. Our data prove that the coagulation time for a latex droplet of the typical size of 10 μl differs significantly between the different tested plant genera and species. For most studied latex-bearing plants (e.g., *H. brasiliensis*, *F. benjamina* and various *Euphorbia* and *Vinca* species) latex droplets

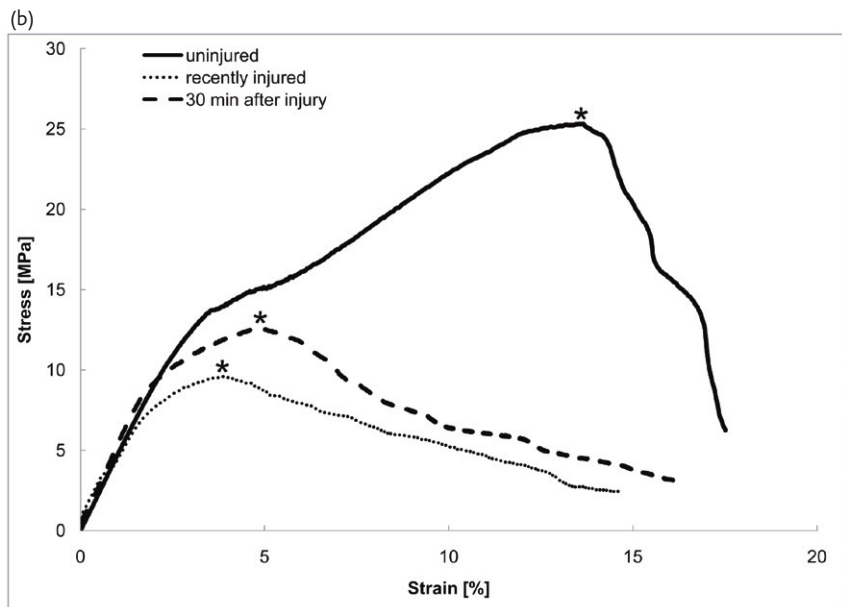
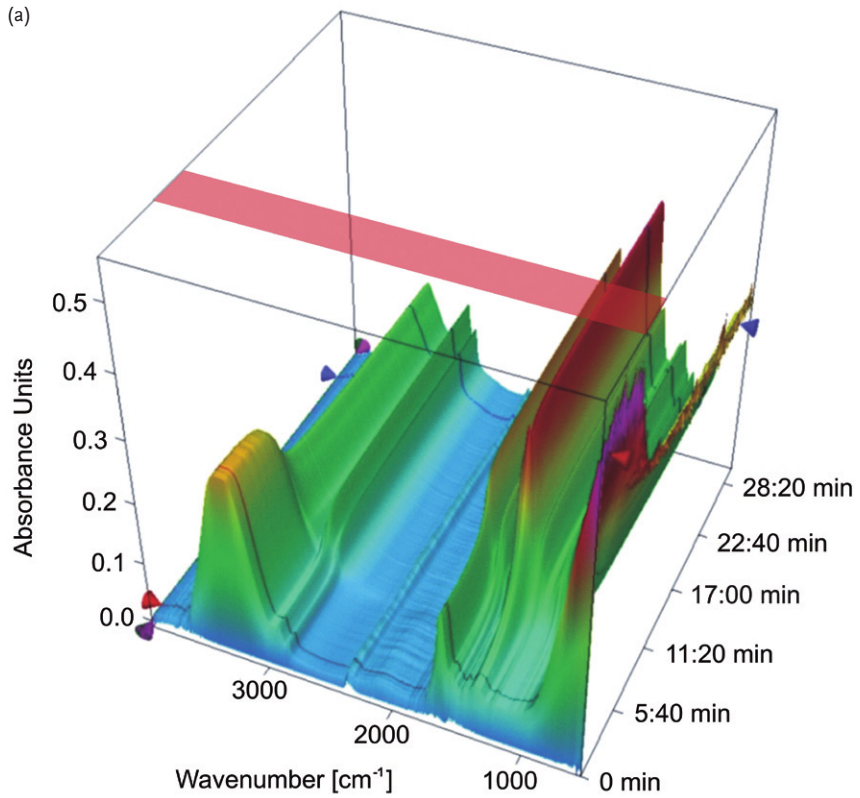


Figure 2.2 (a) IR-spectrum of coagulating *Ficus benjamina* latex, most pronounced changes between 6 and 10 min. (b) Tensile strength (marked by asterisks) of uninjured bark (solid line), recently injured bark (dotted line) and of bark 30 min after injury (dashed line) ((a) from [14]).

coagulate within 20 to 30 min. On the other hand, as found for *Campanula glomerata* and *Campanula latifolia* in the genus *Campanula* a much faster coagulation takes place lasting only a few seconds [14, 16]. Moreover, our findings also support different coagulation mechanisms for “typical” plant latices that coagulate in the same time span between 20 and 30 min. As mentioned above, in latices of the weeping fig (*F. benjamina*) and of the para rubber tree (*H. brasiliensis*) a bimodal size distribution of particles was found in fresh latex. In contrast, the studied spurge (*Euphorbia*) and bell flower (*Campanula*) species possess a markedly different size distribution of latex particles, which also are packed more densely. These differences come along with a different coagulation mechanism which probably is caused mainly by physical changes (e.g., simply by evaporation). The existence of different coagulation mechanisms is also supported by other findings, such as differing rheological behavior during latex coagulation, that is, different patterns concerning the reduction of viscosity [6, 14–19]. Additionally, the wettability of latices differs significantly between latex-bearing plant species and genera. The contact angle of *Ficus benjamina* latex, for example, is much smaller, on both natural and artificial surfaces, than the contact angle of the latices of the various *Euphorbia* species tested. Based on these results we hypothesize that different latex-bearing plants may be adapted to different scenarios of injury, defense or healing [18, 19]. These variations found in the coagulation behavior and other physical and chemical properties of plant latices are especially promising for a transfer into technical self-healing materials as they can be used as concept generators for the development of customizable bio-inspired healing agents for varying different demands [6, 16].

One of the most crucial questions for justifying the use of plant latices as concept generators for the development of self-healing elastomers is, if coagulated plant latices are in addition to their self-sealing function also able to restore the mechanical properties of the injured plant tissue or organ to a satisfactory extent. This self-healing ability of latex coagulation was tested by using bark samples of young *Ficus benjamina* trees. After incising the bark with a prepared razor blade the injured bark was removed from the plant at different latency times after injury and immediately tested under tension (Figure 2.2b) [14, 17]. The recovery of the tensile strength at various latency times after injury was used as a measure to quantify the self-healing ability (Figure 2.3). Compared to the values for uninjured bark, the tensile strength drops immediately after injury to 42% of the initial value. For the first 20 to 25 min following injury the tensile strength does not differ significantly from this value and remains low. It is not before 30 min that the tensile strength increases significantly to a value of 55% of the initial value for uninjured bark. After this (fast) initial increase—representing the mainly physico-chemical phase of self-repair—the tensile strength remains unaltered for several hours or days before, due to other (biological) self-healing mechanisms such as cell growth and cell proliferation, the tensile strength begins to increase slightly again. Our data prove that in the weeping fig a considerable first self-healing effect takes place within the first 30 min after injury, a period that fits well with the time span measured for latex coagulation (cf. Figure 2.1). However, the

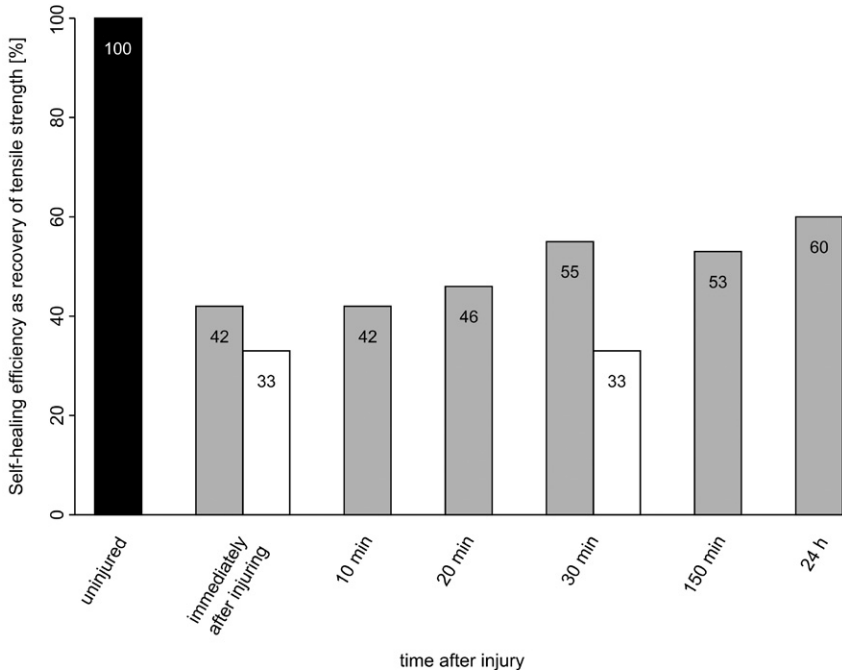


Figure 2.3 Self-healing efficiency of the bark of the weeping fig (*Ficus benjamina*) expressed as recovery of tensile strength at various latency times after injury. White bars represent bark samples where the latex was

cleaned from the samples immediately after the latex was discharged from the lesion. In the latter case the latex cannot contribute to the recovery of the tensile strength.

Young's modulus and, therefore, also the elasticity of the bark remains nearly unaffected by latex coagulation. In additional tests the fresh latex was cleaned immediately after oozing out from the lesion of the injured bark. If the latex was removed, the tensile strength did not increase within the first 30 min after injury, which proves that the first fast self-healing effect results from the coagulation of the latex alone [17]. These results show that—in addition to self-sealing of the cut—the coagulation of plant latices possesses also a significant self-healing function, making reasonable their use as role models for the development of biomimetic self-healing elastomers [6, 16].

The above described results prove that plant latices represent promising concept generators for the design and development of biomimetic self-healing elastomeric materials for technical purposes (see Section 2.3.1). Bio-inspired approaches may include (i) embedding of microcapsules filled with healing agents in technical self-healing elastomers, that burst upon injury thus releasing a healing agent (inspired by vesicular lutoids found in *Hevea brasiliensis* and *Ficus benjamina* latex), and (ii) the development of technical ionomeric elastomers (inspired by the function of Ca^{2+} -ions in *Hevea brasiliensis* latex during coagulation) [26]. Our analyses prove that, in addition to micro- and nano-structural properties assuring a fast

wound sealing, chemical properties of the biological concept generators are of especially high interest for the development of innovative bio-inspired self-healing materials [6, 16, 26].

2.2.2

Lianas as Concept Generators for Bio-Inspired Self-Sealing Membranes for Pneumatic Structures (Role Model: *Aristolochia macrophylla*)

Vines show a drastic change in mechanical properties of their stems during growth. Young axes of vines, which act as searchers spanning the gaps to new supportive structures, are very stiff in bending and torsion. As soon as a liana axis is secured to a new support the stems become increasingly flexible in bending and torsion due to profound alterations in stem anatomy brought about by secondary growth processes [1, 2]. These internal growth processes may cause (micro-)fissures in more peripheral tissues. If these (micro-)fissures run to the outside of the stem they would be perfect entrance doors for harmful fungi and bacteria. Vines of the genus *Aristolochia*, for example, are able to seal these fissures very effectively and very quickly. In order to understand this sealing process in detail and to learn for an abstraction and transfer process into bio-inspired self-healing technical materials, functional anatomy and stem mechanics, and their variations during ontogeny have been studied in detail in different species of *Aristolochia* [3, 27–29].

As a role model the Dutchman's pipe (*Aristolochia macrophylla*), a twining vine native to North-America, was chosen (Figure 2.4). In this species, as in other



Figure 2.4 Dutchman's pipe (*Aristolochia macrophylla*) in the open field of the Botanic Garden Freiburg.

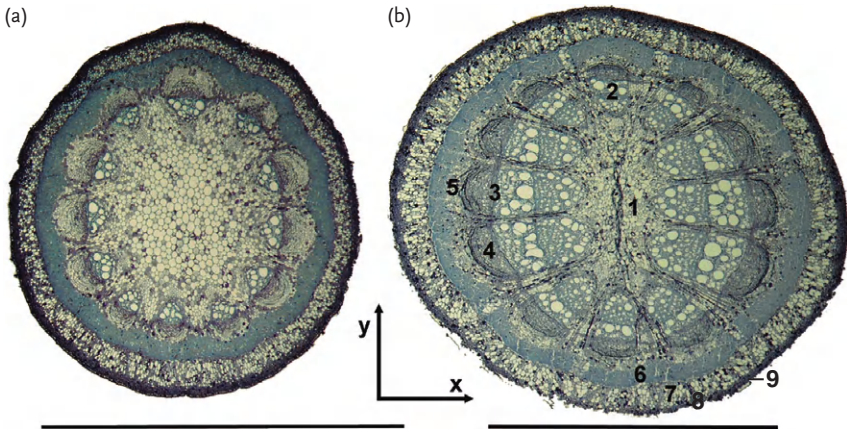


Figure 2.5 Dutchman's pipe (*Aristolochia macrophylla*), cross-sections of a one-year-old stem (a) possessing a closed sclerenchymatous cylinder and of a two-year-old stem (b) with a fragmented sclerenchymatous cylinder due to secondary growth of the vascular tissues. 1: pith, 2: secondary xylem, 3:

cambium, 4: secondary phloem, 5: inner parenchymatous primary cortex, 6: sclerenchymatous cylinder, 7: outer parenchymatous primary cortex, 8: collenchymatous cylinder, 9: epidermis; scale bars: 3 mm (from [29], reproduced with permission from Oxford University Press).

Aristolochia-species, the high bending and torsional stiffness found in young apical searcher twigs is (mainly) caused by a closed ring of stiff sclerenchyma fibers in the stem periphery [27, 30]. Both types of vascular tissues, phloem and xylem, are located close to the stems center around the pith, that is, inside the sclerenchymatous ring. After being secured to a new support the secondary growth of vascular tissues markedly accelerates, the stem significantly increases in diameter, and the elastic modulus in bending and torsion decreases due to the formation of rather flexible secondary xylem and phloem [1, 30]. Additionally, the increase in diameter of the internal vascular tissues causes radial stresses and strains in the soft inner parenchymatous cortex tissues located within the sclerenchymatous ring, and tangential stresses and strains in the sclerenchymatous ring. Due to continuous secondary growth the stresses and strains finally become overcritical and the sclerenchymatous ring ruptures and splits into segments, further decreasing the stem stiffness (Figure 2.5). The (micro-)fissures in the sclerenchymatous ring typically run through the middle lamellas of neighboring sclerenchyma fibers. A rapid sealing mechanism enables *Aristolochia macrophylla* to repair these lesions very efficiently. These repair processes are essential for securing the functional integrity of the plant stem and preventing the fissures running to the outside of the stem [28, 29].

During this self-sealing, and the subsequent healing processes, at least four phases can be discerned [3, 27, 28]. First—due to overcritical tangential stresses and strains—a tiny (micro-)fissure in the sclerenchymatous ring occurs, turgescient parenchyma cells from the surrounding outer cortex tissue swell into the (micro-)fissure and seal it (Figure 2.6a). This initial self-sealing (phase 1) is excited by

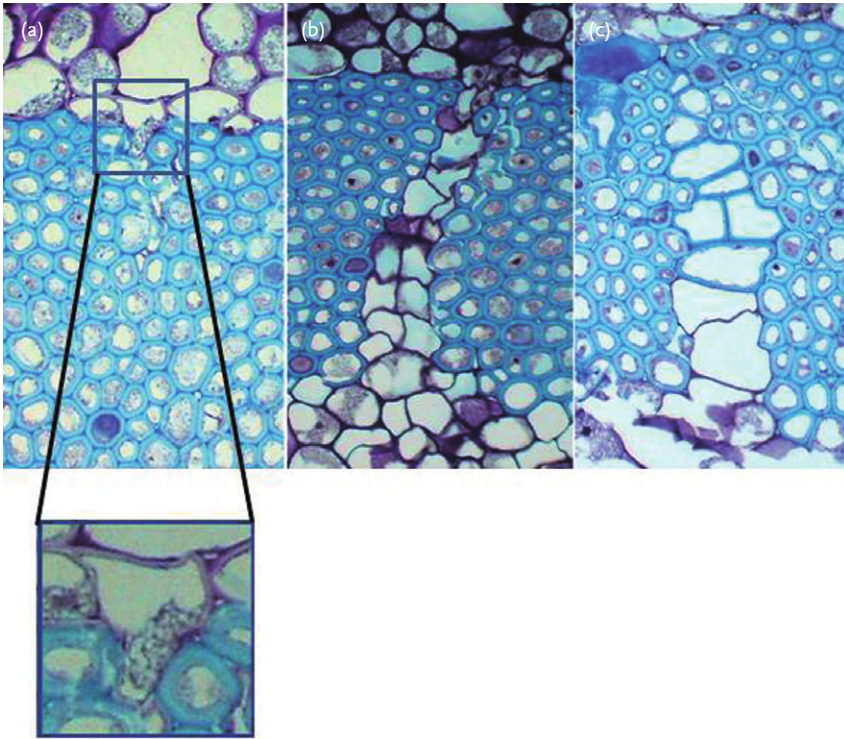


Figure 2.6 Different phases of fissure repair in Dutchman's pipe (*Aristolochia macrophylla*). (a) A micro-fissure in the peripheral sclerenchymatous ring caused by internal growth processes of the central vascular tissues is sealed by a parenchymatous cortex cell swelling into this fissure due to its internal pressure (turgor) (phase I/phase II).

The magnification shows the sealing in detail. (b) A fissure running through the entire sclerenchymatous ring is repaired by cells having the typical irregular shape and being the result of radial and tangential cell divisions (phase III). (c) In the peripheral repairing cells the cell walls are thickened and lignified (phase IV) (from [3]).

changes in the stress–strain field at the contact region between the (micro-)fissure and parenchymatous outer cortex tissue where a turgescent parenchyma cell (“sealing cell”), due to its internal overpressure of several bar, immediately deforms and relaxes, that is, swells into the lesion. This deformation causes elastic and/or viscoelastic deformation of the cell wall and seems to be mainly a passive physical reaction due to relaxation of the parenchymatous sealing cells [12, 27, 28]. According to our studies, physiological reactions do not occur in the repairing cells before the second phase of self-sealing when a plastic deformation of the cell walls appears. This plasticization of the cell is probably effected by cell wall loosening, initiated by hydroxyl radicals and/or oxygen radicals causing non-enzymatic cleavage of cell wall polysaccharides [12, 28]. Healing of the lesion, that is, the actual “biological part” of self-repair, starts in phase three, when, due to ongoing

secondary vascular growth, fissures extend more and more deeply into the sclerenchymatous ring. In this phase pronounced cell wall synthesis and division of the repairing cells (first in a radial direction) takes place. Later, if the fissure runs through the entire sclerenchymatous ring, both radial and tangential cell divisions of the repairing cells occur (see Figure 2.6b). As a consequence of cell division and cell wall plasticization the lesions are sealed with irregularly-shaped and thin-walled repairing cells. Whereas in some fissures the sealing cells remain parenchymatous during further development, in other fissures the walls of the cells sealing the most peripheral region of the fissure gradually become thicker and start to lignify (phase 4). By the latter processes occurring in the fourth and final phase of the self-repairing process (see Figure 2.6c), the mechanical function of the sclerenchymatous ring, that is, stiffening the stem of the vine in bending and torsion, can be restored, at least for a limited period of time [6, 28].

Our analyses suggest that in the initial phase of self-sealing in *Aristolochia macropphylla* mainly physical and chemical processes are involved. This result is especially encouraging for using these processes as inspiration for the development of bio-inspired self-repairing engineering materials. Because of their internal pressure and the concomitant pre-stress in the parenchyma tissue, turgescient parenchymatous cortex cells swell into the (micro-)fissures and seal them very effectively [8, 28]. The functional principle underlying this self-sealing process has been successfully abstracted and transferred into a biomimetic patent-registered closed-cell PU-foam coating for pneumatic structures and other types of membranous hulls [6, 31] (see Section 2.3.2).

2.2.3

Succulent Plants as Concept Generators for Bio-Inspired Self-Sealing Membranes for Pneumatic Structures (Role Model *Delosperma cooperi*)

As specific self-healing mechanisms have evolved many times independently in different systematic groups of plants, a screening process searching for other, up to now unknown modes of self-repair was performed. Using different search criteria which make high selective pressures on efficient self-repair probable, further plant species and genera were identified with self-healing mechanisms promising for a biomimetic transfer into technical materials and structures [9, 32]. Our analysis shows that in succulent plant species which are found in various not closely related evolutionary lineages, distinct and very effective self-healing effects exist. For these plants, which typically grow in arid environments, wounds cause an exceptional drought stress. Therefore, fast self-sealing processes and subsequent efficient self-healing are of high selective advantage for succulent plants as they protect them from dehydration and may secure their survival after wounding [6, 9].

For a detailed analysis we selected *Delosperma cooperi* a member of the Aizoaceae family with succulent leaves, native to South Africa (Figure 2.7). External injuries, caused in the natural environment for example, from feeding or trampling animals, were simulated by an artificial cut caused by incising the leaf with a



Figure 2.7 Flowering pink carpet plants (*Delosperma cooperi*) in the open field of the Botanic Garden Freiburg.

prepared razor blade. For testing the self-sealing capacity the cuts were made in different directions relative to the leaf, including longitudinal cuts (parallel to the longitudinal axis of the leaf), transverse cuts (perpendicular to the longitudinal axis of the leaf), and circular cuts, that is, incisions around the entire leaf perpendicular to the longitudinal axis of the leaf [32, 33]. After each type of cut self-sealing of the wounds takes place in leaves of *Delosperma cooperi* by deformation and movement of the leaf. Two main mechanisms are involved in the self-sealing process. The first mechanism, the rolling in of the fringes of the cut, occurs within a few minutes. The second process typically takes place within a time span of 30 to 90 min and involves—in the case of the two types of straight cuts—curvature of the entire leaf, or—in the case of circular cuts—leaf contraction (Figure 2.8). Subsequent processes of wound healing are characterized by cell growth, cell division and further physiochemical reactions. The entity of self-healing processes led to callus formation in the wound region and a permanent curvature of the leaf (Figure 2.9) [6, 32].

The succulent leaves of *Delosperma cooperi* comprise five main tissue types, are almost cylindrical and possess a centripetal arrangement of tissues. The leaves consist of an outer epidermis with window cells, followed by an outer ring of chlorenchyma, the next tissue zone is a thin net of vascular bundles, followed by an inner ring of parenchymatous tissue and a central strand of vascular tissue (Figure 2.10). The vascular tissue consists in part of wide-band tracheids, a specialized type of tracheids that prevent cell collapse under water stress [32, 34] and allow size changes of leaves and shoots of succulent plants due to “swelling and shrinkage” caused by varying water status. To characterize the mechanical

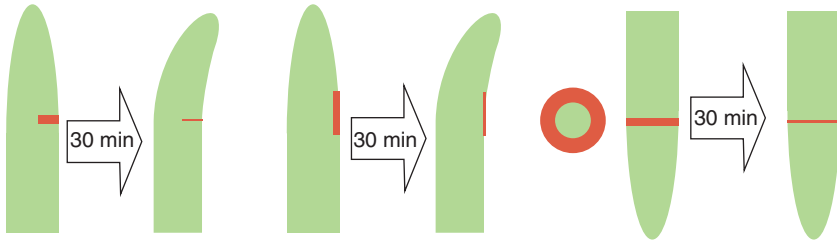


Figure 2.8 Schematic drawings showing the arrangement of artificial cuts made for testing the self-sealing capacity in *Delosperma cooperi* leaves, and of leaf deformation and movement during the process of self-sealing. From left to right: longitudinal cut (parallel

to the longitudinal axis of the leaf), transverse cut (perpendicular to the longitudinal axis of the leaf), and circular cut (around the entire leaf perpendicular to the longitudinal axis of the leaf).



Figure 2.9 Leaf of *Delosperma cooperi* 14 days after being injured by a deep transverse cut showing entire repair of the fissure. A permanent kink of the leaf remains after complete healing (from [32]).

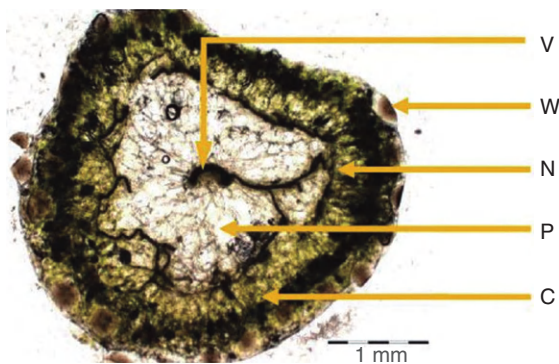


Figure 2.10 Cross-section of a central part of a leaf of *Delosperma cooperi* showing the five main tissue types used for the modeling of the self-healing processes. (V) vascular

bundles in the leaf centre, (W) epidermis with window cells, (N) net of peripheral vascular bundles, (P) parenchyma, (C) chlorenchyma (from [32]).

properties of the leaf, tensile tests of the entire leaf and of single tissue layers were performed. For further characterization of leaf mechanics, in the intact state and during self-healing, tissue pressure in the parenchymatous leaf tissues was quantitatively analyzed using a micro-optic-mechanical-system (samba-sensor), and cell turgor was measured with a pressure probe. Measurements were performed at the moment of injury and during the subsequent sealing and healing phase [35].

Quantitative studies of the functional anatomy of the leaves, as well as measurements of tissue pressure and cell turgor were used to develop an analytical model which allows the description of the self-sealing process in *D. cooperi* based on the dimensions and mechanical properties of five hulls that represent the different tissue layers of the real leaf [32, 33]. As in real leaves, also in the analytical model, intact leaves are supposed to be pre-stressed. The mechanical stability of leaves is based on tension and compression stresses alternating between the different tissue layers. In intact leaves the internal stresses sum up to an overall equilibrium. Stress equilibrium is disturbed by injuries destroying parts of the constitutive tissues. This disturbance causes a net stress which evokes a bending or a contraction, respectively, acting on the leaf close to the incision [32, 33].

The above model was originally developed to describe (semi-)quantitatively the self-sealing processes occurring in the biological role model but it can also be used to characterize and thereby to develop self-sealing biomimetic engineering materials. Based on the model it will become possible to calculate the mechanical properties necessary in the different tissue layers for a successful transfer of ideas into bio-inspired self-sealing materials and structures as, for example, compound polymer membranes. A selection of suitable materials may allow the construction of bio-inspired composite materials with adjustable sealing properties, for example, by using modern foil techniques [6].

Our analyses show that if mainly physical and chemical processes are involved, as in the first rapid phases of self-repair in *Aristolochia macrophylla* and in *Delosperma cooperi*, and in the latex coagulation of latex bearing plants such as *Ficus benjamina* or the various *Euphorbia*- and *Campanula*-species, a transfer into bio-inspired technical materials is especially promising.

2.3

Bio-Inspired Approaches for the Development of Self-Repairing Materials and Structures

In biomimetics two fundamentally different approaches can be discerned describing the process of transferring ideas from biological concept generators to bio-inspired technical products. The first, called the “bottom-up-approach” of biomimetics is driven by initial finding of biologists, whereas the second termed “top-down-approach” of biomimetics is initiated by specific questions and challenges from the side of industry. Between the two fundamental approaches there exists a multiplicity of transitions [4, 5]. The modus operandi in R&D projects on biomimetics has also been specified in recently published guidelines of the

Verein Deutscher Ingenieure (VDI) [36]. The bottom-up-approach starts with the discovery of an interesting function by biologists. By using methods from engineering sciences, physics, and chemistry, a detailed analysis of biological functions and underlying structures is performed, leading to a quantitative understanding of the principles, that is, of the form–structure–function relationship in the biological role model. Already the latter, as all following steps of the project, is performed in close interdisciplinary cooperation between biologists, engineers, material scientists and colleagues from other disciplines of natural sciences. The next step, often crucial for a successful transfer, is the abstraction of basic principles essential for the designated function, that is, the detachment from the biological concept generator. Then technical implementation follows and the production of demonstrators, first on the lab scale and then at pilot plant level. Then prototyping takes place and finally—together with industrial partners—the introduction of the novel product to the market [4, 5]. This approach is characterized by a “biological push”. The second process, to which all developments of self-repairing materials described in the following sections belong, is the top-down-approach which is characterized by a “technology pull”. In this case industry contacts biomimetically working scientists with the request to improve an existing product which may or may not have already been introduced to the market. After carefully defining the technological problem, the biologists start to search for biological analogies with functions appropriate to solving the given technological challenge. At the end of the screening process is the identification of appropriate principles in one or more biological role models, as described in detail for self-sealing and self-healing in plants. Then, similar to the bottom-up-approach, a detailed analysis of the form–structure–function relationship is performed and abstraction takes place. These steps are followed by a test of the technical feasibility and—if successful—by prototyping and introduction of the improved product to the market (see Figure 2.14) [4, 5]. The procedural methods described here have been applied successfully in many biomimetic R&D projects over the last ten years.

As in biology, also for technical materials and systems self-repair is often used as an umbrella term including self-sealing and self-healing, which can again be clearly distinguished by the different processes involved and the different timescales [6]. To generalize, in technical materials self-sealing effects a functional repair causing the closure of a still existing fissure by physical and/or chemical processes acting on the edges of the fissure. As in plants, the structural repair of a lesion is not accomplished until self-healing has taken place, restoring (at least partially) the materials’ structural integrity and its mechanical functioning [37–39]. In self-repairing technical materials self-healing may be effected either by polymerization processes, and/or the formation of ionic bonding or hydrogen bonding structurally healing the fissure [39, 40]. The progressively better understanding of self-repair mechanisms in biology is increasingly stimulating the development of bio-inspired self-repair mechanisms and their integration into industrial engineering materials. Over recent years, in collaboration with other research institutes, the authors have used several bio-inspired strategies for the development of self-

sealing and self-healing of technical rubbers, plastics, coatings, and polymer composite materials.

In the following we briefly summarize some of the recent developments of bio-inspired self-healing concepts realized during the last years, based on the biological role models described above. For a more detailed account explaining the biomimetic transfer process as well as the physical and chemical background of the production methods and of the mode of functioning we refer to Speck *et al.* [6]. Beyond that, additional examples of bio-inspired self-healing materials are depicted in more detail in other chapters of this book (e.g., Chapter 15).

2.3.1

Bio-Inspired Self-Healing Elastomers

The spectrum of technical applications for elastomeric materials is vast and still increasing. Many of these applications are (mechanically) highly demanding and additionally include a wide portfolio of desired properties as for example, UV resistance, recyclability, and prolonged lifetime. Mechanical failure in elastomeric materials—sometimes occurring long before the characteristic limits of loading and lifetime are reached—may be caused by alternating loading cycles which cause micro-cracks that become overcritical in length and finally induce material failure [6]. Biological materials and structures typically “tolerate” micro-cracks but have evolved self-healing mechanisms for keeping these micro-cracks under-critical in length, and thereby insignificant for the functioning of the respective biological tissue or organ. Transferring these mechanisms into technical elastomeric materials would allow exploitation of the full loading and lifetime-limit of the material, and therefore a high industrial demand exists for self-healing elastomers.

Different bio-inspired approaches for self-healing elastomeric materials have been developed and tested, including micro-encapsulation and vesicle-like systems, blends with liquid polymers, and thermoreversible (co)network formation.

2.3.1.1 Micro-encapsulation

Micro-encapsulating of healing agents, that parallels or mimics self-repair processes in latex bearing plants, has been proven to function well in thermoplastics [41–43], but do not work sufficiently well in elastomeric materials [26]. Due to high shear forces and temperature characteristic for compounding processes of elastomeric materials typical micro-capsules used for encapsulating self-healing agents rupture. If the self-healing agents are stored in rigid porous micro-beads and/or covered in capsule walls with increased mechanical strength micro-cracks in the elastomer run around the capsules. The micro-capsules do not burst and do not release the self-healing agents and therefore no self-healing takes place [6, 16, 26].

Similar problems occur by using in elastomeric materials self-repairing systems based on micro-tubes filled with self-healing agents, which again are functioning well in thermoplastics and thermosets [44–46]. Interestingly bio-inspiration for most of these approaches is taken from the blood vessel-system of animals which differs due to the heart driven pumping mechanism basically from most of the

technical implementations (but see [47]). Inspirations from plant systems, as for example, from laticifers of latex-bearing plants in which the self-healing agent is stored under high internal pressure without pumping (see Section 2.2.1), are up to now scarcely used. For a more detailed discussion of methods and potential of micro-encapsulation and micro-channels for the development of self-healing materials we refer to Chapters 10 and 15.

Successful approaches for the development of bio-inspired self-healing elastomers are mainly based on non-covalent interactions and self-assembly processes. Two approaches for non-autonomous self-healing in elastomeric materials based on thermoreversible supramolecular (co)network formation, exploiting directional hydrogen bridging and ionomer formation have been explored.

2.3.1.2 Ionomeric Elastomers

Inspired by the function of Ca^{2+} ions for the formation of Hevein dimers during latex coagulation in the para rubber tree (cf [23].) in a common R&D project with Fraunhofer UMSICHT Oberhausen and the Institute for Physical Chemistry in Cologne a concept for self-healing elastomeric materials based on the incorporation of ionic groups into the elastomer backbone has been developed. The idea is that these ionomers show self-healing after fissure application due to a rearrangement of ionic domains after energy input followed by a certain time of relaxation [16, 26]. The most promising results as to the self-healing capacity after cutting rectangular strips of the ionomeric elastomer in half, rejoining them and annealing them for 24 h at 55 °C were found for carboxylated nitrile butadiene rubber (NBR)-based samples (Figure 2.11). For non-vulcanized samples a restoration of the tensile strength of 50% was obtained, for vulcanized NBR-samples a restoration of 15% (Figure 2.12). For a detailed account of the physico-chemical background of this development and an overview on the ionomer approach in self-healing materials we refer to Chapter 13 “Self-Healing Ionomers” of the book at hand.

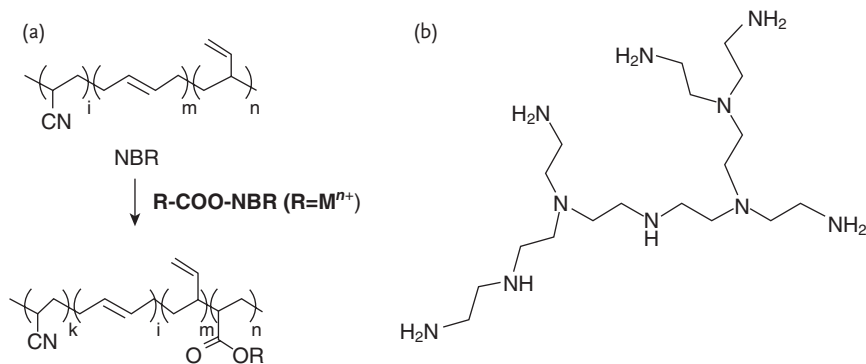


Figure 2.11 (a) Modification route for nitrile butadiene rubber (NBR)-based ionomeric elastomers shown for carboxylated nitrile butadiene rubber (M^{n+} : metal counter ion). (b) Hyperbranched polyethyleneimine (PEI)

used as self-healing component in nitrile butadiene rubber (NBR) blends ((a) modified from [26]; (b) from [6], reproduced with permission of the Royal Society of Chemistry).

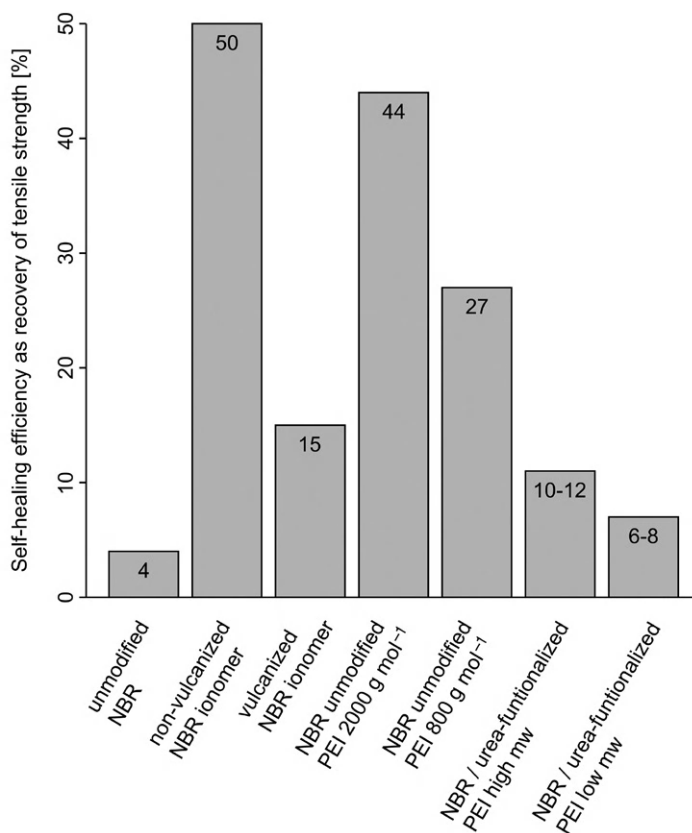


Figure 2.12 Self-healing efficiency of nitrile butadiene rubber (NBR), ionomeric carboxylated nitrile butadiene rubber, and blends of nitrile butadiene rubber with unmodified and urea-functionalized

hyperbranched polyethyleneimines (PEI) expressed as recovery of tensile strength after rejoining samples cut in half and annealed under the conditions described in the text.

2.3.1.3 Supramolecular Co-networks

Other concepts found in biological role models that have inspired material sciences and supramolecular chemistry pioneered by Lehn [48] are self-assembly and self-healing mechanisms based on hydrogen-bridging [49–51]. Inspired by the nature supramolecular (co)networks were developed containing non-covalent bonds. In different approaches the hydrogen-bridging functional groups have been introduced as well in the elastomer back bone as in the side chains [52, 53]. Using PBAN, a commercially available amine-terminated butadiene/acrylonitrile liquid rubber (Hypro™ 1300 × 35 ATBN; Nanoresins Company) a versatile synthetic approach for the assembly of supramolecular network building blocks has been developed. The PBAN is endcapped with aspartic imide (PBAN_MI) and with methyl barbiturate groups (PBAN_BA), respectively [6]. Between the PBAN_BA-end groups very good intermolecular hydrogen bond formation exists as well

as hydrogen bridging of PBAN_MI with PBAN_BA causing a significantly increased shear. As these supramolecular materials do not have the good performance of industrially produced NBR rubbers, the building blocks and their blends have been used as additives for NBR. As consequence of the co-vulcanization of the PBAN a covalent attachment to the NBR network is probably. At 12.5 phr content of the blends only a slight increase in self-healing efficiency of NBR was found [6]. A detailed description of different “Supramolecular Systems” important for self-healing materials is given in Chapter 11.

2.3.1.4 Nitrile Butadiene Rubber (NBR) Blends

Inspired by turgor (internal cell pressure) found in parenchymatous plant cells and tissues [35, 54] an alternative to micro-encapsulation of self-healing agents avoiding the micro-capsule wall was investigated. Based on this concept, bio-inspired multiphase blends of NBR with liquid polymers as self-sealing and self-healing agent were developed [55]. Due to different thermal expansion of rubber and self-healing agent turgor-inspired high internal pressure will built up in the micro-phase separated domains of the liquid polymer. If micro-cracks encounter such domains the liquid polymer serves as self-healing agent and seals the crack [6, 55].

For NBR hyperbranched polyethyleneimine (PEI), as shown in Figure 2.11B, proved to be a suitable self-healing additive (liquid polymer) fulfilling several rather opposing requirements including: (i) immiscibility with NBR to ensure micro-phase separation, (ii) high enough molecular weight to prevent leaching during compounding, (iii) low enough molecular weight for an easy dispersion in NBR and rapid migration into micro-cracks, and (iv) effective sealing of the micro-fissures due to pronounced self-assembly via the large number of end groups and effective bonding of the rubber.

For testing the potential of this approach, molecular weights and substitution patterns of PEI have been varied by converting amine endgroups with alkyl isocyanates into alkyl urea end groups. Non-modified PEI with high molecular weight (2000 g/mol) shows the best performance with respect to micro-phase separation (mean diameter: 5–10 μm) and to self-healing. Phenylurea-modified (PEI-ph) as well as hexylurea-modified (PEI-hex) hyperbranched polyethyleneimine form smaller micro-phases and have a drastically reduced self-healing efficiency [55]. Self-healing efficiency, given as %-recovery of tensile strength, was measured for different NBR/PEI blends after cutting rectangular samples in half, annealing them in a heated sample holder under compression for 12 h at 100 °C and subsequent storing at room temperature without compression for another 12 h (Figure 2.12). Self-healing efficiency varies from 44% for unmodified PEI (2000 g/mol, 12.5 phr) and 27% for unmodified PEI (800 g/mol, 12.5 phr) to 6% (PEI-ph) and 8% (PEI-hex) for urea-functionalized PEI-amphiphile with low molecular weight (12.5 phr); the self-healing efficiency for neat NBR is 4% [55]. The results show that micro-phase separation of liquid hyperbranched (unmodified) PEI renders a promising approach for the development of self-healing NBR that avoids problems occurring in elastomers due to micro-encapsulation of the self-healing agent. Adjusting the design of the self-healing agent will allow to improving the self-healing capacity and will permit expanding this concept to other rubbers of industrial significance [6, 55].

2.3.2

Self-Sealing Foam Coatings for Membranes of Pneumatic Structures

The turgor based self-repair process found in twining lianas of the genus *Aristolochia* [8, 12, 28] was used as inspiration for a biomimetic “foam coating” applied to the inner side of the membranous hull of a pneumatic structure (Figure 2.13A). In case of puncturing of the foam coated membrane, the prestrained foam immediately collapses and stops the air-flow through the punctured hull by sealing the fissure [56]. Based on results of detailed functional and mechanical analyzes of the biological concept generators (see Section 2.2.2), turgor pressure and prestrain

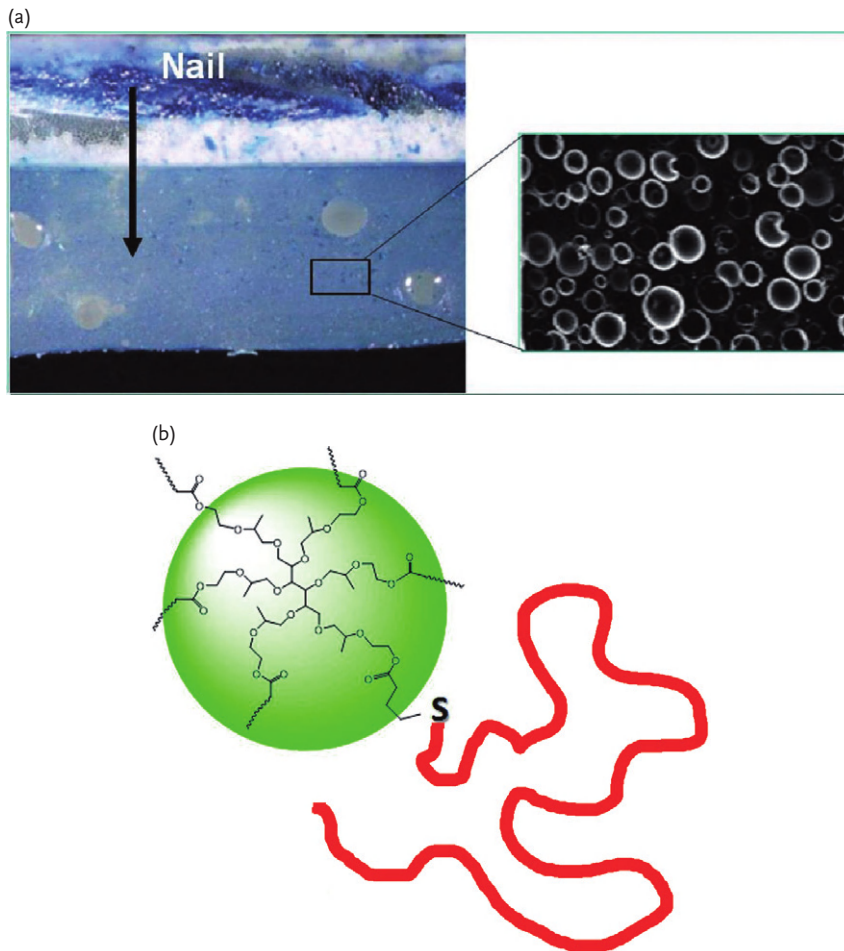


Figure 2.13 (a) Fiber reinforced PVC fabric membrane (at the top) coated with a self-healing polyurethane foam layer cured at 1 bar overpressure. The fissure caused by puncturing with a 2.4 mm diameter nail (parallel to the arrow) is closed by the

self-healing foam. The magnification shows a SEM picture of the PU foam. (b) Polybutylacrylate-grafted branched polyol stearates (hyperPBA) used as additives for self-healing polyurethane foams.

conditions which represent characteristic traits of the biological system, are mimicked either (i) in a bio-inspired physical transfer process by curing the repair foam under external over pressure, or (ii) in a bio-inspired chemical transfer process by the development of innovative self-repairing systems based on skin and blend formations.

For measuring the repair efficiency of the sealing mechanism, a novel testing set-up was build which allows to quantifying the air-flow through punctured foam coated and uncoated hull membranes [3, 6]. The repair efficiency of the foam coating is defined by

$$R_{flow} = 1 - (\dot{m}_{coat} / \dot{m}_{ref}) \quad (2.1)$$

with \dot{m}_{coat} : air flow through the puncture of a foam coated membrane, \dot{m}_{ref} : air flow through the puncture of a uncoated membrane. For $R_{flow} = 1$ complete sealing is achieved; $R_{flow} = 0$ corresponds to no sealing [31].

2.3.2.1 Self-Sealing Membranes of Pneumatic Structures: Bio-Inspired Physical Transfer

The bio-inspired physical transfer process is a typical example of a top-down-approach in biomimetics (Figure 2.14). The self-sealing coating developed during

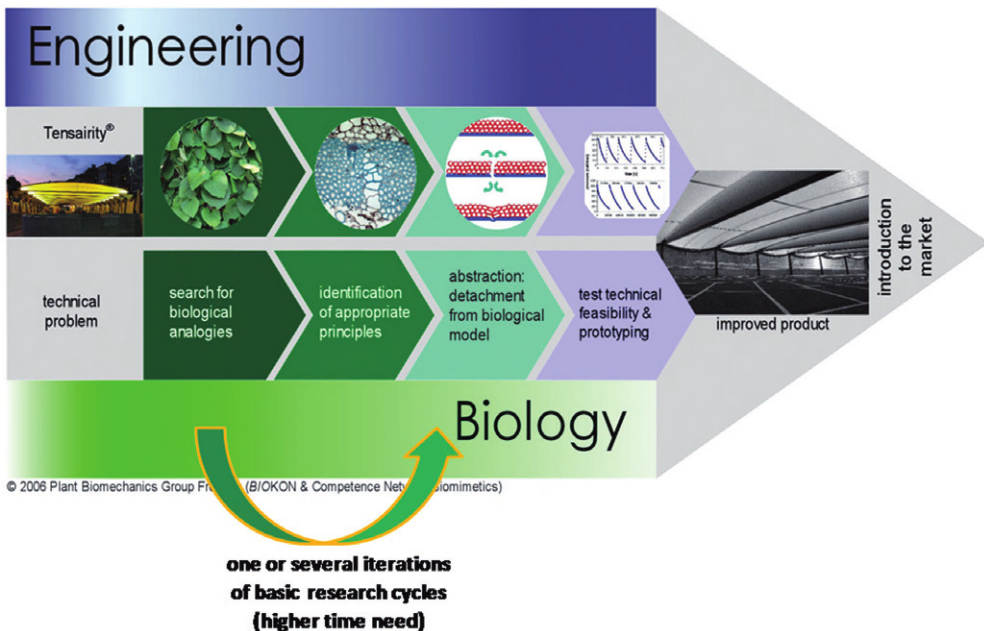


Figure 2.14 (Extended) top-down-process of biomimetics exemplified for the development of bio-inspired self-repairing membranes. Due to the limited knowledge on self-repair processes in plants in this specific case

several iterations of basic research cycles, including search for, identification and abstraction of novel self-repair mechanisms, have been included in the process sequence (from [4]).

this process was based on a commercially available two-component polyurethane foam system (RAKU-PUR® 33-1024-3 black; Rampf Giessharze). Our analyses prove that the amount of overpressure during the foaming and curing reaction is crucial for structure, mechanical properties, and repair efficiency of the self-sealing foam coating [31, 56, 57]. An abrupt transition of porosity from open to closed cell material, mirrored by an increase in closed pore ratio from circa 16 to 75%, was found between 50 and 60% relative density [56]. Polyurethane foam coatings could be produced with very good median repair efficiencies $R_{\text{flow}} \geq 0.999$ (Figure 2.15). Our analyses further show that on the inner surface of the coating layer compressive strains are necessary to yield high repair efficiencies. The air pressure in a pneumatic structure also causes a curvature of the hull with the squeezing of

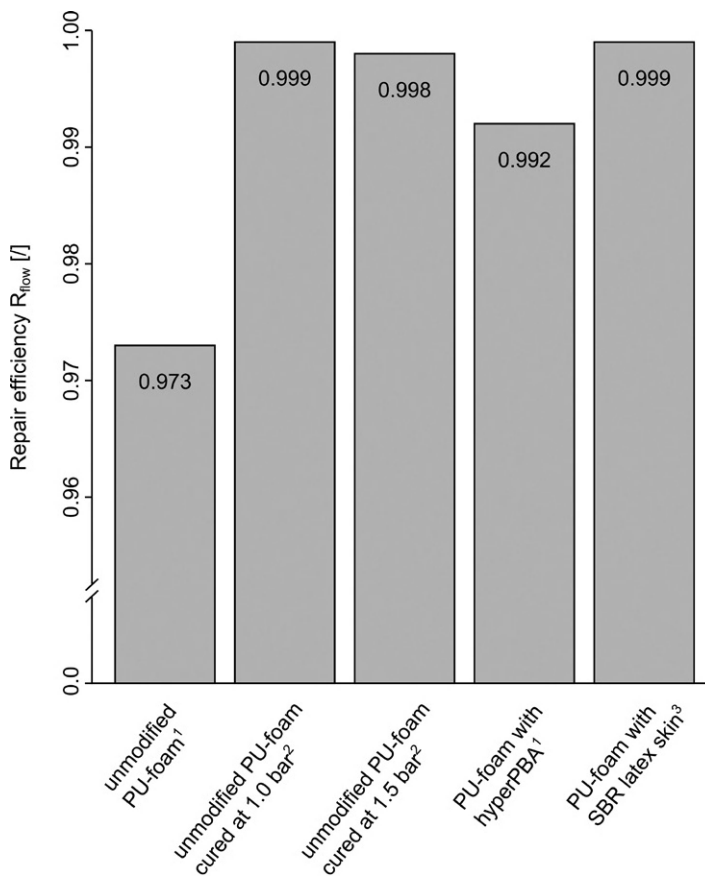


Figure 2.15 Repair efficiency of different types of polyurethane-based foam coatings for pneumatic systems expressed as R_{flow} .¹Average thickness of the self-healing polyurethane foam layer: 1.86 mm, ²average

mass of the self-healing polyurethane foam layer: 0.16 g cm^{-2} (the thickness is dependent on the applied overpressure), ³average thickness of the self-healing polyurethane foam layer: 2.20 mm.

the foam layer, and thereby introduces these compressive strains, if the self-repairing foam layer is placed on the internal side of the hull (Figure 2.13a) [57].

Our analyses prove that, at similar coating thicknesses, foams with more closed pores, that is, foams cured under higher overpressure, yield significantly higher repair efficiencies than foams with more open pores. Therefore, closed cell foams cured under 1 bar overpressure represent an optimal combination of high repair efficiency (0.999), and minimal weight of the foam coating (0.16 g cm^{-2}) which is very important for lightweight pneumatic structures. The results on the laboratory scale are very promising and point to the high potential of this approach for making pneumatic structures more reliable and safer in handling, and for increasing their lifetime [6, 31, 56, 57].

2.3.2.2 Self-Sealing Membranes of Pneumatic Structures: Bio-Inspired Chemical Transfer

A central aim of the research in the Freiburg Materials Research Center was the development of new self-healing additives for polyurethane foams that function without encapsulation. To this end amphiphilic polymers are tailored possessing crystallizable *n*-alkyl chains in the shell and cores with highly branched polyether. Due to their core-shell topology these branched and dendritic polymers may act as vesicle-like molecular transporters and host-guest systems [58]. As described in detail in [6], branched polyether cores can easily be synthesized. In a next step oligomers, for example, liquid rubbers, can be grafted to these core-shell macromolecules which serve simultaneously as molecular transporters and self-healing agent. In one approach star-shaped propoxylated sorbitol (Lupranol™ 3422; Elastogran) served as the core material and was completely esterified in the presence of catalytic amounts of *p*-toluene sulfonic acid at 140°C with stearic acid (90 mol% OH substitution), making the polar polyethers amphiphilic, and with mercaptopropionic acid (10 mol % OH substitution) causing incorporation of thiol groups into the shell [6]. Then a novel graft copolymer (hyperPBA; average molar mass of 3000 g mol^{-1}) was produced by adding 50 wt.% of a butylacrylate/acrylonitrile (80/20) mixture and grafting it at 80°C onto the thiol-functionalized polyol stearate (Figure 2.13b).

For the self-healing effect it is crucial that the amphiphilic hyperbranched polymers can migrate and show self-assembly at interfaces. In a next step polybutylacrylate (PBA) and hyperPBA were added to the commercially available two-component polyurethane foam (RAKU-PUR® 33-1024-3 black, Rampf Giessharze). The repair efficiency R_{flow} was tested in the above described testing device for a polyurethane foam layer cured at ambient pressure (i.e., at 0 bar overpressure) with an average thickness of 1.86 mm coated on a PVC fabric membrane (Ferrari Preconstraint 1002). For a non-modified PU foam a repair efficiency of $R_{\text{flow}} = 0.973$ was found (Figure 2.15). The admixture of 2 wt.% PBA did not increase repair efficiency, the addition of up to 10 wt.% hyperPBA did not influence the foam processing but markedly improved the repair efficiency up to $R_{\text{flow}} = 0.992$ [6]. A further improvement in the repair efficiency is found when the inner surface of the PU foam layer is coated with a SBR latex (Holt Lloyd GmbH), increasing

the thickness of the foam coating to 2.20 mm. By this procedure the repair efficiency is improved to $R_{\text{flow}} = 0.999$ (Figure 2.15), a value matching results found when the polyurethane layer was cured under overpressure [6].

Our results show that both vesicle-like molecular healing agents with core-shell topologies (chemical strategy I) and skin formation on the inner surface of the self-repairing foam coating (chemical strategy I) significantly improve the self-repairing capacity of polyurethane foams without external overpressure during foam curing.

2.4

Bio-Inspired Self-Healing Materials: Outlook

The above mentioned examples show that during the last years plants have proved to be an important source of inspiration for various biomimetic materials and structures with self-repairing properties. The self-sealing and self-healing mechanisms in plants (and other living beings) offer a huge variety of inspirations for developing biomimetic technical materials and structures with self-repairing properties. Important driving forces for the increasing potential of, and the improved interest in the development of biomimetic products are: (i) the availability of more sophisticated analyzing devices and modeling tools allowing a better quantitative understanding of the form-structure-function relationship on different hierarchical levels of the biological role models as well as of the biomimetic materials; and (ii) the availability of production methods allowing the transfer of modes of function and/or the hierarchical structuring typical for biological role models into biomimetic products (e.g., generative methods, 3D-braiding pultrusion techniques, sophisticated micro-laminate and foil techniques, and improved techniques in macromolecular and supramolecular chemistry). Additionally, over the last two decades biomimetic approaches have been increasingly noticed and appreciated by industry due to a generally higher interest in tapping the “treasure trove of nature” for the development of smart and intelligent materials and structures with self-x-properties [4, 5]. An additional aspect often mentioned, especially also for self-repairing materials, is the potential for sustainability of biomimetic products being generally considered as very high. However, the level of sustainability has to be tested separately for each biomimetic product [59].

We think that biomimetic approaches in general, and especially in the field of self-x-materials and structures, as for example, self-repairing materials and structures, are very promising and will become of increasing importance in the near future.

Acknowledgments

These studies were accomplished within the project “Self-healing polymers OSIRIS” (FKZ 01RB0711) that is funded by the German Federal Ministry of Education and Research within the scope of the funding programme BIONA, and the

project “Vom biologischen Vorbild zum bionischen Produkt: Wundheilung bei Pflanzen als Ideengeber für selbstreparierende technische Materialien” (FKZ 0313778A) that is funded by the German Federal Ministry of Education and Research within the scope of the funding programme “Ideenwettbewerb: BIONIK–INNOVATIONEN AUS DER NATUR”, and additionally funded by the EMPA Dübendorf. We thank Dipl.-Biol. Marc Thielen for help with the figures.

References

- 1 Rowe, N.P., Isnard, S., Gallenmüller, F., and Speck, T. (2006) Diversity of mechanical architectures in climbing plants: an ecological perspective, in *Ecology and Biomechanics: A Mechanical Approach to the Ecology of Animals and Plants* (eds A. Herrel, T. Speck, and N.P. Rowe), Dekker Publishers/Taylor & Francis Group, Boca Raton, pp. 35–59.
- 2 Rowe, N.P., and Speck, T. (2013) Liana biomechanics, in *The Ecology of Lianas* (eds S. Schnitzer, F. Bongers, R. Burnham, and F. Putz), Wiley-Blackwell, Chichester. (submitted).
- 3 Speck, T., Luchsinger, R.H., Busch, S., Rüggeberg, M., and Speck, O. (2006) Self-healing processes in nature and engineering: self-repairing biomimetic membranes for pneumatic structures, in *Comparing Design in Nature with Science and Engineering “Design and Nature III”* (ed. C.A. Brebbia), WIT Press, Southampton, pp. 105–114.
- 4 Speck, T., and Speck, O. (2008) Process sequences in biomimetic research, in *Comparing Design in Nature with Science and Engineering “Design and Nature IV”* (ed. C.A. Brebbia), WIT Press, Southampton, pp. 3–11.
- 5 Masselter, T., Barthlott, W., Bauer, G., Bertling, J., Ditsche-Kuru, P., Gallenmüller, F., Gude, M., Hermann, M., Immink, H., Knippers, J., Lienhard, J., Luchsinger, R.H., Lunz, K., Mattheck, C., Milwich, M., Mölders, N., Neinhuis, C., Nellesen, A., Rechberger, M., Schleicher, S., Schmitt, C., Schwager, H., Seidel, R., Speck, O., Stegmaier, T., Tesari, I., Thielen, M., and Speck, T. (2011) Biomimetic products, in *Biomimetics: Nature-Based Innovation* (ed. Y. Bar-Cohen), CRC Press/Taylor & Francis Group, Boca Raton, pp. 377–429.
- 6 Speck, T., Bauer, G., Flues, F., Oelker, K., Rampf, M., Schüssele, A.C., von Tapavicza, M., Bertling, J., Luchsinger, R.H., Nellesen, A., Schmidt, A.M., Mülhaupt, R., and Speck, O. (2013) Bio-inspired self-healing materials, in *Materials Design Inspired by Nature: Function through Inner Architecture* (eds P. Fratzl, J.W.C. Dunlop, and R. Weinkamer), The Royal Society of Chemistry, London, pp. 359–389.
- 7 Fink, S. (1999) *Pathological and Regenerative Plant Anatomy, Encyclopedia of Plant Anatomy XIV*, Gebrüder Borntraeger, Berlin, Stuttgart.
- 8 Busch, S., Schmitt, K., Erhardt, C., and Speck, T. (2010) Analysis of self-repair mechanisms of *Phasaeolus vulgaris* var. *saxa* using near-infrared surface enhanced Raman spectroscopy (SERS). *J. Raman Spectrosc.*, **41**, 490–497.
- 9 Flues, F., Speck, T., Luchsinger, R.H., and Speck, O. (2009) Wundheilung bei Pflanzen als Ideengeber für selbstreparierende technische Materialien – Erste Ergebnisse einer vergleichenden Untersuchung von Selbstreparationsprinzipien in der Pflanzenwelt, in *Tagungsbeiträge zum 4. Bionik-Kongress, 7.-8. November, Bremen, Germany* (eds A.B. Kesel and D. Zehren), Bionik-Innovations-Centrum B-I-C, Bremen, pp. 222–227.
- 10 Wilson, J.W., and Grange, R.I. (1984) Regeneration of tissues in wounded stems: a Quantitative Study. *Ann. Bot. (Lond)*, **53**, 515–525.
- 11 Liskay, A., van der Zalm, E., and Schopfer, P. (2004) Production of reactive oxygen intermediates (O(2)(-), H(2)O(2),

- and (.)OH) by maize roots and their role in wall loosening and elongation growth. *Plant Physiol.*, **136**, 3114–3123.
- 12 Busch, S., Speck, T., Liskay, A., Speck, O., and Luchsinger, R.H. (2006) Self-repair processes in plants as concept generators for innovative biomimetic technical materials with self-repairing functions, in *Proceedings of the 5th International Plant Biomechanics Conference August 28–September 1, 2006, Stockholm, Sweden*, vol. I (ed. L. Salmen), STFI Packforsk AB, Stockholm, pp. 83–88.
 - 13 Lewinsohn, T.M. (1991) The geographical distribution of plant latex. *Chemoecology*, **2**, 64–68.
 - 14 Bauer, G., Nellesen, A., and Speck, T. (2010) Biological latices in fast self-repair mechanisms in plants and the development of bio-inspired self-healing polymers, in *Comparing Design in Nature with Science and Engineering “Design and Nature V”* (eds C.A. Brebbia and A. Carpi), WIT Press, Southampton, pp. 453–459.
 - 15 Bauer, G., Nellesen, A., Sengespeick, A., and Speck, T. (2009) Fast self-repair mechanisms in plants: biological latices as role models for the development of biomimetic self-healing, mechanically loaded polymers, in *Proceedings of the 6th Plant Biomechanics Conference, November 16-21, 2009, Cayenne, French Guyana* (ed. B. Thibaut), ECOFOG, Cayenne, pp. 367–373.
 - 16 Speck, T., Bauer, G., Schüssele, A., Gorb, S., von Tapavicza, M., Nellesen, A., and Mülhaupt, R. (2012) Self-healing elastomers—learning from Nature’s solutions, in *Proceedings of the 7th Plant Biomechanics Conference, August 20–24, 2012, Clermont-Ferrand, France* (eds B. Moulia and M. Fournier), Clermont-Ferrand, pp. 377–380.
 - 17 Bauer, G., and Speck, T. (2012) Restoration of tensile strength in bark samples of *Ficus benjamina* due to coagulation of latex during fast self-healing of fissures. *Ann. Bot. (Lond)*, **109**, 807–811.
 - 18 Bauer, G., Gorb, S., Klein, M.C., Nellesen, A., von Tapavicza, M., and Speck, T. (2012) Comparative study on latex particles and latex coagulation in *Ficus benjamina*, *Campanula glomerata* and three *Euphorbia* species. (submitted).
 - 19 Bauer, G., Friedrich, C., Gillig, C., Vollrath, F., Speck, T., and Holland, C. (2012) Investigating the rheological properties of native plant latex. (submitted).
 - 20 Agrawal, A.A., and Konno, K. (2009) Latex: a model for understanding mechanisms, ecology, and evolution of plant defense against herbivory. *Annu. Rev. Ecol. Evol. Syst.*, **40**, 311–331.
 - 21 Hunter, J. (1994) Reconsidering the functions of latex. *Trees—Struct. Funct.*, **9**, 1–5.
 - 22 Metcalfe, C.R. (1967) Distribution of latex in the plant kingdom. *Econ. Bot.*, **21**, 115–127.
 - 23 D’Auzac, J., Prevot, J.-C., and Jacob, J.-L. (1995) What’s new about lutoids? A vacuolar system model for *Hevea* latex. *Plant Physiol. Biochem.*, **33**, 765–777.
 - 24 Gidrol, X., Chrestin, H., Tan, H.-L., and Kush, A. (1994) Hevein, a Lectin-like protein from *Hevea brasiliensis* (Rubber Tree) is involved in the Coagulation of Latex. *J. Biol. Chem.*, **269**, 9278–9283.
 - 25 Wititsuwannakul, R., Pasitkul, P., Jewtragoon, P., and Wititsuwannakul, D. (2008) *Hevea* latex lectin binding protein in C-serum as an anti-latex coagulating factor and its role in a proposed new model for latex coagulation. *Phytochemistry*, **69**, 656–662.
 - 26 Nellesen, A., von Tapavicza, M., Bertling, J., Schmidt, A.M., Bauer, G., and Speck, T. (2011) Pflanzliche Selbstheilung als Vorbild für selbstreparierende Elastomerwerkstoffe. *GAK—Gummi, Fasern, Kunststoffe*, **64** (8), 472–475.
 - 27 Speck, O., Luchsinger, R.H., Busch, S., Rüggeberg, M., and Speck, T. (2006) Self-repairing membranes for pneumatic structures: transferring nature’s solutions into technical applications, in *Proceedings of the 5th International Plant Biomechanics Conference, August 28–September 1, 2006, Stockholm, Sweden*, vol. I (ed. L. Salmen), STFI Packforsk AB, Stockholm, pp. 115–120.
 - 28 Busch, S., Seidel, R., Speck, O., and Speck, T. (2010) Morphological aspects of self-repair of lesions caused by internal growth stresses in stems of *Aristolochia*

- macrophylla* and *Aristolochia ringens*. *Proc. R. Soc. London Ser. B*, **277**, 2113–2120.
- 29 Masselter, T., and Speck, T. (2008) Quantitative and qualitative changes in primary and secondary stem organization of *Aristolochia macrophylla* during ontogeny: growth analysis and experiments. *J. Exp. Bot.*, **59**, 2955–2967.
- 30 Speck, T., and Rowe, N.P. (1999) A quantitative approach for analytically defining size, form and habit in living and fossil plants, in *The Evolution of Plant Architecture* (eds M.H. Kurmann and A.R. Hemsley), Royal Botanic Gardens Kew, Kew, pp. 447–479.
- 31 Rampf, M., Speck, O., Speck, T., and Luchsinger, R.H. (2011) Self-repairing membranes for inflatable structures inspired by a rapid wound sealing process of climbing plants. *J. Bionic Eng.*, **8**, 242–250.
- 32 Speck, O., Schmich, F., Flues, F., and Speck, T. (2012) Self-healing processes in plants as concept generator for biomimetic self-repairing material, in *Proceedings of the 7th Plant Biomechanics Conference, August 20–24, 2012, Clermont-Ferrand, France* (eds B. Moulia and M. Fournier), Clermont-Ferrand, pp. 373–376.
- 33 Konrad, W., Flues, F., Schmich, F., Speck, T., and Speck, O. (2013) An analytic model of the self-sealing mechanism of the succulent plant *Delosperma cooperi*. *J. Theor. Biol.* (accepted).
- 34 Landrum, V.J. (2006) Wide-band tracheids in genera of Portulacaceae: novel, non-xyllary tracheids possibly evolved as an adaptation to water stress. *J. Plant Res.*, **119**, 497–504.
- 35 Caliaro, M., Flues, F., Speck, T., and Speck, O. (2013) Novel method for measuring tissue pressure in herbaceous plants. *Int. J. Plant Sci.*, **174**, 161–170.
- 36 VDI-Guideline 6220 (2011) *Biomimetics – Conception and strategy, differences between biomimetic and conventional methods/products*. VDI Gesellschaft Technologies and Life Sciences, Verein Deutscher Ingenieure e.V., Düsseldorf. (see also VDI-Guidelines 6221–6225).
- 37 van der Zwaag, S. (ed.) (2007) *Self Healing Materials*, Springer, Dordrecht.
- 38 Ghosh, S.K. (ed.) (2008) *Self-healing Materials: Fundamentals, Design Strategies, and Applications*, Wiley-VCH Verlag GmbH, Weinheim.
- 39 Zhang, M.Q., and Rong, M.Z. (eds) (2011) *Self-Healing Polymers and Polymer Composites*, John Wiley & Sons, Inc., Hoboken.
- 40 Guimard, N.K., Oehlschlaeger, K.K., Zhou, J., Hilf, S., Schmidt, F.G., and Berner-Kowollok, C. (2012) Current trends in the field of self-healing materials. *Macromol. Chem. Phys.*, **213**, 131–143 [and articles in this issue].
- 41 White, S.R., Sottos, N.R., Geubelle, P.H., Moore, J.S., Kessler, M.R., Sriram, S.R., Brown, E.N., and Viswanathan, S. (2001) Autonomic healing of polymer composites. *Nature*, **409**, 794–797.
- 42 Brown, E., Sottos, N.R., and White, S.R. (2002) Fracture testing of a self-healing polymer composite. *Exp. Mech.*, **42**, 372–379.
- 43 Jin, H., Mangun, C.L., Stradley, D.S., Moore, J.S., Sottos, N.R., and White, S.R. (2012) Self-healing thermoset using encapsulated epoxy-amine healing chemistry. *Polymer*, **53**, 581–587.
- 44 Pang, J.W.C., and Bond, I.P. (2004) Bleeding composites' – Damage detection and self-repair using a biomimetic approach. *Compos. Part A: Appl. Sci. Manuf.*, **36**, 183–188.
- 45 Williams, H.R., Trask, R.S., Knights, A.C., Williams, E.R., and Bond, I.P. (2008) Biomimetic reliability strategies for self-healing vascular networks in engineering materials. *J. R. Soc. Interface*, **5**, 735–747.
- 46 Esser-Kahn, A.P., Thakre, P.R., Dong, H., Patrick, J.F., Vlasko-Vlasov, V.K., Sottos, N.R., Moore, J.S., and White, S.R. (2011) Three-dimensional microvascular fiber-reinforced composites. *Adv. Mater.*, **23**, 3654–3658.
- 47 Hamilton, A.R., Sottos, N.R., and White, S.R. (2012) Pressurized vascular systems for self-healing materials. *J. R. Soc. Interface*, **9**, 1020–1028.
- 48 Lehn, J.-M. (1995) *Supramolecular Chemistry*, Wiley-VCH Verlag GmbH, Weinheim.

- 49 Köhler, L., and Spatz, H.-C. (2002) Micromechanics of plant tissues beyond the linear-elastic range. *Planta*, **215**, 33–40.
- 50 Keckes, J., Burgert, I., Frühmann, K., Müller, M., Kölln, K., Hamilton, M., Burghammer, M., Roth, S.V., Stanzl-Tschegg, S., and Fratzl, P. (2003) Cell-wall recovery after irreversible deformation of wood. *Nat. Mater.*, **2**, 810–814.
- 51 Dunlop, J.W.C., and Fratzl, P. (2010) Biological composites. *Annu. Rev. Mater. Res.*, **40**, 1–24.
- 52 Cordier, P., Tournilhac, F., Soulié-Ziakovic, C., and Leibler, L. (2008) Self-healing and thermoreversible rubber from supramolecular. *Nature*, **451**, 977–980.
- 53 Aida, T., Meijer, E.W., and Stupp, S.I. (2012) Functional supramolecular polymers. *Science*, **335**, 813–817.
- 54 Tomos, A.D., and Leigh, R.A. (1999) The pressure probe: a versatile tool in plant cell physiology. *Annu. Rev. Plant Physiol. Plant Mol. Biol.*, **50**, 447–472.
- 55 Schüssele, C., Nübling, F., Thomann, Y., Carstensen, C., Bauer, G., Speck, T., and Mülhaupt, R. (2012) Self-healing rubbers based on NBR blends with hyperbranched polyethylenimines. *Macromol. Mater. Eng.*, **297**, 411–419.
- 56 Rampf, M., Speck, O., Speck, T., and Luchsinger, R.H. (2012) Structural and mechanical properties of flexible polyurethane foams cured under pressure. *J. Cell. Plast.*, **48**, 49–65.
- 57 Rampf, M., Speck, O., Speck, T., and Luchsinger, R.H. (2012) Investigation of a fast mechanical self-repair mechanism for inflatable structures. *Int. J. Eng. Sci.*, **63**, 61–70.
- 58 Yan, D., Gao, C., and Frey, H. (eds) (2011) *Hyperbranched Polymers: Synthesis, Properties, and Applications*, John Wiley & Sons, Inc., Hoboken.
- 59 Antony, F., Mai, F., Speck, T., and Speck, O. (2012) Bionik–Vorbild Natur als Versprechen für nachhaltige Technikentwicklung? *Naturwiss. Rundsch.*, **65/4**, 175–182.

3

Modeling Self-Healing Processes in Polymers: From Nanogels to Nanoparticle-Filled Microcapsules

German V. Kolmakov, Isaac G. Salib, and Anna C. Balazs

3.1

Introduction

Nature has devised a number of highly effective means of both preventing and healing wounds in living organisms. Consider, for example, the abalone shell nacre, where brittle inorganic layers are interconnected by a layer of cross-linked polymers [1]. Under mechanical deformation, the weak cross-links or “sacrificial bonds” are the first to break; these ruptures dissipate energy and thereby mitigate the effects of the deformation. Consequently, the breakage of these sacrificial bonds helps prevent catastrophic damage and maintain the structural integrity of the material. As another example, consider the performance of leukocytes, which offer an elegant biological solution to wound healing. These cells sense injury in the body, migrate to the injured areas and then help initiate the healing process. Both these biological mechanisms can serve as inspiration for creating materials systems that thwart catastrophic mechanical failure and perform some level of self-repair.

We describe recent theoretical and computational studies that have borrowed from the above design principles to devise synthetic self-mending materials. Both the examples described below exploit the properties of nanoparticles. In the first example, we describe how weak sacrificial bonds between cross-linked nanoscopic gel particles lead not only to bond breaking, but also to bond making that forestalls the catastrophic failure of the material [2, 3]. In the second example, we design an artificial “leukocyte” that rolls along a surface and delivers nanoparticles into cracks within this substrate [4–6]. The deposited nanoparticles fill the fissure in the surface and, in this manner, effectively heal the defects on the substrate.

There have been a number of computational studies that yielded guidelines for harnessing both the enthalpic and entropic behavior of nanoparticles dispersed in polymers to create self-healing systems. Using a self-consistent-field/density functional theory (SCF/DFT) [7, 8], Monte Carlo simulations [8] and molecular dynamics [9, 10], Balazs *et al.* examined the behavior of nanoparticle-filled polymer films that are in contact with a cracked wall. If the particles are comparable in size to the radius of gyration of the chains and exhibit an enthalpically favorable

interaction with the host polymer, then the nanoparticles become localized in the cracks within the wall and effectively form “patches” to repair the damaged regions. In these scenarios, the polymers induce an entropic depletion attraction between the particles and wall that drives the nanoparticles into the defects. In this way, the chains gain conformational entropy because they do not have to stretch around particles within the film [7–10]. These predictions were later confirmed in experiments [11, 12] where nanoparticles dispersed in a polymer matrix were observed to migrate to a crack generated at the interface between the polymer and a glassy surface. Together, these computational and experimental findings point to an effective means of improving the lifetime and durability of multilayered systems.

In the following discussion, we describe other approaches for harnessing nanoparticles to create self-healing systems. We start by describing the advantage of introducing weak, labile bonds into a network of cross-linked polymeric nanogels and then detail the design of nanoparticle-filled polymeric microcapsules that behave as artificial leukocytes.

3.2

Designing Self-Healing Dual Cross-Linked Nanogel Networks

Inspired by the utility of weak “sacrificial bonds” [1], we used computational modeling to determine how weak, labile bonds could be harnessed to improve the mechanical behavior of materials composed of nanoscopic, deformable gel particles [2, 3] that are decorated with ligands, which contain a number of functional groups (see Figure 3.1a). Through these functional groups, the gels can form a “dual cross-linked” network; namely, they are interconnected by both strong “stable” bonds and weak labile bonds. The stable bonds could be carbon–carbon linkages and the labile bonds could be provided by thiol groups that enable thiol/disulfide exchange reactions. In prior computational studies [2], we found that the stable bonds provide a rigid backbone, while the labile bonds allow the material to undergo a dynamic reconfiguration in response to stress. In studies described here, we adapted the hierarchical Bell model (HBM) [13] in order to model cases where the ligands on neighboring nanogels interact through multiple sites. For example, the binding interactions between the pairs of sites on the ligands in Figure 3.1 can be modeled via three parallel bonds in the HBM formalism.

The HBM formalism, however, did not include the possibility of bond reformation; once a bond was broken, it could not be reconnected. Though this approximation is appropriate in situations where the material experiences very rapid deformations, it might not be valid in cases where the sample is undergoing a slower stretching or pulling. Furthermore, for nanogels or nanoscale star polymers that are decorated with thiol and disulfide groups [14–18] (as we envision in our system), the ensuing exchange reactions enable the reformation of broken bonds.

We then combined our modified HBM with the lattice spring model (LSM) [19, 20], which is the coarse-grained approach we used to simulate each nanogel par-

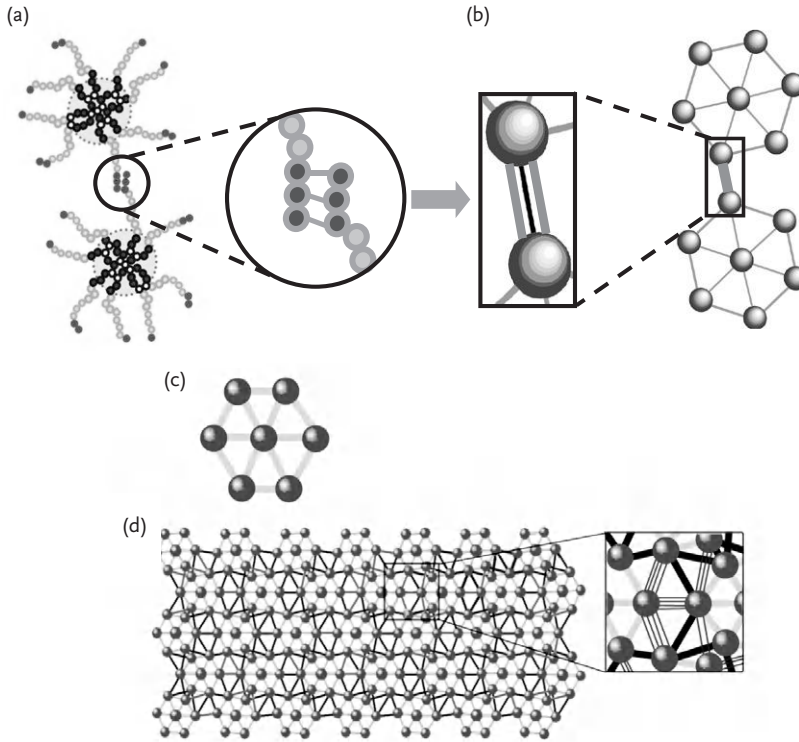


Figure 3.1 (a) Schematic of two nanogels that are decorated with functionalized ligands; the inset indicates three interparticle bonds formed through the interactions of the functional groups on the ligands. (b) An illustration of the HBM/LSM model for the two nanogels in (a); each nanogel is modeled by a seven node network of springs. The nanogels are interconnected by a labile linkage, which encompasses three parallel

labile bonds (see inset). (c) Schematic of a deformable nanogel particle. Each LSM gel particle consists of seven nodes that are interconnected by permanent spring-like bonds. (d) An illustration of a crosslinked nanogel network. The nanogel particles are crosslinked by stable linkages and labile linkages. Each labile linkage can consist of a number of parallel labile bonds (inset).

ticle (see Figure 3.1). The integrated “HBM/LSM” method [3] allows us to model the dual cross-linked nanogels, which are joined by bonds that can break and reform in response to a mechanical deformation and more accurately capture the experiments [14–18] where the ligands on the nanogel particles can subtend multiple reactive groups (see Figure 3.1a).

We focus on systems that contain a relatively high fraction P of stable bonds and hence, a low fraction $(1-P)$ of the labile linkages. Our goal is to determine how the addition of just a small number of chemically reactive species can be harnessed to tailor the mechanical properties of the sample and, importantly, “heal” damage within the material.

3.2.1

Methodology

Figure 3.1c shows the seven-node lattice spring model (LSM) unit that represents an individual nanogel. These units are then interconnected into an extended material by both stable and labile bonds, as demonstrated in Figure 3.1d. Within a single gel unit, the nodes interact through a potential $U(r)$ that involves an attractive Hookean spring interaction and a repulsive force, which mimics an excluded volume around the node, and is written as:

$$U(r) = \frac{\kappa}{2} \left(r^2 + \frac{a}{r} \right) \quad (3.1)$$

with a cut-off distance r_c . Here, κ is the spring stiffness constant, r is the distance between the nodes, and a is the repulsion parameter. The equilibrium distance between the nodes is equal to $d = (a/2)^{1/3}$. For the stable and labile links that can break and reform, the potential $U(r)$ is taken to be a constant at $r > r_c$, so that the bonding interaction is cut off at r_c . The cut-off distance is set to $r_c = 2d \equiv (4a)^{1/3}$. Within each gel unit, the bonds do not break during the course of the simulations.

To model bonds between gel units, we use the same interaction potential, which emanates from each of the surface nodes on the gel pieces. Now, however, the spring constant κ for the inter-gel interactions (both stable and labile) is six times weaker than that for intra-gel bonds. (While different values for the latter spring constants could be chosen, significant differences between the inter- and intra-gel spring constants can give rise to numerical instabilities.) Additionally, κ has the same value for both the stable and labile bonds. (The latter choice allowed us to specifically focus on isolating effects arising from the dual cross-linking.) In the case of a broken bond, the repulsive interaction potential is given by the same dependence as Eq. (3.1) at $r < d = (a/2)^{1/3}$, and U is equal to a constant at $r \geq d$.

Each gel node obeys the following dynamic equation: $\frac{d\mathbf{r}_i}{dt} = \mu\mathbf{F}_i$ (i.e., the dynamics is in the over-damped limit), where μ is the mobility (assumed to be a constant) and the force acting on node i is $\mathbf{F}_i = -\frac{\partial U}{\partial \mathbf{r}_i} + \mathbf{F}_i^{\text{ext}}$. The elastic energy U_{tot}

is equal to $U_{\text{tot}} = \frac{1}{2} \sum_{m,n} 'U(|\mathbf{r}_m - \mathbf{r}_n|)$; the prime denotes that the summation is made

at a given bond configuration at a particular moment of time, and $m \neq n$. The term $\mathbf{F}_i^{\text{ext}}$ is the external tensile force, which is applied to the nodes at the edges of the rectangular samples. We numerically integrate the above equations of motion, using a fourth order Runge–Kutta algorithm with a time step of $\Delta t = 10^{-2}T_0$ where $T_0 = d^2/(k_B T \mu)$ is the unit of time in the simulation, k_B is the Boltzmann constant, and T is the temperature.

In response to the applied deformation, the bonds between the gel units (both labile and stable bonds) can break and reform. To model the rupture and reformation of bonds due to an external force, we utilize the Bell model [21], where the rupture rate, k_r , is an exponential function of the force applied to a single bond and is given by:

$$k_r^{(s,l)} = \nu^{(s,l)} \exp\left[\frac{r_0 F - U_0^{(s,l)}}{k_B T}\right] \quad (3.2)$$

The superscripts s and l refer to the respective stable and labile bonds. The parameter $\nu^{(s,l)}$ is the intrinsic frequency of an unstressed bond, r_0 is a characteristic length that describes the change in the reactivity of the bond under stress and F is the applied force. We used the same value $r_0 = d$ for both stable and labile bonds. The difference between the reactivities of the stable and labile bonds is captured through the term $U_0^{(s,l)}$, which is the potential well depth at zero mechanical stress. We set the potential well depth equal to $U_0^{(l)} = 100k_B T$ for labile bonds and $U_0^{(s)} = 140k_B T$ for the less reactive, stable bonds [3]. (As noted above, the label linkages could represent thiol or disulfide units, and the stable links could model carbon-carbon bonds.)

The reforming rate, k_r , for a single broken bond can be calculated directly from the principle of detailed balance and is given by [3]:

$$\frac{k_r^{(s,l)}}{k_r^{(s,l)}} = \frac{k_{0f}^{(s,l)}}{k_{0r}^{(s,l)}} \exp\left(\frac{\Delta U(r)}{k_B T}\right), \quad (3.3)$$

where r is the bond length and $\Delta U(r)$ is the difference in the potential energies of a connected and broken bond. At small distances, $r < d$, the energy difference is $\Delta U(r) = 0$, whereas at $d \leq r \leq r_c$, $\Delta U(r) = U(r)$ where $U(r)$ is given by Eq. (3.1). At distances larger than r_c , the bonds are ruptured. The k_{0r} and k_{0f} are the respective rates of rupturing and forming a single unstressed bond. The probability for a connected bond to break and the probability for a broken bond to reform within a simulation time step Δt are:

$$w_r^{(s,l)} = 1 - \exp[-k_r^{(s,l)} \Delta t], \quad w_f^{(s,l)} = 1 - \exp[-k_f^{(s,l)} \Delta t] \quad (3.4)$$

As shown schematically in Figure 3.1, we now model the fact that a ligand on a nanogel particle can encompass $n > 1$ reactive sites and bonding between ligands on neighboring nanogels can contribute multiple binding interactions. Thus, an inter-gel spring represents n bonds that lie in parallel. The total force applied to the linkage, F_{tot} , is shared among the connected bonds and hence, the force applied to a single bond is equal to $F = F_{\text{tot}}/n$. To describe this scenario, we take advantage of the HBM [13]. We extended this approach [3] to describe not only bond breaking, but also remaking. As shown below, the remaking of broken bonds plays a vital role in the structural integrity of the samples at late times.

In our modified HBM, the state of each labile interconnection between two gel nodes at a given time is characterized by the number of connected reactive bonds, n , with the maximum number being equal to N . We emphasize that only the labile interconnections between the nodes encompass multiple bonds that lie in parallel; the stable bonds are always described by $N = 1$.

The probability for a single stressed bond to break and reform in our model is described by Eqs. (3.2)–(3.4). Given that n bonds are initially connected, then the probability of rupturing m bonds within a time step Δt is equal to

$$p_r(m, n) = C_m^n w_r^{(l)m} (1 - w_r^{(l)})^{n-m}, \quad (3.5)$$

where C_m^n is the binomial coefficient that accounts for the number of ways that m bonds that break can be chosen from a set of n initially connected bonds, and $w_f^{(l)}$ is defined by Eqs. (3.2)–(3.4) at an applied force equal to F . Similarly, the probability of m' bonds forming (if $n' = N - n$ bonds are initially ruptured) is equal to

$$p_f(m', n') = C_{m'}^{n'} w_f^{(l)m'} (1 - w_f^{(l)})^{n'-m'} \quad (3.6)$$

The rupture and forming of the bonds at the same time step are considered as statistically independent processes. Accordingly, the total probability $W(n_1, n)$ for a link to have n_1 connected bonds at the subsequent time step is computed as a sum over all possibilities of the rupture and formation processes,

$$W(n_1, n) = \sum_m p_r(n - n_1 + m, n) p_f(m, N - n) \quad (3.7)$$

In Eq. (3.7), the probabilities p_r and p_f are set equal to zero if the first argument is negative or is greater than the second argument; in other words, both the probability to break more bonds than were initially connected, and the probability to connect more bonds than were initially ruptured are strictly equal to zero. We use Eqs. (3.2)–(3.7) to update the system of bonds at each time step Δt .

Via the above model, we then constructed the interconnected nanogel samples; a fragment of such a sample is shown in Figure 3.1d. We examined two sample sizes: the smaller samples are composed of 5 layers of clusters with 10 clusters in each layer, and the larger samples are composed of 12 rows of clusters with 15 clusters in a row. The layers were constructed with a lattice spacing of $3d$ between the centers of the gel units, where d is the equilibrium distance between the nodes ($2d$ is the diameter of the unit). The vertical spacing between the layers was equal to $1.3d$. At this step, all possible bonds within the cut-off radius were established, and each node was allowed to subtend at most five interactions (that is, all possible interconnections between the gel units were allowed to form for given r_c and the inter-unit distance). All these interactions were marked as labile linkages, with the number of bonds in each linkage equal to the maximum number N . Then, the sample was equilibrated for 400 time units T_0 . During the equilibration, the initial mechanical stresses relaxed and the most stressed bonds were ruptured in accordance with the probability in Eq. (3.2). In the second step, we specify the types of each inter-gel linkage, assigning stable linkages with a probability P and labile linkages with a probability $(1 - P)$, and equilibrate the sample for additional 400 units of time. (If the linkage is assigned as stable, we set the maximum number of connected reactive bonds in this linkage equal to $N = 1$.) Thus, even for a fixed value of P , each simulation has a different, independent distribution of stable and labile bonds.

Given that N_{stable} and N_{labile} are the respective numbers of stable and labile interconnections in the samples generated as described above, we use the ratio $P = N_{\text{stable}} / (N_{\text{stable}} + N_{\text{labile}})$ to characterize the system. For example, for $P = 1$ the sample is totally interconnected by strong bonds; for $P = 0.7$, 30% of the linkages in the initial sample are labile. We refer to P as the dual cross-link ratio. The total number of labile bonds in the sample is equal to $N_{\text{bonds}} \times N_{\text{labile}}$ where N_{bonds} is the average number of labile bonds between two gel nodes. Using the above model,

we investigated the mechanical behavior and the self-healing mechanism of the dual cross-linked nanogels.

3.2.2

Results and Discussion

3.2.2.1 Applying a Tensile Deformation at Constant Force

Focusing first on the smaller samples (see above), we apply a constant tensile stress σ , which is defined as the ratio of the tensile force to the initial cross section of the sample (or the engineering stress). The critical stress, σ_b , is the tensile stress at which the cross-linked nanogel network is fractured into two pieces and σ_b^* is the critical stress for a sample cross-linked solely by stable bonds (i.e., a $P = 1$ sample). The tensile stress is applied gradually, at a rate of $5.88 \times 10^{-5} (\sigma / \sigma_b^*)$ per one normalized timestep, $\Delta t / T_0$. (Higher rates can result in the breaking of the sample at the ends, the region where the stress is applied.)

Figure 3.2 shows the dependence of the σ_b / σ_b^* on P and N ; the data was obtained by varying P from 0.6 to 1 and altering N from 1 to 4, and averaging over eight independent runs for each data point. Figure 3.2a reveals that the introduction of labile linkages can have a dramatic effect on the strength of the material. For example, for $P = 0.6$ and $N = 4$, the critical stress is roughly 230% greater than that for the $P = 1$. For the range of P considered here, the curves for $N > 1$ do not exhibit a maximum; rather, the strength of the material increases with the introduction of a higher fraction of labile bonds, that is, as P is decreased from $P = 0.9$ to $P = 0.6$. Our previous studies on just the $N = 1$ samples [2] showed that the labile bonds allowed the nanogels to reshuffle and thus, mend voids that appeared within the mechanically deformed system. It is this reshuffling that contributes to the improvement in strength with decreases in P at fixed N seen in Figure 3.2a.

Figure 3.2b shows σ_b / σ_b^* as a function of N for different values of P ; one can see that for a given P , the strength of the material increases considerably with an increase in N . This effect is expected since increases in N introduce more bonds between the nanogels and thus, inherently increase the strength of the material. This effect is more pronounced at lower P because the network encompasses more labile bonds.

3.2.2.2 Applying a Tensile Deformation at Constant Velocity

To probe the ductility and toughness of these materials, we apply a tensile deformation to the sample at constant velocity (strain rate) and thereby determine stress versus strain curves for these dual cross-linked nanogels. These calculations also reveal the self-healing mechanism that is operative in these materials.

Figure 3.3a shows the stress–strain curves for $P = 0.7$, with N being varied from 1 to 4. To obtain these curves, the nodes at the left-most edge of the sample are pulled with a velocity [10] equal to $2.0 \times 10^{-3} d_1 / \mu \kappa$ where $d_1 = 2d$ is the diameter of a cluster, μ is the mobility of the nanogel and κ is the bond stiffness (spring constant). The stress in Figure 3.3a is normalized by the bond stiffness κ . The strain ε is calculated as the ratio of the extension of the sample to its original

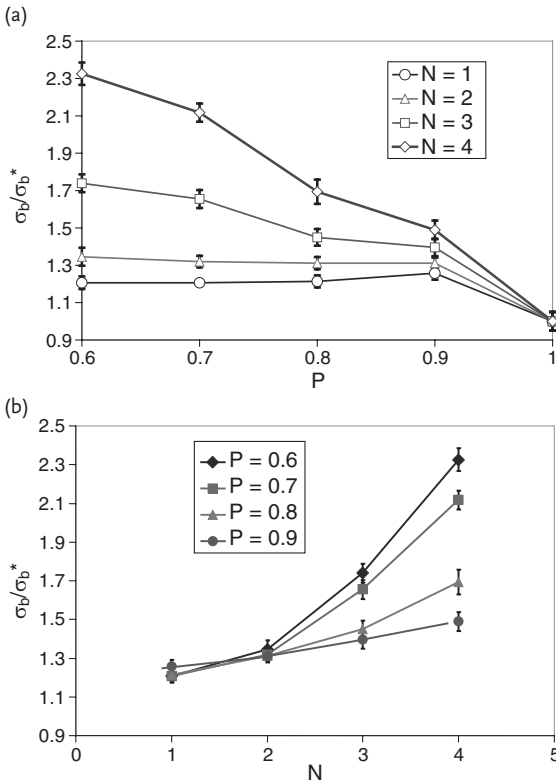


Figure 3.2 Dependence of the critical stress σ_b/σ_b^* for the small sample as a function of (a) P and (b) N . The normalization parameter σ_b^* is the critical stress for a sample with $P = 1$. The critical stress is calculated from constant force simulations.

length. The sharp drop in ε to zero at finite strain indicates that the sample has fractured into two pieces. As can be seen from Figure 3.3a, increases in N lead to decreases in the ductility of the sample. Namely, as N is increased, the sample fractures at smaller strain, meaning that the entire sample cannot be stretched to significant extensions at higher N .

From curves such as Figure 3.3a, we can determine the strain at breakage or the breaking strain ε_b for samples with different values of P . Figure 3.3b shows this data as a function of N for $P = 0.7, 0.8,$ and 0.9 . Again, the samples were pulled with a velocity of $2.0 \times 10^{-3} d_1/\mu\kappa$ and the data in the plot represent averages over five independent runs for each P and N value. All three curves indicate that increasing N from 1 to 4 leads to a monotonic drop in ε_b , the breaking strain.

From the above plots, we can see that while increasing N leads to stronger materials, it also leads to a decrease in the ductility of the sample. As noted above, our prior studies [2] on the $N = 1$ dual cross-linked samples revealed that the introduction of a small fraction of labile bonds led to an improvement in toughness and ductility relative to the $P = 1$ sample. In particular, the labile bonds

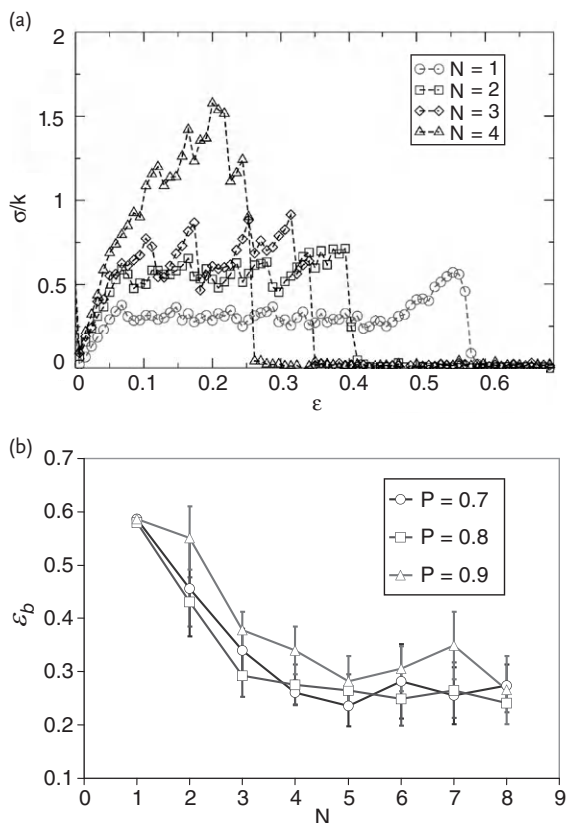


Figure 3.3 (a) Stress–strain curves calculated for the small sample for $N = 1, 2, 3$ and 4. Stress is normalized by the bond stiffness κ . (b) Dependence of the breaking

strain on N for small samples with $P = 0.7, 0.8$ and 0.9 . The breaking strain was calculated from the constant strain rate simulations.

allowed the nanogels to rearrange and thereby mend cavities in the material that were formed due to the tensile deformation. It is this autonomous mending of the cavities that constituted the self-healing mechanism within the materials. We now hypothesize that with the introduction of more labile bonds at higher N , the nanogels are more strongly attached to their neighbors and hence, the nanogel particles cannot readily undergo the structural rearrangement that is necessary for closing the voids formed during the deformation. Consequently, the breaking strain decreases with increases in N . Note that Figure 3.3b also indicates that for $N > 4$, the breaking strains reach a plateau value, suggesting that the nanogel connections are too strong to permit any reshuffling within the network and the breaking strain is solely the result of deformation of the clusters and hole formation.

There might, however, be an optimal range of parameters that yield not only an improved strength relative to the $N = 1$ scenarios, but also provide sufficient ductility that these high strength materials can exhibit the effective reorganizing that

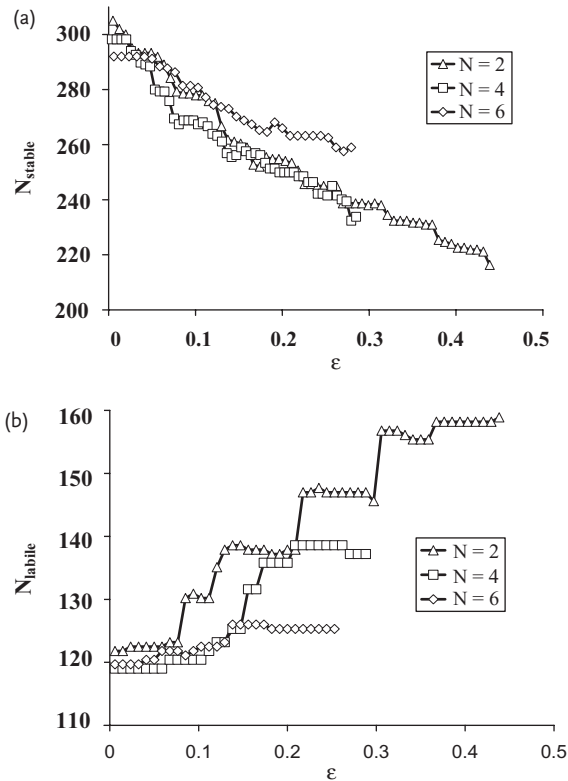


Figure 3.4 (a) Dependence of the number of stable bonds on strain (obtained from the simulations at constant strain rate) for $P = 0.7$ and $N = 2, 4, 6$. (b) Dependence of the number of labile linkages on strain (obtained from the simulations at constant strain rate) at $P = 0.7$ and $N = 2, 4, 6$. The data are displayed up to the strain at which the sample fractures.

produces the desired self-healing behavior. Figure 3.4 displays the dependence of the number of stable, N_{stable} , and labile linkages, N_{labile} , on the applied strain for the $P = 0.7$ samples. The data are plotted up to the point where the samples have become fractured. In the course of the tensile deformation, the vast majority of the stable bonds do not reform after rupturing. As a result, the number of stable bonds decreases as the strain is increased (see Figure 3.4a). For example, the number of stable bonds N_{stable} in the sample with $N = 2$ decreases from 305 to 216 when ϵ is increased from 0 to 0.439. In the sample with $N = 6$, N_{stable} decreases from 292 to 259 bonds when ϵ is increased to 0.279.

The situation, however, is different for the labile bonds. For $N \leq 4$, the nanogels can undergo rearrangements and establish new labile linkages with new neighbors. These new bonding interactions give rise to the overall increase in the number of labile linkages shown in Figure 3.4b. For $N > 4$, however, the labile linkages in the sample are too strong to allow the effective reorganization of the

nanogels. As a consequence, voids formed in the sample are not closed, but rather grow with increasing strain. Thus, the increase in the number of labile linkages for $N = 6$ is much smaller than that for samples with $N = 4$ and $N = 2$ (see Figure 3.4b). The considerable rise in the number of labile linkages during rearrangement for the $N \leq 4$ samples leads to the higher mechanical stability of the material and therefore, these samples can withstand higher deformations than those at $N > 4$, in agreement with the results in Figure 3.3.

Notably, we also applied a tensile deformation at constant strain rate to larger samples, which contain 12 rows with 15 nanogels in each row. The behavior for these larger samples reveals a pattern similar to that shown in Figure 3.3; as the value of N is increased, the strain at fracture decreases for all P considered here. As noted above, this implies that, for higher N values, the gel becomes more brittle and the ability of the nanogels to undergo structural rearrangement decreases.

3.2.2.3 Optimizing the Mechanical Response of the Material

The above results indicate that while increasing N significantly increases the strength of the material, it has a deleterious effect on the ductility and the self-healing attributes of the dual cross-linked nanogels. The results, however, also reveal that the properties of the material can be optimized relative to the $P = 1$ sample through a judicious choice of both P and N . In particular, we have found that for $P = 0.7$ and $N = 4$, we can design a network that is twice as strong as an all stable cross-linked network while preserving its self-healing ability.

These findings provide guidelines for creating dual cross-linked nanogels that forestall the catastrophic failure of the material. These design concepts can significantly extend the lifetime and utility of soft, responsive materials. In the following section, we discuss another means of extending the lifetime of materials.

3.3

Designing “Artificial Leukocytes” That Help Heal Damaged Surfaces via the Targeted Delivery of Nanoparticles to Cracks

The second scenario considered here is inspired by the functionality of biological leukocytes, which localize at wounded tissue and facilitate the repair process. Our aim was to design a biomimetic system that can initiate site-specific repair of cracked surfaces. We recently simulated the three-dimensional interactions of deformable microcapsules with a substrate that contains a 3D crack [5]. We assumed that the surface of the microcapsules is amphiphilic in nature and thus, could have comparable interactions with hydrophilic and hydrophobic domains. Such microcapsules can be fabricated from comb copolymers that encompass a hydrophobic backbone and hydrophilic side-chains [6]. We further assumed that the microcapsules encase an oil phase, which contains dispersed hydrophobic nanoparticles. These encapsulated particles could be quantum dots that are functionalized with hydrophobic ligands [6]. Within an oil/water mixture, the amphiphilic comb copolymers can provide an encapsulating shell for the coated

nanoparticles, which are dispersed in the interior oil phase [6]. Upon crosslinking of the polymer shell, the copolymers form a robust micro-carrier for the nanoparticles, with a very thin (~ 10 nm) wall [6] through which the nanoparticles can permeate under appropriate conditions.

We further assumed that the hydrophilic surface contains a hydrophobic crack. Such a substrate can be fabricated from poly(dimethyl siloxane) (PDMS)-based polymers. PDMS is hydrophobic, but ultraviolet/ozone (UVO) treatment effectively converts the surface of a PDMS film from hydrophobic to hydrophilic, by production of a thin silica-like surface layer [6]. The surface silica layer has a higher modulus than the underlying PDMS; subjecting such PDMS-silica composite films to sufficiently high strain forces leads to cracking at the surface [6].

With the above materials in mind, we simulated the scenario shown in Figure 3.5, where hydrophobic nanoparticles are encapsulated in a fluid-filled microcapsule, which is localized on a substrate in an aqueous solution. The intact portion of the surface is hydrophilic, but this substrate also encompasses cracks, which expose the underlying hydrophobic domains (e.g., the underlying PDMS). The amphiphilic nature of the capsule allows this colloid to be solubilized in water and

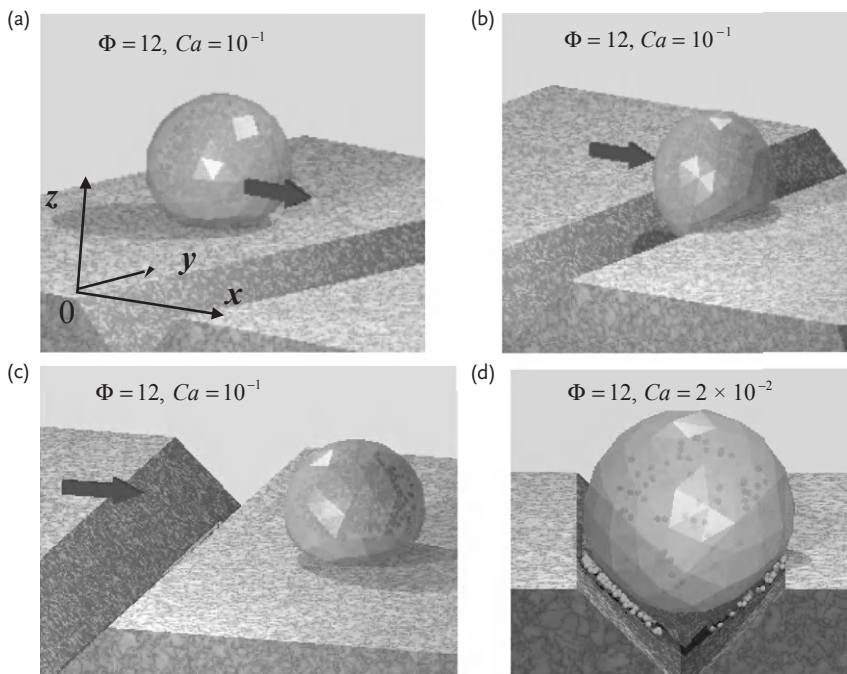


Figure 3.5 Simulation results showing the capsule motion on a damaged surface from its initial position (a) to the interior of the crack (b) and its re-emergence onto the undamaged portion of the surface (c). Here, $Ca = 10^{-1}$ and $\Phi = 12$. (d) Capsule arrested

within the crack at $Ca = 2 \times 10^{-2}$ and $\Phi = 12$. Nanoparticles are visible within the capsules and in the crack under the capsule in (d). Arrows indicate the direction of the imposed shear flow.

attracted to both hydrophilic and hydrophobic portions of the surface. On the other hand, the encapsulated hydrophobic nanoparticles are only attracted to the hydrophobic cracks.

In effect, the enthalpic interactions between the nanoparticles and the hydrophobic crack provide a site-specific response of these particles. As we show below, when the capsule is localized in the crack, the nanoparticles can tunnel through the microcapsule’s shell to bind to and fill the cracked regions. Once the healing nanoparticles are deposited on the desired sites, the fluid-driven capsules can move further along the surface and, for this reason, the strategy was termed “repair-and-go”.

3.3.1

Methodology

To capture the fluid-structure interactions between the flowing fluid and the surface of the compliant capsule, we used our “LBM/LSM” approach [5], which integrates the lattice Boltzmann model (LBM) for the fluid dynamics and the lattice spring model (LSM) for the micromechanics of an elastic solid. The capsule’s elastic, solid shell is represented by a lattice spring model, which consists of a triangular network of harmonic springs that connect regularly spaced mass points, or nodes. The spring force \mathbf{F}_s on node \mathbf{r}_i is equal to $\mathbf{F}_s(\mathbf{r}_i) = -\sum_j k_j [(r_{ij} - r_{ij}^{\text{eq}}) / r_{ij}] \mathbf{r}_{ij}$,

where the summation runs over all nearest- and next-nearest-neighbor nodes. The quantity $\mathbf{r}_{ij} = \mathbf{r}_i - \mathbf{r}_j$ is the radius vector between the i th and j th nodes, r_{ij}^{eq} is the equilibrium length of the spring and k_j is the spring constant. To capture the dynamics of the solid shell, we numerically integrate Newton’s equations of motion, $M(d^2\mathbf{r}_i/dt^2) = \mathbf{F}(\mathbf{r}_i)$, where M is the mass of a node. The total force \mathbf{F} acting on a node consists of the following: the sum of the spring forces between the masses (representing the elastic response of the solid shell), the force exerted by the fluid on the shell at the fluid/solid boundary, and the adhesion forces at the solid substrate (see below).

The capsule’s spherical shell is formed from two concentric layers of LSM nodes; each layer contains $N = 122$ nodes. (A capsule formed from just a single shell is mechanically unstable against finite deformations [19, 20].) These two layers are separated by a distance of $\Delta x_{\text{LSM}} = 1.5\Delta x$, where Δx_{LSM} is the lattice spacing between nearest nodes in the LSM and Δx is the spacing in the LBM (see below). The outer radius of the shell is $R = 5\Delta x$. For small deformations, the LSM system obeys linear elasticity theory and results in a Young’s modulus of $E = 5k_j/2\Delta x_{\text{LSM}}$ [19, 20]. (The use of a larger number of shells or of a larger capsule radius does not change the character of the capsule’s motion [22].)

The LBM can be viewed as an efficient solver for the Navier–Stokes equation [23]. In our LBM/LSM simulations, the fluid and solid phases interact through appropriate boundary conditions. In particular, lattice spring nodes that are situated at the solid/fluid interface impose their velocities on the surrounding fluids; the velocities are transmitted through a linked bounce-back rule [24] to those LBM

distribution functions that intersect the moving solid boundary. In turn, LS nodes at the solid/fluid interface experience forces due to the fluid pressure and viscous stresses at that boundary. We calculate the latter force based on the momentum exchange between the LBM particle and solid boundary, and then distribute this quantity as a load to the neighboring LS nodes. We further assume no-slip boundary conditions at the fluid/solid interface.

The interaction between the capsule and the surface (both the undamaged region and crack wall) is modeled with the following non-specific Morse potential [5]: $\phi(r) = \varepsilon \left(1 - \exp \left[-\frac{(r-r_0)}{\kappa} \right] \right)^2$, where ε and κ characterize the respective strength and range of the interaction potential. Additionally, r is the distance between the LSM node and the substrate surface, and r_0 is the distance at which this force is equal to zero. We set $\kappa = 1$, $r_0 = 1$ and vary ε .

The diffusion of nanoparticles within the encapsulated fluid is described by the following stochastic differential equation: $d\mathbf{r}(t) = \mathbf{u}(\mathbf{r}, t)dt + \sqrt{2D_0}d\mathbf{W}(t)$, where the first term describes the advection due to the local fluid velocity $\mathbf{u}(\mathbf{r}, t)$ and the second term describes the particle's Brownian motion, with D_0 being the particle's diffusion coefficient and $d\mathbf{W}(t)$ being the differential of a Weiner process with unit variance. We neglect backflow effects (i.e., the impact of the particles motion on the flow field); the latter assumption is valid for submicron-sized particles at relatively low concentrations. We also neglect the interactions between the particles. We use a first order Euler scheme to solve the above equation for the particle motion [5].

We simulate the chemisorbtion of nanoparticles onto the crack walls by assigning a probability w_{dep} for a nanoparticle to deposit from the microcapsule's interior onto the surface in a given time step Δt . (Note that the nanoparticles can only bind to the surface when the microcapsule is located in the crack.) This probability has the form $w_{\text{dep}} = k\Delta t e^{-r/r_{\text{tun}}}$. Here r is the distance from the microcapsule's shell to the crack wall, r_{tun} is a characteristic distance over which the probability decays, and k is a characteristic deposition rate, which was set to $k = 1/\Delta t$ in our simulations. We also set the characteristic tunneling distance r_{tun} equal to the distance κ in the Morse potential. A "rejection" rule is applied to those nanoparticles that are not deposited onto the surface at a given time step (i.e., with a probability $[1 - w_{\text{dep}}]$); the variable $\Delta\mathbf{W}$ is set equal to zero for the "rejected" particles and their positions are then updated in accordance with the above equation for the nanoparticle motion.

The profile of the substrate/fluid interface is updated dynamically at each time step; the local elevation of the profile due to the nanoparticle deposition is computed as $h = (4\pi/3)r_{\text{np}}^3 n$ where n is the density of deposited nanoparticles at the wall at a given point. The radius of the nanoparticles, r_{np} , is taken to be 10^3 times smaller than the radius of the microcapsule.

The flat, upper wall of the simulation box is moved with a constant velocity U_{wall} to create a uniform shear rate of $\dot{\gamma} = U_{\text{wall}} / L_z$. We characterize the flow by specifying the dimensionless capillary number $Ca = \dot{\gamma}\mu R / Eh$, where μ is the fluid viscosity, R is the capsule radius, E is the modulus of the shell and h is the shell

thickness. The capillary number represents the relative importance of the viscous stress in the surrounding fluid and the elastic stress in the capsule’s shell. In the simulations, we vary Ca by altering $\dot{\gamma}$, keeping the values of the other relevant parameters fixed. We consider capillary numbers in the range of $10^{-4} \leq Ca \leq 10^{-1}$, which are experimentally reasonable values if we consider the microcapsules to be propelled by an imposed flow in an aqueous solution whose viscosity is $\mu \approx 10^{-3} \text{ kg s}^{-1} \text{ m}^{-1}$ and density is $\rho \approx 10^{-3} \text{ kg m}^{-3}$. Typical velocities in microfluidic devices are of the order of 1 cm s^{-1} and typical channel heights are 100s of microns [25]. For polymeric microcapsules with a diameter of $10 \mu\text{m}$, the stiffness of the shell, Eh , can be of the order of $10^{-3} - 1 \text{ Nm}^{-1}$ [26, 27]. From these values, we obtain capillary numbers of $Ca \sim 10^{-5} - 10^{-2}$, which is approximately the range considered in these simulations.

We also introduce a dimensionless interaction strength $\Phi = \varepsilon N / Eh\kappa^2$, where ε and κ characterize the respective strength and range of the interaction potential; here, N is the number of nodes on the capsule’s outer surface. The parameter represents Φ the ratio of the interaction strength to the membrane stiffness. For $\Phi \gg 1$, this interaction leads to significant deformation of the capsule, while for $\Phi \ll 1$, the effect on the capsule’s shape is small. Herein, we consider $0 < \Phi < 25$, which also corresponds to experimentally realistic values [28].

3.3.2

Results and Discussion

3.3.2.1 Effect of Imposing a Steady Shear Flow

Via the above model, we determined conditions that provide maximal deposition of nanoparticles into the surface crack and thereby, produce effective repair of the substrate. The simulation box is $L_x L_y L_z = 100 \times 40 \times 40$ lattice Boltzmann units in size. Periodic boundary conditions are applied in the x - and y -directions. A well-defined crack is located in the center of the substrate along the y -axis, with the crack tip being located at $x = 0$ (see Figure 3.5). The capsule diameter is equal to $10\Delta x$, where Δx is equal to the lattice spacing in the LBM. The crack depth, d_c , is equal to $5\Delta x$ (i.e., comparable to the capsule radius), and the crack width is equal to $2d_c$.

We focus primarily on the case where the interaction of the microcapsule with the undamaged horizontal substrate and with the crack walls is characterized by the same interaction constant ε . Since the surface of the microcapsule is assumed to be amphiphilic, it can exhibit a comparable interaction with both the intact hydrophilic surface and the hydrophobic crack. We further assume that the deposited hydrophobic nanoparticles do not modify the adhesive properties of the crack walls. (The latter choice is not a necessary constraint of the method: the nanoparticles can dynamically modify the adhesive properties in the simulation [4].)

As shown in Figure 3.5a, the capsule is initially placed on the undamaged, horizontal region of the surface (with its center of mass positioned at $x = -15$) and in the middle of the channel in the y -direction (at $y = 20$). The capsule initially contains $N_{np}(0) = 10^5$ nanoparticles. The particle-filled capsule is propelled toward the

crack by the imposed shear flow; the horizontal arrow in Figure 3.5a shows the direction of the imposed shear. The images in Figure 3.5b,c are for a capillary number of $Ca = 10^{-1}$ and adhesion strength of $\Phi = 12$ and correspond to points in time when the capsule is localized in the crack (Figure 3.5b) and when it has been propelled away from this region by the imposed flow (Figure 3.5c). For the image in Figure 3.5d, the adhesion strength is held fixed, but the shear rate is decreased to $Ca = 2 \times 10^{-2}$ and the figure shows that the capsule has become arrested in the crack as it moved along the surface.

Figure 3.6a shows the time dependence of the capsule's center-of-mass x -coordinate for $\Phi = 2.4$ and for three shear rates, corresponding to $Ca = 2 \times 10^{-2}$, 6×10^{-2} and 1.2×10^{-1} and Figure 3.6b shows a phase map for the system as a

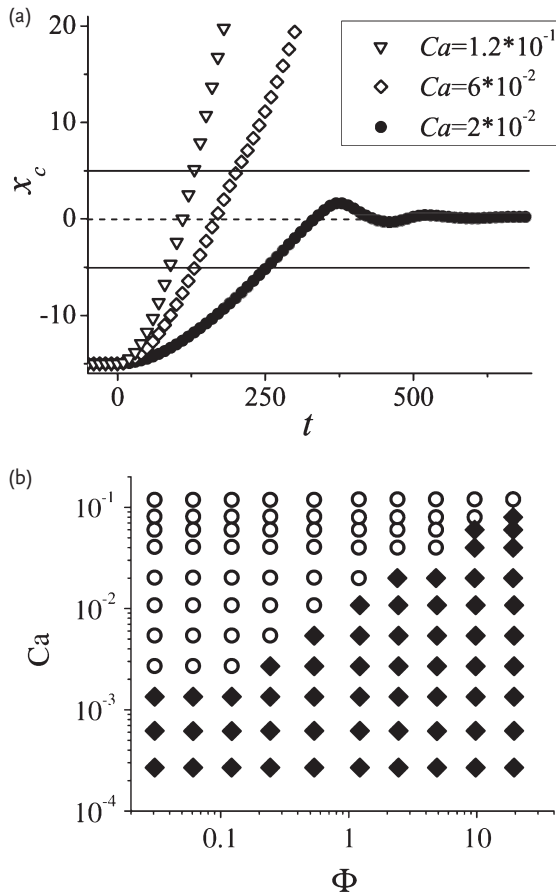


Figure 3.6 (a) Capsule's center-of-mass coordinate x_c as a function of time for different shear rates (expressed in terms of Ca). Solid horizontal lines indicate x -coordinates of the crack boundaries and

the dashed horizontal line indicates the x -coordinate of the crack tip. (b) Phase map as a function of Ca and Φ . In both (a) and (b), open symbols indicate moving capsules and filled symbols indicate arrested capsules.

function of Ca and Φ that indicates the response of the capsules to the imposed flow and the attractive surface. To generate this phase map, we varied the dimensionless interaction strength from weak to strong adhesion, $3 \times 10^{-2} \leq \Phi \leq 24$, and the shear rates, Ca , from 2.7×10^{-4} to 1.2×10^{-1} . For each point, we averaged over three independent runs. These results reveal two general scenarios for the capsule’s motion. For relatively high adhesion or low shear rates (indicated by the solid diamonds in the phase map), the capsule becomes arrested within the crack (as shown in Figure 3.5d). For weaker adhesion and higher shear rates (marked by the empty circles), the capsule moves into the crack, but then exits this region to continue moving along the surface (as seen in Figure 3.5c). In rare events, after the capsule leaves the crack, it bounds off the substrate due to lift forces that arise at high shear rates.

To characterize the nanoparticle layer deposited by the microcapsule onto the crack walls, and, hence, quantify the extent of the repair, we calculated $N_{\text{dep}}(t)$, the total number of nanoparticles deposited by time t . Figure 3.7 shows the behavior

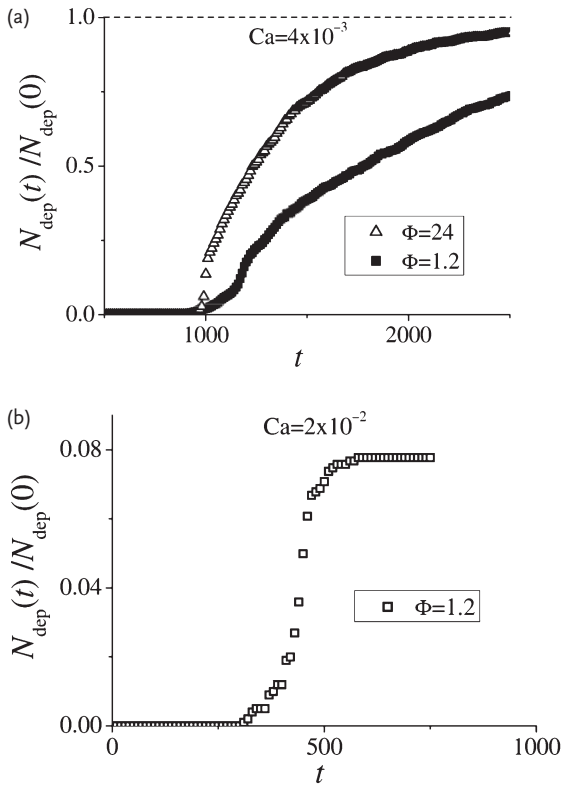


Figure 3.7 Time dependence of $N_{\text{dep}}(t)$, the number of nanoparticles deposited on the crack surface. Number is normalized to the initial number of nanoparticles in the capsule $N_{\text{np}}(0)$. (a) Unfilled triangles and filled

squares indicate arrested capsules. (b) Unfilled squares indicate moving capsules. Respective values of Ca and Φ are marked on the plot.

of $N_{\text{dep}}(t)$ as a function of time for an arrested (Figure 3.7a) and a moving (Figure 3.7b) capsule; here, the quantity is normalized to the total number of nanoparticles initially encased in the microcapsule, $N_{\text{NP}}(0)$. For an arrested capsule, the ratio $N_{\text{dep}}(t)/N_{\text{NP}}(0)$ approaches unity. The total number of deposited nanoparticles provided by a moving capsule, however, is smaller. For example, we obtain $N_{\text{dep}}(t)/N_{\text{NP}}(0) \sim 0.08$ for the case shown in Figure 3.7b.

To summarize, we find that full surface coverage by the nanoparticles can be more readily attained in the case of an arrested capsule, that is, in a “repair” rather than a “repair-and-go” system. In the next section, however, we demonstrate that a pulsatile fluid flow can lead to an effective “repair-and-go” scenario where the micro-carriers not only deliver a high volume fraction of particles into the crack, but also leave the crack and thus, could potentially contribute to repairing additional cracks within the system with the remaining encapsulated particles.

3.3.2.2 Utility of Applying a Pulsatile Flow

We apply a pulsatile shear where the value of the shear rate $\dot{\gamma}(t)$ (and, hence, the capillary number $Ca(t)$) depends on time in the manner shown in Figure 3.8a. In effect, we use the information from the previous section to tailor the motility of the capsule. Specifically, for a fixed Φ , we choose a low capillary number Ca_1 from the region in the phase map where the capsule is arrested within the crack. After a time interval Δt , we then increase the shear rate to Ca_2 so that for the specific Φ , the capsule is in the “free” region of phase space. (We note that the capsule can move along the undamaged portion of the surface for both Ca_1 and Ca_2 .) In the time interval $t_1 < t < t_2$ during which the low shear corresponding to $Ca = Ca_1$ is applied, the capsule can become arrested in a nearby crack, and if this time interval is sufficiently long the micro-carrier can deposit a high density of nanoparticles along the walls of the crack (see below). At $t = t_2$, we increase the shear rate to $Ca = Ca_2$; in other words, we move vertically up in the (Φ, Ca) phase map. The simulations show that at some time $t = t_{\text{out}} > t_2$, the capsule leaves the crack due to the strong drag force from the surrounding fluid and moves further along the surface.

Figure 3.8b shows this behavior for two parameter sets, $Ca_1 = 2 \times 10^{-2}$, $Ca_2 = 6 \times 10^{-2}$ for an adhesion strength of $\Phi = 2.4$ (the case of moderate adhesion), and $Ca_1 = 6 \times 10^{-2}$, $Ca_2 = 1.2 \times 10^{-1}$ for an adhesion strength of $\Phi = 12$ (strong adhesion). The inset in Figure 3.8b shows the variations with time of the center-of-mass x -coordinate of the capsule calculated for the two parameter sets. The capsule is arrested within the crack at a time $t = t_{\text{in}} \sim 100$ and leaves the crack at $t = t_{\text{out}} \sim 1500\text{--}2000$ in both cases. The main plot in Figure 3.8b shows the time dependence of the coverage computed for the two parameter sets. As can be seen, a nearly full deposition $N_{\text{dep}}/N_{\text{NP}}(0)$ (73% for moderate adhesion and 90% for strong adhesion) is obtained for a pulsatile flow. The latter values are significantly above the typical values of $N_{\text{dep}}/N_{\text{NP}}(0)$ ($\sim 10\text{--}20\%$) obtained for a permanently moving or “free” capsule in a steady flow.

As indicated in Figure 3.8, the advantage of using the pulsatile shear is that we can combine high adhesion strength Φ , which provides nearly full nanoparticle

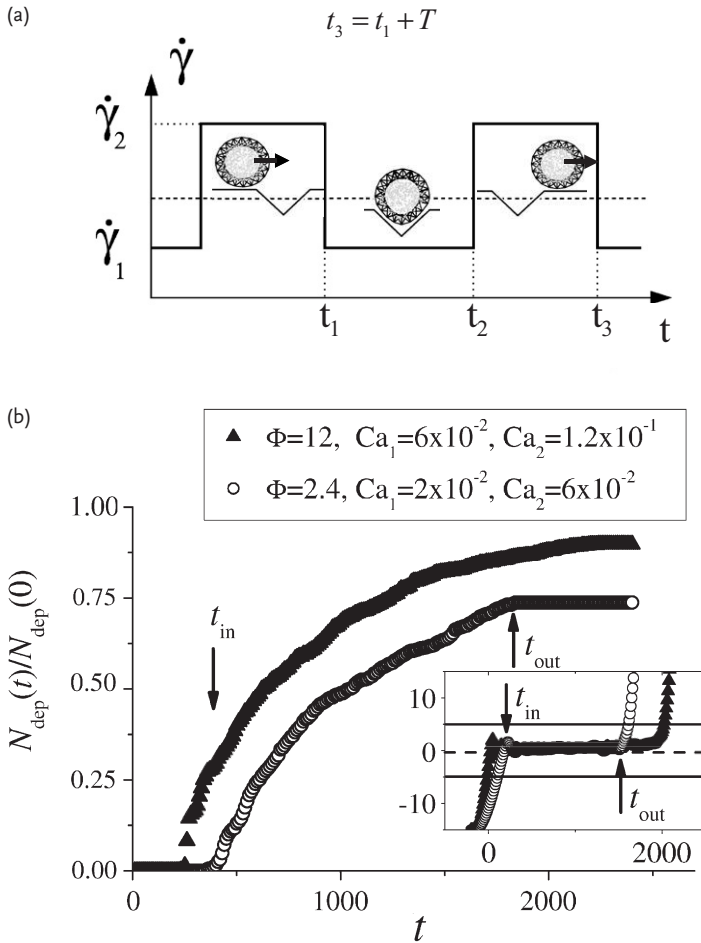


Figure 3.8 (a) Schematic indicating the time dependence of Ca (and thus, $\dot{\gamma}$) for the imposed pulsatile shear flow. The t_1 , t_2 , and t_3 are the points in time when the shear rate is switched. Ca_1 corresponds to an arrested state and the capillary number Ca_2 corresponds to a moving state of the capsule. (b) Time dependence of the nanoparticle coverage calculated for the pulsatile shear

shown for two different sets of parameters. Inset shows the time dependence of the capsule's center-of-mass x -coordinate calculated for the same parameter set as in the main plot. Arrows mark the times when the capsule was arrested in (t_{in}) and exits the crack (t_{out}) for $\Phi = 2.4$. In the simulations, $t_1 = 0$, $t_2 = 1500$, $t_3 = 2500$.

coverage of the crack, with the possibility for a capsule to remain moving along the surface, therefore realizing the basic ideas of a “repair-and-go” system. Additionally, by applying a pulsatile flow, we can control the effective exposure time $t_{exp} = t_{out} - t_{in} \approx t_2 - t_1$ (see Figure 3.8a); that is, the exposure time can be set manually and independently, and can be varied over wide limits. (In the repair-and-go system with a pulsatile shear, the exposure time t_{exp} is defined by the duration of

the low shear portion t_2-t_1 .) Furthermore, we can exploit the attractive features offered by the case of relatively high adhesion strength; namely, the higher Φ affords a more deformable capsule, which in turn contributes to an increased healing rate [5].

3.4 Conclusions

In the first biologically inspired study, our goal was to determine how structural rearrangements arising from the breaking and remaking of labile bonds within a network of cross-linked nanogels could contribute to the mechanical properties and self-healing behavior of the material. We found that the introduction of a small number of labile linkages with $N > 1$ bonds per linkage significantly increased the strength of the material relative to samples that were cross-linked solely by the stable bonds. For example, for $P = 0.7$ and $N = 4$, the critical stress needed to fracture the sample was roughly 200% of that needed to fracture the $P = 1$ sample (where $N = 1$ for these strong bonds).

On the other hand, if we set $N > 4$ for samples in the range $0.6 \leq P < 1$, the nanogel pieces become so strongly inter-connected that they are hindered from shuffling to a new position. Consequently, the material becomes more brittle and the self-healing abilities of the system are effectively lost. The above results indicate that there is an optimal range of labile interconnections that provide high-strength, tough materials that are capable of self-repair.

In the second study, our aim was to design an artificial leukocyte that could affect the repair of a synthetic wound, namely a crack in a surface. Our ultimate goal was to design a system where the nanoparticle-filled capsule would not only aid in the repair of one site, but also travel on to heal other cracks. To this end, we introduced a pulsatile shear flow that involves alternating low and high shear rates. In the low shear rate phase, the pulsatile flow enables the capsule to be localized within a crack for a time Δt . With an increase in the shear rate, however, this capsule is propelled to leave the fissure and thus, be available to carry out further healing of the damaged substrate. Hence, by utilizing the pulsatile flow field, we could achieve the desired “repair and go” functionality in our simulations. (An attractive feature of this system is that the user can tailor the flow profile in order to control the value of Δt .)

We note that in the above studies, we focused on the action of a single microcapsule, allowing us to isolate the factors that control the dynamic behavior of this micro-carrier. In the actual physical system, which involves a solution of microcapsules moving in a microchannel, there is a high volume fraction of microcarriers available to repair the surface and thus, the cracks could potentially be completely filled by deposited nanoparticles. For the chosen interaction parameters, the amphiphilic capsules would then move over these repaired areas and go onto other locations where they are needed.

References

- 1 Smith, B.L., Schäffer, T.E., Viani, M., *et al.* (1999) *Nature*, **399**, 761–763.
- 2 Kolmakov, G.V., Matyjaszewski, K., and Balazs, A.C. (2009) *ACS Nano*, **3**, 885–892.
- 3 Salib, I.G., Kolmakov, G.V., Gnegy, C.N., Matyjaszewski, K., and Balazs, A.C. (2011) *Langmuir*, **27**, 3991–4003.
- 4 Verberg, R., Dale, A.T., Kumar, P., Alexeev, A., and Balazs, A.C. (2007) *J. R. Soc. Interface*, **4**, 349–357.
- 5 Kolmakov, G.V., Revanur, R., Tangirala, R., Emrick, T., Russell, T.P., Crosby, A.J., and Balazs, A.C. (2010) *ACS Nano*, **4**, 1115–1123.
- 6 Kratz, K., Narasimhan, A., Tangirala, R., Moon, S.C., Revanur, R., Kundu, S., Kim, H.S., Crosby, A.J., Russell, T.P., Emrick, T., Kolmakov, G., and Balazs, A.C. (2012) *Nat. Nanotechnol.*, **7**, 87–90.
- 7 Lee, J.Y., Shou, Z., and Balazs, A.C. (2003) *Phys. Rev. Lett.*, **91**, 136103.
- 8 Lee, J.Y., Buxton, G.A., and Balazs, A.C. (2004) *J. Chem. Phys.*, **121**, 5531.
- 9 Smith, K.A., Tyagi, S., and Balazs, A.C. (2005) *Macromolecules*, **38**, 10138–10147.
- 10 Tyagi, S., Lee, J.Y., Buxton, G.A., and Balazs, A.C. (2004) *Macromolecules*, **37**, 9160–9168.
- 11 Gupta, S., Zhang, Q., Emrick, T., Balazs, A.C., and Russell, T.P. (2006) *Nat. Mater.*, **5**, 229–233.
- 12 Balazs, A.C., Emrick, T., and Russell, T.P. (2006) *Science*, **314**, 1107–1110.
- 13 Ackbarow, T., Chen, X., Keten, S., and Buehler, M.J. (2007) *Proc. Natl Acad. Sci. U. S. A.*, **104**, 16410–16415.
- 14 Oh, J.K., Tang, C., Gao, H., Tsarevsky, N.V., and Matyjaszewski, K. (2006) *J. Am. Chem. Soc.*, **128**, 5578–5584.
- 15 Min, K., Gao, H., Yoon, J.A., Wu, W., Kowalewski, T., and Matyjaszewski, K. (2009) *Macromolecules*, **42**, 1597–1603.
- 16 Oh, J.K., Drumright, R., Siegwart, D.J., and Matyjaszewski, K. (2008) *Prog. Polym. Sci.*, **33**, 448–477.
- 17 Tsarevsky, N.V., Min, K., Jahed, N.M., Gao, H., and Matyjaszewski, K. (2006) *ACS Symp. Ser.*, **939**, 184–200.
- 18 Kamada, J., Koynov, K., Corten, C., Juhari, A., Yoon, J.A., Urban, M.W., Balazs, A.C., and Matyjaszewski, K. (2010) *Macromolecules*, **43**, 4133–4139.
- 19 Buxton, G.A., Care, C.M., and Cleaver, D.J. (2001) *Model. Simul. Mater. Sci. Eng.*, **9**, 485–497.
- 20 Ladd, A.J.C., Kinney, J.H., and Breunig, T.M. (1997) *Phys. Rev. E*, **55**, 3271–3275.
- 21 Bell, G.I. (1978) *Science*, **200**, 618–627.
- 22 Maresov, E.A., Kolmakov, G.V., Yashin, V.V., Van Vliet, K.J., and Balazs, A.C. (2012) *Soft Matter*, **8**, 77–85.
- 23 Succi, S. (2001) *The Lattice Boltzmann Equation for Fluid Dynamics and Beyond*, Clarendon Press, Oxford.
- 24 Lallemand, P., and Luo, L.-S. (2000) *Phys. Rev. E*, **61**, 6546–6562.
- 25 Stone, H.A., Stroock, A.D., and Ajdari, A. (2004) *Annu. Rev. Fluid Mech.*, **36**, 381–411.
- 26 Dubreuil, F., Elsner, N., and Fery, A. (2003) *Eur. Phys. J. E*, **12**, 215–221.
- 27 Elsner, N., Kozlovskaya, V., Sukhishvili, S.A., and Fery, A. (2006) *Soft Matter*, **2**, 966–972.
- 28 Alexeev, A., Verberg, R., and Balazs, A.C. (2005) *Macromolecules*, **38**, 10244–10260.

Part Two
Polymer Dynamics

4

Structure and Dynamics of Polymer Chains

Ana Rita Brás, Wim Pyckhout-Hintzen, Andreas Wischnewski, and Dieter Richter

4.1

Foreword

Polymers form a sub-class of typical soft matter systems and exhibit a wealth of dynamical and mechanical properties which are intimately related to their particular molecular structure or constitution. On a higher level a supramolecular association of them is able to assemble spontaneously by reversible noncovalent connections, of which hydrogen bonds are an example. One of the fascinating aspects of a self-assembly of supramolecular polymers is the possibility of controlling the structure, adding functionalities, adjusting the macroscopic properties and taking profit from the non-trivial dynamics associated with the reversibility of hydrogen-bond links. Such supramolecular polymers carrying functional end-groups are named telechelic. In this predominantly introductory treatise we will present a combined approach of macroscopic and neutron scattering techniques, the latter of which profits from the controlled exchange of hydrogen by deuterium atoms. We will show that neutron scattering plays a unique role due to the exquisite sensitivity to the local and global structure. The associated dynamics sheds light on details of the relaxation mechanisms and in view of this contribution also on the reversibility character of self-healing materials, the inherent nanostructuring and its implication for emerging new elastic macroscopic properties. Since a basic knowledge of polymer dynamics is a prerequisite for the final understanding of these systems on the microscopic level we will review descriptions of the structure and the dynamic relaxation behavior of simple polymeric systems, covering all relevant length and time scales, always in the combination of rheology and neutron scattering. The transition of short unentangled chains to tube-controlled dynamics is treated. Subsequently the class of functionalized telechelic polymers will be reviewed from the same aspect. Questions of molecular interpretations, in particular on which length and time scales the dynamics of the telechelic group or hydrogen bonding in such polymers control or change the parent material by the presence of a reversible non-covalent link and some key experiments will be addressed, with particular emphasis on the self-healing mechanisms. Finally, in the conclusion we will give an outlook on future developments and opportunities with the help of neutron scattering techniques.

4.2 Techniques

Soft matter is a broadly defined complex topic which covers biological materials, macromolecules and colloidal systems. The interest in soft matter has increased considerably in recent years due to the fact that new developments for special purposes have become available like for example, intelligent and shape-memory polymers, stimuli-responsive gels and the self-healing materials described in this book.

The typical dynamical range in which mechanisms display their activity covers generally more than 10 decades in the time and at the same time length scales, from atomic dimensions like conformational transitions up to global chain dimension in flow. The present contribution will not be dedicated to the standard techniques of characterization, like dynamic mechanical analysis, dielectric spectroscopy and so on, but merely will introduce the strength of neutron-based methods in a complementary way. The neutron is an outstanding tool as it probes the time scale at the particular spatial scale at which the dynamical process takes place. Typical limits of resolution are femtoseconds up to microseconds, controlled by the characteristic energies of the neutron beam (see Figure 4.1). The sensitivity comes from the different scattering which deuterium shows compared to that of hydrogen, which allows one to investigate single (macro)molecule physics by applying sophisticated labeling schemes. Neutron investigations correlate extraordinarily well with the following techniques:

- Dynamic mechanical analysis (DMA), which in the broadest sense relates the answer of the system to some small external perturbation, is able to separate the total complex modulus $G^*(\omega)$ into contributions which are in phase or out

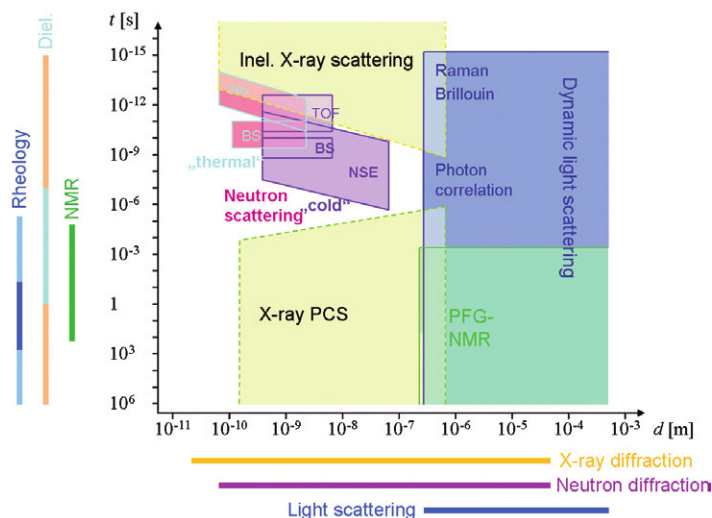


Figure 4.1 Comparison between different inelastic scattering methods and standard techniques for polymer characterization.

of phase with the perturbation, highlighting the pronounced viscoelasticity of the systems. By temperature variation the accessible time range can be roughly shifted from 1 μ s up to 1 Ms. However, no microscopic detail on the process concerning spatial scales is within reach.

- Dielectric spectroscopy (DR) makes use of the dynamic electric permittivity $\epsilon^*(\omega)$. Whereas the method is rather limited to type A polymers in order to study global dynamics it covers the broader range of times from 1 ns up to 10 Ms. Even though the lack of structural aspects is prominent too, this technique can distinguish which of the observed dynamics is either segmental or global. Also their time scales are widely separated. Particularly, in this context it allows one to study the influence of intra- and intermolecular hydrogen bonds in the dynamics of functionalized polymers. At the same time it is complementary to calorimetry in glass transition studies.
- Nuclear magnetic resonance (NMR) techniques measure the response of nuclear spins but the information cannot compete with the isotopic substitution in neutron scattering. The information is very local and very atomic-bound. Particularly useful in the present context is the pulsed field gradient nuclear magnetic resonance (PFG-NMR) which measures molecular diffusion in the range of μ m in a time range that exceeds that of dynamic neutron scattering by at least 1 or 2 orders of magnitude.

Therefore this contribution will try to bring and link together rather well known aspects of polymer dynamics with neutron investigations. It should be noted as well that the neutron is extremely gentle. The strength of this approach to understanding how matter flows lies in the use of complementary techniques. This chapter is not meant as a course but should stimulate the reader to further study of the literature.

4.3

Structure

Polymers are simple coiled molecules, the structure of which varies from flexible to rigid in the case of rods [1–4]. Their configuration is the result of brownian dynamics, which therefore leads to an enormous amount of possible configurations. This necessitates one to determine both the static structure of their time-averaged structures and their dynamic behavior to complete the understanding. How can we calculate the size? For this, basic models for linear chains were developed in the past with different levels of sophistication and approximations. We will simply summarize this here and introduce at this stage also the corresponding length scales.

The simplest model to deal with is the freely jointed chain (FJC). An example of such a configuration is shown in Figure 4.2 and illustrates the idea that polymer chains are performing random walks. With this, the ensemble of systems can be characterized by average quantities. One is the so-called end-to-end vector,

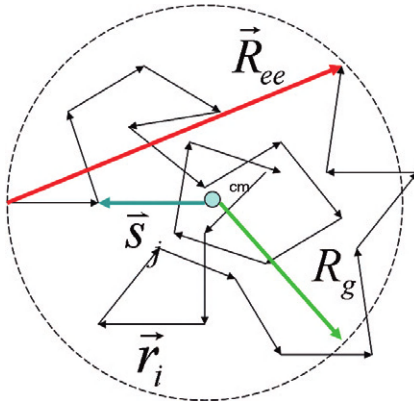


Figure 4.2 A freely jointed chain and definitions.

$$\bar{R}_{ee} = \sum_{i=1}^N \bar{r}_i \quad \text{with} \quad R_{ee}^2 = \sum_{i,j=1}^N \bar{r}_i \bar{r}_j \quad (4.1)$$

The bond vector connecting two atoms is \bar{r}_i with average length l_0 . A parameter which has its counterpart in classical mechanics is the radius of gyration:

$$R_g^2 = \frac{1}{N+1} \sum_{i=0}^N \bar{s}_i^2 \quad (4.2)$$

where now the vectors \bar{s}_i are the distance vectors with respect to the center of mass and N is the total number of bonds (or steps).

Averaging over all conformations leads, for the case of a fully freely jointed chain, to a mean squared end-to-end distance of

$$\langle R_{ee}^2 \rangle = \sum_{i,j=1}^N \langle \bar{r}_i \bar{r}_j \rangle = Nl_0^2 + 2 \sum_{i<j} \langle \bar{r}_i \bar{r}_j \rangle \quad (4.3)$$

The average end-to-end distance $\langle R_{ee} \rangle = 0$ due to the ensemble average. The calculation of $\langle R_{ee}^2 \rangle$ which characterizes the full size of a chain, constituting about the diameter of a hypothetical sphere including the full chain, can now be performed for different chain models. The FJC chain model assumes an equal probability in 3D of all bond vectors, random bond rotation angles, while keeping the bond length constant. The orientation of each segment or bond is therefore independent of all others and as a consequence the second term, which is the scalar product in Eq. (4.3), averages out to zero. The mean radius of gyration can then generally be obtained as

$$\langle R_g^2 \rangle = \frac{Nl_0^2}{6} \quad (4.4)$$

From both end-to-end distance and radius of gyration, an important conclusion which applies to polymer chains in the bulk or theta state can be drawn: the size

depends on the square root of the number of basic steps, \sqrt{N} . This is a result which has its equivalent in the random walk statistics where now the position of the monomers is replaced by the trajectory of a randomly-diffusing particle and so the variable becomes the time, \sqrt{t} .

However, real polymers are not connected freely jointed. Instead, bond angles assume well-defined values, and correlations between bonds within the chain as well as from the environment will affect the size. Intuitively it can be understood that these correlations will vanish with increasing separation distance. In addition, the flexibility of polymer chains is restricted by the fact that rotations with so-called bond rotation or torsional angles are enabled within a certain range only, due to steric reasons. If we take the FJC model as the reference then the difference to real polymers can be quantified in terms of a local stiffness parameter, C_∞ . This is defined as

$$C_\infty = \frac{\langle R_{ee}^2 \rangle}{Nl_0^2} \quad (4.5)$$

Thus, for perfect flexibility, $C_\infty = 1$.

Experimentally, the parameter as determined from small angle neutron scattering (SANS) investigations is found to be in the range between 3 and 10. Highly-coiled polymers are characterized by low C_∞ values, whereas extended or loosely-coiled chains show, on the contrary, high values. If we consider real chains to be built up from N monomers (instead of bonds), then the chain end-to-end distance becomes

$$\langle R_{ee}^2 \rangle = C_\infty N n_b l_0^2 = Nl^2 \quad (4.6)$$

Here, n_b is the number of backbone bonds per monomer with mean squared bond length l_0^2 and l is the statistical segment length per monomer. The often used Kuhn segment step length, l_k is defined as the minimum length scale above which a real chain behaves again like the freely jointed one. Whereas $l = \sqrt{C_\infty n_b} l_0$, the latter is determined by $l_k = C_\infty l_0$ and $N_K = N/C_\infty$. Due to the direct comparison of molecular weights, provided by the synthetic chemists, with computations for the end-to-end distance, the definition of the statistical segment length per monomer is more favored but this is, however, not a strict rule [3]. Further, it can be shown that the distribution of the end-to-end vector is Gaussian, a result which is valid for any intramolecular distance as

$$p(R) = \left(\frac{3}{2\pi \langle R^2 \rangle} \right)^{3/2} \exp(-3R^2 / 2 \langle R^2 \rangle) \quad (4.7)$$

The chain dimension and characteristic lengths of a polymer chain can be measured by means of the static structure factor $S(Q)$ as obtained from SANS [5, 6]. Here, Q is the scattering vector, that is, the norm of the difference between the incoming k_i and scattered k_f wave vectors, which in the elastic case, that is, no exchange of energy with $k_i = k_f$, is given by

$$Q = |\vec{k}_i - \vec{k}_f| = \frac{4\pi}{\lambda} \sin\left(\frac{\theta}{2}\right) \quad (4.8)$$

where θ is the scattering angle. With the scattering vector a length scale of typically $2\pi/Q$ is connected, which immediately can be assigned to the chain dimension parameters. The SANS method is reviewed in several text books and it suffices to state here that the accessible wavelength range that is obtained from a typical reactor equipped with a cold neutron source matches the size and resolution from the nm to μm scale. Its power resides especially in the property that single polymers, or just pieces of them, can be highlighted without modifying the mechanical or flow properties. Deuterium scatters neutrons very differently from hydrogen and does not affect in good approximation any property.

For a dilute single chain in a melt that is, without inter-chain correlations the static structure factor is written by a sum over all possible pairs of intra-chain monomers i, j reflecting all possible interferences of elementary waves originating from monomer pairs. For a Gaussian distribution of the $\vec{R}_i - \vec{R}_j$ we write that

$$S(Q) = \frac{1}{N} \sum_{i,j}^N \langle \exp(i\vec{Q}(\vec{R}_i - \vec{R}_j)) \rangle \quad (4.9)$$

$$= \frac{1}{N} \int_0^N di \int_0^N dj \exp\left(-\frac{1}{6}Q^2 \cdot |i - j| \cdot l^2\right) \quad (4.10)$$

The result of this double integral reads:

$$S(Q) = \frac{2N}{R_g^4 Q^4} [\exp(-R_g^2 Q^2) - 1 + (R_g^2 Q^2)] \quad (4.11)$$

which is the so-called Debye function. Asymptotic forms of $S(Q)$ are given by:

$$S(Q) = N(1 - R_g^2 Q^2 / 3) \text{ for } QR_g \ll 1 \quad (4.12)$$

$$= 2N / R_g^2 Q^2 \text{ for } QR_g \gg 1 \quad (4.13)$$

Since R_g^2 scales with N , the high Q -expansion yields directly C_∞ , or equivalently the statistical segment l .

Whereas the above applies to linear chains only, the SANS method is also extremely sensitive to different architectures. Within the Gaussian chain statistics form factors $S(Q)$ can be derived as well for star-like, comb-like or, for example, also ring-like structures, which differ in well-defined scattering vector ranges. They allow investigations of branched polymers or cyclics which, in the light of the subject of self-healing, may well appear. Figure 4.3 shows the normalized form factor for a star polymer in both log-log and Kratky representation. The stars differ only in the number of arms, whereas the linear chain is retrieved in the limit as a 2-arm star. It is clear how the architecture influences the observed scattering intensity.

4.4 Dynamics

In Section 4.3 we introduced the important length scales in polymers and briefly discussed the static structure which can be measured in a dense system by means

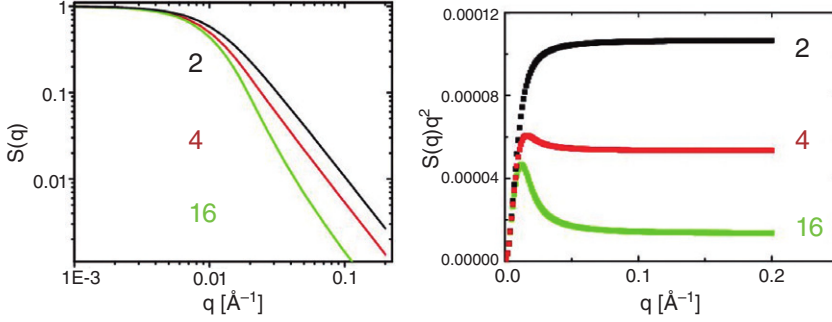


Figure 4.3 Log-log and Kratky representation of theoretical star form factors with varying functionality. The linear chain is a 2-arm star and yields the upper Debye function. For high functionality the form factor approaches the limit of a spherical particle.

of the SANS technique. Quasi-elastic dynamic scattering by, for example, the neutron spin echo (NSE) technique, however, is now able to resolve energies in the μeV – neV range. Motions of scatterers are detectable by velocity changes of the neutron, whereas the spatial character of the motion is inferred from the angular distribution of the scattered neutrons. The energy and momentum which were transferred by the scattering process are characterized by the initial (suffix i) and final state (suffix f):

$$\Delta E = \hbar\omega = E_i - E_f \quad (4.14)$$

$$\Delta \vec{p} = \hbar\vec{Q} = \hbar(\vec{k}_i - \vec{k}_f) \quad (4.15)$$

For the case of $E_i = E_f$, the scattering process is called elastic. This also means that $k_i = |\vec{k}_i| = k_f = |\vec{k}_f| = \frac{2\pi}{\lambda}$. Q was defined before.

We refrain from further details which can be found in the specialized scattering literature.

NSE spectroscopy directly measures the coherent scattering function in the time domain on the SANS-length scale, also called the intermediate scattering function, and is calculated similarly as

$$S_{\text{coh}}(Q, t) = \frac{1}{N} \sum_{i,j=1}^N \langle e^{-i\vec{Q}\vec{R}_i(0)} e^{i\vec{Q}\vec{R}_j(t)} \rangle \quad (4.16)$$

Note that for $t = 0$ the $S(Q)$ as measured by SANS is obtained.

The respective incoherent scattering function is given as

$$S_{\text{inc}}(Q, t) = \frac{1}{N} \sum_{i=1}^N \langle e^{-i\vec{Q}\vec{R}_i(0)} e^{i\vec{Q}\vec{R}_i(t)} \rangle \quad (4.17)$$

Note the difference in the indices. Whereas the coherent scattering from blends of labeled and unlabeled chains yields directly the single chain dynamic structure factor, the incoherent version from unlabeled systems allows one to directly extract

the segmental mean-squared displacement. It is a matter of choice which to use depending on what physical property is looked for. However, since in the coherent case the form factor shifts the intensity into the NSE-Q-region, whereas in the incoherent case it is scattered in 4π , the former is much easier to measure. We will not discuss the incoherent application in this context.

The developed Gaussian chain picture can now be exploited as a good basis for the observed macroscopic dynamics of polymers which is pronounced viscoelastic, that is, contains both properties that resemble rubbers and those similar to viscous fluids. They occur over a wide range of length and time scales. The relaxation modulus $G(t)$, and $G'(\omega)$ which is the real part of the Fourier transformation of $G(t)$, as shown in Figure 4.4 displays several regions with characteristic time dependences. Note that $G(t)$ is in good approximation equal to $G'(1/\omega)$. The strong decay of the shortest times, that is, highest frequencies in total complex modulus $G^*(\omega)$ is due to local fast equilibration mechanisms on typical length scales of 10–50 Å within the chain. The intermediate to long times can be discussed in a mean field-like approach of particular interactions between chains. The concept shows a strong analogy to that of a chain which is restricted locally and dynamically to a soft confinement channel with an interaction radius that must depend on the local stiffness and statistics of the chain under consideration. This tube model, as depicted in Figure 4.5, was constructed by DeGennes and Doi and Edwards [7] originally for networks and melts. The chain itself is Gaussian that is, performs random walk statistics. The allowed motions are curvilinear along and perpendicular to the mean path of the polymer, the latter, however, are limited by

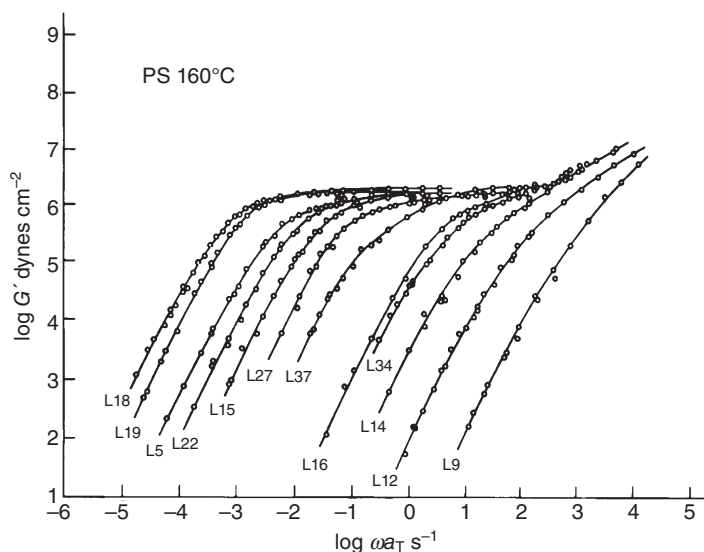


Figure 4.4 The mastercurve of the storage modulus $G'(\omega)$ of PS at reference temperature of 160°C for molecular weights between 9 and 600 kg mol⁻¹, showing Rouse and entangled dynamics. Taken from [7].

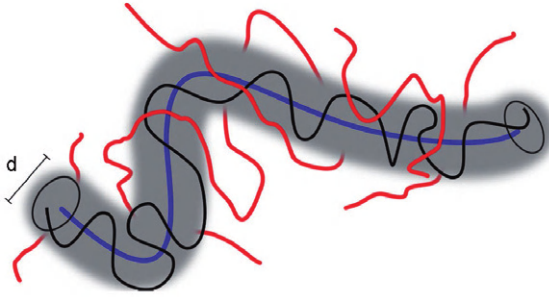


Figure 4.5 Schematic illustration of the tube concept. The lateral confinement of a polymer chain is represented by a tube with diameter d formed by adjacent chains. Figure taken from [8].

the tube diameter. As this chapter is not intended to be a review, we could use the size of this tube to separate between Rouse and tube models. Logically in the reviewing literature the tube concept is introduced only after the simplest treatment of phantom chains in a heat bath.

4.4.1

The Rouse Model

This model is best viewed to be a limiting case: topological inter-chain interactions are fully absent and a working hypothesis would be to assign to the tube diameter a larger length scale than the path length of the chain itself. Connected with the used Gaussian model for chains, the elasticity is of entropic character and any perturbations are counteracted by harmonic restoring spring forces. Thus the Rouse model is that of an artificial chain, which consists of beads and spring connectors. Furthermore, for the beads to move, a local friction, which is determined by the identical polymer surrounding, is to be overcome. This friction is the sum of all frictions in the chains. The equation of motion of such a Rouse chain in a heat bath can be solved analytically using normal coordinates and can be found in the text books. The main outcome of this is

$$\eta_0 = \frac{\xi_0 l^2 N \rho}{36} \quad D = \frac{kT}{\xi_0 N} \quad (4.18)$$

which can be easily verified from rheological and dielectric spectroscopy investigations. l is the statistical segment length and N the number of monomeric beads. Here η_0 is the zero shear viscosity and D is the diffusion coefficient. The zero-shear rate viscosity η_0 depends obviously directly on the molecular weight via N with monomeric friction coefficient ξ_0 . The translational diffusion coefficient of the center of mass is inversely proportional to the molecular weight.

A first microscopic proof of this is provided by means of neutron scattering through the coherent intermediate Rouse scattering function. The segmental

friction determines the relaxation time $\tau_R = \frac{\xi_0 N^2 l^2}{3\pi^2 k_B T}$ in $S(Q, t)$:

$$S(Q, t) = \frac{1}{N} \sum_{i,j} \exp \left[-Q^2 D t - \frac{1}{6} Q^2 |i - j| l^2 - \frac{2Q^2 N l^2}{3\pi^2} \sum_{p=1} \frac{1}{p^2} \cos \left(\frac{p\pi j}{N} \right) \cos \left(\frac{p\pi i}{N} \right) [1 - \exp(-t p^2 / \tau_R)] \right] \quad (4.19)$$

The global dynamics is determined by the center-of-mass diffusion in the first term, the second term describes the correlation due to the structure of the Gaussian chain and the internal dynamic contributions by means of the Rouse modes are given in the third term. τ_R is the longest characteristic time corresponding to the first mode with the longest wavelength $p = 1$.

The Rouse model provides a good description of the dynamics of a Gaussian chain on an *intermediate* length scale in terms of two parameters $Nl^2 = 6R_g^2$ and l^2/ξ , that is, the dimension of the chain and an effective friction.

The friction parameter ξ/l^2 is often expressed in terms of the so-called *Rouse-rate*:

$$Wl^4 = 3k_B T l^2 / \xi \quad (4.20)$$

and the center-of-mass diffusion may be expressed as:

$$D = \frac{k_B T (l^2 / \xi)}{6R_g^2} = \frac{Wl^2}{3N} \quad (4.21)$$

Figure 4.6 shows an example of a PEE melt single chain dynamic structure factor at $M_w = 2 \text{ kg mol}^{-1}$ described with Eq. (4.19).

4.4.2

The Tube Model

The dynamics of short unentangled polymer melts (i.e., in the former simulated by letting the topological tube $d \rightarrow \infty$) has been proven to follow the Rouse model, which is a simple but very successful ansatz to describe the segmental motion of a polymer chain in a heat bath by a balance of viscous and entropic forces [1], as described above. Longer polymer chains mutually interpenetrate, that is, they entangle (see the sketch represented in Figure 4.5). The significantly slowed down dynamics of long chain melts as observed in for example, $G(t)$ can now be successfully described by means of the introduced reptation/tube model.

For short times the chain segments undergo free Rouse dynamics until their mean squared displacement (m.s.d.) becomes comparable to the diameter of the tube. After the so-called entanglement time τ_e the segmental fluctuations are forced to equilibrate along the full tube profile, a process which is called local reptation ($\sim \tau_R$). Finally, the chain may diffuse out of the tube, the true reptation process ($\sim \tau_d$), before it can undergo free Fickian diffusion. In fact it is straightforward to predict the time dependences of the m.s.d. for these different regimes:

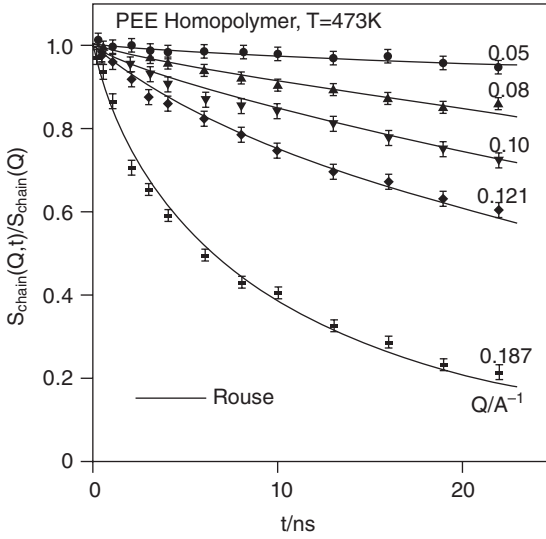


Figure 4.6 Single chain dynamic structure factor from a PEE melt at 473 K. The numbers along the curves represent the experimental Q -values in \AA^{-1} . The solid lines are a joint fit with the Rouse model (Eq. 4.19). Figure taken from [9].

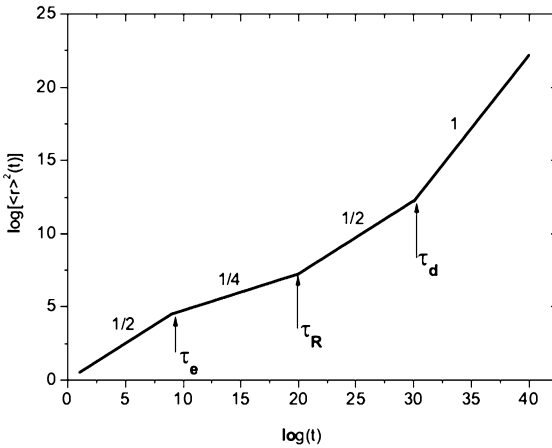


Figure 4.7 Schematic representation of the segmental mean square displacements versus time in a double logarithmic plot. Taken from [10].

Since the tube is a random walk in space, the segmental fluctuations following the tube profile in the local reptation regime have a time dependence which is the square root of that in the Rouse model, that is, $\sqrt{t^{1/2}} = t^{1/4}$. The same argument holds for the reptation process, where a free diffusion (m.s.d. $\sim t^1$) is forced to take place along the random walk tube, yielding a $t^{1/2}$ dependence before the region of free diffusion is reached (proportional t^1). Figure 4.7 shows the m.s.d. predicted by the reptation model as explained. We refer to the literature.

The distinct t -independent plateau in $G(t)$ is the immediate signature of the topological constraints in a network-like system. The subsequent nearly single-exponential decay with flow at long times describes the disentangling and dissolution of the tube. Whereas in the Rouse model for short chains the melt viscosity at zero shear rate, that is, at long times, was found to scale with $\eta_0 \sim N$, now for long chains with entanglement interaction $\eta_0 \sim N^{3.4}$ is found.

The transition between the two different regimes is at a critical molecular weight, M_c which is roughly twice the molecular weight between pair-wise entangled chains, called the entanglement molecular weight M_e .

This allows us to specify the three different time scales which are connected with the relaxation on a certain length scale of the structure. The cross-over times are respectively τ_e , τ_R and τ_d , which denote the entanglement time, the longest Rouse chain relaxation time, and the time to reptate out of the tube. The new parameter is the tube diameter d . Assuming Gaussian statistics, the diameter is equivalent to the end-to-end distance of a chain with a number of segments N_e that spans this distance, and therefore is written as $R_{ee}^2(M_e) = d^2 = N_e l^2$. This length scale is directly related to τ_e . Although slightly different definitions for the latter entanglement time are found throughout the literature, mainly due to their special derivation from different asymptotic representations, we would like to stick to that which complies with the mean square displacements of the reptation model. In terms of the parameters used in the Rouse description this yields

$$\tau_e = \frac{\pi d^4}{36Wl^4} \quad (4.22)$$

This point in time marks the transition from free Rouse-behavior to restricted motion.

Similarly to the polymer chain which is a succession of monomers, the longitudinal tube can be viewed as a succession of isotropic segments of length and diameter d , and its structure is identical to that of a coarse-grained Gaussian random walk chain with persistent length d . The number of entanglements Z per chain is given by:

$$Z = \frac{N}{N_e} = \frac{Nl^2}{d^2} \quad (4.23)$$

and therefore the length L_0 of the tube is:

$$L_0 = Zd = \frac{Nl^2}{d} \quad (4.24)$$

Thus the entanglement time τ_e is the longest relaxation times τ_R of a chain with N_e segments $\tau_e = \tau_R(N_e)$. The longest time needed by a polymer to escape completely its tube (before undergoing normal Fickian diffusion), τ_d becomes

$$\tau_d = \frac{1}{\pi^2} \frac{\zeta N^3 l^4}{k_B T d^2} \quad (4.25)$$

comparing τ_R to τ_d delivers the relation:

$$\frac{\tau_d}{\tau_R} = 3 \cdot Z \quad (4.26)$$

The non-relaxed stress is expressed by the tube occupation function $\mu(t)$ as:

$$\mu(t) = \frac{L(t)}{L_0} \quad (4.27)$$

where L_0 is the initial length and $L(t)$ the remaining occupied tube length after a time t . Considering only pure reptation, $\mu(t)$ decays almost single-exponentially as [7]:

$$\mu_{\text{rep}}(t) = \sum_{p=1, \text{odd}} \frac{8}{p^2 \pi^2} \cdot e^{-\frac{p^2 t}{\tau_d}} \quad (4.28)$$

By Fourier transformation of $G(t) = G_e \mu(t)$, with G_e the modulus of the plateau region, it can be shown that for times $t < \tau_d$ or $\omega > \omega_d = 1/\tau_d$ [7, 11, 12]:

$$G''_{\text{rep}}(\omega) \propto \omega^{-1/2} \quad (4.29)$$

Since the melt viscosity $\eta_0 = \pi^2/12 G_e \tau_d$ it therefore should scale with N^3 . Experimentally η_0 scales with N^α (with $\alpha \geq 3.4$). Therefore the reptation model must be improved taking into account higher order relaxation processes. The most important are contour length fluctuations (CLF) and constraint release (CR).

The effective tube length $L(t)$ is a function of time because chain fluctuations ΔL liberate tube portions at both ends of the tube: each time a chain end is retracted into the tube, the vacated tube segment is lost. The number of tube segments confining the chain under consideration is, therefore, reduced with increasing time. The free ends lose their orientation and “dilute” the entanglement network. Here, no motion of the center of mass is involved. The shortening of the occupied tube implies a reduction of the reptation time as well. A renormalized time τ_{dr} (affecting Eq. 4.28) has been proposed from a solution of the first passage problem [13] according to Likhtman as:

$$\tau_{\text{dr}} \sim \tau_d \left(1 - \frac{C}{\sqrt{Z}} \right) \quad (4.30)$$

with C of the order of 1. The correction is quickly saturated by the $1/\sqrt{Z}$ dependence. For the calculation of the time-dependent tube segment occupation function accounting for contour length fluctuations we refer to the original literature. Figure 4.8 summarizes how reptation and contour length fluctuations both affect the dynamic modulus ($G''(\omega)$) and the dielectrical permittivity loss moduli ($\epsilon''(\omega)$).

Since the tube is a topological entity constituted itself of chains undergoing the same dynamics as the confined chain under consideration, it cannot be described as fixed in time. While exploring their surrounding, free ends are interacting with their neighbors and remove the constraints that they may have been exerting: therefore entanglements can be released. The most accurate description of CR was delivered by Rubinstein and Colby [2] who defined a relaxation spectrum of the tube $R(t)$ self-consistently to the tube survival relaxation spectrum, $\mu(t)$ (already

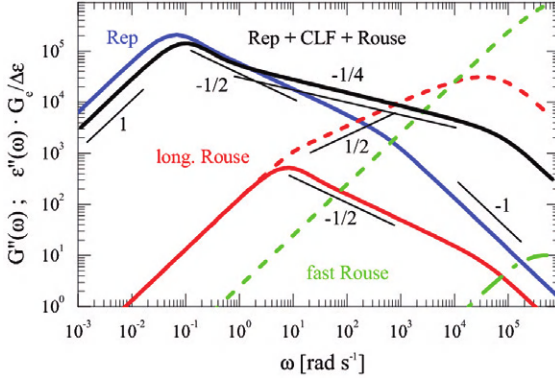


Figure 4.8 Calculated contributions to the normalized $G''(\omega)/G_e$ and $\varepsilon''(\omega)$ for an entangled polymer according to the Likhtman approach [13]. G_e is the plateau modulus and Δ_ε the dielectric relaxation strength. The different mechanisms with corresponding time dependence are included and discussed at full length in the reference [14].

containing the effect of CLF). A distribution of mobilities is used instead of a constant time τ_d as in the double reptation model. The main difficulty in describing the CR effect analytically is related to its many chain character.

Quasi-elastic NSE spectroscopy measurements were performed in the past to microscopically investigate the above described mechanisms.

After the expected initial decay of $S(Q, t)$ by a free 3-dimensional Rouse motion up to roughly τ_e , the relaxation slows down. This slowing down should start when the m.s.d. of the chain segments becomes comparable to the diameter squared of the tube (Figure 4.5). The scattering function for a single chain in a melt is given by [7, 15]:

$$\frac{S(Q, t)}{S(Q)} = (1 - F(Q))S_{\text{locrep}}(Q, t) + F(Q)S_{\text{esc}}(Q, t) \quad (4.31)$$

Here, $F(Q)$ is the (cross-sectional) form-factor of the tube:

$$F(Q) = \exp[-(Qd/6)^2] \quad (4.32)$$

The local reptation and the creeping of the entire chain out of the tube where the chain follows its own profile, are given as:

$$S_{\text{locrep}}(Q, t) = \exp\left(\frac{t}{\tau_0}\right) \text{erfc}(\sqrt{t/\tau_0}) \quad (4.33)$$

$$S_{\text{esc}}(Q, t) = \sum_{p=1}^{\infty} \frac{2AN\mu}{\alpha_p^2(\mu^2 + \alpha_p^2 + \mu)} \sin^2(\alpha_p) \exp\left(-\frac{4t\alpha_p^2}{\pi^2\tau_d}\right) \quad (4.34)$$

where $\mu = Q^2 N l^2 / 12$ and α_p are the solutions of equation $\alpha_p \tan(\alpha_p) = \mu$. A is a normalization constant, so that $S_{\text{esc}}(Q, 0) = 1$. The two time scales in Eqs (4.33) and (4.34) are given by $\tau_0 = 36/(Wl^4 Q^4)$ for Rouse-type segment diffusion along the

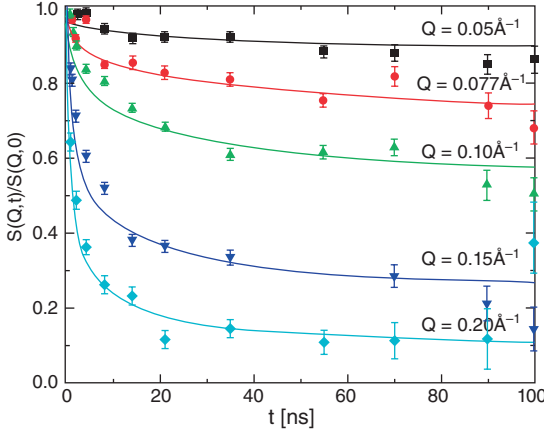


Figure 4.9 NSE data of PEO sample with $M_w = 81 \text{ kg mol}^{-1}$ at $T = 413 \text{ K}$. Symbols show the data measured for various Q values. The solid lines represent a fit with the reptation

model simultaneously to all Q values. The data were fitted in the time range $t > 10 \text{ ns}$ and then extrapolated to $t = 0$. Figure taken from K. Niedzwiedz [16].

tube; the second time scale is the so-called disentanglement time $\tau_d = 3N^3l^2/(\pi^2 Wd^2)$ for the reptation type escape of the chain from the tube (creep).

In the high Q -limit, that is, $R_g Q \gg 1$, $\alpha_p \approx (p - 1/2)\pi$ and $S_{\text{esc}}(Q, t)$ in Eq. (4.34) can be approximated by:

$$S_{\text{esc}}(Q, t) = \frac{8}{\pi^2} \sum_{p, \text{odd}} \frac{1}{p^2} \exp\left(-\frac{p^2 t}{\tau_d}\right) =: \mu_{\text{rep}}(t) \quad (4.35)$$

As before, $S_{\text{esc}}(Q, 0)$ is normalized to 1.

Figure 4.9 shows an example of the fit to a PEO single chain dynamic structure factor data at $M_w = 81 \text{ kg mol}^{-1}$ with the reptation model.

It is beyond the scope of this chapter to discuss the corrections of the reptation model for the CLF and CR mechanism in more detail. However, a rather complete expression for the complex modulus has been derived by Likhtman [13]. There the impact of CLF and CR on the complex modulus has been derived and compared to experimental data. The model successfully describes mechanical stress relaxation data over a large range of molecular weights.

The contribution of CLF to the relaxation spectrum, as measured in the single chain dynamic structure factor $S(Q, t)$, has also been developed [17]. The agreement with experimental NSE data is very good over a wide range of molecular weights.

But even without any theoretical model it was possible to demonstrate the influence of CLF by a key experiment [18]: the dynamic structure factor was measured by NSE for a fully labeled long chain and compared to a chain of the same molecular weight where the chain ends were not labeled. In the latter case the ends did not contribute to the structure factor since they had no contrast to the matrix. The

data showed the significantly faster relaxation of the fully labeled chain due to CLF, whereas the $S(Q, t)$ of the partly labeled chain was slower and indistinguishable from an extremely long polymer where CLF does not play a role.

In a similar way the CR effect has been verified [18]: a long labeled chain was measured by NSE in matrix polymers with different molecular weight. Very short matrix chains could not establish a tube, in consequence the long labeled chain showed pure Rouse behavior, although its molecular weight was much higher than M_e . The longer the matrix chains, the more they were able to build a tube, yielding a significant slowing down of the dynamics of the long labeled chain.

4.5

Application to Self-Healing

Supramolecular polymers that are built up from a strong directional interaction between end groups can show some similarity to the formerly treated linear class of covalently bonded chain molecules, given there is no specific interaction between the linking molecules themselves which leads to higher-level aggregation or stacking. The latter complicates the analysis and hinders investigation of the structure and the dynamics of the macromonomeric building blocks and the new contribution due to the transient connectivity between them. In the following section we will attempt to review only a few studies performed in the melt state, based on H-bonding interactions, and refer to literature for further treatments of other metal- or dynamic-covalent involving interactions in solutions and gels. We note that the transition between a simple linear structure and network-like behavior is strongly controlled then by the architecture of the moieties bearing the interaction site. If the active end groups are strictly telechelic and no nanostructuring is occurring, only linear aggregates (or cyclic if dilute) are formed. A typical parameter then is the degree of polymerization N_{agg} like in polycondensation reactions. N_{agg} is determined by the concentration of active sites and the equilibrium association constant K_{ass} via $\sim\sqrt{K_{\text{ass}}c}$. This is limited by several factors of which the integrity of the functionality per chain is the dominating one. Mono-functional contaminants serve as chain stoppers and decrease the total average length of the living chains. On the other hand, if the active groups are distributed comb-like along a polymeric backbone the system inter-molecularly associates, which leads to considerable gelling into a physical network. Then the dynamics of the sub-unities is thus seriously affected. Several studies on purely hydrogen-bonded systems have been presented in the literature and we restrict ourselves to some which in our opinion are particular relevant and representative:

- Lehn *et al.* [19–21] developed hierarchical self-assemblies mediated by multiple hydrogen-bonded homoditopic heterocomplementary monomers induced by solvent-specific effects. It was demonstrated that increasing the number of hydrogen bonds per functional end group results in a change in the degree of association and structure. SANS has been used to investigate these systems. Aggregates and fibrillar structures have been observed. Specifically in the case

of the fibers the nanostructures formed in decane were found to be rigid, with an average length that increased upon increasing concentration and/or decreasing temperature, containing on average several monomolecular wires.

- Sijbesma and Meijer *et al.* [22–30] showed that with well-defined interaction sites, that is, chain ends, by means of a highly directional interaction—in this case using ureidopyrimidinone (UPy)—new and unique properties can be obtained, compared to the previously discussed linear polymers. The formation of intramolecular loops in solution or diluted in the melt as the only competitive interaction was thought to be controllable via a suitable sterically-chemical substitution in the chain. Also the properties of telechelic poly(ethylene/butylene) changed dramatically upon functionalization, in this case with ureidotriazine (UTr). Already a SANS experiment was reported to investigate the aggregation of the above compounds in dodecane-d₂₆. It was observed that supramolecular triblock copolymer in the form of rigid rod structures was formed. PDMS using the same functionalization showed typical viscoelastic behavior in $G^*(\omega)$ and $\eta^*(\omega)$ that is, a rubbery plateau and terminal flow. The first ideas to tune new polymers with special properties as well as application for coating or rubbers were discussed.
- Elkins *et al.* [31], for example, showed that polymer stars, which were modified at the tips with the above UPy, show very well defined solid-like behavior through the interlinkage of star polymers into a rubberlike organization.
- Ruokolainen *et al.* [32] were able to bridge the theory of microphase separation known for polymer block copolymers into a study of a new class of copolymeric systems, obtained by hydrogen-bonding (H-bonding) between homopolymers and end-functionalized oligomers. The interaction is comb-like and leads to a lamellar-like morphology. Crossing the order–disorder temperature changes the system from a more solid-like phase separated to a liquid-like. This could be verified by the unique dependence of the observed dynamical moduli in the respective time-domains. Related is also the work of Noro *et al.* [33] on H-bonded thermoplastic block copolymers.
- The unwanted nanophase aggregation of end groups was encountered for example, also in PTHF, terminated with nucleobased compounds, as shown by Sivakova [34]. In the melt, hard domains of H-bond actors aggregate in stacks, witnessed from SAXS, and disperse within a soft polymer matrix.
- Binder *et al.* [35–43] have taken up the incompatibility argument together with the attractive H-bonding supramolecular interaction in the example of PIB and PEEK which are immiscible. Both components can be brought together in multiblock copolymers by means of appropriate heteroditopic interactions in the end groups, based on diaminotriazine and thymine for example, or hamilton-barbituric acid configurations. They showed that in this way both microphase separation or macrophase separation can be induced by varying the temperature. At high T all supramolecular bonds have opened and both polymers segregate.

Also, the same author has recently [44–46] reported the synthesis of a truly self-healing two-component system forming three-arm star polyisobutylene networks as well as a layered donor–acceptor material based on perylenes and ter(thiophen)es ordered by hydrogen-bonding moieties.

- A new contribution to this field was published by Herbst *et al.* [47–49]. From symmetric mixtures of PIB functionalized with both diaminotriazine and thymine, small angle X-ray (SAXS) and rheological measurements proved the existence of large-scale extended structures, similar to block copolymers. It was found that the triazine (dat) compound influences the overall behavior in the most decisive way, whereas thymine has less influence. The latter being weakly associated with itself affects the complexation in the mixture. They came to the conclusion that both H-bonding and nanophase structuring are responsible for the enhanced viscosity and the overall time–temperature dependence in the relaxation time spectrum. More recently [50] the influence of the different functionalization pyridinium/pyridine end-groups interaction has been compared with the former systems. A difference between weaker and stronger interaction, respectively, was observed through the effective cluster lifetime coming from rheological measurements. At the same time with increasing backbone molecular weight an increase in the plateau modulus, pointing to the formation of supramolecular networks, was noticed.
- In a related polymer using the very same end-group functionalities, but now based on the polar PPG, by Cortese *et al.* [51] the thymine component seemed to be the most important contributor in that it crystallizes in rather thin layers or sheets. The melting behavior reminds once again of normal microphase-separated block copolymers. Cortese [52] also treated the case of the dat and thy complexation. There it is found that the complementary interaction prevents thymine from crystallizing and keeps the assembled material in a viscoelastic state. The kinetic chain is largely increased judging by the viscosity and its temperature dependence controlled by the H-bond activation energy.
- In parallel, the same group developed new, non-covalent supramolecular networks based on interacting polymers supported on bio-based fatty acid chemistry [53–57]. Recently, the observed dynamo-mechanical properties have been investigated in the same biocompatible self-healing networks where two parts of the supramolecular rubber are simply brought into contact and then taken apart. It was observed that the self-healing capability can be activated after 12 h from the fracture but deactivated when at high temperatures. This can provide data to investigate the efficiency and kinetics of self-healing in these soft rubbers [58].
- A first NSE study on UPy-terminated macromonomers of PTHF was published by Muresan *et al.* [59]. The chain linkers led to highly-reduced mobility but proved microscopically the existence of long, associated chains.

- With respect to this, as one of the pioneers, Stadler *et al.* [60] showed that the modification of simple PB with urazol-based H-bonding groups, affected the local dynamics severely in that no simple master curve for the dynamic moduli could be constructed anymore, implying different activation schemes for both monomer and active sites.

This list is not meant to be complete and it is suggested that the reader looks up the specialized literature. It merely presents important issues, which are relevant for the structure and the dynamics in H-bonded polymers and networks which have the unique property of self-healing. The latter mechanism is discussed at full length in various topical contributions in this book.

This brings us to the fundamental question: how can the combination of rheology and neutron scattering unravel the microscopic mechanisms of the self-healing process?

The above introduced techniques of rheology and neutron scattering are ideal complementary techniques to study the molecular-based microscopic aspects of damage-repairing properties in new polymeric systems. These are based on well-defined and tuneable supramolecular interactions. Neutron scattering techniques are the method of choice since they resolve both relevant length scales and time scales. The cross-correlation with mechanical-dynamical methods allows one to address reversible hydrogen bonding in polymers, both in solution and especially in the bulk state, which is a prerequisite for the design of new elastic smart responsive materials. The goal is to reach generalization and finally controlled design of new adaptive high-performance composites.

4.6

Conclusions and Outlook

In this final section an outlook is presented, to exemplify the possible applications of neutron scattering and rheology on specifically adapted and labeled samples. The selective deuteration of polymer molecules without altering the macroscopic properties of the system provides an ideal tool and unique method for structural and dynamical studies of tailored soft materials. With sophisticated labeling schemes, selected parts of molecules can be made even invisible while other sections can be highlighted, as exemplified in Figure 4.10. The number of systems and parameters to be investigated is enormous: They include variation of the concentration of functionalized building blocks in solution (or even in a melt of covalent polymer chains), the architecture of the functionalized macromolecules (linear, combs, stars), temperature, molecular weight, the composition with respect to the hydrogenated and deuterated fraction, even the size and position of hydrogenated sections within one macromolecule, to name just a few. As described, SANS covers the relevant length scales under equilibrium conditions to access the single chain structure factor of the aggregate. These length scales range between 1 and 1000 Å. By NSE, microscopic times up to several hundred nanoseconds are

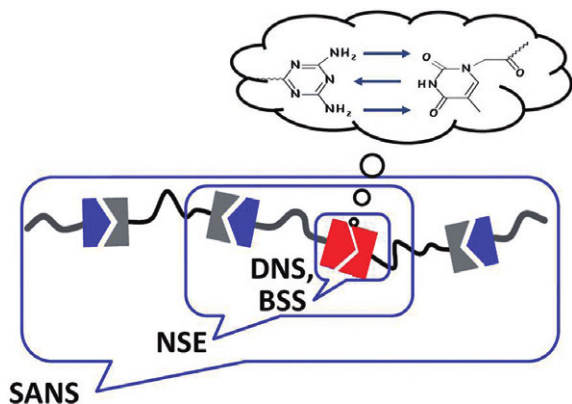


Figure 4.10 Scheme exemplifying which length scales are accessible by different neutron scattering techniques in relation to the polymer chain as well as the selective deuteration of polymer molecules shown by

the highlighted functional groups in red. DNS and BSS are structural and dynamical neutron scattering methods for the small length scales.

available. If these experiments are performed at high temperatures, these times correspond to typically the range of milliseconds at room temperature. NSE on these polymers, as described, allows one to study the single chain dynamic structure factor, which is determined by the diffusion as well as the intra-chain (segmental) dynamics of the macromolecules. Both depend strongly on the number of building blocks in the case of telechelic chains. Added to this diffuse neutron scattering (DNS) allows access to the coherent scattering (by neutron polarization analysis the incoherent scattering will be quantitatively removed) in a higher Q -range that is, to resolve the structure on the length scale between 1 and 10 Å. DNS overlaps partially with and complements the SANS method, especially in this local range. By the combination of SANS, DNS and NSE on the dissolved aggregating reactive polymers, both overall chain and local aggregation mechanisms can be characterized in dependence on temperature, concentration, and binding constant (functional group). At the same time incoherent quasielastic neutron scattering of the protons in the reactive groups on an Angstrom scale (backscattering) will allow one to identify the state of aggregation in the melt state, since the dynamics of the protons depends strongly on the immediate environment. The starting point for interpretation of the collected data is the fundamental theories available to describe the structure and dynamics of polymeric systems. Here, tremendous progress has been achieved in the last decades. As an example, the consistent description of polymer dynamics starting from the center of mass diffusion and segmental relaxation as addressed in the Rouse model for short polymer chains may be mentioned. It is continued by reptation dynamics, including higher order processes like contour length fluctuations and constraint release for long, entangled polymers, as described by the tube model and its increments. However, the progress is not limited to simple linear chains, but can also be found in more

complex architectures. In all cases the combination of neutron scattering with complementary, in particular broad-band techniques was effective.

In Ref. [59] it was shown that by neutron spin echo spectroscopy the dynamics of hydrogen bonded macromolecules can indeed be accessed. The results could be described in terms of a significantly higher stiffness of the supra-chain, reflected in the suppression of long wavelength Rouse modes.

Recent NSE data [61] of two different polymer melts have been measured and compared. One is a conventional short chain polymer melt and it is compared with a melt of similar molecular weight with functionalized end groups at the same temperature. While the first can be nicely described by the Rouse model center of mass diffusion, the second clearly does not have the same diffusion and is significantly slowed down. This effect can be modeled by taking into account the higher segmental friction due to the functional end groups and the aggregation process. The influence of the functional groups on the segmental friction in turn has been independently determined by measuring the diffusion of these in a covalent matrix. This example just serves to illustrate how a combination of experiments on simple systems facilitates the understanding of underlying basic mechanisms and sets the stage for the investigation of more complex systems, for example, network-like systems representing real self-healing materials [62, 63]. Particularly in the latter, NSE has never been attempted and offers a great opportunity to improve knowledge on self-assembly and self-healing mechanisms in network-like environments. It is desirable to conduct more systematic experimental studies on microscopic and macroscopic scales on the structure and the dynamics of both supramolecular polymer melts and networks. Extensive work basing on a Random Phase Approximation approach typical for block-copolymers [61] is presently under way to close these gaps, and future discoveries can be anticipated to shed more light on these fascinating materials.

References

- 1 Flory, P. (1953) *Principles of Polymer Chemistry*, Cornell University Press, Ithaca, NY.
- 2 Rubinstein, M., and Colby, R.H. (1988) *Polymer physics*. *J. Chem. Phys.*, **89**, 5291.
- 3 Graessley, W.W. (2004) *Polymeric Liquids and Networks*, Taylor and Francis: Structure and Properties.
- 4 Teraoka, I. (2002) *Polymer Solutions: An Introduction to Physical Properties*, Wiley-Interscience.
- 5 Higgins, J.S., and Benoit, H. (1994) *Polymers and Neutron Scattering*, Clarendon Press.
- 6 Hammouda, B. (2010) *Probing Nanoscale Structures-The SANS Toolbox*. http://www.ncnr.nist.gov/staff/hammouda/the_sans_toolbox.pdf (accessed October 17, 2012).
- 7 Doi, M., and Edwards, S.F. (1986) *The Theory of Polymer Dynamics*, Clarendon Press, Oxford.
- 8 Wischniewski, A., and Richter, D. (2006) Chapter 1, *Polymer Dynamics in Melts*, Wiley-VCH Verlag GmbH, Weinheim, Germany.
- 9 Richter, D. (2006) *J. Phys. Soc. Jpn.*, **75**, 111004–111012.
- 10 Niedzwiedz, K. (2007) *Polymer dynamics in miscible polymeric blends*. Phd thesis, University of Münster.
- 11 Milner, S., and McLeish, T. (1998) *Rev. Lett.*, **81**, 725–728.

- 12 McLeish, T.C.B. (2002) *Adv. Phys.*, **51**, 1379–1527.
- 13 Likhtman, A.E., and McLeish, T.C.B. (2002) Quantitative theory for linear dynamics of linear entangled polymers. *Macromolecules*, **35**, 6632–6643.
- 14 Glomann, T., Schneider, G.J., Bras, A.R., Pyckhout-Hintzen, W., Wischnewski, A., Zorn, R., Allgaier, J., and Richter, D. (2010) *Macromolecules*, **44** (18), 7430–7437.
- 15 DeGennes, P.G. (1981) *J. Phys.*, **42**, 735.
- 16 Niedzwiedz, K., Wischnewski, A., Pyckhout-Hintzen, W., Allgaier, J., Richter, D., and Faraone, A. (2008) *Macromolecules*, **41**, 4866–4872.
- 17 Wischnewski, A., Monkenbusch, M., Willner, L., Richter, D., Likhtman, A., McLeish, T., and Farago, B. (2002) *Phys. Rev. Lett.*, **88**, 058301–058304.
- 18 Zamponi, M., Wischnewski, A., Monkenbusch, M., Willner, L., Richter, D., Likhtman, A., Kali, G., and Farago, B. (2006) Molecular observation of constraint release in polymer melts. *Phys. Rev. Lett.*, **96**, 238–302.
- 19 Fouquey, C., Lehn, J.M., and Levelut, A.M. (1990) *Adv. Mater.*, **2**, 254.
- 20 Kolomiets, E., Buhler, E., Candau, S.J., and Lehn, J.M. (2006) *Macromolecules*, **39**, 1173–1181.
- 21 Lehn, J.M. (2002) *Polym. Int.*, **51**, 825.
- 22 Sijbesma, R.P., Beijer, F.H., Brunsveld, L., Folmer, B.J.B., Hirschberg, J.H.K.K., Lange, R.F.M., Lowe, J., and Meijer, E. (1997) *Science*, **278** (5343), 1601–1604.
- 23 Hirschberg, J.H.K.K., Beijer, F.H., van Aert, H.A., Magusin, P.C.M.M., Sijbesma, R.P., and Meijer, E. (1999) *Macromolecules*, **32**, 2696–2705.
- 24 Hirschberg, J.H.K.K., Brunsveld, L., Ramzi, A., Vekemans, A.J.M., Sijbesma, R.P., and Meijer, E.W. (2000) *Nature*, **407**, 167–170.
- 25 Sontjens, S.H.M., Sijbesma, R.P., van Genderen, M.H.P., and Meijer, E.W. (2000) *Journal of the American Chemical Society*, **122** (31), 7487–7493
- 26 Brunsveld, L., Folmer, B.J.B., Meijer, E.W., and Sijbesma, R.P. (2001) *Chem. Rev.*, **101**, 40–71.
- 27 Bosman, A., Brunsveld, L., Folmer, B., Sijbesma, R.P., and Meijer, E.W. (2003) *Macromol. Symp.*, **201**, 143–154.
- 28 Bosman, A., Sijbesma, R.P., and Meijer, E.W. (2004) *Mater. Today*, **7** (4), 34–39.
- 29 Brett, H., and Meijer, E.W. (2006) *Science*, **313**, 929–930.
- 30 de Greef, T., and Meijer, E.W. (2008) *Nature*, **453**, 1731–1739.
- 31 Elkins, C.L., Viswanathan, K., and Long, T.E. (2006) *Macromolecules*, **39**, 3132.
- 32 Ruokolainen, J., Torkkeli, M., Serimaa, R., Komanschek, E., ten Brinke, G., and Ikkala, O. (1997) *Macromolecules*, **30**, 2002–2007.
- 33 Noro, A., Matsushita, Y., and Lodge, T.P. (2008) *Macromolecules*, **41**, 5839–5844.
- 34 Sivakova, S., Bohnsack, D.A., Mackay, M.E., Suwanmala, P., and Rowan, S.J. (2005) *J. Am. Chem. Soc.*, **127**, 18202–18211.
- 35 Binder, W.H., Bernstorff, S., Kluger, C., Petraru, L., and Kunz, M. (2005) *Adv. Mater.*, **23**, 2824.
- 36 Binder, W.H., and Zirbs, R. (2007) *Advances in Polymer Science-Hydrogen Bonded Polymers*, Springer-Verlag Berlin, Berlin, Germany.
- 37 Kluger, C., and Binder, W.H. (2007) *J. Polym. Sci. A*, **45** (3), 485–499.
- 38 Binder, W.H. (2008) *Rapid Commun.*, **29** (12–13), 951.
- 39 Kurzhals, S., and Binder, W.H. (2010) *J. Polym. Sci. A*, **48** (23), 5522–5532.
- 40 Enders, C., Tanner, S., and Binder, W.H. (2010) *Macromolecules*, **43** (20), 8436–8446.
- 41 Gragert, M., Schunack, M., and Binder, W.H. (2011) *Macromol. Rapid Commun.*, **32** (5), 419–425.
- 42 Ostaš, E., Schroter, K., Beiner, M., Yan, T.Z., Thurn-Albrecht, T., and Binder, W.H. (2011) *J. Polym. Sci. A*, **49** (15), 3404–3416.
- 43 Binder, W.H. (2005) *Monatsh. Chem.*, **136** (1), 1–19.
- 44 Nia, A.S., Enders, C., and Binder, W.H. (2012) *Tetrahedron*, **68** (2), 722–729.
- 45 Schunack, M., Gragert, M., and Binder, W.H. (2012) *Macromol. Chem. Phys.*, **213** (2), 205–214.
- 46 Doehler, D., Michael, P., and Binder, W.H. (2012) *Macromolecules*, **45** (8), 3335–3345.
- 47 Herbst, F., Schröter, K., Gunkel, I., Gröger, S., Thurn-Albrecht, T., Balbach,

- J., and Binder, W.H. (2010) *Macromolecules*, **43**, 10006–10016.
- 48 Adekunle, O., Herbst, F., Hackethal, K., and Binder, W.H. (2011) *J. Polym. Sci. A*, **49** (13), 2931–2940.
- 49 Herbst, F., Schulz, M., and Binder, W.H. (2010) *J. Polym. Sci. A*, **58** (7–8), 734–739.
- 50 Hacketal, K., Herbst, F., and Binder, W.H. (2012) *J. Polym. Sci. A*, **50** (21), 4494–4506.
- 51 Cortese, J., Soulié-Ziakovic, C., Cloitre, M., Tencé-Girault, S., and Leibler, L. (2011) *J. Am. Chem. Soc.*, **133**, 19672–19675.
- 52 Cortese, J., Soulié-Ziakovic, C., Tencé-Girault, S., and Leibler, L. (2012) *J. Am. Chem. Soc.*, **134**, 3671–3674.
- 53 Cordier, P., Tournilhac, F., Soulié-Ziakovic, C., and Leibler, L. (2008) *Nature*, **451**, 977–980.
- 54 Montarnal, D., Cordier, P., Soulié-Ziakovic, C., Tournilhac, F., and Leibler, L. (2008) *J. Polym. Sci. A*, **46**, 7925–7936.
- 55 Montarnal, D., Tournilhac, F., Hidalgo, M., Couturier, J.L., and Leibler, L. (2009) *J. Am. Chem. Soc.*, **131**, 7966–7967.
- 56 Tournilhac, F., Cordier, P., Montarnal, D., Soulié-Ziakovic, C., and Leibler, L. (2010) *Macromol. Symp.*, **291–292**, 84–88.
- 57 Montarnal, D., Tournilhac, F., Hidalgo, M., and Leibler, L. (2011) *Actual. Chim.*, **348–349**, 49–53.
- 58 Maes, F., Montarnal, D., Cantournet, S., Tournilhac, F., Corte, L., and Leibler, L. (2012) *Soft Matter*, **8** (5), 1681–1687.
- 59 Muresan, A.S., Dubbeldam, J.L.A., Kautz, H., Monkenbusch, M., Sijbesma, R.P., van der Schoot, P., and de Jeu, W.H. (2006) *Phys. Rev. E*, **74**, 031804(1–7).
- 60 Stadler, R., and de Lucca Freitas, L. (1986) *Colloid Polym. Sci.*, **264** (9), 773–778.
- 61 Brás, A.R., Hövelmann, C., Antonius, W., Radulescu, A., Pyckhout-Hintzen, W., Wischniewski, A., and Richter, D. (2013) Microscopic insights into supramolecularly linearly-assembled telechelic polymers. In preparation; Brás, A.R., Antonius, W., Hövelmann, C., Radulescu, A., Lindner, P., Farago, B., Pyckhout-Hintzen, W., Wischniewski, A., and Richter, D. (2013) Structure and dynamics in supramolecular polymers by neutron scattering. In preparation.
- 62 Kautz, H., van Beek, D.J.M., Sijbesma, R.P., and Meijer, E.W. (2006) *Macromolecules*, **39** (13), 4265–4267.
- 63 Lange, R.F.M., Gulp, M.V., and Meijer, E.W. (2000) *J. Polym. Sci. A*, **37** (19), 3657–3670.

5 Physical Chemistry of Cross-Linking Processes in Self-Healing Materials

Joerg Kressler and Hans-Werner Kammer

5.1 Introduction

Nature, in animals and plants, frequently uses self-healing materials, mainly composites, which are based on integrated, hierarchical structures often formed over several length scales [1]. Thus, it seems reasonable to mimic nature in order to improve the performance of polymer-based materials [2, 3]. In recent years several reviews on theoretical and experimental aspects of self-healing polymers have been published [4–8]. Key points for the understanding of self-healing materials are the diffusion of polymer chains below the glass transition temperature in thermoplastics, for example, after crack formation, or the network formation which can be achieved either by chemical cross-linking reactions leading to covalent bonds between the polymer chains, or by strong physical interactions as for example, in supramolecular polymer networks [9]. A practical approach for autonomous healing is the dispersion of microencapsulated healing agents which are released upon crack intrusion [10]. A typical system consists of dicyclopentadiene (DCPD) and a Grubbs' catalyst which yields PDCPD, a highly cross-linked polymer, after ring-opening metathesis polymerization (ROMP) [10, 11]. The DCPD is located in the microcapsules, whereas the catalyst, which tolerates a wide range of functional groups, water, and oxygen, is dispersed in the polymer matrix. This polymerization is highly useful due to its strong exothermal reaction enthalpy as a result of the relief of ring strain energy. The self-healing efficiency is then obtained by measuring for example, the fracture toughness of tapered double-cantilever (TBCD) specimens or by dynamic mechanical analysis [10, 12]. The cross-linking kinetics is followed either by differential scanning calorimetry or by rheokinetic measurements [13, 14]. Meanwhile a large variety of different chemical cross-linking reactions has been employed [15], including copper(I)-catalyzed alkyne-azide cycloaddition reactions, known as "click" chemistry [16].

In general, the formation of networks is a key element for spontaneous repair of polymer specimens as a response to mechanical damage. For autonomous healing, one has to select a balanced dynamic approach for formation of a network. In other words, one has to establish a sufficiently high molecular dynamics for

formation of high modulus, load-bearing networks. These are conflicting requirements. Strong interactions in the supramolecular system result in mechanical stability but also in slowing down dynamics. Weak interactions enhance molecular dynamics but generate only soft materials. In what follows, physical-chemical aspects of gelation processes will be discussed. Polymer gels are a state of matter intermediate between liquid and solid. A polymer solution, where individual chains are dissolved, forms a liquid. When a fraction of chains is cross-linked to a huge cluster pervading the entire sample, then the liquid turns into a gel. Thus, the gel is a mixture of at least one huge cluster extending over the whole system and inclusions of finitely linked clusters. It becomes obvious that such a mixture exhibits both elasticity and fluidity. In addition, we note that gelation always implies the tendency of phase separation in the solution. It might be suppressed by sufficiently strong excluded-volume repulsion, that is, the energy of this interaction per network section exceeds the thermal energy $k_B T$.

To what extent viscoelastic response occurs in the gel system depends on the specific process of gel formation. We distinguish chemically and physically linked gels. Suppose the cross-linking process is irreversible, that is we have chemical cross-linking. The fraction of cross-links increases up to a critical value which corresponds to occurrence of the infinite cluster covering the whole system. This happens, for example, in associating polymers. Gelation is marked by the time of reaction where the system may exhibit quite abrupt increase in viscosity. We introduce the fraction of associative bonds, p , formed in the system. Then, gelation occurs at $p = p_{\text{gel}}$. Beyond this point, reaction proceeds up to the saturation value of p which defines the glass transition at conversion $p = p_{\text{glass}}$. We recognize

$$p_{\text{gel}} < p_{\text{glass}} < 1 \quad (5.1)$$

Gelation is in the sketched sense a connectivity transition. If we have an assembly of independent particles, there will be no transition on the horizon. But if this assembly of particles is linearly connected to a chain molecule then, depending on conditions, the chain may exhibit a (reversible) transition swollen to collapsed conformation due to connectivity [17]. The same mechanism rules gelation. The difference here being that chemical gelation is not reversible. Formation of the infinite cluster is associated with an abrupt change in properties. This calls percolation theory onto the stage [18]; gelation is reflected as a threshold. The infinite life-time of the bonds relates the gel point to the formation of an infinite cluster which can be described in the spirit of percolation theory. In other words, percolation is defined in terms of connectivity or bonds and their life-times. In that sense, percolation is closely related to dynamics. We note that this process is not an equilibrium process marked by the gelation threshold because in the range beyond the threshold the chemical reaction proceeds in the finite-cluster inclusions and leads eventually to the glass.

Reversible gelation proceeds under different circumstances. A physical gel might be defined as a low density, disordered and arrested state of matter. Stable networks are formed owing to reversible bonding with a long life-time. Chains

associate by physical interactions, for example, H-bonding, complex formation, covalently reversible Diels–Alder reaction, and so on. These cross-links are weaker than in the case of irreversible gelation and their life-time τ_b differs markedly from irreversible gels:

$$\begin{aligned} \text{Irreversible gel } \tau_b &\rightarrow \infty \\ \text{Reversible gel } \tau_b &\text{ – large, but finite} \end{aligned} \quad (5.2)$$

Moreover, we have an equilibrium situation. Bond energies in thermo-reversible gels are of the order of $k_B T$. Hence, clusters form and dissociate permanently. When we perform some relaxation experiment, for example periodic stress excitation in dynamic-mechanic analysis, then we monitor a typical relaxation response. In the range of low frequencies, the gel will display liquid-like behavior. However, one observes the transition from liquid-like to elastic response over a range of frequencies rather than at an abrupt gelation threshold. At low frequencies the system can follow the imposed variation of stress, and cross-links are destroyed. But, the system cannot follow these stress variations at higher frequencies, cross-links are kept and elastic response is observed. This transition from liquid-like to elastic behavior is not an equilibrium transition. It is similar to a relaxation transition, like the glass transition. As a consequence, employing such a gel for self-healing is only useful against damage caused by externally imposed actions lasting over a long time.

5.2 Thermodynamics of Gelation

Polymer chains endowed with functional groups are capable of forming associations in solution. Branched aggregates grow in the course of time and their distribution becomes broader. Eventually, a macroscopic cluster, a gel, results, covering the whole system. This transition from the sol state, that is the polydispersed system of chain associations, to the gel state, the mixture of those aggregates and a macroscopic gel, is termed gelation. As mentioned before, this process might proceed reversibly or irreversibly. An adequate approach is percolation theory [18]. Mean-field versions of this theory were provided by Flory [19] and Stockmayer [20]. The mean-field approach is only realistic when concentration fluctuations are sufficiently small, that is, the concentration of the solution should be sufficiently above the overlapping concentration, $c > c^*$.

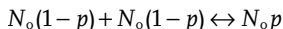
In the following, we will discuss only the fundamentals of these approaches. Chains, having the degree of polymerization N , are dissolved in a low-molecular weight solvent and form a semi-dilute solution with monomer concentration c or chain concentration c/N . Each chain comprises f associating groups with $f \ll N$. The number of associating groups in volume v of solution amounts to

$$N_{\text{assoc}} = f \frac{c}{N} v \quad (5.3)$$

The number of groups bound in pairs relates to the fraction of associative bonds p

$$N_{\text{pair}} = \frac{1}{2} p f \frac{c}{N} \nu \quad (5.4)$$

The equilibrium



between free and paired groups is characterized by the equilibrium constant $K = \frac{p}{(1-p)^2} \frac{1}{N_o}$. It follows with Eq. (5.3) the implicit relationship for the fraction of bonds (next is Eq. (5.5)):

$$\frac{p}{(1-p)^2} = f \frac{c}{N} K \text{ with } K = \nu_b \exp\left(-\frac{f_b}{k_b T}\right) \quad (5.5)$$

Quantities f_b and ν_b represent the free energy of bond formation and the volume of a single bond, respectively. Eq. (5.5) may be used to calculate the equilibrium gel line as a function of T and c . We abbreviate K by $\nu_b \kappa$ and may recast Eq. (5.5) as

$$\frac{p}{(1-p)^2} = \frac{\nu_{\text{bond}}}{\nu} \kappa \quad (5.6)$$

where ν_{bond} represents the total bond volume. The volume ratio describes an entropy effect, the driving force to densification of the system. Formation of branched polymers or formation of clusters is accompanied by enhanced segment density or one may also say by some precipitation. This is reflected by the first factor of Eq. (5.6). In general terms, one may say the entropy term controls bonding. Hence, it rules the association process.

What is the gel point in this approximation? A continuous path through a cluster may lead to a chain. Then this chain has $(f-1)$ bonds open for continuation of the network. When the fraction of bonds is p , we have the probability $p(f-1)$ for extension of the cluster. Formation of an infinite cluster characterizes the gel point. The probability at the gel point becomes unity, $p_g(f-1) = 1$. It is

$$p_g = \frac{1}{f-1} \quad (5.7)$$

The concentration at the gel point becomes, after Eq. (5.5)

$$c_g = \frac{f-1}{(f-2)^2} \frac{N}{f \kappa} \quad (5.8)$$

The percolation point is characterized by islands of finite clusters immersed in a matrix of connected molecules. Let us mention also in that context a quantity called extent of polymerization, $\Phi(t)$. It is usually experimentally determined by spectroscopic methods. The quantity Φ is defined as the fraction of chains linked in clusters, $\Phi = 1 - \rho_1/\rho$, where ρ_1 and ρ refer to monomer and total density, respectively; Φ acts as an order parameter in the connectivity transition. For monomer density ρ_1 , it follows $\rho_1 = \rho(1-p)^f$ and Φ becomes

$$\Phi = 1 - (1 - p)^f \quad (5.9)$$

One recognizes that $\Phi(p)$ is a monotonically increasing function in the range $0 \leq \Phi \leq 1$ that becomes steeper with increasing f . This is equivalent to Eq. (5.6).

The free energy density of associated chains, with degree of association p and with reference to non-interacting chains, reads in the language of Ref. [21, 22]

$$\begin{aligned} \frac{f_{\text{assoc}}}{\nu k_{\text{B}} T} = & \left[\frac{c}{N} \ln \left(\frac{c}{eN} \nu_{\text{ref}} \right) - p \frac{fc}{2N} \ln \left(\frac{fc}{eN} \nu_{\text{b}} \right) \right] \\ & + \frac{fc}{2N} [p \ln p + 2(1 - p) \ln(1 - p) - p \ln \kappa] \end{aligned} \quad (5.10)$$

The first line refers to non-interacting polymer chains. They have only entropy. The second line gives the free energy of the linked chains. It is straightforward that minimization of free energy Eq. (5.10) with respect to p yields Eq. (5.5). In Ref. [22] it is demonstrated that Eq. (5.10) agrees completely with the free energy approximations used in the classic papers by Flory and Stockmayer [19, 20].

With respect to cluster distribution, the sol phase is described in the same way in both classic approaches. Distribution of finite clusters gets narrower on approaching the gel point. However, the mixture of sol and gel fraction above the gel point is considered differently. Flory makes the natural assumption that the chemical reaction, the bonding reaction, proceeds also above the gel point, leading to narrowing of the distribution as below the gel point. Moreover, the gel state, according to Flory, may comprise cycles, in contrast to Stockmayer's approach. In addition Stockmayer assumes that development of cluster distribution is arrested at the gel point. The two approaches are different in another important point. Gelation is not a thermodynamic transition according to Flory whereas reversible gelation is a third order transition in the context of Stockmayer's version; the derivative of isothermal osmotic compressibility, Π/Π_{ideal} , displays a discontinuity. Detailed analyses support the Flory approach and come to the result that reversible gelation is not a thermodynamic transition [23–26]. As Eq. (5.10) shows, the free energy of the system and all its derivatives are analytical functions at the gel point. This fact supports strongly that gelation is a connective transition. It turns out that the mean-field version, given by Eq. (5.10) as combination of lattice-gas and Flory–Huggins approximation, is able to describe this transition well above the overlap concentration in solutions of associative polymers.

5.3

Viscoelastic Properties of the Sol–Gel Transition

Dynamics of associative polymers is closely related to changes in viscoelastic properties. Gel transition is accompanied by marked changes in viscosity. A sol is a liquid and remains a liquid when cross-linking starts. Above the gel point the liquid is arrested, fluidity goes down and elasticity develops with enhanced crosslink density. Thus, sol–gel transition in a solution of associating chains

manifests itself in a change in physical properties at a particular temperature or concentration. In the following we will discuss changes in viscoelastic properties near the gelation point.

From a theoretical point of view gel formation is characterized by the existence of a long chain running through the whole system and having infinite molecular mass. Formation of an infinite cluster is accompanied by a sudden loss of flow. This effect may serve to determine the sol–gel transition. Viscoelastic properties change markedly from liquid-like to solid-like behavior. We observe changes over a range of temperature or concentration. The transition may also be accompanied by vitrification, chain entanglement, and even phase separation in the polymer solution. In general terms, we have to classify it as a relaxation transition; in that sense it is similar to a glass transition.

Viscoelastic properties of cross-linking polymers may be characterized by the complex shear modulus as a function of frequency, $G^*(\omega)$. This can be determined under harmonic strain excitation. Many experiments on associating polymers revealed that this quantity follows a power law at the gelation point over a wide range of frequencies

$$G^*(\omega) \propto (i\omega)^n \quad (5.11)$$

with $0 < n < 1$. Equation (5.11) implies a constant phase angle, independent of frequency, between stress and strain. This constancy of loss tangent with respect to frequency might be used to obtain experimentally the gelation point. Adoption of the frequency law Eq. (5.11) for gelation was first suggested by Winter and Mours [27]. Accordingly, the gel point is located at a loss tangent independent of frequency.

Dynamic mechanical experiments were carried out for end-linking poly(dimethyl siloxane) and poly(urethane) [28]. Near the gel point, it resulted in agreement with Eq. (5.11)

$$\begin{aligned} G'(\omega) &\propto \omega^n \\ G''(\omega) &\propto \omega^n \end{aligned} \quad (5.12)$$

The process of gelation is quite complex. For elucidation, we subdivide it into three states:

Pre-gel, critical gel and post-gel state

The gelation process may be monitored via the complex dynamic viscosity

$$|\eta^*| = \frac{|G^*|}{\omega} \quad (5.13)$$

Below the cross-over frequency ω_0 between the critical gel and the pre-gel state, we observe just linear viscoelastic behaviour. Close to the gel point the complex modulus turns to a power law response in a certain frequency range. Thus, the pre-gel shows ω^{-n} -behavior for $\omega > \omega_0$ and liquid-like viscoelasticity for $\omega < \omega_0$. It is

$$\begin{aligned} G'(\omega) &\propto \omega^2 \text{ and } G''(\omega) \propto \omega \text{ for } \omega < \omega_0 \\ G'(\omega), G''(\omega) &\propto \omega^n \text{ for } \omega > \omega_0 \end{aligned} \quad (5.14)$$

The cross-over frequency decreases with progressing cluster formation. It is quite natural that it approaches zero at the gel point since we can no longer observe liquid-like behavior.

$$\omega_0 \rightarrow 0 \text{ at gel point} \quad (5.15)$$

As a consequence, modulus G^* of the critical gel displays power-law dependence over the entire frequency range

$$G'(\omega) = \frac{G''(\omega)}{\tan(n_0\pi/2)} \propto \omega^{n_0} \quad (5.16)$$

In the post-gel stage, cross-over frequency increases to a finite value ω^* . For frequencies above ω^* , we observe power-law dependence of the complex modulus, whereas solid-like behavior with a finite equilibrium modulus, G_0 , is found for frequencies below ω^* . Instead of Eq. (5.14), we have

$$\begin{aligned} G'(\omega) &\propto G_0 \text{ and } G''(\omega) \propto \omega \text{ for } \omega < \omega^* \\ G'(\omega), G''(\omega) &\propto \omega^n \text{ for } \omega > \omega^* \end{aligned} \quad (5.17)$$

Inserting Eq. (5.16) in Eq. (5.13), we obtain for the critical gel

$$|\eta^*| \propto \frac{1}{\omega^{1-n_0}} \quad (5.18)$$

We may use the critical gel as reference for the pre-gel and post-gel stages. In the pre-gel state, Eq. (5.13) approaches zero-shear viscosity for $\omega \rightarrow 0$ after Eq. (5.14)

$$|\eta^*| \rightarrow \eta_0 < \frac{C}{\omega^{1-n_0}} \text{ for } \omega \rightarrow 0 \quad (5.19)$$

It merges into Eq. (5.18) at $\omega \approx \omega_0$ under condition $n_0 = n$. With progressing cross-linking in the system, one can no longer observe the limiting zero-shear viscosity.

The dynamic viscosity of the post-gel tends towards solid-like behaviour for $\omega \rightarrow 0$

$$|\eta^*| \rightarrow \frac{G_0}{\omega} > \frac{C}{\omega^{1-n_0}} \text{ for } \omega \rightarrow 0 \quad (5.20)$$

It approaches Eq. (5.18) at $\omega \approx \omega^*$ again under $n_0 = n$. In a double-logarithmic plot of $|\eta^*|$ versus ω , pre-gel shows negative deviation from the linear reference line of the critical gel at $\omega \rightarrow 0$, whereas post-gel displays positive deviation in the same limit.

The foregoing discussion leads us directly to the dependence of the complex modulus on the concentration of the associating polymer. In the pre-gel state liquid-like behavior dominates. It results that $G''(c) > G'(c)$ at $\omega = \text{const}$. The

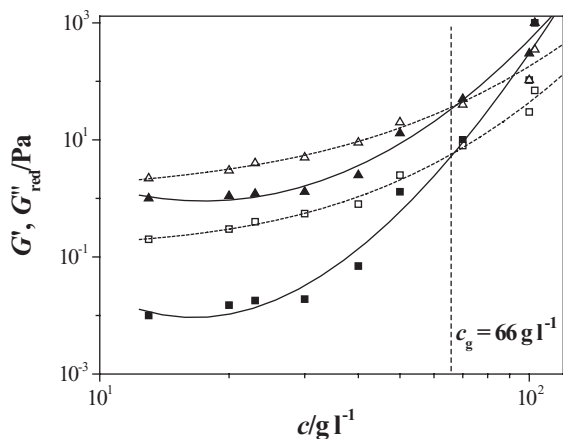


Figure 5.1 Storage and loss modules, G' (solid markers) and G''_{red} (open markers), versus polymer concentration for solutions of PVC in DOP at room temperature; squares: $\omega = 10 \text{ rad s}^{-1}$, triangles: $\omega = 100 \text{ rad s}^{-1}$ (data taken from Ref. [29]).

opposite is observed in the post-gel state, $G'(c) > G''(c)$, since solid-like response occurs. Hence, it is straightforward and in accordance with Eq. (5.16) that, for $\omega = \text{const}$, functions $G'(c)$ and $G''_{\text{red}}(c) \equiv \frac{G''(c)}{\tan(n_o\pi/2)}$ should cross at concentration c_g marking the critical gel

$$G'(c_g) = G''_{\text{red}}(c_g)$$

Moreover, the crossing points should appear at c_g , independent of frequency, since $\tan(n_o\pi/2)$ does not depend on frequency at the gel point, as we stated in the context of Eq. (5.11). This is nicely demonstrated in Figure 5.1 for solutions of poly(vinyl chloride) (PVC), $M_w = 40 \text{ kg mol}^{-1}$, in bis(2-ethyl hexyl) phthalate (DOP) under $\omega = \text{const}$ [29].

One may also discuss the temperature dependence of dynamic modules at constant frequency and concentration. In the low-frequency range corresponding to long-time behavior, $\omega = 1 \text{ Hz}$, and at a concentration around c_g , one observes dominant elastic response $G' \gg G''$. The storage module G' diminishes with increasing temperature, whereas G'' displays a maximum. In many cases, the two modules cross at the maximum of G'' , which is seen as the “melting” point of the gel. One observes liquid-like behavior at temperatures beyond the intersection that is $G'' \gg G'$. It has also been observed that the intersection temperature decreases when the frequency of the temperature sweep decreases, say from $\omega = 3 \text{ Hz}$ to 1 Hz [30]. This might be caused by growth of larger clusters during extended external action.

One may discuss this dynamic behavior qualitatively also in terms of different relaxation characteristics. In physical gels the ruling dynamic quantities are the life-time of growing clusters, τ_{life} , and their relaxation time τ_{relax} under external

action. In the pre-gel stage, far below the gel point, only small clusters develop during reversible gelation. However, these clusters may live sufficiently long

$$\tau_{\text{life}} > \tau_{\text{relax}} \quad (5.21)$$

Under these conditions, rheological experiments are not suitable for distinguishing clusters formed in reversible or irreversible gelation.

Near the critical gel, large clusters develop and condition (5.21) becomes unlikely. Large clusters have a shorter life-time than small ones since with increasing size the probability of bond breaking increases. This means that condition (5.21) changes to

$$\tau_{\text{life}} \approx \tau_{\text{relax}} \quad (5.22)$$

Condition (5.22) indicates that we have a solution of polydisperse dynamic clusters or precipitates. This situation exists close to the gel point and beyond.

After relationship (5.22), the network in reversible gels is a fluctuating system of growing and dissociating bonds. The gel exhibits a finite modulus of elasticity in the low frequency region (1–100 Hz). More precisely, we may state that the non-uniformity of the gel phase, coined by aperiodic structures, generates both liquid and solid properties. As mentioned above, Eq. (5.17), the non-uniform microstructures have solid-like elasticity over long time scales. The aperiodic structures are not thermally stable; with increasing temperature they exhibit liquid-like response. This behavior brings the gel in the vicinity to amorphous glass. Both states behave like a solid but they do not have periodic molecular arrangements. In addition, both transitions are characterized by crossing of dynamic responses. Gelation might be seen as a micro-phase order–disorder transition in an associating polymer solution. This solution consists of polydisperse clusters having different sizes. Therefore, their ordering leads to a random arrangement rather than periodic microstructures. In that sense, reversible gelation is a smooth transition from a disordered liquid phase to a solid-like state with a random aperiodic network. This view of the gel state is strongly supported by scattering studies on aqueous solutions of poly(vinyl alcohol) [31, 32] and poly(*n*-isopropyl acrylamide) [33]. It was found that random fluctuations in scattered intensity appear only in the gel state. They disappear with increasing temperature or decreasing concentration below the gel point.

5.4

Phase Separation and Gelation

Polymer solutions exhibit remarkable property changes in response to small changes in external conditions, temperature, or composition of the solution. In good solvents, polymers form stable solutions with respect to phase decay. However, solutions become suddenly unstable and show phase separation in a polymer-poor and polymer-rich phase when the quality of the solvent changes from good to poor due to a change in temperature. One observes an upper critical

solution temperature (UCST) when phase separation occurs upon cooling of the homogeneous solution. The opposite route, heating of the homogeneous solution, leads to phase behavior termed as a lower critical solution temperature (LCST). Polymer solutions, which are homogeneous below a certain temperature and decay above that temperature in two coexisting phases, are promising candidates for biomedical applications [34].

An aqueous solution of poly(*N*-isopropyl acrylamide) (PNIPAM) constitutes an interesting example of a polymer solution with LCST behavior. It displays an LCST in dilute solutions at around 30 °C. From a molecular view, the PNIPAM chains are swollen in water below the LCST since water is a good solvent for the polymer. In the unstable region above the LCST, when water turns into a poor solvent for the polymer, the chains collapse. This on–off mechanism seems to be attractive for drug delivery operations. Eventually, phase separation leads to coexistence of a highly diluted phase in polymer and a phase rich in polymer.

Two phase separation processes of this kind of gelation might be superimposed. Thus, competition of two rate processes rules the morphology formation in the system, the rate of phase separation and the rate of gelation. In the limit

$$Rate_{\text{phase sep}} \gg Rate_{\text{gelation}} \quad (5.23)$$

gelation will proceed in the polymer-rich phase that is under equilibrium conditions. Considering the opposite limit to (5.23)

$$Rate_{\text{phase sep}} \ll Rate_{\text{gelation}} \quad (5.24)$$

the situation becomes more complex. Phase separation in a polymer solution is a diffusion-driven process. Gelation on the other hand involves growing connectivity of chains, which leads to solid-like behavior or a dramatic increase in viscosity. Hence, progression of gelation will dramatically slow down the kinetics of phase separation, as indicated in (5.24). As a possibility, one may control the morphology of a polymer solution by inducing cross-linking during phase separation under the condition that gelation occurs in the same temperature range as liquid–liquid phase separation. This opens a wide field of intelligent structure manipulation. Superposition of phase separation and gelation under condition of inequality (5.24) generates the possibility for pinning down phase-separated morphology at some transient stage in the unstable region of the phase diagram upon gelation. In other words, it is pinning down of non-equilibrium morphologies. The morphology of these gels is kinetically controlled. Coupling of the two processes may also generate phase-separated gels. The procedures discussed here in general terms have been successfully applied in the preparation of membranes [35, 36].

Sol–gel reversible hydrogels have also been prepared by utilizing disorder–order transitions in block copolymers with amphiphilic balance. We mention here the triblock copolymers of poly(ethylene oxide) (PEO) and poly(propylene oxide) (PPO) sequences, PEO-PPO-PEO (trade name, Pluronic®). In aqueous solution, microphase-separation leads to micelle-like aggregates consisting of a hydrophobic PPO core and a swollen hydrated PEO corona with dangling PEO chains. The dangling PEO chains drive toward network-like packing of the micelles. As a result, gel

networks, consisting of interconnected micelles with entangled PEO chains, are established in concentrated Pluronic solutions. The polymer concentration necessary for gelation is relatively high; it is around 15 wt% for a triblock with total molecular mass of $12\,500\text{ g mol}^{-1}$ [37]. Surprisingly, the gelation process in the Pluronic solution was not influenced by adding poly(acrylic acid) (PAA) [38], despite the fact that a high tendency to cross-linking of PAA leads to a hydrogel with an enormous hydration ability. But, obviously, these effects do not affect network formation in the triblock copolymer. The PAA chains are swollen and screened from the PEO-PPO-PEO micelles. Both polymers form independent networks.

The situation changes remarkably when PAA is grafted to the triblock backbone. Studies were carried out with PEO-PPO-PEO-g-PAA where PAA stands for poly(sodium acrylate) [38]. In the grafted polymer the hydrated, dramatically swollen PAA belongs to the molecule and is no longer screened from the triblock. They do not form separate networks as in the blend solution. The PAA acts as the “director” for network formation. This gelation process is obviously not accompanied by phase separation as indicated above with the PNIPAM. It means that PAA grafted to the triblock does not collapse during gelation. Responses to oscillatory shear experiments are shown in Figure 5.2 after the data of Ref [39]. The study was made with a grafted polymer of the following composition (EO100-PO65-EO100)-g-AA170. It means we are close to a 50/50 composition of triblock and grafted PAA. Figure 5.2 shows that in the 1 wt% polymer solution, one obtains Newtonian liquid-like behavior with $G'' > G'$ at low temperature, with increasing temperature the storage modulus increases by two orders of magnitude within a narrow range of temperature and exceeds the loss modulus G'' .

The dramatic reduction in polymer concentration able to gelate as compared to the triblock copolymer is caused by the network-like packing of micelles controlled by highly hydrated PAA.

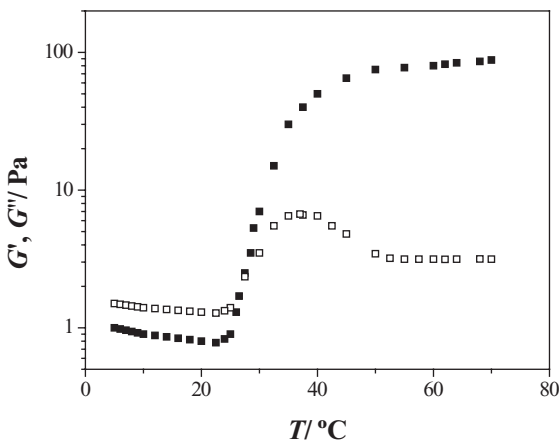


Figure 5.2 Storage (solid square) and loss moduli of aqueous solutions of PEO-PPO-PEO-g-PAA, with 1 wt% of polymer, as a function of temperature; shear frequency 1 Hz, stress 0.6 Pa (after data from Ref. [39]).

5.5

Conclusions

It has been demonstrated that the classical theory of the thermodynamics of gelation is a useful tool in order to describe self-healing processes in polymers quantitatively. The theory is applied in conjunction with viscoelastic properties at the sol-gel transition and with phase separation processes during gelation. It is assumed that in the near future the applications for polymers, polymer alloys and polymer composites can be expanded considerably by using modern concepts of self-healing materials. It will increase the reliability of plastic materials and rubbers for applications in areas such as electronics and transportation.

References

- 1 Bruck, H.A., Evan, J.J., and Peterson, M.L. (2002) *Exp. Mech.*, **42**, 361–371.
- 2 Kassner, M.E., Nemat-Nasser, S., Suo, Z., Bao, G., et al. (2005) *Mech. Matr.*, **37**, 231–259.
- 3 Trask, R.S., Williams, H.R., and Bond, I.P. (2007) *Bioinsp. Biomim.*, **2**, 1–9.
- 4 Wool, R.P. (2008) *Soft Matter*, **4**, 400–418.
- 5 Wu, D.Y., Meure, S., and Solomon, D. (2008) *Prog. Polym. Sci.*, **33**, 479–522.
- 6 Zhang, M.Q., and Rong, M.Z. (2012) *J. Polym. Sci. Polym. Phys.*, **50**, 229–241.
- 7 Yuan, Y.C., Yin, T., Rong, M.Z., and Zhang, M.Q. (2008) *eXPRESS Polym. Lett.*, **2**, 238–250.
- 8 Blaiszik, B.J., Kramer, S.L.B., Olugebefola, S.C., Moore, J.S., Sottos, N.R., and White, S.R. (2010) *Annu. Rev. Mater. Res.*, **40**, 179–211.
- 9 Seiffert, S., and Sprakel, J. (2012) *Chem. Soc. Rev.*, **41**, 909–930.
- 10 White, S.R., Sottos, N.R., Geubelle, P.H., Moore, J.S., Kessler, M.R., Sriram, S.R., Brown, E.N., and Viswanathan, S. (2001) *Nature*, **409**, 794–797.
- 11 Kessler, M.R., and White, S.R. (2002) *J. Polym. Sci. Polym. Chem.*, **40**, 2372.
- 12 Sheng, X., Lee, J.K., and Kessler, M.R. (2009) *Polymer*, **50**, 1264–1269.
- 13 Liu, X., Sheng, X., Lee, J.K., Kessler, M.R., and Kim, J.S. (2009) *Compos. Sci. Technol.*, **69**, 2102–2107.
- 14 Mauldin, T.C., Leonhard, J., Earl, K., Lee, J.K., and Kessler, M.R. (2012) *ACS Appl. Mater. Interfaces*, **4**, 1831–1837.
- 15 Caruso, M.M., Davis, D.A., Shen, Q., Odom, S.A., Sottos, N.R., White, S.R., and Moore, J.S. (2009) *Chem. Rev.*, **109**, 5775.
- 16 Schunack, M., Gragert, M., Döhler, D., Michael, P., and Binder, W.H. (2012) *Macromol. Chem. Phys.*, **213**, 205–214.
- 17 Di Marzio, E.A. (1999) *Prog. Polym. Sci.*, **24**, 329–377.
- 18 Stauffer D., (1976) *J. Chem. Soc. Faraday Trans. II*, **72**, 1354–1364; Stauffer, D., and Aharoni, A. (1992) *Introduction to Percolation Theory*, Taylor and Francis, London.
- 19 Flory, P.J. (1941) *J. Am. Chem. Soc.*, **63**, 3083–3094.
- 20 Stockmayer, W.H. (1943) *J. Chem. Phys.*, **11**, 45–56.
- 21 Wertheim, M.S. (1984) *J. Stat. Phys.*, **35**, 19–34.
- 22 Semenov, A.N., and Rubinstein, M. (1998) *Macromolecules*, **31**, 1373–1385.
- 23 Conglio, A., Stanley, E.H., and Klein, E.H. (1982) *Phys. Rev. B*, **25**, 6805.
- 24 Drye, T.J., and Cates, M.E. (1992) *J. Chem. Phys.*, **96**, 1367–1375.
- 25 Semenov, A.N., Nyrkova, I.A., and Cates, M.E. (1995) *Macromolecules*, **28**, 7879–7885.
- 26 Sciortino, L.F., and Zaccarelli, E. (2011) *Curr. Opin. Solid State Mater. Sci.*, **15**, 246–253.
- 27 Winter, H.H., and Mours, M. (1997) *Adv. Polym. Sci.*, **134**, 165.
- 28 Winter, H.H. (1987) *Progr. Colloid Polym. Sci.*, **75**, 104.

- 29 Li, L., and Aoki, Y. (1997) *Macromolecules*, **30**, 7835.
- 30 Zhao, Y., Cao, Y., Yang, Y., and Wu, C. (2003) *Macromolecules*, **36**, 855.
- 31 Ikkai, F., Shibayama, M., and Han, C.C. (1998) *Macromolecules*, **31**, 3275.
- 32 Kanaya, T., Okhura, M., Kaji, K., and Furusaka, M. (1994) *Macromolecules*, **27**, 5609.
- 33 Shibayama, M., Tanaka, T., and Han, C.C. (1992) *J. Chem. Phys.*, **97**, 6842.
- 34 Zhang, X., Zhuo, R., and Yang, Y. (2002) *Biomaterials*, **26**, 1313.
- 35 Reuvers, A.J., Altena, F.W., and Smolders, C.A. (1986) *J. Polym. Sci.*, **24**, 793.
- 36 Boom, R.M., van den Boomgaard, T., and Smolders, C.A. (1994) *J. Membr. Sci.*, **90**, 231.
- 37 Malmsten, M., and Lindman, B. (1992) *Macromolecules*, **25**, 5440.
- 38 Alexandridis, P., and Hatton, T.A. (1995) *Colloids Surf. A*, **96**, 1–14.
- 39 Huibers, P.D.T., Bromberg, L.E., Robinson, B.H., and Hatton, T.A. (1999) *Macromolecules*, **32**, 4889–4894.

6 Thermally Remendable Polymers

Tom Engel and Guido Kickelbick

6.1 Principles of Thermal Healing

6.1.1 Physical Methods

Physical self-healing mechanisms involve a repair of physical damage by interdiffusion of polymer chains at crack interfaces. No chemical bonds are formed or broken during this process. Only physical links between entangled macromolecular chains are released, rearranged and new entanglements form after diffusion of chain segments across crack interfaces.

6.1.1.1 Molecular Diffusion across a Crack Interface

Self-healing of thermoplastic polymers through molecular diffusion across crack interfaces was studied extensively in the 1980s. The research covers amorphous, semi-crystalline, block copolymers, and composites. Bringing two pieces of the same polymer into contact at a temperature higher than the glass transition temperature T_g , results in a gradual disappearance of the crack interface and an increase in strength at the healing site due to interdiffusion of polymer chains [1].

Jud and Kausch investigated the crack-healing behavior of a series of PMMA samples differing in their molecular weights. They figured out that interpenetration depended strongly on the temperature, the healing-time and the molecular weight of the polymer [2]. Healing occurred already at 5 K above T_g but the effect was much faster if the system was heated to 15 K above T_g . A slight normal pressure on the sample was required to insure the initial contact between fracture surfaces. The amount of pressure depended on the molecular weight because the stiffness increased with M_w . After 1 min penetration time, two surfaces brought together established a bond, which was considerably stronger than that of pure adhesion [2]. In short time experiments, fracture strength comparable to the initial strength of the material was regained quickly. On the other hand, long time experiments showed that the optically healed samples failed 10 times faster than the original material. This means that no fully entangled network has been established in the

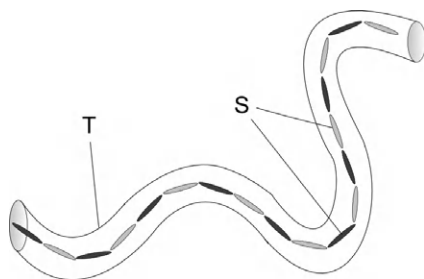


Figure 6.1 A polymer chain P composed of segments S cannot move sideways. The chain is trapped in a virtual tube T and can only move by reptation.

crack region and an interdiffusion of chain segments rather than that of whole polymer chains was responsible for the regain of strength [1]. The effect of the time expired between the formation of the crack and the re-healing was investigated. Immediate (several minutes) penetration led to a much faster healing process than a penetration delay of several days. There has to be some reorganization of chain ends at the crack surfaces and surface reactions cannot be excluded [2].

Different models were established to explain the dynamics of concentrated polymer systems and the phenomenon of crack healing at thermoplastic interfaces [3–5]. According to the reptation model (a chain in a tube) introduced by de Gennes (Figure 6.1), the molecular diffusion coefficient D of a polymer chain is proportional to M^{-2} [3]. The reptation model predicts the dependence between thermal motions and the molecular weight of entangled macromolecules in polymer melts or concentrated polymer solutions. Movements of chains are constrained and, therefore, the macromolecules need to move in a snake-like fashion. In particular, Wool and O'Connor used the reptation model to determine a recovery ratio of mechanical properties. Their five stages model consists of rearrangement, surface approach, wetting, diffusion and randomization [5].

6.1.1.2 Interpenetrating Networks

Another physical thermally engaged self-healing mechanism uses thermoplastic polymers as a system to heal thermosets. These interpenetrating polymer networks (IPN) are composed of a cross-linked thermosetting polymer network and an interpenetrating linear polymer (Figure 6.2). Upon heating, diffusion of linear polymer to the crack interface could aid in closing the rupture.

Palmese *et al.* formulated an *in situ* sequential synthesis of an IPN using diglycidyl ether of bisphenol A (DGEBA) cured with 4,4'-methylene biscyclohexanamine as the crosslinked phase and poly(methacrylated phenyl glycidyl ether) (pMPGE) as the linear polymer phase [6]. Using soxhlet extraction, they showed first that the linear polymer is mobile within the network, which is a necessary condition for the self-healing mechanism. The incorporation of the linear polymer chains allowed increasing retention of healing capacity over additional healing cycles.

Hayes *et al.* mixed a commercially available thermosetting epoxy resin with a linear thermoplastic poly(bisphenol-A-co-epichlorohydrin). The matrix system could be

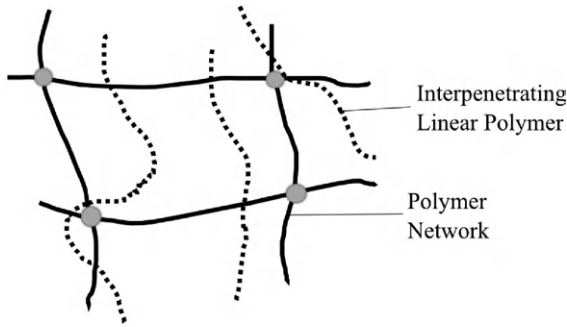


Figure 6.2 Semi-interpenetrating polymer network (SIPN).

induced to regain up to 70% of its virgin properties upon healing by raising the temperature above 140 °C after a fracture event has been demonstrated [7].

Luo *et al.* blended two non-miscible materials, an epoxy network and poly(ϵ -caprolactone) (PCL). The phase-separated blend had “a bricks and mortar” morphology with polyepoxide spheres in a PCL matrix. On heating, the PCL “mortar” melted and wetted all free surfaces and cracks. On cooling, recrystallization of PCL closed the cracks and even two separated pieces could be reattached to each other [8].

6.1.1.3 Shape Memory Assisted Self-Healing

The shape memory effect in polymers permits a polymeric piece to be deformed to a temporary shape until later being triggered to return to its original shape when stimulated by external heating or other means [9, 10].

For semi-crystalline networks, crystallites serve as physical cross-links that can temporarily fixate a deformation below the melting point T_m , and the permanent shape may be recovered when the sample is heated above T_m . Beyond the melting point, rubber elasticity, resulting from permanent covalent cross-links, is responsible for the return to the initial shape. In particular, the crosslinks serve as permanent anchors for the network chains to return to their state of highest conformational entropy [11].

Mather *et al.* used the shape memory effect to assist in the self-healing process. Their strategy was demonstrated in a blend system consisting of a crosslinked poly(ϵ -caprolactone) network and linear poly(ϵ -caprolactone) interpenetrating the network. The shape memory closed any cracks formed during deformation and the linear chains diffused to the crack interface where they re-entangled during the same heating step [12].

6.1.2

Chemical Methods

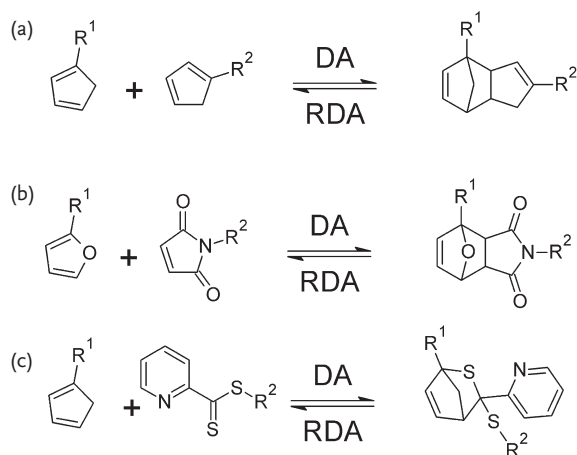
Contrary to physical self-healing mechanisms, chemical methods require breaking and regeneration of new bonds. In this chapter, we will only mention mechanisms

involving covalent bonds. For ionic and supramolecular systems, please consider the chapters dedicated to these topics (Chapters 11 and 13).

6.1.2.1 Thermoreversible Mechanisms

Thermoreversible mechanisms involve chemical reactions forming reversible bonds. Formation or breakage of covalent bonds is controlled by temperature. At low temperature cross-linking or polymerization occurs. Increase in temperature above a critical temperature causes the back reaction, breaking up the previously formed bonds. This critical temperature dictates a temperature range for application. The material can only be employed at temperatures below which the material does not lose any of its mechanical stability. Ideally the back reaction occurs at a higher temperature to allow application at or above room temperature.

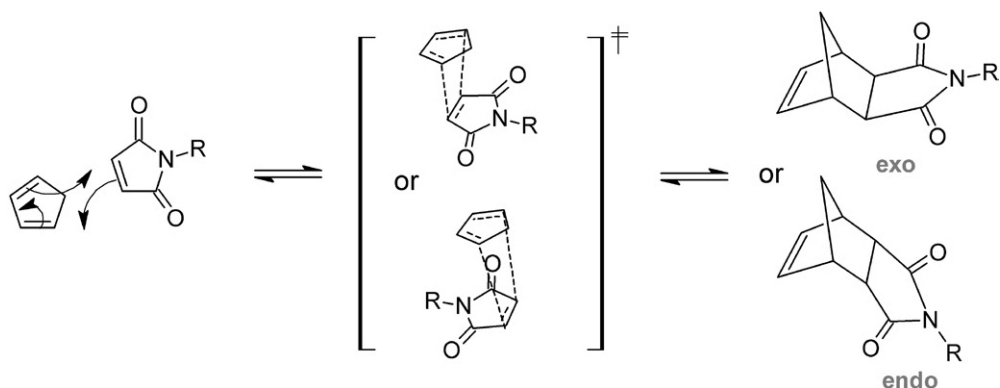
Diels–Alder Reactions DA chemistry has been widely used to synthesize self-healing materials. One of the most relevant aspects of the DA reaction for remendable polymers is its thermal reversibility, known as the retro-Diels–Alder (RDA) reaction [13]. Different systems were investigated for example, dicyclopentadiene, maleimide/furan, hetero-DA. (Scheme 6.1)



Scheme 6.1 Diels–Alder/retro-Diels–Alder equilibrium between (a) two cyclopentadienes, (b) furan and maleimide, (c) cyclopentadiene and pyridinyldithioformate (HDA).

The DA reaction is a thermoreversible [4+2]-cycloaddition involving diene and dienophile reactants. DA reaction enables the formation of two carbon–carbon bonds in a specific manner to form a cyclic (bicyclic) product. Electrons move simultaneously in a cyclic fashion without the need of intermediates. The DA reaction proceeds in a single step, simply on heating. The transition state has six delocalized π -electrons and is, therefore, somewhat aromatic in character, stabilizing the transition to the DA product (Scheme 6.2)

DA reactions occur between a conjugated diene and an alkene called the dienophile, in the example above, cyclopentadiene and a maleimide. Cyclic dienes, like



Scheme 6.2 Schematic DA reaction between a diene and a dienophile. There are two possible six-centered transition states, resulting in the kinetically favored endo-product and the thermodynamically favored exo-product.

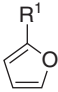
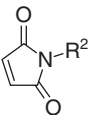
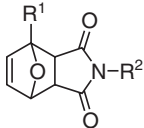
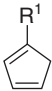
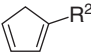
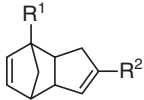
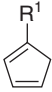
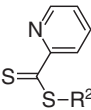
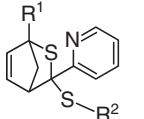
furan or cyclopentadiene, are exceptionally good DA reagents because the conjugated diene in cyclic systems is trapped in the cis-position. Butadiene normally prefers the trans-conformation, making it necessary to rotate around the σ -bond. Because the involved orbitals are normally the HOMO of the diene and the LUMO of the dienophile, it is preferable to approach the energy level of these two orbitals. This can happen with electron-donating functional groups at the 1-position of the diene. The HOMO of furan is higher in energy than that of cyclopentadiene because of the extra electron density brought to the system by the oxygen. That is why, normally, furan and maleimide are reacted together because the energies of the involved molecular orbitals are closer together, permitting faster DA reaction at lower temperatures.

On the other hand, the dienophile reactant needs some kind of conjugation of the alkene for the DA reaction to occur. Simple alkenes have relatively high energy LUMOs and do not react well with nucleophiles. In the case of the maleimide ring, the π -system is extended onto two carbonyl-functional groups and the cyclopentadiene is both the diene and the conjugated dienophile.

DA cycloaddition reaction forms not only carbon-carbon bonds but also heteroatom-carbon bonds (hetero-DA) and it is widely used synthetically to prepare six-membered rings [14]. Dithioesters are very reactive dienophiles when reacted with cyclic dienes. They react even very fast at temperatures below room temperature and in bulk, especially when the reaction is catalyzed by a Lewis acid or trifluoroacetic acid [15, 16]. These catalysts coordinate to sulfur atoms of the dithioester end-group in order to increase the electrophilicity on the thiocarbonyl bond [14]. Table 6.1 summarizes the different reaction partners and reaction conditions for DA reactions used in preparation of thermally remendable polymers.

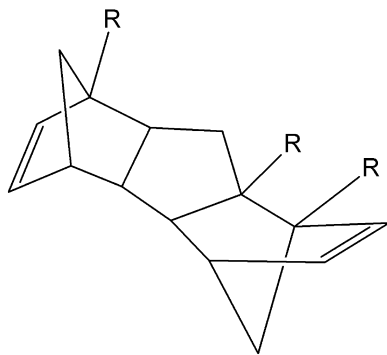
The system using cyclopentadiene as both the diene and the alkene demonstrates a distinctive feature that none of the other DA couples show. Wudl *et al.* demonstrated that the cyclopentadiene dimer (dicyclopentadiene, DCP) is able to

Table 6.1 Summary of different DA reaction partners and the corresponding reaction conditions.

Diene	Dienophile	Conditions	Adduct
 Furan	 Maleimide	DA: between RT and 120 °C RDA: >120 °C Several hours to days	
 Cyclopentadiene	 Cyclopentadiene	DA: between 80 °C and 120 °C ^{a)} RDA: >120 °C or >180 °C ^{a)} Several hours to days	
 Cyclopentadiene	 Dithioester	HDA: between RT and 80 °C RHDA: >80 °C Minutes (Cat: Trifluoroacetic acid)	

a) Depending on R¹ and R².

react as a dienophile with a third CP molecule to form a trimer (Scheme 6.3) [17]. In fact, even linear molecules with telomeric CP-units are able to form network-like materials.



Scheme 6.3 Representation of a cyclopentadienyl trimer responsible for crosslinks in CP polymers [17].

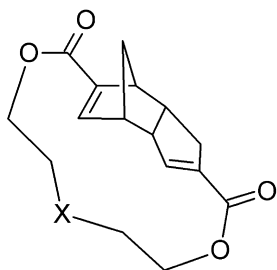
The reactivity of the functional groups in a polymeric material is strongly dependent on the mobility of these groups in the bulk of the polymer. In order to afford a DA-adduct, the reactants must be able to reach the six-centered transition state required to undergo the concerted cycloaddition. If the reactive units are trapped in a rigid matrix, not able to reach one another, no DA reaction will be observed. This can be the case if too many cross-linking points are present, or

if the temperature is lower than the glass transition temperature of the linear polymer chains.

Polymers of cyclopentadiene have been known since Staudinger and Bruson [18]. They discovered not only that CP undergoes a self-DA reaction to produce DCP, but also that DCP is an even better DA substrate, and therefore continues to react with itself to produce a polymer. The major advantage of CP as DA-active units for polymer materials is the fact that CP acts as both the diene and the dienophile [19]. In 1961, Stille and Plummer investigated the polymerization of 1,6-bis(cyclopentadienyl)hexane, 1,9-bis(cyclopentadienyl)nonane and α,α' -bis(cyclopentadienyl)-*p*-xylenes in a homopolymerization and in copolymerization with bismaleimides [20].

CP derivatives of common chlorinated polymers have been widely synthesized and have been used as crosslinkers for the DA reaction. They are easily obtained by reacting the chlorinated polymers for example, poly(vinyl chloride) (PVC) or polychloromethylstyrene (PCMS) with the sodium or lithium salts of CP [21]. The first to demonstrate the thermal reversibility of the DCP-system were Kennedy and Castner [22]. They thermally reversed via RDA at 215 °C, but these systems were not very stable at temperatures this high.

Recently, Wudl *et al.* reported the synthesis of two DA-monomers starting from DCP, which was first transformed to dicyclopentadiene dicarboxylic acid. Afterwards, the monomer was obtained by bislactonization with variable diols (Scheme 6.4). Mechanical and thermal properties of the resulting material could be tuned by varying the nature of the backbone of the diol [17].



Scheme 6.4 Dicyclopentadienyl monomer for single-component self-healing polymer [14].

By heating to the RDA reaction temperature of 120 °C, the monomer opened, releasing two cyclopentadiene units, which could react intermolecularly to form a remendable polymer. The same authors could demonstrate that these systems tend to form crosslinked networks when a DCP unit acts like the dienophile in the DA reaction and reacts with a third CP [17]. Compression tests followed by healing showed remarkable shape recovery (Figure 6.3).

The first to use maleimide and furan moieties, as crosslinking species for polymeric materials, were Stevens and Jenkins [23]. They incorporated maleimide functional groups into a polystyrene backbone by Friedel–Crafts alkylation and

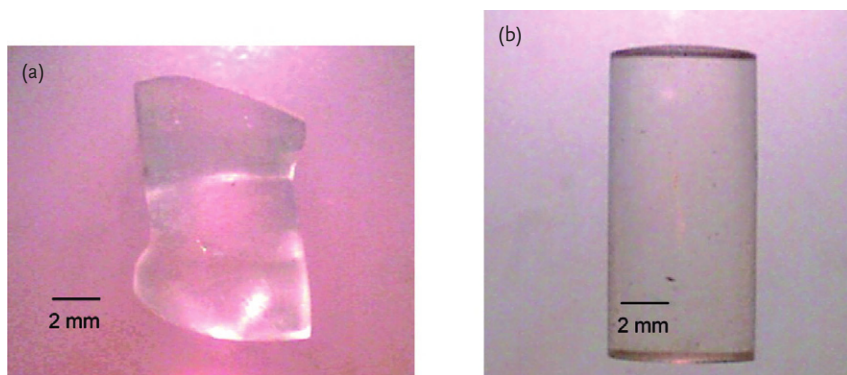


Figure 6.3 CPD polymer, (a) after compression testing and (b) after healing. Reprinted with permission from [17]. Copyright (2008) American Chemical Society.

envisioned the creation of a self-healing material using DA reactivity with a bifunctional furan linker. However this idea was not exploited until a decade later, when Stevens and Canary mixed maleimide-modified polystyrene with difurfuryl adipate [24]. They achieved a remendable crosslinked material with a RDA temperature of 150 °C. Thermal instability of the furfuryl groups, however, limited healing cycles. Wudl *et al.* widely investigated maleimide and furan moieties to develop a remendable polymeric network [25–27]. The materials had equal mechanical properties to commercially available epoxy resins, but a thermal treatment at a temperature above 120 °C allowed disconnecting 30% of the crosslinking, which reconnected upon cooling [25]. Monomers were composed of divalent, trivalent or tetravalent maleimides and furans, varying also in the nature of the spacer backbone. Diethyleneglycol segments were used for example, to lower the glass transition temperature of the resulting polymer, which increased the mobility of polymer chains within the material. Both Wouters *et al.* and Singha *et al.* used furfuryl methacrylate as a co-monomer for co-polymerization with butyl methacrylate or methyl methacrylate, respectively [28, 29]. In the first example, free radical polymerization was used to synthesize the polymethacrylate backbone bearing pendant furan-groups [28]. This led to a polymer gel because, under these reaction conditions, some of the furfuryl-groups crosslinked. By mixing the swollen polymer with a bismaleimide as crosslinking agent a powder coating system was obtained. The powder was applied onto a substrate and melted at elevated temperatures above 120 °C to form a coating which solidified upon cooling. Subsequent heating and cooling cycles revealed reversible behavior and no significant loss of properties [28]. On the other hand, Singha *et al.* used atom transfer radical polymerization (ATRP) to prepare furfuryl methacrylate co-polymers together with methyl methacrylate. Thereby they achieved a better polydispersity index of 1.3 [29], and no crosslinking of the pendant furfuryl-groups was observed. The resulting linear co-polymer was crosslinked via DA reaction using bismaleimides.

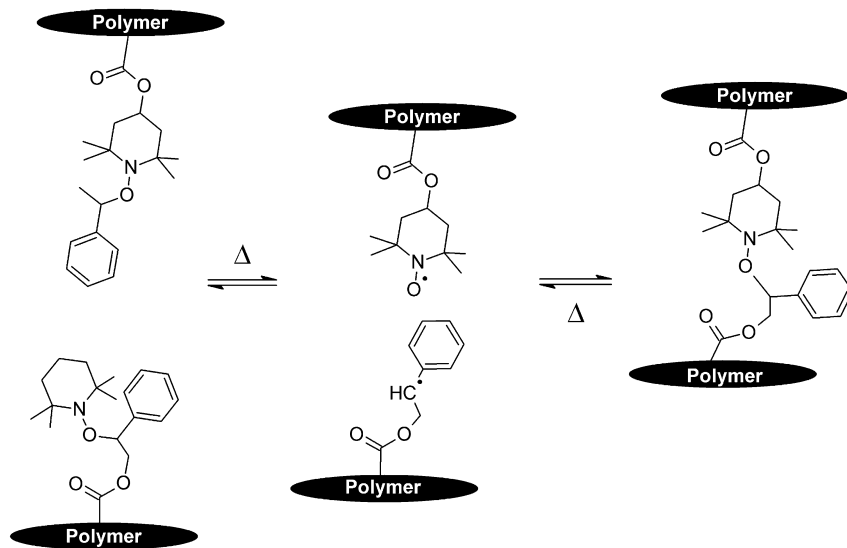
Within the wide variety of dienes and dienophiles usable for self-healing based on DA chemistry, there are very few that allow fast crosslinking or polymerization. Reaction times of several days can be necessary for the DA reaction in the bulk of a polymer. Probably the fastest DA reaction reported until now, is the hetero-DA reaction between CP and pyridinyldithioformate linkers [15, 16]. The monomers could be crosslinked in the solid state within minutes at room temperature and de-crosslinked at temperatures above 80 °C within minutes. Disadvantages for the application of these fast-healing systems are the small window of temperatures, relatively high costs, and instability at higher temperatures limiting the number of healing-cycles [16].

NO–C Bonds Self-healing polymeric materials, using dynamic covalent bonds like the NO–C bonds as a healing mechanism, are based on the same principles as stable free radical polymerization (SFRP) first mentioned by Kazmeier *et al* [30]. SFRP is a living polymerization technique using reversible termination of radical chain growth. Reversible terminators, such as 2,2,6,6-tetramethyl-1-piperidinyloxy (TEMPO), must have an endothermic enthalpy of reaction with styrene monomer so that they are not able to initiate new chains once they are liberated.

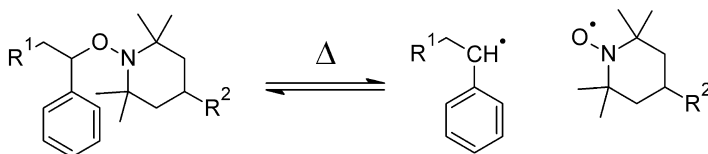
During SFRP, TEMPO is required to capture reversibly any radical at the chain ends to prevent preliminary chain termination. To use this procedure as a self-healing mechanism the NO–C bonds have to be used as crosslinking points in the thermosetting material. Therefore, it is necessary to attach pendant styryl groups captured by TEMPO, as well as pendant TEMPO units linked to styryl moieties onto the backbone of polymer chains [31–33]. By heating to a temperature of >60 °C, two complementary radicals, which are attached to the polymer backbone, are released. These free TEMPO and styryl radicals can recombine through a radical exchange reaction, thereby crosslinking the material (Scheme 6.5). The biggest advantage is the rate at which the bonds dissociate and reform, leaving the material with all its mechanical properties, even above the dissociation temperature.

Stable organic radicals have received much attention over the last years. The advantages of these systems are that the C–ON bonds of alkoxyamines quite easily break and reform (Scheme 6.6). The resulting N–O radicals are stable enough to give the material the apparent dynamic features of a supramolecular system and the mechanical strength of a covalently bonded polymer [19]. For the first time, Otsuka *et al.* demonstrated the dynamic covalent bond between a TEMPO and a styrylradical [31, 34, 35].

Model compounds were used to demonstrate the exchange reaction after breaking the bond [31]. Otsuka *et al.* prepared linear polymers containing dynamic bonds in their backbone [35] or as pendant groups on a PMMA chain [31]. Zhang *et al.* developed a synthetic pathway to attach the dynamic unit on a PCMS polymer [32]. Both Zhang and Otsuka demonstrated the gelation of these systems by radical exchange reaction (Figure 6.4). By heating the polymer, the covalent bonds broke up into two radicals, which could recombine with a different radical to form



Scheme 6.5 Schematic representation of the thermodynamic formation of crosslinked polymers via radical exchange reaction of alkoxyamines.



Scheme 6.6 Dissociation/association of alkoxyamine-derivatives.

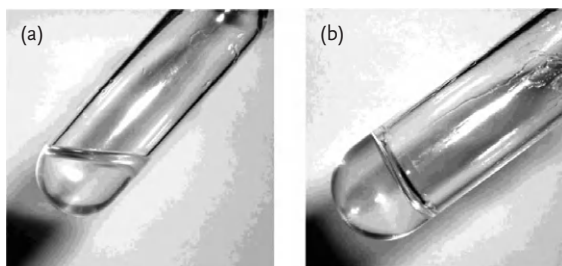


Figure 6.4 Pictures of the solution of the polymer in anisole (10wt%) (a) before and (b) after heating at 100°C for 24 h. Reprinted with permission from [31]. Copyright (2006) American Chemical Society.

chemical crosslinks. These crosslinks could easily be cleaved by adding an excess amount of free alkoxyamine [31].

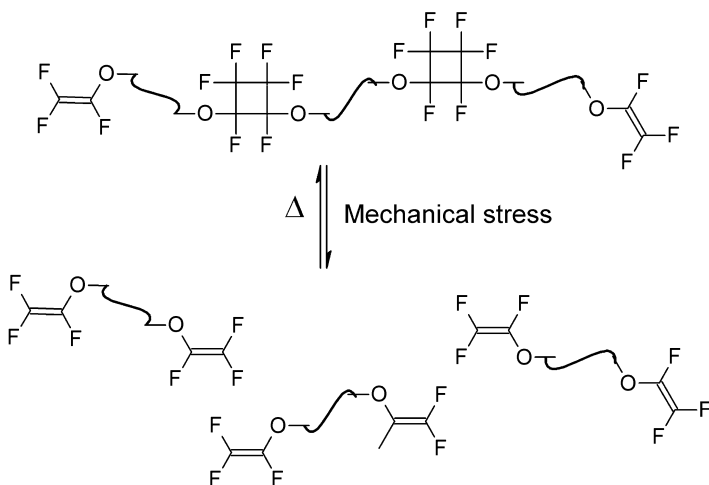
6.1.2.2 Alternative Mechanism

Thermal decomposition of PFCB is an effectively irreversible reaction yielding different products [36]. On the other hand, pure mechanical decomposition, like in the case of ultrasonic pulses, lead to breaking the cyclobutane into two vinyl ethers. These can be thermally triggered to form PFCB bonds once again. The perfluorocyclobutane healing mechanism is technically not a thermoreversible mechanism and, therefore, it is treated separately.

6.1.2.3 Perfluorocyclobutanes

The C–F bonds in fluoroalkenes are 460–540 kJ mol⁻¹ very strong bonds (450–540 kJ mol⁻¹). But vicinal fluorination has been shown to weaken the strength of the alkene. Tetrafluoroethene has a π -dissociation energy of only 220 kJ mol⁻¹. The double bond instability is responsible for the well-known propensity of fluorinated alkenes to undergo [2+2]-cycloaddition. Thermal [2+2]-cycloaddition is normally forbidden, because of molecular orbital symmetry. In simple alkenes a biradical intermediate product has to be induced photochemically, which recombines into a cyclobutane [37]. The weakness of the π -bond in fluorinated alkenes enables thermal dissociation into a biradical transition state.

Craig *et al.* investigated the self-healing properties of poly(perfluorocyclobutane) (PPFCB), an important class of polymers for aerospace and electronics [36]. PFCB units were interesting because they break under mechanical stress to form trifluorovinylethers (TFVE), which are the starting material for the formation of PPFCB. A simple thermal treatment (>150 °C) led to remending (Scheme 6.7). The breaking mechanism involved a diradical transition state, which enabled



Scheme 6.7 PFCB polymers are cleaved by mechanical chain stress into smaller parts containing TFVE groups that can be repolymerized thermally.

secondary self-healing mechanisms. The 1,4-diradical makes stress-induced crosslinking a possible self-healing mechanism and stress-induced isomerization, from *cis* to *trans*, could be a mechanism for stress-release, like in the case of *gem*-dibromocyclopropane [38].

It must be distinguished between a thermal decomposition and a mechanical decomposition, because they do not yield the same decomposition product [36]. The major thermal decomposition products are hexafluorocyclobutene and phenol, an effectively irreversible reaction that is not suitable for remending. Only pure mechanical decomposition results in a cycloreversion of PFCB moieties to thermally remendable TFVE units. Ultrasonic pulses simulated these pure mechanical reaction conditions.

6.2 Inorganic–Organic Systems

In inorganic–organic composite and nanocomposite materials, properties of different material classes can be combined to increase thermal stability, mechanical strength, electrical conductivity and/or the index of refraction. Inorganic particles or fibers have been widely used in the field of (nano)composites. These principles can be expanded to self-healing (nano)composites.

In particle or fiber-reinforced materials, the adhesion of the filler to the polymer matrix is important to guarantee load transfer from the polymer matrix to the reinforcement material [39]. Normally surface modification of the filler particles with polymerizable groups allows chemical binding between both phases.

Peterson and coworkers attached dienophile maleimido functional groups to the surface of glass fibers. These glass fibers were combined with a thermosetting furan-functionalized epoxy resin [39]. Reversible DA reaction was used to impart reversible covalent binding at the polymer/glass interface. Mechanical stress was followed by complete failure of the interface. Significant healing could be observed after thermal treatment for 1 h at 90 °C.

Kwok and Hahn proposed to use carbon fibers as a resistive heating network for use in self-healing composites based on the DA mechanism [40]. An electrical current passing through fibers of a carbon fiber-filled polymer matrix caused heat through resistance heating. The heat created in the composite was then transferred to the insulating resin, utilizing DA reaction to heal itself. Removal of any resin-rich top layer may be necessary to expose the fibers and reduce local contact resistance as much as possible [40].

Bowman *et al.* were interested in using the magnetic properties of metal oxide nanoparticles to trigger self-healing by an external alternating magnetic field. Therefore chromium oxide CrO₂, which has an ideal Curie temperature for retro-DA reaction (113 °C), was mixed with a trifuran monomer. To this mixture, a diphenylbismaleimide was added and, upon melting at 150 °C and re-cooling, the monomers combined to a thermoreversible network. The black thermoset melted within a magnetic field and crosslinked again upon slow cooling. The maximum

temperature depended on the weight-percentage of CrO₂ and the magnetic field strength [41]. The incorporation of magnetically susceptible particles in a thermoreversible gel resulted in a material that underwent a reversible gel-to-sol transition when placed in an alternating magnetic field. The gel-to-sol transition allowed the material to flow, and upon cooling macroscopic fractures were healed by diffusion.

6.3

Efficiency, Assessment of Healing Performance

In this section, popular methods for the control of healing performance will be mentioned. First, there are general analytical methods, like nuclear magnetic resonance (NMR) and infrared (IR) spectroscopy, differential scanning calorimetry (DSC), size-exclusion chromatography (SEC), or mechanical tests. On the other hand, some specialized tools are used, depending on the system and the self-healing mechanism.

Beside liquid NMR and IR spectroscopy, solid-state ¹³C NMR spectroscopy is another general method to study self-healing polymers [25, 26]. NMR allows one to investigate the thermally reversible DA reaction in the macromolecular solid by differentiating for example, between free furan groups and the pericyclic DA product.

In the case of perfluorocyclobutane as a healing mechanism, ¹⁹F NMR is a useful tool to distinguish between the PFCB unit and free fluoroalkenes [36]. SEC is especially useful in the analysis of soluble uncrosslinked macromolecules [15, 16, 36]. If a thermoreversible reaction like DA, hetero-DA or the thermal cyclization of fluoroalkenes is used to polymerize beginning from monomers, SEC allows to monitor reversibility by checking for de-polymerization, by retro-DA reaction or mechanical damage.

DSC was also utilized to monitor DA and retro-DA reaction in self-healing polymers [25, 26, 42]. Wudl and coworkers used a specialized DSC technique called temperature-modulated DSC. Employing this method they could differentiate between reversible and non-reversible effects. Non-reversible effects, like degradation of the material, tend to overlap with signals of the reaction of interest.

Dynamic mechanical analysis (DMA) has been proven helpful for self-healing performance assessment [17, 33]. It is applicable for all types of thermally self-healing materials, physical methods or chemical methods. In the case of dynamic covalent bonds, Yuan *et al.* used DMA to compare the temperature dependence of the loss factor $\tan \delta$ of reversibly crosslinked polystyrene and permanently crosslinked polystyrene. Both systems showed similar glass transition temperature signals at 125 °C. The dynamic equilibrium of dissociation/association was very fast and the apparent molecular weight did not change, allowing the part to retain the shape and mechanical properties even during the healing process [33].

Mechanical testing is very important to study the bulk properties of a healed material, which should be as similar as possible to the original material properties.

Table 6.2 Summary of healing efficiencies of self-healing materials determined with different mechanical tests.

Healing mechanism	Mechanical test	Healing conditions	Maximum healing efficiency
Cyclopentadiene Diels–Alder [17]	Three-point bending test	120 °C, 12 h	≈60%
Maleimide/furan Diels–Alder with CrO ₂ [41]	Three-point bending test	110 °C, 12 h	≈100%
C–ON bond [33]	Double cleavage drilled compression test	130 °C, 2.5 h	≈75%
Maleimide/furan Diels–Alder epoxy resin [42]	Double cleavage drilled compression test	120 °C, 20 min 80 °C, 72 h	≈96%
Maleimide/furan Diels–Alder [25]	Compact tension test	120–150 °C, 24 h	≈57%
Interpenetrating Network (IPN) [7]	Compact tension test	130 °C, 1 h	≈70%
Interpenetrating Network (IPN) [6]	Compact tension test (modified)	165 °C, 1 h	≈52%
Maleimide/furan Diels–Alder coatings [28]	Rheology, measurement of viscosity during heating cycles	175 °C, 1 h	≈100%

Table 6.2 summarizes healing efficiencies of some materials using different mechanical tests. A general method to study these properties is the three-point bending flexural test [41]. Three-point bending was used in the nanocomposite using CrO₂ as magnetic susceptible particles transferring the energy of an alternating magnetic field into the polymer matrix in the form of heat. The flexural test was used to determine the flexural strength of a specimen before and after several healing cycles. In these experiments, complete recovery of the flexural modulus and ultimate strength was demonstrated.

Fracture toughness is an indication of the amount of stress required to propagate a pre-existing flaw. It is a very important material property since the occurrence of flaws is not completely avoidable in the processing, fabrication, or service of a material/component. There are different popular fracture test specimen geometries. Double cleavage drilled compression (DCDC) specimens are particularly suitable for brittle materials (Figure 6.5a) [43]. Janssen originally designed DCDC fracture tests for measuring the fracture toughness of glass [44]. DCDC sample refers to a rectangular column with a circular hole drilled through its center that is subjected to axial compression [43]. This geometry was used by

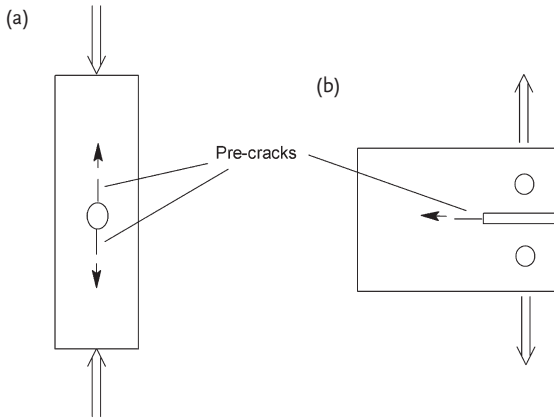


Figure 6.5 Fracture test sample geometries: (a) double cleavage drilled compression (DCDC) test, (b) compact tension test. Pre-cracks are formed by tapping with a razor blade.

Zhang and coworkers to evaluate the healing efficiency of their maleimide and furan modified epoxy resin. The design allowed controlled incremental crack growth so that the cracked specimen remained in one piece after the test, ensuring realignment of the fracture surfaces prior to healing. A blade was wedged into the central hole of the DCDC specimen before the test to create pre-cracks at the upper and lower extremities [42]. The same method was used in the case of the radical mechanism using alkoxyamines for self-healing. Healing efficiency was calculated from the ratio of critical stress required to propagate the crack to a given length in the healed material and in the virgin material. Nearly complete rehabilitation was observed for the cured resin, as characterized by the average healing efficiency of 96% [33].

Wudl *et al.* used a different geometry to test the fracture toughness of their DA self-healing materials [25, 26]. Hayes *et al.* investigated with the same test the properties of an IPN [7]. They chose compact tension test specimen geometry (Figure 6.5b). Gently tapping a fresh razor blade into a machined starter notch of the sample created a sharp pre-crack.

Application of a tension perpendicular to the pre-crack, led to a complete fracture of the specimen by crack propagation. After structural failure, the two pieces were matched and held together with a clamp, treated at 120° to 150°C under nitrogen for about 2h, and cooled to room temperature (Figure 6.6). Fracture tests before and after healing showed recovery of about 57% of fracture strength [25]. Palmese *et al.* used the same geometry for the assessment of healing properties of their IPN, with the addition of a crack-arresting hole drilled in the middle of the crack-propagation pathway [6].

The free stable radical approach developed by Otsuka and Takahara allows a special analytical tool, which detects free radicals [31, 34, 35]. Electron spin resonance (ESR) spectroscopy was first used by Rong *et al.* and later by Zhang *et al.* to examine fission behavior of alkoxyamine moieties at increasing temperatures

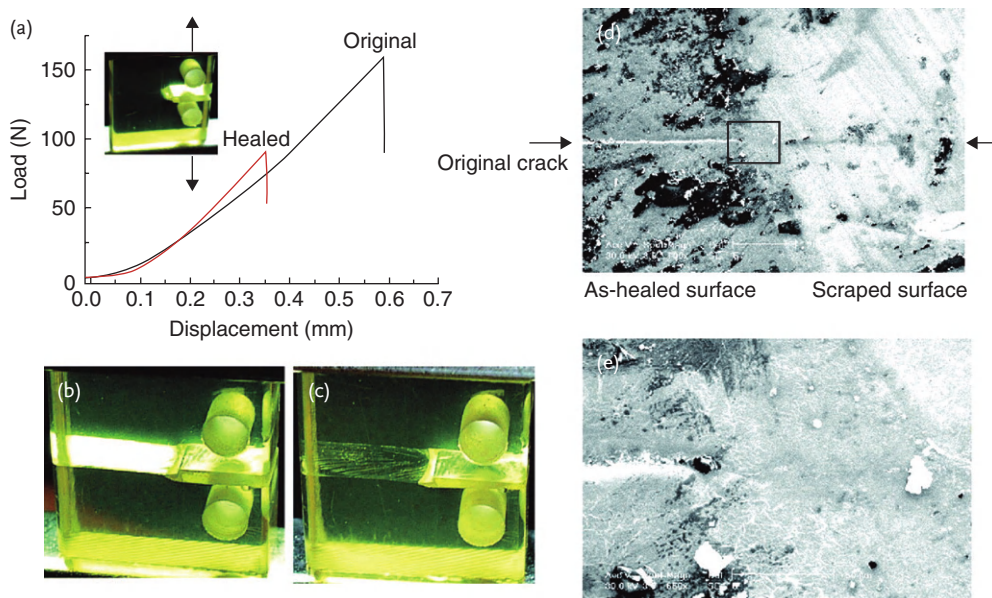


Figure 6.6 (a) Mending efficiency obtained by fracture toughness testing. Values for the original and healed fracture toughness at the critical load. (b) Image of a broken specimen before thermal treatment. (c) Image of the specimen after thermal treatment. (d) SEM

image of the surface of a healed sample: the left side is the as-healed surface and the right side is the scraped surface. (e) Enlarged image of the boxed area in (d). Reprinted with permission from [25]. Copyright (2002) Science Magazine.

[32, 33]. Starting from a temperature of 100°C, free radical concentration increased gradually. Cyclic ESR measurement between 20 and 130°C showed that the relative intensity of the radical signal fluctuated and that the process was fully reversible apart from irreversible recombinations of styrene radicals [33].

6.4 Conclusions

In recent years substantial progress has been observed in the field of thermally remendable polymers. A comparison between thermally reversible polymerization or thermoplastic diffusion and autonomous healing mechanisms reveals both advantages and disadvantages. The advantages of thermally remendable polymers are clearly the repeatability of the crack-healing process and the single-component nature of the systems, which makes manufacturing easy. No healing agents and/or capsules are required because the necessary functionalities are included in the polymer chains. The fact that thermally remendable polymers demand external energy intake, in the form of heat, in order to heal damage is clearly a disadvantage. Monomers for the chemical approaches using reversible polymerization are not

commercially available. Another disadvantage is the quite long healing times in some cases, which makes the search for accelerating mechanisms one of the major research tasks. The future of chemically based self-healing materials appears to be bright, particularly once they leave academic research and enter the world of applications. Physical healing mechanisms on the other hand, do not need expensive starting materials. These materials are more likely to find large-scale implementations because commercially available polymers can be mixed together to obtain self-healing properties.

Acknowledgments

We thank the grant DFG KI 1066/2-1 (within the SPP 1568 “Design and Generic Principles of Self-Healing Materials” for financial support.

References

- 1 Wu, D.Y., Meure, S., and Solomon, D. (2008) Self-healing polymeric materials: a review of recent developments. *Prog. Polym. Sci.*, **33**, 479–522.
- 2 Jud, K., and Kausch, H.H. (1979) Load transfer through chain molecules after interpenetration at interfaces. *Polym. Bull.*, **1**, 697–707.
- 3 Gennes, P.G.D. (1971) Reptation of a polymer chain in the presence of fixed obstacles. *J. Chem. Phys.*, **55**, 572–579.
- 4 Doi, M., and Edwards, S.F. (1978) Dynamics of concentrated polymer systems. Part 1. Brownian motion in the equilibrium state. *J. Chem. Soc. Faraday Trans. 2*, **74**, 1789–1801.
- 5 Wool, R.P., and O'Connor, K.M. (1981) A theory of crack healing in polymers. *J. Appl. Phys.*, **52**, 5953–5963.
- 6 Peterson, A.M., Kotthapalli, H., Rahmathullah, M.A.M., and Palmese, G.R. (2012) Investigation of interpenetrating polymer networks for self-healing applications. *Compos. Sci. Technol.*, **72**, 330–336.
- 7 Hayes, S.A., Jones, F.R., Marshiya, K., and Zhang, W. (2007) A self-healing thermosetting composite material. *Compos. Appl. Sci. Manuf.*, **38A**, 1116–1120.
- 8 Luo, X., Ou, R., Eberly, D.E., Singhal, A., Viratyporn, W., and Mather, P.T. (2009) A thermoplastic/thermoset Blend exhibiting thermal mending and reversible adhesion. *ACS Appl. Mater. Interfaces*, **1**, 612–620.
- 9 Rousseau, I.A. (2008) Challenges of shape memory polymers: a review of the progress toward overcoming SMP's limitations. *Polym. Eng. Sci.*, **48**, 2075–2089.
- 10 Lendlein, A., and Kelch, S. (2002) Shape-memory polymers. *Angew. Chem. Int. Ed.*, **41**, 2034–2057.
- 11 Lendlein, A., Schmidt, A.M., Schroeter, M., and Langer, R. (2005) Shape-memory polymer networks from oligo(ϵ -caprolactone)dimethacrylates. *J. Polym. Sci. Part A Polym. Chem.*, **43**, 1369–1381.
- 12 Rodriguez, E.D., Luo, X., and Mather, P.T. (2011) Linear/Network Poly(ϵ -caprolactone) blends exhibiting Shape Memory Assisted Self-Healing (SMASH) *ACS Appl. Mater. Interfaces*, **3**, 152–161.
- 13 Diels, O., and Alder, K. (1928) Syntheses in the hydroaromatic series. I. Addition of “diene” hydrocarbons. *Justus Liebigs Ann. Chem.*, **460**, 98–122.
- 14 Tasdelen, M.A. (2011) Diels-Alder “click” reactions: recent applications in polymer and material science. *Polym. Chem.*, **2**, 2133–2145.
- 15 Inglis, A.J., Sinnwell, S., Stenzel, M.H., and Barner-Kowollik, C. (2009) Ultrafast click conjugation of macromolecular

- building blocks at ambient temperature. *Angew. Chem. Int. Ed.*, **48**, 2411–2414.
- 16 Inglis, A.J., Nebhani, L., Altintas, O., Schmidt, F.G., and Barner-Kowollik, C. (2010) Rapid bonding/debonding on demand: reversibly cross-linked functional polymers via Diels-Alder chemistry. *Macromolecules*, **43**, 5515–5520.
- 17 Murphy, E.B., Bolanos, E., Schaffner-Hamann, C., Wudl, F., Nutt, S.R., and Auad, M.L. (2008) Synthesis and characterization of a single-component thermally remendable polymer network: Staudinger and Stille revisited. *Macromolecules*, **41**, 5203–5209.
- 18 Staudinger, H., and Bruson, H.A. (1926) Highly polymerized compounds. VIII. Polymerization of cyclopentadiene. *Justus Liebigs Ann. Chem.*, **447**, 110–122.
- 19 Bergman, S.D., and Wudl, F. (2008) Mendable polymers. *J. Mater. Chem.*, **18**, 41–62.
- 20 Stille, J.K., and Plummer, L. (1961) Polymerization by the Diels-Alder reaction. *J. Org. Chem.*, **26**, 4026–4029.
- 21 Miura, M., Akutsu, F., Usui, T., Ikebukuro, Y., and Nagakubo, K. (1985) Soluble cyclopentadienylated polymers. *Makromol. Chem.*, **186**, 473–481.
- 22 Kennedy, J.P., and Castner, K.F. (1979) Thermally reversible polymer systems by cyclopentadienylation. I. A model for termination by cyclopentadienylation of olefin polymerization. *J. Polym. Sci. Polym. Chem. Ed.*, **17**, 2039–2054.
- 23 Stevens, M.P., and Jenkins, A.D. (1979) Crosslinking of polystyrene via pendant maleimide groups. *J. Polym. Sci. Polym. Chem. Ed.*, **17**, 3675–3685.
- 24 Canary, S.A., and Stevens, M.P. (1992) Thermally reversible crosslinking of polystyrene via the furan-maleimide Diels-Alder reaction. *J. Polym. Sci. Part A Polym. Chem.*, **30**, 1755–1760.
- 25 Chen, X., Dam, M.A., Ono, K., Mal, A., Shen, H., Nutt, S.R., Sheran, K., and Wudl, F. (2002) A thermally re-mendable cross-linked polymeric material. *Science*, **295**, 1698–1702.
- 26 Chen, X., Wudl, F., Mal, A.K., Shen, H., and Nutt, S.R. (2003) New thermally remendable highly cross-linked polymeric materials. *Macromolecules*, **36**, 1802–1807.
- 27 Wudl, F., and Chen, X. (2004) Thermally re-mendable crosslinked polymers, monomers, their manufacture, and thermally mending. US Patent 20040014933, filed July 12, 2002 and issued January 22, 2004.
- 28 Wouters, M., Craenmehr, E., Tempelaars, K., Fischer, H., Stroeks, N., and van Zanten, J. (2009) Preparation and properties of a novel remendable coating concept. *Prog. Org. Coat.*, **64**, 156–162.
- 29 Kavitha, A.A., and Singha, N.K. (2007) A tailor-made polymethacrylate bearing a reactive diene in reversible Diels-Alder reaction. *J. Polym. Sci. Part A Polym. Chem.*, **45**, 4441–4449.
- 30 Kazmaier, P.M., Moffat, K.A., Georges, M.K., Veregin, R.P.N., and Hamer, G.K. (1995) Free-radical polymerization for narrow-polydispersity resins. Semiempirical molecular orbital calculations as a criterion for selecting stable free-radical reversible terminators. *Macromolecules*, **28**, 1841–1846.
- 31 Higaki, Y., Otsuka, H., and Takahara, A. (2006) A thermodynamic polymer crosslinking system based on radically exchangeable covalent bonds. *Macromolecules*, **39**, 2121–2125.
- 32 Wang, F., Rong, M.Z., and Zhang, M.Q. (2012) Reversibility of solid state radical reactions in thermally remendable polymers with C-ON bonds. *J. Mater. Chem.*, **22**, 13076–13084.
- 33 Yuan, C.E., Rong, M.Z., Zhang, M.Q., Zhang, Z.P., and Yuan, Y.C. (2011) Self-healing of polymers via synchronous covalent bond fission/radical recombination. *Chem. Mater.*, **23**, 5076–5081.
- 34 Higaki, Y., Otsuka, H., and Takahara, A. (2004) Dynamic formation of graft polymers via radical crossover reaction of alkoxyamines. *Macromolecules*, **37**, 1696–1701.
- 35 Otsuka, H., Aotani, K., Higaki, Y., Amamoto, Y., and Takahara, A. (2007) Thermal reorganization and molecular weight control of dynamic covalent polymers containing alkoxyamines in their main chains. *Macromolecules*, **40**, 1429–1434.
- 36 Klukovich, H.M., Kean, Z.S., Iacono, S.T., and Craig, S.L. (2011) Mechanically

- induced scission and subsequent thermal remending of perfluorocyclobutane polymers. *J. Am. Chem. Soc.*, **133**, 17882–17888.
- 37 Banks, R.E., Smart, B.E., Tatlow, J.C. (eds) (1994) *Organofluorine Chemistry: Principles and Commercial Applications*, Springer
- 38 Wu, D., Lenhardt, J.M., Black, A.L., Akhremitchev, B.B., and Craig, S.L. (2010) Molecular stress relief through a force-induced irreversible extension in polymer contour length. *J. Am. Chem. Soc.*, **132**, 15936–15938.
- 39 Peterson, A.M., Jensen, R.E., and Palmese, G.R. (2011) Thermoreversible and remendable glass-polymer interface for fiber-reinforced composites. *Compos. Sci. Technol.*, **71**, 586–592.
- 40 Kwok, N., and Hahn, H.T. (2007) Resistance heating for self-healing composites. *J. Compos. Mater.*, **41**, 1635–1654.
- 41 Adzima, B.J., Kloxin, C.J., and Bowman, C.N. (2010) Externally triggered healing of a thermoreversible covalent network via self-limited hysteresis heating. *Adv. Mater.*, **22**, 2784–2787.
- 42 Tian, Q., Rong, M.Z., Zhang, M.Q., and Yuan, Y.C. (2010) Synthesis and characterization of epoxy with improved thermal remendability based on Diels-Alder reaction. *Polym. Int.*, **59**, 1339–1345.
- 43 Pallares, G., Ponson, L., Grimaldi, A., George, M., Prevot, G., and Ciccotti, M. (2009) Crack opening profile in DCDC specimen. *Int. J. Fracture*, **156**, 11–20.
- 44 Janssen, C. (1974) Specimen for fracture mechanics on glass. 10th International Congress on Glass, pp. 23–30.

7

Photochemically Remendable Polymers

Jun Ling, Ming Qiu Zhang, and Min Zhi Rong

7.1

Background

Inspired by naturally occurring species, self-healing polymers have been prepared as a member of the intelligent materials family [1–5]. Of these, self-healing based on photoreversible reaction is quite attractive because the use of light is clean, cheap, and readily available. It would be advantageous to have polymers that unconsciously mend when exposed to environmental conditions like sunlight [6].

Covalently bonded polymers are welcome in many applications due to their balanced mechanical performance. To provide covalent bonds with reversibility for building up intrinsic self-healing polymers, cycloaddition reactions are certainly the first choice. Besides the thermally initiated Diels–Alder reaction, photoinitiated cycloaddition is also possible (Figure 7.1). Photochemical [2+2] and [2+4] cycloaddition are the most common photodimerization reactions and can be used for photochemical healing of polymers as the reversion of the cycloaddition resultant to C=C bonds occurs readily in the solid state [7]. Photoinduced cyclodimerization of cinnamic acid in its crystalline form even traces back to as early as 1919 [8]. Nevertheless, photocycloaddition-aided self-healing polymers were not documented until recently.

In 2004, Chung *et al.* synthesized a photo-crosslinkable cinnamate monomer, 1,1,1-tris-(cinnamoyloxymethyl) ethane (TCE) bearing three optically active moieties (Figure 7.2a) [9]. It can crosslink to form a very hard solid via [2+2] photocycloaddition upon ultraviolet (UV) irradiation at $\lambda > 280$ nm. When the sample of TCE suffers an impact, propagating microcracks result in cleavage of the cyclobutane ring due to its low bond strength. Re-irradiation with UV light allows recovery of the crosslinked networks (Figure 7.2b). Healing efficiencies in terms of flexural strength up to 14 and 26% were obtained in the case of UV stimulus or a combination of UV light and heating (100 °C).

Urban and Ghosh developed a heterogeneous polyurethane (PUR) network containing an oxetane-substituted derivative of chitosan (OXE-CHI) via the reaction with hexamethylene diisocyanate (HDI) and polyethylene glycol (PEG) (Figure 7.3) [10]. Upon mechanical damage of the material, the four-membered oxetane

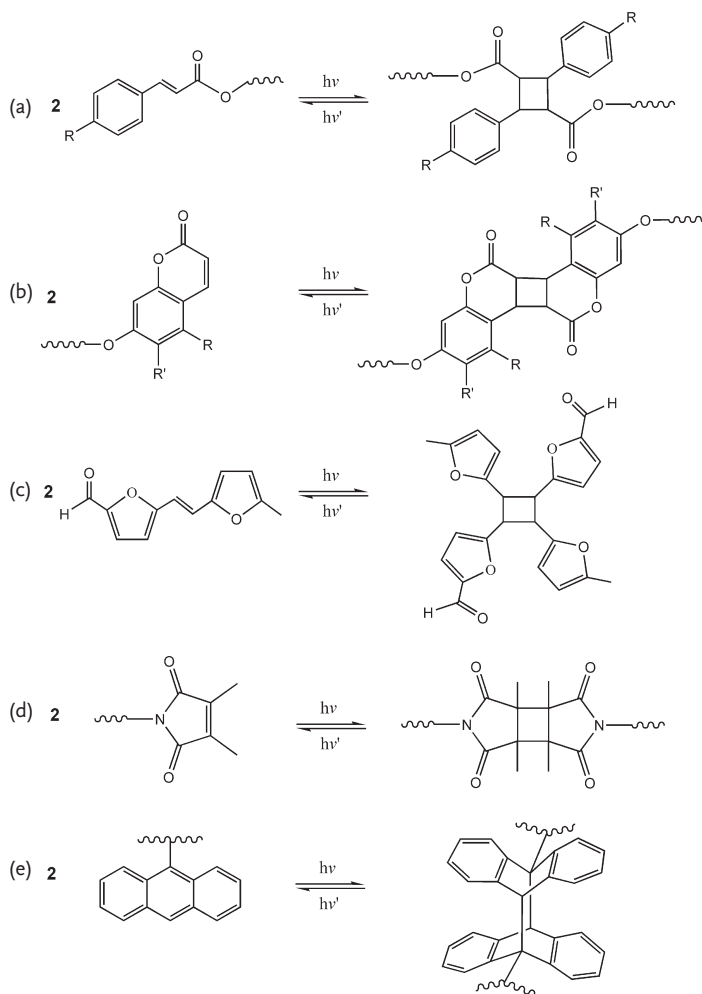


Figure 7.1 Most common photocycloaddition dimerization reactions used in polymer and materials science, specifically dimerization of (a) cinnamate, (b) coumarins, (c)

vinyl, (d) maleimides, and (e) anthracene derivatives [7] (Reproduced by permission of Wiley-VCH Verlag GmbH & Co. KGaA).

rings open to create two reactive ends. When exposed to UV light at 302 nm wavelength, a series of covalent bond rearrangements including chitosan chain scission occurs, generating crosslinks with the reactive oxetane ends, so that the network acquires one way healability. Visual inspection of the cut on a filmy sample indicated that the material was capable of repairing itself in less than an hour.

Amamoto *et al.* [11] prepared macroscopic self-healing crosslinked polyurethanes based on radical reshuffling of thiuram disulfide (TDS) units under the stimulation of visible light at room temperature and without solvent. Since the S–S bonds in the incorporated TDS units homolytically dissociate in visible light, the radical

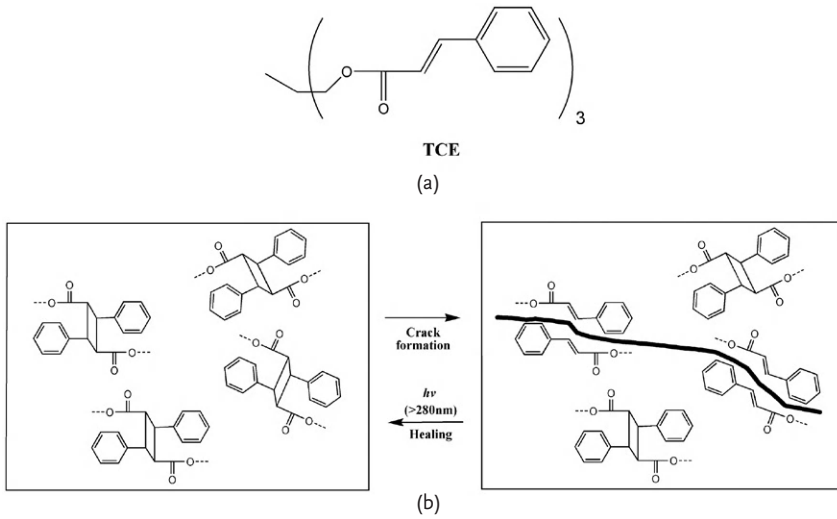


Figure 7.2 (a) Chemical structure of TCE. (b) Schematic illustration of the healing concept [9] (Reproduced by permission of American Chemical Society).

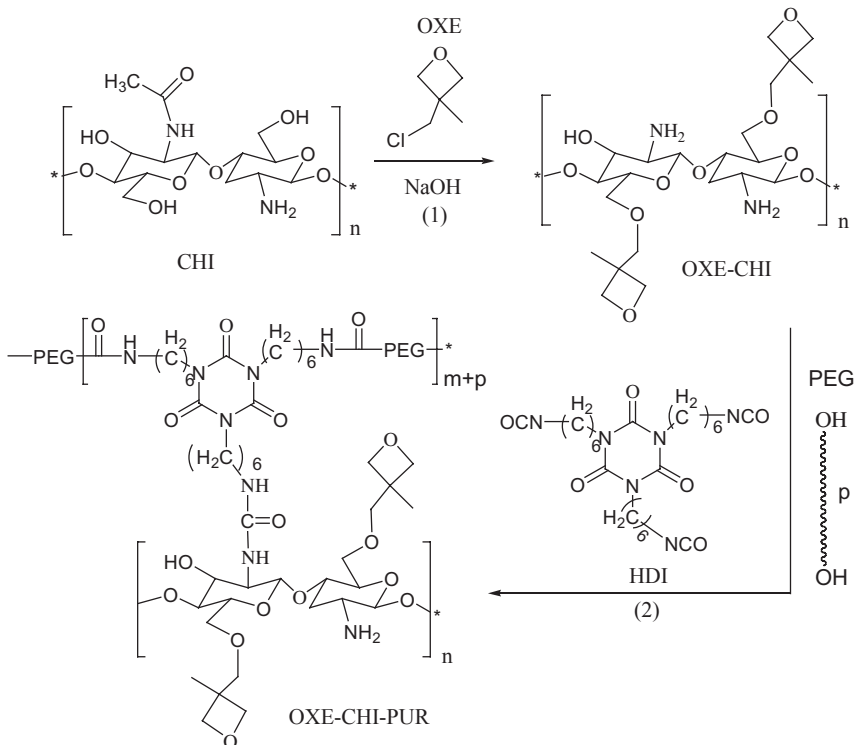


Figure 7.3 Synthetic steps involved in the formation of OXE-CHI [10]. 1. Reactions of OXE with CHI, leading to the formation of OXE-CHI precursor. 2. Reactions of OXE-CHI with HDI and PEG, leading to formation of remendable OXE-CHI-PUR network.

reshuffling reactions enable the reorganization of the linking units in the covalently crosslinked polymers and self-healing of significantly damaged polymers. In the meantime, to carry out the self-healing reaction in a bulk material at room temperature, the reactive TDS units, capable of re-shuffling, were incorporated in the main chain of a low- T_g polyurethane.

Amamoto *et al.* also reported repeatable photoinduced self-healing of covalently crosslinked polymer through reshuffling of trithiocarbonate (TTC) units [12]. The polymer was prepared by reversible addition fragmentation chain transfer (RAFT) copolymerization of *n*-butyl acrylate and a TTC crosslinker. Healing of cracked parts (i.e., dynamic chain transfer), which were swollen in acetonitrile, was completed with UV light in nitrogen protection under catalysis of 2,2'-azobis(isobutyronitrile). The authors considered that this approach could be applied to recycle covalently crosslinked polymers into complex-shaped parts.

Froimowicz *et al.* introduced anthracene into dendritic macromonomer to create a photo-reversible material, which was proven to build up networks possessing a reversible self-healing property under successive UV irradiations at 254 and 366 nm [13]. The self-healing ability of their system was tested by introducing an artificial scratch in a previously crosslinked film of anthracene containing hyperbranched polyglycerol (PG-An). This film was then de-crosslinked for 15 min with 254 nm light to regenerate the building block. Afterwards, PG-An in the form of a colorless and viscous liquid was kept over night in the dark at room temperature. The low T_g (~46 °C) allowed the PG-An to reorganize itself over the entire area. Finally, the bulk film was irradiated with 366 nm light to restore the crosslinked film.

Burnworth *et al.* proposed optically healable metallosupramolecular polymers based on macromolecules with pyridine derivative termini and Zn^{2+} ions complexes [14]. Liquefaction of the polymers due to photo-dissociation of Zn^{2+} motifs under irradiation at the wavelength of 320–390 nm and the subsequent re-complexation offer the self-healing function, as characterized by stress–strain data. Upon exposure to ultraviolet light, the metal–ligand motifs are electronically excited and the absorbed energy is converted into heat. This causes temporary disengagement of the metal–ligand motifs and a concomitant reversible decrease in the polymers' molecular mass and viscosity, thereby allowing defect healing. Dong *et al.* prepared a novel class of A_2 – B_3 type photoreversible supramolecular hyperbranched polymer (SHP) through the host–guest complexation of azobenzene dimer (diazo) and β -cyclodextrin trimer (β -CD₃) [15]. The supramolecular polymer exhibits a branched structure and interesting optical properties that can be switched reversibly by alternating UV/Vis light irradiation through the reversible association and disassociation of the non-covalent connection in the backbone. Accordingly, the photo-reversible SHP might act as a candidate for a photochemically self-healing polymer.

Moreover, trans–cis photoisomerization of azobenzene has also been found to be a useful measure of photochemical healing. Yamamoto and Yoshida [16] proved self-healing of surface damage of polymeric microparticles/liquid crystal gels containing a photochromic azobenzene dopant. The healing mechanism is based on the site-selective gel–sol transition induced by the photochemical modulation of

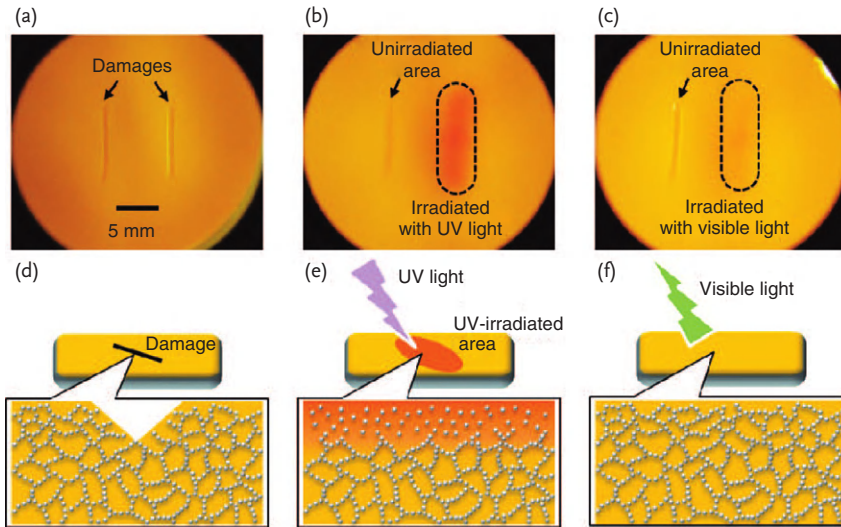


Figure 7.4 Photographs and schematic representations of the photochemical healing of surface damage on the particle/liquid crystal composite gel [16]: (a,d) before irradiation with UV light, (b,e) just after 10 s of irradiation with UV light ($\lambda = 365$ nm;

intensity: 10 mW cm^{-2}), and (c,f) after 10 s irradiation with visible light ($\lambda = 435$ nm; intensity: 10 mW cm^{-2}) at 32°C (Reproduced by permission of American Chemical Society).

the phase structure of the host liquid crystal between nematic and isotropic (Figure 7.4). The surface damage was repaired repeatedly and rapidly through the reconstruction of microparticle networks in the fluidic sol-state.

In summary, the healing strategies presented in Ref. [12–16] have one thing in common—they include fluidification in the course of bond rearrangement, which is different from the works described in Ref. [9–11].

Hereinafter, we mainly demonstrate that reversible photochemical reaction can effectively occur in solid polyurethane by introducing hanging coumarin groups into the main chains. Owing to the photosensitive nature and improved mobility of coumarin that serves as a reversible crosslinker in the polyurethane network, not only cracks in the polymer but also the mechanical strength of the ruptured parts can be recovered for multiple times under ultraviolet irradiation or even direct sunlight.

Coumarin, a traditional perfume substance from plants, possesses attractive photo-responsiveness, which was first discovered in solutions or crystals of coumarin derivatives. Since the 1990s, reversible photochemical reaction between coumarin moieties, which were incorporated into polymeric chains, has been investigated in the liquid phase. It was found that they are capable of photodimerization via [2+2] photocycloaddition with $\lambda > 300$ nm UV irradiation and photocleavage upon irradiation at 254 nm (Figure 7.5) [17, 18]. These photoreactions are fully reversible, and can thus be used to repair damaged polymers. In this context,

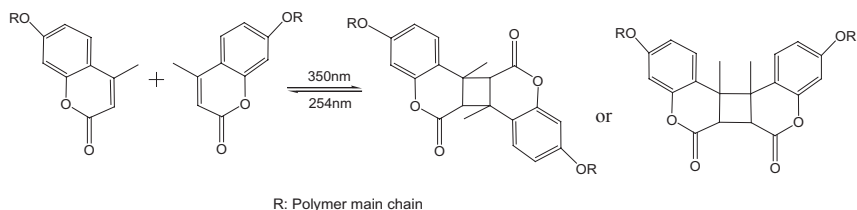


Figure 7.5 Photodimerization and photocleavage of coumarin derivatives in polymer.

biomimetic self-healing might be available, based on the photo-responsive behavior in nature. So far, however, most of the previous works on this aspect have been concerned with the reaction mechanism, and only a few have dealt with applied studies, including photo-controlled drug release within solvents [19, 20] and photo-alignment of liquid crystalline polymers [21, 22].

7.2 Molecular Design

7.2.1 Polyurethane Containing Monohydroxy Coumarin Derivatives

As the first proof-of-concept material, polyurethane networks containing monohydroxy coumarin side groups (THHPEG400) are prepared (Figure 7.6a), which is the polymeric product of the tri-functional homopolymer of hexamethylene diisocyanate (tri-HDI) with polyethylene glycol (PEG400, $M_w = 400$) as the skeleton and 7-(hydroxyethoxy)-4-methylcoumarin (HEOMC) as the pendant group. Unlike most coumarin derivatives, HEOMC can carry out photodimerization even in the solid state. The coumarin moieties in HEOMC help to establish photoreversible crosslinks among linear THHPEG400 by forming cyclobutane rings via photodimerization under UV light at $\lambda = 350$ nm (Figure 7.6b). As the bond strength of cyclobutane rings is lower than other covalent bonds, scission of cyclobutane rings would preferentially occur in the case of crack propagation, reproducing coumarin moieties. By re-applying UV light at $\lambda = 350$ nm, the above photodimerization proceeds again and heals the damage. If the mechanically induced cleavage of cyclobutane rings is not efficient enough, UV irradiation at $\lambda = 254$ nm can be introduced to initiate photocleavage of the rest of the cyclobutane rings on the damaged surface, which further increases the amount of coumarin moieties and healing efficiency.

It is worth noting that the monomer HEOMC is obtained by modifying 7-hydroxy-4-methylcoumarin (HMC) with 2-bromoethanol to convert the aromatic hydroxy group into an aliphatic one, which is easier to react with isocyanate. The resultant ether linkage on the side chain is believed to increase the mobility of coumarin moieties, which would facilitate photodimerization (i.e., healing reaction) of cleft coumarin dimers in bulk polyurethane.

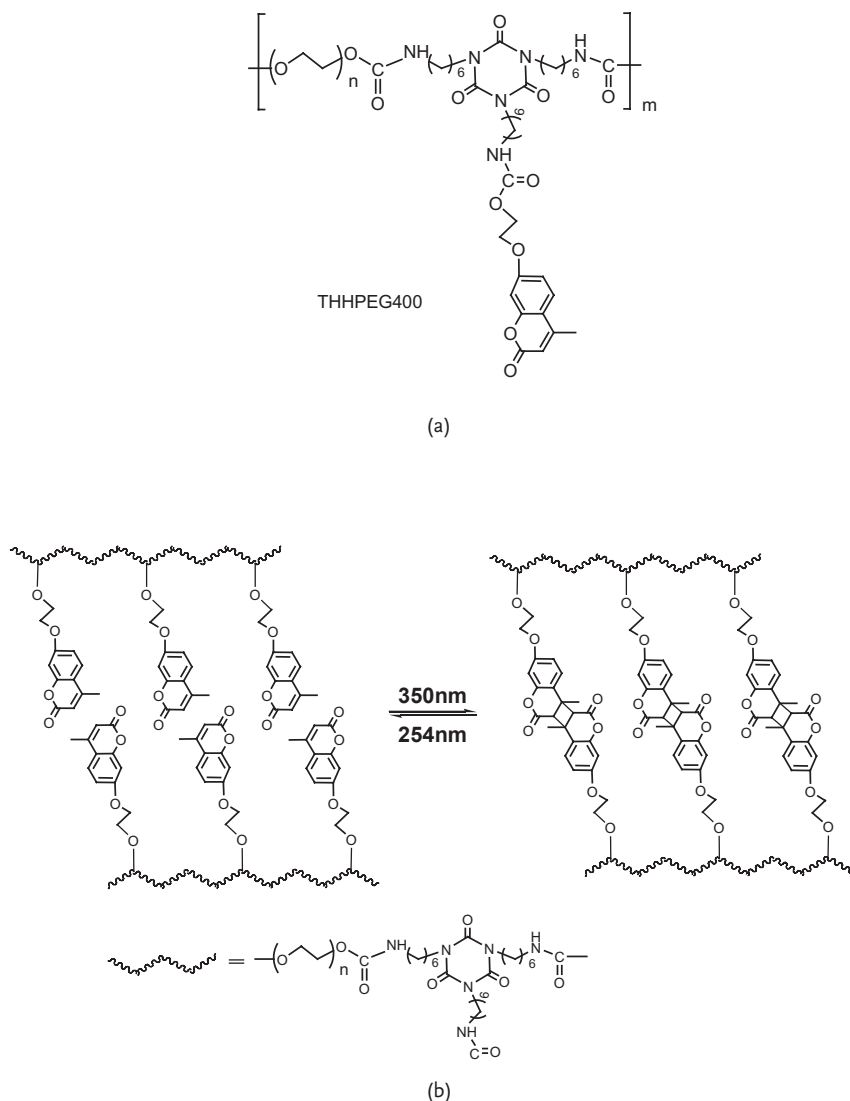


Figure 7.6 (a) Chemical structure of THHPEG400, (b) reversible photodimerization and photocleavage of coumarin moieties in THHPEG400 upon alternating irradiation with 350 and 254 nm UV light.

7.2.2

Polyurethane Containing Dihydroxy Coumarin Derivatives

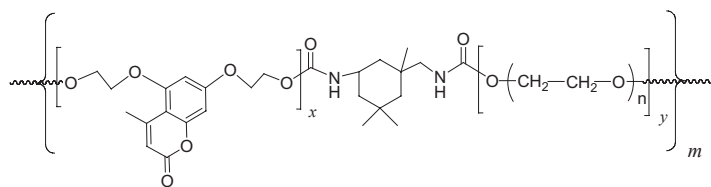
With respect to synthesis control of the above photo-remendable polyurethane, however, the system with monohydroxy coumarin derivatives needs to be upgraded to prevent gelation and facilitate structural adjustment. According to the structural

requirements for imparting photochemical reactivity to polyurethane, monohydroxy coumarin derivatives should play a dual-role as side groups and crosslinkers. This means that free NCO groups have to be present on the main chains of the polymer for the reaction with monohydroxy coumarin derivatives. As a result, tri-HDI that contains three NCO groups per molecule is introduced. Ideally, monohydroxy coumarin first reacts with one NCO group of tri-HDI, and then polyethylene glycol is incorporated for chain extension, producing the desired polyurethane. Because the reactivities of the three NCO groups of tri-HDI are almost identical, synthesis of the aforesaid intermediate from the reaction between monohydroxy coumarin and tri-HDI is hard to control. In many cases, all the three NCO groups of one tri-HDI molecule have reacted with monohydroxy coumarin, so that excessive unreacted tri-HDI is left. When bifunctional PEG is added for the subsequent reaction, detrimental gelation of the system appears. On the other hand, monohydroxy coumarin derivatives are attached to the hard segments of polyurethane (i.e., tri-HDI). Since both soft and hard segments should have the same equivalent, as required by stoichiometry, the ratio of soft and hard segments in the polyurethane carrying monohydroxy coumarin can be regulated only by changing the molar mass of PEG, but not by changing the content of PEG with a given molar mass.

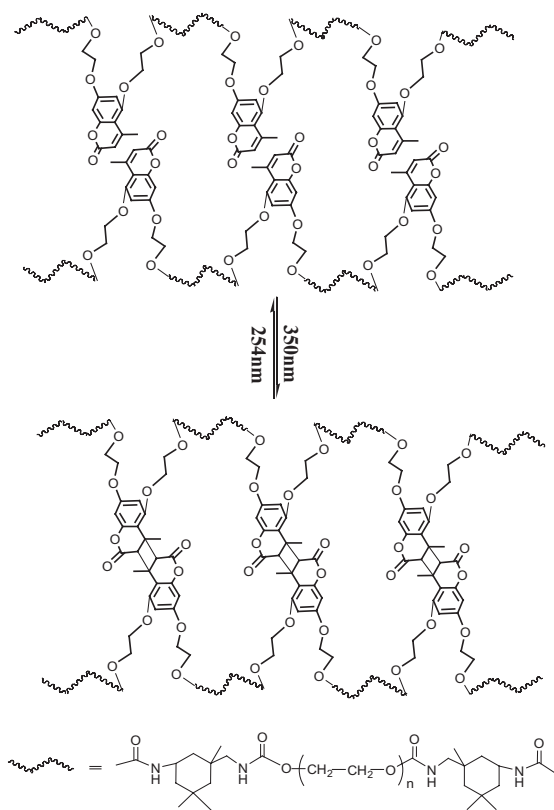
To overcome these shortcomings, dihydroxy coumarin derivatives are employed as a substitute for their monohydroxy counterparts. Similar to the case of conventional polyether diols, polycondensation of dihydroxy coumarin derivatives with bifunctional isocyanate only gives rise to linear polyurethane. Moreover, the ratio of soft and hard segments in the polyurethane can be regulated by changing the ratio of dihydroxy coumarin derivatives and PEG, as well as by changing the molar mass of PEG. Comparatively, the synthesis becomes more flexible, favoring optimization of polyurethane structure and the integrated photoreversibility.

Accordingly, a dihydroxy coumarin derivative 5,7-bis(2-hydroxyethoxy)-4-methylcoumarin (DHEOMC) is synthesized by the reaction between 5,7-dihydroxy-4-methylcoumarin (DHMC) and 2-bromoethanol. Then, a novel optical stimuli-responsive polyurethane (IDHPEG, meaning a condensation polymer of isophorone diisocyanate (IPDI), DHEOMC and PEG) is yielded (Figure 7.7a), which consists of IPDI and DHEOMC moieties as hard segments, and PEG ($M_w = 400$ or 800 g mol^{-1}) as the soft segments. Upon UV irradiation, the photo-reversible DHEOMC moieties are crosslinked, forming cyclobutane structures. When products made from the crosslinked version of the polyurethane are scratched or cut, it is hoped that the cracked parts could be re-bound through UV-induced reversible photoreaction of coumarin moieties (Figure 7.7b). The ether linkages offered by DHEOMC that connect coumarin moieties with the macromolecules are believed to increase the localized mobility of the former, favoring photodimerization (i.e., healing reaction) of cleft coumarin dimers in bulk polyurethane.

Eventually, three types of polyurethane: IDHPEG400-0.5, IDHPEG800-0.5 and IDHPEG800-0.25 were produced. Here, PEG400 and PEG800 refer to PEG with $M_w = 400$ and 800 g mol^{-1} , respectively. The corresponding molar feed ratios are



(a)



(b)

Figure 7.7 (a) Chemical structure of IDHPEG, (b) reversible photodimerization and photocleavage reactions of coumarin moieties in IDHPEG upon alternating irradiation with 350 and 254 nm UV light.

$n_{\text{IPDI}}:n_{\text{DHEOMC}}:n_{\text{PEG400}} = 1.05:0.5:0.5$, $n_{\text{IPDI}}:n_{\text{DHEOMC}}:n_{\text{PEG800}} = 1.05:0.5:0.5$, and $n_{\text{IPDI}}:n_{\text{DHEOMC}}:n_{\text{PEG800}} = 1.05:0.25:0.75$, respectively.

7.3 Reversible Photo-Crosslinking Behaviors

As mentioned in Section 7.1, coumarin possesses inherent reversible photoreactivity. To check whether and to what extent the habit is inherited by the polyurethanes in the solid state, UV-vis spectroscopic analysis was performed. The issue is closely related to photo-remendability of the polymers.

It is seen from Figure 7.8a, under UV irradiation ($\lambda = 350 \text{ nm}$, 14.4 mW cm^{-2}), typical absorptions of coumarin and its derivatives appear: a $\pi-\pi^*$ transition between 250 and 300 nm attributed to electrons of the conjugated benzene nucleus,

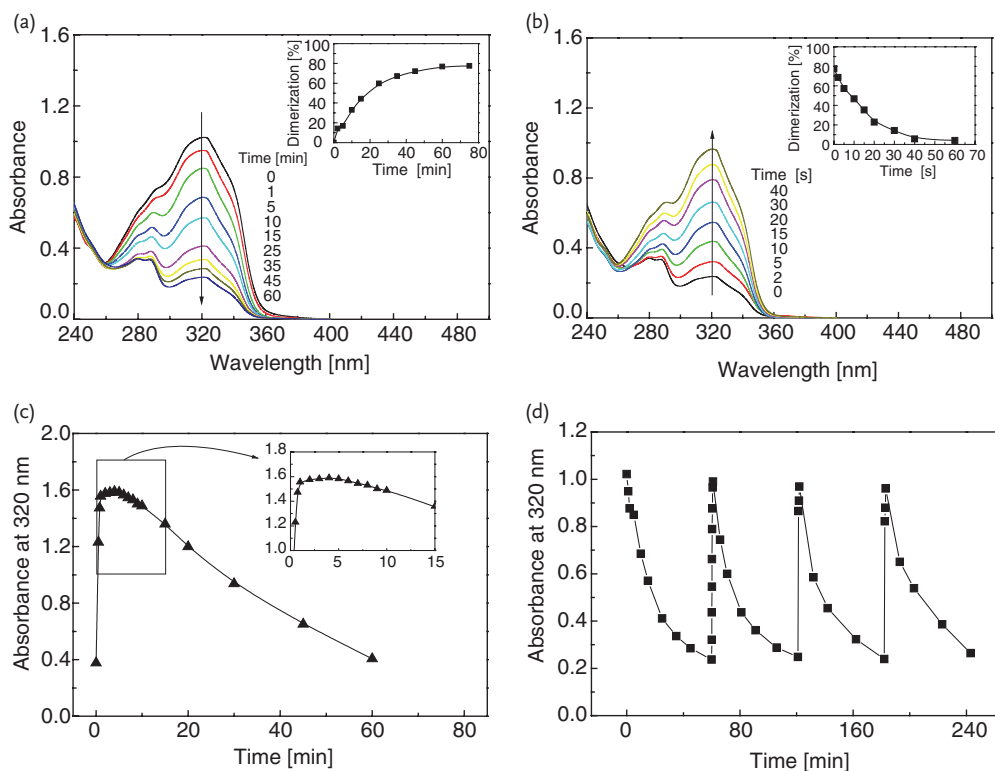


Figure 7.8 UV-vis spectra of THHPEG400 [23] (Reproduced by permission of The Royal Society of Chemistry). (a) Photodimerization upon irradiation at 350 nm; (b) photocleavage upon irradiation at 254 nm; (c) absorbance at 320 nm versus time under irradiation

at 254 nm (the specimen had been exposed to 350 nm UV light for 70 min in advance allowing maximization of photodimerization); (d) absorbance at 320 nm upon alternating irradiations at 350 nm (for 70 min) and 254 nm (for 1 min).

and another π - π^* transition between 310 and 340 nm assigned to the pyrone nucleus [24, 25]. With an increase in irradiation time, the absorption at 320 nm decreases because the double bonds of 4-methylcoumarin dimerize to form cyclobutane rings, which destroys the conjugated π -system. Therefore, the maximum absorbance at 320 nm can be used to describe the dimerization degree of 4-methylcoumarin moieties of THHPEG400 (i.e., dimerization degree = $1 - A_t/A_0$, where A_t and A_0 denote the absorbance at 320 nm at times t and 0 of UV irradiation, respectively). The inset shows that at the time of 70 min a maximum of 77.5% of coumarin moieties are dimerized.

When the light source changes to 254 nm (15.6 mW cm^{-2}), the dimerization degree decreases rapidly (Figure 7.8b), but the minimum does not reach zero as a few 4-methylcoumarin groups may be photo-crosslinked in the last stage of photocleavage [26]. Figure 7.8c shows that a short plateau appears on the time dependence of maximum absorbance at 320 nm due to the dynamic equilibrium between photocrosslinking and photocleavage. This means that prolonged exposure to 254 nm light would result in an irreversible crosslinked structure. A reasonable irradiation time with 254 nm UV light is critical for multiple reversible photoresponse and remending of THHPEG400.

Photodimerization and photocleavage cycles of THHPEG400 were repeatedly tested to investigate the reversibility (Figure 7.8d). The maximum absorbance at 320 nm of each cycle decreases slightly with time, probably due to the appearance of a small amount of asymmetric fission products of coumarin dimer during photocleavage under 254 nm light [27].

As for IDHPEGs (i.e., IDHPEG400-0.5, IDHPEG800-0.25 and IDHPEG800-0.5), similar reversible photoreactivity is observed. Supposing the peak absorbance at 320 nm of the specimen exposed to 254 nm UV light is represented by A'_0 , its reversibility can be characterized by the percentage recovery as follows:

$$\text{Recovery} = (A'_\infty - A_\infty) / (A'_0 - A_\infty) \times 100\% \quad (7.1)$$

where A_∞ denotes the minimum absorbance at 319 nm after exposure to 350 nm UV light, and A_0 the absorbance at 320 nm at time zero. Table 7.1 lists the values of degree of dimerization and percentage recovery of all the three polyurethanes during the first photodimerization and photocleavage cycle. Comparatively, IDHPEG400-0.5 exhibits the poorest reversibility. Although the percentage recovery of IDHPEG800-0.5 is the highest, it is only 59.1%.

According to the results of ^1H NMR measurement, the initial concentrations of coumarin moieties in the polyurethanes are calculated (Table 7.1). It can be concluded that the amount of available coumarin moieties is not the controlling factor for photoreversibility. Otherwise, IDHPEG400-0.5 should have a percentage recovery superior to the other two polymers. When looking at the glass transition temperatures of the polymers, we can see different phase structures and viscoelastic states are involved for the room temperature photoreactions in the present work. In the case of IDHPEG400-0.5, only one glass transition temperature is perceived before and after exposure to 350 nm UV light, owing to the good miscibility between soft and hard segments. Moreover, the glass transition temperature

Table 7.1 Characterization of the first cycle of photodimerization and photocleavage of IDHPEGs in relation to their structural information [28] (Reproduced by permission of Elsevier).

Polymer	Dimerization (%)	Recovery (%)	Initial coumarin content ($\times 10^{-1} \text{ mol dm}^{-3}$)	Rate constant ($\times 10^{-3} \text{ dm}^3 \text{ mol}^{-1} \text{ min}^{-1}$)	M_c (g mol^{-1})	T_g^1 ($^{\circ}\text{C}$)	T_g^2 ($^{\circ}\text{C}$)
IDHPEG400-0.5	50.5	16.2	9.91	8.052	1754	34.6	53.2
IDHPEG800-0.5	93.6	59.1	6.92	328.0	1539	-26.8	-24.8 (43.7)
IDHPEG800-0.25	86.3	35.2	2.94	412.5	15413	-37.1	-35.1 (47.1)

Rate constant: parameter quantifying the speed of photocrosslinking (refer to the Electronic Supplementary Data for more details of the calculation based on the UV-vis spectroscopic data).

M_c : average molar mass between crosslinks of the photocrosslinked polyurethanes.

T_g^1 : glass transition temperatures of the polyurethanes prior to photocrosslinking, measured by differential scanning calorimetry (DSC).

T_g^2 : glass transition temperatures of the polyurethanes that had been exposed to 350 nm UV irradiation for 60 min, measured by DSC. The data outside and inside the parentheses are glass transition temperatures of soft and hard segments, respectively.

of the photocrosslinked version is increased from 34.6 to 53.2 $^{\circ}\text{C}$, following the general law of crosslinking. This means that either photodimerization or photocleavage of the crosslinkages has to occur in the glass state. Molecular mobility that is related to the kinetics of photoreaction is thus reduced. With respect to IDHPEG800-0.25 and IDHPEG800-0.5, however, their glass transition temperatures are lower than room temperature before being exposed to 350 nm UV light. Photocrosslinking leads to the appearance of two glass transition temperatures as a result of microphase separation of soft and hard domains. Although the glass transition temperatures of the soft segments are slightly increased, they are still far lower than room temperature. Clearly, the longer molecular chain of PEG800 compared to that of PEG400 should account for the results. Since the soft segments in IDHPEG800-0.25 and IDHPEG800-0.5 exhibit a rubbery feature at room temperature, the neighboring coumarin dimers or moieties must be much more mobile as compared to the case of IDHPEG400-0.5. The analysis is supported by the rate constants of dimerization (Table 7.1), and explains the higher dimerization degrees and percentage recovery of the former two polymers.

On the other hand, Table 7.1 reveals that the molar mass between crosslinks of crosslinked IDHPEG800-0.5 resembles that of crosslinked IDHPEG400-0.5, which is obviously smaller than that of crosslinked IDHPEG800-0.25. If viewed merely from the restriction effect exerted by crosslinked networks, coumarin dimers or moieties in the latter polymer have the highest mobility and, hence, we should observe the highest dimerization degree and percentage recovery, but this is not the case. By taking all factors into consideration, it is known that the appearance of rubbery domains resulting from microphase separation is the most important condition for the reversible photoreactions. Once this prerequisite is satisfied, the initial concentration of coumarin moieties attached to the polymer plays the leading role, so that IDHPEG800-0.25 exhibits poorer reversibility than IDHPEG800-0.5.

In short, reversibility of photodimerization and photocleavage reactions in the polyurethanes turns out to be a function of the photoreactivity of coumarin itself, the fraction of the coumarin group, the phase separation structure, molecular mobility, glass transition temperature, and so on. This finding might help to further improve the photoreversibility of the polymers.

7.4 Evaluation of Photo-Remendability

On the basis of the above study of photochemical reactivity, crack remendability of the crosslinked polyurethane was quantified in terms of tensile tests. After testing, the fractured surfaces of specimens were firstly irradiated with 254 nm UV light, kept in alignment and intimate contact without pressure, and illuminated by 350 nm UV light. Then, the healed specimens were tested again and the healing efficiency was estimated by the ratio of tensile strengths of the healed and virgin specimens. Figure 7.9 shows that the tensile strength of crosslinked THHPEG400 can be repeatedly restored, and the efficiency of the first healing event is 70.2%. The decline in efficiency of the second and third remending might originate from reduction in photoreversibility (Figure 7.8d) and misalignment of fractured surfaces.

In fact, photocleavage of coumarin dimers (i.e., de-crosslinking of the polyurethane network) led by the irradiation at 254 nm only occurs at the fractured surface layer of the specimen used for the tensile tests, due to the limited

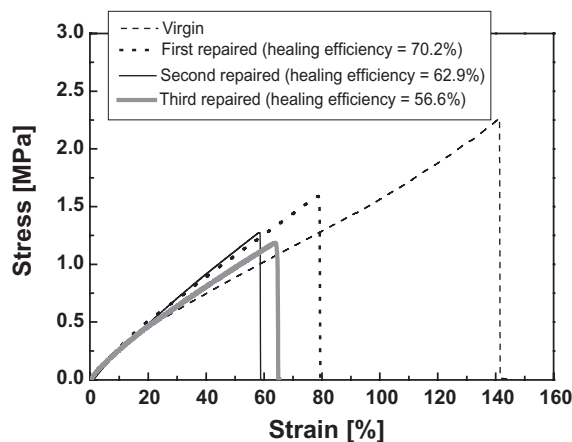


Figure 7.9 Typical tensile stress–strain curves of virgin and repaired THHPEG400 [23] (Reproduced by permission of The Royal Society of Chemistry). Healing conditions: irradiation with 254 nm UV light for 1 min followed by irradiation with 350 nm for 90 min. Because the tensile strength of the

virgin specimen cannot be fully restored, the reconnected interface became the weakest part, and had to break again during the subsequent tensile tests. This ensured that the second and third tensile failures happened to the same healed portion.

penetration depth of short-wave UV light in the material. The dangling chains carrying cleft coumarin moieties on the fracture surface are highly mobile, which favors wetting and diffusion of molecules at the solid–solid contact of the damaged specimen, and helps to meet the molecular level movement requirement of crack healing [29]. Meantime, they are still bound to the inner crosslinked structure that is not influenced by photo-treatment and retains the original network of the film specimen, so that macroscopic flow of the material is prohibited. The above feature of the crosslinked THHPEG400 ensures its dimensional stability during repeated crack healing.

To clarify whether photoreaction of coumarin moieties attached to the polyurethane is fully responsible for the restoration of tensile strength, control experiments were carried out as follows. The tensile failed specimens of crosslinked THHPEG400 were reconnected in a similar way to the above photo-healed specimens and healed at 40 °C for 90 min. In this case, the healing temperature was identical to the environmental temperature inside the UV chamber caused by UV illumination and the healing time equaled that of 350 nm irradiation (refer to the caption of Figure 7.9), while no UV light was applied. Afterwards, the tensile test was re-performed to evaluate the effect of rehabilitation. The results of three successive control experiments indicate that the polymer exhibits slight remendability in the absence of UV light, as characterized by the healing efficiencies of 16.8, 13.9 and 11.3%. Intermolecular interactions, including hydrogen bonding and entanglements of dangling chains [30, 31] across the intimately contacted fractured surfaces, might account for the healing. Accordingly, the contribution made by photodimerization of coumarin moieties can be roughly estimated by deducting the healing efficiencies offered by the physical interactions from those listed in Figure 7.9, that is, 53.4, 49.0 and 45.3% for the repeated healing events.

Relatively, when coumarin is integrated into the main chain of polyurethane (i.e., IDHPEGs), photochemical remendability of the polymer has to be greatly affected by the surrounding molecular structures. When the specimens of IDHPEG400-0.5 underwent tensile tests and the subsequent healing treatment as mentioned above, no healing effect was detected because coumarin dimers in the polymer are difficult to be recovered to original coumarin moieties under 254 nm light (Table 7.1). Moreover, its higher T_g should be detrimental to the molecular motion and contacts at the fractured surfaces. The situation is changed in the case of IDHPEG800-0.5 and IDHPEG800-0.25. The ruptured specimens can indeed be reconnected due to UV stimulus (Figure 7.10). Due to the declined coumarin reversibility revealed by the above UV–vis spectroscopy study and misalignment of fractured surfaces, however, healing efficiency has to be successively reduced.

It is interesting to see that full restoration of tensile strength is achieved for IDHPEG800-0.25 (Figure 7.10b). A close view of the re-fractured surface of a healed specimen indicates that some parts of the failure path generated during the first tensile test were so well re-bonded that crack propagation during the second failure has to deviate from the original fracture plane. Moreover, the rate of decline of healing efficiency becomes not that obvious in comparison with that of IDHPEG800-0.5 (Figure 7.10a).

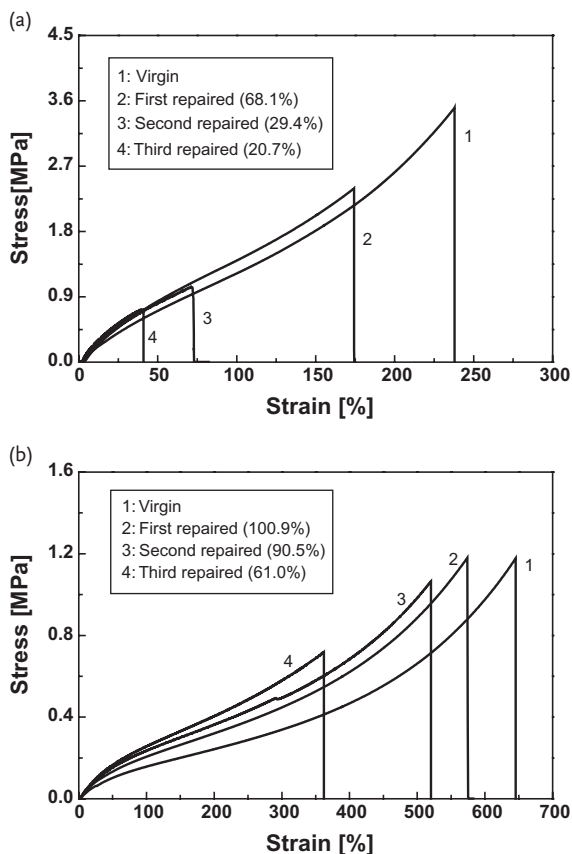


Figure 7.10 Typical stress–strain curves of virgin and repeatedly repaired specimens (a: IDHPEG800-0.5, b: IDHPEG800-0.25) [28] (Reproduced by permission of Elsevier). Healing conditions: irradiation with 254 nm

UV light for 1 min followed by irradiation with 350 nm for 90 min. The data inside the parentheses in the legend are healing efficiencies.

Although the result is encouraging, it seems to be contradictory to the partial data in Table 7.1, where the dimerization degree and percentage recovery of IDHPEG800-0.25 are lower than those of IDHPEG800-0.5. To understand the discrepancy both (i) the difference between the constrained state of the coumarin moieties inside bulk polyurethane and that on the fractured surface of the polymer, and (ii) wetting and diffusion between the cracked surfaces to be re-bound [29], which are prerequisites for the mechanical property recovery due to interfacial photoreaction, should be considered. The UV–vis spectroscopic data in Table 7.1 only deal with densely packed molecules in the as-cast specimens, rather than the contact problem of molecules from broken materials. Because IDHPEG800-0.25 has lower T_g and greater M_c than IDHPEG800-0.5, the mobility of the dangling chains [30, 31] carrying cleft coumarin moieties on the fracture surface of the

former is higher. This is proved by the higher photo-reaction rate constant of IDHPEG800-0.25 than that of IDHPEG800-0.5 (see Table 7.1). The interdiffusion-induced chain entanglements and hydrogen bonding furnish the basis for the subsequent development of strong links across the interface via photodimerization. The higher healing efficiency of IDHPEG800-0.25 than that of IDHPEG800-0.5 (or IDHPEG400-0.5) demonstrates that this is a critical factor.

For verification of the analysis, control experiments were done. The tensile failed specimens were no longer exposed to UV light, but directly reconnected and heated in an oven at 40°C for 90 min. The thermal treatment temperature simulated the environment temperature inside the UV chamber, and the healing process excludes the contribution of photochemistry. In the case of IDHPEG800-0.25, healing efficiencies for the successive three cycles of such control failure-repair tests are: 30.3, 28.4 and 24.3%; while for IDHPEG800-0.5, the values are: 15.4, 12.6 and 11.2%. This means that the mechanism of entanglements between the opposite sides of the damaged specimen did take effect, and molecular mobility on the fractured surfaces of IDHPEG800-0.25 is superior to that of IDHPEG800-0.5. The attached coumarin moieties in IDHPEG800-0.25 have more opportunities to encounter with each other for the photodimerization, despite the low initial coumarin content.

On the other hand, by comparing the results of the control tests with those of authentic tests in Figure 7.10, it is known that both photochemical reactions and localized viscoelastic flow are responsible for tensile strength restoration, but the latter makes less contribution. After all, the polyurethanes are photocrosslinked in advance, and photocleavage of coumarin dimers (i.e., de-crosslinking of the polyurethane networks) only takes place on a superficial layer due to the limited penetration depth of short-wave (254 nm) UV light.

7.5

Concluding Remarks

The coumarin crosslinked polyurethane possesses multiple photo-remendability, transparency and mechanical performance similar to conventional polyurethane. Its synthesis route is simple and consistent with the general route of polyurethane synthesis. It can replace conventional polyurethane in a variety of products, such as next generation coatings, films and sheets where esthetic, structural and functional requirements should be met. Repeated damages are very common in daily life, like scratches on cars made by automatic brush washing and those on touch screens by fingernails. The above work provides a possible solution to induce multiple cycles of self-repairing with UV exposure at room temperature, which has shown the potential to be developed into a practical technique simply based on sunlight stimulus.

Dependence of healing efficiency on the structure of the macromolecules reveals that chain mobility on fracture surfaces plays an important role for crack healing. In this context, crosslinked polyurethane is ideal for making UV-stimulated self-

healing products. On the one hand, the soft segments provide the photochemical groups with the possibility of moving about at ambient conditions (i.e., microscopic flow localized at fracture surfaces is allowed); on the other hand, the majority of the crosslinked structure in the bulk material is not affected by short-wave UV irradiation so that the material would not flow and would still have load bearing ability even during crack repair.

On the whole, photochemically self-healing polymers represent a brand new category of intelligent materials. Research in this area has not yet boomed, while the reported explorations showed bright prospects. Taking advantage of easy control, rapidness and specific wavelength selectivity of light sources of photochemical reactions, positioned (localized) crack healing is allowed without additional catalysts. Supplementary heating would further raise the healing efficiency. Due to the limited penetrating power of light, their future applications would be mostly found in surface engineering. At present, four main tasks have to be fulfilled: (i) Development of feasible and cost effective techniques of synthesis, processing, end-product manufacturing, and crack repairing, which is a critical step towards practical usage. (ii) Improvement of long term reproducibility of photochemical remending performance. (iii) Synthesis of proper derivatives from existing photoresponsive chemicals, which are capable of taking effect in polymers for crack healing. For example, Scott *et al.* proved that introduction of radicals via photocleavage of residual photoinitiator in crosslinked polymer matrix, which diffused via addition-fragmentation chain transfer of midchain functional groups, allowed chain rearrangement [32]. Nevertheless, it has not been shown how the methodology works as a measure of intrinsic self-healing. (iv) Working out new photochemical reactions that could be integrated into macromolecules. Diels–Alder reaction that is known for its sensitivity to temperature, for example, has been lately provided with molecular photoswitches in 3,4-dithienylfuran systems with suitable dienophiles [33]. It is these new findings that push forward self-healing polymers, including photochemically remendable polymers.

Acknowledgments

The authors acknowledge the support of the Natural Science Foundation of China (Grants: 51273214, 20874117, 50903095, 51073176 and U0634001), Doctoral Fund of Ministry of Education of China (Grant: 20090171110026), and the Science and Technology Program of Guangdong Province (Grant: 2010B010800021).

References

- 1 Zhang, M.Q., and Rong, M.Z. (2011) *Self-Healing Polymers and Polymer Composites*, John Wiley & Sons, Inc, Hoboken.
- 2 Yuan, Y.C., Yin, T., Rong, M.Z., and Zhang, M.Q. (2008) Self healing in polymers and polymer composites. Concepts, realization

- and outlook: a review. *Express Polym. Lett.*, **2**, 238–250.
- 3 Zhang, M.Q., Rong, M.Z., and Yin, T. (2009) Self-healing polymers and polymer composites, in *Self-Healing Materials: Fundamentals, Design Strategies, and Applications* (ed. S.K. Ghosh), Wiley-VCH Verlag GmbH, pp. 29–71.
- 4 Zhang, M.Q., and Rong, M.Z. (2012) Design and synthesis of self-healing polymers. *Sci. China Chem.*, **55**, 648–676.
- 5 Zhang, M.Q., and Rong, M.Z. (2012) Theoretical consideration and modeling of self-healing polymers. *J. Polym. Sci. B Polym. Phys.*, **50**, 229–241.
- 6 Bergman, S.D., and Wudl, F. (2008) Mendable polymers. *J. Mater. Chem.*, **18**, 41–62.
- 7 Cardenas-Daw, C., Kroeger, A., Schaertl, W., Froimowicz, P., and Landfester, K. (2012) Reversible photocycloadditions, a powerful tool for tailoring (nano) materials. *Macromol. Chem. Phys.*, **213**, 144–156.
- 8 Stobbe, H. (1919) Light reactions of the allo- and iso-cinnamic acids. *Ber. Dtsch. Chem. Ges.*, **52B**, 666–672.
- 9 Chung, C.-M., Roh, Y.-S., Cho, S.-Y., and Kim, J.-G. (2004) Crack healing in polymeric materials via photochemical [2+2] cycloaddition. *Chem. Mater.*, **16**, 3982–3984.
- 10 Ghosh, B., and Urban, M.W. (2009) Self-repairing oxetane-substituted chitosan polyurethane networks. *Science*, **323** (5920), 1458–1460.
- 11 Amamoto, Y., Otsuka, H., Takahara, A., and Matyjaszewski, K. (2012) Self-Healing of covalently cross-linked polymers by reshuffling thiuram disulfide moieties in air under visible light. *Adv. Mater.*, **24**, 3975–3980.
- 12 Amamoto, Y., Kamada, J., Otsuka, H., Takahara, A., and Matyjaszewski, K. (2011) Repeatable photoinduced self-healing of covalently cross-linked polymers through reshuffling of trithiocarbonate units. *Angew. Chem. Int. Ed.*, **50**, 1660–1663.
- 13 Froimowicz, P., Frey, H., and Landfester, K. (2011) Towards the generation of self-healing materials by means of a reversible photo-induced approach. *Macromol. Rapid Commun.*, **32**, 468–473.
- 14 Burnworth, M., Tang, L., Kumpfer, J.R., Duncan, A.J., Beyer, F.L., Fiore, G.L., Rowan, S.J., and Weder, C. (2011) Optically healable supramolecular polymers. *Nature*, **472**, 334–337.
- 15 Dong, R.J., Liu, Y., Zhou, Y.F., Yan, D.Y., and Zhu, X.Y. (2011) Photo-reversible supramolecular hyperbranched polymer based on host-guest interactions. *Polym. Chem.*, **2**, 2771–2774.
- 16 Yamamoto, T., and Yoshida, M. (2012) Viscoelastic and photoresponsive properties of microparticle/liquid-crystal composite gels: tunable mechanical strength along with rapid-recovery nature and photochemical surface healing using an azobenzene dopant. *Langmuir*, **28**, 8463–8469.
- 17 Chen, Y., and Wu, J.D. (1994) Preparation and photoreaction of copolymers derived from N-(1-phenylethyl)acrylamide and 7-acryloyloxy-4-methyl coumarin. *J. Polym. Sci. Part A Polym. Chem.*, **32**, 1867–1875.
- 18 Trenor, S.R., Shultz, A.R., Love, B.J., and Long, T.E. (2004) Coumarins in polymers: from light harvesting to photo-cross-linkable tissue scaffolds. *Chem. Rev.*, **104**, 3059–3077.
- 19 Ren, B.Y., Zhao, D.L., Liu, S.S., Liu, X.X., and Tong, Z. (2007) Synthesis and characterization of poly(ferrocenylsilanes) with coumarin side groups and their photochemical reactivity and electrochemical behavior. *Macromolecules*, **40**, 4501–4508.
- 20 Jiang, J.Q., Qi, B., Lepage, M., and Zhao, Y. (2007) Polymer micelles stabilization on demand through reversible photo-cross-linking. *Macromolecules*, **40**, 790–792.
- 21 Gangadhara, and Kishore, K. (1995) A new class of photo-cross-linkable side chain liquid crystalline polymers containing bis(benzylidene)cyclohexanone units. *Macromolecules*, **28**, 806–815.
- 22 Jackson, P.O., O'Neill, M., Duffy, W.L., Hindmarsh, P., Kelly, S.M., and Owen, G.J. (2001) An investigation of the role of crosslinking and photodegradation of side-chain coumarin polymers in the photoalignment of liquid crystals. *Chem. Mater.*, **13**, 694–703.
- 23 Ling, J., Rong, M.Z., and Zhang, M.Q. (2011) Coumarin imparts repeated

- photochemical remendability to polyurethane. *J. Mater. Chem.*, **21**, 18373–18380.
- 24 Moore, T.A., Harter, M.A., and Song, P.-S. (1971) Ultraviolet spectra of coumarins and psoralens. *J. Mol. Spectrosc.*, **40**, 144–157.
- 25 Kehrlösser, D., Träger, J., Kim, H.-C., and Hampp, N. (2010) Synthesis and photochemistry of coumarin-based self-assembled monolayers on silicon oxide surfaces. *Langmuir*, **26**, 3878–3882.
- 26 Chen, Y., and Jean, C.-S. (1997) Polyethers containing coumarin dimer components in the main chain: (I) Synthesis by photopolymerisation of 7,7'-(polymethylenedioxy) dicoumarins. *J. Appl. Polym. Sci.*, **64**, 1749–1758.
- 27 Yonezawa, N., Yoshida, T., and Hasegawa, M. (1983) Symmetric and asymmetric photocleavage of the cyclobutane rings in head-to-head coumarin dimers and their lactone-opened derivatives. *J. Chem. Soc., Perkin Trans. 1*, 1083–1086.
- 28 Ling, J., Rong, M.Z., and Zhang, M.Q. (2012) Photo-stimulated self-healing polyurethane containing dihydroxyl coumarin derivatives. *Polymer*, **53**, 2691–2698.
- 29 Wool, R.P., and O'Connor, K.M. (1981) A theory of crack healing in polymers. *J. Appl. Phys.*, **52**, 5953–5963.
- 30 Yamaguchi, M., Ono, S., and Terano, M. (2007) Self-repairing property of polymer network with dangling chains. *Mater. Lett.*, **61**, 1396–1399.
- 31 Yamaguchi, M., Ono, S., and Okamoto, K. (2009) Interdiffusion of dangling chains in weak gel and its application to self-repairing material. *Mater. Sci. Eng. B*, **162**, 189–194.
- 32 Scott, T.F., Schneider, A.D., Cook, W.D., and Bowman, C.N. (2005) Photoinduced plasticity in cross-linked polymers. *Science*, **308**, 1615–1617.
- 33 Erno, Z., Asadirad, A.M., Lemieux, V., and Branda, N.R. (2012) Using light and a molecular switch to “lock” and “unlock” the Diels–Alder reaction. *Org. Biomol. Chem.*, **10**, 2787–2792.

8

Mechanophores for Self-Healing Applications

Charles E. Diesendruck and Jeffrey S. Moore

8.1

Introduction

The transformation of chemical energy into mechanical energy is elementary in our lives, not only moving cars and airplanes, but pumping blood in our bodies and moving our eyeballs as we read these lines. The reverse action, defined as mechanochemistry [1–3], is to make chemical transformations using mechanical force, and finding simple examples may be challenging for people unfamiliar with the subject.

Certainly one can think of petroleum or diamonds as examples. Millions of years of small chemical changes under high pressure produced these valuable materials, but more elementary examples are necessary in order to study these transformations. Indeed, the first reported example of mechanochemistry was demonstrated by Staudinger in the 1930s, where he demonstrated that masticating a polymeric material caused not only the expected conformational and positional changes in the polymer chains, but it also cleaved covalent chemical bonds, causing a decrease in the molecular weight of the polymer [4–6]. Indeed, this phenomenon was studied in the rubber industry, revealing that when rubber was masticated in the presence of oxygen (from air), the rubber would “soften”, while in the absence of oxygen the rubber properties would not change [7]. The explanation suggested then was based on the homolytic cleavage of cross-linking bonds to produce two radicals. In the absence of oxygen these radicals recombine and reform cross-linking bonds, restoring the properties of the material; on the other hand, if oxygen is present the radicals are quenched as peroxy radicals and the cross-linking bonds are lost, causing the material to soften [8]. Remarkably, one of the first studies in mechanochemistry provided a synthetic self-healing material, demonstrating the broad potential technologies that could evolve from this science.

In order to understand the effect of mechanical stress in materials, it was necessary to study the changes at the molecular level, in addition to examining macroscopic properties. The analytical challenge of looking at few chemical changes in macromolecules was unrealistic at the time, and was achieved only several years later. For example, the hypothesis that the chemical bonds broke homolytically



Figure 8.1 Possible positioning of mechanophores: chain end, side chain, and chain center. Activation is highest when the mechanophore is at the chain center and the polymer chain passes through both ends of the activated bond.

was directly demonstrated only in the 1960s, using electron spin resonance (ESR) to study mechanically damaged materials [9].

An important step to ease the study of mechanochemistry of polymers was the development of mechanical stressing in solution, where chemical changes are distributed homogeneously through the chains. Moreover, classical analytical chemistry methods to analyze the chemical changes, such as spectrometers, laser light scattering and others could be used, giving the possibility to study molecular weight change and kinetics of the mechanochemical reactions. This important breakthrough came early and was achieved through the use of flow fields [10] and ultra-sound cavitation that caused high shear stress on the chains through flow induced elongation [11].

A key discovery that came from the study in solution was the observation that certain bonds cleave more easily than others [12]. If one of these bonds is present in the main chain, close to its center (Figure 8.1), it can be selectively cleaved. This originated the concept of mechanophores—bonds or chemical functionalities that are especially susceptible to undergoing a chemical change caused by mechanical stress. Mechanophores, when placed into a polymeric molecule where the mechanical force is highest, selectively undergo a chemical reaction [13].

In this chapter we will describe how polymeric materials deal with mechanical stress, methods to mechanically stress materials in a controlled manner to study the chemical changes, and the development of mechanophores that direct mechanical energy to molecular constituents to produce positive effects on the material, such as self-healing.

8.2 Mechanochemical Damage

8.2.1 Deformation

The response of a polymeric material to mechanical stress depends on its chemical composition as well as the chain architecture [14]. The primary mechanism used by a material to dissipate mechanical energy is through deformation, including displacement of chains as a group or in relation to each other, as well as conformational changes. Thermoplastic polymers (linear or branched chains which are

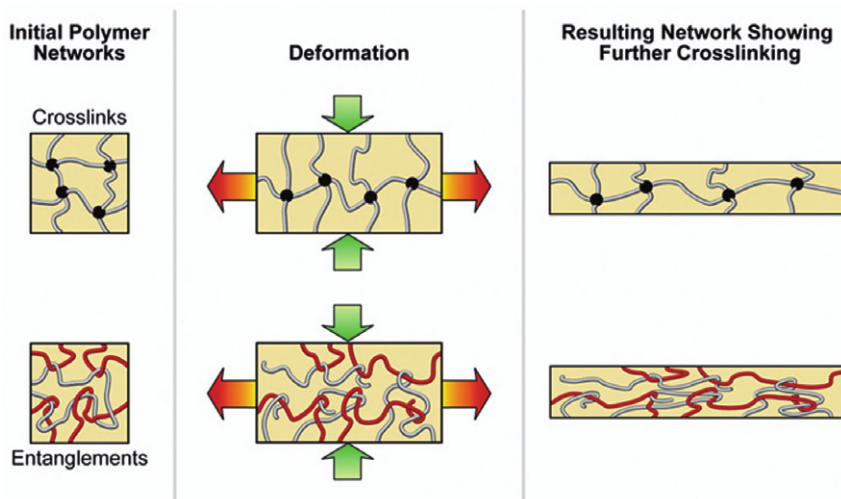


Figure 8.2 Deformation of polymers in the solid state (above T_g) [1]. Reprinted with permission from reference [1]. Copyright 2009 American Chemical Society.

entangled in the solid state) may undergo permanent displacement of chains, while in thermosets (cross-linked polymers) this displacement may be limited due to covalent constraints (Figure 8.2). The chemical composition defines the non-covalent interactions between chains and the feasibility of energy dissipation through conformational changes, but other factors are also very influential: molecular mass, density of chain entanglements/cross-linkages, chain alignment, and degree of crystallinity.

Non-covalent forces between chains, such as van der Waals forces, hydrogen bonds and electrostatic interactions determine the ease by which the chains move independently. Calculating the energy of these interactions for a specific chain or chain segment is very complicated, and mostly unnecessary. The macroscopic effect of these interactions is clearly observed by studying the glass transition temperature (T_g) and melting point of the polymeric material, both of which can be used as a method to compare between materials and their ability to dissipate mechanical energy through displacement of chain segments.

Above the T_g the polymer chains present more mobility, facilitating their displacement and increasing their ability to dissipate mechanical force. On the other hand, below the T_g the mobility is restricted and the polymer behaves like an elastic solid, that is, strain energy is reversibly stored in the polymer until the chains finally deform irreversibly, as in viscous flow [15]. In the solid state, stress on particular polymer chains is mainly localized in the entanglements or cross-links in the material [16] and, above a certain stress, more energetic movements become significant in the dissipation of the concentrated stress.

The second, more energetic way polymer chains dissipate energy is by intramolecular geometry changes. There are three internal motions by which molecules

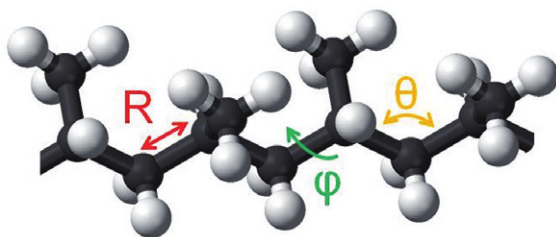


Figure 8.3 Different directions for force dissipation at the molecular level: rotation of dihedral angles φ , bending of bond angles θ , and stretching of bond length R .

deform when acted upon by mechanical force: rotation of dihedral angles, bending of bonds, and stretching of bonds (Figure 8.3).

The effect of mechanical force on the molecular geometry was studied by infrared (IR) spectrometry of polypropylene [17]. Using a polarizer to examine parallel and perpendicular dichroic bands, and analyzing first-order peak shift and difference spectra, this seminal work was able to simultaneously verify the changes in these three parameters and quantitatively compare them. As expected, the change in dihedral angle ($\Delta\varphi$), being the easiest deformation, underwent the steepest change, up to 9 times more than the changes observed in bond length (ΔR), while valence angle bending ($\Delta\theta$) was around 2.4 times the change in bond length. The authors were also able to show that these changes could be significantly different for different C–C bond types. For example, axial bonds were more easily stretched than equatorial bonds. This indicates that the conformation, which changes under mechanical force, is an important factor in this method of energy dissipation.

8.2.2

Homolytic Bond Cleavage

When high stress is applied to a material, chemical bond stretching becomes a significant method for dissipating this energy. The potential caused by mechanical stretching, when added to the original Morse potential, changes the energy versus distance relationship (Figure 8.4). Above a certain stress level, bonds may stretch to a distance where the interaction between the electronic orbitals of the two atoms becomes negligible, leading to the cleavage of the bond.

Most bond cleavages caused by stretching are homolytical in nature, as demonstrated by the presence of radicals [9]. Radicals have high chemical potential and are unstable. They dissipate their potential through several pathways, such as recombination, disproportionation, reaction with atmospheric oxygen, or reacting with another chemical bond. Sonication experiments of polymers in the presence of spin traps demonstrated the creation of radicals in solution using UV–Vis spectroscopy [18, 19]. This indirect method to observe bond cleavage turned out to be very useful, and was one of the first means to study mechanochemical kinetics.

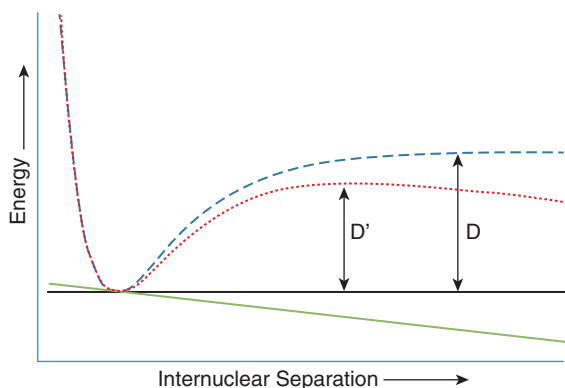


Figure 8.4 Energy as a function of intermolecular distance. Normal Morse potential (blue), potential owing to mechanical force (green) and sum of the potentials (red). The dissociation energy D is changed by the mechanical force to D' [8].

The high reactivity of the radicals produced under mechanical force can be used for productive chemistry. For example, they were used as radical initiators for polymerization, creating co-polymers [20], or used as an effective method to produce H_2O_2 [21]. In special cases, they can even recombine, healing the broken bond (with heat being released).

8.2.3

Heterolytic Bond Cleavage

Homolytic bond cleavage is the generally accepted mechanism when high stress is applied to polymers, and it was demonstrated by direct and indirect detection methods. Heterolytic bond cleavage, while not demonstrated directly, appears occasionally as a proposed mechanism, especially for the cleavage of supramolecular bonds, and when bonds are cleaved in a rearrangement reaction. For example, in the widely studied spiropyran–merocyanine rearrangement by mechanical force [22, 23], the carbon–oxygen bond is cleaved into a phenolate, that is, the oxygen takes both the electrons. In polymers containing coordinating organometallic systems (described below), the ligand is cleaved supposedly taking both the electrons. A molecular dynamics study also proposed that heterolytic bond cleavage may become a major factor when functional groups stabilizing the produced ions are interacting with one of the atoms in the stretched bond [24]. In this study, water molecules interacted through hydrogen bonds with the non-bonding electrons of the oxygen in PEG chains, and the calculations indicated a preference towards heterolytical bond cleavage. One can imagine that other functional groups in polymer side-chains may cause similar effects, but a direct experimental demonstration of this effect has not been reported.

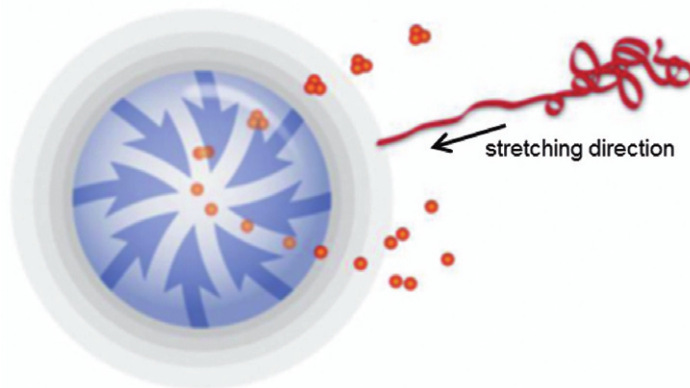


Figure 8.5 Implosion of cavitation bubble pulling the solvent and polymer towards it. Reprinted with permission from reference [1]. Copyright 2009 American Chemical Society.

8.3

Activation of Mechanophores

8.3.1

Ultrasound

Acoustic fields generated by an ultrasound transducer are the most common method to stretch dissolved polymers and the standard method used for testing polymer shear stability [25]. Putatively, the dissolved polymer is mechanically stressed by solvodynamic shear caused by the nucleation, growth and collapse of bubbles in solution. When a bubble is collapsing (implosion), the solvent and the dissolved polymer chains are pulled towards the forming cavity, resulting in elongational flow. The atoms closer to the bubble will move faster than those away from it, causing the polymer to uncoil. Due to the different relative motion of the polymer segments and small solvent molecules, shear stress is produced in the polymer chain (Figure 8.5) [26]. In homopolymers, the stress level can be described by a gaussian distribution with the polymer center as peak [27, 28]. Scission (bond cleavage) generally is achieved through high-energy sonication, occurring within the middle 15% of the chain [29].

The rate of mechanochemical reactions caused by acoustic fields increases with sonication intensity [30] and initial molecular weight of the polymer [31, 32]; but decreases with temperature [33], polymer concentration [26], viscosity [26], and vapor pressure of the solvent [34]. Other factors that influence the rate are polymer chemical composition [12] and architecture [18, 35, 36].

8.3.2

Tensile Testing

Studying the mechanochemical activation in the solid state is fundamental to the development of mechanophores for self-healing applications. Tensile testing is

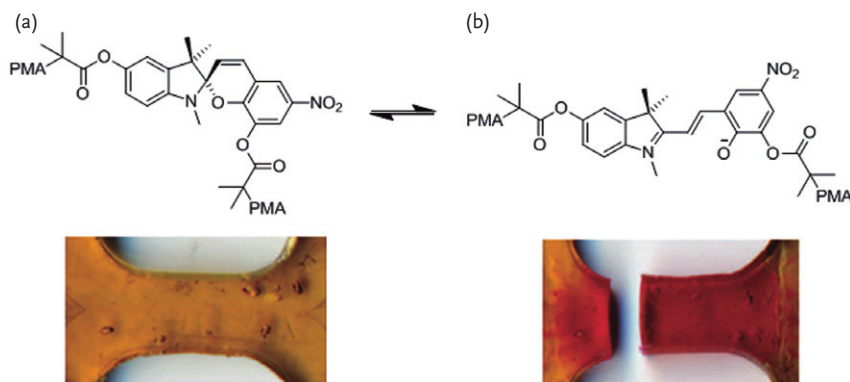


Figure 8.6 Dogbone samples of PMA-linked SP samples before (a) and after (b) stretching to failure [22].

one of the simplest and most effective ways to test mechanochemical activation through stretching solid samples of material. Tensile strains can be amplified in the area of a crack and may lead to its propagation, thus tensile testing is applicable to self-healing instances. Spiropyran (SP) was used as a mechanophore model in order to study the necessary conditions for mechanochemical activation during a stress–strain measurement [22]. This mechanophore undergoes a rearrangement to merocyanin (MC) which has a different color and is fluorescent, working as a probe for direct observation of the stress distribution in the solid material (Figure 8.6).

The stress state, as well as polymer mobility, are the most important factors to be considered for activating mechanophores in bulk polymers. In elastomers, stress levels are low and large deformations are necessary to achieve activation. As an example, when linear PMA ($T_g = 12^\circ\text{C}$) was tested at room temperature, activation was observed only after several hundreds of percent strain. In glassy systems, where $T_{\text{test}} \ll T_g$, no activation is observed (and no yielding occurs). Significant mechanochemical activation was only achieved when test temperatures were below but close to T_g , and only after material yields, that is, plastic deformation is necessary in order to have mechanochemical changes [37]. Using linear PMMA ($T_g = 128^\circ\text{C}$), a significant color change was observed during tensile testing between 90 and 105°C , starting at as low as 10% strain. Interestingly, the authors demonstrated that reducing the T_g by the use of a plasticizer caused the temperature of effective mechanochemical activation to be reduced. The addition of 15% MeOH as a plasticizer to linear PMMA reduced its T_g to 80°C and mechanochemical activation of SP was observed while stretching at room temperature.

Another important factor demonstrated using SP is the alignment of the mechanophores with the force direction. The dipole moment of MC groups can be used to measure their orientation via the anisotropy of fluorescence polarization [38]. Indeed, during tensile testing, the chains (and the mechanophore which is part of them) tend to align themselves with the force direction, especially in the places where stress is higher. This important work provides a mechanochemical method

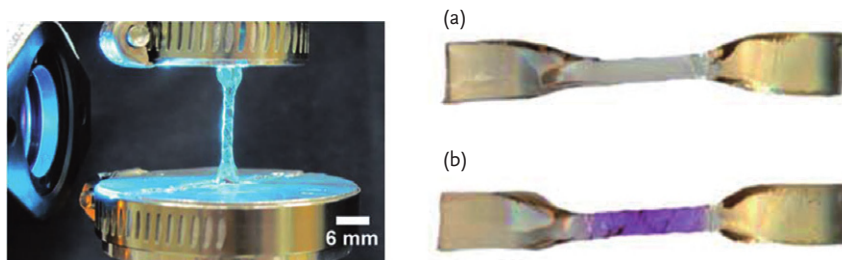


Figure 8.7 PMMA–EGDMA–SP samples before (a) and after (b) torsional testing [39]. Reproduced by permission of The Royal Society of Chemistry.

to ascertain both deformation (leading to chain alignment), and mechanophore activation (bond cleavage), and demonstrated that mechanochemical reaction is more significant when the chains are aligned with the force.

8.3.3

Torsional Shear Testing

Shear stress was used as a method to activate mechanophores in polymers. Using SP as a model mechanophore, a torsional (shear) strain was applied and was demonstrated to be very efficient for mechanophore activation, being able to cause yield and high stress before sample failure [39]. SP was used as a cross-linker in PMMA, and as in the case of tensile testing, mechanophore activation was observed only after the polymer yielded, again indicating that plastic deformation is necessary (Figure 8.7).

8.3.4

Compression

Compression is another common loading condition for solid state materials. Similarly to the previous cases, SP was used in order to study compression in mechanophore activation [22]. PMMA beads cross-linked with SP and ethyleneglycol dimethacrylate (EGDMA) were prepared by suspension radical polymerization, and compressed with a stepper actuator coupled to a load cell, which allowed strain rate control. The MC coloring was localized in the center of the spheres, regions of highest deformation and tensile stresses, indicating activation under diametric compressive loading is actually through tensile forces actuating transverse to the compression axis (Figure 8.8).

The advantage of this method is that large stresses are conveniently applied, allowing the activation of mechanophores which may be difficult to activate by tensile testing. For example, the exothermic ring-opening of *gem*-dihalocyclopropanes was demonstrated in linear polybutadiene, while no activation was observed during tensile testing [40]. The authors noticed that keeping the material under compressive loading for longer times did not lead to higher mechanophore activa-

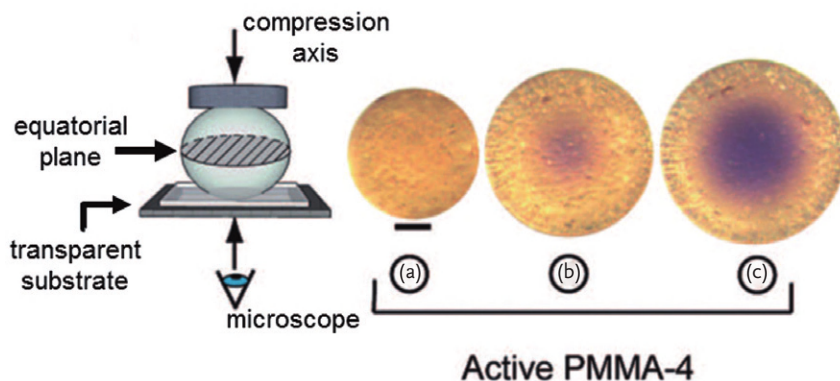


Figure 8.8 The sample configuration and experimental set-up for diametric compressive loading is illustrated schematically. Tensile forces develop in the equatorial plane

normal to compression axis. Cross-linked PMMA-SP beads before (a), during (b), and after (c) compression [22].

tion, but folding and re-compressing to the same load did. This implies that the activation occurs during the initial application of load, coinciding with when plastic deformation and considerable polymer flow occurs.

8.3.5 Others

Several other methods for mechanically stressing materials have been used in order to study mechanochemistry of polymers. Classical examples are turbulent flow [41], elongational flow [42], and repeating freeze–thaw [43]. The disadvantages of these methods are that they are non-uniform and, thus, difficult to control/calculate the forces applied to the dissolved polymers. In contrast, ultrasound is simple to use, and, although it provides excessive mechanical energy, there are several parameters which can be changed in order to change the energy transferred to the chains (see above).

A modern and more sophisticated, precise method to apply force to a macromolecule is using single molecule force spectroscopy measurements (SMES) with the help of atomic force microscopy [44]. This method provides a precise measure of the force applied to the chain and, therefore, can be used to calculate the energy necessary for a mechanochemical reaction in a specific chain. On the other hand, force-induced structure changes cannot be validated by direct spectroscopic methods but rather, must be inferred indirectly. Another interesting method for activating mechanophores was the development of a molecular device where photoinduced geometry change causes stretching of the mechanophore [45]. This technique, while limited in mechanophore size, uses small molecules to apply mechanical force and allows simple chemical analysis, which is a challenging issue when studying mechanochemical reactions in macromolecules.

Finally, theoretical modeling of mechanical forces is a significant method to study mechanochemical reactions. For example, “constrained geometries simulate external force” (COGEF) is a simple method to predict the mechanochemical reaction products, and calculate activation energy and thermodynamic parameters [46]. More complicated, but more revealing theoretical studies include the combination of COGEF with “external force is explicitly included” (EFEI) [47], the combination of molecular dynamics with *ab initio* techniques [48] and others.

8.4 Mechanochemical Self-Healing Strategies

Mechanophores are promising functionalities for the development of self-healing materials. As described above, mechanical energy causes localized changes in the chemical structure, activating a materials system at the molecular level even before macroscopic failure. One of the first discovered mechanochemical reactions was the self-healing of vulcanized rubber. Damaging mechanical force, which is concentrated in the rubber’s cross-linkages, cleaves several S–S bonds into long-lived reactive sulfur radicals that, in the absence of oxygen, recombine reforming the cross-linking bonds [7].

While self-healing is defined as the recovery of mechanical properties at the macroscopic level [49–51]; in this section, damage and healing are described at the molecular level; that is, mechanical damage leading to chemical bond cleavage, and healing systems based on chemical bond formation. It is important to emphasize that the cleavage of some chemical bonds does not necessarily affect the mechanical properties of the material. In addition, forming chemical bonds may change the material in different ways, not necessarily restoring the original mechanical properties, especially if the new chemical bonds are different from the bond cleaved by the mechanochemical damage.

Several mechanophores were not intentionally designed for self-healing applications but contain the basic chemistry to form new chemical bonds, and therefore have potential self-healing features. Using the serendipitous case of rubber as a model, mechanophores that produce reactive species under mechanical stress, with the possibility of reacting with a different chain to form new chemical bonds, provide a basic strategy. Improving on the original strategy, mechanophores that produce active catalysts instead of reactants can increase the healing effect by turnover. Finally, disrupting a chemical equilibrium with mechanical force provides a third strategy, where the system heals by reforming chemical bonds when the system re-equilibrates. These strategies are described in more detail in the following sections.

8.4.1 Production of Reactive Species

As described before, under high mechanical stress, covalent bonds may be cleaved homolytically in polymeric materials, producing two radicals. Radicals, as a highly

reactive species, may react with different surrounding molecules or decay through disproportionation or reaction with oxygen. This strategy works well with vulcanized rubber, since it has a high concentration of the mechanophore. The reactive species produced is long-lived in the absence of oxygen, and the material is soft enough that the chains have sufficient mobility to bring the reactive radicals together to form new bonds.

While the same kind of reaction (cleavage to radicals) can occur in most polymers, this unique self-healing feature is rare. For glassy polymers below T_g , mobility is limited and thus, the likelihood two radicals will meet and combine is small. In addition, in the case of polymers where carbon–carbon or carbon–heteroatom bonds compose the main chain, short-lived carbon radicals are produced, which tend to decay through non-productive chemistry. In order to get the same effect that was serendipitously incorporated in rubber, judiciously designed mechanophores that produce reactive species with longer life-times need to be incorporated.

Polyethylene glycol having a single azo mechanophore per chain was used to study the effects of polymer molecular weight and mechanophore positioning on the mechanochemical reaction rate [52]. This mechanophore produces tertiary carbon radicals with an α -nitrile group, which are relatively long-lived radicals, used often for radical polymerization. When the azo group was released from the chain thermally (heating to 82 °C), recombination of the radicals was observed, indicating that the two radicals could potentially rebind and restore the chain's molecular weight. However, during sonication, the recombination product was not observed. Instead, a cyanohydrin was produced as the only product, probably from the reaction of the radical with oxygen or hydroxyl radical (Figure 8.9). The activation of this mechanophore was studied only in dilute solutions, and the

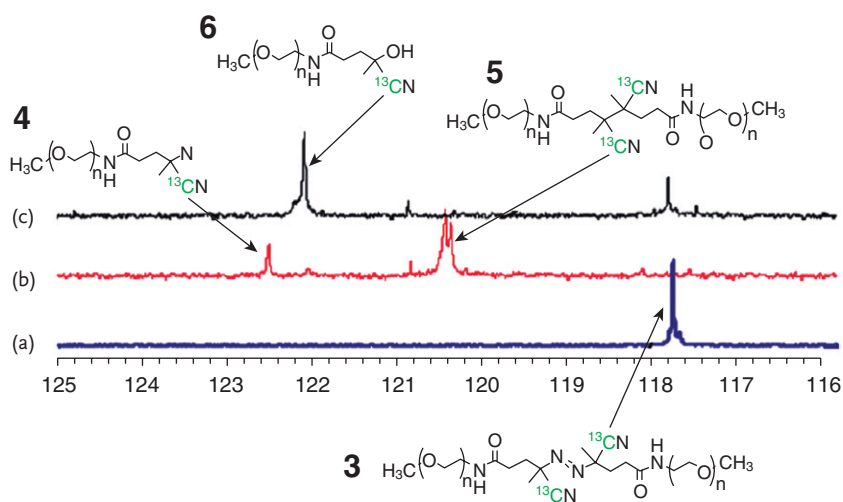
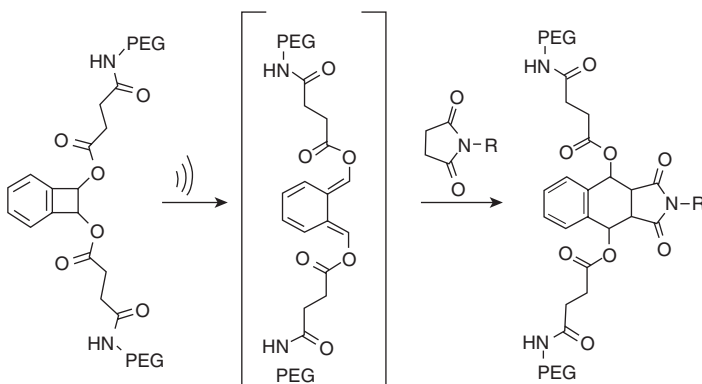


Figure 8.9 ^{13}C NMR spectra of (a) polymer 3, (b) thermal activation products 4 and 5, and (c) sonication product polymer 6 (c) [1, 52]. Reprinted with permission from reference [1]. Copyright 2009 American Chemical Society.

reaction pathway of this mechanophore in bulk polymers, where the concentration of the radicals is higher and access to water/oxygen limited, was not reported.

Strained cyclic molecules, such as cyclobutanes and cyclopropanes, were shown to selectively undergo ring-opening under mechanical force when incorporated close to the center of a polymer chain. Benzocyclobutene, for example, produces a reactive *ortho*-quinodimethide diene under sonication (Scheme 8.1) [13]. While the paper's focus was on the interesting fact that mechanical force can take a reaction to a different pathway compared to the thermal reaction, the identification of the reactive product was done by "trapping" using a Diels–Alder (DA) reaction, achieved by sonicating in the presence of excess of a dienophile. Several successful self-healing systems based on DA reactions have already been demonstrated (see Section 8.4.3); this mechanophore, which produces a very reactive diene, in combination with a polymer having dienophiles in side chains, may be developed into another successful system.



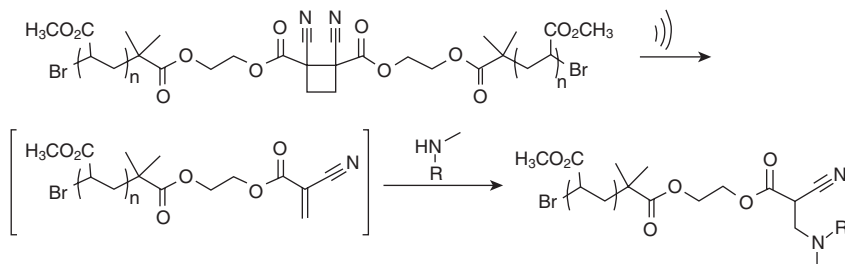
Scheme 8.1 Sonication of a polymer containing a chain center benzocyclobutene affording a reactive *ortho*-quinodimethide diene, which is trapped by a DA reaction with a dienophile [13].

Cyanoacrylates are a stable but very reactive functional group, and constitute the next attempt to develop a mechanophore which could be used for self-healing materials [53]. Using a substituted cyclobutane precursor as a mechanophore, sonication selectively cleaves the polymer into two chains of half the original size, each having one cyanoacrylate as a terminus (Scheme 8.2). Excess secondary amine as a trapping reagent confirmed the presence of cyanoacrylates, reacting only when sonication was started. A polymer having secondary amine side groups may produce new covalent bonds when the cyanoacrylates are released, but no report has been published.

8.4.2

Activation of Catalytic Species

The mechanochemical activation of catalysts stands by itself as a novel method for triggering latent catalysts. Polymers containing different catalysts were prepared,



Scheme 8.2 Production of reactive cyanoacrylates by sonication, and subsequent trapping with a secondary amine [53].

and shown to be inactive towards reagents until mechanical force (sonication) is applied [54, 55]. If the reagents for the activated reactions are part of the polymer side chains, catalyst activation under mechanical force could lead to cross-linking between chains. No example of this reaction has been reported yet, but several reactions using small molecule reagents were demonstrated in both solution and the solid state.

In 2008, a mechanophore was designed to undergo Bergman cyclization and generate radicals without causing scission to the polymer backbone [56]. This mechanophore was used as a cross-linker in PMMA and was mechanically activated by swelling in methyl methacrylate (MMA). Although the evidence was not fully conclusive, the findings suggest that swelling initiated the mechanochemical reaction, producing the desired di-radical. This, in turn, initiated the polymerization of the MMA. While not described as a self-healing system, this mechanophore catalyzed the production of new polymer chains around the mechanically stressed area (Figure 8.10).

Homogeneous organometallic complexes are the finest in chemical catalysis, achieving the best selectivities, turnover numbers and rates [57], making them suitable candidates for mechanically activated catalysts. The first study reported was a ruthenium olefin metathesis catalyst where two of the ligands are telechelic polymer chains [54]. Under mechanical force, the weaker ligand–metal bond is cleaved, leaving the metal with an open coordinating spot, effectively activating it (Scheme 8.3). As in the previous case, the authors were able to show that the activated catalyst can start a polymerization reaction [58]. Following this example, several other organometallic reagents were incorporated into polymers and shown to be activated only under mechanical force, such as palladium [59] which can catalyze several different carbon–carbon and carbon–heteroatom bond formations, and silver [54, 60] which can catalyze trans-esterification reactions.

Mechanical generation of less complex catalysts has the advantages of stability and lower costs compared to organometallic reagents. By cleaving a boronium–pyridine bond, a Brønsted base can be produced (Scheme 8.4) that is able to initiate the anionic polymerization of α -trifluoromethyl-2,2,2-trifluoroethyl acrylate [61].

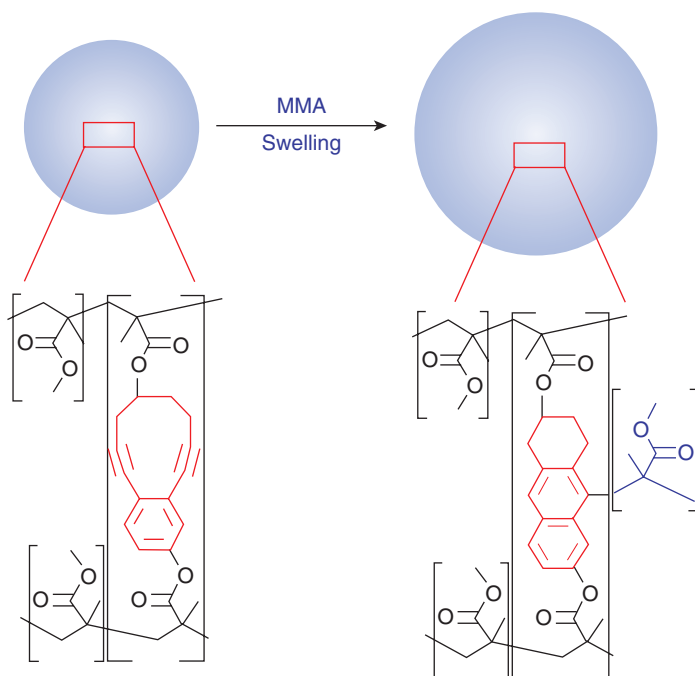
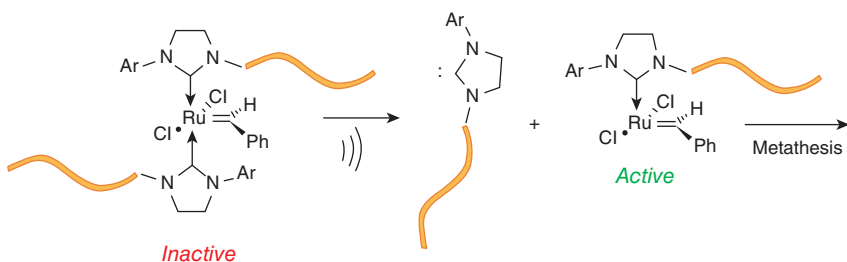
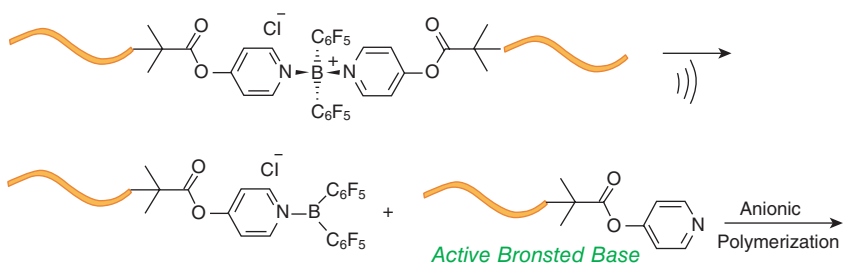


Figure 8.10 Swelling activation of a Bergman cyclization followed by radical polymerization [56].

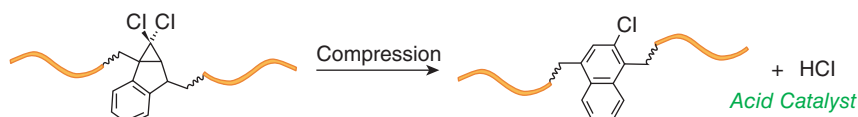


Scheme 8.3 Latent bis-NHC ruthenium olefin metathesis precatalysts activated by sonication [54].



Scheme 8.4 Anionic polymerization initiated by a Brønsted base, which is produced by sonication [61].

A drawback of the catalytic systems described above is that the activated catalysts are bound to a polymer chain, and therefore have very limited mobility in the solid state, which limits the turnover they are intended to achieve. In order to address this problem, an acid-releasing mechanophore was developed. The acid produced is not part of the polymer chain, but is released by elimination as a small molecule (Scheme 8.5) [62]. The inorganic acid has a larger mobility even in the solid state (as demonstrated in photoresists based on photoacid generators) and has the potential to catalyze different chemical reactions, including polymerizations.



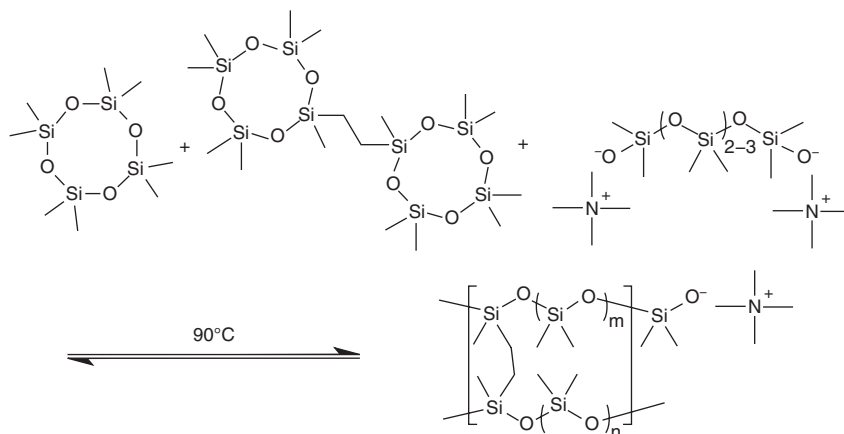
Scheme 8.5 Production of an inorganic acid by mechanical force, the acid is not bound to the polymer chain and may diffuse to reach numerous substrates [62].

8.4.3

Disruption of Equilibrium

Chemical equilibrium is the state in which both reactants and products are present at concentrations which have no further tendency to change with time [63]. When the equilibrium is disrupted, for example by partially cleaving chemical bonds and changing the concentrations of the different components, the system presents a chemical potential to return to the equilibrated state.

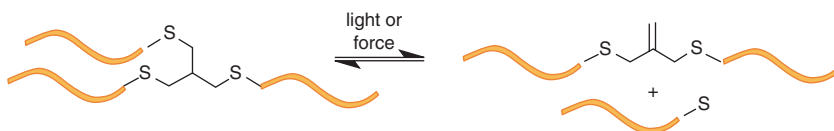
Living polymerizations in which the propagating species is relatively stable towards the environment is one approach to using chemical equilibrium as a method to heal polymers. In the 1950s, cross-linked polydimethylsiloxane (PDMS)—described in Scheme 8.6—was prepared by anionic polymerization [65].



Scheme 8.6 Equilibrium between cyclic monomer and linear oligomers in anionic polymerization to produce cross-linked PDMS [64].

The system contains tetramethylammonium dimethylsilanolate termini as propagating species, which are stable towards air and water. During polymerization at 90 °C, the system equilibrates between linear chains, cross-linkers and cyclic oligomers [66]. If covalent bonds on the linear chains are cleaved by mechanical damage, the equilibrium between the constituents is disrupted, meaning that, given the conditions where they have enough mobility to react, the system will re-equilibrate by sacrificing cyclic oligomers to reform linear chains. Heating the damaged polymer for 24 h causes complete healing of the system [64].

In a similar approach, cross-linked networks made by thiol-ene polymerization undergo chemical changes to adapt to imposed mechanical stress, without losing mechanical properties [67]. When irradiated (320 to 500 nm, 30 mW cm⁻²) the thioether groups can undergo reversible addition–fragmentation through a sulfur radical mechanism, effectively moving the covalent bonds through the irradiated area (Scheme 8.7). Using a polymer that contains a large quantity of thioether groups, it was demonstrated that the material could keep constant mechanical properties while being deformed and irradiated.

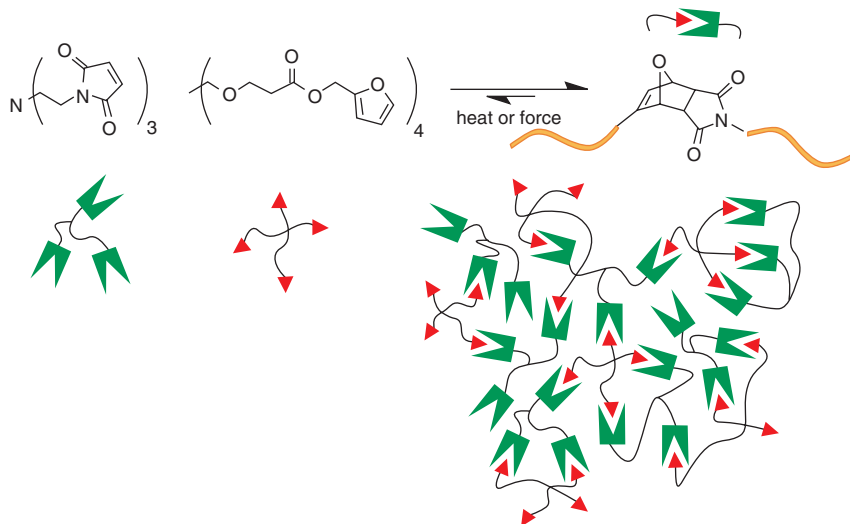


Scheme 8.7 Reversible fragmentation (caused by light or mechanical force)-addition in thioether containing polymers [67].

This strategy was recently expanded by post-polymerization addition of catalysts that allow the metathesis of strong covalent bonds. In these materials, the bonds re-equilibrate as directed by the mechanical potential. For example, transesterification of cross-linked epoxies at high temperatures is possible by addition of Zn(acac)₂, allowing this “thermoset” to be molded or mended, while maintaining its strong mechanical properties upon return to room temperature [68].

Addition of a small quantity of Grubbs catalyst to cross-linked polybutadiene allows room-temperature metathesis of the double bonds in the polymer backbone [69]. Mechanical stress applied to this material triggers metathesis between the chains, causing the strain to increase constantly with time at constant stress, or the dissipation of the stress at constant strain.

The second approach to equilibrium-based healing is centered on systems where the bound state is more energetically stable than the unbound state, but the unbound state is long-lived and mostly unreactive towards other reagents in the system. The original idea was demonstrated for the cross-linked polymer shown in Scheme 8.8, prepared by DA reaction [70]. Interestingly, this material has mechanical properties similar to epoxy resins. A crack was induced in the material and healed by a heating/cooling cycle. During the heating period, the equilibrium is disrupted toward the reagents, while during a slow cooling these would react again in their new position, mending the crack. However, the authors did not know at that time that mechanical damage by itself is enough to break DA products

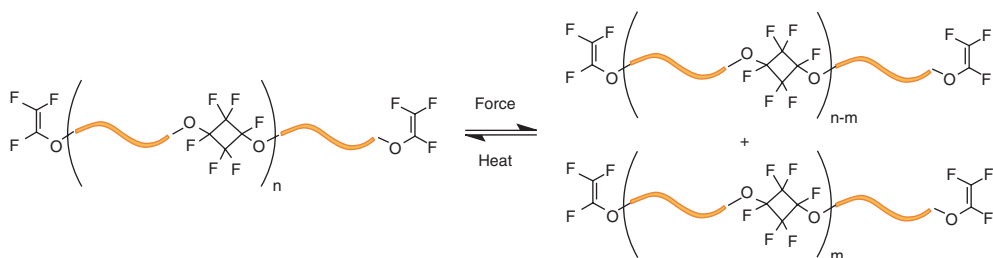


Scheme 8.8 Reversible DA reaction in cross-links of a polymer network [70].

into their reagents, as demonstrated several years later [71]. While heating is still necessary (increases chain mobility, activation energy), a high concentration of “reagents” was already present on the surface of the crack.

This approach was also shown to work for other cycloadditions. A crack was induced in a thermoset prepared by photochemical [2+2] cycloaddition of a tris-cinnamoyl monomer [72]. Assuming most mechanochemical damage was cyclobutane cleavage, the material was healed by photoirradiation to re-form the cyclobutanes. Better healing was achieved when the photoirradiation was conducted under heating, however, heating alone did not provide any healing.

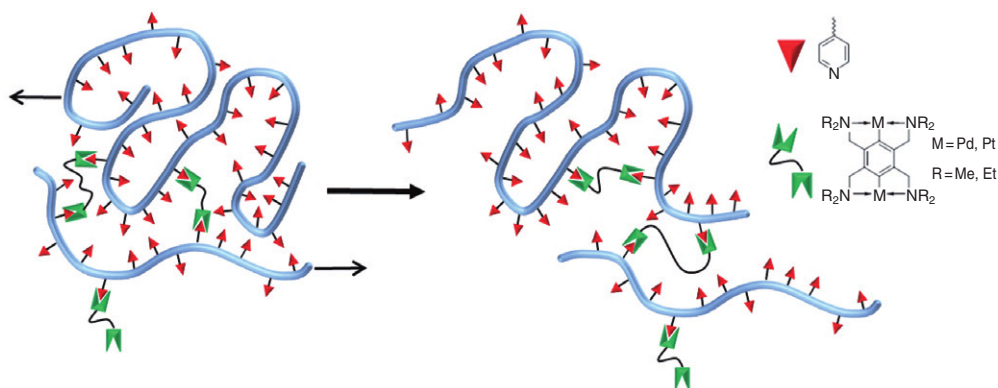
This strategy works also in linear soft thermoplastics. A perfluorocyclobutane aryl ether polymer was prepared by step-growth [2+2] cycloaddition containing several mechanophores along the chains [73]. Mechanical force induced the retro [2+2] cycloaddition into shorter linear segments with trifluorovinyl ether termini. These, given enough energy, can rebind, mending the linear chains (Scheme 8.9). Interestingly, the linear chains do not necessarily return to their original size—the



Scheme 8.9 Reversible cycloaddition of trifluorovinyl groups to form and cleave a linear thermoplastic [73].

size of the product depends on the equilibrium between open and closed forms, which depends on concentration and temperature.

Weaker non-covalent bonds were used as an alternative to cycloaddition reactions. Poly(4-vinylpyridine) (PVP) was cross-linked by addition of Pd or Pt (Scheme 8.10) [74]. The authors demonstrated that these cross-linkers bound reversibly, changing between inter and intra-chain cross-links in accordance to the mechanical stress. In another example, a telechelic polytetrahydrofuran with terminal phosphines was used to make networks using rhodium and iridium, each metal binding up to four different phosphines [75]. These systems undergo sol-gel transition under sonication, but given enough time, revert to the original state.



Scheme 8.10 Cross-linking of PVP by organometallic complexes forming reversible coordinative bonds [74].

Supramolecular polymers held together by hydrogen bonds make efficient self-healing systems. A rubber-like polymer formed from polyfunctional carboxylic acids and diethylenetriamine further functionalized with urea could be cut and rebound [76]. If the two pieces were immediately rejoined, complete recovery of some mechanical properties was achieved. Healing efficiency was decreased if the parts were rejoined after a delay, supposedly as a consequence of new hydrogen bonds re-formed in the separate parts.

8.5

Conclusions and Outlook

Modern mechanochemistry, the development of productive chemistry by mechanical stimuli, is a relatively new scientific direction with the potential to impact several technologies. The development of mechanochemically activated self-healing systems is just one of the various applications under development. The mechanophore concept allowed localization of the mechanical force into selective chemical reactions, and the production of high energy intermediates which are

able to form new chemical bonds. The study of mechanophores in solution allows an easy and fast screening of new mechanophores, while their study in the solid state is useful in the direct observation of mechanical stress in materials, as well as the simulation of the materials' response to damaging mechanical stress.

The biggest limitation to a mechanochemical self-healing system is the activation in the solid state, which is constrained to certain environmental conditions, directly related to the T_g of the material. On the other hand, a mechanochemical system can be incorporated into a material without changing its mechanical properties, which is a limitation when using larger scale self-healing systems. Mechanophores display a homogeneous distribution throughout the material, and actuate at the molecular level even before a crack is produced, restricting their effect to the places where mechanical stress is maximized.

Several self-healing systems based on mechanochemistry have already been reported and were described here. A challenge still unmet by mechanophores is in the development of an autonomic self-healing system, where the mechanical energy will initiate the cascade which eventually leads to chemical bond formation without any additional energy or human intervention. An autonomic self-healing mechanochemical system will give access to the ultimate self-healing material, which will expand the lifetime of structural materials by maintaining their mechanical properties and adapting itself to the changes in mechanical stress.

References

- 1 Caruso, M.M., Davis, D.A., Shen, Q., Odom, S.A., Sottos, N.R., White, S.R., and Moore, J.S. (2009) Mechanically-induced chemical changes in polymeric materials. *Chem. Rev.*, **109**, 5755–5798.
- 2 Wiggins, K.M., Brantley, J.N., and Bielawski, C.W. (2012) Polymer mechanochemistry: force enabled transformations. *ACS Macro Lett.*, **1**, 623–626.
- 3 Black, A.L., Lenhardt, J.M., and Craig, S.L. (2011) From molecular mechanochemistry to stress-responsive materials. *J. Mater. Chem.*, **21**, 1655–1663.
- 4 Staudinger, H., and Bondy, H.F. (1930) Isoprene and rubber. XIX. The molecular size of rubber and balata. *Ber. Dtsch. Chem. Ges.*, **63**, 734–736.
- 5 Staudinger, H., and Heuer, W. (1934) Highly polymerized compounds. XCIII. The breaking up of the molecular fibers of the polystyrenes. *Ber. Dtsch. Chem. Ges.*, **67**, 1159–1164.
- 6 Staudinger, H., and Leupold, E.O. (1930) Isoprene and rubber. XVIII. Studies of the viscosity of balata. *Ber. Dtsch. Chem. Ges.*, **63**, 730–733.
- 7 See for example: Busse, W.F., and Cunningham, R.N. (1938) Mastication of rubber: a study of some of the oxidation processes involved. Proceedings of the Rubber Technology Conference, London, 288–301.
- 8 Kauzmann, W., and Eyring, H. (1940) The viscous flow of large molecules. *J. Am. Chem. Soc.*, **62**, 3113–3125.
- 9 For a review on ESR studies of mechanically stressed materials see: Sohma, J. (1989) Mechanochemistry of polymers. *Prog. Polym. Sci.*, **14**, 451–596.
- 10 Staudinger, H., and Schweitzer, O. (1930) Highly polymerized compounds. XLVIII. Molecular size of cellulose. *Ber. Dtsch. Chem. Ges.*, **63**, 3132–3154.
- 11 Schmid, G., and Rommel, O. (1939) Zerreißen von makromolekülen mit ultraschal. *Z. Phys. Chem.*, **185** (2), 97–139.
- 12 Encina, M.V., Lissi, E., Sarasúa, M., Gargallo, L., and Radic, D.J. (1980)

- Ultrasonic degradation of polyvinylpyrrolidone: effect of peroxide linkages. *Polym. Sci. Polym. Lett. Ed.*, **18**, 757–760.
- 13 Hickenboth, C.R., Moore, J.S., White, S.R., Sottos, N.R., Baudry, J., and Wilson, S.R. (2007) Biasing reaction pathways with mechanical force. *Nature*, **446**, 423–427.
- 14 Stevens, M.P. (1999) *Polymer Chemistry: An Introduction*, 3rd edn, Oxford University Press.
- 15 Kausch, H.H., and Plummer, C.J.G. (1994) The role of individual chains in polymer deformation. *Polymer*, **35**, 3848–3857.
- 16 Svaneborg, C., Everaers, R., Grest, G.S., and Curro, J.G. (2008) Connectivity and entanglement stress contributions in strained polymer networks. *Macromolecules*, **41**, 4920–4928.
- 17 Wool, R.P., and Boyd, R.H. (1980) Molecular deformation of polypropylene. *J. Appl. Phys.*, **51**, 5116–5124.
- 18 Thomas, J.R., and deVries, L. (1959) Sonically induced heterolytic cleavage of poly(methyl siloxane). *J. Phys. Chem.*, **63**, 254–256.
- 19 Henglein, V.A. (1955) The reaction of 2,2-diphenyl-1-picrylhydrazyl with long-chain free radicals produced from ultrasonic degradation of polymethyl methacrylate. *Makromol. Chem.*, **15**, 188–210.
- 20 Melville, H.W., and Murray, A.J.R. (1950) Ultrasonic degradation of polymers. *Trans. Faraday Soc.*, **46**, 996–1009.
- 21 Baytekin, H.T., Baytekin, B., and Grzybowski, B.A. (2012) Mechanoradicals created in “polymeric sponges” drive reactions in aqueous media. *Angew. Chem. Int. Ed.*, **51**, 3596–3600.
- 22 Davis, D.A., Hamilton, A., Yang, J., Cremar, L.D., Van Gough, D., Potisek, S.L., Ong, M.T., Braun, P.V., Martínez, T.J., White, S.R., Moore, J.S., and Sottos, N.R. (2009) Force-induced activation of covalent bonds in mechanoresponsive polymeric materials. *Nature*, **459**, 68–72.
- 23 Potisek, S.L., Davis, D.A., Sottos, N.R., White, S.R., and Moore, J.S. (2007) Mechanophore-linked addition polymers. *J. Am. Chem. Soc.*, **129**, 13808–13809.
- 24 Aktah, D., and Frank, I. (2002) Breaking bonds by mechanical stress: when do electrons decide for the other side? *J. Am. Chem. Soc.*, **124**, 3402–3406.
- 25 ASTM (2007) D2603. Standard test method for sonic shear stability of polymer-containing oils. American Society for Testing and Materials, Pennsylvania.
- 26 Price, G.J., and Smith, P.F. (1993) Ultrasonic degradation of polymer solutions. III. The effect of changing solvent and solution concentration. *Eur. Polym. J.*, **29**, 419–424.
- 27 Glynn, P.A.R., van der Hoff, B.M.E., and Reilly, P.M. (1972) A general model for prediction of molecular weight distributions of degraded polymers. Development and comparison with ultrasonic degradation experiments. *J. Macromol. Sci., Part A*, **6**, 1653–1664.
- 28 Basedow, A.M., and Ebert, K.H. (1977) Ultrasonic degradation of polymers in solution. *Adv. Polym. Sci.*, **22**, 83–148.
- 29 Suslick, K.S., and Price, G.J. (1999) Applications of ultrasound to materials chemistry. *Annu. Rev. Mater. Sci.*, **29**, 295–326.
- 30 Price, G.J. (1990) The use of ultrasound for the controlled degradation of polymer solutions, in *Advances in Sonochemistry*, 1st vol (ed. T.J. Mason), JAI Press Ltd, Cambridge, pp. 231–287.
- 31 Nguyen, T.Q. (1994) Kinetics of mechanochemical degradation by gel permeation chromatography. *Polym. Degrad. Stab.*, **46**, 99–111.
- 32 Florea, M. (1993) New use of size exclusion chromatography in kinetics of mechanical degradation of polymers in solution. *J. Appl. Polym. Sci.*, **50**, 2039–2045.
- 33 Price, G.J., and Smith, P.F. (1993) Ultrasonic degradation of polymer solutions. 2. The effect of temperature, ultrasound intensity and dissolved gases on polystyrene in toluene. *Polymer*, **34**, 4111–4117.
- 34 Basedow, A.M., and Ebert, K.H. (1975) Mechanism of the degradation of polymers in solution by ultrasound. *Makromol. Chem.*, **176**, 745–757.
- 35 Schittenhelm, N., and Kulicke, W.-M. (2000) Producing homologous series of

- molar masses for establishing structure–property relationships with the aid of ultrasonic degradation. *Macromol. Chem. Phys.*, **201**, 1976–1984.
- 36 Striegel, A.M. (2003) Influence of chain architecture on the mechanochemical degradation of macromolecules. *J. Biochem. Biophys. Methods*, **56**, 117–139.
- 37 Beiermann, B.A., Davis, D.A., Kramer, S.L.B., Moore, J.S., Sottos, N.R., and White, S.R. (2011) Environmental effects on mechanochemical activation of spiropyran in linear PMMA. *J. Mater. Chem.*, **21**, 8443–8447.
- 38 Beiermann, B.A., Kramer, S.L.B., Moore, J.S., White, S.R., and Sottos, N.R. (2012) Role of mechanophore orientation in mechanochemical reactions. *ACS Macro Lett.*, **1**, 163–166.
- 39 Kingsbury, C.M., May, P.A., Douglas, D.A., White, S.R., Moore, J.S., and Sottos, N.R. (2011) Shear activation of mechanophore-crosslinked polymers. *J. Mater. Chem.*, **21**, 8381–8388.
- 40 Lenhardt, J.M., Black, A.L., Beiermann, B.A., Steinberg, B.D., Rahman, F., Samborski, T., Elsagr, J., Moore, J.S., Sottos, N.R., and Craig, S.L. (2011) Characterizing the mechanochemically active domains in gem-dihalocyclopropanated polybutadiene under compression and tension. *J. Mater. Chem.*, **21**, 8454–8459.
- 41 Horn, A.F., and Merrill, E.W. (1984) Midpoint scission of macromolecules in dilute solution in turbulent flow. *Nature*, **312**, 140–141.
- 42 Porter, R.S., and Johnson, J.F. (1959) Laminar flow degradation of polyisobutene. *J. Phys. Chem.*, **63**, 202–205.
- 43 Zysman, V., Nguyen, T.Q., and Kausch, H.-H. (1994) Degradation on freezing dilute polystyrene solutions in p-xylene. *J. Polym. Sci., Part B: Polym. Phys.*, **32**, 1257–1269.
- 44 Binnig, G., Quate, C.F., and Gerber, C. (1986) Atomic force microscope. *Phys. Rev. Lett.*, **56**, 930–933.
- 45 Yang, Q.-Z., Huang, Z., Kucharski, T.J., Khvostichenko, D., Chen, J., and Boulatov, R. (2009) A molecular force probe. *Nat. Nanotechnol.*, **4**, 302–306.
- 46 Beyer, M.K. (2000) The mechanical strength of a covalent bond calculated by density functional theory. *J. Chem. Phys.*, **112**, 7307–7312.
- 47 Ribas-Arino, J., Shiga, M., and Marx, D. (2009) Understanding covalent mechanochemistry. *Angew. Chem. Int. Ed.*, **48**, 4190–4193.
- 48 Ong, M.T., Leiding, J., Tao, H., Virshup, A.M., and Martínez, T.J. (2009) First principles dynamics and minimum energy pathways for mechanochemical ring opening of cyclobutene. *J. Am. Chem. Soc.*, **131**, 6377–6379.
- 49 Blaiszik, B.J., Kramer, S.L.B., Olugebefola, S.C., Moore, J.S., Sottos, N.R., and White, S.R. (2010) Self-healing polymers and composites. *Annu. Rev. Mater. Res.*, **40**, 179–211.
- 50 Wool, R.P. (2008) Self-healing materials: a review. *Soft Matter*, **4**, 400–418.
- 51 Wu, D.Y., Meure, S., and Solomon, D. (2008) Self-healing polymeric materials: a review of recent developments. *Prog. Polym. Sci.*, **33**, 479–522.
- 52 Berkowski, K.L., Potisek, S.L., Hickenboth, C.R., and Moore, J.S. (2005) Ultrasound-induced site-specific cleavage of azo-functionalized poly(ethylene glycol). *Macromolecules*, **38**, 8975–8978.
- 53 Kryger, M.J., Ong, M.T., Odom, S.A., Sottos, N.R., White, S.R., Martinez, T.J., and Moore, J.S. (2010) Masked cyanoacrylates unveiled by mechanical force. *J. Am. Chem. Soc.*, **132**, 4558–4559.
- 54 Piermattei, A., Karthikeyan, S., and Sijbesma, R.P. (2009) Activating catalysts with mechanical force. *Nat. Chem.*, **1**, 133–137.
- 55 Karthikeyan, S., Potisek, S.L., Piermattei, A., and Sijbesma, R.P. (2008) Highly efficient mechanochemical scission of silver-carbene coordination polymers. *J. Am. Chem. Soc.*, **130**, 14968–14969.
- 56 Hickenboth, C.R., Rule, J.D., and Moore, J.S. (2008) Preparation of enediyne-crosslinked networks and their reactivity under thermal and mechanical conditions. *Tetrahedron*, **64**, 8435–8448.
- 57 Astruc, D. (2007) *Organometallic Chemistry and Catalysis*, Springer, Berlin.
- 58 Jakobs, R.T.M., and Sijbesma, R.P. (2012) Mechanical activation of a latent olefin metathesis catalyst and persistence of its

- active species in ROMP. *Organometallics*, **31** (6), 2476–2481.
- 59 Tennyson, A.G., Wiggins, K.M., and Bielawski, C.W. (2010) Mechanical activation of catalysts for C-C bond forming and anionic polymerization reactions from a single macromolecular reagent. *J. Am. Chem. Soc.*, **132**, 16631–16636.
- 60 Rooze, J., Groote, R., Jakobs, R.T.M., Sijbesma, R.P., Iersel, M.M., van Rebrov, E., Schouten, J.C., and Keurentjes, J.T.F. (2011) Mechanism of ultrasound scission of a silver-carbene coordination polymer. *J. Phys. Chem. B*, **115** (38), 11038–11043.
- 61 Wiggins, K.M., Hudnall, T.W., Tennyson, A.G., and Bielawski, C.W. (2011) Selective scission of pyridine-boronium complexes: mechanical generation of brønsted bases and polymerization catalysts. *J. Mater. Chem.*, **21**, 8355–8359.
- 62 Diesendruck, C.E., Steinberg, B.D., Sugai, N., Silberstein, M.N., Sottos, N.R., White, S.R., Braun, P.V., and Moore, J.S. (2012) Proton-coupled mechanochemical transduction: a mechanogenerated acid. *J. Am. Chem. Soc.*, **134**, 12446–12449.
- 63 Atkins, P., and de Paula, J. (2006) *Physical Chemistry*, 8th edn, W.H. Freeman.
- 64 Zheng, P., and McCarthy, T.J. (2012) A surprise from 1954: siloxane equilibration is a simple, robust, and obvious polymer self-healing mechanism. *J. Am. Chem. Soc.*, **134**, 2024–2027.
- 65 Kantor, S.W., Grubb, W.T., and Osthoff, R.C. (1954) The mechanism of the acid- and base-catalyzed equilibration of siloxanes. *J. Am. Chem. Soc.*, **76**, 5190–5197.
- 66 Gilbert, A.R., and Kantor, S.W. (1959) Transient catalysts for the polymerization of organosiloxanes. *J. Polym. Sci.*, **40**, 35–58.
- 67 Scott, T.F., Schneider, A.D., Cook, W.D., and Bowman, C.N. (2005) Photoinduced plasticity in cross-linked polymers. *Science*, **308**, 1615–1617.
- 68 Montarnal, D., Capelot, M., Tournilhac, F., and Leibler, L. (2011) Silica-like malleable materials from permanent organic networks. *Science*, **334**, 965–968.
- 69 Lu, Y.-X., Tournilhac, F., Leibler, L., and Guan, Z. (2012) Making insoluble polymer networks malleable via olefin metathesis. *J. Am. Chem. Soc.*, **134**, 8424–8427.
- 70 Chen, X., Dam, M.A., Ono, K., Mal, A., Shen, H., Nutt, S.R., Sheran, K., and Wudl, F. (2002) A thermally re-mendable cross-linked polymeric material. *Science*, **295**, 1698–1702.
- 71 Wiggins, K.M., Syrett, J.A., Haddleton, D.M., and Bielawski, C.W. (2011) Mechanically facilitated retro [4 + 2] cycloadditions. *J. Am. Chem. Soc.*, **133**, 7180–7189.
- 72 Chung, C.-M., Roh, Y.-S., Cho, S.-Y., and Kim, J.-G. (2004) Crack healing in polymeric materials via photochemical [2+2] cycloaddition. *Chem. Mater.*, **16**, 3982–3984.
- 73 Klukovich, H.M., Kean, Z.S., Iacono, S.T., and Craig, S.L. (2011) Mechanically induced scission and subsequent thermal remending of perfluorocyclobutane Polymers. *J. Am. Chem. Soc.*, **133**, 17882–17888.
- 74 Xu, D., Hawk, J.L., Loveless, D.M., Jeon, S.L., and Craig, S.L. (2010) Mechanism of shear thickening in reversibly cross-linked supramolecular polymer networks. *Macromolecules*, **43**, 3556–3565.
- 75 Paulusse, J.M.J., van Beek, D.J.M., and Sijbesma, R.P. (2007) Reversible switching of the sol-gel transition with ultrasound in rhodium(I) and iridium(I) coordination networks. *J. Am. Chem. Soc.*, **129** (8), 2392–2397.
- 76 Cordier, P., Tournilhac, F., Soulie-Ziakovic, C., and Leibler, L. (2008) Self-healing and thermoreversible rubber from supramolecular assembly. *Nature*, **451**, 977–980.

9

Chemistry of Crosslinking Processes for Self-Healing Polymers

Roberto F.A. Teixeira, Xander K.D. Hillewaere, Stijn Billiet, and Filip E. Du Prez

9.1

Introduction

This chapter will give the reader an overview of the crosslinking chemistries that have been used for self-healing purposes until now. The described chemistries are used in a self-healing concept that envisages a recovery of all types of material properties, such as fracture toughness, corrosion resistance, or conductivity, to improve the durability and reliability of the polymeric materials. Damage due to impact, wear, or fatigue initiates a healing mechanism that – preferentially without external stimulus – can recover any functionality. For this, crosslinking chemistries used in extrinsic and intrinsic self-healing materials will be discussed in detail. The first part of this chapter will focus on the chemistries used in extrinsic materials (Section 9.2), where the self-healing property is obtained by adding healing agents to the material to be healed. The second part will highlight chemistries used for intrinsic self-healing materials (Section 9.3), where self-healing is achieved by the material itself through its chemical nature.

9.2

Extrinsic Self-Healing Materials

In this section, a vast summary of the chemistries (conditions, limitations, benefits, efficiencies. . .) that have been used in extrinsic self-healing materials will be addressed. An overview of all the discussed extrinsic self-healing systems can be found in Table 9.1. These materials can be divided, according to their healing mechanism, into catalytic and non-catalytic systems. In both cases, the healing agent (or catalyst) is sequestered in one or more capsules, or in a vascular network in the shape of capillaries or hollow channels, which, depending on the system complexity, can interconnect in one (1D), two (2D) or three dimensions (3D). A third option is the use of meltable healing agent particles. In either a capsule or a vascular-based system, upon a damage-induced cracking, the self-healing mechanism is triggered by the rupture of the capsules or vascular network and

Table 9.1 Extrinsic self-healing systems.

Healing agent	Method of healing	Material to be healed	Healing conditions ^{a)}	Healing eff. (% ^{b)})	Ref.
DCPD/ENB	Microcapsules	Epoxy	Grubbs cat. [wax], 0–125 °C, 1–2 d	18–93 (100)	[1–16]
			WCl ₆ cat., RT, 2 d	20 (107)	[17]
Siloxanes	Vascular Microcapsules	Epoxy/vinyl ester PMMA PS- <i>block</i> -PBD- <i>block</i> -PS Epoxy	Grubbs cat., SMA wires (80 °C), RT, 1 d	80 (98)	[18, 19]
			Grubbs cat., RT, 2.5 min–2 d	46–50	[20]
			Grubbs cat., RT	80	[21–23]
			Grubbs cat., RT	Not mentioned	[24]
			Grubbs cat., RT, 2 d	38–58	[25, 26]
			Organotin cat., RT, 1 d	11–51	[27]
Epoxy	Microcapsules	Epoxy/vinyl ester PDMS	Organotin cat. [PU], 20–50 °C, 1 d	24–46	[28, 29]
			Pt cat., siloxane initiator, RT, 5 h–2 d	70–120 (57–84)	[30, 31]
			Organotin cat. [PU], RT, 1 d	33–100	[32]
			Imidazole init., 120–180 °C, 30 min–1 h	68–111	[33–38]
Epoxy	Vascular Meltable ^{c)} Thermoplastic additive	Epoxy/polyimide Epoxy	BF ₃ ·OEt ₂ cat., 20–30 °C, 30 min–2 h	76–89	[39]
			Sc(OTf) ₃ cat., solvent, 45–80 °C, 2 d	49–86 (78)	[40]
			Solvent, RT, 1 d	82–100	[41, 42]
			UV, 1 min	Not mentioned	[43]
			100 °C, 10 min	100	[44]
		MWCNT, 150 °C	55–70	[45]	
		130–185 °C, 1–2 h	50–75	[46–51]	

Thiol-epoxy	Microcapsules	Epoxy	Amine cat., RT, 3 h–1 d	80–105	[52–58]
Amine-epoxy	Microcapsules	Epoxy	RT, 2 d	Not mentioned	[59]
			RT, 2 d	77–91 (136)	[60]
	Fibers/Vascular	Epoxy	(acetone), RT–100°C, 2 h–5 d	82–100	[61–70]
			30°C, 2 d	64–86	[71–73]
			RT, 36 h–2 d	82–114	[74, 75]
GMA	Microcapsules	Polymethacryl imide	(Excess amine), RT, 3 d	75–90 (95)	[76]
Thiol-maleimide	Manual	Epoxy	m-cresol, RT, 3–5 d	(50–121)	[77]
Isocyanates	Microcapsules	Epoxy	H ₂ O	Not mentioned	[78]
	Fibers/Vascular	Polyisocyanurate	Polyol, RT, 30 min–1 d	43–88 (120–160)	[79]
Thiol-ene	Microcapsules	Acrylates	Photoinit., UV, RT, 1 h	Not mentioned	[80, 81]
Azide-alkyne	Microcapsules	Poly(isobutylene)	CuBr(PPh ₃) ₃ cat., 25–60°C, 5 d	91–107	[82, 83]
Vinyl ester	Fibers	Epoxy/vinyl ester	–	Not mentioned	[84]
PEMAA	Meltable ^(c)	Epoxy	150°C, 30 min	85–121	[85–87]
Copolyester	Meltable ^(c)	SMP polystyrene	150°C, 20 min	65	[88]

a) The shell material of the catalyst microcapsules is indicated in square brackets.

b) Healing efficiency obtained using manual injection of healing agents is indicated in parentheses; healing efficiencies higher than 100% indicate a healed network that fails at a higher load value than the original matrix network; multiple healing cycle values are not added to allow comparison between the different delivery systems.

c) Meltable particles are added to the matrix.

subsequent release and reaction of the healing agent in the affected region. On the other hand, in the case of meltable particles or thermoplastic additives, heat is required to initiate flow of the healing agent. In contrast to a capsule or meltable particle-based system, a vascular system may allow refilling of the network with more healing agents by an external source/or by an undamaged region, and thus multiple local healing events can occur. However, due to the complexity in the design/manufacturing of vascular networks, the use of capsule-based systems has attracted more attention during the last decade.

The majority of the capsules used in self-healing materials are prepared by *in situ* and interfacial polymerization techniques in an oil-in-water (o/w) emulsion. Typical compositions used for the shell material are poly(urea-formaldehyde) (PUF) [30, 89–93], poly(melamine-formaldehyde) (PMF) [52, 94], poly(melamine-urea-formaldehyde) (PMUF) [95], polyurethane (PU) [28] and acrylates [96]. On the other hand, vascular networks usually consist of hollow glass fibers (HGFs), carbon fiber plies, or are made via direct-write assembly of a fugitive organic ink [97]. An overview of encapsulation methods as well as the assembly of vascular network structures is outside the scope of this section and will be discussed in chapter 10.

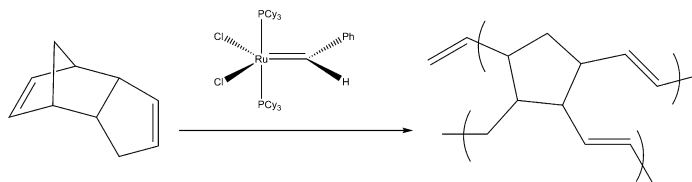
In what follows, the discussed crosslinking chemistries during the self-healing process will be divided into catalytic and non-catalytic systems.

9.2.1

Catalytic Systems

9.2.1.1 Dicyclopentadiene (DCPD) + Grubbs' Catalyst Healing System

The most known and extensively explored capsule-catalytic self-healing system was proposed by White *et al.* [1]. The system comprises an epoxy matrix with urea-based microcapsules containing dicyclopentadiene (DCPD). Upon release, DCPD can undergo ring-opening metathesis polymerization (ROMP) when coming into contact with a pre-embedded, dispersed Grubbs' catalyst (Scheme 9.1). This pioneering work was then fully characterized and extended toward higher healing efficiencies (up to 93% as indicated in Table 9.1) [2–13]. The Grubbs' catalyst was encapsulated with wax to overcome the deactivation problem of the catalyst [14, 15]. Proton NMR analysis showed that Grubbs' catalyst retained 69% of its reactivity, which is a significant improvement compared to the previous system, and also showed a more uniform distribution of the wax microcapsules throughout the



Scheme 9.1 Ruthenium-based Grubbs' catalyst initiates ROMP of DCPD [1].

epoxy matrix. Moll *et al.* also developed a self-healing composite using wax-protected Grubbs' catalyst and DCPD-filled capsules dispersed into a glass fiber-reinforced epoxy composite, obtaining similar results [98]. Biggs and coworkers extended the first generation Grubbs' catalyst ROMP toward the use in cement joint replacements [21–23]. PUF microcapsules containing DCPD and particles of Grubbs' catalyst were dispersed into a PMMA-based bone cement, yielding a healing efficiency of 80%. At 37°C, it was verified that the polymerization rate of the bone cement is dependent on the Grubbs' catalyst particle size, increasing significantly with size reduction. Wilson and Chipara further expanded the DCPD self-healing system to epoxy vinyl ester [20] and polystyrene-*block*-polybutadiene-*block*-polystyrene (PS-*block*-PBD-*block*-PS) [24] matrix materials.

The ROMP between DCPD and a Grubbs' catalyst was studied kinetically by Aldridge and collaborators [99]. In their work, the evolution of the curing network was monitored as a function of network connectivity and chemical composition. It was noted that the ROMP reaction rate correlated with the square of Grubbs' catalyst concentration and that a minimum amount of catalyst was always required.

Inspired by nature, Toohey *et al.* [25, 26]. created a 3D microvascular network embedded in an epoxy matrix via the direct-write assembly method. The microvascular network was filled with DCPD, while Grubbs' catalyst particles were dispersed in the matrix. The self-healing mechanism is the same as indicated before but, due to the presence of the vascular network, multiple repair cycles were possible.

In order to improve the DCPD/Grubbs' catalyst self-healing efficiency, Kirkby *et al.* [18, 19]. embedded shape-memory alloy (SMA) wires within an epoxy matrix. In this system, the presence of SMA wires decreased the crack volume, thus increasing the fill factor (DCPD volume divided by crack volume). Consequently, lower amounts of DCPD are required for crack filling, leading to better healing performances for the same amount of DCPD. With the use of SMA wires, the healing efficiency increased from 49 to 77%.

One important issue with regard to the industrial use of a Grubbs' catalyst in self-healing applications is its price and low versatility. In order to overcome these problems, Wilson *et al.* compared three variations of Grubbs' catalyst: a first, second, and Hoveyda–Grubbs' second generation catalyst for use in self-healing materials [16, 100]. This study demonstrated that the second generation Grubbs' catalyst was the most versatile, especially at high temperatures. Additionally, Kessler *et al.* investigated the rheological behavior of the ROMP triggered by the first and second generation Grubbs' catalyst [101]. They showed that the first generation Grubbs' catalyst was more effective in all studied epoxy matrices. In an attempt to establish a cost effective and widely available self-healing chemistry, Kamphaus and coworkers used WCl_6 , a widely available compound, as a ROMP catalyst to improve thermal stability in self-healing epoxy matrices [17]. With this combination, a healing efficiency of only 20% was obtained. The Kessler group also screened different diene monomers that could be cost effective and developed a model to predict the solubility of Grubbs' catalyst in different norbornenyl-based monomers with potential use in self-healing materials [102, 103].

To further improve and better understand the healing mechanism of the DCPD/Grubbs' catalyst system, Blaiszik *et al.* [104]. measured the bonding recovery of a fiber/matrix interface. Upon damage, microcapsules of circa 1.5 μm in diameter, filled with DCPD and recrystallized Grubbs' catalyst, present at the glass fiber surface, released their content, initiating a healing polymerization. The healing efficiency was measured by the interfacial shear strength, a measure of interfacial bond strength, and increased to 44% after full interfacial debonding. Similar work was performed by Sanada *et al.*, who measured the healing efficiency of the interface of a carbon fiber/epoxy matrix [105]. The Grubbs' catalyst and microcapsules with DCPD were manually injected in between both layers, reaching a healing efficiency up to 19%, when the capsules were broken.

The lack of interfacial bonding between the microcapsules containing the healing agent and the polymer matrix could be one plausible reason for the low healing efficiencies reported by Blaiszik and Sanada. To enhance interfacial bonding between filled microcapsules and the surrounding polymer matrix, Wang *et al.* functionalized the surface of PUF DCPD-filled microcapsules with 3-aminopropyltriethoxy silane or γ -glycidoxypropyltrimethoxysilane [106–108]. Both hydrogen bonds and Si–O–C covalent bonds were formed at the interface by the interaction between Si–OH and hydroxy groups of PUF microcapsules, resulting in an improvement in the tensile strength and impact resistance of the epoxy composites.

9.2.1.2 DCPD/5-Ethylidene-2-Norbornene (ENB)+Grubbs' Catalyst Healing System

Besides the improvements in the DCPD/Grubbs' catalyst system, some limitations had to be solved. The low melting point of the DCPD and the high cost of the Grubbs' catalyst have been recognized as the main obstacles to overcome. Therefore, attempts to reduce the amount of Grubbs' catalyst and increase the reactivity of the ROMP have been explored. Liu and collaborators replaced the DCPD-filled microcapsules by 5-ethylidene-2-norbornene (ENB) [109]. They showed that, under the same conditions, the curing of ENB was much faster when compared to DCPD and a lower amount of Grubbs' catalyst was required. It is known that DCPD is capable of forming crosslinking structures while the ENB polymerizes faster in the presence of lower amounts of Grubbs' catalyst, but polymerizes in a linear chain structure so less rigidity of the healing networks is expected [110–112]. Hence, the study of Liu and coworkers was extended for the combination of DCPD and ENB with a Grubbs' catalyst [102]. Differential scanning calorimetry analysis (DSC) indicated that the DCPD has a melting temperature ($T_m = 15^\circ\text{C}$), while the blend mixture and ENB shows no T_m and consequently produces a resin with a higher glass transition temperature (T_g) [109]. Dynamic mechanical analysis (DMA) of various ratios of DCPD and ENB showed that the healing reaction becomes faster with increase in the ENB content. In addition, it was stated that the mixture of 1:3 DCPD/ENB had the highest rigidity after 120 min of curing time. Improvements in the healing efficiencies in automatic damage repairing applications were then expected by using this blend

mixture. However, the healing efficiency of the proposed system was not investigated by the authors.

The use of ENB-loaded microcapsules and Grubbs' catalyst was also investigated by other authors. Guadagno *et al.* showed that ENB can form a metathesis product at low temperatures in a damaged epoxy material region [113]. Sheng *et al.* synthesized a norbornene-based crosslinker to mix with two monomers: ENB and endo-DCPD [114]. The authors noted that the use of norbornene as a crosslinker increased the T_g and accelerated the network formation as evidenced by the shorter gelation times. Kessler and collaborators also investigated the ROMP of DCPD and ENB at different ratios in the presence of Grubbs' catalyst [115]. They confirmed that the ENB has a higher reactivity than DCPD, even at much lower catalyst quantities. It was also demonstrated that the maximum T_g of the fully cured samples was lower with ENB (120 °C) than with DCPD (160 °C), showing a linear decrease with increasing ENB content.

9.2.1.3 Siloxane-Based Healing System

Despite the improvements on the self-healing mechanism first proposed by White [1], the Grubbs' catalyst is always required, leading to problems with chemical efficiency due to side reactions between the catalyst and air, which limits the use of this approach for long-term applications. Various attempts have been made in order to find new, cost-effective self-healing chemical approaches. Cho *et al.* [28], proposed a new self-healing mechanism based on the polycondensation of hydroxy end-functionalized polydimethylsiloxane (HOPDMS) and polydiethoxysiloxane (PDES) in the presence of a tin catalyst (di-*n*-butyltindilaurate (DBTL)). In this system, HOPDMS and PDES are present as phase-separated droplets in a vinyl ester matrix, while the DBTL is encapsulated in PU microcapsules that are also embedded in the vinyl ester matrix. This direct blended mixture of the siloxane-based polymers in the matrix is possible because of its low solubility in the matrix. Upon damage, the DBTL-containing microcapsules break, initiating the polycondensation between the two siloxane-based polymers. This system allowed use of a simple blend mixture of the healing agent with the matrix, while the previous approaches always required the encapsulation of the monomeric healing agent. Besides this process simplification, the authors stated other advantages such as (i) a stable chemistry at high temperatures (>100 °C) enabling healing in thermoset systems, (ii) the stability of the healing chemistry in humid or wet environments, and (iii) a large accessibility of the siloxane-based polymers and tin catalyst that can make the system economically feasible. The concept was later extended to prevent corrosion in self-healing polymer coatings [29]. However, the direct contact of the siloxane-based healing agent with an epoxy-amine matrix also caused some matrix-initiated reactions. To overcome this issue, the authors encapsulated the PDMS healing agent and catalyst in PUF microcapsules, proposing a dual microcapsule system approach. The results demonstrated that the dual capsule PDMS healing system approach can provide healing and corrosion protection under ambient temperatures. Nevertheless, in both studies, lower healing efficiencies (ca. 24%) were obtained when compared to the DCPD and Grubbs' catalyst system.

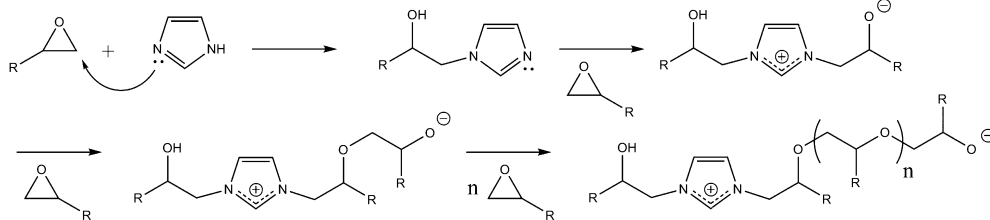
Recently, Mangun *et al.* reported the self-healing of an epoxy matrix at high temperatures (177 °C) using the same dual capsule PDMS healing system [27]. The healing efficiencies were low, ranging from 11 to 35%, and increasing with a higher PDMS resin molecular weight. To further improve the healing efficiency, two sets of silane-based adhesion promoters were used. The first, called “amino silane”, contained two primary amine groups to bond with the epoxy matrix and three methoxy groups on both sides with the ability to react with the silanol-terminated PDMS. The second was a mixture of two coupling agents (called “mixed silane”), one containing equal amounts of amine/methoxy groups and the other with no amine functional groups (only the three methoxy groups on each end). The use of both adhesion promoters had a positive impact on the healing efficiency that improved up to 45 and 52% for the “amino silane” and “mixed silane” promoters, respectively. Besides these improvements, the described work was stated to be the first presentation of a microcapsule-based healing system able to repair at such high cure temperature (177 °C).

Sottos and collaborators studied the self-healing behavior of a PDMS healing agent in an elastomeric PDMS matrix [30]. PUF microcapsules containing high molecular weight vinyl functionalized PDMS and the platinum catalyst on the one hand and PUF microcapsules with a PDMS copolymer that serves as a crosslinker to the functional PDMS on the other hand were used. The trigger for the healing reaction is analogous to the previous examples (rupture of the capsules), and healing efficiencies between 70 and 100% were obtained after recovery of the original tear strength, measured under quasi-static conditions. The healing performance was later tested under dynamic fatigue loading, also with substantial recovery effects [31]. This PDMS self-healing approach has the benefit of having the same polymeric nature in both the crack region and the host matrix.

Beiermann *et al.* reported a self-healing system capable of healing puncture damage based on tin-catalyzed PDMS chemistry [32]. A liquid silanol-terminated PDMS resin, 25% of PUF microcapsules containing silanol-terminated PDMS resin, a liquid poly(diethoxysilane) crosslinker and 0–6 wt% of tin catalyst containing microcapsules were sandwiched between two layers of polyurethane coated nylon. Samples were damaged using a hypodermic needle or a razor blade and the healing process was defined as the ability to reseal the damage. Recorded healing efficiencies were up to 100%, depending on the microcapsule size and puncture diameter.

9.2.1.4 Epoxy + Latent Hardener/Catalyst Healing System

The use of ring-opening polymerization of epoxide prepolymers with a latent catalyst for self-healing was introduced by Yin *et al.* in 2007 [33]. In this system, the epoxy resin was encapsulated in PUF microcapsules and the complex of CuBr_2 with four 2-methylimidazole units, serving as the latent hardener, was dispersed in an epoxy matrix. Upon fracture, the epoxy comes into contact with the hardener, but the curing reaction (Scheme 9.2) only takes place when the imidazole is released from the latent hardener complex by heating to 130–180 °C. Healing at 130 °C for 1 h was evaluated for both the epoxy thermoset matrix and its glass fabric



Scheme 9.2 Curing of epoxy with imidazole [33, 116].

composite counterpart, yielding a fracture toughness healing efficiency of 111 and 68% respectively.

Further work fully analyzed this system [34–36] and extended the mechanical characterization to impact damage [37]. When the durability of the self-healing laminates at room temperature was checked, a decrease in healing efficiency was noted at first, but then leveled out and remained the same for over two months [38].

Later, Xiao *et al.* devised a strategy using $\text{BF}_3 \cdot \text{OEt}_2$ as a strong Lewis-acid catalyst for cationic ring-opening polymerization of an epoxy monomer [39]. The epoxy healing agent in this concept is encapsulated using a new methodology with epoxy diacrylates and a polymerizable emulsifier as shell formers [117]. The latent $\text{BF}_3 \cdot \text{OEt}_2$ hardener on the other hand, would lose its activity when encapsulated in a conventional approach due to being highly hygroscopic. This resulted in the use of porous plant fibers to absorb the hardener, followed by coating the fibers with polystyrene to protect the content. When the fibers were inserted in the epoxy material, the hardener gradually spread out into the matrix, providing easy contact with the epoxy healing agent. Immediate mixing into the matrix resulted in processing issues due to fast curing of the epoxy material. In spite of the moisture sensitivity of the hardener, the activity is retained within the epoxy composite for at least 12 months. An additional advantage of this latent hardener system is that a stoichiometric epoxy/hardener ratio and even distribution of both compounds is not required, since cationic polymerization proceeds as long as contact with the latent hardener is maintained. The fast healing rate (76% impact strength recovery after 30 min at 20°C) is indicative of the high speed of the reaction. After 2 h at 20°C, a maximum healing efficiency of 85% is reached. Increasing the temperature slightly to 30°C further raised the efficiency to 89%. Meanwhile, hollow microcapsules infiltrated with $\text{BF}_3 \cdot \text{OEt}_2$ were synthesized to further improve the system [96].

Coope *et al.* published another system with $\text{Sc}(\text{OTf})_3$ as the Lewis-acid catalyst and epoxy co-encapsulated with ethyl phenylacetate in PUF microcapsules [40]. In this case, the catalyst particles were inserted in the epoxy matrix without problems of deactivation. With manual injection of the healing agent mixture, a healing efficiency of 78% could be obtained after healing at 45°C for 2 days. Using the same healing temperature and time with microcapsule-catalyst loaded epoxy samples rendered a decrease in fracture toughness recovery to 49%. When the temperature was elevated to 80°C, the efficiency improved again to 86%. Finally,

tests at ambient temperature were performed, but limited self-healing (recovery <20%) was observed due to the increased viscosity of the epoxy healing agent in comparison to the higher temperature range.

9.2.1.5 Thiol-Epoxy Healing System

A second possibility for the use of an epoxy healing agent is by combining it with a hardener. Both amines and thiols are an option since they can react with epoxides through addition polymerization. Because the amine hardeners do not require a catalyst, this chemistry is further discussed in Section 9.2.2. The thiols however, have to be deprotonated by a tertiary amine catalyst in order to increase their nucleophilicity. Therefore, Yuan *et al.* infiltrated a tetrafunctional thiol-containing PMF microcapsule with a tertiary amine [52–58, 94]. As a thiol pentaerythritol tetrakis(3-mercaptopropionate) (PMP) was used, while benzyl dimethylamine (BDMA) or 2,4,6-tris(dimethylaminomethyl)phenol (DMP-30) was chosen as an amine base. Triphenylphosphine (TPP) was also tested, but due to immiscibility with the PMP, infiltration into the capsule was not possible and the base had to be mixed straight into the epoxy matrix. Epoxy was encapsulated using the same procedure. Reaction rates appeared to be highest with the amine DMP-30 and lowest with the phosphine TPP, resulting in the highest and lowest healing efficiency, respectively. Typically, samples were healed for 1 day at room temperature, reaching up to 105% of fracture toughness recovery. Healing at lower (down to -10°C) and higher temperatures (up to 110°C) was also checked and followed over time. After 36 h, the lowest temperature still yields a recovery of 86–88%. The highest healing efficiency obtained with thermal healing was 171% at 55°C , which could be explained by the close proximity to the curing temperature of the thiol-epoxy system (57°C). Below 200°C , no loss of performance due to thermal degradation or leakage of the microcapsules is noticed. Research on impact [55] and fatigue damage [57] revealed that also in these situations, healing to the extent of full recovery can be achieved.

9.2.1.6 Thiol-Ene Healing System

Van den Dungen *et al.* turned to the use of thiol-ene chemistry in order to avoid the amine infiltration step of microcapsules [80, 81]. In this strategy, both a diacrylate (1,6-hexanediol diacrylate) and a dinorbornene reagent (1,6-hexanediol di(norborn-2-ene-5-carboxylate)) were combined with the tetrafunctional PMP mentioned above. Although this reaction does not require an activator or a catalyst, the network formation is accelerated by using UV irradiation for 1 h and 2,2-dimethoxy-2-phenylacetophenone (DMPA) as a radical photoinitiator. The diacrylate and PMP were incorporated in PUF micro- or nanocapsules, while the dinorbornene was encapsulated with a polystyrene shell for the use in poly(methyl acrylate), polystyrene-acrylate or pure acrylic coatings. DMPA is dispersed as such in the acrylate matrix. With scanning electron microscopy, only partial recovery of the cut in the coating is noted due to aggregation of the diacrylate capsules, thus leading to a lower healing efficiency. Incomplete healing is also registered with dinorbornene microcapsules. This observation is even more pronounced with nanocapsules, leading to the conclusion that the amount of healing agent delivered

to the rather large cut is not sufficient for full healing to occur. Unfortunately, no degree of healing efficiency has been mentioned in this study.

9.2.1.7 Thiol-Maleimide Healing System

The combination of thiols with maleimides for self-healing was recently introduced in our research group by Billiet *et al.*, though so far only manual injection has been used to heal epoxy materials [77]. In this concept, the tertiary amines present in the epoxy matrix are sufficient to catalyze the fast thiol-maleimide Michael addition, thus no additional tertiary amines had to be added to the reaction mixture. The maleimides also react with residual amines at the crack surface, thus covalently linking the healed network to the surrounding matrix. The reaction kinetics are shown to be faster than the amine-epoxy and amine-acrylate chemistry. For healing, PMP is utilized as a multifunctional thiol and combined with solid, aromatic bismaleimides dissolved in *m*-cresol. This solvent was chosen because of the lack of solubility of the bismaleimides in other media, and additionally prevented homopolymerization of the double bonds. Epoxy matrices with a stoichiometric ratio of epoxy resin and amine hardener were healed with different thiol-maleimide combinations. After 3 days of healing at room temperature, up to 92% recovery is obtained. If the healing time was increased, the healing efficiency went up to 121%. Amine-maleimide reactions with DETA were also investigated, but rendered lower efficiencies (up to 70%), even after 5 days.

9.2.1.8 Azide-Alkyne Healing System

The Cu(I)-catalyzed azide-alkyne cycloaddition reaction was applied by Gragert *et al.* in poly(isobutylene) matrices [82, 83]. Both a trivalent polymeric azide and alkyne were encapsulated in separate PUF microcapsules, due to immiscibility. The $\text{CuBr}(\text{PPh}_3)_3$ catalyst was dispersed as such in the polymer matrix. Healing was performed for 5 days at 25 or 60 °C, yielding a recovery of 91 and 107%, respectively. In a further investigation, both acrylate copolymers containing multiple alkyne functions and three-arm-star alkyne-telechelic poly(isobutylene)s have been reacted with three-arm-star azido-telechelic poly(isobutylene)s to form low- T_g networks suitable for self-healing. This system works at room temperature due to the autocatalytic effect of the 1,3-triazole rings on subsequent “click” reactions [118].

9.2.2

Non-Catalytic Systems

9.2.2.1 Amine-Epoxy Healing System

As stated before, epoxy-containing chemicals can be used as healing agents to form networks with themselves or with thiols. The very first attempts however, were made by Dry in 1996 using amines as hardeners for the epoxy resin [61]. Both reagents were delivered to the crack by hollow glass fibers embedded in an epoxy matrix material. Mixing of the compounds was assured by pairing the resin and hardener containing glass fibers together in the same fiber layer. After allowing time to heal (up to 8 months), broken composites containing these healing agents

had greater strength, and showed the ability to deflect the crack from the original crack path in contrast to the ones without added adhesives. Two patents were filed for this system [62, 63]. Bleay and coworkers studied the vacuum filling of smaller hollow glass fibers through capillary action in epoxy composites, which indicated that heating to 60 °C and a solvent (acetone) were needed to fill the tubes with the viscous epoxy resin [64]. This research mainly focused on lowering the hollow glass fiber dimensions to reinforcing fiber size. The hardener and accelerator also had to be diluted with acetone for successful filling of the secondary fibers. Both Dry and Bleay also used cyanoacrylates as healing agents, but this was not further elaborated due to issues with the glass tube filling. Pang *et al.* continued work on this system, adding a fluorescent dye to visualize the flow of healing agents in the epoxy sample [65, 66]. Four-point bend flexural testing followed by healing for 24 h at room temperature yielded a healing efficiency up to 97%, indicating that the amine-epoxy reaction proceeds rapidly and can fully restore the strength of the broken epoxy composite. The research was further extended by Trask [67, 68] and G. Williams [69, 70], making use of different epoxy resins, other mechanical analysis techniques, and additional carbon fiber reinforcement. Full recovery (100%) of the self-healing laminates was obtained after heating for 2 h at 100 °C, a temperature chosen to simulate the application's conditions.

In a next stage, the amine-epoxy chemistry was inserted into microvascular networks similar to the DCPD system. Toohey *et al.* could achieve over 60% healing efficiency for up to 16 healing cycles with this chemistry, where in each cycle the sample was healed for 2 days at 30 °C [71]. The temperature was slightly increased above room temperature to lower the time of healing between cycles. Further investigation increased the recovery up to almost 100% in some cycles, although single cycle healing did not exceed 86%, as indicated in Table 9.1 [72, 73]. Eventually, more than 50% healing efficiency could be retained over 30 cycles.

H. R. Williams *et al.* investigated the use of microvascular networks in sandwich panels, comprising a polymethacrylimide core with epoxy skin material [74, 75]. In the core material, horizontal PVC tubes and vertically drilled channels connected to these tubes were added to deliver the healing agents to any damage area. The tubing again was paired and contained the epoxy resin and the amine hardener separately. Impact damage and flexural testing revealed a healing efficiency of 82% after 2 days of healing at room temperature. If the sample tubing was pressurized, the recovery went up to 114% due to increased mixing of the healing agents and delivery to the crack.

Due to problems with the encapsulation of amine hardeners, the first microcapsule amine-epoxy system was not published until 2009, when Kirk *et al.* made nanoporous silica capsules infiltrated with both amines and epoxy [59]. Unfortunately, due to the low volume of healing agent delivered to the damage area, only partial self-healing was observed in most cases. Later, Jin *et al.* devised a method to encapsulate amine hardeners in PUF microcapsules using vacuum infiltration of a hollow polymeric capsule [60]. In this work, the healing efficiencies (77–91%) obtained for the first healing cycle were in the same range as those of the fibers and microvascular networks, when the sample was again allowed to heal for 2 days at ambient temperature.

Instead of incorporating additional amine hardeners in microcapsules, fibers or vascular networks, the residual unreacted amines present in the epoxy matrix can also be used for self-healing, as demonstrated by Caruso *et al.* [41]. By wetting the damage area with a whole range of solvents, molecular mobility in the crack is increased, promoting further curing of unreacted functionalities. Although nitrobenzene, NMP, DMA, DMF and DMSO gave the best results in manual healing of epoxy, chlorobenzene was the most suitable solvent for encapsulation, still rendering proper healing results. One day of room temperature healing yielded a fracture toughness recovery of 82%. In order to optimize this system, a mixture of chlorobenzene and additional epoxy resin was incorporated in the microcapsules [42, 91]. This epoxy resin allowed additional crosslinking with the residual amine functionalities and led to an increase up to 100% of fracture toughness healing. Evidence for the amine-epoxy reaction was given by changing the ratio of the amine hardener in the matrix, leading to increased covalent linking and thus healing efficiency. Phenyl- and ethyl phenylacetate were also successfully tested as solvents, being less toxic than chlorobenzene.

Meng *et al.* also made use of this residual amine concept in combination with glycidyl methacrylate (GMA), a monomer with an epoxide and an acrylate functional group susceptible to nucleophilic attack [76]. GMA was encapsulated in PMF microcapsules and inserted in the epoxy material. Since this monomer is miscible with epoxy, it is stated that a small solvent effect is present when released in the crack. However, the main part of healing is related to hydrogen bonding and covalent bonding with amines. This is again evidenced by adding an excess of amine hardener to the epoxy matrix, leading to increased healing efficiencies. Recovery up to 75% was obtained after 3 days at 25 °C with a stoichiometric matrix composition of 12:100 wt% DETA/epoxy, but over 90% healing was observed with 20:100 wt% DETA/epoxy. Healing at 160 °C, a temperature above the T_g of the matrix, was also tested with stoichiometric matrices and in this case the healing efficiency increased to 120% for manual injection and up to 90% for the microcapsule system, most likely due to further increased mobility and infiltration at the crack interface.

9.2.2.2 Epoxy-Based Healing System

In 1999, Zako and Takano published a healing concept based on the use of meltable epoxy resin particles [44], whereby a volume fraction of 40% in meltable epoxy resin was added to a cold-curing epoxy matrix. The epoxy material was mechanically tested for static fracturing and fatigue. Full recovery of the fracture toughness was obtained when the samples were heated to 100 °C for 10 min, allowing the epoxy additive to melt and react at the damage site. This concept was taken up by Zhang *et al.* and combined with resistive heating of multi-walled carbon nanotubes (MWCNT) [45]. At the interface, the melting temperature of the epoxy particles (150 °C) was reached within 15 s when a current was applied, due to local resistive heating. In this way, adding 25 wt% of the meltable, heat-curing resin yielded a healing efficiency of 55%, while with 30 wt% of epoxy particles a recovery of 70% was achieved.

In order to avoid heating the matrix, ultraviolet light (UV) has been explored by Carlson *et al.* to start the polymerization of a UV-curable epoxy reagent [43]. A

self-healing sensor skin was made with a solid epoxy core and a polyimide surface, encasing a liquid epoxy chamber network. When the surface is punctured, the liquid healing agent is exposed to sunlight and cured at the site of the damage. No healing efficiencies were mentioned in this study, but it is stated that successful healing is attained after 1 min.

9.2.2.3 Isocyanates-Based Healing System

Isocyanates are very reactive compounds that can react with water or simply with air moisture. Yang and Huang developed a catalyst-free self-healing system by preparing PU microcapsules containing hexamethylenediisocyanate (HDI) in the core, via an interfacial polymerization technique between methylene diphenyldiisocyanate (MDI) prepolymer and 1,4-butanediol in an oil-in-water emulsion [78]. The PU microcapsules with HDI in the core were mixed into an epoxy resin to create a self-healing coating on a steel panel surface. The surfaces were scratched, then the panels were immersed in a salt solution. After 48 h, the steel panel coated with self-healing epoxy was practically free of corrosion, while in the blank experiments corrosion was clearly visible.

Patrick *et al.* reported a catalyst-free self-healing chemistry to repair a rigid polyisocyanurate (PIR) foam [79]. A microvascular network was used to load the matrix with two commercially available PU foam formulations. Upon fracture, the vascular network released the polyurethane-based healing agents, creating a new foam in the cracked region. Due to the heat generation and the presence of the liquid blowing agents that start to evaporate, gas bubbles were formed, expanding the mixture towards foam production and subsequent healing of the PIR foam. This allowed self-repair of macro-scale damages.

9.2.2.4 Vinyl Ester Healing System

Motuku and coworkers showed that healing of epoxy or vinyl ester matrix materials with vinyl ester resins inserted in hollow glass fibers also has great potential [84]. Release of the healing agent in the damaged area was visualized and several determining factors, such as the spatial distribution of the fibers, were investigated. The system can heal impact damage to a certain extent, but neither healing conditions nor efficiencies are mentioned in this publication.

9.2.2.5 Molecular Interdiffusion

In this subsection, the main mechanism of healing is molecular interdiffusion of thermoplastics, which is also described in Section 9.3.1 under intrinsic self-healing materials. However, the systems mentioned below use additives to obtain self-healing, *de facto* generating an extrinsic self-healing material.

Meure and coworkers blended thermoplastic polyethylene-co-methacrylic acid (PEMAA) additives into an epoxy thermosetting material [85]. When damage has occurred, heating to 150 °C for 30 min was applied to liquefy the thermoplastic, allowing the PEMAA to fill the cracks via a pressure-driven delivery mechanism. This was explained by the expansion of bubbles in the PEMAA particles, most likely containing volatile products of reactions between the thermoplastic and the

surrounding epoxy [87, 119]. After cooling, over 100% recovery of the peak load was obtained, which was mainly attributed to hydrogen bonding between both polymer materials. Carbon fiber laminates could also be healed completely by inserting a PEMAA mesh into the material [86]. Additionally, this could be maintained over 10 damage-healing cycles.

Nji and coworkers combined melttable copolyester particles with a Veriflex polystyrene shape-memory polymer (SMP) matrix to provide a two-step self-healing mechanism [88]. When a fractured sample was gradually heated to 150°C, it first passed the T_g of the shape-memory matrix, thereby lowering the crack volume. At 114°C, the copolyester particles start to melt and fill the remaining crack, bonding both surfaces back together at temperatures higher than 125°C, due to diffusion of the copolyester into the surrounding network. When retested after being kept at 150°C for 20 min and subsequently allowed to set, the material revealed a healing efficiency of 65%.

Increasing the temperature above the T_g in thermoplastics, as further highlighted in Section 9.3.1, is sufficient to restore damage. For thermoset materials, this is of course not a straightforward approach, since the crosslinked nature of the material prevents healing when brought above the T_g . In 2007, the group of Hayes *et al.* came up with the idea to use the interesting capabilities of the thermoplastic materials in combination with an epoxy thermoset [49, 50]. A poly(bisphenol-A-co-epichlorohydrin) thermoplastic was dissolved into the thermosetting network. When brought above the T_g , the thermoplastic additive will provide the healing when damage occurs. Other groups improved the epoxy system to reach healing efficiencies up to 75% [46, 47, 51].

9.3

Intrinsic Self-Healing Materials

This section will focus on the chemistries that have been used in intrinsic self-healing materials. These materials contain chemical bonds that have the ability to re-form after having sustained damage. This re-formation can be triggered by an external stimulus, such as heat, light and oxygen. A division of these materials will be made based on the healing mechanism used. First the systems based on molecular diffusion will be addressed, followed by the largest group of materials, making use of reversible bonds in the crosslinking of the matrix. Finally, other systems that do not fit in the already mentioned categories will be discussed. An overview of all the discussed intrinsic self-healing materials can be found in Table 9.2.

9.3.1

Molecular Interdiffusion

The easiest polymers to heal are thermoplastic materials. Wool and McGarrel came up with a theory to describe healing at different stages [177]. In this case, bringing the polymer above its T_g will suffice to restore damage contracted during

Table 9.2 Intrinsic self-healing systems.

Method of healing	Material to be healed	Healing conditions	Healing eff. (%)	Ref.
<i>Molecular Interdiffusion</i>	PMMA	Above T_g	100	[120]
	PMMA	Solvent + 40–60 °C (1–10 min)	100	[121–125]
	PMMA – PS	125 °C (30 min)	100	[126]
<i>Diels–Alder/retro-Diels–Alder</i>	Polycarbonate	CCl ₄ + 40–60 °C (2 min)	50	[127]
	Polyurethane	RT, p' (10 min)	80	[128–130]
	–	100–150 °C (30 min–1 h)	50–100	[131–138]
	Epoxy	90–120 °C (1–3 d)	37–100	[139–144]
	Polyketone	120–150 °C (5 min–1 h)	100	[145, 146]
	Polystyrene	150 °C (2.5 min)	80	[147]
	Polyethylene	60 °C–140 °C (20 min–5 d)	100	[148–150]
	Polyamides	100–150 °C (10 min–2 h)	Not mentioned	[151, 152]
	PMMA	100–150 °C (4 h)	80–100	[153–155]
	–	100–200 °C (1–3 d)	50	[156, 157]
<i>Photochemical</i>	Anthracene-maleimide	120 °C (20 h)	63	[158, 159]
	DCPD	$h\nu$ (>250 nm) (90 min)	14–65	[160, 161]
	2+2	$h\nu$ (280–400 nm) (15–30 min)	100	[162, 163]
	4+4	$h\nu$ (>360 nm) (15 min)	NM	[164]
	Triithio-carbonate	$h\nu$ (330 nm) (4 h)	100	[165, 166]
	Radical formation	$h\nu$ (320–500 nm) (15 min)	Not mentioned	[167]
<i>Disulfides</i>	–	Reduction/oxidation(1–2 h)	90	[168–170]
	–	120 °C (2.5 h)	75	[171]
<i>Radical fission/recombination</i>	Diarylbenzo-furanone	DMF + RT (24 h)	98	[172]
	Polycarbonate	130 °C	98	[173]
<i>Anionic</i>	Siloxanes	90 °C (24 h)	100	[174]
	Acylhydrazone materials	Solvent + pH < 4 (7 h)	Not mentioned	[175]
<i>pH-responsive</i>	–	95% H ₂ O/30 °C (12 h)	100	[176]
<i>Water-based healing</i>	copolymer	–	–	–

the lifetime of the material. This was already recognized as early as 1981 by Williams *et al.* for the healing of polymethylmethacrylate (PMMA) [120]. This will of course consume a lot of energy in the case of high- T_g materials. For this reason, research was conducted to lower the effective T_g with the aid of solvents. Thanks to the plasticizing effect of methanol [121, 124, 125], ethanol [122] or a combination of both [123], the effective T_g of PMMA was lowered to a more easily accessible range (40–60°C). The same effect was reached for polycarbonate [127]. Here the effective T_g was lowered from 147°C to 40–60°C with the aid of CCl_4 . Sibener *et al.* synthesized a block copolymer of PMMA and polystyrene, which had the ability to heal itself when brought above the T_g of PMMA [126].

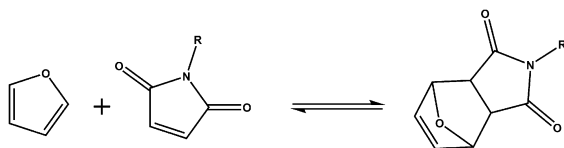
Yamaguchi *et al.* were able to incorporate a self-healing mechanism in a weak polyurethane gel with the aid of dangling chains [128–130]. The weak gel was obtained by eliminating the sol-fraction of the gel just beyond the sol–gel transition point. This gel reached healing efficiencies up to 80% within a significantly short time at room temperature, due to the strong topological interactions of the dangling chains.

9.3.2

Reversible Bond Formation

9.3.2.1 Diels–Alder/Retro-Diels–Alder

Probably the most well known chemical reaction used for intrinsic self-healing materials is the Diels–Alder (and retro-Diels–Alder) reaction [178]. The reaction allows control of bond formation and breaking by making use of temperature (see Scheme 9.3). The first study on thermally reversible polymeric networks containing Diels–Alder functionalities was reported by Craven in 1969 [179], but it took more than 30 years before Chen *et al.* reported the use of furan–maleimide systems as an efficient self-healing material [131, 132, 180]. The system was formed at 75°C (for 3 h) and, when cooled, had nice thermosetting properties. Damage that was inflicted to the material could be healed with a thermal treatment at 145°C for 25 min. Other groups have investigated and improved this same furan–maleimide chemistry [133–138].



Scheme 9.3 Diels–Alder reaction between a furan component and a maleimide component.

This concept was also used in more well-known thermoset materials such as epoxy [139–144, 181], polyketones [145, 146], polystyrene [147], polyethylene [148–150], polyamides [151, 152] and PMMA [153–155].

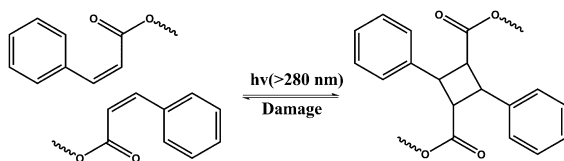
In an attempt to shift the healing temperature range of furan–maleimide (100–150°C), other chemistries were investigated. Already in 1999 Schiraldi *et al.* were

able to crosslink a polyethylene derivative containing anthracene moieties with bismaleimides at higher temperatures (125 °C) [182]. This knowledge was used by different groups to make a self-healing polymer based on anthracene-maleimide crosslinks [156, 157]. This chemistry made it possible to make thermoset materials at a higher temperature (>100 °C) and heal sustained damage at even higher temperature (>200 °C).

For self-healing purposes, mostly cyclic dienes are used because the diene is always locked in the desired *s-cis* conformation. Besides furan, there are a lot of different dienes that could be useful for this reaction [159]. For example, Murphy *et al.* described the self-healing behavior of dicyclopentadiene polymers [158]. Here, cyclic monomers containing two cyclopentadiene moieties were used. Upon heating (120 °C), the cycles opened and were able to react with a cyclopentadiene unit of another molecule to form a polymer. It was also found that dicyclopentadiene can undergo a second Diels–Alder reaction, leading to the formation of trimers and resulting in crosslinked networks. Upon damage the healing cycle could be repeated to re-form the original network.

9.3.2.2 Photochemical Trigger

In 2004, Chung *et al.* came up with a completely new idea for self-healing: light-induced crack healing [160]. Although photoreactions are generally fast, simple and environmentally friendly, this was never used before in self-healing. Chung *et al.* described the first polymeric sample that could be healed with the aid of a light source. For this, the photochemical [2+2] cycloaddition of cinnamoyl groups was chosen, because the photocycloaddition to form cyclobutane structures and the conversion of cyclobutane to C=C bonds readily occurs in the solid state (see Scheme 9.4). A crosslinker with three cinnamoyl groups was synthesized by reacting 1,1,1-tris(hydroxymethyl)ethane with cinnamoyl chloride. This crosslinker was then polymerized by irradiating with UV (>280 nm) for 120 s (99% conversion). The obtained film was hard, transparent, and insoluble in organic solvents such as chloroform. When damage was inflicted to this film, the weakest links (cyclobutane bonds) were broken, resulting in free cinnamoyl groups. Irradiation for 2 min with UV light (>280 nm) allowed recovery of the crosslinked network. Additional heating (100 °C) helped to obtain a higher healing efficiency.



Scheme 9.4 UV-based healing system based on [2+2] cycloaddition of cinnamoyl groups.

This pioneering work was quickly followed by the research of Bowman *et al.* in 2005 [167]. A rubbery network with a T_g of about -25 °C was formed from a stoichiometric mixture of pentaerythritol tetrakis(3-mercaptopropionate) and triethyl-ene glycol divinylether. This thiol-ene crosslinking resulted in a residual amount

of photoinitiator being present, which played an important role in the healing process. During irradiation (15 min at 320 to 500 nm, 30 mW cm^{-2}), homolytic photolysis of the photoinitiator produced radicals in the specimens. Diffusion of these radicals occurred via addition–fragmentation chain transfer through the allyl sulfide functionalities. As a result, the polymer backbone was repeatedly cleaved, stress was alleviated, and the backbone was re-formed in a less stressed conformation. In 2009, Ghosh and Urban reported the development of a polyurethane network that exhibited self-repairing characteristics upon exposure to UV light [162]. The network consisted of an oxetane-substituted chitosan precursor incorporated into a two-component polyurethane. Upon mechanical damage of the network, the four-member oxetane rings opened to create two reactive ends. When exposed to ultraviolet light (120 W fluorescent UV lamp at 302 nm), chitosan chain scission occurred, forming crosslinks with the reactive oxetane ends and thus repairing the network. These materials were capable of repairing themselves in less than 1 h. Further investigation was conducted on the precise role of every component, temperature and pH [163].

Matyjaszewski *et al.* reported in 2010 the self-healing reactions of polymer gels based on reshuffling reactions of trithiocarbonate (TTC) units through chemical stimulation procedures [165]. The TTC units have the potential to undergo photo-stimulated reshuffling reactions because they can act as photoinitiators in RAFT polymerizations. It was shown that the covalently crosslinked gels could achieve repeatable self-healing and macroscopic fusion of separate pieces simultaneously [166]. A polymer crosslinked with TTC units was synthesized by a RAFT copolymerization of *n*-butyl acrylate (BA) and a TTC crosslinker. Poly(*n*-butyl acrylate) (PBA), a polymer with a low T_g value (-50°C), was selected as the matrix polymer because of its high chain mobility at room temperature. This sample was first healed with the aid of acetonitrile as a solvent, because it does not absorb UV light and it does not excessively swell the crosslinked polymers. After cutting into pieces and irradiating with UV for 4 h, the network was fused into a single sample again. The experiment was repeated for reaction in the bulk state. Considering the lower chain mobility in the bulk state than that in solution, or solvent swollen state, the reaction was performed for 48 h, and under pressure of a 10 g weight. Again the macroscopic crack almost completely disappeared after UV irradiation.

Froimowicz *et al.* reported the first use of a dendritic polymer as a scaffold for reversible photo-dimerizable chromophores toward the generation of building blocks and its application in self-healing materials [164]. Building blocks were designed from hyperbranched polyglycerols with incorporated anthracenes. Anthracene has the ability for a reversible dimerization, where an irradiation with 366 nm light induces a forward [4 + 4] dimerization (or crosslinking in the case of anthracene-containing polymers), while an irradiation with 254 nm light produces the backward decomposition of the dimer (or de-crosslinking). The self-healing ability of the system was tested by introducing an artificial scratch in a previously crosslinked film of anthracene containing polyglycerol. This film was then irradiated for 15 min with 254 nm light to regenerate the building block. Afterwards, the sample was kept overnight in the darkness and at room temperature. The low T_g value (-46°C) allowed the material to reorganize itself covering the entire area.

Finally, the bulk film was irradiated with 366 nm light in order to restore the crosslinked film.

In 2012, Ling *et al.* [161] described a self-mending polyurethane network based on isophoronediiisocyanate, polyethyleneglycol and the photo-reversible moiety 5,7-bis(2-hydroxyethoxy)-4-methylcoumarin. By taking advantage of the reversible photodimerization and photocleavage property of coumarin, the polyurethane can be repeatedly crosslinked and de-crosslinked under successive UV irradiations at 350 and 254 nm. More importantly, damage in a crosslinked version of the polyurethane can be partially re-bonded (65%) through chain reconnection on the fracture surfaces, resulting from the photochemical reactions.

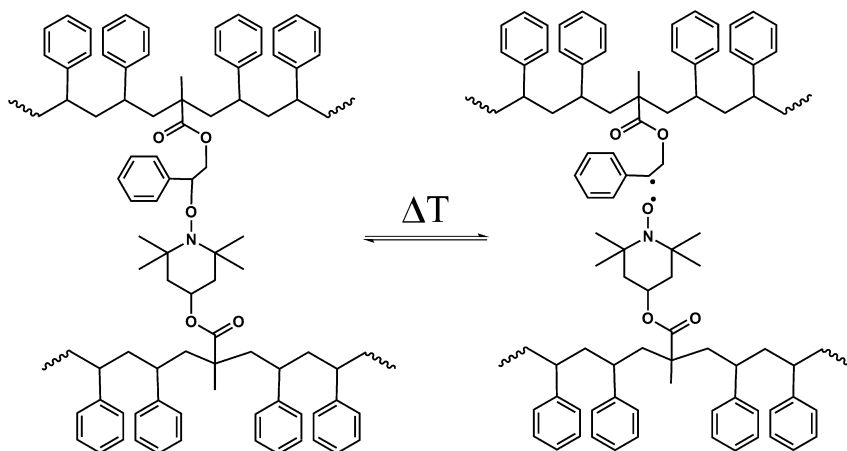
9.3.2.3 Disulfide Bridges

Klumperman *et al.* came up with a new self-healing concept that is based on the use of disulfide links incorporated in a rubber network, which is able to fully restore its mechanical properties at moderate temperatures [168]. The exchange reaction of disulfide groups at moderate temperatures can lead to a renewal of crosslinks across damaged surfaces. An epoxy resin containing disulfide groups in its structure was crosslinked with a tetrafunctional thiol. When a sample of this network was damaged and the fracture surfaces were immediately put into close contact and heated at 60 °C, the mechanical properties were fully restored in just 1 h. As expected, longer healing times led to better healing, but even when the contact time between the two broken parts was as short as 15 min, healing was observed. The results indicated that the healed samples had elastic properties similar to the original material, even after multiple healing cycles.

Around the same period, Matyjaszewski *et al.* reported a self-healing star-shaped polymer containing disulfide connections [169]. Again, a redox reaction is the basis of the healing strategy. While it can be accelerated by the presence of catalysts, it can, in principle, also proceed under ambient conditions without the need for any external triggers. Since bond formation/re-formation essentially needs intimate contact of materials, the flow properties of materials should be seriously considered, so that the surfaces of the damaged materials can easily approach each other for bond re-formation. Because of that, polymers with a branched architecture that are characterized by a low intrinsic viscosity, were selected in this study, eventually resulting in the development of a self-healing polyurethane system based on the reshuffling of thiuram disulfide groups in visible light and without solvent [170]. Both a radical transfer reaction in which the generated radical reacts with a thiuram disulfide group and a simple radical crossover reaction can lead to reshuffling. To heal this material, the broken surfaces were firmly held together for 1 min and then kept under visible light for 12 h. After this treatment, the material regained its original properties.

9.3.2.4 Radical Fission/Recombination

In 2006, Takahara *et al.* reported the use of alkoxyamines as a reversible crosslinker for poly(methacrylic esters) [183]. This led Yuan *et al.* to develop a crosslinked polystyrene with alkoxyamines as crosslinker (see Scheme 9.5) [171]. Upon heating



Scheme 9.5 Representation of the alkoxyamine system of Yuan *et al.* [171].

(120–200 °C), covalent bond fission and radical recombination synchronously occurred among the alkoxyamine moieties. The radical concentration can be increased by working at higher temperature but this is not unlimited due to thermal degradation of the polymer itself. Healing efficiencies up to 75% could be reached with these materials. In 2012, Otsuka *et al.* made an improvement to this system by developing a dynamic material that had the ability to autonomously self-heal under mild conditions, such as under air at room temperature, using a novel dynamic covalent bond unit, diarylbibenzofuranone, which is a dimer of arylbenzofuranone, a known antioxidant [170]. The nice feature of this dynamic bond is the fact that it reaches an equilibrium without special stimuli and the formed radicals can tolerate the presence of oxygen. For healing, the fresh surfaces were first wetted with a small amount of DMF (to ensure close contact between the surfaces) and were then immediately placed together without applying any excessive pressure. The samples were kept at room temperature under air. After 24 h, self-healing of the contacted samples could be observed and the scars had almost disappeared (healing efficiency up to 98%).

9.3.2.5 Anionic Reactions

In 2004, Zhang *et al.* came up with the development of a self-healing polycarbonate [173]. This polymer obtained its self-healing properties with the addition of Na_2CO_3 . Polycarbonate can be hydrolyzed when heated (130 °C). This resulted in polymer chains with phenyl and phenolic ends with the release of CO_2 . The phenolic end, generated by the hydrolysis, reacted with a phenyl end with the aid of a sodium carbonate group. Sodium phenoxide is probably eliminated from the chain because the observation of a slight smell of phenol. The hydrolysis was simultaneously accelerated with sodium carbonate. Due to these reactions polycarbonate can heal and restore its original properties up to 98%. In 2012, McCarthy *et al.* also used

anionic species to heal their system [174]. The work presented the re-discovery of the anionic equilibration of crosslinked poly(dimethylsiloxane), which had already been known for more than 60 years. Tetramethylammonium silanolate-initiated ring-opening copolymerization of octamethylcyclotetrasiloxane and bis(heptamethylcyclotetrasiloxanyl)ethane resulted in a cross-linked network that contains ethylene bridges and active silanolate end groups. These living reactive anionic species are stable to water, oxygen, CO₂ and promote thermally activated equilibration among different network isomers and cyclic oligomers. When a sample of this material is damaged, it can be healed by wrapping it in tape (to keep the surfaces together) and putting in an oven at 90 °C for 24 h. The obtained properties of the material were exactly the same as the original.

9.3.2.6 pH-Responsive Systems

Deng *et al.* constructed a novel reversible polymer gel based on dynamic covalent chemistry [175]. By condensation of acylhydrazines at the two ends of a poly(ethylene oxide) chain with aldehyde groups in tris[(4-ormylphenoxy)methyl]ethane, a network with acylhydrazone bonds as cross-links is generated. Acylhydrazone bonds are covalent in nature and, therefore, the polymer network should be stable under normal conditions. But more importantly, acylhydrazone formation displays reversibility under mild conditions with acid catalysis, breaking down the network and regenerating the starting reagents. By adjusting the acidity of the system, this chemical gel revealed reversible sol–gel phase transitions. Moreover, the chemical gel possessed a self-healing property based on the reversible breaking and regenerating of acylhydrazone bonds. For this, the gel had to be put in a solvent containing an acidic catalyst. When the gel was broken into two pieces, it could be healed again by simply putting them together and keeping them in contact for 7 h without any external intervention.

9.3.3

Other Systems

Guo *et al.* [176]. developed a homogeneous self-repairing copolymer system that exhibited self-healing characteristics upon exposure to a moisture holding environment. The copolymer consisted of two components: a monomer containing isocyanate groups (the repairing component) and a fluorinated monomer, 2,2,3,4,4,4-hexafluorobutyl methacrylate (the protective component). In this system, the fluorine-containing segments are prone to gather on the solid/air interface, to form a good water barrier during the coating preparation and application process while the isocyanate-containing segments, due to their strong polarity, are prone to settle on the solid substrate interface, forming a repairable layer. Upon mechanical damage of the copolymer, the isocyanate groups will resurface to generate reactive ends (that can react with environmental water), thus forming new (urea) crosslinks and repairing the material. For this healing to take place, an ideal environment is required (65% water humidity and a temperature of 30 °C).

9.4

Concluding Remarks and Future Outlook

Polymeric materials are susceptible to mechanical damage, such as degradation or crack damage, resulting in loss of functionality and reduction of mechanical properties. To overcome these limitations, a new class of materials has emerged, with the ability to (autonomously) repair themselves. These materials are classified as extrinsic or intrinsic self-healing materials, whether or not an additional healing agent is added.

This chapter aimed to give an overview of the cross-linking chemistries used in both approaches. Most work has been done for the extrinsic materials, more specifically for the microencapsulation approach. This approach, pioneered by White *et al.* [1], demonstrated that epoxy materials can be repaired via the ring-opening metathesis polymerization (ROMP) of dicyclopentadiene (DCPD) in the presence of Grubbs' catalyst. The system was then optimized toward a higher healing efficiency. However, problems with the Grubbs' catalyst stability and reactivity, and the autopolymerization of the DCPD monomer has driven researchers towards alternative cross-linking chemistries for the microencapsulation approach, such as poly(dimethylsiloxane) (PDMS), epoxy, thiol-ene or azide-alkyne-based healing systems. Lately, a new type of extrinsic self-healing system, where the use of a catalyst is not required, has attracted attention. In these types of systems, unreacted monomers, air humidity or meltable particles are the healing precursors.

The search for intrinsic self-healing materials is an increasing area of research, where the presence of a catalyst is not a requisite and the healing is a result of molecular interactions after exposure to an external stimulus. The most well-known intrinsic self-healing system is the one based on the Diels–Alder (and retro-Diels–Alder) reaction. The reaction allows control of bond formation and breaking by making use of temperature. Chen *et al.* [131, 132, 180] demonstrated this by making use of the furan-maleimide reaction as an efficient self-healing approach. The material is formed at 75 °C and, when cooled, has nice thermosetting properties. Other intrinsic self-healing approaches have been reported, such as UV-based healing systems, disulfide bridge formation healing systems, radical fission/recombination healing systems or anionic reactions.

Nevertheless, despite the fast and encouraging improvements, there are still unsolved technical issues for an accelerated industrial breakthrough, such as repair of macro-scratches, healing by sunlight or contact with air, healing at low temperatures, and the use of cost effective chemistries. Many of these require multidisciplinary studies, covering the molecular level up to the final material characterization. This is of course challenging as it requires numerous refined preparative and analytical methods. This multifaceted approach is expected to result in a rapidly expanding class of new materials that have the ability to repair more than one functionality and even better mimic biologic systems. This will eventually lead to the tailor-made development of self-healing polymeric systems that can be used for a wide range of applications, including in fields such as (bio) medical materials and electronics.

References

- 1 White, S.R., Sottos, N.R., Geubelle, P.H., Moore, J.S., Kessler, M.R., Sriram, S.R., Brown, E.N., and Viswanathan, S. (2001) Autonomic healing of polymer composites. *Nature*, **409** (6822), 794.
- 2 Brown, E.N., Sottos, N.R., and White, S.R. (2002) Fracture testing of a self-healing polymer composite. *Exp. Mech.*, **42** (4), 372.
- 3 Brown, E.N., Sottos, N.R., and White, S.R. (2004) Microcapsule induced toughening in a self-healing polymer composite. *J. Mater. Sci.*, **39** (5), 1703.
- 4 Brown, E.N., Sottos, N.R., and White, S.R. (2005) Retardation and repair of fatigue cracks in a microcapsule toughened epoxy composite – part I: manual infiltration. *Compos. Sci. Technol.*, **65** (15–16), 2466.
- 5 Brown, E.N., Sottos, N.R., and White, S.R. (2005) Retardation and repair of fatigue cracks in a microcapsule toughened epoxy composite – part II: in situ self-healing. *Compos. Sci. Technol.*, **65** (15–16), 2474.
- 6 Rule, J.D., Sottos, N.R., and White, S.R. (2007) Effect of microcapsule size on the performance of self-healing polymers. *Polymer*, **48** (12), 3520.
- 7 Jones, A.S., Rule, J.D., Moore, J.S., Sottos, N.R., and White, S.R. (2007) Life extension of self-healing polymers with rapidly growing fatigue cracks. *J. R. Soc. Interface*, **4** (13), 395.
- 8 Mauldin, T.C., Rule, J.D., Sottos, N.R., White, S.R., and Moore, J.S. (2007) Self-healing kinetics and the stereoisomers of dicyclopentadiene. *J. R. Soc. Interface*, **4** (13), 389.
- 9 White, S.R., Sottos, N.R., Geubelle, P.H., Moore, J.S., Sriram, S.R., Kessler, M.R., and Brown, E.N. (2003) Multifunctional autonomically healing composite material, WO2003060569.
- 10 Skipor, A., Scheifer, S., and Olson, B. (2004) Self-healing polymer compositions, WO2004007608.
- 11 Kessler, M.R., and White, S.R. (2001) Self-activated healing of delamination damage in woven composites. *Compos. Part A-Appl. Sci. Manuf.*, **32** (5), 683.
- 12 Kessler, M.R., Sottos, N.R., and White, S.R. (2003) Self-healing structural composite materials. *Compos. Part A-Appl. Sci. Manuf.*, **34** (8), 743.
- 13 Patel, A.J., Sottos, N.R., Wetzel, E.D., and White, S.R. (2010) Autonomic healing of low-velocity impact damage in fiber-reinforced composites. *Compos. Part A-Appl. Sci. Manuf.*, **41** (3), 360.
- 14 Rule, J.D., Brown, E.N., Sottos, N.R., White, S.R., and Moore, J.S. (2005) Wax-protected catalyst microspheres for efficient self-healing materials. *Adv. Mater.*, **17** (2), 205.
- 15 Jones, A.S., Rule, J.D., Moore, J.S., White, S.R., and Sottos, N.R. (2006) Catalyst morphology and dissolution kinetics of self-healing polymers. *Chem. Mater.*, **18** (5), 1312.
- 16 Wilson, G.O., Caruso, M.M., Reimer, N.T., White, S.R., Sottos, N.R., and Moore, J.S. (2008) Evaluation of ruthenium catalysts for ring-opening metathesis polymerization-based self-healing applications. *Chem. Mater.*, **20** (10), 3288.
- 17 Kamphaus, J.M., Rule, J.D., Moore, J.S., Sottos, N.R., and White, S.R. (2008) A new self-healing epoxy with tungsten (VI) chloride catalyst. *J. R. Soc. Interface*, **5** (18), 95.
- 18 Kirkby, E.L., Rule, J.D., Michaud, V.L., Sottos, N.R., White, S.R., and Manson, J.A.E. (2008) Embedded shape-memory alloy wires for improved performance of self-healing polymers. *Adv. Funct. Mater.*, **18** (15), 2253.
- 19 Kirkby, E.L., Michaud, V.J., Manson, J.A.E., Sottos, N.R., and White, S.R. (2009) Performance of self-healing epoxy with microencapsulated healing agent and shape memory alloy wires. *Polymer*, **50** (23), 5533.
- 20 Wilson, G.O., Moore, J.S., White, S.R., Sottos, N.R., and Andersson, H.M. (2008) Autonomic healing of epoxy vinyl esters via ring opening metathesis polymerization. *Adv. Funct. Mater.*, **18** (1), 44.
- 21 Biggs, P., Jones, I.L., and Lewis, G. (2009) An autonomically-healed PMMA

- bone cement: influence of the crystal size of Grubbs' catalyst on fracture toughness and polymerisation rate. *Int. J. Nano Biomater.*, **2** (6), 494.
- 22 Biggs, P., Jones, I.L., and Lewis, G. (2007) Incorporation of microencapsulated dicyclopentadiene into an acrylic bone cement matrix. PMSE Division, 233rd ACS National Meeting, ACS Polymeric Materials: Science and Engineering, **96**, 498
 - 23 Lewis, G., Wellborn, B., Jones, L., and Biggs, P. (2009) *J. Appl. Biomater. Biomech.*, **7** (2), 90.
 - 24 Chipara, M.D., Chipara, M., Shansky, E., and Zaleski, J.M. (2009) Self-healing of high elasticity block copolymers. *Polym. Adv. Technol.*, **20** (4), 427.
 - 25 Toohey, K.S., Sottos, N.R., Lewis, J.A., Moore, J.S., and White, S.R. (2007) Self-healing materials with microvascular networks. *Nat. Mater.*, **6** (8), 581.
 - 26 Toohey, K.S., Sottos, N.R., and White, S.R. (2009) Characterization of microvascular-based self-healing coatings. *Exp. Mech.*, **49** (5), 707.
 - 27 Mangun, C.L., Mader, A.C., Sottos, N.R., and White, S.R. (2010) Self-healing of a high temperature cured epoxy using poly(dimethylsiloxane) chemistry. *Polymer*, **51** (18), 4063.
 - 28 Cho, S.H., Andersson, H.M., White, S.R., Sottos, N.R., and Braun, P.V. (2006) Polydimethylsiloxane-based self-healing materials. *Adv. Mater.*, **18** (8), 997.
 - 29 Cho, S.H., White, S.R., and Braun, P.V. (2009) Self-healing polymer coatings. *Adv. Mater.*, **21** (6), 645.
 - 30 Keller, M.W., White, S.R., and Sottos, N.R. (2007) A self-healing poly(dimethyl siloxane) elastomer. *Adv. Funct. Mater.*, **17** (14), 2399.
 - 31 Keller, M.W., White, S.R., and Sottos, N.R. (2008) Torsion fatigue response of self-healing poly(dimethylsiloxane) elastomers. *Polymer*, **49** (13–14), 3136.
 - 32 Beiermann, B.A., Keller, M.W., and Sottos, N.R. (2009) Self-healing flexible laminates for resealing of puncture damage. *Smart Mater. Struct.*, **18** (8), 085001.
 - 33 Yin, T., Rong, M.Z., Zhang, M.Q., and Yang, G.C. (2007) Self-healing epoxy composites – preparation and effect of the healant consisting of microencapsulated epoxy and latent curing agent. *Compos. Sci. Technol.*, **67** (2), 201.
 - 34 Rong, M.Z., Zhang, M.Q., and Zhang, W. (2007) A novel self-healing epoxy system with microencapsulated epoxy and imidazole curing agent. *Adv. Compos. Lett.*, **16** (5), 167.
 - 35 Yin, T., Zhou, L., Rong, M.Z., and Zhang, M.Q. (2008) Self-healing woven glass fabric/epoxy composites with the healant consisting of micro-encapsulated epoxy and latent curing agent. *Smart Mater. Struct.*, **17** (1), 015019.
 - 36 Yin, T., Rong, M.Z., and Zhang, M.Q. (2008) Self-healing of cracks in epoxy composites, in *Multi-Functional Materials and Structures, Pts 1 and 2* (eds A.K.T. Lau, *et al.*), Trans Tech Publications Ltd, Stafa-Zurich, p. 282.
 - 37 Yin, T., Rong, M.Z., Wu, J.S., Chen, H.B., and Zhang, M.Q. (2008) Healing of impact damage in woven glass fabric reinforced epoxy composites. *Compos. Part A-Appl. Sci. Manuf.*, **39** (9), 1479.
 - 38 Yin, T., Rong, M.Z., Zhang, M.Q., and Zhao, J.Q. (2009) Durability of self-healing woven glass fabric/epoxy composites. *Smart Mater. Struct.*, **18** (7), 074001.
 - 39 Yin, T., Rong, M.Z., Zhang, M.Q., and Zhao, J.Q. (2009) A facile strategy for preparing self-healing polymer composites by incorporation of cationic catalyst-loaded vegetable fibers. *Adv. Funct. Mater.*, **19** (14), 2289.
 - 40 Coope, T.S., Mayer, U.F.J., Wass, D.F., Trask, R.S., and Bond, I.P. (2011) Self-healing of an epoxy resin using scandium(III) triflate as a catalytic curing agent. *Adv. Funct. Mater.*, **21** (24), 4624.
 - 41 Caruso, M.M., Delafuente, D.A., Ho, V., Sottos, N.R., Moore, J.S., and White, S.R. (2007) Solvent-promoted self-healing epoxy materials. *Macromolecules*, **40** (25), 8830.
 - 42 Caruso, M.M., Blaiszik, B.J., White, S.R., Sottos, N.R., and Moore, J.S. (2008) Full recovery of fracture toughness using a nontoxic solvent-based self-healing system. *Adv. Funct. Mater.*, **18** (13), 1898.

- 43 Carlson, J.A., English, J.M., and Coe, D.J. (2006) A flexible, self-healing sensor skin. *Smart Mater. Struct.*, **15** (5), 129.
- 44 Zako, M., and Takano, N. (1999) Intelligent material systems using epoxy particles to repair microcracks and delamination damage in GFRP. *J. Intell. Mater. Syst. Struct.*, **10** (10), 836.
- 45 Zhang, W., Sakalkar, V., and Koratkar, N. (2007) In situ health monitoring and repair in composites using carbon nanotube additives. *Appl. Phys. Lett.*, **91** (13), 1.
- 46 Rahmathullah, M.A.M., and Palmese, G.R. (2009) Crack-healing behavior of epoxy-amine thermosets. *J. Appl. Polym. Sci.*, **113** (4), 2191.
- 47 Peterson, A.M., Kotthapalli, H., Rahmathullah, M.A.M., and Palmese, G.R. (2012) Investigation of interpenetrating polymer networks for self-healing applications. *Compos. Sci. Technol.*, **72** (2), 330.
- 48 Outwater, J.O., and Gerry, D.J. (1969) On the fracture energy, rehealing velocity and refracture energy of cast epoxy resin. *J. Adhes.*, **1** (4), 290.
- 49 Hayes, S.A., Jones, F.R., Marshiya, K., and Zhang, W. (2007) A self-healing thermosetting composite material. *Compos. Part A: Appl. Sci. Manuf.*, **38** (4), 1116.
- 50 Hayes, S.A., Zhang, W., Branthwaite, M., and Jones, F.R. (2007) Self-healing of damage in fibre-reinforced polymer-matrix composites. *J. R. Soc. Interface*, **4** (13), 381.
- 51 Luo, X., Ou, R., Eberly, D.E., Singhal, A., Viratyaporn, W., and Mather, P.T. (2009) A thermoplastic/thermoset blend exhibiting thermal mending and reversible adhesion. *ACS Appl. Mater. Interfaces*, **1** (3), 612.
- 52 Yuan, Y.C., Rong, M.Z., Zhang, M.Q., Chen, J., Yang, G.C., and Li, X.M. (2008) Self-healing polymeric materials using epoxy/mercaptan as the healant. *Macromolecules*, **41** (14), 5197.
- 53 Coope, T.S., Mayer, U.F.J., Wass, D.F., Trask, R.S., and Bond, I.P. (2009) Study of factors related to performance improvement of self-healing epoxy based on dual encapsulated healant. *Polymer*, **50** (24), 5771.
- 54 Yuan, Y.C., Rong, M.Z., Zhang, M.Q., Yang, G.C., and Zhao, J.Q. (2010) Healing of fatigue crack in epoxy materials with epoxy/mercaptan system via manual infiltration. *Express Polym. Lett.*, **4** (10), 644.
- 55 Yuan, Y.C., Ye, Y.P., Rong, M.Z., Chen, H.B., Wu, J.S., Zhang, M.Q., Qin, S.X., and Yang, G.C. (2011) Self-healing of low-velocity impact damage in glass fabric/epoxy composites using an epoxy-mercaptan healing agent. *Smart Mater. Struct.*, **20** (1), 015024.
- 56 Yuan, Y.C., Ye, X.J., Rong, M.Z., Zhang, M.Q., Yang, G.C., and Zhao, J.Q. (2011) Self-healing epoxy composite with heat-resistant healant. *ACS Appl. Mater. Interfaces*, **3** (11), 4487.
- 57 Yuan, Y.C., Rong, M.Z., Zhang, M.Q., Yang, G.C., and Zhao, J.Q. (2011) Self-healing of fatigue crack in epoxy materials with epoxy/mercaptan system. *Express Polym. Lett.*, **5** (1), 47.
- 58 Lee, J., Bhattacharyya, D., Zhang, M.Q., and Yuan, Y.C. (2011) Fracture behaviour of a self-healing microcapsule-loaded epoxy system. *Express Polym. Lett.*, **5** (3), 246.
- 59 Kirk, J.G., Naik, S., Moosbrugger, J.C., Morrison, D.J., Volkov, D., and Sokolov, I. (2009) Self-healing epoxy composites based on the use of nanoporous silica capsules. *Int. J. Fracture*, **159** (1), 101.
- 60 Jin, H.H., Mangun, C.L., Stradley, D.S., Moore, J.S., Sottos, N.R., and White, S.R. (2012) Self-healing thermoset using encapsulated epoxy-amine healing chemistry. *Polymer*, **53** (2), 581.
- 61 Dry, C. (1996) Procedures developed for self-repair of polymer matrix composite materials. *Compos. Struct.*, **35** (3), 263.
- 62 Dry, C. (2006) Self-repairing, reinforced matrix materials, US7022179.
- 63 Dry, C. (2007) Multiple function, self-repairing composites with special adhesives, US2012009391.
- 64 Bleay, S.M., Loader, C.B., Hawyes, V.J., Humberstone, L., and Curtis, P.T. (2001) A smart repair system for polymer matrix composites. *Compos. Part A-Appl. Sci. Manuf.*, **32** (12), 1767.
- 65 Pang, J.W.C., and Bond, I.P. (2005) A hollow fibre reinforced polymer composite encompassing self-healing

- and enhanced damage visibility. *Compos. Sci. Technol.*, **65** (11–12), 1791.
- 66 Pang, J.W.C., and Bond, I.P. (2005) “Bleeding composites” – damage detection and self-repair using a biomimetic approach. *Compos. Part A-Appl. Sci. Manuf.*, **36** (2), 183.
- 67 Trask, R.S., and Bond, I.P. (2006) Biomimetic self-healing of advanced composite structures using hollow glass fibres. *Smart Mater. Struct.*, **15** (3), 704.
- 68 Trask, R.S., Williams, G.J., and Bond, I.P. (2007) Bioinspired self-healing of advanced composite structures using hollow glass fibres. *J. R. Soc. Interface*, **4** (13), 363.
- 69 Williams, G., Trask, R., and Bond, I. (2007) A self-healing carbon fibre reinforced polymer for aerospace applications. *Compos. Part A-Appl. Sci. Manuf.*, **38** (6), 1525.
- 70 Williams, G.J., Bond, I.P., and Trask, R.S. (2009) Compression after impact assessment of self-healing CFRP. *Compos. Part A-Appl. Sci. Manuf.*, **40** (9), 1399.
- 71 Toohey, K.S., Hansen, C.J., Lewis, J.A., White, S.R., and Sottos, N.R. (2009) Delivery of two-part self-healing chemistry via microvascular networks. *Adv. Funct. Mater.*, **19** (9), 1399.
- 72 Hansen, C.J., Wu, W., Toohey, K.S., Sottos, N.R., White, S.R., and Lewis, J.A. (2009) Self-healing materials with interpenetrating microvascular networks. *Adv. Mater.*, **21** (41), 4143.
- 73 Hamilton, A.R., Sottos, N.R., and White, S.R. (2010) Self-healing of internal damage in synthetic vascular materials. *Adv. Mater.*, **22** (45), 5159.
- 74 Williams, H.R., Trask, R.S., and Bond, I.P. (2007) Self-healing composite sandwich structures. *Smart Mater. Struct.*, **16** (4), 1198.
- 75 Williams, H.R., Trask, R.S., and Bond, I.P. (2008) Self-healing sandwich panels: restoration of compressive strength after impact. *Compos. Sci. Technol.*, **68** (15–16), 3171.
- 76 Meng, L.M., Yuan, Y.C., Rong, M.Z., and Zhang, M.Q. (2010) A dual mechanism single-component self-healing strategy for polymers. *J. Mater. Chem.*, **20** (29), 6030.
- 77 Billiet, S., Van Camp, W., Hillewaere, X.K.D., Rahier, H., and Du Prez, F.E. (2012) Development of optimized autonomous self-healing systems for epoxy materials based on maleimide chemistry. *Polymer*, **53** (12), 2320.
- 78 Huang, M., and Yang, J. (2011) Facile microencapsulation of HDI for self-healing anticorrosion coatings. *J. Mater. Chem.*, **21** (30), 11123.
- 79 Patrick, J.F., Sottos, N.R., and White, S.R. (2012) Microvascular based Self-healing polymeric foam. *Polymer*, **53** (19), 4231.
- 80 van den Dungen, E.T. (2009) A Self-healing coatings based on thiol-ene chemistry, PhD thesis (Department of Chemistry and Polymer Science), University of Stellenbosch: Stellenbosch.
- 81 van den Dungen, E.T.A., and Klumperman, L. (2010) Self Healing Composition, WO2010081713.
- 82 Gragert, M., Schunack, M., and Binder, W.H. (2011) Azide/Alkyne-“click”-reactions of encapsulated reagents: toward self-healing materials. *Macromol. Rapid Commun.*, **32** (5), 419.
- 83 Schunack, M., Gragert, M., Döhler, D., Michael, P., and Binder, W.H. (2012) Low-temperature Cu(I)-catalyzed “click” reactions for self-healing polymers. *Macromol. Chem. Phys.*, **213** (2), 205.
- 84 Motuku, M., Vaidya, U.K., and Janowski, G.M. (1999) Parametric studies on self-repairing approaches for resin infused composites subjected to low velocity impact. *Smart Mater. Struct.*, **8** (5), 623.
- 85 Meure, S., Wu, D.Y., and Furman, S. (2009) Polyethylene-co-methacrylic acid healing agents for mendable epoxy resins. *Acta Mater.*, **57** (14), 4312.
- 86 Meure, S., Furman, S., and Khor, S. (2010) Poly ethylene-co-(methacrylic acid) healing agents for mendable carbon fiber laminates. *Macromol. Mater. Eng.*, **295** (5), 420.
- 87 Meure, S., Varley, R.J., Wu, D.Y., Mayo, S., Nairn, K., and Furman, S. (2012) Confirmation of the healing mechanism in a mendable EMAA-epoxy resin. *Eur. Polym. J.*, **48** (3), 524.
- 88 Nji, J., and Li, G.Q. (2010) A biomimic shape memory polymer based

- self-healing particulate composite. *Polymer*, **51** (25), 6021.
- 89 Brown, E.N., Kessler, M.R., Sottos, N.R., and White, S.R. (2003) In situ poly(urea-formaldehyde) microencapsulation of dicyclopentadiene. *J. Microencapsul.*, **20** (6), 719.
- 90 Blaiszik, B.J., Sottos, N.R., and White, S.R. (2008) Nanocapsules for self-healing materials. *Compos. Sci. Technol.*, **68** (3–4), 978.
- 91 Blaiszik, B.J., Caruso, M.M., McIlroy, D.A., Moore, J.S., White, S.R., and Sottos, N.R. (2009) Microcapsules filled with reactive solutions for self-healing materials. *Polymer*, **50** (4), 990.
- 92 Yuan, L., Liang, G., Xie, J., Li, L., and Guo, J. (2006) Preparation and characterization of poly(urea-formaldehyde) microcapsules filled with epoxy resins. *Polymer*, **47**, 5338.
- 93 Cosco, S., Ambrogi, V., Musto, P., and Carfagna, C. (2007) Properties of poly(urea-formaldehyde) microcapsules containing an epoxy resin. *J. Appl. Polym. Sci.*, **105**, 1400.
- 94 Yuan, Y.C., Rong, M.Z., and Zhang, M.Q. (2008) Preparation and characterization of microencapsulated polythiol. *Polymer*, **49** (10), 2531.
- 95 Liu, X., Sheng, X., Lee, J.K., and Kessler, M.R. (2009) Synthesis and characterization of melamine-urea-formaldehyde microcapsules containing ENB-based self-healing agents. *Macromol. Mater. Eng.*, **294** (6–7), 389.
- 96 Xiao, D.S., Yuan, Y.C., Rong, M.Z., and Zhang, M.Q. (2009) Hollow polymeric microcapsules: preparation, characterization and application in holding boron trifluoride diethyl etherate. *Polymer*, **50** (2), 560.
- 97 Therriault, D., Shepherd, R.F., White, S.R., and Lewis, J.A. (2005) Fugitive inks for direct-write assembly of three-dimensional microvascular networks. *Adv. Mater.*, **17** (4), 395.
- 98 Moll, J.L., White, S.R., and Sottos, N.R. (2010) A self-sealing fiber-reinforced composite. *J. Compos. Mater.*, **44** (22), 2573.
- 99 Aldridge, M., Shankar, C., Zhen, C., Sui, L., Kieffer, J., Caruso, M., and Moore, J. (2010) Combined experimental and simulation study of the cure kinetics of DCPD. *J. Compos. Mater.*, **44** (22), 2605.
- 100 Wilson, G.O., Porter, K.A., Weissman, H., White, S.R., Sottos, N.R., and Moore, J.S. (2009) Stability of second generation Grubbs' alkylidenes to primary amines: formation of novel ruthenium-amine complexes. *Adv. Synth. Catal.*, **351** (11–12), 1817.
- 101 Liu, X., Sheng, X., Lee, J.K., Kessler, M.R., and Kim, J.S. (2009) Rheokinetic evaluation of self-healing agents polymerized by Grubbs catalyst embedded in various thermosetting systems. *Compos. Sci. Technol.*, **69** (13), 2102.
- 102 Liu, X., Lee, J.K., Yoon, S.H., and Kessler, M.R. (2006) Characterization of diene monomers as healing agents for autonomic damage repair. *J. Appl. Polym. Sci.*, **101** (3), 1266.
- 103 Mauldin, T.C., and Kessler, M.R. (2010) Enhanced bulk catalyst dissolution for self-healing materials. *J. Mater. Chem.*, **20** (20), 4198.
- 104 Blaiszik, B.J., Baginska, M., White, S.R., and Sottos, N.R. (2010) Autonomic recovery of fiber/matrix interfacial bond strength in a model composite. *Adv. Funct. Mater.*, **20** (20), 3547.
- 105 Sanada, K., Yasuda, I., and Shindo, Y. (2006) Transverse tensile strength of unidirectional fiber-reinforced polymers and self-healing of interfacial debonding. *Plast. Rubber Compos.*, **35** (2), 67.
- 106 Li, H., Wang, R., Hu, H., and Liu, W. (2008) Surface modification of self-healing poly(urea-formaldehyde) microcapsules using silane-coupling agent. *Appl. Surf. Sci.*, **255** (5 Pt 1), 1894.
- 107 Wang, R., Li, H., Hu, H., He, X., and Liu, W. (2009) Preparation and characterization of self-healing microcapsules with poly(urea-formaldehyde) grafted epoxy functional group shell. *J. Appl. Polym. Sci.*, **113** (3), 1501.
- 108 Wang, R., Li, H., Liu, W., and He, X. (2010) Surface modification of poly(urea-formaldehyde) microcapsules and the effect on the epoxy composites performance. *J. Macromol. Sci. A*, **47** (10), 991.

- 109 Lee, J.K., Hong, S.J., Liu, X., and Yoon, S.H. (2004) Characterization of dicyclopentadiene and 5-ethylidene-2-norbornene as self-healing agents for polymer composite and its microcapsules. *Macromol. Res.*, **12**, 478.
- 110 Grubbs, R.H., and Stanford, M. (2002) Mechanism of ruthenium based olefin metathesis catalyst, in *Ring Opening Metathesis Polymerization and Related Chemistry: State of the Art and Vision for the New Century* (eds E. Khosravi and T. Szymanska Buzar), Kluwer Academic Publishers, Boston, p. 17.
- 111 Mol, J.C. (2004) Industrial applications of olefin metathesis. *J. Mol. Catal. A: Chem.*, **213**, 39.
- 112 Yang, Y.-S., Lafontaine, E., and Mortaigne, B. (1997) Curing study of dicyclopentadiene resin and effect of elastomer on its polymer network. *Polymer*, **38**, 1121.
- 113 Guadagno, L., Longo, P., Raimondo, M., Mariconda, A., Naddeo, C., Sorrentino, A., Vittoria, V., Iannuzzo, G., Russo, S., and Calvi, E. (2009) A composite material which is self-repairing even at low temperature. WO2009/113025.
- 114 Sheng, X., Lee, J.K., and Kessler, M.R. (2009) Influence of cross-link density on the properties of ROMP thermosets. *Polymer*, **50**, 1264.
- 115 Lee, J.K., Liu, X., Yoon, S.H., and Kessler, M.R. (2007) Thermal analysis of ring-opening metathesis polymerized healing agents. *J. Polym. Sci. B: Polym. Phys.*, **45**, 1771.
- 116 Ham, Y.R., Lee, D.H., Kim, S.H., Shin, Y.J., Yang, M., and Shin, J.S. (2010) Microencapsulation of imidazole curing agent for epoxy resin. *J. Ind. Eng. Chem.*, **16** (5), 728.
- 117 Xiao, D.S., Rong, M.Z., and Zhang, M.Q. (2007) A novel method for preparing epoxy-containing microcapsules via UV irradiation-induced interfacial copolymerization in emulsions. *Polymer*, **48** (16), 4765.
- 118 Döhler, D., Michael, P., and Binder, W.H. (2012) Autocatalysis in the room temperature copper(I)-catalyzed alkyne-azide "click" cycloaddition of multivalent poly(acrylate)s and poly(isobutylene)s. *Macromolecules*, **45** (8), 3335.
- 119 Meure, S., Wu, D.Y., and Furman, S.A. (2010) FTIR study of bonding between a thermoplastic healing agent and a mendable epoxy resin. *Vib. Spectrosc.*, **52** (1), 10.
- 120 Jud, K., Kausch, H.H., and Williams, J.G. (1981) Fracture mechanics studies of crack healing and welding of polymers. *J. Mater. Sci.*, **16** (1), 204.
- 121 Lin, C.B., Lee, S., and Liu, K.S. (1990) Methanol-Induced crack healing in poly(methyl methacrylate). *Polym. Eng. Sci.*, **30** (21), 1399.
- 122 Wang, P.-P., Lee, S., and Harmon, J.P. (1994) Ethanol-induced crack healing in poly(methyl methacrylate). *J. Polym. Sci. B Polym. Phys.*, **32** (7), 1217.
- 123 Hsieh, H.-C., Yang, T.-J., and Lee, S. (2001) Crack healing in poly(methyl methacrylate) induced by co-solvent of methanol and ethanol. *Polymer*, **42** (3), 1227.
- 124 Liu, C.K., Yang, T.J., Shen, J.S., and Lee, S. (2008) Some recent results on crack healing of poly(methyl methacrylate). *Eng. Fract. Mech.*, **75** (17), 4876.
- 125 Kawagoe, M., Nakanishi, M., Qiu, J., and Morita, M. (1997) Growth and healing of a surface crack in poly(methyl methacrylate) under case II diffusion of methanol. *Polymer*, **38** (24), 5969.
- 126 Yufa, N.A., Li, J., and Sibener, S.J. (2009) Diblock copolymer healing. *Polymer*, **50** (12), 2630.
- 127 Wu, T., and Lee, S. (1994) Carbon tetrachloride-induced crack healing in polycarbonate. *J. Polym. Sci. B Polym. Phys.*, **32** (12), 2055.
- 128 Yamaguchi, M., Ono, S., and Okamoto, K. (2009) Interdiffusion of dangling chains in weak gel and its application to self-repairing material. *Mater. Sci. Eng. B*, **162** (3), 189.
- 129 Yamaguchi, M., Ono, S., and Terano, M. (2007) Self-repairing property of polymer network with dangling chains. *Mater. Lett.*, **61** (6), 1396.
- 130 Ho, C. (1996) Reactive two part polyurethane compositions and optionally self-healable and scratch resistant coatings prepared therefrom, MX9702420.

- 131 Chen, X., Dam, M.A., Ono, K., Mal, A., Shen, H., Nutt, S.R., Sheran, K., and Wudl, F. (2002) A thermally re-mendable cross-linked polymeric material. *Science*, **295** (5560), 1698.
- 132 Chen, X., Wudl, F., Mal, A.K., Shen, H., and Nutt, S.R. (2003) New thermally remendable highly cross-linked polymeric materials. *Macromolecules*, **36** (6), 1802.
- 133 Plaisted, T.A., and Nemat-Nasser, S. (2007) Quantitative evaluation of fracture, healing and re-healing of a reversibly cross-linked polymer. *Acta Mater.*, **55** (17), 5684.
- 134 Park, J.S., Darlington, T., Starr, A.F., Takahashi, K., Riendeau, J., and Thomas Hahn, H. (2010) Multiple healing effect of thermally activated self-healing composites based on Diels–Alder reaction. *Compos. Sci. Technol.*, **70** (15), 2154.
- 135 Ax, J., and Wenz, G. (2012) Thermoreversible networks by Diels–Alder reaction of cellulose furoates with bismaleimides. *Macromol. Chem. Phys.*, **213** (2), 182.
- 136 Zhang, J., Niu, Y., Huang, C., Xiao, L., Chen, Z., Yang, K., and Wang, Y. (2012) Self-healable and recyclable triple-shape PPDO-PTMEG co-network constructed through thermoreversible Diels–Alder reaction. *Polym. Chem.*, **3** (6), 1390.
- 137 Harris, K.M., and Rajagopalan, M. (2003) Self-healing polymers in sports equipment, US20030032758.
- 138 Wudl, F., and Chen, X. (2004) Thermally Re-mendable cross-linked polymers, US2004014933.
- 139 Peterson, A.M., Jensen, R.E., and Palmese, G.R. (2009) Reversibly cross-linked polymer gels as healing agents for epoxy–amine thermosets. *ACS Appl. Mater. Interfaces*, **1** (5), 992.
- 140 Liu, Y.-L., and Hsieh, C.-Y. (2006) Crosslinked epoxy materials exhibiting thermal remendability and removability from multifunctional maleimide and furan compounds. *J. Polym. Sci. Part A Polym. Chem.*, **44** (2), 905.
- 141 Tian, Q., Yuan, Y.C., Rong, M.Z., and Zhang, M.Q. (2009) A thermally remendable epoxy resin. *J. Mater. Chem.*, **19** (9), 1289.
- 142 Tian, Q., Rong, M.Z., Zhang, M.Q., and Yuan, Y.C. (2010) Synthesis and characterization of epoxy with improved thermal remendability based on Diels–Alder reaction. *Polym. Int.*, **59** (10), 1339.
- 143 Scheltjens, G., Brancart, J., De Graeve, I., Van Mele, B., Terryn, H., and Van Assche, G. (2011) Self-healing property characterization of reversible thermoset coatings. *J. Therm. Anal. Calorim.*, **105** (3), 805.
- 144 Peterson, A.M., Jensen, R.E., and Palmese, G.R. (2010) Room-temperature healing of a thermosetting polymer using the Diels–Alder reaction. *ACS Appl. Mater. Interfaces*, **2** (4), 1141.
- 145 Zhang, Y., Broekhuis, A.A., and Picchioni, F. (2009) Thermally self-healing polymeric materials: the next step to recycling thermoset polymers? *Macromolecules*, **42** (6), 1906.
- 146 Toncelli, C., De Reus, D.C., Picchioni, F., and Broekhuis, A.A. (2012) Properties of reversible Diels–Alder furan/maleimide polymer networks as function of crosslink density. *Macromol. Chem. Phys.*, **213** (2), 157.
- 147 Canary, S.A., and Stevens, M.P. (1992) Thermally reversible crosslinking of polystyrene via the furan–maleimide Diels–Alder reaction. *J. Polym. Sci. Part A Polym. Chem.*, **30** (8), 1755.
- 148 Magana, S., Zerroukhi, A., Jegat, C., and Mignard, N. (2010) Thermally reversible crosslinked polyethylene using Diels–Alder reaction in molten state. *React. Funct. Polym.*, **70** (7), 442.
- 149 Watanabe, M., and Yoshie, N. (2006) Synthesis and properties of readily recyclable polymers from bisfuranic terminated poly(ethylene adipate) and multi-maleimide linkers. *Polymer*, **47** (14), 4946.
- 150 Yoshie, N., Watanabe, M., Araki, H., and Ishida, K. (2010) Thermo-responsive mending of polymers crosslinked by thermally reversible covalent bond: polymers from bisfuranic terminated poly(ethylene adipate) and tris-maleimide. *Polym. Degrad. Stab.*, **95** (5), 826.
- 151 Liu, Y.-L., Hsieh, C.-Y., and Chen, Y.-W. (2006) Thermally reversible cross-linked

- polyamides and thermo-responsive gels by means of Diels–Alder reaction. *Polymer*, **47** (8), 2581.
- 152 Liu, Y.-L., and Chen, Y.-W. (2007) Thermally reversible cross-linked polyamides with high toughness and self-repairing ability from maleimide- and furan-Functionalized aromatic polyamides. *Macromol. Chem. Phys.*, **208** (2), 224.
- 153 Kavitha, A.A., and Singha, N.K. (2007) A tailor-made polymethacrylate bearing a reactive diene in reversible diels–alder reaction. *J. Polym. Sci. Part A Polym. Chem.*, **45** (19), 4441.
- 154 Kavitha, A.A., and Singha, N.K. (2009) “Click Chemistry” in tailor-made polymethacrylates bearing reactive furfuryl functionality: a new class of self-healing polymeric material. *ACS Appl. Mater. Interfaces*, **1** (7), 1427.
- 155 Wouters, M., Craenmehr, E., Tempelaars, K., Fischer, H., Stroeks, N., and van Zanten, J. (2009) Preparation and properties of a novel remendable coating concept. *Prog. Org. Coat.*, **64** (2–3), 156.
- 156 Yoshie, N., Saito, S., and Oya, N. (2011) A thermally-stable self-mending polymer networked by Diels–Alder cycloaddition. *Polymer*, **52** (26), 6074.
- 157 Syrett, J.A., Mantovani, G., Barton, W.R.S., Price, D., and Haddleton, D.M. (2010) Self-healing polymers prepared via living radical polymerisation. *Polym. Chem.*, **1** (1), 102.
- 158 Murphy, E.B., Bolanos, E., Schaffner-Hamann, C., Wudl, F., Nutt, S.R., and Auad, M.L. (2008) Synthesis and characterization of a single-component thermally remendable polymer network: staudinger and stille revisited. *Macromolecules*, **41** (14), 5203.
- 159 Takeshita, Y., Uoi, M., Hirai, Y., and Uchiyama, M. (1975) Reversibly crosslinked polymers, US3890253.
- 160 Chung, C.-M., Roh, Y.-S., Cho, S.-Y., and Kim, J.-G. (2004) Crack Healing in polymeric materials via photochemical [2+2] cycloaddition. *Chem. Mater.*, **16** (21), 3982.
- 161 Ling, J., Rong, M.Z., and Zhang, M.Q. (2012) Photo-stimulated self-healing polyurethane containing dihydroxyl coumarin derivatives. *Polymer*, **53** (13), 2691.
- 162 Ghosh, B., and Urban, M.W. (2009) Self-repairing oxetane-substituted chitosan polyurethane networks. *Science*, **323** (5920), 1458.
- 163 Ghosh, B., Chellappan, K.V., and Urban, M.W. (2011) Self-healing inside a scratch of oxetane-substituted chitosan-polyurethane (OXE-CHI-PUR) networks. *J. Mater. Chem.*, **21** (38), 14473.
- 164 Froimowicz, P., Frey, H., and Landfester, K. (2011) Towards the generation of self-healing materials by means of a reversible photo-induced approach. *Macromol. Rapid Commun.*, **32** (5), 468.
- 165 Nicola, R., Kamada, J., Van Wassen, A., and Matyjaszewski, K. (2010) Responsive gels based on a dynamic covalent trithiocarbonate cross-linker. *Macromolecules*, **43** (9), 4355.
- 166 Amamoto, Y., Kamada, J., Otsuka, H., Takahara, A., and Matyjaszewski, K. (2011) Repeatable photoinduced self-healing of covalently cross-linked polymers through reshuffling of trithiocarbonate units. *Angew. Chem. Int. Ed.*, **50** (7), 1660.
- 167 Scott, T.F., Schneider, A.D., Cook, W.D., and Bowman, C.N. (2005) Photoinduced plasticity in cross-linked polymers. *Science*, **308** (5728), 1615.
- 168 Canadell, J., Goossens, H., and Klumperman, B. (2011) Self-healing materials based on disulfide links. *Macromolecules*, **44** (8), 2536.
- 169 Yoon, J.A., Kamada, J., Koynov, K., Mohin, J., Nicolaÿ, R., Zhang, Y., Balazs, A.C., Kowalewski, T., and Matyjaszewski, K. (2011) Self-healing polymer films based on thiol–disulfide exchange reactions and self-healing kinetics measured using atomic force microscopy. *Macromolecules*, **45** (1), 142.
- 170 Amamoto, Y., Otsuka, H., Takahara, A., and Matyjaszewski, K. (2012) Self-healing of covalently cross-linked polymers by reshuffling thiuram disulfide moieties in air under visible light. *Adv. Mater.*, **3975**.
- 171 Yuan, C.E., Rong, M.Z., Zhang, M.Q., Zhang, Z.P., and Yuan, Y.C. (2011)

- Self-healing of polymers via synchronous covalent bond fission/ radical recombination. *Chem. Mater.*, **23** (22), 5076.
- 172 Imato, K., Nishihara, M., Kanehara, T., Amamoto, Y., Takahara, A., and Otsuka, H. (2012) Self-healing of chemical gels cross-linked by diarylbibenzofuranone-based trigger-free dynamic covalent bonds at room temperature. *Angew. Chem. Int. Ed.*, **51** (5), 1138.
- 173 Takeda, K., Unno, H., and Zhang, M. (2004) Polymer reaction in polycarbonate with Na₂CO₃. *J. Appl. Polym. Sci.*, **93** (2), 920.
- 174 Zheng, P., and McCarthy, T.J. (2012) A surprise from 1954: siloxane equilibration is a simple, robust, and obvious polymer self-healing mechanism. *J. Am. Chem. Soc.*, **134** (4), 2024.
- 175 Deng, G., Tang, C., Li, F., Jiang, H., and Chen, Y. (2010) Covalent cross-linked polymer gels with reversible Sol–Gel transition and self-healing properties. *Macromolecules*, **43** (3), 1191.
- 176 Zhang, Z., Hu, Y., Liu, Z., and Guo, T. (2012) Synthesis and evaluation of a moisture-promoted healing copolymer. *Polymer*, **53** (14), 2979.
- 177 Wool, R.P., and O'Connor, K.M. (1981) A theory crack healing in polymers. *J. Appl. Phys.*, **52** (10), 5953.
- 178 Diels, O., and Alder, K. (1928) Synthesen in der hydroaromatischen Reihe. *Justus Liebigs Ann. Chem.*, **460** (1), 98.
- 179 Craven, J.M. (1969) Cross-linked thermally reversible polymers produced from condensation polymers with pendant furan groups cross-linked with maleimides, US3435003.
- 180 Chen, X. (2003) Novel polymers with thermally controlled covalent cross-linking. PhD Thesis, University of California: Los Angeles.
- 181 Tian, Q. (2009) Thermally remendable epoxy resin. PhD Thesis, University of Guangzhou: Zhongshan.
- 182 Jones, J.R., Liotta, C.L., Collard, D.M., and Schiraldi, D.A. (1999) Cross-linking and modification of poly(ethylene terephthalate-co-2,6-anthracenedicarboxylate) by Diels–Alder reactions with maleimides. *Macromolecules*, **32** (18), 5786.
- 183 Higaki, Y., Otsuka, H., and Takahara, A. (2006) A thermodynamic polymer cross-linking system based on radically exchangeable covalent bonds. *Macromolecules*, **39** (6), 2121.

10

Preparation of Nanocapsules and Core–Shell Nanofibers for Extrinsic Self-Healing Materials

Daniel Crespy and Yi Zhao

Since the pioneering publication of White *et al.* [1], the preparation of containers encapsulating chemicals suitable for self-healing (SH) reactions has been extensively investigated for the restoration of materials mechanical properties, electrical conductivity, or for the inhibition of corrosion.

Capsules, that is, core–shell structures with a liquid core, are still widely used to load SH agents due to the simple preparative procedure and their potential for up-scaling. One of the most interesting features compared to intrinsic SH materials remains that already existing and commercial materials can be employed as matrixes to embed the capsules, enabling possible use in current industrial processes. A second decisive advantage is the possibility to implement a stimulus-responsive release of the SH agents from the capsules [2]. This feature allows the release to be activated on demand and avoids unnecessary and non-environmentally friendly release of the SH agent into the surrounding environment. Fibers encapsulating SH agents, as high aspect ratio pendants for the capsules, are also currently investigated in extrinsic SH materials.

Since some of the failures in materials start at the nanoscale level and then are amplified to micro- and macro- levels, nanocontainers such as nanocapsules or nanofibers allowing the encapsulation of SH agents are interesting for healing cracks or delaminations at their very initial stages [3–5].

The present chapter discusses in a non-comprehensive manner the current and possible future use of nanocapsules and nanofibers for self-healing materials.

10.1

Selected Preparation Methods for the Encapsulation of Self-Healing Agents

10.1.1

Emulsion Droplets as Templates

Suspension polymerization is the method employed to synthesize most of the microcapsules reported so far in the literature. The polymerization, usually a radical polymerization, a polyaddition, or a polycondensation, is carried out in

micro- or milli-droplets created by shearing a liquid phase in another immiscible liquid phase in the presence of a stabilizer. In the case of microcapsules transporting apolar SH agents, the apolar liquid droplets are usually surrounded by an aqueous solution. Because there is no major diffusion of the apolar liquid through the continuous phase, as is the case for emulsion polymerization [6], suspension polymerization allows the encapsulation of large quantities of liquid in a straightforward process.

The pendant of suspension polymerization for preparing submicron particles is miniemulsion polymerization [7, 8]. Miniemulsions are created by dispersing a liquid phase in another immiscible liquid phase in the presence of a surface-active molecule and an additional substance that hinders Ostwald ripening. Direct and inverse miniemulsions are usually oil-in-water and water-in-oil miniemulsions, respectively. However, many other possibilities are available to prepare non-aqueous miniemulsions [9], which can be useful if the SH agents to be encapsulated are water-sensitive. The miniemulsions are efficiently stabilized against coalescence with an appropriate surfactant while the introduction of a *hydrophobe* for direct miniemulsions or a *lipophobe* for inverse miniemulsions prevents Ostwald ripening [10].

Nanocapsule morphology, that is, a core–shell structure with a liquid core, can be formed by different methods from submicron droplets [11, 12]. We discuss here only the methods that are relevant for self-healing materials. Interfacial reactions to create nanocapsules rely on the reaction between molecules mainly present in the dispersed phase and molecules mainly present in the continuous phase. Both molecules react then at the interface of the droplets to build an organic or an inorganic capsule wall. In miniemulsions, interfacial step-growth polymerizations have been performed in direct [13, 14] and inverse systems for the encapsulation of apolar and polar substances in polymer nanocontainers, respectively [15]. With this method, the shell thickness can be conveniently controlled by the concentration of the monomers in the miniemulsion (Figure 10.1a,b), whereas the size of the nanocapsules is controlled by the amount of surfactant employed to emulsify the dispersed phase. Inorganic containers can

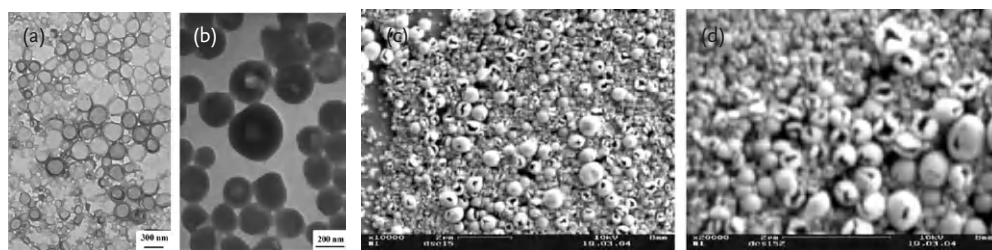


Figure 10.1 (a,b) TEM micrographs of capsules with different shell thickness prepared by interfacial polyaddition. Reprinted with permission from reference [15]. Copyright (2007) American Chemical

Society. (c,d) SEM micrographs of internal phase separation driven by radical polymerization of divinylbenzene [16]. With kind permission from Springer Science and Business Media.

be formed by the same method. For instance, the hydrolysis and condensation of alkoxy silanes in direct [17–19] and inverse [20] miniemulsion yielded also silica nanocontainers with a liquid core.

The layer-by-layer method proposed by Decher [21] was found to be also applicable to curved materials such as spherical particles and droplets [22]. The method is based on the alternate deposition of polyelectrolytes of opposite charges on a solid or liquid substrate. The concept is general and can be derived to macromolecules or colloids possessing interactions strong enough to allow the formation of a shell. The same method was also applied to fabricate functional nanocapsules [23].

Internal phase separation induced by a reaction performed in the dispersed phase and/or the evaporation of a solvent from the dispersed phase can also lead to the formation of nanocapsules. For instance, it was shown that free-radical polymerizations in miniemulsion droplets in the presence of a high amount of alkanes allowed their encapsulation in polymer shells (Figure 10.1c,d) [16, 24, 25]. Phase separation within emulsion droplets can also be triggered by the evaporation of a solvent from the dispersed phase. The principle was shown by Loxley and Vincent for PMMA microcapsules containing a poor solvent for PMMA [26]. The dispersed phase of the emulsion contained the polymer, a good low-boiling solvent, and a poor solvent for the polymer. When the good solvent is removed by evaporation, phase separation of the polymer occurs within the droplets.

The success for the formation of the capsules is guided by the values of the spreading coefficients defined by:

$$S_i = g_{jk} - (g_{ij} + g_{ik})$$

$$S_w = \gamma_{OP} - (\gamma_{OW} + \gamma_{PW})$$

$$S_p = \gamma_{OW} - (\gamma_{OP} + \gamma_{PW})$$

with $g_{12} > g_{ik}$ and 1,2,3 the symbols for the three different phases. According to the theory developed by Torza and Mason [27], several morphologies can be obtained, as described in Figure 10.2, among which only the core–shell with liquid core is of interest for the encapsulation of self-healing agents. As shown in the subsequent part of this chapter, the fabrication of core–shell structures can be implemented to lower length scales to prepare nanocapsules. Compared to the internal

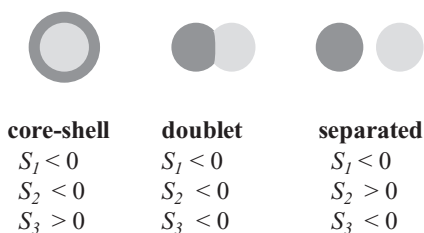


Figure 10.2 Predicted morphology of the colloids according to the sign of the spreading coefficients.

phase separation induced by a reaction (e.g., polymerization), solvent evaporation-induced phase separation has the advantage of being free of non-reacted species because the polymer can be purified before the emulsification.

10.1.2

Electrospinning

Nanofibers can be conveniently prepared by the electrospinning technique [28]. The method is very versatile and can be applied to synthesize inorganic, organic, or composites meshes [29, 30] not only from solutions, but also from emulsions and dispersions [31]. A typical set-up for electrospinning is schematized in Figure 10.3. It is usually composed of a spinneret, a high voltage power supply, and an electrically conductive collector placed opposite to the spinneret. The electrospinning solution or dispersion is fed through the spinneret with the help of a syringe pump or by gravity. In the presence of a strong electrical field, the droplet formed at the end of the spinneret undergoes a conical deformation called Taylor cone. The cone deforms further and the electrified liquid is ejected toward the collector. Because of evaporation of the solvent and strong electrostatic repulsion forces, the jet is stretched and thinned to yield fibers that are deposited on the collector. Core–shell nanofibers are ideal candidates for the encapsulation of self-healing materials and can be produced either by coaxial or emulsion-electrospinning [32]. Coaxial electrospinning relies on the simultaneous electrospinning of two different jets from two spinnerets arranged in a coaxial manner. The electrospin-

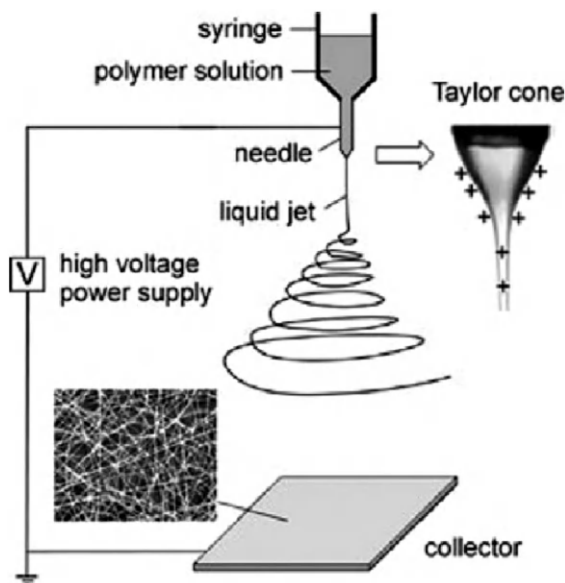


Figure 10.3 Schematics of an electrospinning set-up with an enlargement of the Taylor cone and a typical SEM micrograph of polymer fibers deposited on the collector [29].

ning of emulsions can lead to core-shell structures when the concentration of droplets in the spinning feed is sufficiently high. The droplets can be deformed during the electrospinning process and coalesce in the jet to form a continuous domain in the core of the fibers.

10.2

Mechanically Induced Self-Healing

10.2.1

Nanocapsules

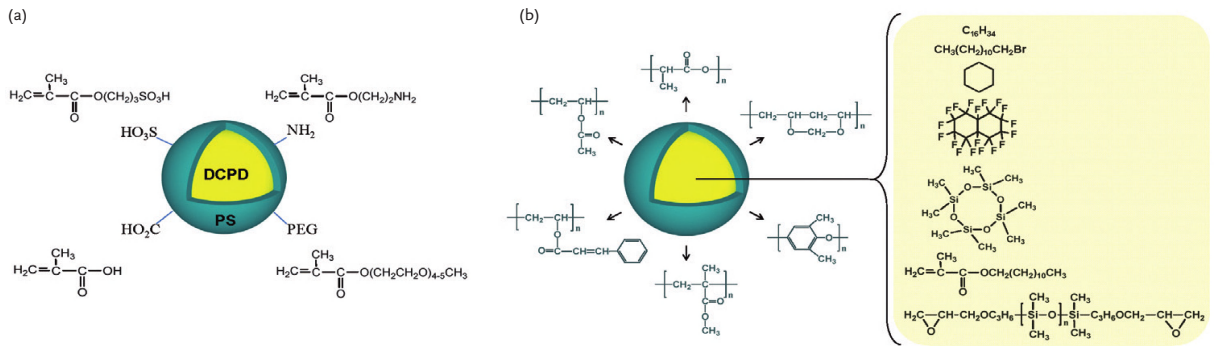
Mechanical damage was the first investigated trigger for the release of SH agents. According to the composition of the shells, nanocapsules for SH materials can be divided into polymer nanocapsules, inorganic nanocapsules, or hybrid nanocapsules. Table 10.1 summarizes the characteristics of capsules for SH materials.

Blaiszik *et al.* reported the first application of nanocapsules for SH materials [33, 34]. Dicyclopentadiene (DCPD) was encapsulated in poly(urea-formaldehyde) (PUF) nanocapsules by interfacial polycondensation. With the help of ultrasonication, 1.65 μm PUF capsules were prepared. The capsule size could be further decreased to 220 nm by introducing hexadecane (HD) in DCPD droplets to prevent Ostwald ripening. The PUF were subsequently embedded in an epoxy matrix and its fracture toughness was found to be increased by ~59% when the capsules volume fraction was ~15%. In this case, no Grubbs' catalyst was employed during the material fabrication. The enhancements of mechanical properties were mainly due to the active crack pinning by DCPD when the capsules were broken. A similar approach was developed to encapsulate triethylene glycol dimethacrylate (TEGDMA) in polyurethane (PU) nanocapsules for self-healing in dentistry [35]. The bond strength of the dental adhesive was significantly increased when 9 wt.% TEGDMA nanocapsules were incorporated in the matrix.

Klumperman *et al.* successfully encapsulated tetrathiol in PUF nanocapsules with styrene-maleic anhydride copolymer (PSMA) or poly(styrene-maleic anhydride)-*block*-polystyrene (PSMA-*b*-PS) as surfactants [37]. The nanocapsules had a size range of 150 ~500 nm. It was found that the nanocapsules had better stability when block copolymers were used as surfactants instead of random copolymers. The authors also reported the encapsulation of dinorbornene in PS nanocapsules by miniemulsion radical polymerization of styrene. The encapsulated substances, tetrathiol and dinorbornene, are candidates for self-healing reactions based on thiol-ene click chemistry and ROMP, respectively. Fickert *et al.* encapsulated DCPD in copolymers of styrene and hydrophilic monomers by miniemulsion polymerization [36]. The surface chemistry and charge of the capsules could be easily controlled by varying the nature of the hydrophilic comonomer, which included methacrylic acid (MAA), the potassium salt of 3-sulfopropyl methacrylate (SMA), 2-aminoethylmethacrylate hydrochloride (AEMA), and poly(ethylene glycol) methyl ether methacrylate (PEGMA) (see Figure 10.4a). Holes

Table 10.1 Characteristics of the capsules, types of SH agents and reactions. The abbreviations are summarized at the end of the chapter.

Capsules		Self-healing compounds		Ref.
Materials	Size	Materials	Healing method	
PUF	1.65 ± 0.79 μm	DCPD	ROMP	[33]
	220 ± 110 nm			
	300 nm			[34]
PU	260–340 nm	TEGDMA	Radical polymerization	[35]
PS	290 ± 100 nm	DCPD	ROMP	[36]
P(S-co-SMA)	310 ± 90 nm			
P(S-co-MAA)	260 ± 80 nm			
P(S-co-AEMA)	440 ± 170 nm			
P(S-co-SMA-co-PEGMA)	240 ± 30 nm			
P(S-co-AEMA-co-PEGMA)	490 ± 170 nm			
PDVB	340 ± 90 nm			
P(S-co-PEGMA)	280 ± 80 nm			
P(S-co-MAA-co-PEGMA)	270 ± 80 nm			
P(DVB-co-SMA)	320 ± 60 nm			
P(S-co-DVB-co-SMA-co-PEGMA)	300 ± 30 nm			
PUF/PSMA	150–500 nm	Tetrathiol	Click chemistry	[37]
PS	60–150 nm	Dinorbornene	ROMP	
PLLA	320 ± 140 nm	HD	Solvent induced	[38]
PMMA	335 ± 80 nm			
PVAc	250 ± 90 nm			
PVF	250 ± 50 nm			
PPO	320 ± 110 nm			
PVCi	240 ± 70 nm			
PLLA	360 ± 200 nm	1-Bromododecane		
	240 ± 60 nm	Cyclohexane		
	320 ± 180 nm	Perfluorodecane		
PVF	240 ± 110 nm	D4	Ionic polymerization	
	260 ± 120 nm	LMA	Radical polymerization	
	230 ± 70 nm	PDMS-DE	Polycondensation	
Silica/PUF	1.5 μm	DCPD	ROMP	[39]
Silica/PS	1.5 μm	Grubbs' catalyst		
Silica/PS/PMMA	0.4 μm			
Silica(TEOS)	140 ± 60 nm	DCPD		[19]
Silica(TEOS/MPTMS 9:1)	120 ± 60 nm			
Silica(TEOS/MPTMS 8:2)	110 ± 60 nm			
Silica(TEOS/MPTMS 5:5)	130 ± 50 nm			
Silica(TEOS/APTES 95:5)	120 ± 60 nm			
silica	180 ± 90 nm	Grubbs' 1st/TOL		
	190 ± 100 nm	Grubbs' 2nd/TOL		
	320 ± 130 nm	Grubbs' 1st/XYL		
	300 ± 150 nm	Grubbs' 2nd/XYL		
	170 ± 90 nm	Grubbs' 2nd/CHCl ₃		
	210 ± 80 nm	Grubbs' 1st/CHCl ₃		
	100–150 nm	MBT	Corrosion inhibitor	[40]



were observed in scanning electron micrographs and were attributed to the evaporation of the liquid core in the vacuum during coating of the substrates or/and during the observation in the scanning electron microscope. To prove that the holes were not present on the surface of particles in the dispersion, and thus that the SH agent was successfully encapsulated, atomic force microscopy (AFM) was carried out in the absence or presence of water. Some holes were also observed with AFM when the dispersion of nanocapsules was measured without surrounding water. On the contrary, the shells of the nanocapsules were found to remain intact when they were surrounded by water. This finding has important implications for the applications of nanocapsules in self-healing materials. Indeed, it means that encapsulated substances should be processed as a dispersion or that substances with lower vapor pressure should be encapsulated when the drying occurs at room temperature.

Besides the formation of nanocapsules involving reactions, SH agents can be encapsulated in pre-synthesized polymers via the mild miniemulsion-solvent evaporation technique [38]. This method was found to be general and a large variety of polymers with completely different chemical structures and physical properties could be used as shells, such as poly(L-lactide) (PLLA), poly(methyl methacrylate) (PMMA), poly(vinyl formal) (PVF), poly(vinyl acetate) (PVAc), poly(2,6-dimethyl-1,4-phenylene oxide) (PPO), and poly(vinyl cinnamate) (PVCi) (see Figure 10.4b). Different hydrophobic oils, such as hexadecane, 1-bromododecane, cyclohexane and perfluorodecaline, were successfully encapsulated in PLLA nanocapsules which could be used in solvent-induced self-healing. Furthermore, octamethylcyclotetrasiloxane (D4), lauryl methacrylate (LMA) and diglycidyl ether terminated poly(dimethylsiloxane) (PDMS-DE) were also encapsulated in PVF nanocapsules for self-healing reactions based on ionic, radical, and condensation polymerizations, respectively.

Although polymer capsules are widely used in SH materials, they are usually less mechanically and thermally stable than inorganic capsules. During the processing, the polymer shells may collapse or the polymer capsules form large aggregates above their glass transition temperature. These problems can be addressed either by coating a thin inorganic layer on the polymer capsules, or by directly encapsulating SH agents in inorganic nanocontainers. Jackson *et al.* encapsulated DCPD in PUF nanocapsules and entrapped Grubbs' catalysts in PS or PS/PMMA nanoparticles by an emulsion–solvent evaporation technique [39]. These solid nanoparticles were further coated with a thin silica layer (20 ~ 40 nm) by hydrolysis and condensation of tetraethylorthosilicate (TEOS). These silica-protected containers showed high stability and less aggregation when mixing with epoxy matrix, which could make the containers disperse in the matrix at high concentration only with little loss of reactivity. Another approach is to carry out interfacial reaction between TEOS present in the dispersed phase and the surrounding aqueous medium at the surface of miniemulsion droplets containing either DCPD or Grubbs' catalysts (Figure 10.5a) [19]. The surfaces were functionalized with thiol or amine groups by copolymerizing TEOS with 3-mercaptopropyl trimethoxysilane (MPTMS) and 3-aminopropyltriethoxysilane (APTES), respectively. In order to increase the solubility and mobility of Grubbs' catalysts during

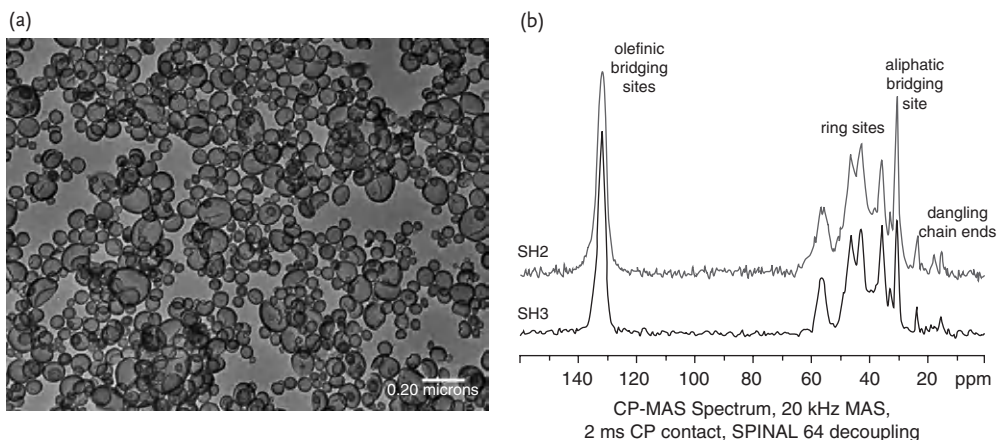


Figure 10.5 (a) TEM micrographs of silica nanocapsules prepared by the hydrolysis and condensation of alkoxysilanes at the interface of miniemulsion droplets. The Grubbs' catalyst and the monomer dicyclopentadiene (DCPD) for ring-opening metathesis polymerization were separately encapsulated in silica nanocontainers. After mixing the two dispersions, breaking the capsules walls by

ultrasonication, and drying the mixture, the polymer poly(DCPD) could be recovered as shown by ^{13}C CP-MAS NMR spectroscopy (b). The experiments could be carried out under air (SH2) or argon (SH3) without significant difference between both cases. Reproduced from reference [19] with permission from The Royal Society of Chemistry.

a possible self-healing reaction, different hydrophobic organic solvents were used to dissolve the catalysts, including toluene, xylene, chloroform and dichloromethane. The self-healing reaction was carried out via an *in vitro* method. The nanocapsules containing DCPD and Grubbs' catalysts were mixed and sonicated to open the capsules mechanically. Poly(DCPD) was formed, as revealed by solid-state NMR (Figure 10.5b) and TGA measurements. Besides monomers and catalysts for self-healing reactions based on polymerizations, corrosion inhibitors were also encapsulated in silica nanocontainers. For instance, Zheludkevich *et al.* encapsulated 2-mercaptobenzothiazole (MBT) in silica nanocapsules for active corrosion protection [40]. A self-healing effect was detected when defects were intentionally created in the modified coatings. The self-healing and self-repairing approach is described in more detail in Sections 10.3.2 and 10.3.3.

10.2.2

Nanofibers and Nanotubes

Incorporating containers encapsulating SH agents without deteriorating the properties of the matrix is an important prerequisite for their application. A suitable container should keep or even enhance the properties of the matrix. Fibers are routinely used to improve the toughness of polymer materials for many years. Among the different fibers morphologies, core–sheath (or core–shell) fibers allow the entrapping of large amount of SH agents in their core. Once they are

Table 10.2 Characteristics of the fibers employed to encapsulate SH agents in nanofibers.

Fibers/tubes		Self-healing agents		Ref.
Materials	Diameter ^{a)}	Materials	Healing method	
Glass	60 μm (ext)	Ciba MY750 epoxy resin	Polyaddition	[41]
	30–100 μm (ext)	Cycom 823 epoxy resin		[42]
	60 ± 3 μm (ex)			[43]
	60 ± 3 μm (ex)/40 μm (int)			[44]
Sisal	150–200 μm (ext)	(C ₂ H ₅) ₂ O·BF ₃	Cationic polymerization	[45]
Glass	5 μm (int)/15 μm (ext)	Ciba LY5120 epoxy resin	Polyaddition	[46]
	5 μm (int)/15 μm (ext)	Ciba MY750 epoxy resin		
	5 μm (int)/15 μm (ext)	cynoacrylate	Anionic polymerization	
Halloysite	15 nm (int)/50 nm (ext)	BTA	Anti-corrosion	[47]
	15 nm (int)/50 nm (ext)	8HQ		[47]
	15 nm (int)/50 nm (ext)	BTA		[48]
CNT	50–100 nm (ext)	DCPD	ROMP	[49]
	50–100 nm (ext)	IPDI	Polycondensation	
PAN	0.4–1.5 μm (int)/1.5–3 μm (ext)	DCPD	ROMP	
	0.4–1.5 μm (int)/1.5–3 μm (ext)	IPDI	Polycondensation	

a) ext = external diameter, int = internal diameter.

embedded in the matrix to be healed, reinforcement and self-healing abilities can be simultaneously achieved. The different strategies and materials reported in the literature are summarized in Table 10.2.

Various hollow fibers have been used for SH materials, including glass fibers [41–46, 50, 51], halloysite nanotubes [47, 48, 52], carbon nanotubes [53] and polymer fibers [49]. Bond *et al.* filled different uncured epoxy resins in glass fibers [41–44]. The filled glass fibers were further incorporated in an epoxy matrix for reinforcement and self-healing. The results of mechanical tests showed that the fraction strength of the matrix was restored by the self-healing effect. To avoid the deactivation of the catalysts during materials fabrication, Xiao *et al.* loaded boron trifluoride diethyl etherate ((C₂H₅)₂O·BF₃) in sisal fibers [45]. After mixing the fibers with the epoxy matrix, the catalysts diffused in the whole system and healing occurred when epoxy resin-filled capsules were broken upon mechanical damage. Since glass fibers and sisal fibers are usually in the micrometer range or above, they are not suitable for healing cracks in a smaller length scale. Halloysites nanotubes are much smaller, cheap, durable, biocompatible and display high mechanical strength [52]. Fix *et al.* successfully encapsulated corrosion inhibitors, such as benzotriazole and 8-hydroxyquinoline, in halloysite nanotubes [47]. The filled halloysites were dispersed in a sol–gel coating to protect the aluminum alloy. A self-healing effect was successfully demonstrated by an *in situ* scanning vibrating electrode technique, showing a rapid decrease in the maximal anodic activity within 1–2 h after corrosion.

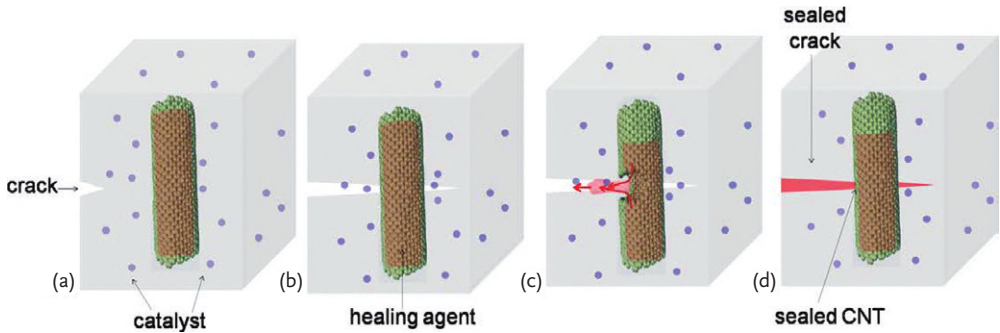


Figure 10.6 Scheme illustrating the concept of the self-healing process using carbon nanotubes as reservoirs for SH agents. Copyright Institute of Physics and IOP Publishing 2010.

Others promising nanocontainers for SH materials are carbon nanotubes (CNTs) because they have extremely large interfacial area and very good mechanical properties. Therefore, CNTs are considered as ideal filler materials for mechanical reinforcement and as nanocontainers for SH agents at the same time. The challenges for their applications are whether the cracks can form on the sidewall of CNTs and if the healing agents will release from CNTs when cracks happen. To answer these questions, Lanzara *et al.* investigated the application of CNTs as nanocontainers for SH materials through a molecular dynamics (MD) study [53]. The concept of proposed self-healing with CNTs is illustrated schematically in Figure 10.6. CNTs loaded with SH agents were embedded in a hosting matrix. Crack healing was achieved through chemical reactions between the healing molecules and triggered catalysts. The simulation results showed that the number of molecules released depends on the size of the cracks that formed on the CNT wall. Moreover, the release was temperature-dependent and exhibited saturation. This study showed that CNTs were not only able to load SH agents for repairing the matrix but could also be used as filler materials for mechanical reinforcement before and after delivery of the active compounds.

Although CNTs are theoretically suitable as multifunctional nanocontainers, they have not yet been used for SH application due to the experimental difficulties in loading the SH agents and sealing the two ends of the CNTs. Polymer nanofibers produced by electrospinning are good alternatives since they possess a much higher aspect ratio and the surface of the non-closed cross-section of the fibers (extremities) is negligible compared to the total surface of the fibers. Sinha-Ray *et al.* recently reported the encapsulation of SH agents in core-shell polymer nanofibers by the electrospinning method [49]. Two types of healing agents, DCPD and isophorone diisocyanate were successfully loaded in polyacrylonitrile (PAN) fibers. As shown in Figure 10.7, the fibers had an average internal diameter 0.4–1.5 μm and an average external diameter 1.5–3 μm . The presence of the healing materials in the fiber core was proved by polymerization of the monomers under squeezing, energy dispersive X-ray spectroscopy, and preferential imprinting of a

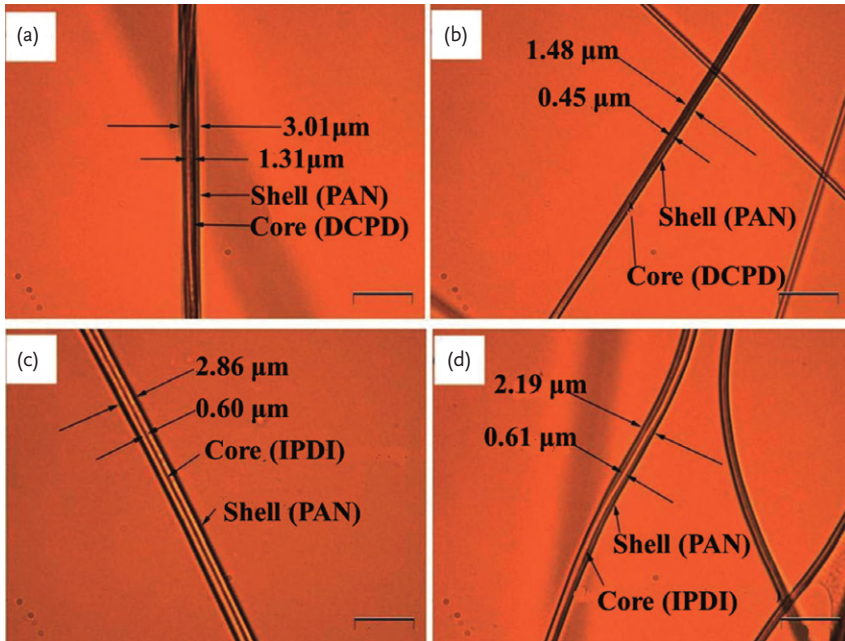


Figure 10.7 Optical microscopy images of core–shell fibers: (a,b) PAN fibers loaded with DCPD; (c,d) PAN fibers loaded with IPDI. The scale bar in all images is 10 μm. Reproduced from reference [49] with permission from The Royal Society of Chemistry.

fluorescent dye. Hybrid polymer composites reinforced with healant-loaded PAN nanofibers have been fabricated, and the toughening mechanisms and delivery of self-healing agents examined and validated. This study provided a simple way for encapsulation of SH agents to be used in the production of smart composites.

10.3 Stimuli-Responsive Self-Healing Materials

Nanocontainers with the ability to release the SH or so-called self-repairing agents in a controlled way have already been used to prepare active SH materials [54–56]. These nanocontainers not only have a passive functionality but also rapid feedback activity upon external stimuli.

10.3.1 Light-Responsive Capsules

Light is becoming an appealing external stimulus to release substances encapsulated in polymer capsules because it has a broad range of tunable parameters (intensity, irradiation time and location) and it does not require additional chemical

substances [57]. To the best of our knowledge, there is, however, no report about the application of photoresponsive capsules in SH materials until now. As photoresponsive capsules have already been widely studied for controlled release, they could also be applied in SH materials. Usually photoresponsive capsules are made with photoresponsive polymers [58–61] and dyes [62], or by incorporating metal nanoparticles [63–67] and carbon nanotubes [68] in polymer shells. A straightforward method would be to prepare photoresponsive capsules from photoresponsive polymers. Photodegradable polymers are a good choice when burst release of the encapsulated compounds is needed because it can be achieved upon photoirradiation. Kitano *et al.* prepared photodegradable polymer microcapsules by a coupling reaction of disuccinimido 4,4'-azobis(4-cynovalerate), L-lysine and polyallylamine [58]. Due to the decomposition of polymer chains under photoirradiation, encapsulated succinylated bovine serum albumin was observed to be released. Following the same strategy, Almutairi *et al.* prepared UV and near-IR responsive polymer nanoparticles encapsulating the dye Nile Red [61]. The polymer was composed of a self-immolative quinone-methide backbone and photocleavable nitrobenzyl alcohol groups as trigger. Controlled release of payload upon irradiation at 365 or 700 nm and subsequent degradation of polymers were observed. Compared with burst release of compounds, releasing the encapsulated compounds in a controlled manner allows a prolonged delivery of the encapsulated substance. Kono *et al.* prepared crosslinked poly(acrylic acid)-poly(ethyleimide) capsules containing a copolymer of acrylic acid and bis[4-(dimethylamino)phenyl](4-vinylphenyl)methyl leucohydroxide [59]. In weak alkaline conditions, the triphenylmethane derivative could dissociate into an ion pair under UV irradiation. The permeation of *p*-toluene sulfonate through the membrane was then enhanced significantly. The permeation of the substance could be controlled simply by switching on/off the UV light.

Another important type of photoresponsive capsules is prepared from polymers and inorganic particles which have optothermal or photocatalytic properties. Gold and silver nanoparticles are commonly used in capsule shells to convert light to heat. By generating sufficient heat, the capsule can be collapsed and burst release occurs, as shown in Figure 10.8. An alternative is generating heat to increase the temperature above the glass transition temperature of the polymer shell, thereby accelerating the permeation rate of the payload. Caruso *et al.* prepared photoresponsive capsules built from PSS/PAH multilayers and gold nanoparticles [63]. The encapsulated fluorescein isothiocyanate-labeled dextran could be released on demand from the capsules by irradiating with a 10 ns pulse of laser light at 1064 nm. Pastine *et al.* prepared toluene-filled polyamide microcapsules containing 1% carbon nanotubes and 5% Grubbs' catalyst (II) [68]. These microcapsules were dispersed in neat DCPD (1:100 by weight) for weeks without noticeable increase in viscosity. However, a laser irradiation at 785 nm was found to open the capsule shell, resulting in the gelation of the dispersion in several minutes. This phenomenon was explained by the optothermal effect of CNTs, which absorbed and converted the light to heat to break the capsule shell, inducing a release of the Grubbs' catalyst. Besides the optothermal effect, a photocatalyst effect could also be applied to prepare photoresponsive capsules. Katagiri *et al.* prepared

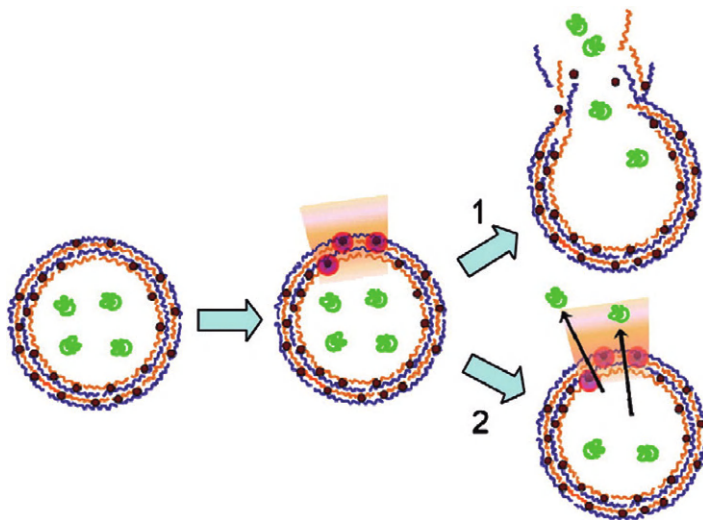


Figure 10.8 Scheme illustrating two possible release routes due to the optothermal effect: 1) large amount of heat can break the capsule wall; 2) lower amount of heat allows the local temperature of the shell to exceed

the glass transition temperature of the polymer shell and accordingly increase the permeability. Reprinted from reference [57], Copyright (2010), with permission from Elsevier.

UV-responsive microcapsules based on poly(sodium 4-styrenesulfonate) (PSS) and poly(diallyldimethylammonium chloride) (PDDA) multilayers, which were subsequently coated with a cationic bilayer of dioctadecyldimethylammonium bromide and $\text{SiO}_2\text{-TiO}_2$ prepared by sol–gel chemistry [66]. The encapsulated Phenol Red was released by irradiating at 550 nm. As a control test, the capsules without TiO_2 were unaffected by UV irradiation. This was explained by the photocatalytic activity of the TiO_2 component decomposing polyelectrolytes, which causes the capsules to rupture.

10.3.2

pH-Responsive Systems

In some cases, for instance when metal corrosion occurs, the generation of cracks in a material is accompanied by local pH changes. Therefore, pH-responsive capsules active nanocontainers have been investigated for anticorrosion applications [69–83]. Mesoporous SiO_2 [69–76] and ZnO [77] were used as nanocontainers to load corrosion inhibitors. The surface was then decorated via the layer-by-layer technique, with pH-responsive polymers such as poly(ethyleneimine) (PEI), poly(styrene sulfonate) (PSS), poly(acrylic acid) (PAA), poly(methacrylic acid) (PMA), and poly(allylamine hydrochloride) (PAH). As shown in Table 10.3, various organic and inorganic corrosion inhibitors were successfully encapsulated, including benzotriazole (BTA), cerium cation, 2-mercaptobenzothiazole (MBT), ben-

Table 10.3 Characteristics of pH responsive nanocontainers for self-healing materials.

Containers		Self-healing compounds		Ref.
Materials	Diameter	Materials	Healing method	
SiO ₂ /PEI/(PSS/BTA) _n	150 nm	BTA	Corrosion inhibitor	[69]
SiO ₂ /PAH/(PSS/BTA) _n	60–140 nm			[70]
SiO ₂ /PAH/(PMA/BTA) _n	60–140 nm			
SiO ₂ /PAH/(PSS+PMA/BTA) _n	60–140 nm			
SiO ₂ /PEI/(PSS/BTA) _n	70 nm			[71]
	70–100 nm			[73]
Zeolite	<2 μm	Cerium cation		[74]
SiO ₂ /CB[6]/bisammonium stalks	0.5–0.8 μm	BTA		[75]
SiO ₂	60–80 nm	MBT		[76]
ZnO/PANI/BTA/PAA	950 nm	BTA		[77]
Zn–Al LDH	50–100 nm	Benzoate anion		[78]
	200–400 nm	MBT		[79]
	200–400 nm	Vanadate		
	200–400 nm	Phosphate		
Cerium molybdate	140 ± 10 nm	8-HQ		[80]
	140 ± 10 nm	1-BSA		
Zn–Al LDH	–	MBT		[81]
Mg–Al LDH	–			

zoate anion, vanadate, phosphate, 1-H-benzotriazole-4-sulfonic acid (1-BSA), and 8-hydroxyquinoline (8-HQ).

Grigoriev *et al.* loaded benzotriazole (BTA) as a corrosion inhibitor into mesoporous SiO₂ nanoparticles [68]. The particles were further coated with PEI/PSS/(BTA/PSS)_n multilayers. Then the decorated SiO₂ nanocontainers were combined with zirconia and organosiloxane sols to form a sol–gel anticorrosion coating on an aluminum alloy substrate. When corrosion occurred, the local pH changed, becoming either acidic or alkaline, depending on the corrosion mechanism, and on impurities and surface properties of the metals. The change in pH induced a loosening of the shell structure and, as a result, the inhibitor located in the shell or mesoporous SiO₂ was released into the corrosion sites and stopped the corrosion. After healing, the capsule shells closed again due to the recovery of the initial pH and the release of inhibitor was stopped. The evolution of the corrosion process and self-healing efficiency of protected aluminum dipped in 0.1 M NaCl solution was analyzed by the scanning vibrating electrode technique (SVET). As shown in Figure 10.9, no corrosion current was observed during the experiment. After 42 h of immersion of the metal, anodic activity was detected (Figure 10.9b) due to corrosion. After another 18 h, the corrosion was suppressed because of the release of inhibitors (Figure 10.9c). Following the same strategy, polyelectrolytes-modified nanocarriers based on halloysite nanotubes and SiO₂ nanoparticles were prepared

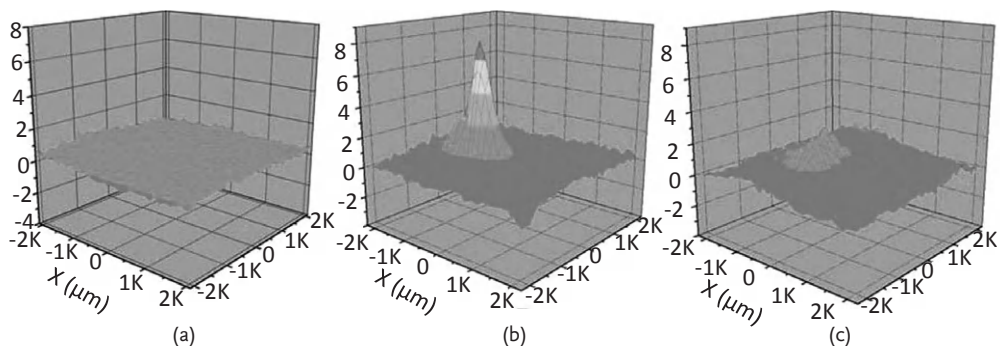


Figure 10.9 SVET curves of the anticorrosion coating on aluminum substrate doped with $\text{SiO}_2/\text{PEI}/\text{PSS}/(\text{BTA}/\text{PSS})_n$ particles dipped in 0.1 M NaCl solution for (a) 0 h, (b) 42 h, and (c) 60 h. z-coordinates in all figures represent

the local current density due to the development of the corrosion process. Reproduced from reference [69] with permission from The Royal Society of Chemistry.

[70]. Benzotriazole (BTA) was chosen as corrosion inhibitor and loaded in these carriers that were further used to protect copper from corrosion. Electrochemical measurements were carried out to analyze the anticorrosion effect by using a copper specimen as the working electrode. The corrosion medium was 0.5 M NaCl aqueous solution and BTA-loaded nanoparticles were added before the measurement. It was discovered that lower pH, stronger stirring, and higher temperature could accelerate the release of BTA, and consequently increase the efficiency of the nanocontainers against corrosion. Instead of polyelectrolyte layers, CB[6] and bisammonium stalks were used as pH-responsive nanovalves in SiO_2 shells [75]. The release rate of corrosion inhibitors increased above pH 7 because of the detachment of CB[6] rings from bisammonium stalks. ZnO particles could be sequentially modified with PANI, BTA and PAA layers [77]. The corrosion testing results showed that 5 wt.% nanoparticles in the matrix would be enough for sustained release of inhibitors in applications. Other inorganic particles such as, SiO_2 [76], zeolite particles [74], cerium molybdate particles [80], Zn-Al LDHs [78, 79, 81] and Mg-Al LDH [81] could also be used for encapsulation of different corrosion inhibitors without surface decoration. Zeolite particles loaded with Ce(III) as corrosion inhibitor were embedded into silica-zirconia sol-gel film to protect an aluminum substrate [74]. When corrosion happened, the local pH decreased due to the hydrolysis of metal cations and Ce^{3+} was released and precipitated in the cathodic areas to heal the corrosion. Lower pH value increased the amount of Ce^{3+} released from the zeolite. In another approach, Kartsonakis *et al.* loaded 8-HQ and 1-BSA in cerium molybdate nanocontainers [80]. The loaded amount was found to be ~5 wt.% for 8-HQ and ~16 wt.% for 1-BSA. These nanocontainers were further applied to protect aluminum alloy and carbon steel from corrosion. The releases of the inhibitors were studied in a corrosion environment by potentiodynamic measurement and spectrophotometer. The results showed that the release of inhibitors suppressed the corrosion activity.

An important kind of containers are layered double hydroxides (LDHs) [78, 79, 81], including Zn–Al LDHs and Mg–Al LDHs. Ferreira *et al.* synthesized Zn–Al LDHs loaded with different corrosion inhibitors, such as vanadate, phosphate and MBT [79]. The nanocontainers were incorporated into commercial coatings to test the anti-corrosion effect. The study showed that the combination of LDH containers loaded with vanadate and phosphate anions, or vanadate and MBT showed a synergistic anticorrosion effect on aluminum alloy. The best anti-corrosion performance was found for a sol–gel coating doped with LDH-MBT and a primer doped with LDH-vanadate.

10.3.3

Temperature-Responsive Systems

Temperature is another possible stimulus to trigger the release of SH agents from nanocapsules. As already mentioned, the release of payload from capsules is influenced by the glass transition temperature (T_g) of the capsule's shell. Increasing temperature above the T_g accelerates the releasing rate. Most of the temperature-responsive capsules have been studied in aqueous solution and used for controlled drug delivery study [84–90]. Thermally responsive capsules usually have sharp changes of morphologies in response to a small change in temperature around the lower critical solution temperatures (LCSTs) or upper critical solution temperatures (UCSTs) of the polymers. Figure 10.10 shows an example of thermo-responsive core–shell microcapsules with a porous membrane and poly(*N*-isopropylacrylamide) gates [84]. The polyamide microcapsules were prepared by interfacial polymerization, and grafting of PNIPAM in the pores was achieved by plasma-graft pore-filling polymerization. The microcapsules showed positive and negative thermo-responsive controlled release by changing the PNIPAM grafting yield. When the grafting yield was low, the release rate was higher at $T > \text{LCST}$ than $T < \text{LCST}$ due the opening and closing of the pores. When the graft yield was high, the release rate was lower at $T > \text{LCST}$ than $T < \text{LCST}$ due to the hydrophilic/hydrophobic phase transitions of the PNIPAM gates. However, temperature has not yet been used in SH materials as a stimulus to open nanocapsules.

10.3.4

Redox-Responsive Systems

Capsules with permeability sensitive to the redox of the shell have also been reported. The layer-by-layer technique was employed on colloidal templates with polyanions and polycations based on poly(ferrocenylsilane) [91]. The microcapsule wall permeability could be controlled by the redox states of the ferrocene units in the shell. Chemical oxidation yielded swelling of the capsule and a drastic change in the permeability of the capsule wall. Another approach was investigated by Staff *et al.* and is based on the design of polymer nanocapsules with redox-responsive nanopatches [92]. The nanopatches were formed by poly(vinylferrocene) blocks of poly(methyl methacrylate)-block-poly(vinylferrocene). The selective

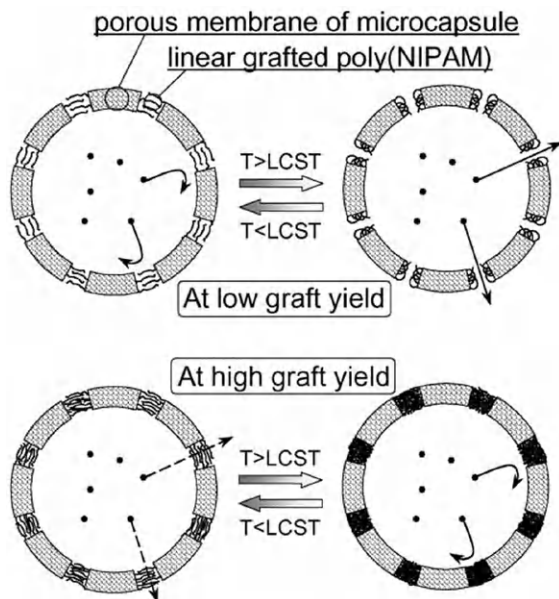


Figure 10.10 Schematic illustration of the thermo-responsive release in core–shell microcapsules with a porous membrane and thermoresponsive polymer gates having different grafting density. Reprinted from reference [87], Copyright (2001), with permission from Elsevier.

oxidation of the patches led to the release of substances encapsulated in the nanocontainers.

10.4

Novel Approaches and Perspectives

Core–shell particles and fibers with encapsulated self-healing agents are suitable components for thin extrinsic self-healing materials. While mechanical- and pH-induced opening of the nanocapsules are predominant in the literature, light-, temperature-, and redox-triggered delivery of encapsulating self-healing agents are promising alternatives.

Elongated nanocapsules, as a bridge between spherical nanocapsules and core–sheath nanofibers are also interesting fillers for self-healing materials. Indeed, simulations carried out by Mookhoek *et al.* have shown that a combination of high aspect ratio of capsules and preferential orientation of such capsules was advantageous for self-healing applications [93]. Recently, it was shown that nanocapsules could be elongated by embedding them in a film and subsequently heating and drawing the film [94], or during the electrospinning process [95]. However, there are up to now no reports about applications of elongated nanocapsules for self-healing materials.

Remarkably, metallic nanoparticles dispersed in a polymer matrix were found to migrate at the interface between the matrix and a silica layer [96]. The optimal size for the diffusion of the nanoparticles was related to the gyration radius of the polymer of the matrix, and therefore to its molecular weight. Indeed, larger particles induce an increase in entropic penalty for the incorporation of the nanoparticles in the matrix. This phenomenon favored the migration of the nanoparticles from the matrix to the crack area. On the other hand, particles that were too large diffused much shorter distances in the same time and did not reach the crack. Such a feature could be advantageously used for very small nanocontainers to deliver preferentially the payload to the crack.

Some of the challenges and limits for self-healing materials based on nanocapsules and nanofibers are common with other extrinsic self-healing materials. The main problem is the fact that the encapsulated self-healing agents are consumed once the capsule's shell is opened. Several solutions with different levels of complexity could overcome this major issue. The nanocontainers could be re-filled after use. Although it is probably very delicate in the case of nanocapsules, it might be possible for nanofibers if the extremities of the fibers are available to feed again their core with self-healing agents after use, similarly to the approach followed for self-healing materials based on a vascular network [97]. A second possibility would be to create multicompartment materials with compartments that are locally or selectively opened and, therefore, would allow a repeated release of self-healing agents. The methods to produce multicompartment nanoparticles [98] or fibers [31] are available and, hence, could be used for self-healing materials. Another option is to follow a long-lasting dream for many chemists, which is the synthesis of self-reproducing, self-healing materials. Since the amount of self-healing agent is limited by the volume of the core in core-shell structures, artificial self-replicators [99] would be needed to allow a repeated self-healing of the matrix.

Abbreviations

1-BSA: 1-H-benzotriazole-4-sulfonic acid

8HQ: 8-hydroxyquinoline

AEMA: 2-aminoethylmethacrylate hydrochloride

AFM: atomic force microscopy

APTES: 3-aminopropyltriethoxysilane

BTA: benzotriazole

CB[6]: cucurbit[6]uril

D4: octamethylcyclotetrasiloxane

DCPD: dicyclopentadiene

Dinorbornene: 1,6-hexanediol di(endo, exo-norborn-2-ene-5-carboxylate)

DVB: 1,2-divinylbenzene and 1,4-divinylbenzene

LDH: layered double hydroxide

IPDI: isophorone diisocyanate

LMA: lauryl methacrylate

MAA: methacrylic acid
 MBT: 2-mercaptobenzothiazole
 MPTMS: 3-mercaptopropyltrimethoxysilane
 PAH: poly(allylamine hydrochloride)
 PAN: polyacrylonitrile
 PDDA: poly(diallyldimethylammonium chloride)
 PDMS-DE: poly(dimethylsiloxane) diglycidyl ether terminated
 PEG-MA: poly(ethylene glycol) methyl ether methacrylate
 PEI: polyethyleneimine
 PLLA: poly(L-lactide)
 PMA: poly(methacrylic acid)
 PMMA: poly(methyl methacrylate)
 PPO: poly(2,6-dimethyl-1,4-phenylene oxide)
 PSMA: poly(styrene-co-maleic anhydride)
 PSS: poly(sodium 4-styrenesulfonate)
 PU: poly(urethane)
 PUF: poly(urea-formaldehyde)
 PVAc: poly(vinyl acetate)
 PVCi: poly(vinyl cinnamate)
 PVF: poly(vinylformal)
 ROMP: ring-opening metathesis polymerization
 S: styrene
 SH: self-healing
 SMA: potassium salt of 3-sulfopropyl methacrylate
 TEGDMA: triethylene glycol dimethacrylate
 TEOS: tetraethylorthosilicate
 Tetrathiol: pentaerythritol tetrakis(3-mercaptopropionate)

References

- White, S.R., Sottos, N.R., Geubelle, P.H., Moore, J.S., Kessler, M.R., Sriram, S.R., Brown, E.N., and Viswanathan, S. (2001) Autonomic healing of polymer composites. *Nature*, **409**, 794–798.
- Esser-Kahn, A.P., Odom, S.A., Sottos, N.R., White, S.R., and Moore, J.S. (2011) Triggered release from polymer capsules. *Macromolecules*, **44**, 5539–5553.
- Amendola, V., and Meneghetti, M. (2011) *Self-Healing at the Nanoscale: Mechanisms and Key Concepts of Natural and Artificial Systems*. CRC Press Inc.
- Amendola, V., and Meneghetti, M. (2009) Self-healing at the nanoscale. *Nanoscale*, **1**, 74–88.
- Jackson, A.C. (2011) Novel encapsulation technologies for small size-scale self-healing applications, Dissertation, Urbana, Illinois, University of Illinois at Urbana-Champaign.
- Lovell, P.A., and El-Aasser, M.S. (1997) *Emulsion Polymerization and Emulsion Polymers*, Wiley-VCH.
- Landfester, K., and Crespy, D. (2012) in *Synthesis of Polymers* (eds D.A. Schlüter, C. Hawker, and J. Sakamoto), Wiley-VCH, p. 449.
- Crespy, D., and Landfester, K. (2010) Miniemulsion polymerization as a versatile tool for the synthesis of functionalized polymers. *Beilstein J. Org. Chem.*, **6**, 1132–1148.
- Crespy, D., and Landfester, K. (2011) Making dry fertile: a practical tour of non-aqueous emulsions and

- mini-emulsions, their preparation and some applications. *Soft Matter*, **7**, 11054–11064.
- 10 Landfester, K. (2000) Recent developments in mini-emulsions – formation and stability mechanisms. *Macromol. Symp.*, **150**, 171–178.
 - 11 Meier, W. (2000) Polymer nanocapsules. *Chem. Soc. Rev.*, **29**, 295–303.
 - 12 Landfester, K. (2009) Mini-emulsion polymerization and the structure of polymer and hybrid nanoparticles. *Angew. Chem. Int. Ed.*, **48**, 4488–4507.
 - 13 Scott, C., Wu, D., Ho, C.C., and Co, C.C. (2005) Liquid-core capsules via interfacial polymerization: a free-radical analogy of the nylon rope trick. *J. Am. Chem. Soc.*, **127**, 4160–4161.
 - 14 Torini, L., Argillier, J.F., and Zydowicz, N. (2005) Interfacial polycondensation encapsulation in mini-emulsion. *Macromolecules*, **38**, 3225–3236.
 - 15 Crespy, D., Stark, M., Hoffmann-Richter, C., Ziener, U., and Landfester, K. (2007) Polymeric nanoreactors for hydrophilic reagents synthesized by interfacial polycondensation on mini-emulsion droplets. *Macromolecules*, **40**, 3122–3135.
 - 16 Crespy, D., Musyanovych, A., and Landfester, K. (2006) Synthesis of polymer particles and nanocapsules stabilized with PEO/PPO containing polymerizable surfactants in mini-emulsion. *Colloid Polym. Sci.*, **284**, 780–787.
 - 17 Peng, M., Chen, M., Zhou, S., Wu, L., and Ma, X. (2008) Fabrication of hollow silica spheres using droplet templates derived from a mini-emulsion technique. *J. Colloid Interface. Sci.*, **321**, 67–73.
 - 18 Pang, H.B., Zhou, S.X., Wu, L.M., Chen, M., and Cu, G.X. (2010) Fabrication of silicone oil microcapsules with silica shell by mini-emulsion method. *Colloid Surf. A*, **364**, 42–48.
 - 19 Fickert, J., Rupper, P., Graf, R., Landfester, K., and Crespy, D. (2012) Design and characterization of functionalized silica nanocontainers for self-healing materials. *J. Mater. Chem.*, **22**, 2286–2291.
 - 20 Cao, Z.H., Dong, L.Z., Li, L., Shang, Y., Qi, D.M., Lv, Q., Shan, G.R., Ziener, U., and Landfester, K. (2012) Preparation of mesoporous submicrometer silica capsules via an interfacial sol-gel process in inverse mini-emulsion. *Langmuir*, **28**, 7023–7032.
 - 21 Decher, G. (1997) Fuzzy nanoassemblies: toward layered polymeric multicomposites. *Science*, **277**, 1232–1237.
 - 22 Caruso, F., Caruso, R.A., and Mohwald, H. (1998) Nanoengineering of inorganic and hybrid hollow spheres by colloidal templating. *Science*, **282**, 1111–1114.
 - 23 Sukhorukov, G., Fery, A., and Mohwald, H. (2005) Intelligent micro- and nanocapsules. *Prog. Polym. Sci.*, **30**, 885–897.
 - 24 Tiarks, F., Landfester, K., and Antonietti, M. (2001) Preparation of polymeric nanocapsules by mini-emulsion polymerization. *Langmuir*, **17**, 908–918.
 - 25 Luo, Y.W., and Zhou, X.D. (2004) Nanoencapsulation of a hydrophobic compound by a mini-emulsion polymerization process. *J. Polym. Sci. Polym. Chem.*, **42**, 2145–2154.
 - 26 Loxley, A., and Vincent, B. (1998) Preparation of Poly(methylmethacrylate) microcapsules with liquid cores. *J. Colloid Interface. Sci.*, **208**, 49–62.
 - 27 Torza, S., and Mason, S.G. (1970) *J. Colloid Interface. Sci.*, **33**, 67–83.
 - 28 Ramakrishna, S., Fujihara, K., Teo, W.-E., Lim, T.C., and Ma, Z. (2005) *An Introduction to Electrospinning and Nanofibers*, World Scientific Publishing Co. Pte. Ltd.
 - 29 Li, D., and Xia, Y. (2004) Electrospinning of nanofibers: reinventing the wheel? *Adv. Mater.*, **16**, 1151–1170.
 - 30 Greiner, A., and Wendorff, J.H. (2007) Wendorff electrospinning: a fascinating method for the preparation of ultrathin fibers. *Angew. Chem. Int. Ed.*, **46**, 5670–5703.
 - 31 Crespy, D., Friedemann, K., and Popa, A.-M. (2012) Colloid-electrospinning: fabrication of multicompartiment nanofibers by the electrospinning of organic or/and inorganic dispersions and emulsions. *Macromol. Rapid Commun.*, **33**, 1978–1995.
 - 32 Yarin, A.L. (2010) Coaxial electrospinning and emulsion electrospinning of core-shell fibers. *Polym. Adv. Technol.*, **22**, 310–317.
 - 33 Blaiszik, B.J., Sottos, N.R., and White, S.R. (2008) Nanocapsules for self-healing

- materials. *Compos. Sci. Technol.*, **68**, 978–986.
- 34 Jackson, A.C., Blaiszik, B.J., McIlroy, D., Sottos, N.R., and Braun, P.V. (2008) New capsule chemistries for nanoscale self-healing. *Polym. Prepr.*, **49**, 967–968.
- 35 Ouyang, X.B., Huang, X.Q., Pan, Q.H., Zuo, C.Q., Huang, C., Yang, X.L., and Zhao, Y.B. (2011) Synthesis and characterization of triethylene glycol dimethacrylate nanocapsules used in a self-healing bonding resin. *J. Dent.*, **39**, 825–833.
- 36 Fickert, J., Makowski, M., Kappl, M., Landfester, K., and Crespy, D. (2012) Efficient encapsulation of self-healing agents in polymer nanocontainers functionalized by orthogonal reactions. *Macromolecules*, **45**, 6324–6332.
- 37 van den Dungen, E.T.A., and Klumpermann, B. (2011) Synthesis of liquid-filled nanocapsules via the miniemulsion technique. *J. Polym. Sci. Polym. Chem.*, **48**, 5215–5230.
- 38 Zhao, Y., Fickert, J., Landfester, K., and Crespy, D. (2012) Encapsulation of self-healing agents in polymer nanocapsules. *Small*, **8**, 2954–2958.
- 39 Jackson, A.C., Bartelt, J.A., Marczewski, K., Sottos, N.R., and Braun, P.V. (2011) Silica-protected micron and sub-micron capsules and particles for self-healing at the microscale. *Macromol. Rapid Commun.*, **32**, 82–87.
- 40 Maia, F., Tedim, J., Lisenkov, A.D., Salak, A.N., Zheludkevich, M.L., and Ferreira, M.G.S. (2012) Silica nanocontainers for active corrosion protection. *Nanoscale*, **4**, 1287–1298.
- 41 Pang, J.W.C., and Bond, I.P. (2005) Bleeding composites' damage detection and self-repair using a biomimetic approach. *Compos. Part A-Appl. Sci. Manuf.*, **36**, 183–188.
- 42 Williams, G., Trask, R., and Bond, I. (2007) A self-healing carbon fibre reinforced polymer for aerospace applications. *Compos. Part A-Appl. Sci. Manuf.*, **38**, 1525–1532.
- 43 Trask, R.S., and Bond, I.P. (2006) Biomimetic self-healing of advanced composite structures using hollow glass fibres. *Smart Mater. Struct.*, **15**, 704–710.
- 44 Trask, R.S., Williams, G.J., and Bond, I.P. (2007) Bioinspired self-healing of advanced composite structures using hollow glass fibres. *J. R. Soc. Interface*, **4**, 363–371.
- 45 Xiao, D.S., Yuan, Y.C., Rong, M.Z., and Zhang, M.Q. (2009) A facile strategy for preparing self-healing polymer composites by incorporation of cationic catalyst-loaded vegetable fibers. *Adv. Funct. Mater.*, **19**, 2289–2296.
- 46 Bleay, S.M., Loader, C.B., Hawyes, V.J., Humberstone, L., and Churtis, P.T. (2001) A smart repair system for polymer matrix composites. *Compos. Part A-Appl. Sci. Manuf.*, **32**, 1767–1776.
- 47 Fix, D., Andreeva, D.V., Lvov, Y.M., Shchukin, D.G., and Möhwald, H. (2009) Application of inhibitor-loaded halloysite nanotubes in active anti-corrosive coatings. *Adv. Funct. Mater.*, **19**, 1720–1727.
- 48 Abdullayev, E., and Lvov, Y. (2010) Clay nanotubes for corrosion inhibitor encapsulation, release control with end stoppers. *J. Mater. Chem.*, **20**, 6681–6687.
- 49 Sinha-Ray, S., Pelot, D.D., Zhou, Z.P., Rahman, A., Wu, X.F., and Yarin, A.L. (2012) Encapsulation of self-healing materials by coelectrospinning, emulsion electrospinning, solution blowing and intercalation. *J. Mater. Chem.*, **22**, 9138–9146.
- 50 Wang, C.H., Sidhu, K., Yang, T., Zhang, J., and Shanks, R. (2012) Interlayer self-healing and toughening of carbon fibre/epoxy composites using copolymer films. *Compos. Part A-Appl. Sci. Manuf.*, **43**, 512–518.
- 51 Kousourakis, A., and Mouritz, A.P. (2010) The effect of self-healing hollow fibres on the mechanical properties of polymer composites. *Smart Mater. Struct.*, **19**, 085021.
- 52 Lvov, Y.M., Shchukin, D.G., Möhwald, H., and Price, R.R. (2008) Halloysite clay nanotubes for controlled release of protective agents. *ACS Nano*, **2**, 814–820.
- 53 Lanzara, G., Yoon, Y., Liu, H., Peng, S., and Lee, W.I. (2009) Carbon nanotube reservoirs for self-healing materials. *Nanotechnology*, **20**, 335704.

- 54 Zheludkevich, M.L., Tedim, J., and Ferreira, M.G.S. (2012) "Smart" coatings for active corrosion protection based on multi-functional micro and nanocontainers. *Electrochim. Acta.*, **82**, 314–323.
- 55 Shchukin, D.G., and Möhwald, H. (2011) Smart nanocontainers as depot media for feedback active coatings. *Chem. Commun.*, **47**, 8730–8739.
- 56 Shchukin, D.G., and Möhwald, H. (2007) Self-repairing coatings containing active nanoreservoirs. *Small*, **3**, 926–943.
- 57 Bédard, M.F., Geest, B.G.D., Skirtach, A.G., Möhwald, H., and Sukhorukov, G.B. (2010) Polymeric microcapsules with light responsive properties for encapsulation and release. *Adv. Colloid Interface*, **158**, 2–14.
- 58 Litano, H., Oehmichen, T., and Ise, N. (1991) Photo-degradable polymer microcapsules. *Makromol. Chem.*, **192**, 1107–1114.
- 59 Kono, K., Nishihara, Y., and Takacishi, T. (1995) Photoresponsive permeability of polyelectrolyte complex capsule membrane containing triphenylmethane leucohydroxide residues. *J. Appl. Polym. Sci.*, **56**, 707–713.
- 60 Park, M.K., Deng, S., and Advincula, R.C. (2005) Sustained release control via photo-cross-linking of polyelectrolyte layer-by-layer hollow capsules. *Langmuir*, **21**, 5272–5277.
- 61 Fomina, N., McFearin, C., Sermsakdi, M., Edigin, O., and Almutairi, A. (2010) UV and near-IR triggered release from polymeric nanoparticles. *J. Am. Chem. Soc.*, **132**, 9540–9542.
- 62 Tao, X., Li, J.B., and Möhwald, H. (2004) Self-assembly, optical behavior, and permeability of a novel capsule based on an azo dye and polyelectrolytes. *Chem. Eur. J.*, **10**, 3397–3403.
- 63 Angelatos, A.S., Radt, B., and Caruso, F. (2005) Light-responsive polyelectrolyte/gold nanoparticle microcapsules. *J. Phys. Chem. B*, **109**, 3071–3076.
- 64 Radt, B., Smith, T.A., and Caruso, F. (2004) Optically addressable nanostructured capsules. *Adv. Mater.*, **16**, 2184–2189.
- 65 Javier, A.M., del Pino, P., Bedard, M.F., Ho, D., Skirtach, A.G., Sukhorukov, G.B., Plank, C., and Parak, W.J. (2008) Photoactivated release of cargo from the cavity of polyelectrolyte capsules to the cytosol of cells. *Langmuir*, **24**, 12517–12520.
- 66 Katagiri, K., Koumoto, K., Iseya, S., Sakai, M., Matsuda, A., and Caruso, F. (2009) Tunable uv-responsive organic-inorganic hybrid capsules. *Chem. Mater.*, **21**, 195–197.
- 67 Skirtach, A.G., Antipov, A.A., Shchukin, D.G., and Sukhorukov, G.B. (2004) Remote activation of capsules containing ag nanoparticles and IR dye by laser light. *Langmuir*, **20**, 6988–6992.
- 68 Pastine, S.J., Okawa, D., Zettl, A., and Fréchet, J.M.J. (2009) Chemicals on demand with phototriggerable microcapsules. *J. Am. Chem. Soc.*, **131**, 13586–13587.
- 69 Grigoriev, D.O., Köhler, K., Skorb, E., Shchukin, D.G., and Möhwald, H. (2009) Polyelectrolyte complexes as a "smart" depot for self-healing anticorrosion coatings. *Soft Matter*, **5**, 1426–1432.
- 70 Jafari, A., Hosseini, S., and Jamalizadeh, E. (2010) Investigation of smart nanocapsules containing inhibitors for corrosion protection of copper. *Electrochim. Acta*, **55**, 9004–9009.
- 71 Shchukin, D.G., Zheludkevich, M., Yasakau, K.A., Lamaka, S., Ferreira, M.S.G., and Möhwald, H. (2006) Layer-by-layer assembled nanocontainers for self-healing corrosion protection. *Adv. Mater.*, **18**, 1672–1678.
- 72 Shchukin, D.G., Zheludkevich, M.L., and Möhwald, H. (2006) Feedback active coatings based on incorporated nanocontainers. *J. Mater. Chem.*, **16**, 4561–4566.
- 73 Zheludkevich, M.L., Shchukin, D.G., Yasakau, K.A., Möhwald, H., and Ferreira, M.G.S. (2007) Anticorrosion coatings with self-healing effect based on nanocontainers impregnated with corrosion inhibitor. *Chem. Mater.*, **19**, 402–411.
- 74 Dias, S.A.S., Lamak, S.V., Nogueira, C.A., Diamantino, T.C., and Ferreira, M.G.S. (2012) Sol-gel coatings modified with zeolite fillers for active corrosion protection of AA2024. *Corros. Sci.*, **62**, 153–162.

- 75 Chen, T., and Fu, J. (2012) pH-responsive nanovalves based on hollow mesoporous silica spheres for controlled release of corrosion inhibitor. *Nanotechnology*, **23**, 235605.
- 76 Borisova, D., Möhwald, H., and Shchukin, D.G. (2012) Influence of embedded nanocontainers on the efficiency of active anticorrosive coatings for aluminum alloys part i, influence of nanocontainer concentration. *ACS Appl. Mater. Interfaces*, **4**, 2931–2939.
- 77 Sonawanec, S.H., Bhanvasea, B.A., Jamalia, A.A., Dubeya, S.K., Kalea, S.S., Pinjari, D.V., Kulkarnic, R.D., Gogateb, P.R., and Pandit, A.B. (2012) Improved active anticorrosion coatings using layer-by-layer assembled ZnO nanocontainers with benzotriazole. *Chem. Eng. J.*, **189–190**, 464–472.
- 78 Wang, Y., and Zhang, D. (2011) Synthesis, characterization, and controlled release anticorrosion behavior of benzoate intercalated Zn–Al layered double hydroxides. *Mater. Res. Bull.*, **46**, 1963–1968.
- 79 Tedim, J., Poznyak, S.K., Kuznetsova, A., Raps, D., Hack, T., Zheludkevich, M.L., and Ferreira, M.G.S. (2010) Enhancement of active corrosion protection via combination of inhibitor-loaded nanocontainers. *ACS Appl. Mater. Interfaces*, **2**, 1528–1535.
- 80 Kartsonakis, I.A., and Kordas, G. (2010) Synthesis and characterization of cerium molybdate nanocontainers and their inhibitor complexes. *J. Am. Ceram. Soc.*, **93**, 65–73.
- 81 Poznyak, S.K., Tedim, J., Rodrigues, L.M., Salak, A.N., Zheludkevich, M.L., Dick, L.F.P., and Ferreira, M.G.S. (2010) Novel inorganic host layered double hydroxides intercalated with guest organic inhibitors for anticorrosion applications. *ACS Appl. Mater. Interfaces*, **1**, 2353–2362.
- 82 Andreeva, D.V., Fix, D., Möhwald, H., and Shchukin, D.G. (2008) Self-healing anticorrosion coatings based on pH-sensitive polyelectrolyte/inhibitor sandwichlike nanostructures. *Adv. Mater.*, **20**, 2789–2794.
- 83 Andreeva, D.V., Fix, D., Möhwald, H., and Shchukin, D.G. (2008) Buffering polyelectrolyte multilayers for active corrosion protection. *J. Mater. Chem.*, **18**, 1738–1740.
- 84 Wang, W., Liu, L., Ju, X.J., Zerrouki, D., Xie, R., Yang, L.H., and Chu, L.Y. (2009) A novel thermo-induced self-bursting microcapsule with magnetic-targeting property. *Chem. Phys. Chem.*, **10**, 2405–2409.
- 85 Čjková, J., Hanuš, J., and Štěpánek, F. (2010) Investigation of internal microstructure and thermo-responsive properties of composite PNIPAM/silica microcapsules. *J. Colloid Interface. Sci.*, **346**, 352–360.
- 86 Volz, M., Walther, P., Ziener, U., and Landfester, K. (2007) Nano-explosions of nanoparticles for sudden release of substances by embedded azo-components as obtained via the miniemulsion process. *Macromol. Mater. Eng.*, **292**, 1237–1244.
- 87 Chu, L.Y., Park, S.H., Yamaguchi, T., and Nakao, S. (2001) Preparation of thermo-responsive core-shell microcapsules with a porous membrane and poly(N-isopropylacrylamide) gates. *J. Memb. Sci.*, **192**, 27–39.
- 88 Gao, Q.X., Wang, C.Y., Liu, H.X., Wang, C.H., Liu, X.X., and Tong, Z. (2009) Suspension polymerization based on inverse Pickering emulsion droplets for thermo-sensitive hybrid microcapsules with tunable supracolloidal structures. *Polymer*, **50**, 2587–2594.
- 89 Gao, H.F., Yang, W.L., Min, K., Zhao, L.S., Wang, C.C., and Fu, S.K. (2005) Thermosensitive poly(N-isopropylacrylamide) nanocapsules with controlled permeability. *Polymer*, **46**, 1087–1093.
- 90 Du, P., Mu, B., Shen, R., and Liu, P. (2010) Well-defined thermo-responsive polymeric nanocapsules by a one-pot method via surface-initiated atom transfer radical copolymerization. *IET Nanobiotechnol.*, **4**, 72–76.
- 91 Ma, Y., Dong, W.-F., Hempenius, M.A., Mohwald, H., and Vancso, G.J. (2006) Redox-controlled molecular permeability of composite-wall microcapsules. *Nat. Mater.*, **5**, 724–729.
- 92 Staff, R.H., Gallei, M., Mazurowski, M., Rehahn, M., Berger, R., Landfester, K.,

- and Crespy, D. (2012) Patchy nanocapsules of Poly(vinylferrocene)-based block copolymers for redox-responsive release. *ACS Nano.*, **6**, 9042–9049.
- 93 Mookhoek, S.D., Fischer, H.R., and Van der Zwaag, S. (2009) A numerical study into the effects of elongated capsules on the healing efficiency of liquid-based systems. *Comput. Mater. Sci.*, **47**, 506–511.
- 94 Herrmann, C., Bannwarth, M.B., Landfester, K., and Crespy, D. (2012) Re-dispersible anisotropic and structured nanoparticles: formation and their subsequent shape change. *Macromol. Chem. Phys.*, **213**, 829–838.
- 95 Herrmann, C., Turshatov, A., and Crespy, D. (2012) Fabrication of polymer ellipsoids by the electrospinning of swollen nanoparticles. *ACS Macro Lett.*, **1**, 907–909.
- 96 Gupta, S., Zhang, Q., Emrick, T., Balazs, A.C., and Russell, T.P. (2006) *Nat. Mater.*, **5**, 229–233.
- 97 Toohey, K.S., Sottos, N.R., Lewis, J.A., Moore, J.S., and White, S.R. (2007) Self-healing materials with microvascular networks. *Nat. Mater.*, **6**, 581–585.
- 98 Crespy, D., Staff, R.H., Becker, T., and Landfester, K. (2012) Chemical routes toward multicompartiment colloids. *Macromol. Chem. Phys.*, **213**, 1183–1189.
- 99 Vidonne, A., and Philp, D. (2009) Making molecules make themselves – the chemistry of artificial replicators. *Eur. J. Org. Chem.*, 593–610.

Part Three
Supramolecular Systems

11

Self-Healing Polymers via Supramolecular, Hydrogen-Bonded Networks^{*)}

Florian Herbst and Wolfgang H. Binder

11.1

Introduction

The technological design of self-healing polymers also demands the possibility to achieve multiple healing cycles, thus requesting more complex strategies than those just relying on covalent bonding. This chapter deals with concepts and realizations to generate polymeric materials capable of executing multiple self-healing cycles due to the supramolecular nature of the interactions between their chains.

The concept of supramolecular self-healing materials relies on the use of noncovalent, transient bonds to generate networks, which are able to heal the damaged site. Thus, the aspect of reversibility and dynamics of a network [1, 2] and its underlying supramolecular bonds is crucial for the understanding and design of self-healing polymers via this concept. Supramolecular interactions [3–8] can affect material properties, such as the polymers' strength (moduli), viscosity and flow, as well as the intrinsic ordering of polymer chains. The additional dynamic behavior in turn adds new features of stimuli-responsiveness towards external damage to the material properties, thus making them ideal candidates for self-healing materials.

A general process of self-healing is depicted in Figure 11.1, demonstrating the basic steps of self-healing in supramolecular polymers. First (see Figure 11.1a) the undamaged material, consisting of polymer chains with attached supramolecular bonds, forms a network by bonds able to connect and reconnect via reversible “sticker-like” behavior. Thus, in contrast to “conventional” polymeric materials, the strength of the material is generated by the “stickiness” of the supramolecular bonds, and is not a consequence of covalent bonds or chain entanglement. Crucial for the network formation is a specific interaction between the two different supramolecular bonds linking the different polymer chains. After damage has occurred via external forces, leading to a crack (Figure 11.1b), the generated new interface contains a multitude of now unbound supramolecular bonds, which remain “sticky” at the fractured surface for a certain period of time. Thus,

*) This chapter is partially based on thoughts published in *Macromol. Rapid Commun.* (2013), **34** (3), 203–220, written and designed by the very same authors.

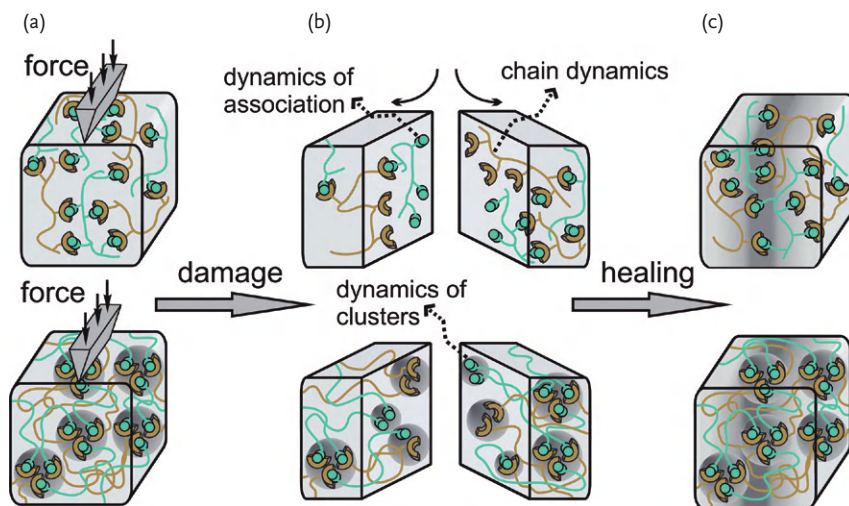


Figure 11.1 Self-healing mechanism for a supramolecular polymer: (a) When the material is cut into two halves the weak supramolecular bonds (top) or clusters (bottom) are broken preferentially; (b) the hydrogen-bonding motifs stay unassociated

on the fractured surface for a certain period of time, but can rearrange as well; (c) after being brought into contact again the supramolecular bonds or clusters are re-formed, thus the crack is healed.

recombination of the two fragments leads to reformation of the supramolecular bonds, closing the gap and healing the damaged site (Figure 11.1c).

The possibility of repeatedly conducting the healing event even after multiple damages have occurred is a central advantage of supramolecular self-healing materials, putting them on the frontline for application in industry.

One can imagine that the possibility and time to heal the damaged site depends at least on two factors, the first being the time by which the supramolecular “stickers” recombine, the second being sufficient chain dynamics of the individual polymer chains, necessary to enable mobility of the supramolecular groups. Thus, controllable dynamics of the supramolecular interactions within or attached to a polymer with sufficient chain mobility and overall good mechanical properties are required for the design of such self-healing polymers [9, 10]. Particularly, rubbery behavior can be a direct consequence of either supramolecular association [11–13], or concomitant phase separation processes active within the polymeric materials [14–17]. Both principles can contribute to a successful design of the self-healing supramolecular material and are, therefore, considered in this chapter.

The dynamics of the attached polymer chains and the dynamic behavior of supramolecular networks in gels [18, 19] and in bulk are discussed separately. The underlying models [20–22] to understand the dynamics and strength of polymeric supramolecular networks (sticky-Rouse- [20, 23–26], sticky-reptation- [21] or “living”-reptation-model [27]) have been referred to already. In this chapter examples of self-healing polymers are described, focusing on hydrogen-bonds and π - π interactions as supramolecular interactions.

Hydrogen bonds [29] have emerged as one of the most important supramolecular bonds in chemistry and polymer science [3–5], since their binding strength (“stickiness”) as well as their association dynamics can be tuned over a large range of orders of magnitude. Additionally, due to their high structural variability hydrogen bonds have attracted many scientists in the past. A special feature of hydrogen bonds is their ability to assemble in a directional and specific mode of association, which is most brilliantly demonstrated in biomimetic polymers [30] where their self-aggregation generates hydrogen-bonded networks [11, 31].

In order to apply supramolecular interactions, for example, for the formation of networks, one main challenge is to deal with the weak binding energy of a supramolecular interaction $0.5\text{--}40\text{ kJ Mol}^{-1}$ for a hydrogen bond (an ordinary C–C-bond has a binding energy of $\sim 345\text{ kJ Mol}^{-1}$) [29]. Therefore, the main parameters to control self-healing in supramolecular polymers are the strength and number of the involved hydrogen bonds. For relevant hydrogen-bonding motifs (see Figure 11.2), as a rule of the thumb, an additional hydrogen bond implies a stronger interaction with a value of about 7.4 kJ Mol^{-1} per bond [3]. This challenge has led to the development of different hydrogen-bonding motifs which exhibit a strong directed association (several hydrogen bonds involved). Due to their dynamic feature materials containing these groups were often called “dynamers”, a term introduced by Nobel prize winner Jean-Marie Lehn [32, 33]. Some prominent examples of supramolecular bonds used for self-healing materials are shown in Figure 11.2, including Meijer’s 2-ureido-4[1H]-pyrimidinone dimers [34] (self-complementary) (a), the thymine (b, left)/2,6-diaminotriazine (b, right) interaction [11, 16, 17, 35], the Hamilton wedge (c, right)/barbituric acid system (c, left) [18, 36], Zimmerman’s 2,7-diamido-1,8-naphthyridine (d, right)/guanosine motif (d, left) [37], the association of Bouteiller’s [38] 2,4-bis(2-ethylhexyl-ureido)toluene (e, EHUT) and a strong quadruple hydrogen bonding motif (g) invented by Blight *et al.* [39]. The stacking of electron-poor naphthalene-diimide (g, top and bottom) and electron-rich pyrene groups (g, middle), as published by Greenland *et al.* [40], is shown as an example utilizing $\pi\text{--}\pi$ -interactions.

Even the strongest of the above-mentioned interactions (Figure 11.2f) with a binding free energy (ΔG) of -71 kJ Mol^{-1} reaches only $\sim 20\%$ of the thermodynamic stability of a carbon–carbon covalent bond [39]. Hence, when both covalent bonds and supramolecular bonds are present in a material and mechanical stress is applied, it will be the weaker supramolecular bond which fails. Due to the inherent dynamic reversible character of the supramolecular bond its re-formation is possible, thus enabling recovery of the pristine properties. The extent of “healing” can be expressed by the healing efficiency:

$$\text{Healing efficiency} = \frac{\text{Mechanical value}_{\text{healed}}}{\text{Mechanical value}_{\text{pristine}}} * 100$$

and must be determined separately for each mechanical property.

To create a supramolecular network from smaller building blocks different concepts can be applied (see Figure 11.3). Linear chain extension of unentangled polymers bearing associative groups can lead to the formation of significantly longer

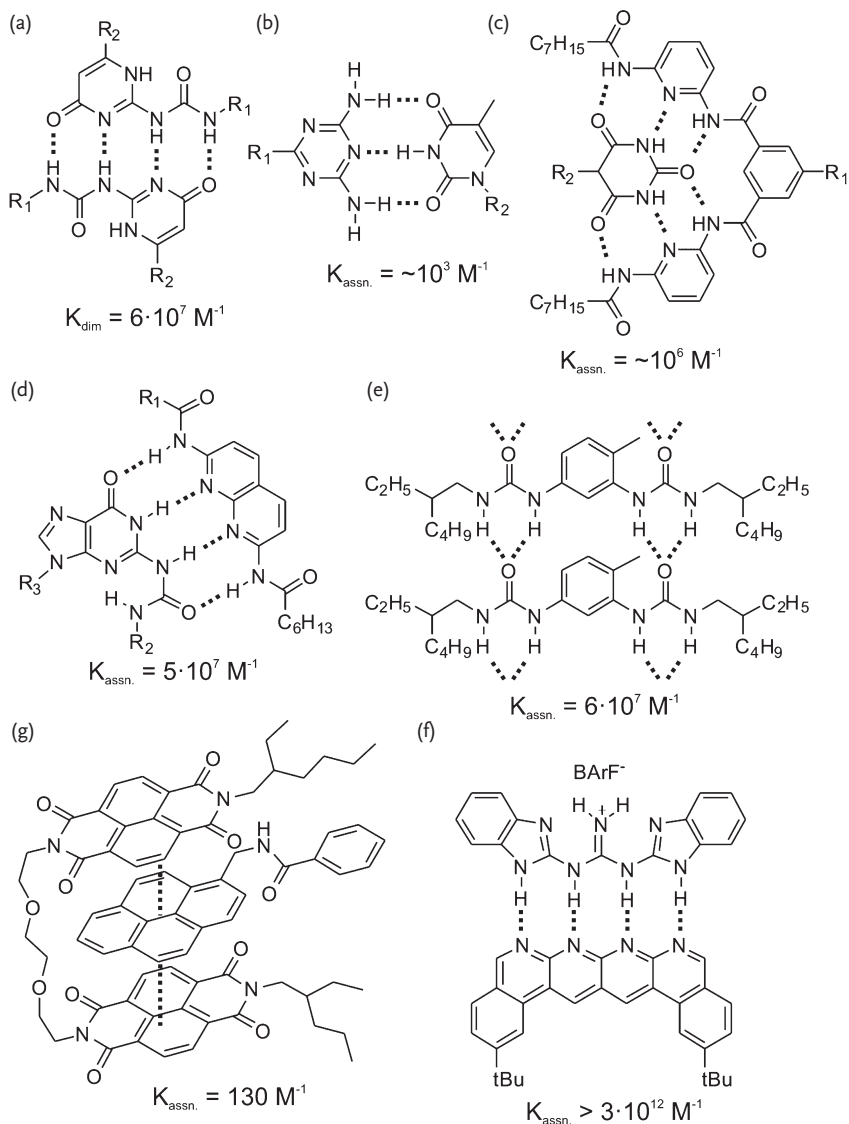


Figure 11.2 Different supramolecular binding motifs utilizing hydrogen bonds (a–f) and π - π -stacking (g). Values for $K_{\text{assn.}}$ are provided in an inert solvent (CHCl_3).

entangled supramolecular chains (expressed by a virtual degree of polymerization) (Figure 11.3a) [41], thus creating a network due to effective entanglements.

In the case of association of more than two functional groups, network formation occurs due to the formation of tie-points (crosslinks) connecting several polymer strands (Figure 11.3b) [11, 42]. Furthermore, polymer chains where several functional groups are distributed along the polymer chain form supramo-

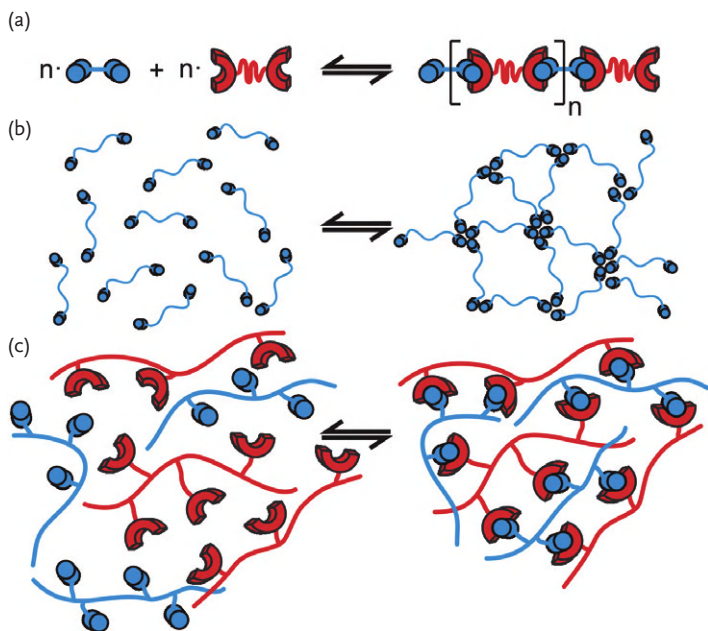


Figure 11.3 Different modes of association leading to the formation of a supramolecular network.

lecular networks (Figure 11.3c) [43]. These graft-polymers can also be interconnected via low molecular weight bifunctional spacers [44].

Not only the binding energy, which dictates the extent of network formation, but also the dynamics of each binding system, the influence of temperature, concentration, and, most importantly, the effect of the surrounding polymer matrix, which by itself can act as a “solvent” for the supramolecular bonding motif in polymeric melts and in the bulk, can influence the “stickiness” of a hydrogen bond. We will discuss these influences in the following sections, first shedding light on the dynamics of hydrogen bonds in polymer solutions.

11.2 Dynamics of Hydrogen Bonds in Solution

For a specific set of supramolecular associating groups A and B the possible modes of aggregation are as simple as displayed in (Figure 11.4). Besides the desired A–B formation the dimerization of each group, A–A and B–B, is possible. Each species is in a permanent dynamic equilibrium, which is expressed by the association constant $K_{\text{assn.}}$ (for the formation of A–B) or the dimerization constant $K_{\text{dim.}}$ (A–A or B–B). Since $K_{\text{assn.}}$ is often large (see Figure 11.2) in comparison to $K_{\text{dim.}}$ (usually in the range of $K_{\text{dim.}} < 100 \text{ M}^{-1}$) the dimerization can be neglected in solution.

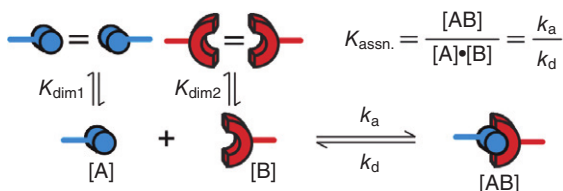


Figure 11.4 Modes of aggregation in solution for complementary groups A and B.

According to this model the association constant $K_{\text{assn.}}$ is defined by the ratio of the rate of association (k_a) and rate of dissociation (k_d), k_a/k_d (see Figure 11.4). It was shown by Hammes *et al.* [45] that the rate of association in solution is often a diffusion-controlled process, thus expressing the rate of dissociation (k_d) as a direct measure of the strength of the hydrogen bond, also expressed by the bond lifetime τ_d ($\tau_d = 1/k_d$). This observation holds true for many binding motifs, except for a few systems where, for example, tautomers [46], or an energetic conformation bias [47] are significant, where the rate of association (k_a) is not diffusion controlled.

For bifunctional monomers (Figure 11.3a) the formation of supramolecular chains consisting of numerous initial building blocks takes place. The extent of aggregation can be described by a virtual degree of polymerization (DP), which is dependent on $K_{\text{assn.}}$, the concentration (c) of the monomer, the solvent and the temperature. To calculate the relation between DP, $K_{\text{assn.}}$ and c it is necessary to control the monomer concentration independently from the DP. This was accomplished by the use of chain-stoppers [6], revealing the following correlation:

$$DP = [K_{\text{assn.}} \cdot c]^{0.5}$$

Thus, the attachment of a hydrogen-bonding motif onto both chains ends of a polymer will cause a remarkable change in the viscoelastic properties in comparison to the blank polymer, for example, an increase in the solution viscosity [48, 49].

In order to create a strong *and* dynamic supramolecular network (as a basic requirement for a self-healing material), the DP must be sufficiently high to form effective entanglements. For an arbitrary binding motif (fixed $K_{\text{assn.}}$ and solvent) this can be achieved by an increase in the concentration, by a decrease in the temperature ($DP \sim T^{-1}$) or by using multivalent monomers (acting as crosslinkers). Under certain critical conditions ($c_{\text{crit.}}$ or $T_{\text{crit.}}$) one will observe a transition from the solution or sol-phase to a gel-phase. Supramolecular self-healing gels will be discussed in the next section.

11.3 Supramolecular Gels

Important for determining the strength of a supramolecular network is the timescale of opening/closing (τ_b) of the supramolecular crosslinks, the statistical

chain length between two crosslinking points (M_c), and the temperature dependence of the supramolecular interaction. Control of the relation between the strength of the network and the dynamics of the supramolecular bonds is thus crucial [50]. The plateau modulus (G_N) resulting from reversible (e.g., supramolecular) crosslinks and those crosslinks resulting from entanglements can be used to estimate the number of permanent and transient crosslinks (n_{plat}) within a supramolecular (rubbery) network. An expansion of this concept was reported [51–54], which allows to calculate bond-lifetimes in metallo-supramolecular gels by monitoring the plateau modulus in oscillatory, frequency-dependent measurements. This concept can further be extended to hydrogen-bonded graft-polymers in the melt state, so that both, the network strand density (ν_2) and the segment length between two supramolecular crosslinking points (M_c), [50] can be determined.

As stated above, a supramolecular network can be formed by the formation of either effective entanglements [55] or crosslinks (or both) [56]. For given conditions (temperature, concentration and binding motif) the existence of the network is dictated by the lifetime of the hydrogen bond. A suitable tool to investigate the time-dependent mechanical properties in the solvent free state is available by frequency-dependent rheology measurements. A typical frequency sweep measurement for a supramolecular gel is sketched in Figure 11.5. At high frequencies (short times) the bond lifetime τ_d is long in comparison to the applied frequency ($\tau_d > \tau$). As a result, the supramolecular bonds are monitored in the closed state and the material behaves similar to a permanently crosslinked network. At lower frequencies (long times), the supramolecular bonds are monitored in the open state ($\tau_d < \tau$, slope of $G' = 2$, slope of $G'' = 1$), thus the materials properties are dictated by the middle segments (between the hydrogen-bonding motifs). The transition between these two states ($\tau_d = \tau$) is called the gel point.

However, it is the density of the network, and thus the mobility of the polymer chains, which influences the lifetime of the reversible bonds. To break a tie-point, first the supramolecular bond must be in the open state, and secondly both groups must depart from each other. Since the chain mobility is limited by the network

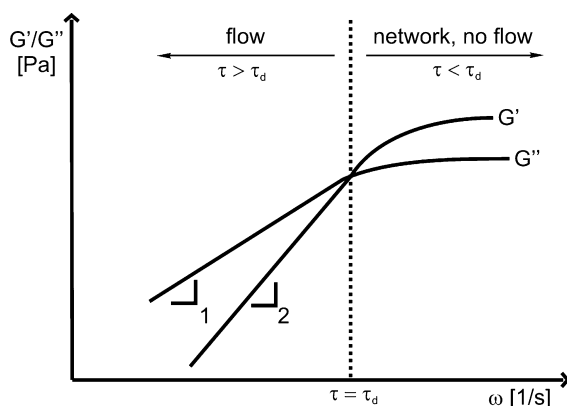


Figure 11.5 Typical frequency sweep measurement for a dynamic supramolecular gel.

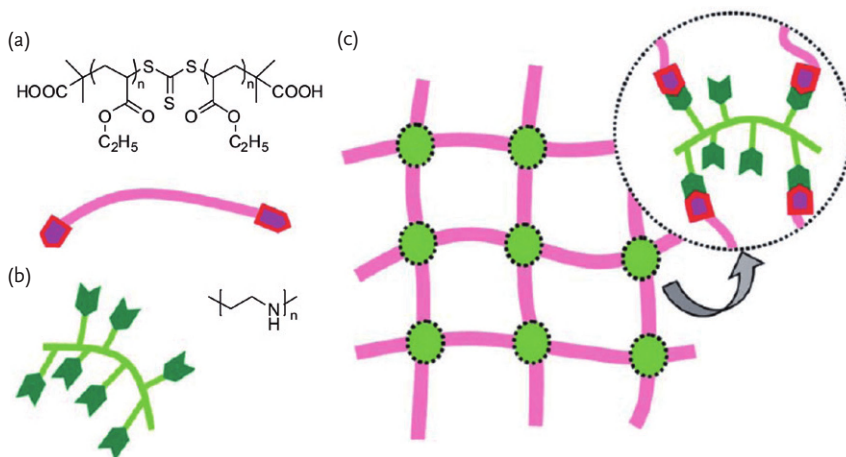


Figure 11.6 Formation of a supramolecular gel, reported by Noro *et al.* [44]. Reproduced with permission from RSC Publishing.

density (or the limited mobility of surrounding chains due to supramolecular bonding) an individual bond can open and close several times before the two groups finally depart from each other. As a result, it is rather the effective bond lifetime τ_d^* than the “ordinary” bond lifetime τ_d ($\tau_d^* > \tau_d$) that is crucial for understanding the network-dynamics. Therefore, it is not necessary to use strong hydrogen-bonding motifs (with high K_{assn} and slow τ_d), since even weak systems are reasonably applicable as soon as their effective bond lifetime is in the range of $1 \mu\text{s} < \tau_d^* < 1 \text{min}$ [57]. As a result, for creation of a self-healing supramolecular material one has to find a compromise between a sufficiently high number of tie-points and sufficient mobility of the polymer chains. While tie-points give mechanical strength to the material (in terms of a high G_N , tensile strength, etc.), the mobility of the polymer chains is constricted, thus slowing the self-healing dynamics [58].

It was shown by Noro *et al.* [44], that carboxyl-terminated telechelic poly(ethylacrylate) (PEA) (Figure 11.6a) and poly(ethyleneimine) (PEI) (Figure 11.6b) form a supramolecular network in THF/methanol ($v:v = 1:1$) (Figure 11.6c), although only one hydrogen bond is formed between both groups. PEA and PEI are immiscible under these conditions, leading to the formation of PEI cores surrounded by the PEA matrix (swollen with the solvent). Therefore, it is the connection of the PEI cores via hydrogen bonding which leads to the formation of the supramolecular network. As a result one has to refrain from using the simple association model in solution, since in polymeric gels additional effects emerge, including microphase separation [44], stacking [59–61], or fiber formation [62, 63].

Vidvasagar *et al.* reported on self-healing gels made from mannitol-based diols flanked by two ketal moieties (Figure 11.7a) [62]. Although only weak hydrogen bonds are involved these low molecular weight molecules form gels in different

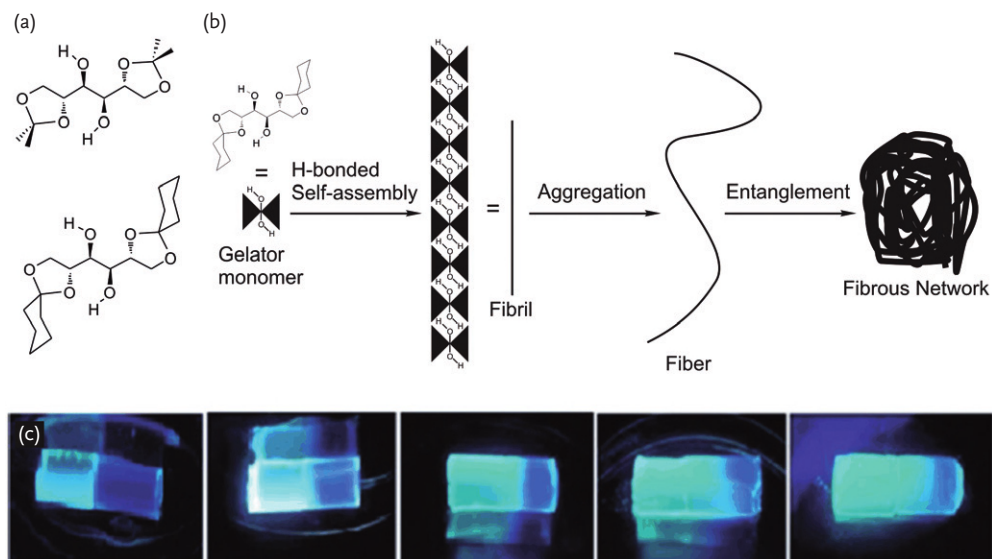


Figure 11.7 (a) Mannitol-based diols. (b) Aggregation of diols into a fibrous network. (c) Self-healing experiment of a pyrene-doped gel fused to an undoped gel. Both gels are made from the upper diol in pump oil at 1 wt% concentration. Figure reproduced according to Vidyasagar *et al.* [62]. With permission from John Wiley & Sons, Inc.

solvents, due to the aggregation into long fibers which can entangle to form a fibrous network (Figure 11.7b). Figure 11.7c shows a self-healing experiment of the diol (Figure 11.7a top) in pump oil (at 1 wt% concentration). A pyrene-doped part (left side) was fused to an undoped part and left for several days, showing the blue glowing color migrating into the undoped part. The dynamic equilibrium between free dissolved and assembled molecules leads to a continuous formation and dissociation of fibers, allowing the pyrene molecules to move into the undoped part. It is noteworthy that these gels, although dynamic in nature, exhibit a permanent shape. However, no mechanical analysis of these gels was reported.

A reasonable improvement for the use of gels would be the use of water as a non-toxic, inexpensive and easy accessible “green” solvent, to form hydrogels [64]. However, a main disadvantage of water is its ability to form hydrogen bonds with the hydrogen-bonding motifs, reducing the association constant $K_{\text{assn.}}$ by orders of magnitude. One attempt to solve this problem was reported by the company *SupraPolix BV* utilizing Meijer’s quadruple hydrogen bond (UPy), producing and merchandising this concept already on an industrial scale [65]. The UPy motif was attached to hydrophilic poly(ethylene glycol) (PEG) which can accommodate water, whereby the UPy motifs can assemble into hydrogen-bonded arrays, giving the gel elasticity and strength (Figure 11.8a). In this way, UPy groups were shielded from the water-swollen PEG chains by apolar isophorone spacers [66]. A heart made of the hydrogel (Figure 11.8b), consisting of 15 wt% UPy-polymer (and a

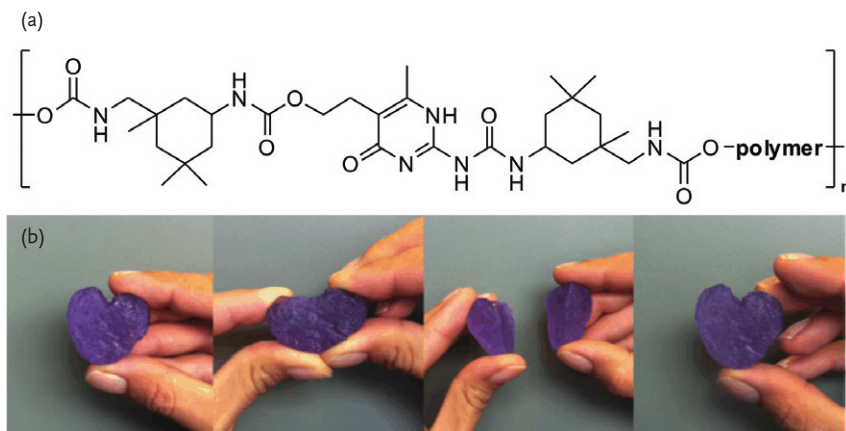


Figure 11.8 (a) UPy-containing polymer. (b) Supramolecular hydrogel made of PEG-UPy polymer 15 wt% in water. Reproduced according to van Gemert *et al.* [66]. With permission from John Wiley & Sons, Inc.

small amount of purple dye) in water, shows self-healing behavior at ambient temperatures. After being cut in half the broken heart heals when the parts are slightly pressed together, recovering almost immediately its ability to be stretched without breaking.

Although these examples show spontaneous self-healing behavior, there are several limitations for the technical application of supramolecular gels. As mentioned above, the use of organic solvents and the sensitivity towards water (if not designed specifically) might be critical. Furthermore, the self-healing dynamics (chain mobility) are strongly dependent on the polymer/solvent ratio, which can change (e.g., by evaporation of the solvent) in long-term applications. For this kind of application an increased thermal stability and long-term shape persistence are desirable. While the thermal stability is limited to the thermal properties of the solvent, shape persistence is not necessarily given.

As a logical consequence one has to seek supramolecular methods capable of self-healing without the presence of a solvent. A crucial aspect, thus, is to guarantee sufficient chain mobility, which in supramolecular gels is introduced by an excess of solvent, making supramolecular gels inherently self-healing. As a consequence, for bulk materials sufficient chain mobility can only be introduced by using polymers or oligomers with low glass transition temperatures (or a composite of at least one low- T_g material).

11.4 Self-Healing Bulk Materials

In a polymeric bulk material the hydrogen-bonding groups are surrounded by either the polymer matrix or by other hydrogen-bonding groups. Therefore, a vast

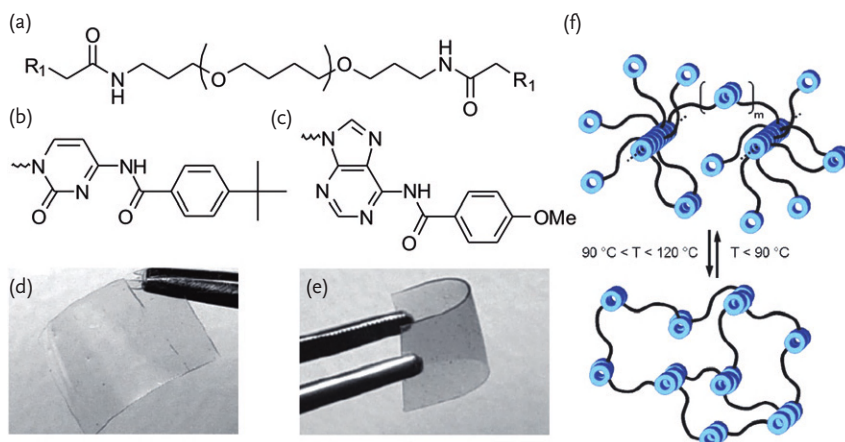


Figure 11.9 (a) Telechelic poly(THF) with nucleobase end groups, (b) adenine, (c) cytosine, (d) film of poly(THF) with adenine end groups, (e) film of poly(THF) with cytosine end group, (f) model of the

assembly of poly(THF) with adenine end groups. Figure reproduced according to Sivakova *et al.* [42]. With permission from ACS Publications.

variety of different effects can additionally influence the supramolecular aggregation, including stacking [42, 67–70], fiber formation [59, 63, 67–69, 71], microphase separation/cluster formation [1, 9, 11, 12, 14, 15, 42, 72, 73], crystallization effects of the supramolecular group or the polymer chain [74–76], as well as secondary effects [42, 70, 72] (such as dipole–dipole interactions or secondary hydrogen bonds).

Sivakova *et al.* reported on telechelic low molecular weight poly(THF) polymers ($M_n < 2000\text{ g mol}^{-1}$) bearing different nucleobases on both chain ends (Figure 11.9a–c) [42, 68]. Although the interaction of these derivatives is weak in solution, ($K < 50\text{ M}^{-1}$) materials with film and fiber-forming capability (Figure 11.9d,e) were obtained, demonstrating that a combination of phase segregation between the poly(THF) matrix and the nucleobase chain ends yielded highly thermo-sensitive flexible supramolecular films. In the case of an adenine-capped poly(THF) (Figure 11.9c) a transition from a linear system (fibers of the adenine stacks by π – π -interaction) to a gel-like cross-linked system at $\sim 90^\circ\text{C}$ consisting of smaller disordered stacks connected via hydrogen bonding (Figure 11.9f) was observed.

Herbst *et al.* reported on a similar system consisting of low- T_g poly(isobutylene)s (PIBs) ($T_g \sim -70^\circ\text{C}$) bearing either thymine (Thy) or 2,6-diaminotriazine (DAT) groups at both chain ends (Figure 11.10a–c) [11]. The aggregation of the end groups in the melt is strongly different from the association in solution. While the Thy–Thy and DAT–DAT interactions are weak (3.8 and 1.7 M^{-1}) in comparison to the Thy–DAT interaction ($\sim 10^3\text{ M}^{-1}$; see Figure 11.2b) in solution, the bifunctional PIB–Thy₂ shows the strongest effect in the melt. Figure 11.10e shows the frequency-dependent measurements at 20°C , revealing that all samples are strong



Figure 11.10 (a) Structure of supramolecular polyisobutylene (PIB); (b) PIB bearing 2,6-diaminotriazine groups; (c) PIB bearing thymine groups; (d) equimolar mixture of PIB-Thy and PIB-DAT; (e) frequency sweep

measurements for bifunctional supramolecular PIBs. Figure reproduced according to Herbst *et al.* [11]. With permission from ACS Publications.

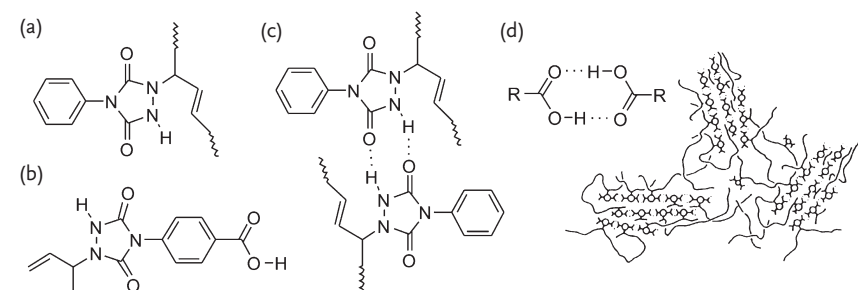


Figure 11.11 (a) 4-Phenyl-1,2,4-triazolidine-3,5-dione group (urazole), (b) 4-urazoylbenzoic acid group, (c) hydrogen bonding between two urazol groups attached to a PBD, (d) phase separation of 4-

urazoylbenzoic acid groups due to additional hydrogen bonding between carboxylic acid groups. Figure reproduced according to Hilger *et al.* With permission from Elsevier Ltd.

rubbers at room temperature. It was confirmed by SAXS measurements, that microphase separation of the end groups (cluster formation) leads to the formation of a thermoreversible, supramolecular crosslinked network. At high temperatures ($T > 100^\circ\text{C}$) the materials are low viscous polymer melts due to the deaggregation of these clusters.

In an early work Stadler and coworkers investigated the influence of different functional groups attached to linear poly(butadiene)s (PBDs) [1, 77–79]. Although 4-phenyl-1,2,4-triazolidine-3,5-dione (urazole) (Figure 11.11a) and 4-urazoylbenzoic acid (Figure 11.11b) are quite similar in their chemical structure, the effect when distributed along the PBD chains is strikingly different. PBDs with urazole groups show for example, a broadening of the rubbery plateau zone and an increase in the zero-shear viscosity due to the formation of two hydrogen bonds between a

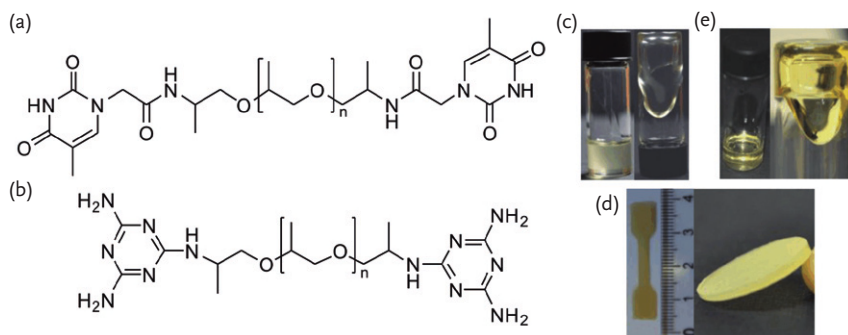


Figure 11.12 (a) Thymine (Thy) functionalized PPO; (b) 2,6-diaminotriazine (DAT) functionalized PPO; (c) DAT-PPO-DAT; (d) Thy-PPO-Thy; (e) 1:1 mixture of DAT-PPO-DAT and Thy-PPO-Thy. Figure reproduced according to Cortese *et al.* [72]. With permission from ACS Publications.

pair of urazole groups (Figure 11.11c) [1, 77]. For these materials a thermorheologically simple behavior is observed and their temperature dependence of $\log a_T$ (shift factor) can be described by the Williams–Landel–Ferry [80] (WLF) equation. In contrast, PBDs with urazolebenzoic acid groups, which only differ from the urazole group by the presence of the carboxyl group, show a considerably more complex behavior due to cooperative aggregation. For these polymers the time–temperature superposition fails [78, 79]. The secondary forces introduced by the carboxyl groups (Figure 11.11d) lead to the formation of extended aggregates of the 4-urazolebenzoic acid groups, which phase separate from the polymer matrix, while the urazole groups are homogeneously distributed within the polymer matrix.

Cortese *et al.* studied the influence of the Thy-DAT motif (see Figure 11.2b) attached to the chain ends of unentangled low molecular weight ($M_n = 2200 \text{ g Mol}^{-1}$) poly(propylene oxide) (PPO) (Figure 11.12) [72, 81]. A PPO bearing two 2,6-diaminotriazine groups (DAT; Figure 11.12b) was observed as a low viscous liquid (Figure 11.12c), since only weak hydrogen bonds were formed between two DAT groups. Surprisingly, a PPO bearing two Thy-groups (Figure 11.12a) was obtained as a solid (Figure 11.12d) due to the crystallization of the Thy-groups, as confirmed by SAXS and DSC measurements. It is claimed, that the crystallization was promoted by weak hydrogen bonding (secondary forces) of the amide groups in close vicinity to the Thy-group. An equimolar mixture of both polymers was again obtained as a liquid (Figure 11.12e), since the strong hydrogen bonding between Thy and DAT prevents the Thy-groups from crystallization. The viscosity of an equimolar mixture is significantly higher than for pure 2,6-diaminotriazine-capped PPO because the stronger hydrogen bonds lead to the formation of longer supramolecular chains (higher virtual DP). However, this behavior is in contrast to the association in solution, where the Thy–Thy interaction is weak, and in contrast to the results of Herbst *et al.* [11].

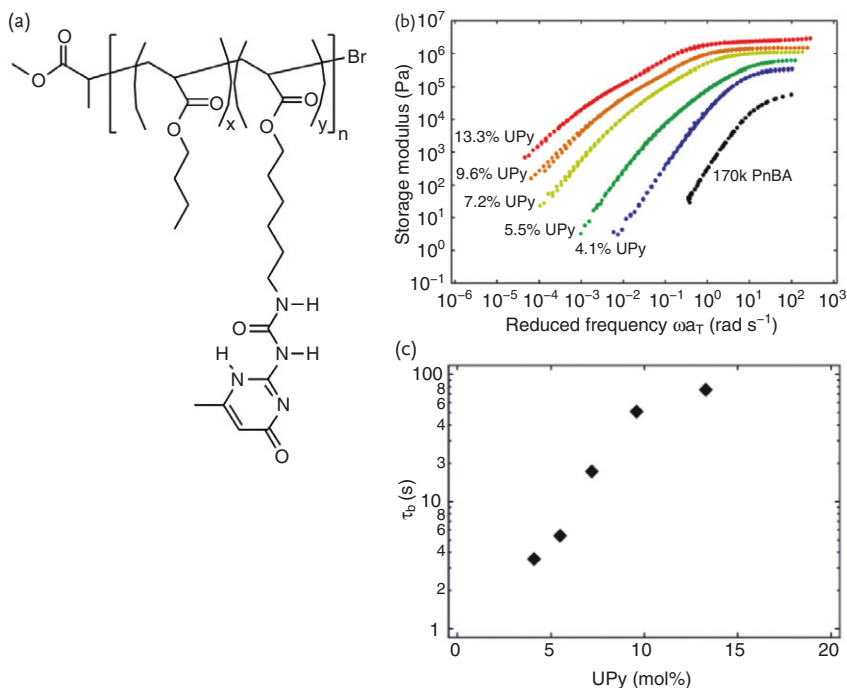


Figure 11.13 (a) Poly(*n*-butyl acrylate) (PnBA) containing different amounts of UPy groups. (b) Storage modulus (G') versus reduced frequency (ωa_T) for PnBA with increasing UPy content. (c) Effective bond

lifetime (τ_b^*) increases with UPy content. Figure reproduced according to Feldman *et al.* [43]. With permission from ACS Publications.

Feldman *et al.* investigated random copolymers consisting of a poly(*n*-butyl acrylate) (PnBA) backbone bearing UPy side chains (Figure 11.13a) [15, 43, 82]. SAXS and DSC measurements revealed that there is no phase separation of the UPy groups. Therefore, the supramolecular groups are homogeneously distributed within the polymer matrix, a crucial requirement for investigating the dynamics of a “simple” aggregation of two functional groups per supramolecular tie-point. The bond lifetime τ_b^* was calculated from the frequency at which the storage modulus dropped to 90% of its plateau modulus. These effective bond lifetimes were significantly larger than the bare bond lifetimes τ_b measured in solution [46]. Therefore, each supramolecular bond can open and close several times before the two involved groups can finally diffuse away from each other [21]. The process is limited by the mobility of the polymer chains and, thus, by the presence of further tie-points (which reduce chain mobility), making the release of a tie-point dependent on other binding events. Increasing the amount of UPy per chain (keeping M_n constant) increases the effective bond lifetimes τ_b^* (see Figure 11.13c) since concurrent unbinding of more tie-points becomes less likely. As a result, the onset of the

terminal flow region (drop in the storage modulus) is shifted towards lower frequencies (longer timescales) (see Figure 11.13b).

In the above-mentioned examples it is obvious that different factors are responsible when constructing a supramolecular self-healing material. On the one hand several systems show “simple” and expected aggregation behavior, but on the other hand even similar systems show strikingly different properties, thus making it almost impossible to forecast the materials properties, and making experimental proof always necessary. Although different models have been developed for describing supramolecular gels and melts [83], a generally valid model is still not available.

Summarizing supramolecular bulk materials with self-healing potential, one has to distinguish between autonomous self-healing materials and “healable” or “mendable” materials, which display self-healing ability, but need an external force in order to recover or regain their initial properties. This stimulus can be triggered by, for instance, thermal energy (heat), irradiation (UV or visible light), or ultrasound. In contrast, autonomous self-healing materials show spontaneous self-healing at ambient conditions without an external stimulus. Often fractured surfaces just have to be brought into contact again and slightly pressed together (which we do not judge as an external “force”) to recover their pristine properties. Since such a macroscopic failure of a material is preceded by the formation of microcracks, an autonomous self-healing material would spontaneously heal such defects, thus reducing the threat of macrocracks and extending the materials lifetime significantly.

One of the most impressive examples of a self-healing material based on hydrogen bonding was shown by Cordier *et al.* who reported on the self-healing behavior of functionalized fatty di- and triacids [9]. In a simple two-step synthesis fatty dimer acids, made from natural renewable resources, were condensed with diethylene triamine and then reacted with urea. The resulting compound was plasticized with 11 wt% dodecane in order to decrease the T_g from 28 to 8°C. Three types of hydrogen bonding motifs were formed, namely the amidoethyl imidazolidone, di(amido ethyl)ureas, and diamido tetraethyl triureas (Figure 11.14). The resulting rubbery material was not crystalline, easily synthesized on a 100 g scale and capable of being molded or extruded at high temperatures. It reveals rheological and mechanical properties typical for ordinary rubbers. Figure 11.15a shows the frequency dependence of storage (G') and loss (G'') moduli, revealing a rubber plateau at low frequencies, and the close proximity to the glass transition at high frequencies. Stress–strain experiments show a strain at break exceeding 500% and after creep–recovery experiments the residual strain is less than $5 \cdot 10^{-2}\%$ (see Figure 11.15b). Although similar to an ordinary rubber with respect to its mechanical properties, the material behaves strikingly differently after being cut into two pieces and the fractured surfaces were brought in contact again. While this event causes permanent rupture of covalent bonds in ordinary rubbers, weak supramolecular bonds were ruptured in this particular rubber. Due to the dynamic reversible character of the hydrogen bonds these bonds can be re-formed when the functional groups are brought into close vicinity together again while

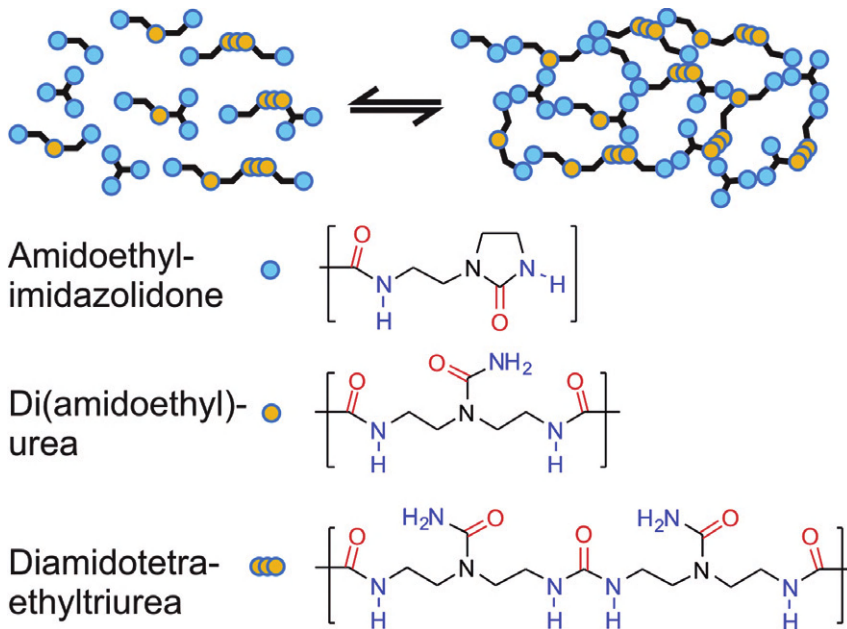


Figure 11.14 Low molecular weight building blocks, based on multivalent fatty acids, form a supramolecular network due to hydrogen bonding. Figure reproduced according to Cordier *et al.* [9]. With permission from Nature Publishing Group.

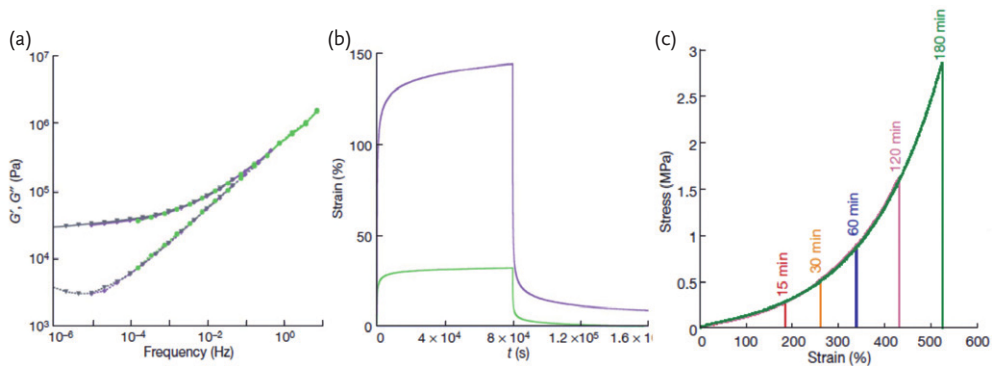


Figure 11.15 Different mechanical measurements of a supramolecular rubber reported by Cordier *et al.*: (a) frequency sweep measurements; (b) creep-recovery experiments for an applied stress of 5000 Pa

(green) and 20000 Pa (purple); (c) stress-strain experiments after different healing times. Figure reproduced according to Cordier *et al.* [9]. With permission from Nature Publishing Group.

autonomically healing and recovering the mechanical properties. Figure 11.15c shows the stress–strain behavior after different healing times. Longer healing times lead to better healing and all healing curves superpose, showing only changes in the strain at break. This stretching–breaking–healing cycle can be repeated many times, again confirming dynamic reversible hydrogen bonds being involved. One has to mention that the healing efficiency is strongly dependent on the waiting time between cut and mending. While the material recovers its initial properties if the waiting time is less than 5 min, the healing efficiency decreases with increasing waiting time. Sufficient efficiency was still observed after 18 h waiting time (at ambient temperature), but after a maximum waiting time of more than one week (at 23 °C) no healing was observed anymore, as the free hydrogen bonds can rearrange and associate with other free hydrogen bonds in the fractured surface, thus reducing the available amount of free bonds for subsequent healing with the corresponding surface. An elevated temperature increases the dynamics of the molecules and the equilibrium is reached faster, the maximal healing time is, for instance, decreased to 5 Min at 120 °C.

Self-healing materials based on aromatic π – π -stacking interactions were first reported by Burattini *et al.* who took advantage of combining π -electron-rich and π -electron-poor moieties [40, 84–86], obtaining supramolecular complexes with chain-folded secondary structures, and thus with a maximum amount of possible interactions. As a result, low molecular weight precursors can be converted into medium molecular weight species in a highly dynamic manner. Moreover, the so-obtained responsive products show physical properties, like high tensile strength, which are more commonly related to covalent bonds but tunable for various self-healing applications [70]. Burattini *et al.* synthesized a polyimide bearing π -electron-deficient naphthalene-diimide units (Figure 11.16a) and a pyrenyl end-capped polyamide bearing π -electron-rich pyrene groups (Figure 11.16b). Complementary π – π stacking of the naphthalene-diimide and pyrene groups leads to chain folding of the polyimide (in solution and melt), confirmed by spectroscopic and crystallographic methods (Figure 11.16c), and thus, to the formation of a supramolecular network. The interaction was easily confirmed by

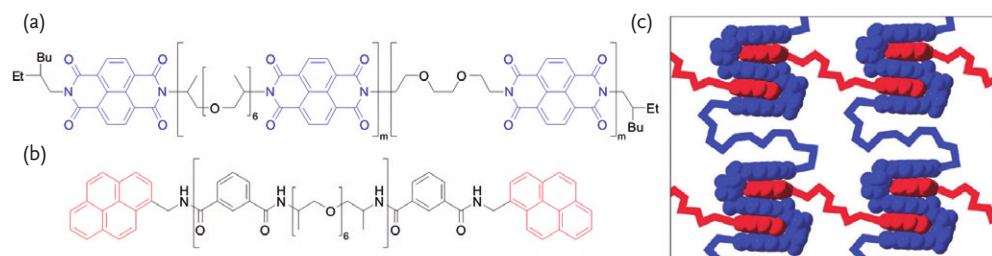


Figure 11.16 (a) Polyimide copolymer containing π -electron-deficient naphthalene-diimide units; (b) pyrenyl end-capped polyamide bearing π -electron-rich pyrene

groups; (c) folding of the two polymers due to attractive π – π stacking. Figure reproduced according to Burattini *et al.* [84]. With permission from RSC Publishing.

mixing a pale yellow solution of the polyimide and a colorless solution of the polyamide. Upon mixing, a deep red color immediately arises, indicating charge transfer between the two groups. The complex exhibits a binding constant ($K_{\text{assn.}}$) of 130 M^{-1} and is strongly thermosensitive, for example, fading of the deep red color was observed upon heating, but the deep red color recovered on cooling again. This simple experiment reveals the dynamic, reversible character of the complex formation, typical for supramolecular interactions.

When films of the polyimide copolymer (tan powder; $T_g = 190^\circ\text{C}$) and the polyamide (pale yellow oil; $T_g = -7^\circ\text{C}$) were prepared by solution casting, a flexi-

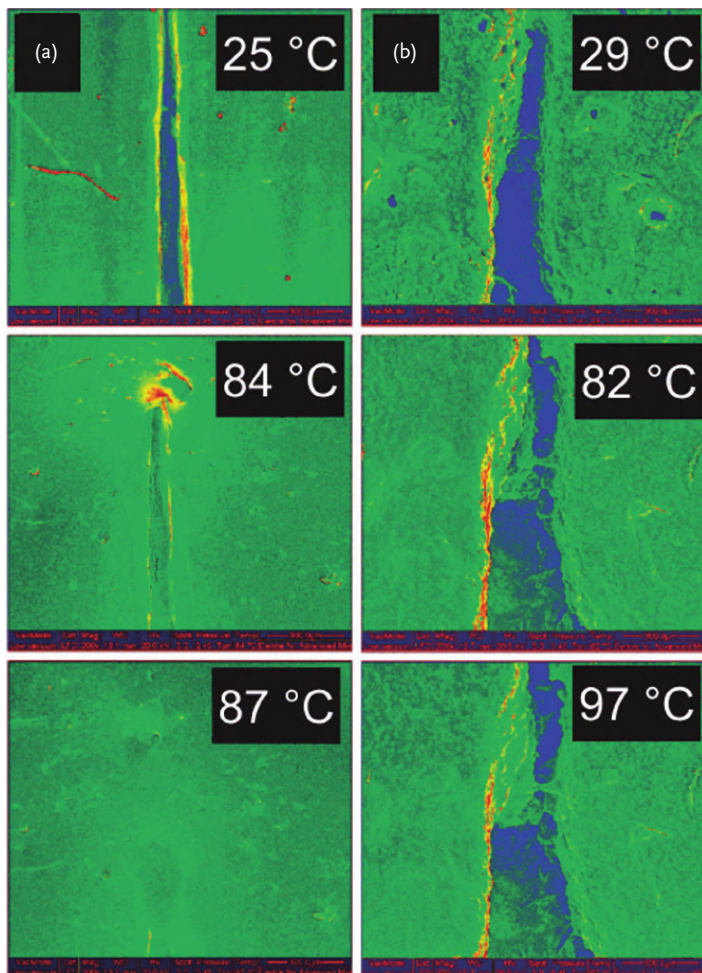


Figure 11.17 Self-healing experiment of a mixture of polyimide and polyamide polymers according to Burattini *et al.* With (a) attractive π - π stacking (healing), and

(b) no attractive π - π stacking (no healing/control experiment). Figure reproduced according to Burattini *et al.* [84]. With permission from RSC Publishing.

ble, homogenous, self-supporting film with a deep red color was obtained. A broken film could be re-healed by simple pressing the broken parts gently together and heating briefly to 80 °C (see Figure 11.17a). Although self-healing was triggered by heat, healing occurs almost immediately (at 80 °C). One hundred percent recovery of the tensile modulus was achieved and the healing after damage could be repeated several times. In comparison, a similar polymer mixture without complementary π - π -interactions (the pyrene moiety was exchanged by a benzyl group) was obtained as a phase-separated material (control experiment) with no self-healing ability (see Figure 11.17b). Therefore, the supramolecular interaction does not only enable self-healing, it further promotes the miscibility of otherwise immiscible polymers as well.

Another temperature-triggered approach toward self-healing materials is commercially available under the brand name *SupraB*[®] (by *Suprapolix BV* [41, 65]), based on Meijer's quadruple hydrogen bond (see Figure 11.2a). Due to the thermo-reversible hydrogen bonding of UPy groups the material combines strong elastic behavior at room temperature (hydrogen bonds closed) and low viscous melt behavior at elevated temperatures (bonds open) (Figure 11.18b). Therefore, these polymers can be dissolved in an adequate solvent and sprayed or cast to form flexible films of different thickness with outstanding mechanical properties (upon evaporation of the solvent) (Figure 11.18b). After a film is damaged by scratching (Figure 11.18a) it spontaneously self-heals by heating briefly to 140 °C. Furthermore, unlimited cycles of healing illustrate the advantages in terms of for example, material lifetime and recyclability.

We have reported on a related system utilizing hydrogen bonding, but revealing spontaneous self-healing at ambient temperatures [12]. Bivalent poly(isobutylene)s ($T_g \sim -70$ °C) with different molecular weights (3k, 8k, 14k and 30k g mol⁻¹) were functionalized with barbituric acid groups (see Figure 11.19b) via the azide-alkyne "click" reaction [87, 88]. Rheology experiments in the melt state (20 °C; Figure 11.19a) show a pronounced rubbery plateau at high frequencies and a terminal flow region in the low-frequency range. Although the polymers consist of unentangled chains ($M_n < M_e$ for 3k, 8k and 14k) a rubbery plateau even higher than for linear high molecular weight PIBs was observed, easily explained by the formation of dynamic supramolecular tie-points, consisting of several barbituric acid groups, within the polymer matrix. These tie-points are closed at short timescales (high frequencies) and partially open at long timescales (low frequencies), combining both elastic and viscous behavior. Surprisingly, the rheological behavior (plateau modulus G_N^0 , zero-shear viscosity and crossover of G'/G'') was found to be almost independent of the molecular weight of the polymer, although varied from 3k to 30k Da. Using the frequency at the crossover of G'/G'' one can calculate the lifetime of the supramolecular aggregates, which is in the range of 31–51 s for the four samples. This lifetime depends on the strength of the supramolecular interaction, the mobility of the polymer chains and the size of the aggregate. While the strength of the supramolecular interaction is the same for all four samples, the chain mobility decreases with increasing molecular weight. Therefore, the size of the aggregates must decrease with increasing molecular weight. In this very special case the two

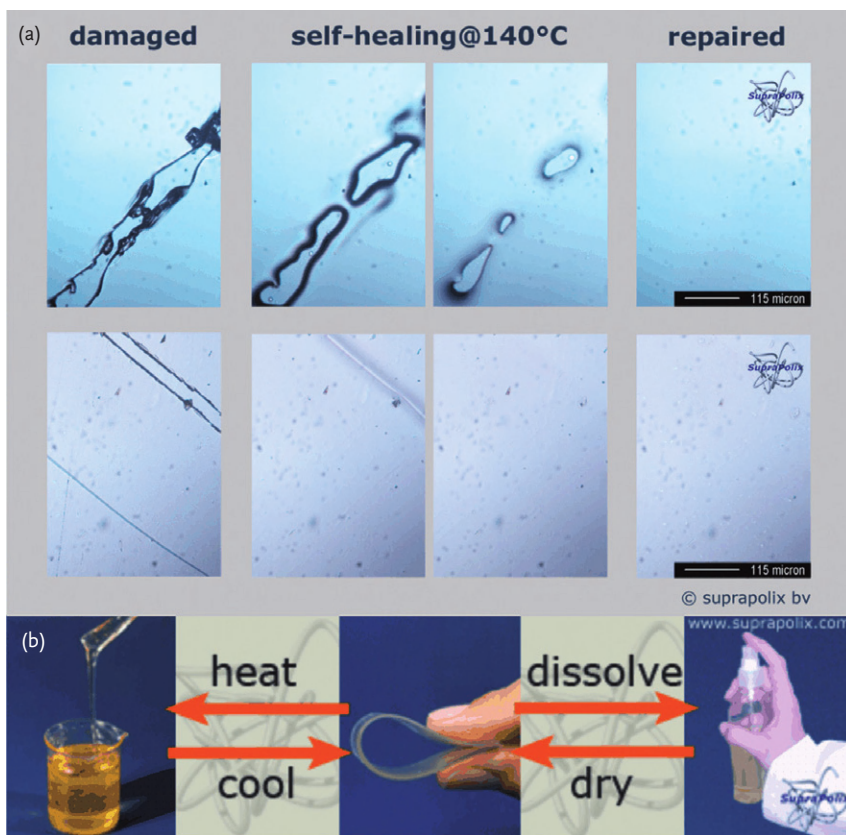


Figure 11.18 (a) Self-healing of *SupraB*[®] at elevated temperatures; (b) unique behavior of *SupraB*[®] upon heating/cooling or dissolving/drying. Figure reproduced with permission from *Suprapolix BV* [65].

opposing effects (decrease in chain mobility and decrease in aggregate size) seem to balance each other, so the resulting lifetime is virtually unaffected by the molecular weight. Small discs prepared from the barbituric acid-telechelic PIBs show autonomous self-healing within several hours at ambient temperatures after the two halves are brought in contact again (see Figure 11.19c). While the association of barbituric acid groups is weak in solution ($K_{\text{assn.}} = 12 \text{ M}^{-1}$), they reveal a complex aggregation in the melt state, drastically influencing the polymer properties, although only two groups per chain are present.

Another approach toward novel self-healing materials was reported by Guan and coworkers [73], combining both the classical TPE (thermoplastic elastomer) approach and the supramolecular concept. They synthesized a hydrogen-bonding brush copolymer (HBP; Figure 11.20a) consisting of a poly(styrene) (PS) backbone grafted with PA-amide (PAA) chains. The immiscibility of the two domains led to phase-separation into hard PS nanospheres (high T_g) surrounded by a soft PAA

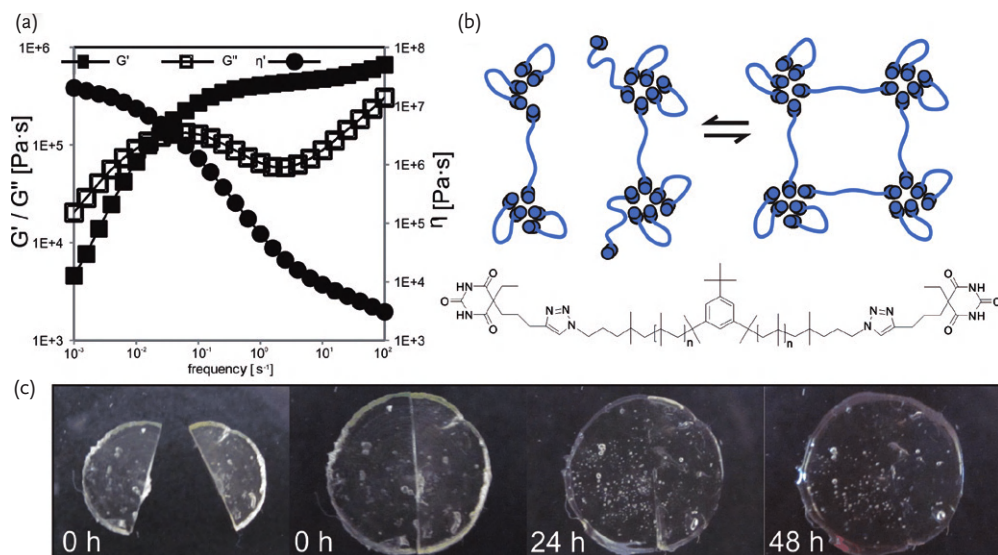


Figure 11.19 (a) Frequency sweep measurement of a PIB bearing two barbituric acid groups; (b) formation of a dynamic, reversible supramolecular network of a barbituric acid functionalized PIB; (c)

self-healing experiment of a barbituric acid functionalized PIB with $M_n = 28\,000\text{ g mol}^{-1}$. Figure reproduced according to Herbst *et al.* [12]. With permission from RSC Publishing.

marix (low T_g) (see Figure 11.20a). Therefore, the material combines both good mechanical stiffness (hard PS cores) and dynamic, elastomeric behavior (soft supramolecular PPA matrix). Due to the presence of amide groups, reversible hydrogen bonding between the PPA-grafts is possible (see Figure 11.20b), bestowing the material self-healing properties.

When the HBP is damaged the weak hydrogen bonds are preferentially ruptured (Figure 11.20b), but due to the low glass transition of the PAA matrix ($T_g = 2\text{--}5\text{ }^\circ\text{C}$) the PPA chains can easily rearrange and thus re-form the amide hydrogen bonds. Long healing times (24 h, see Figure 11.21) lead to a maximum healing recovery of 92% related to the extensibility of the pristine sample. Although the healing efficiency is markedly below the ideal value of 100%, the system is doubtless noteworthy, since the HBP were made from cheap, commercially available chemicals, using simple effective polymerization methods (free radical polymerization and ATRP) and improving the mechanical properties due to the presence of hard and soft domains (TPE attempt).

Thus, this attempt is an excellent example for the improvement of the material properties due to the combination of different chemical concepts (hydrogen bonding and phase separation). It is, therefore, of course possible to combine two different supramolecular approaches to create new self-healing materials. Very recently they extended this work by using a similar approach, applying and the UPy-groups (see Figure 11.2a) as the supramolecular binding motif [89].

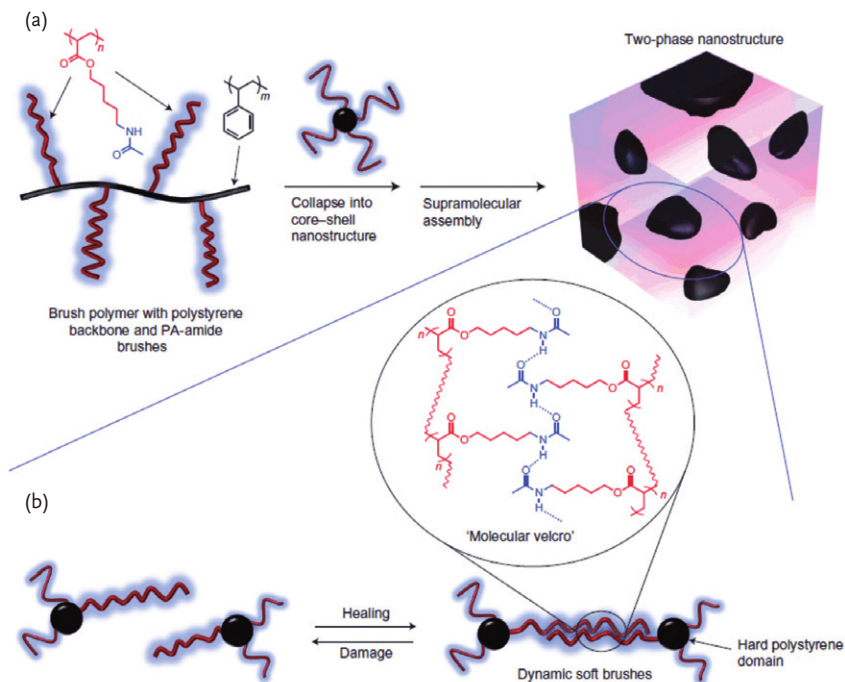


Figure 11.20 (a) Hydrogen-bonding brush copolymer (HBP), consisting of a poly(styrene) (PS) backbone and PA-amide (PAA) side-chains, shows microphase separation into hard PS cores and a soft PAA matrix. (b) PAA chains can rearrange after

rupture due to the dynamic character of the amide hydrogen bonds and sufficient chain mobility (low T_g). Figure reproduced according to Chen *et al.* [73]. With permission from Nature Publishing Group.

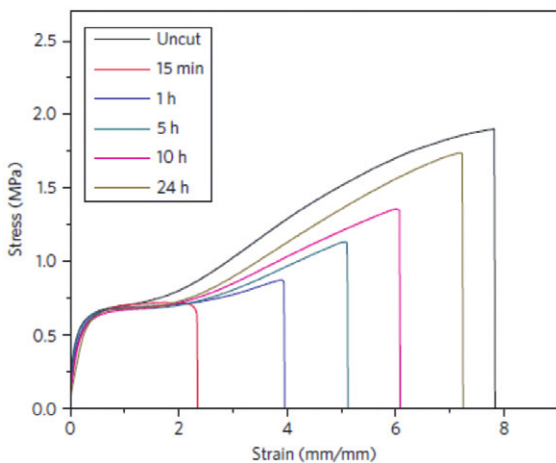


Figure 11.21 Stress-strain experiments on a hydrogen-bonding brush copolymer (HBP) reported by Chen *et al.* after different healing times. Figure reproduced according to Chen *et al.* [73]. With permission from Nature Publishing Group.

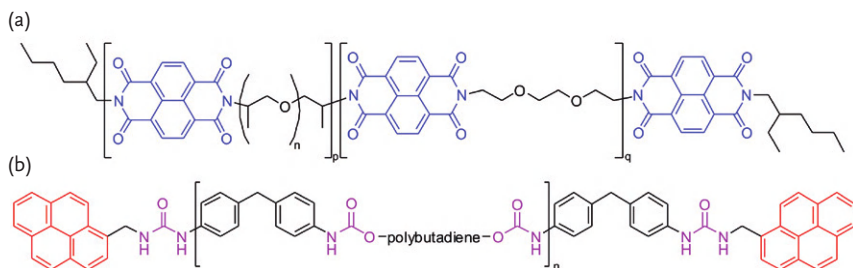


Figure 11.22 (a) polyimide copolymer containing π -electron-deficient naphthalene-diimide units; (b) pyrenyl end-capped polyamide bearing π -electron-rich pyrene groups and urea groups in close vicinity for additional hydrogen bonding.

Burattini *et al.* have extended their work by combining π - π -interactions, between polyimide copolymer bearing π -electron-deficient naphthalene-diimide units (Figure 11.22a) and a pyrenyl end-capped polyamide bearing pyrene groups, and hydrogen bonding between urea groups in the vicinity of the pyrene groups (Figure 11.22b) [70]. Upon mixing these two polymers, the resulting material revealed hydrogen bonding which complements the π - π -stacking interactions (shown by different methods). The resulting material (with a deep red color of the charge-transfer complex) reveals again triggered self-healing at elevated temperatures, with healing efficiencies of 77% (elongation at break) up to 95% (tensile modulus).

11.5

Conclusions

The presented examples of supramolecular polymers based on either hydrogen bonding or π - π -interactions convincingly show the advantages and versatility of these reversible dynamic forces for the generation of self-healing polymers, enabling multiple healing cycles. Although the interplay is simple to describe in solution, it becomes increasingly complex with decreasing amounts of solvent (from solution to the gel-state, and finally the bulk-state). Several excellent models and theories have been developed to describe and predict the properties of such supramolecular materials, but none of them was found to be generally valid. Therefore, it is the scientist's task to invent and characterize novel self-healing systems by utilizing known and developing new ideas, always keeping in mind the main challenge: To combine sufficient structural integrity with sufficient dynamics [58].

Acknowledgment

We acknowledge the grant DFG BI 1337/7-1 (FH, WHB), the project DFG BI 1337/8-1 within the framework of the SPP 1568 "Design and Generic Principles of Self-Healing Materials" and the EU-project IASS for financial support.

References

- 1 de Lucca Freitas, L.L., and Stadler, R. (1987) *Macromolecules*, **20**, 2478.
- 2 Stadler, R., and de Lucca Freitas, L. (1986) *Colloid Polym. Sci.*, **264**, 773.
- 3 Binder, W., and Zirbs, R. (2007) *Adv. Polym. Sci.*, **207**, 1.
- 4 Binder, W.H., Enders, C., Herbst, F., and Hackethal, K. (2011) in *Complex Macromolecular Architectures: Synthesis, Characterization and Self Assembly* (eds N. Hadjichristidis, Y. Tezuka, and A. Hirao), John Wiley & Sons (Asia) Pte Ltd, p. 53.
- 5 Bosman, A., Sijbesma, R.P., and Meijer, E.W. (2004) *Mater. Today*, **7**, 34.
- 6 Brunsveld, L., Folmer, B.J.B., Meijer, E.W., and Sijbesma, R.P. (2001) *Chem. Rev.*, **101**, 4071.
- 7 de Greef, T.F.A., and Meijer, E.W. (2008) *Nature*, **453**, 171.
- 8 Hoeben, F.J.M., Jonkheijm, P., Meijer, E.W., and Schenning, A.P.H.J. (2005) *Chem. Rev.*, **105**, 1491.
- 9 Cordier, P., Tournilhac, F., Soulie-Ziakovic, C., and Leibler, L. (2008) *Nature*, **451**, 977.
- 10 Montarnal, D., Cordier, P., Soulié-Ziakovic, C., Tournilhac, F., and Leibler, L. (2008) *J. Polym. Sci. A: Polym. Chem.*, **46**, 7925.
- 11 Herbst, F., Schröter, K., Gunkel, I., Gröger, S., Thurn-Albrecht, T., Balbach, J., and Binder, W.H. (2010) *Macromolecules*, **43**, 10006.
- 12 Herbst, F., Seiffert, S., and Binder, W.H. (2012) *Polym. Chem.*, **3**, 3084.
- 13 Hackethal, K., Herbst, F., and Binder, W.H. (2012) *J. Polym. Sci. A: Polym. Chem.*, **50**, 4494.
- 14 Binder, W.H., Bernstorff, S., Kluger, C., Petraru, L., and Kunz, M. (2005) *Adv. Mater.*, **17**, 2824.
- 15 Feldman, K.E., Kade, M.J., Meijer, E.W., Hawker, C.J., and Kramer, E.J. (2010) *Macromolecules*, **43**, 5121.
- 16 Binder, W.H., Kunz, M.J., and Ingolic, E. (2004) *J. Polym. Sci. A: Polym. Chem.*, **42**, 162.
- 17 Kunz, M.J., Hayn, G., Saf, R., and Binder, W.H. (2004) *J. Polym. Sci. A: Polym. Chem.*, **42**, 661.
- 18 Binder, W.H., Petraru, L., Roth, T., Groh, P.W., Pálfi, V., Keki, S., and Ivan, B. (2007) *Adv. Funct. Mater.*, **17**, 1317.
- 19 Yount, W.C., Loveless, D.M., and Craig, S.L. (2005) *J. Am. Chem. Soc.*, **127**, 14488.
- 20 Baxandall, L.G. (1989) *Macromolecules*, **22**, 1982.
- 21 Leibler, L., Rubinstein, M., and Colby, R.H. (1991) *Macromolecules*, **24**, 4701.
- 22 Rubinstein, M., and Semenov, A.N. (1998) *Macromolecules*, **31**, 1386.
- 23 Green, M.S., and Tobolsky, A.V. (1946) *J. Chem. Phys.*, **14**, 80.
- 24 Tanaka, F., and Edwards, S.F. (1992) *Macromolecules*, **25**, 1516.
- 25 Tanaka, F., and Edwards, S.F. (1992) *J. Non-Newtonian Fluid Mech.*, **43**, 247.
- 26 Tanaka, F., and Edwards, S.F. (1992) *J. Non-Newtonian Fluid Mech.*, **43**, 273.
- 27 Cates, M.E. (1987) *Macromolecules*, **20**, 2289.
- 28 Zare, P., Stojanovic, A., Herbst, F., Akbarzadeh, J., Peterlik, H., and Binder, W.H. (2012) *Macromolecules*, **45**, 2074.
- 29 Desiraju, G.R. (2011) *Angew. Chem.*, **123**, 52.
- 30 Binder, W.H., Pulamagatta, B., Schunack, M., and Herbst, F. (2012) in *Bioinspiration and Biomimicry in Chemistry* (ed. G. Swiegers), Wiley-VCH Verlag GmbH, p. 323.
- 31 Hackethal, K., Döhler, D., Tanner, S., and Binder, W.H. (2010) *Macromolecules*, **43**, 1761.
- 32 Lehn, J.-M. (2005) *Prog. Polym. Sci.*, **30**, 814.
- 33 Lehn, J.-M. (1988) *Angew. Chem.*, **100**, 91.
- 34 Sijbesma, R.P., Beijer, F.H., Brunsveld, L., Folmer, B.J.B., Hirschberg, J.H.K.K., Lange, R.F.M., Lowe, J.K.L., and Meijer, E.W. (1997) *Science*, **278**, 1601.
- 35 Beijer, F.H., Sijbesma, R.P., Vekemans, J.A.J.M., Meijer, E.W., Kooijman, H., and Spek, A.L. (1996) *J. Org. Chem.*, **61**, 6371.
- 36 Chang, S.K., and Hamilton, A.D. (1988) *J. Am. Chem. Soc.*, **110**, 1318.
- 37 Park, T., and Zimmerman, S.C. (2006) *J. Am. Chem. Soc.*, **128**, 11582.
- 38 Knochen, W., Besseling, N.A.M., Bouteiller, L., and Cohen-Stuart, M.A. (2005) *Phys. Chem. Chem. Phys.*, **7**, 2390.

- 39 Blight, B.A., Hunter, C.A., Leigh, D.A., McNab, H., and Thomson, P.I.T. (2011) *Nat. Chem.*, **3**, 246.
- 40 Greenland, B.W., Burattini, S., Hayes, W., and Colquhoun, H.M. (2008) *Tetrahedron*, **64**, 8346.
- 41 Folmer, B.J.B., Sijbesma, R.P., Versteegen, R.M., van der Rijt, J.A.J., and Meijer, E.W. (2000) *Adv. Mater.*, **12**, 874.
- 42 Sivakova, S., Bohnsack, D.A., Mackay, M.E., Suwanmala, P., and Rowan, S.J. (2005) *J. Am. Chem. Soc.*, **127**, 18202.
- 43 Feldman, K.E., Kade, M.J., Meijer, E.W., Hawker, C.J., and Kramer, E.J. (2009) *Macromolecules*, **42**, 9072.
- 44 Noro, A., Hayashi, M., Ohshika, A., and Matsushita, Y. (2011) *Soft Matter*, **7**, 1667.
- 45 Hammes, G.G., and Park, A.C. (1968) *J. Am. Chem. Soc.*, **90**, 4151.
- 46 Sontjens, S.H.M., Sijbesma, R.P., van Genderen, M.H.P., and Meijer, E.W. (2000) *J. Am. Chem. Soc.*, **122**, 7487.
- 47 Pellizzaro, M.L., Barrett, S.A., Fisher, J., and Wilson, A.J. (2012) *Org. Biomol. Chem.*, **10**, 4899.
- 48 Bertrand, A., Chen, S., Souharce, G.G., Ladavière, C., Fleury, E., and Bernard, J. (2011) *Macromolecules*, **44**, 3694.
- 49 Lillya, C.P., Baker, R.J., Hutte, S., Winter, H.H., Lin, Y.G., Shi, J., Dickinson, L.C., and Chien, J.C.W. (1992) *Macromolecules*, **25**, 2076.
- 50 Müller, M., Seidel, U., and Stadler, R. (1995) *Polymer*, **36**, 3143.
- 51 Yount, W.C., Loveless, D.M., and Craig, S.L. (2005) *Angew. Chem. Int. Ed.*, **44**, 2746.
- 52 Xu, D., Liu, C.-Y., and Craig, S.L. (2011) *Macromolecules*, **44**, 2343.
- 53 Xu, D., Hawk, J.L., Loveless, D.M., Jeon, S.L., and Craig, S.L. (2010) *Macromolecules*, **43**, 3556.
- 54 Serpe, M.J., and Craig, S.L. (2007) *Langmuir*, **23**, 1626.
- 55 Shikata, T., Nishida, T., Isare, B., Linares, M., Lazzaroni, R., and Bouteiller, L. (2008) *J. Phys. Chem. B*, **112**, 8459.
- 56 Nair, K.P., Breedveld, V., and Weck, M. (2008) *Macromolecules*, **41**, 3429.
- 57 Aida, T., Meijer, E.W., and Stupp, S.I. (2012) *Science*, **335**, 813.
- 58 Hoogenboom, R. (2012) *Angew. Chem. Int. Ed.*, **51**, 11942.
- 59 Kolomiets, E., Buhler, E., Candau, S.J., and Lehn, J.M. (2006) *Macromolecules*, **39**, 1173.
- 60 Courtois, J., Baroudi, I., Nouvel, N., Degrandi, E., Pensec, S., Ducouret, G., Chanéac, C., Bouteiller, L., and Creton, C. (2010) *Adv. Funct. Mater.*, **20**, 1803.
- 61 Choi, I.S., Li, X., Simanek, E.E., Akaba, R., and Whitesides, G.M. (1999) *Chem. Mater.*, **11**, 684.
- 62 Vidyasagar, A., Handore, K., and Sureshan, K.M. (2011) *Angew. Chem. Int. Ed.*, **50**, 8021.
- 63 Hunley, M.T., Karikari, A.S., McKee, M.G., Mather, B.D., Layman, J.M., Fornof, A.R., and Long, T.E. (2008) *Macromol. Symp.*, **270**, 1.
- 64 Naficy, S., Brown, H.R., Razal, J.M., Spinks, G.M., and Whitten, P.G. (2012) *ChemInform*, **43** (2).
- 65 SupraPolix BV. <http://www.suprapolix.com/> (accessed December 10, 2012).
- 66 van Gemert, G.M.L., Peeters, J.W., Söntjens, S.H.M., Janssen, H.M., and Bosman, A.W. (2012) *Macromol. Chem. Phys.*, **213**, 234.
- 67 van Beek, D.J.M., Spiering, A.J.H., Peters, G.W.M., te Nijenhuis, K., and Sijbesma, R.P. (2007) *Macromolecules*, **40**, 8464.
- 68 Rowan, S.J., Suwanmala, P., and Sivakova, S. (2003) *J. Polym. Sci. A: Polym. Chem.*, **41**, 3589.
- 69 Botterhuis, N.E., van Beek, D.J.M., van Gemert, G.M.L., Bosman, A.W., and Sijbesma, R.P. (2008) *J. Polym. Sci. A: Polym. Chem.*, **46**, 3877.
- 70 Burattini, S., Greenland, B.W., Merino, D.H., Weng, W., Seppala, J., Colquhoun, H.M., Hayes, W., Mackay, M.E., Hamley, I.W., and Rowan, S.J. (2010) *J. Am. Chem. Soc.*, **132**, 12051.
- 71 Dankers, P.Y.W., Hermans, T.M., Baughman, T.W., Kamikawa, Y., Kiełtyka, R.E., Bastings, M.M.C., Janssen, H.M., Sommerdijk, N.A.J.M., Larsen, A., van Luyn, M.J.A., Bosman, A.W., Popa, E.R., Fytas, G., and Meijer, E.W. (2012) *Adv. Mater.*, **24**, 2703.
- 72 Cortese, J., Soulié-Ziakovic, C., Tencé-Girault, S., and Leibler, L. (2012) *J. Am. Chem. Soc.*, **134**, 3671.
- 73 Chen, Y., Kushner, A.M., Williams, G.A., and Guan, Z. (2012) *Nat. Chem.*, **4**, 467.

- 74 Ostas, E., Schröter, K., Beiner, M., Yan, T., Thurn-Albrecht, T., and Binder, W.H. (2011) *J. Polym. Sci. A: Polym. Chem.*, **49**, 3404.
- 75 Colombani, O., Barioz, C., Bouteiller, L., Chanéac, C., Fompérie, L., Lortie, F., and Montès, H. (2005) *Macromolecules*, **38**, 1752.
- 76 Müller, M., Dardin, A., Seidel, U., Balsamo, V., Ivan, B., Spiess, H.W., and Stadler, R. (1996) *Macromolecules*, **29**, 2577.
- 77 de Lucca Freitas, L., and Stadler, R. (1988) *Colloid Polym. Sci.*, **266**, 1095.
- 78 Hilger, C., and Stadler, R. (1991) *Polymer*, **32**, 3244.
- 79 Hilger, C., Stadler, R., Liane, L., and Freitas, D.L. (1990) *Polymer*, **31**, 818.
- 80 Williams, M.L., Landel, R.F., and Ferry, J.D. (1955) *J. Am. Chem. Soc.*, **77**, 3701.
- 81 Cortese, J., Soulié-Ziakovic, C., Cloitre, M., Tencé-Girault, S., and Leibler, L. (2011) *J. Am. Chem. Soc.*
- 82 Feldman, K.E., Kade, M.J., de Greef, T.F.A., Meijer, E.W., Kramer, E.J., and Hawker, C.J. (2008) *Macromolecules*, **41**, 4694.
- 83 Seiffert, S., and Sprakel, J. (2012) *Chem. Soc. Rev.*, **41**, 909.
- 84 Burattini, S., Colquhoun, H.M., Fox, J.D., Friedmann, D., Greenland, B.W., Harris, P.J.F., Hayes, W., Mackay, M.E., and Rowan, S.J. (2009) *Chem. Commun.*, 6717.
- 85 Burattini, S., Colquhoun, H.M., Greenland, B.W., and Hayes, W. (2009) *Faraday Discuss.*, **143**, 251.
- 86 Burattini, S., Greenland, B.W., Hayes, W., Mackay, M.E., Rowan, S.J., and Colquhoun, H.M. (2010) *Chem. Mater.*, **23**, 6.
- 87 Binder, W.H., and Sachsenhofer, R. (2007) *Macromol. Rapid Commun.*, **28**, 15.
- 88 Binder, W.H., and Sachsenhofer, R. (2008) *Macromol. Rapid Commun.*, **29**, 952.
- 89 Hentschel, J., Kushner, A.M., Ziller, J., and Guan, Z. (2012) *Angew. Chem. Int. Ed.*, **51**, 10561.

12

Metal-Complex-Based Self-Healing Polymers

Stefan Bode, Benedict Sandmann, Martin D. Hager, and Ulrich S. Schubert

In 1987 the fundamental work of J.-M. Lehn, C. J. Pedersen and D. J. Cram was honored with the Nobel Prize in chemistry “for their development and use of molecules with structure-specific interactions of high selectivity” – namely the investigations in the field of crown ethers and host–guest interactions [1]. It was the beginning of supramolecular chemistry as a new research field in chemistry. Lehn defined supramolecular chemistry as the chemistry “beyond the molecule” [2]. Structures of higher complexity are constructed and held together by a wide range of interactions, like hydrophobic interactions [3], π – π stacking interactions [4], hydrogen bonding [5], and metal–ligand interactions [6]. Thereby nature acts as a role model by providing many inspiring examples of supramolecular structures, like the DNA structure (double helix), metallo-proteins, and so on.

In recent years, an area of special interest has been identified in metallo (supramolecular) polymers. These materials have been utilized also for the fabrication of stimuli-responsive structures resulting in reversible polymeric materials with a high dependence on the environment [7]. Due to this fact, metallopolymers have also been discussed in the context of self-healing materials. Their structural elements can feature also reversible interactions, like those known from hydrogen-bonding polymers (see Chapter 11) [8] or reversible covalently-linked polymers (see Chapter 6) [9, 10].

The afore-mentioned properties, that is, reversibility and stimuli-responsiveness, are directly related to the metal–ligand binding strength. By changing the ligand and the metal ion, respectively, the intrinsic properties of the final material can be adjusted within a certain range.

First, Ciardelli classified the architecture of metallopolymers into three types (Figure 12.1) [11, 12]. In Type I, the metal–ligand pairs are attached to the polymer side-chain or as an end group of the backbone by electrostatic interactions, covalent bonds or metal–ligand coordination (Type I a–c, Figure 12.1). In Type II, the metal ions/complexes are embedded into the main chain by coordinative or covalent associations. Type III depicts the assembling of metal ions into the polymeric arrangement (i.e., the matrix) by physical interactions [13]. In particular, polymers of Types I and II are interesting candidates for self-healing polymers.

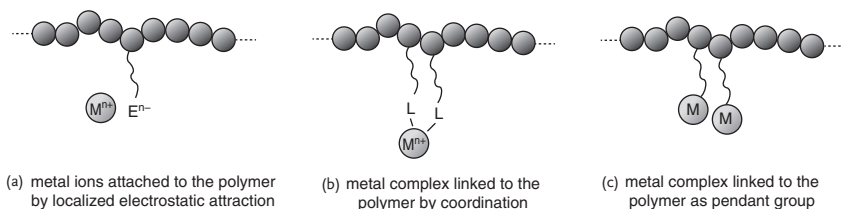
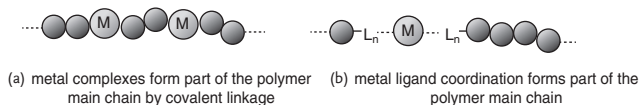
Type I: Metal ions/complexes linked to a chain or surface of a polymer molecule**Type II: Metal complexes as a part of the polymer chain****Type III: Metal ions/complexes interact with polymer physically**

Figure 12.1 Various approaches in preparing metal-containing polymers (the counter ions are omitted for clarity) (Copyright 2012 The Royal Society of Chemistry) [11].

The application of metallopolymers gained significant importance as redox-active materials to create, highly efficiently, redox conductivity for chemo- and biosensors [14], catalytic, and electroluminescent applications [15]. The magnetic properties of coordination polymers play an important role in the construction of multifunctional magnetic materials, such as nanoporous magnets and chiral magnets for advanced functions [16]. In addition, the alignment of the magnetic moments, as well as providing ferromagnetic-, ferrimagnetic- or superparamagnetic properties (solid state), make metallopolymers interesting materials for a wide range of applications [17].

For metal–ligand interactions, the conjunction of both a high binding constant and sufficient reversibility, represents a complicated task. The stability of a certain complex, a thermodynamic property, is represented by the individual binding constant K . In the case of a very high binding constant between the ligand(s) and the corresponding metal ion, thermodynamically stable polymers are formed. Their polymer physics and the properties of these polymers are comparable to classical covalent polymers. For a low binding constant, polymeric assemblies only form in the solid state, not in solution (classical inorganic coordination polymers). On the contrary, medium binding constants enable the formation of macromolecular assemblies also in solution. The binding constant K depends on several external parameters, such as pH, temperature, solvent, as well as on the ligand design and the corresponding metal ion. K can be increased by multiple interacting binding sites, such as chelating ligands or multivalent metal ions. Thus, for

Table 12.1 Binding constants for Zn²⁺-complexed pyridine-based ligands [16].

Ligand type	K_1 (M ⁻¹)	Bn (M ⁻¹)	Solvent/counterion
Pyridine/ZnTPP (5,10,15,20-tetraphenylporphyrin)	4.1×10^3	4.1×10^3 (n - 1)	CHCl ₃ /-
	3.3×10^3	3.3×10^3 (n - 1)	CHCl ₃ /-
	3.8×10^3	3.8×10^3 (n - 1)	Benzene/-
	2.0×10^4	2.0×10^4 (n - 1)	CCl ₄ /-
bpy/Zn ²⁺	2.5×10^5	2×10^{13} (n - 3)	Aqueous KNO ₃
	2.0×10^5	4.2×10^{13} (n - 3)	0.1 M aqueous NaNO ₃
phen/Zn ²⁺	2.7×10^6	1×10^{17} (n - 3)	Aqueous KNO ₃
	3.5×10^6	2.5×10^{17} (n - 3)	0.1 M aqueous NaNO ₃
tpy/Zn ²⁺	2.7×10^6	>10 ⁸	CH ₃ CN/ClO ₄ ⁻
	3.5×10^6	8×10^9 (n - 2)	CH ₃ CN/ClO ₄ ⁻
	2.5×10^8	2×10^{14} (n - 2)	CH ₃ CN/ClO ₄ ⁻ /TBAPF

every metal–ligand pair, a detailed investigation of the thermodynamic and kinetic properties is required when a suitable metal–ligand combination is chosen.

It is possible to investigate soluble metallo-supramolecular polymers in a defined manner by choosing the exact boundary conditions of the self-assembly process. A variety of polymers relying on kinetically inert transition-metal complexes were simply characterized in solution by prevalent analytical methods. In contrast, the successful characterization of polymers formed by kinetically labile transition-metal complexes in solution has only become possible in recent years [18, 19]. Würthner *et al.* investigated, for example, the increase in the binding constant of different pyridine-based chelate ligands complexed with Zn²⁺ ions (Table 12.1) [18]. Kinetic labile metal–ligand interactions open a field for materials with remarkable properties by assembling, disassembling, and reconstructing in a dynamic way. These weak interactions are utilized in materials which have the ability to self-repair [20], self-anneal and self-correct under certain conditions [21]. In 1996 Lehn *et al.* delivered the proof of the dynamic reversibility of labile metal–ligand interactions in their work on metallohelicates [22].

The structural moieties of metal complexes within polymers can be distinguished into main-chain and side-chain attached systems (Figure 12.2). There are some more structural units which will not be discussed in detail in this chapter. The review of Whittell *et al.* provides a good overview of the structural diversities of metal complexes in polymers [9]. Usually the focus is placed on the metal ion when developing a desired property into a main-chain organometallic polymer. However, the matrix of the organic moieties, linking metal centers along the polymer backbone, has to be chosen accurately. These bridging units are primary components of the polymer backbone and influence the intrinsic properties of the

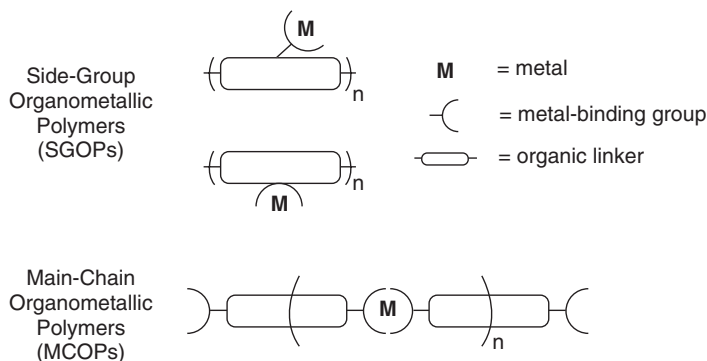


Figure 12.2 Design of side-chain (a) and main-chain (b) metallo-polymers (Copyright 2012 The Royal Society of Chemistry) [23].

particular metallo-polymer in an essential manner. It is important that the ligands exhibit high binding affinities toward the metal ions, so that a sufficient thermodynamic driving force exists to support polymerization, and to achieve polymers with high molar masses. For the respective polymers it has to be taken into account that every intrinsic property (interacting among each other), often ends up impacting others. Therefore, it is necessary to adjust both transition metal and monomer to design a new organometallic polymer. Several examples have been published in the last 20 years. In 1992 Constable *et al.* introduced terpyridyl-functionalized telechelic moieties into polymeric block structures [24]. Rehahn and coworkers described the synthesis and characteristic properties of well-defined tetrapyrrophenanzin-, and bipyridine-based Ru(II) metallo-polymers [25].

Metal incorporation in side-group metallo-polymers is achieved by attaching a ligand moiety to a polymeric backbone. The features of the metal center and the polymer main-chain can generally be tuned independently. For instance, organic monomers containing an appropriate ligand can be polymerized by using standard polymerization techniques (e.g., ionic, radical, ring-opening, or various types of condensation polymerization reactions) [26]. Once the resulting polymer is prepared, the addition of a transition metal precursor leads to the linked ligand and completes the synthesis of the side-group organometallic polymer. Moreover, complexation of these polymers with metal ions yields crosslinked networks. The groups of Schubert [27] and Tew [28] intensively studied grafting copolymers containing terpyridine moieties in the side chain.

Most metallo-polymers contain ionic metal complexes. The combination of these positively charged moieties and the corresponding counter ions can lead to interesting properties. The melt morphology of diblock copolymers with central metal complexes as the linking unit depends strongly on the type and size of the counterions. The groups of Schubert and Gohy investigated the self-assembly of systems which have ruthenium ions as the metal, complexed with terpyridine ligands attached to PS and PEO [29]. In bulk, the electrostatic interactions between

the metal–ligand complex ions and their counter ions drive them to form aggregates [30]. This leads to morphologies that are different to their covalent counterpart. Al-Hussein *et al.* reported highly ordered lamellar structures in the melt of a PS₂₀-[Ru]-PEO₇₀ diblock copolymer when bulky counterions are used. Thereby the metal–ligand complex acting as ionomer is responsible for triggering the microphase separation. This observation can be used to tune the morphology of the metallo-supramolecular copolymers [31]. The electrostatic interaction between the metal–ligand ions and their associated counterions drives them to form aggregates. The described morphology features for metallopolymers show some parallels with the situation in common ionomers, in which the ionic clusters contribute strongly to the healing process. This finding has also to be considered for self-healing metallopolymers.

12.1

Stimuli-Responsive Metallopolymers

The introduction of metal complexes into polymeric materials can lead to interesting properties and, particularly, the structural properties of these complexes are of importance concerning self-healing materials [9]. It is important for the self-healing process that special properties can be changed upon application of an external stimulus, for example, light, heat or pH. These stimuli-responsive metallopolymers can be affected in many different ways. Therefore, they are not only interesting candidates for self-healing polymers but also several other application fields have been discussed [32].

Suzuki *et al.* showed, for example, that the different oxidation states of ruthenium ions influence other properties of the metallopolymer, for example, hydrophilic properties [33]. For this purpose, (4-vinyl-4'-methyl-2,2'-bipyridine)*bis*(2,2'-bipyridine) ruthenium(II) *bis*(hexafluorophosphate) was copolymerized with *N*-isopropylacrylamide and a crosslinker. The resulting metallopolymer was used as a catalyst for the Belousov–Zhabotinsky reaction, which leads to rhythmical redox change. As result, the hydrophilic properties of the polymer change with the different oxidation states of the ruthenium ion, furthermore, it could be shown that the chemical oscillation of the metal oxidation state leads to a mechanical oscillation (swelling/deswelling). The amplitude and the period of the Belousov–Zhabotinsky reaction, which is catalyzed by the ruthenium metallopolymer, can be controlled by visible light [34]. As a consequence, a second stimulus which can influence the metallopolymer, is introduced.

Eloi and coworkers described a polystyrene-*block*-polyferrocenylsilane copolymer, which changes its three-dimensional structure [35]. In dichloromethane the formation of spherical micelles could be observed, if the iron center is oxidized (Figure 12.3).

This change in the three-dimensional structure represents an interesting feature for self-healing processes, because an external stimulus leads to a kind of mobility of the polymeric material which could promote a self-healing process. Moreover,

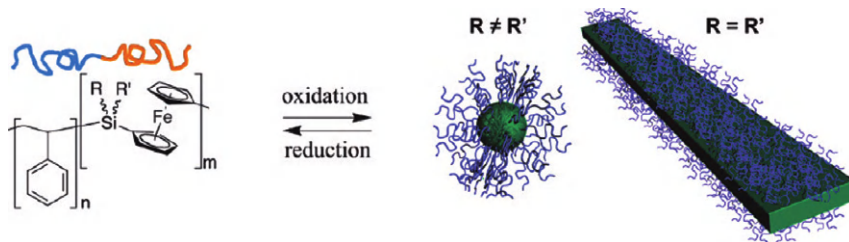


Figure 12.3 Changes in the three-dimensional structure by reversible redox processes (Copyright 2012 American Chemical Society) [35].

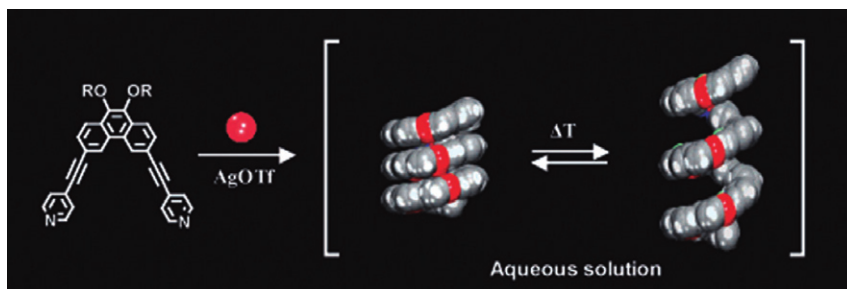


Figure 12.4 Schematic representation of the helical spring (Copyright 2012 American Chemical Society) [39].

mechanical damage (e.g., cracks, scratches) could be closed by movement or volume changes.

Beside the stimulation by redox processes, the properties of a metallopolymer can also be influenced by other stimuli. An interesting change in metallopolymer was shown by Peng *et al.* [36]. The authors used the external stimulus light in order to influence the properties of an iron metallopolymer; a redox process from iron(III) to iron(II) could be induced by light and this process changes the consistency of the polymer. In this case, a metallopolymer gel, which contains iron(III) ions, was converted into a liquid polymer by simply reducing the iron ions. The following reoxidation by air leads to the original “solid” state system.

Furthermore, the supply of thermal energy could also be used to influence the properties of a metallopolymer and to yield the desired effects. For this purpose, Zhou and coworkers utilized ruthenium-containing polymers with two glass transition temperatures and a phase separation could be observed [37]. These transitions induce the kind of mobility which is required for the self-healing process [38].

Kim *et al.* described another fascinating example [39]. In this case, a ligand based on pyridine and phenanthrene was mixed with a silver salt, forming helical structures in aqueous solution. The distance between the windings increased if the solution was heated (Figure 12.4). The observed mobility could also be used for self-healing processes if it could also be applied in the solid state.

Beside the mentioned external stimuli there are also several other possibilities which can influence the polymer properties and structures, leading to changes on the molecular scale and to other properties of the metallopolymer. Beck and Rowan showed, for example, that mechanical energy is adequate (e.g., simple shaking) to generate a change in the properties of the polymer [40]. The authors used an oligo-ethyleneglycol, which was functionalized with two 2,6-bis(1'-methylbenzimidazolyl)pyridine units at the termini. In a second step a metallopolymer was formed by the addition of a lanthanoid (lanthanum or europium) and a transition metal ion (cobalt or zinc). In further studies it was shown that these metallopolymers could also be influenced by other external stimuli [41, 42], for example, by changes in the pH. The influence of light and temperature have also been reported.

This all-embracing example shows that many different stimuli can affect a metallopolymer, resulting in the desired property. In particular, the reversibility of the metal–ligand interaction and the mobility of a metallopolymer are the key factors for the implementation of self-healing properties [43]. Additionally, the addressability by other stimuli features the possibility to trigger healing processes in metallopolymers.

12.2 Self-Healing Metallopolymers

The afore-mentioned properties of metallopolymers are the basic requirements for the generation of self-healing behavior. It is possible to generate a reversible system and to imply self-healing mechanisms, which is the principle of intrinsic self-healing systems [44].

The self-healing possibilities based on metal–ligand interactions were first described in natural systems in 2001 when Vaccaro and Waite reported the ability of mussels to repair their mussel threads after an inflicted damage [45]. In the following decade more insights into the mechanism and the parameters influencing this natural system with external stimuli were collected. It was shown that the self-healing is based on an interaction between iron(III)-ions and 3,4-dihydroxyphenylalanine (dopa) [46]. The iron center can bind one, two or three catechol-based ligands, which are connected to a polymer backbone. The number of bonded ligands depends on the pH (Figure 12.5) [47, 48]. At low pH (below 5) the mono-dopa iron(III) complex is formed, which leads to no crosslinking of the polymer chains. The result is an extensible material. Increasing the pH leads to a more crosslinked polymer network with increased hardness [46, 49].

This principle, which can be found in nature, could be mimicked by synthetic polymers. For this purpose polyethylene glycol was functionalized with catechol units and Holten-Andersen *et al.* were able to show the reversibility of the metal–ligand interaction [47].

It was shown that the zinc histidine system also leads to a self-healing behavior of mussel byssus threads [50, 51]; a fiber containing a middle block of collagen,

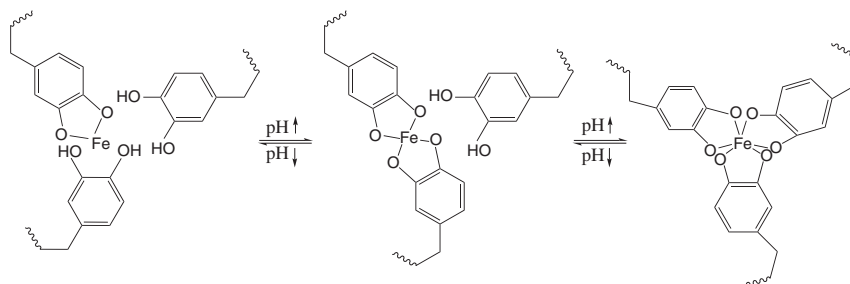


Figure 12.5 Schematic representation of the pH-dependent stoichiometry of iron(III)-catechol complexes [47].

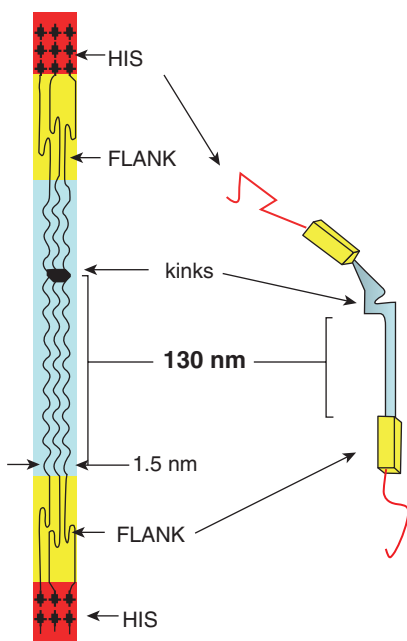


Figure 12.6 Schematic representation of a mussel fiber, which consists of a collagen part flanked by histidine-rich parts (Copyright 2012 American Chemical Society) [51].

which is flanked by histidine-rich parts, in an environment with a high content of zinc leads to reversible crosslinking (Figure 12.6) [51, 52].

Furthermore, several synthetic metallopolymer have been synthesized to obtain self-healing behavior based on metal–ligand interactions. Already in 2005 Varghese *et al.* showed that a gel, based on acryloyl-6-amino caproic acid (A6ACA), could heal scratches, if the polymer is dipped into an aqueous copper(II) chloride solution [53]. However, the performed study does not answer the question of the influence of the hydrogen bonds on the self-healing effect, of particular importance because a medium was selected in which hydrogen bonds exist. Beside that the mobility of

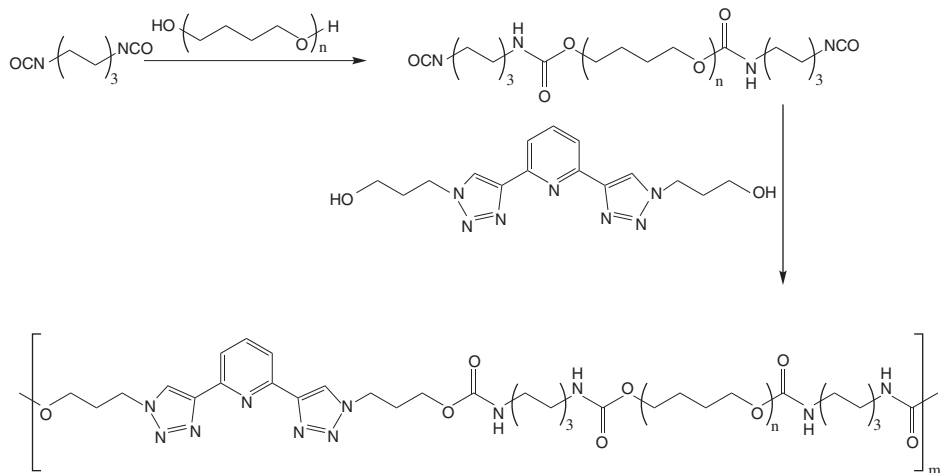


Figure 12.7 Schematic representation of the synthesis of a polymer with a ligand function in the main chain [54].

the gel itself could also affect the self-healing behavior, therefore the particular influence of the metal–ligand interaction on the self-healing process is unclear.

Beside the incorporation of the ligand function in the side chain, it is also possible to install the ligand in the main chain of the polymer. Yuan *et al.* showed that self-healing behavior can be generated by polymers which feature ligands within the main chain [54]. The authors used polyurethane analog polymers as the backbone, in which *bis*(1,2,3-triazol-4-yl) pyridine was incorporated as ligand (Figure 12.7). These polymers were then complexed with zinc(II) and europium(III) ions, respectively, which led to self-healing properties. In this case there is also a question as to whether the metal–ligand interaction is the reason for the self-healing process. There is also the possibility of hydrogen bond formation, which could also contribute to the self-healing properties. In addition, the self-healing efficiency was not quantified.

In 2011 Rowan, Weder *et al.* described the self-healing properties of a linear metallopolymer using UV-light [20]. For this purpose, poly(ethylene-*co*-butylene) was functionalized with two 2,6-*bis*(1'-methylbenzimidazolyl)pyridine at the termini and the following addition of zinc di[*bis*(trifluoromethylsulfonyl)imide] or the lanthan tri[*bis*(trifluoromethylsulfonyl)imide] led to a linear metallopolymer. This metallopolymer showed self-healing behavior when irradiated with UV-light with a wavelength situated in the absorption band of the polymer. In this case, energy transfer could be followed by the heating curve (see Figure 12.8). A proposed mechanism for the self-healing process is based on the reversibility of the metal–ligand interaction (Figure 12.9). The cleavage of the metal complexes increases the mobility of the polymer, which leads to self-healing of inflicted damage. Subsequently, the complexes will be re-formed upon cooling, resulting in an immobilization of the mobile phase and a (complete) healing of the scratch.

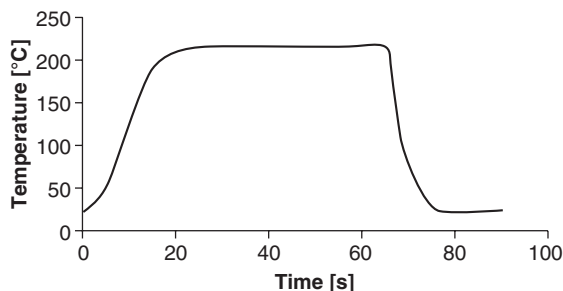


Figure 12.8 Surface temperature of the polymer on irradiation for 60 s [20].

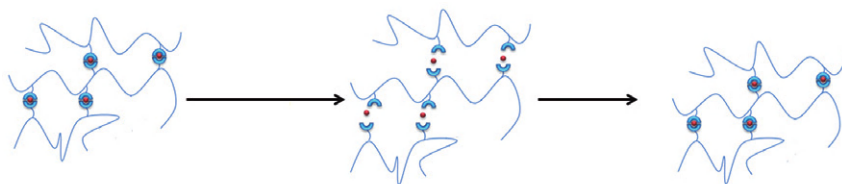


Figure 12.9 Purposed healing mechanism of a linear metallopolymer.

12.3

Summary and Outlook

The fascinating material class of metallopolymers features interesting properties due to the combination of polymeric properties with the distinct properties of metal complexes. The combination of a wide variation of different metal ions with the corresponding ligands allows tuning of the desired properties. In the field of stimuli-responsive polymers metallopolymers have been frequently applied. These properties would allow the utilization of interesting triggers (e.g., light) for a self-healing process. However, in contrast to other non-covalent interactions, in particular in comparison to the prime example of hydrogen bonds, metal complexes have been applied less frequently in self-healing materials. First examples confirm the great potential of these materials and significant improvement can be expected in the future. Nature, which utilizes successfully these interactions (e.g., mussel byssus threads), reveals another important issue: the order and arrangement of the metal complexes.

Currently, the healing of some synthetic materials (see examples described above) can be described on the molecular as well as the macroscopic level.

Starting on the macroscopic level, the deformation of the metallopolymer has to be mainly elastic (in particular, when coatings and thin films are considered). However, plastic deformation will not provide a restoring force. The elastic recovery is important for self-healing, representing the first step in the self-healing process [55].

The healing mechanism on a molecular scale within metallopolymers can be based on the ionic structure of the complexes and/or on the reversibility of the metal complexes.

Most metal–ligand complexes are positively charged and this could lead to an ionic structure and to the formation of ionic clusters. Comparable to “classic” ionomers, a healing process within metallopolymers could be supported by the ionic interactions of positively charged metal complexes and the corresponding counter ions [56].

Furthermore, the strength of the metal–ligand bonding can be tuned and, thereby, it is possible to identify a system where the metal–ligand bonding is weaker than the bonds of the polymer backbone. After mechanical damage it is possible to break the metal–ligand interaction and induce flexibility and mobility. This change leads to a healing of the mechanical damage; however, the breaking of the bonds requires energy. The phenomenon is known from metal–ligand bonds in solution, but the study of the behavior of the metal–ligand interaction in the solid state is difficult [57].

Metallopolymers, as one of the youngest members of the self-healing polymer family, are a rather new research field. Many possibilities for the design of self-healing polymers are imaginable. Moreover, further intense research is required to clarify the detailed mechanisms of the healing within these materials.

Acknowledgments

The authors thank the Deutsche Forschungsgemeinschaft (DFG, SPP 1568) and the Dutch Polymer Institute (DPI, technology area HTE) for financial support.

References

- 1 Brunsveld, L., Folmer, B.J.B., Meijer, E.W., and Sijbesma, R.P. (2001) Supramolecular polymers. *Chem. Rev.*, **101**, 4071–4097.
- 2 Lehn, J.-M. (1994) Supramolecular chemistry. *Proc. Indian Natl. Sci. Acad.*, **106**, 915–922.
- 3 Kästner, U. (2001) The impact of rheological modifiers on water-borne coatings. *Colloids Surf.*, **183**, 805–821.
- 4 Lehn, J.-M., Meric, R., Vigneron, J.-P., Cesario, M., Guilhem, J., Pascard, C., Asfari, Z., and Vicens, J. (1995) Binding of acetylcholine and other quaternary ammonium cations by sulfonated calixarenes. Crystal structure of a [choline-tetrasulfonated calix[4]arene] complex. *Supramol. Chem.*, **5**, 97–103.
- 5 ten Tessa Cate, A., and Sijbesma, R.P. (2002) Coils, rods and rings in hydrogen-bonded supramolecular polymers. *Macromol. Rapid Commun.*, **23**, 1094–1112.
- 6 (a) Hinderberger, D., Schmelz, O., Rehahn, M., Jeschke, G. (2004) Electrostatic site attachment of divalent counterions to rodlike ruthenium(II) coordination polymers characterized by EPR spectroscopy. *Angew. Chem. Int. Ed.*, **43**, 4616–4621; (b) Schmatloch, S., van den Berg, A.M.J., Alexeev, A.S., Hofmeier, H., and Schubert, U.S. (2003) Soluble high-molecular-mass poly(ethylene oxide)s via self-organization. *Macromolecules*, **36**, 9943–9949; (c) South, C.R., Burd, C., and Weck, M. (2007)

- Modular and dynamic functionalization of polymeric scaffolds. *Acc. Chem. Res.*, **40**, 63–74.
- 7 Weng, W., Beck, J.B., Jamieson, A.M., and Rowan, S.J. (2006) Understanding the mechanism of gelation and stimuli-responsive nature of a class of metallo-supramolecular gels. *J. Am. Chem. Soc.*, **128**, 11663–11672.
- 8 (a) Cordier, P., Tournilhac, F., Soulié-Ziakovic, C., and Leibler, L. (2008) Self-healing and thermoreversible rubber from supramolecular assembly. *Nature*, **451**, 977–980; (b) Kitagawa, S., and Uemura, K. (2005) Dynamic porous properties of coordination polymers inspired by hydrogen bonds. *Chem. Soc. Rev.*, **34**, 109–119.
- 9 Whittell, G.R., Hager, M.D., Schubert, U.S., and Manners, I. (2011) Functional soft materials from metalopolymers and metallosupramolecular polymers. *Nat. Mater.*, **10**, 176–188.
- 10 (a) Zhang, Y., Broekhuis, A.A., and Picchioni, F. (2009) Thermally self-healing polymeric materials: the next step to recycling thermoset polymers? *Macromolecules*, **42**, 1906–1912; (b) Yuan, Y.C., Yin, T., Rong, M.Z., and Zhang, M.Q. (2008) Self healing in polymers and polymer composites. Concepts, realization and outlook: a review. *Expr. Polym. Lett.*, **2**, 238–250.
- 11 Happ, B., Winter, A., Hager, M.D., and Schubert, U.S. (2012) Photogenerated avenues in macromolecules containing Re(I), Ru(II), Os(II), and Ir(III) metal complexes of pyridine-based ligands. *Chem. Soc. Rev.*, **41**, 2222–2255.
- 12 Ciardelli, F., Tsuchida, E., and Wöhrle, D. (eds) (1996) *Macromolecule-Metal Complexes*, Springer-Verlag, Heidelberg.
- 13 Chan, W. (2007) Metal containing polymers with heterocyclic rigid main chains. *Coord. Chem. Rev.*, **251**, 2104–2118.
- 14 McQuade, D.T., Pullen, A.E., and Swager, T.M. (2000) Conjugated polymer-based chemical sensors. *Chem. Rev.*, **100**, 2537–2574.
- 15 Holliday, B.J., and Swager, T.M. (2005) Conducting metalopolymers: the roles of molecular architecture and redox matching. *Chem. Commun.*, 23–36.
- 16 Batten, S.R., Neville, S.M., and Turner, D.R. (2009) *Coordination Polymers: Design, Analysis and Application*, Royal Society of Chemistry, Cambridge.
- 17 Manners, I. (2002) *Synthetic Metal-Containing Polymers*, John Wiley & Sons, Ltd, Chichester.
- 18 Dobrawa, R., and Würthner, F. (2005) Metallosupramolecular approach toward functional coordination polymers. *J. Polym. Sci. Part A: Polym. Chem.*, **43**, 4981–4995.
- 19 Kurth, D.G. (2008) Metallo-supramolecular modules as a paradigm for materials science. *Sci. Technol. Adv. Mater.*, **9**, 14103.
- 20 Burnworth, M., Tang, L., Kumpfer, J.R., Duncan, A.J., Beyer, F.L., Fiore, G.L., Rowan, S.J., and Weder, C. (2011) Optically healable supramolecular polymers. *Nature*, **472**, 334–337.
- 21 Kurth, D.G., and Higuchi, M. (2006) Transition metal ions: weak links for strong polymers. *Soft Matter*, **2**, 915.
- 22 Hasenknopf, B., Lehn, J.-M., Baum, G., and Fenske, D. (1996) Self-assembly of a heteroduplex helicate from two different ligand strands and Cu(II) cations. *PNAS*, **93**, 1397–1400.
- 23 Williams, K.A., Boydston, A.J., and Bielawski, C.W. (2007) Main-chain organometallic polymers: synthetic strategies, applications, and perspectives. *Chem. Soc. Rev.*, **36**, 729–744.
- 24 (a) Constable, E.C., and Thompson, A.M.W.C. (1992) Multinucleating 2,2′-terpyridine ligands as building blocks for the assembly of coordination polymers and oligomers. *J. Chem. Soc. Dalton Trans.*, **24**, 3467–3475; (b) Constable, E.C., and Thompson, A.M.W.C. (1992) A new ligand for the self assembly of starburst coordination oligomers and polymers. *J. Chem. Soc., Chem. Commun.*, **8**, 617–619; (c) Constable, E.C. (1995) Towards helical coordination polymers: molecular wires in chiral coats. *Macromol. Symp.*, **98**, 503–524.
- 25 (a) Knapp, R., Schott, A., and Rehahn, M. (1996) A novel synthetic strategy toward soluble, well-defined ruthenium(II) coordination polymers. *Macromolecules*, **29**, 478–480; (b) Kelch, S., and Rehahn,

- M. (1997) High-molecular-weight ruthenium(II) coordination polymers: synthesis and solution properties. *Macromolecules*, **30**, 6185–6193.
- 26 Oadian, G. (2004) *Principles of Polymerization*, John Wiley & Sons, Ltd, Chichester.
- 27 (a) Hofmeier, H., and Schubert, U.S. (2005) Combination of orthogonal supramolecular interactions in polymeric architectures. *Chem. Commun.*, **19**, 2423–2432; (b) Heller, M., and Schubert, U.S. (2002) Polystyrene with pendant mixed functional ruthenium(II)-terpyridine complexes. *Macromol. Rapid Commun.*, **23**, 411–415.
- 28 (a) Aamer, K.A., and Tew, G.N. (2007) Synthesis, dynamic light scattering, and luminescence properties of copolymers containing iridium(III) bisterpyridine in the side chain. *J. Polym. Sci. Part A: Polym. Chem.*, **45**, 1109–1121; (b) Aamer, K.A., and Tew, G.N. (2007) Supramolecular polymers containing terpyridine–metal complexes in the side chain. *Macromolecules*, **40**, 2737–2744.
- 29 Fustin, C.-A., Guillet, P., Schubert, U.S., and Gohy, J.-F. (2007) Metallo-supramolecular block copolymers. *Adv. Mater.*, **19**, 1665–1673.
- 30 Al-Hussein, M., Lohmeijer, B.G.G., Schubert, U.S., and de Jeu, W.H. (2003) Melt morphology of polystyrene–poly(ethylene oxide) metallo-supramolecular diblock copolymer. *Macromolecules*, **36**, 9281–9284.
- 31 Al-Hussein, M., de Jeu, W.H., Lohmeijer, B.G.G., and Schubert, U.S. (2005) Phase behavior of the melt of polystyrene–poly(ethylene oxide) metallo-supramolecular diblock copolymer with bulky counterions. *Macromolecules*, **38**, 2832–2836.
- 32 Stuart, M.A.C., Huck, W.T.S., Genzer, J., Müller, M., Ober, C., Stamm, M., Sukhorukov, G.B., Szleifer, I., Tsukruk, V.V., Urban, M., Winnik, F., Zauschner, S., Luzinov, I., and Minko, S. (2010) Emerging applications of stimuli-responsive polymer materials. *Nat. Mater.*, **9**, 101–113.
- 33 Suzuki, D., Sakai, T., and Yoshida, R. (2008) Self-flocculating/self-dispersing oscillation of microgels. *Angew. Chem. Int. Ed.*, **47**, 917–920.
- 34 Shinohara, S.-I., Seki, T., Sakai, T., Yoshida, R., and Takeoka, Y. (2008) Photoregulated wormlike motion of a gel. *Angew. Chem. Int. Ed.*, **47**, 9039–9043.
- 35 Eloi, J.-C., Rider, D.A., Cambridge, G., Whittell, G.R., Winnik, M.A., and Manners, I. (2011) Stimulus-responsive self-assembly: reversible, redox-controlled micellization of polyferrocenylsilane diblock copolymers. *J. Am. Chem. Soc.*, **133**, 8903–8913.
- 36 Peng, F., Li, G., Liu, X., Wu, S., and Tong, Z. (2008) Redox-responsive gel–sol/sol–gel transition in poly(acrylic acid) aqueous solution containing Fe(III) ions switched by light. *J. Am. Chem. Soc.*, **130**, 16166–16167.
- 37 Zhou, G., Harruna, I.I., and Ingram, C.W. (2005) Ruthenium-centered thermosensitive polymers. *Polymer*, **46**, 10672–10677.
- 38 Wool, R.P. (2008) Self-healing materials: a review. *Soft Matter*, **4**, 400–418.
- 39 Kim, H.-J., Lee, E., Park, H.-S., and Lee, M. (2007) Dynamic extension–contraction motion in supramolecular springs. *J. Am. Chem. Soc.*, **129**, 10994–10995.
- 40 Beck, J.B., and Rowan, S.J. (2003) Multistimuli, multiresponsive metallo-supramolecular polymers. *J. Am. Chem. Soc.*, **125**, 13922–13923.
- 41 Weng, W., Li, Z., Jamieson, A.M., and Rowan, S.J. (2009) Effect of monomer structure on the gelation of a class of metallo-supramolecular polymers. *Soft Matter*, **5**, 4647–4657.
- 42 Rowan, S.J., and Beck, J.B. (2005) Metal-ligand induced supramolecular polymerization: a route to responsive materials. *Faraday Discuss.*, **128**, 43–53.
- 43 (a) Murphy, E.B., and Wudl, F. (2010) The world of smart healable materials. *Prog. Polym. Sci.*, **35**, 223–251; (b) Wang, F., Zhang, J., Ding, X., Dong, S., Liu, M., Zheng, B., Li, S., Wu, L., Yu, Y., Gibson, H.W., and Huang, F. (2010) Metal coordination mediated reversible conversion between linear and cross-linked supramolecular polymers. *Angew. Chem. Int. Ed.*, **49**, 1090–1094.
- 44 Hager, M.D., Greil, P., Leyens, C., van der Zwaag, S., and Schubert, U.S. (2010)

- Self-healing materials. *Adv. Mater.*, **22**, 5424–5430.
- 45 Vaccaro, E., and Waite, J.H. (2001) Yield and post-yield behavior of mussel byssal thread: a self-healing biomolecular material. *Biomacromolecules*, **2**, 906–911.
- 46 Harrington, M.J., Masic, A., Holten-Andersen, N., Waite, J.H., and Fratzl, P. (2010) Iron-clad fibers: a metal-based biological strategy for hard flexible coatings. *Science*, **328**, 216–220.
- 47 Holten-Andersen, N., Harrington, M.J., Birkedal, H., Lee, B.P., Messersmith, P.B., Lee, K.Y.C., and Waite, J.H. (2011) pH-induced metal-ligand cross-links inspired by mussel yield self-healing polymer networks with near-covalent elastic moduli. *PNAS*, **108**, 2651–2655.
- 48 Harrington, M.J., and Waite, J.H. (2008) pH-dependent locking of giant mesogens in fibers drawn from mussel byssal collagens. *Biomacromolecules*, **9**, 1480–1486.
- 49 (a) Harrington, M.J., Gupta, H.S., Fratzl, P., and Waite, J.H. (2009) Collagen insulated from tensile damage by domains that unfold reversibly: in situ X-ray investigation of mechanical yield and damage repair in the mussel byssus. *J. Struct. Biol.*, **167**, 47–54; (b) Harrington, M.J., and Waite, J.H. (2009) How nature modulates a fiber's mechanical properties: mechanically distinct fibers drawn from natural mesogenic block copolymer variants. *Adv. Mater.*, **21**, 440–444.
- 50 (a) Waite, J.H., Qin, X.-X., and Coyne, K.J. (1998) The peculiar collagens of mussel byssus. *Matrix Biol.*, **17**, 93–106; (b) Carrington, E., and Gosline, J.M. (2004) Mechanical design of mussel byssus: load cycle and strain rate dependence. *Am. Malacol. Bull.*, **18**, 135–142.
- 51 Waite, J.H., Lichtenegger, H.C., Stucky, G.D., and Hansma, P. (2004) Exploring molecular and mechanical gradients in structural bioscaffolds. *Biochemistry*, **43**, 7653–7662.
- 52 Waite, J.H., and Broomell, C.C. (2012) Changing environments and structure-property relationships in marine biomaterials. *J. Exp. Biol.*, **215**, 873–883.
- 53 Varghese, S., Lele, A., and Mashelkar, R. (2006) Metal-ion-mediated healing of gels. *J. Polym. Sci. Part A: Polym. Chem.*, **44**, 666–670.
- 54 Yuan, J., Fang, X., Zhang, L., Hong, G., Lin, Y., Zheng, Q., Xu, Y., Ruan, Y., Weng, W., Xia, H., and Chen, G. (2012) Multi-responsive self-healing metallo-supramolecular gels based on “click” ligand. *J. Mater. Chem.*, **22**, 11515–11522.
- 55 Wool, R.P. (2008) Self-healing materials: a review. *Soft Matter*, **4**, 400–418.
- 56 (a) Varley, R.J., and van der Zwaag, S. (2008) Towards an understanding of thermally activated self-healing of an ionomer system during ballistic penetration. *Acta Mater.*, **56**, 5737–5750; (b) Kalista, S.J., and Ward, T.C. (2007) Thermal characteristics of the self-healing response in poly(ethylene-co-methacrylic acid) copolymers. *J. R. Soc. Interface*, **4**, 405–411.
- 57 (a) Lohmeijer, B.G.G., and Schubert, U.S. (2003) Water-soluble building blocks for terpyridine-containing supramolecular polymers: synthesis, complexation, and pH stability studies of poly(ethylene oxide) moieties. *Macromol. Chem. Phys.*, **204**, 1072–1078; (b) Gohy, J.-F., Lohmeijer, B.G.G., and Schubert, U.S. (2002) Metallo-supramolecular block copolymer micelles. *Macromolecules*, **35**, 4560–4563; (c) Gohy, J.-F., Lohmeijer, B.G.G., and Schubert, U.S. (2002) Reversible metallo-supramolecular block copolymer micelles containing a soft core. *Macromol. Rapid Commun.*, **23**, 555–560; (d) Gohy, J.-F., Lohmeijer, B.G.G., Varshney, S.K., Décamps, B., Leroy, E., Boileau, S., and Schubert, U.S. (2002) Stimuli-responsive aqueous micelles from an ABC metallo-supramolecular triblock Copolymer. *Macromolecules*, **35**, 9748–9755.

13

Self-Healing Ionomers

Nico Hohlbein, Max von Tapavicza, Anke Nellesen, and Annette M. Schmidt

13.1

Introduction

Non-covalent ionic bindings play an important role in nature's self-healing procedures. One example is the role of cations in the coagulation of natural latex. These cations are needed to dimerize two protein molecules and in this way enable the proteins to attach to latex particles, initiating the coagulation-based wound repair process (Figure 13.1) [1, 2]. A possibility to transfer this concept to synthetic polymers is to equip polymer chains with ionic groups and to add an adequate counterion to the polymer matrix. These ionic groups aggregate to larger complexes, which contribute strongly to the intermolecular binding capacity. When such a complex is destroyed due to a crack, it can be reformed after a short relaxation period. For this concept to be successful, it is necessary that the polymer matrix provides enough mobility on a molecular level, so that the polymer chains can rearrange and interpenetrate. The properties of a self-healing ionomeric polymer can be easily varied by adapting the ionic content and by using different counterions. In contrast to other self-healing concepts, that are based on a chemical healing-reaction, the ionomeric healing process is reproducible and provides the material with a persistent and repeated self-healing functionality.

13.2

Basic Principles of Ionomers

Ionomers are polymers with organic or inorganic main chains, composed of repeating units that are partially decorated with ionic groups and their counterions. According to Eisenberg and Rinaudo, they are defined as "polymers in which the bulk properties are governed by ionic interactions in discrete regions of the material" [3]. As such, the ionic content is generally between 1 and 15%, and hence ionomers represent an interim position between neutral polymers and polyelectrolytes. Even though inorganic ionomers are also known, for self-healing purposes mainly ionomers with an organic backbone are proposed.

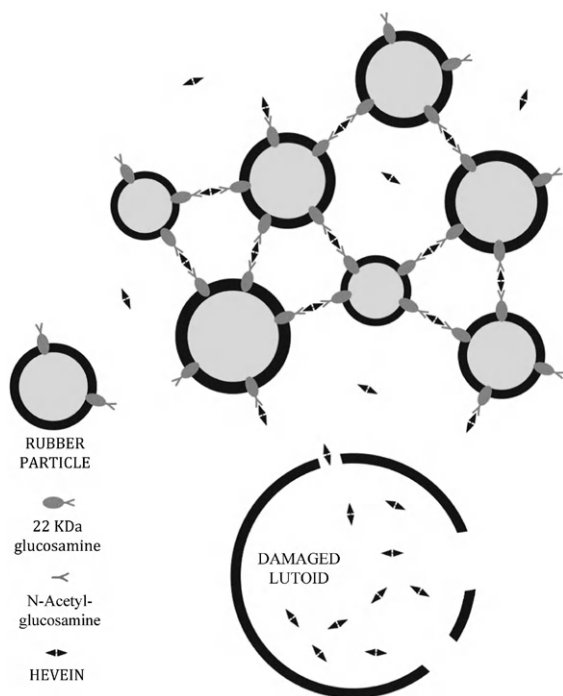


Figure 13.1 Coagulation of caoutchouc from *Hevea brasiliensis*. Reprinted with permission from [1]. Copyright 1995, Elsevier.

Ionic groups, as a consequence of their charged nature, are generally of dipolar character, while the main component of organic ionomers is often constituted of chain segments with a low polarity and dielectric constant. The resulting strong interaction between ionic moieties leads to the separation of polar and nonpolar phases, comparable to the well-investigated microphase separation observed in block copolymers [4–7]. Consequently, every ionic pair is part of a supramolecular network of physical crosslinks, resulting in unique structural, mechanical and dynamic properties. As the phase separation can be overcome thermally in most ionomers, the network formation is thermally reversible.

Various anionic and cationic functional groups have been considered for the purpose of ionic crosslinks. Carboxylates and sulfonates are commonly used and have a huge importance for today's industrial ionomer production [8, 9]. These anionomers are typically neutralized with alkaline, alkaline earth or transition metal cations. Other ionic groups employed are based on thioglycolate or phosphonate, and cationomers, e. g. containing quaternary ammonium groups are also known [9–11].

From a structural point of view, the ionic groups can be distributed either randomly along the main chain or systematically arranged in block copolymers. Principally they can be attached directly to the backbone, in the side chains or at the end of the polymer chains, as shown in Figure 13.2.

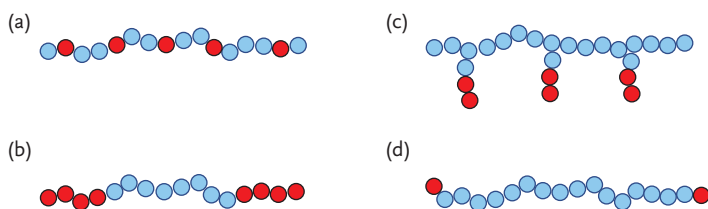


Figure 13.2 Examples of different ionomer architectures: (a) random, (b) block-like, (c) side chain and (d) telechelic distribution of ionic groups.

The morphology of polymers that combine ionic and non-ionic regions in the same macromolecule raised the interest of many scientists in the late 1960s. Initiated by the experimental and theoretical studies on ionic aggregation of Wilson, Longworth and Vaughn [12, 13], several model systems were developed to elucidate the structure–property correlations [14–17]. In 1989, Tadano *et al.* proposed the concept for an order–disorder transition of ionic clusters in ionomers that is based on differential scanning calorimetry (DSC) and thermal expansion studies of methacrylate-based ionomers [18]. Based on this idea, the theoretical model of Eisenberg–Hird–Moore (EHM) was developed in 1990, and is an established concept today [15]. Their comprehensive theory describes the formation of ionic aggregates from the molecular to the micro- and macro-size level, thus implementing the morphology as well as the mechanical and dynamic properties. Referring to this theory, several important factors govern the structural formation, such as the ionic content, the coordination of counter-ions, the flexibility of the polymer backbone, and the dielectric constant of the polar and nonpolar segments. According to the model, multiplets are the smallest ionic aggregates, consisting of up to ten ion pairs (Figure 13.3). The ionic association causes a restriction of mobility of the surrounding polymer backbone on a scale of about 10–50 Å. The average size of multiplets is determined by the number and size of the involved ionic groups, and by the elastic properties of the polymer backbone. In the very low ion content regime, the multiplet size increases with ion concentration along the main chain, as more and more ion pairs are included in the aggregate [14]. Experimental results show that these multiplets have a sharp interface, and that their structure is almost insensitive to the addition of organic nonpolar solvents [19].

For a given system, the size of the multiplets is usually limited due to the steric demand of the polymeric “substituents”. Thus, simultaneously with increasing ion concentration, the number of multiplets increases and, finally, clusters are formed by overlapping of the restricted chain segments and electrostatic interaction between different multiplets [20]. Figure 13.4 illustrates the development of multiplet clusters in the course of increasing multiplet density [15, 21]. The formation of multiplets and clusters is supported by the observation of a second distinctive glass transition temperature T_i . The ionic crosslinking and the region of reduced mobility from uncharged chain segments results in a higher glass transition of clusters compared to the matrix. Several studies have been performed on the correlation

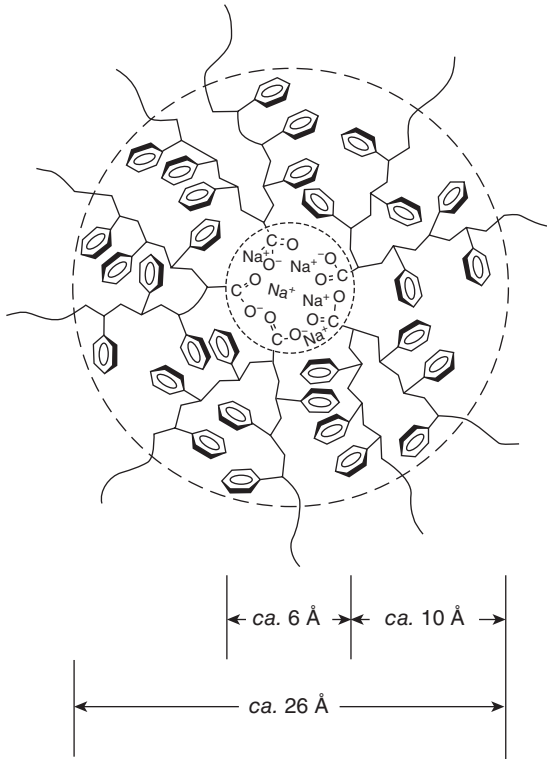


Figure 13.3 Scheme of a multiplet in poly(styrene-co-sodium-methacrylate) ionomer encircled by a region of restricted polymer mobility. Reprinted with permission from [15]. Copyright 1990, American Chemical Society.

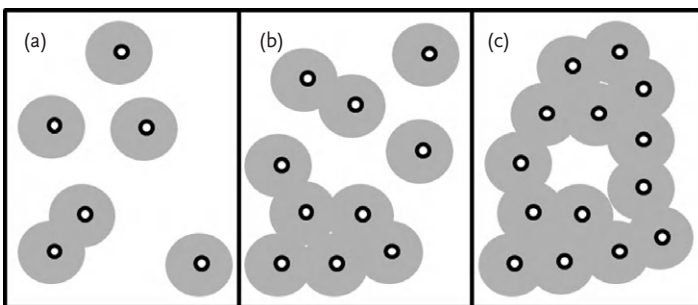


Figure 13.4 Cluster formation by multiplet overlap as observed with increasing ion concentration (a to c). Adapted with permission from [15]. Copyright 1990, American Chemical Society.

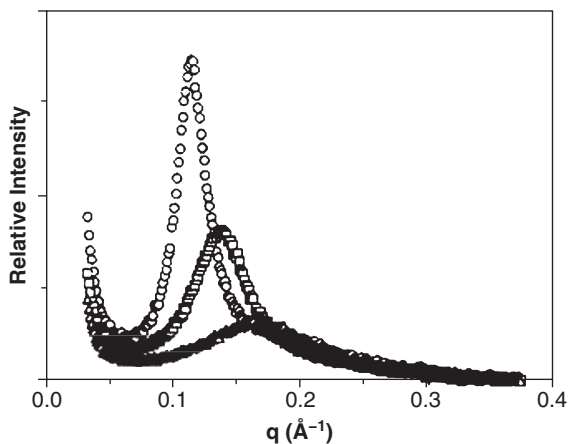


Figure 13.5 SAXS data for partially hydrolyzed ionomers with alkyl side chains, neutralized with Cs^+ . (\circ) C_{11} ; (\square) C_6 ; (Δ) C_2 -side chains. Reprinted with permission from [24]. Copyright 1991, American Chemical Society.

of transition temperature and the nature of the counter-ion, or the distance between cation and anion. Eisenberg observed a sigmoidal increase of the ionic cluster transition temperature T_i with rising ion content of ethyl-acrylic acid ionomers, and similar results were obtained from other materials [22, 23]. According to several studies it can be generalized that sulfonated systems show a higher cluster transition temperature T_i compared to carboxylated ones, possibly due to stronger interactions of ion and counter-ion [21].

Today, the concept of EHM is strongly supported by experimental results. Small-angle X-ray scattering (SAXS) measurements show the appearance of discrete regions of high electron density within the otherwise more transparent bulk phase [24]. The angular variation of the scattered intensity can be attributed to ion groups, and can be used to extract detailed information on the cluster (Figure 13.5). The occurrence of an ionic peak is an evidence of clusters, and can be observed for a wide range of ionic groups, counter-ions, and matrix materials. Another method to directly image the ionic clusters is based on transmission electron microscopy (TEM) [8]. By staining the organic, nonpolar phase with osmium tetroxide, the phase structure of the ionomer can be imaged with the ionic phase imaged unstained. The unstained phase can be observed to change its size and quantity with neutralization degree and ionic content.

13.2.1

Properties

The presence of ionic aggregates, like multiplets and clusters, leads to a number of unique structural and dynamic properties. The basic common feature of all ionomeric polymers is the formation of a thermally reversible crosslinked system

where the microstructure governs the properties. The understanding of the microphase separation processes is thus fundamental to controlling the mechanical and dynamic performance of the material. Depending on the composition of the ionomer, transparency or an improved adhesion can also be achieved.

In general, ionomers show an improved tensile strength, toughness and flexibility compared to conventional copolymers. Many factors have influence on the properties of ionomers, including the nature of ionic groups and counter-ions, the neutralization degree, the elastic behavior of the main chain, the dielectric constant, and the presence of polar impurities, to name a few. From melt rheology experiments it is known that a higher content of acid groups as well as a higher neutralization degree can lead to higher stiffness and increasing melt viscosity and relaxation time by several orders of magnitude, resulting from enhanced network integrity. The association strength and the content of ionic groups also play a significant role. Methods like rheology or dynamic mechanical spectroscopy are suitable to measure the complex dynamic modulus of the material as a function of temperature and frequency. The loss angle ($\tan \delta$) exhibits a maximum at the temperature of relaxation (Figure 13.6). Often two relaxations α and β are observed, with the α -relaxation being characteristic for the nature of the ionic groups. Young's and torsion modulus measurements are likewise sensitive to crosslinks at higher temperatures. For highly crosslinked materials, a plateau is observed, accompanied by a second drop in modulus at higher temperatures, well known from rubber-like materials (Figure 13.6). Under certain circumstances, the crosslink density can be calculated from the mechanical response using relationships from elasticity theory [26]. When the temperature increases, the crosslinks weaken, resulting in a flow of the material and a drop after the rubber plateau.

An extended study was presented by Otocka and Eirich on polybutadiene-methacrylic acid lithium polymers [26]. They observed that the material shows glassy properties at low temperatures, while behaving like a rubber with elastic deformation well above the glass transition temperature of the matrix. At temperatures above the cluster glass transition, the material was processible like a viscous fluid. Furthermore, it has been evidenced that the addition of plasticizers extends the rubbery plateau and thus increases the range of material properties.

Solutions of ionomers reveal remarkably dynamic mechanical properties. More specifically, they show extensive viscoelasticity, thixotropy, and shear thickening [27]. A linear thickening effect was observed in the form of a dramatic increase in the viscosity of ionomer solutions in the range of a critical ion concentration [27]. Shearing induces the appearance of a reversible network, leading to a shift of the gelation point. Higher shear rates break the network mechanically, resulting in a drop in viscosity [6]. For more concentrated systems a shear-thinning and thixotropic behavior is usual [28].

13.2.2

Applications and Availability

The long lifetime of the ionic association shows parallels to properties of permanently crosslinked material. On the other hand, the thermal reversibility of

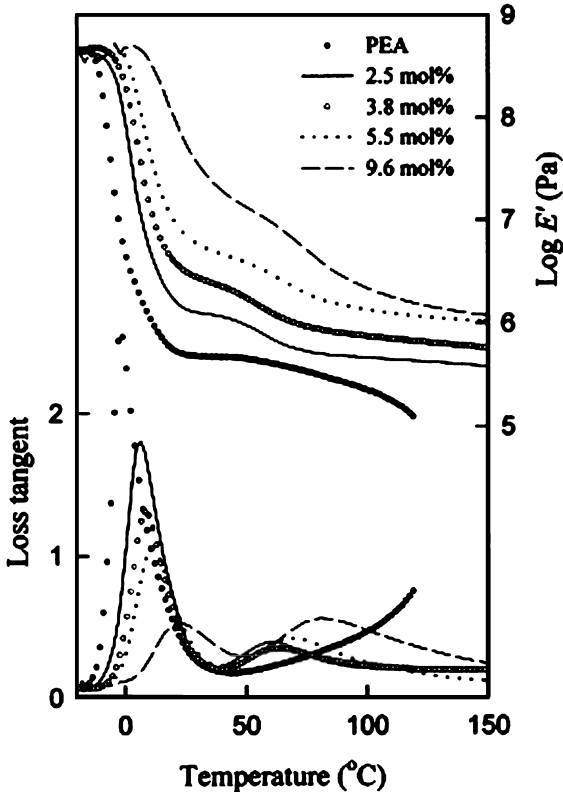


Figure 13.6 Storage modulus ($\log E'$) and loss angle (tangent) of poly(ethylene acrylate) homopolymer and ionomers with different degrees of neutralization as a function of temperature, measured at 1 Hz. The numbers

given in the legend give the ion content. Reprinted with permission from [25]. Copyright 2001 with permission from Elsevier.

ionically crosslinked polymers makes them suitable for processes via compression-molding. The versatility in the composition of ionomer polymers, such as the matrix, the molecular weight, the ionic content, the nature of counter-ions, and the neutralization degree, results in multiple applications. This requires understanding of the structure–property relationship to gain the desired material performance. In addition, several studies show that the method of preparation can affect the properties of ionomers to a great extent. The use of additives in melt processes or residual molecules from solution processes have influence on the formation of ionic aggregates and the related viscoelastic properties [6, 29].

In general, ionomers are used in electrochemical, petrochemical, mechanical, and biotechnological and medical fields. The most significant applications are in packaging films for consumable goods, in molded coatings, and as membranes in fuel cells, but ionomers are also used as adhesives, additives, and as polymer modifiers or catalysts.

In packaging and other non-durable products in the food and cosmetic industry, the stiffness and transparency of ionomers are especially important. For these

purposes, they are processed as blow films and extrusion coatings. Commercially available ionomers include Surlyn[®] from DuPont, and Iotek[®] from Exxon, and are mostly based on thermoplastics with carboxylate side groups, with sodium (Na⁺) or zinc (Zn²⁺) as counter-ions. They combine useful properties such as impact strength, abbreviation durability, and chemical resistance, and are useful for a wide range of sport equipment, like bowling pin covers, golf ball covers, or athletic dresses and shoes [30–33].

In several composites and blends, ionomers are used as additives to modify the properties of coatings. Synergistically blending often leads to properties that are superior to those of the individual components. Sandwiched by two layers of glass, bullet-proof composites based on ionomers were developed [34]. In the last decade, the potential of ionomer-based materials and composites as intrinsically self-healing materials was addressed with increasing activity.

13.3 Ionomers in Self-Healing Systems

It was early speculated that the ionic interaction in poly(ethylene-co-methacrylic acid)/Na⁺ ionomers (EMAA) is involved in the observed self-healing ability of this material class under certain conditions [35]. In particular, the ability of specific EMAA-based ionizable polymers to reseal damages was first observed when the puncture was caused by ballistic bombardment [35]. The sealing of the fresh bullet hole happens immediately after discharge of the penetrating projectile [35, 36], and only a slight scar remains, that appears solid and withdraws pressure treatment [36, 37]. Immediately, the potential of this behavior to be applied in aerospace applications, especially to self-seal destructive micrometeorite impacts at space stations or space shuttles, was envisaged.

Shortly after this discovery, initial studies were performed in order to better understand the underlying healing mechanism, investigating the influence of the environmental temperature, the degree of crosslinking, and the nature of the counter-ion [36–43]. While initially the role of intrinsic self-healing processes due to the thermoplastic nature of the systems was addressed, it quickly turned out that the ionic groups, even if present only as a small fraction, are of high importance, and first experiments concerning the healing behavior as a mainly ionic phenomenon were performed and published by Fall and Kalista at the beginning of this century [35, 36]. They investigated commercially available ionic polymers based on EMAA with different degrees of neutralization with sodium (DuPont[™] Surlyn[®] 8940 and DuPont[™] Surlyn[®] 8920) and compared the observations to the respective, uncharged counterpart (DuPont[™] Nucrel[®]).

For the purpose of a systematic investigation of different parameters concerning the material as well as the healing process, a range of set-ups has been developed that allow the reproducible bombardment experiments [35, 36]. In particular, a pistol range high-speed impact set-up was employed [35]. The testing sample made of the respective thermoplastic was placed at a constant distance from the muzzle

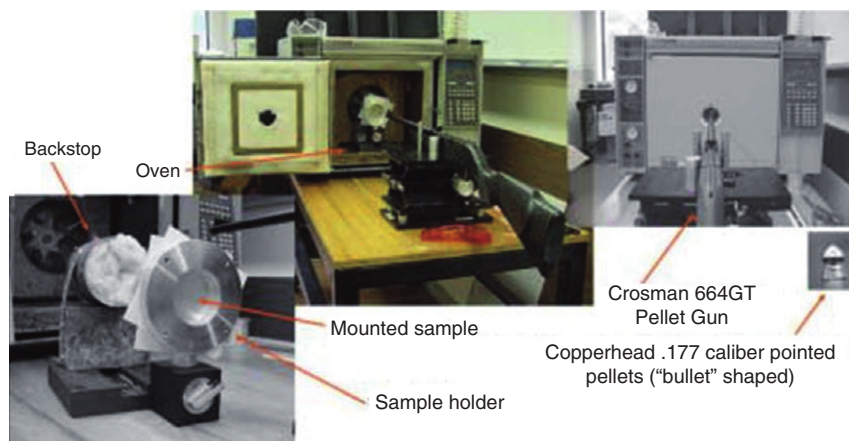


Figure 13.7 Projectile testing station for ballistic self-healing ionomers. Reprinted with permission from [38]. Copyright 2007, Taylor & Francis.

of the pistol. As it was early realized that temperature plays a key role in the process, the set-up allowed the measurement of local heating caused by the impact of the projectile with an infrared camera installed next to the sample.

Later, the set-up was improved by modifying a projectile testing station (Figure 13.7). Specifically, the polymer samples were placed in an oven to maintain constant temperature, and the test shooting occurred via the open oven door [36, 38].

The most relevant observations of these experiments concern the impact of temperature as well as of the concentration of the ionic groups. Under systematic control of the environmental temperature, it was found that elevated temperatures do not positively influence the healing process, but that a local temperature rise due to the ballistic impact is of crucial importance for the closing of the punctured area [36–38, 42]. Recordings via infrared camera revealed a local heating of the sample up to 90°C in the area around the bullet hole, resulting in local melting. After passing of the projectile, the polymer melt rebounds and seals the hole.

It was found that the influence of the ionic group content on the self-healing efficiency in these materials is non-trivial. While self-healing was also observed in the case of the uncharged polymer, and optimal self-healing behavior was qualitatively found for partially neutralized materials (Figure 13.8). For higher degrees of neutralization (60%), the healing efficiency was decreased again [36, 38, 42].

13.3.1

General Mechanism

Based on these findings, Kalista *et al.* postulated a self-healing mechanism for this class of materials that can be divided into three steps [36, 37, 42]. Initiated by the impact of the projectile, part of its kinetic energy is locally transferred to the polymeric material. While one part is converted to local heat caused by friction,

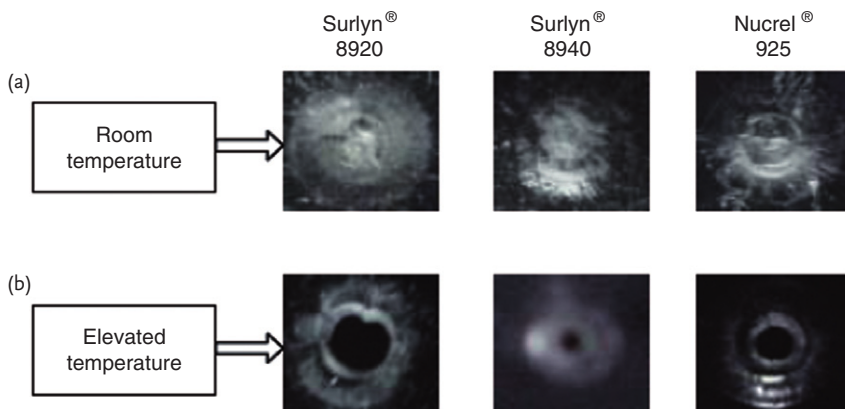


Figure 13.8 Images of the puncture site for four EMAA materials after ballistic tests at ambient (a) and at 70 °C (b) for different degrees of neutralization; Surlyn 8920: 60%,

Surlyn 8940: 30%; Nucrel 925: 0%. Adapted with permission from [36]. Copyright 2003, Virginia State University.

resulting in the observed confined melting of the matrix, another part of the energy is stored elastically, depending on the properties of the polymer matrix. In the following healing process, the first stage is characterized by the elastic rebound of the molten material, while the glassy or semicrystalline zone surrounding the bullet hole serves as a solid frame. The second stage is comprised of the sealing of the hole by interdiffusion of the melt. The ionic clusters act as additional crosslinking points with unique dynamics, contributing to the overall healing process, provided its concentration is optimized. Finally, in the third phase the mechanical properties of the damaged area are gradually restored by progressive interdiffusion, crystallization and the formation of new ionic aggregates [35, 40].

Although initially restricted to the ballistically initiated healing process in certain ionic thermoplasts, this view can be generalized to result in a comprehensive healing mechanism for ionic systems [39, 41]. According to this, an intrinsic healing process based on interdiffusion is dominating during the critical phase, and thus sufficient mobility of the polymer segments at the healing spot is essential. In addition, a particular elasticity of the polymeric structure is required. For both prerequisites, the reversible formation of ionic clusters in dependence on temperature is crucial.

With this model in mind, many experimental observations can be explained, including the need for an optimized ion content [36, 38]. The latter point occurs because, for an efficient healing process, the molecular architecture has to offer a certain mobility and flexibility of polymeric chains. Ionization leads to a higher integrity, but also to a stiffening of the molecular framework [36, 38, 42].

Figure 13.9 shows the general healing mechanism for an ionic thermoplastic polymer as it was postulated by Fall, Kalista and Ward [35–37]. After elastic and plastic deformation, the damaged area is restored by elastic recovery supported by

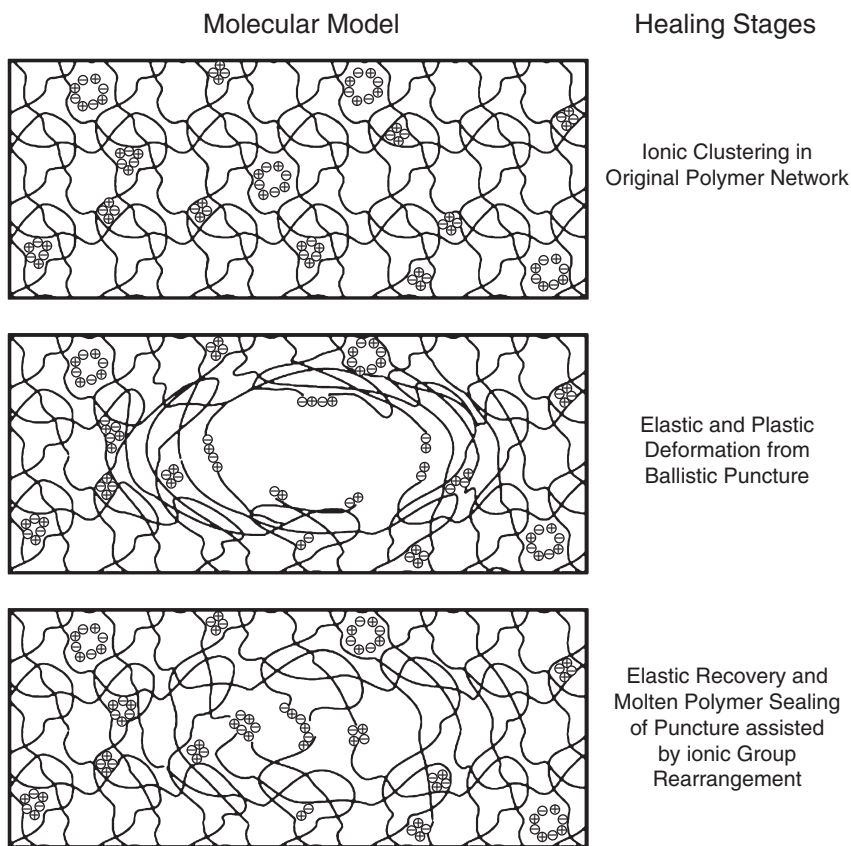


Figure 13.9 Postulated healing mechanism in ionomers. Reprinted with permission from [43]. Copyright 2008, Elsevier.

ionic group rearrangement, resulting in the re-formation of ionic multiplets and finally ionic clusters. These processes on different time scales further promote the elastic setback, as well as the reinforcement of the previously damaged area, and the restoration of mechanical properties by the creation of non-covalent bonds. Bergman and Wudl suggested that certain uncharged polymers develop similar aggregates, making use of microsegregation and / or hydrogen bonds, and showing a transition temperature comparable to the transition temperature T_i of ionic aggregates [44].

All ionomers or blend systems employed and described as self-healing polymeric materials are based on neutralized carboxylic groups [35–40, 42, 43, 45–48], and thus not much is known about the role of the nature of the ionic groups on the self-healing efficiency.

As counter-ion, mainly sodium is used. Although sodium is a monovalent positively charged metal ion, (ratio $\text{Na}^+:\text{COO}^-:1:1$), it is known that sodium ions are

coordinated by more than one carboxylate group in the multiplets [15]. Following the initial reports, carboxylate-based self-healing materials are reported that are neutralized by other alkali and alkaline earth metals or by transition group metals such as zinc (Zn^{2+}) [39].

The impact of the counter-ion nature should not be underestimated; however, no simple correlation between the nature of the cation or its properties, and the resulting healing properties of the ionomer is yet accessible. From the basic studies on ionomers it is known that the structure of the multiplets and their size is influenced cooperatively by the coordination number, the charge of the counter-ion, the ratio of the cation/anion radii, and the distance between cation and anion [15, 21, 49]. In addition, the nature of the counter-ion shows a significant influence on the degree of neutralization, and on the affinity for water absorption – a pronounced tendency to absorb water is considered to have a major effect on the healing effectiveness as it influences the interaction between the ionic groups toward multiplets. Large and hard counter-ions show less water absorption compared to small and soft ions [50]. Zinc is a good candidate, as it is observed that Zn^{2+} -based ionomers are often characterized by a high degree of neutralization, and low water absorption.

The thermal properties of the ionomers are determined by the cluster transition temperature T_i [18]. The relaxation process of separated ionic aggregates (order–disorder transition) is regarded to promote viscoelastic rebound and chain mobility during restoration of ionic aggregates (Figure 13.10) [35, 36, 38]. In addition, ion-rich multiplets exhibit the feature of ion-hopping, characterized by ionic groups that are able to jump between different multiplets within one cluster. A crack can be closed by such a process if affected multiplets, located at the interface, are restored by ion-hopping.

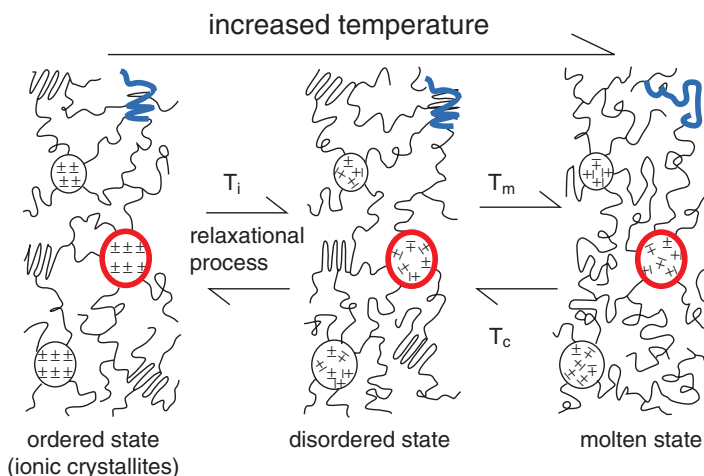


Figure 13.10 Model for order–disorder transition of ionic clusters. Reprinted with permission from [18]. Copyright 1989, American Chemical Society.

13.4

Actual Developments and Future Trends in Ionomeric and Related Self-Healing Systems

As ionomers already today are a technically relevant class of polymers with dynamic bonds, the concept is of increasing interest in view of materials with self-assembling, adjustable, and/or self-healing properties. While, in general, non-covalent dynamic bonds include a wide range of interactions, such as π - π stacking, hydrogen bonding, and metal-ligand interactions [51], their common ground is that they are thermodynamically rather weak in the range of several $k_{\text{B}}T$, yet their relevance is provided by additive or even cooperative impact. As such, they are generally in the state of dynamic equilibrium, and often react highly susceptibly to the thermal conditions, solvents, reagent residues, and concentrations. At the same time, when dynamic bonds are attached to polymers, the dynamic process can be dramatically slowed down by kinetically trapping, for example, due to crystallization, glass transition, or gelation within the polymer matrix, to achieve a virtually fixed state [52]. Thus, under non-reversible conditions, they behave like traditional materials, and the equilibrium can be manipulated. If properly designed, these characteristics can be used to yield structurally dynamic materials sensitive to a range of stimuli.

In structurally dynamic polymeric materials employed as self-healing materials, the nature of the dynamic bond determines to a large extent what stimulus the material will respond to, and how the thermodynamic and the kinetic parameters of the response are affected by the structural parameters. In the ideal case, the functionality of choice is suitable for a fully reversible and selective break that leads to re-formation in response to thermal energy without side reaction. However, under normal working conditions, the material is required to perform as requested, thus the bonds should be intact in order to prevent creep and relaxation phenomena. On the other hand, an ideal healing process can only be achieved, when the dynamic bonds exclusively are cleaved and re-healed. According to Leibler [53], an optimal reversible healing process can thus only be realized when the relative strength of the supramolecular associations is lower than that of the covalent bonds, in order to prevent covalent bond breakage as far as possible, and to ensure the availability of mender sites. Or, to express it on the level of dynamics, self-healing systems based on supramolecular assembly rely on dissociation rates that are favorable when compared to covalent bond scission and association rates.

Another structural parameter of importance is the number of groups available to associate after fracture. The healing rate, as well as the ultimate strength of the lesion closure, are positively influenced by a high volume density of healable units. According to a similar argumentation, autonomous self-healing is typically accomplished in polymers with a low glass transition temperature. Due to the flexibility of the molecular chains they can easily access the free volume, thus initiating the healing process [54, 55]. However, an increasing number of crosslinks restricts the chain motion. For thermosets, consequently, the difficulty of introducing an appropriate healing strategy still needs to be overcome.

When thermally sensitive functionalities are employed – such as present in ionic polymers in the form of cluster-based crosslinks – the material will be able to reorganize its architectures post-synthesis upon exposure to heat. However, in order not to be restricted to self-healing processes after ballistic impact, we need to take into account the healing mechanism and its possible triggers.

Thus the interaction process is ideally characterized by a high density of interaction points, a strong binding strength once the crosslink is formed, and a high degree of dynamic and re-forming affinity once a lesion has occurred. When designing novel systems that are based on dynamic bond-dominated polymers, this has to be taken into account in a straight-forward way.

For example, an interesting new polymeric material reported by Aboudzadeh *et al.* is based on low-molecular precursors (bi-/trisamines and bis-/tris carboxylic acids) that are self-assembled into a supramolecular material by ionic interactions [56]. The material shows unique rheological properties (Figure 13.11), with a sharp transition between a viscoelastic gel and a viscous liquid at the transition temperature of the ionic groups. This concept can be of potential use also for self-healing materials.

Interestingly, ionic interactions leading to reversibly crosslinked materials are not necessarily restricted to one type of material component. Wang *et al.* developed

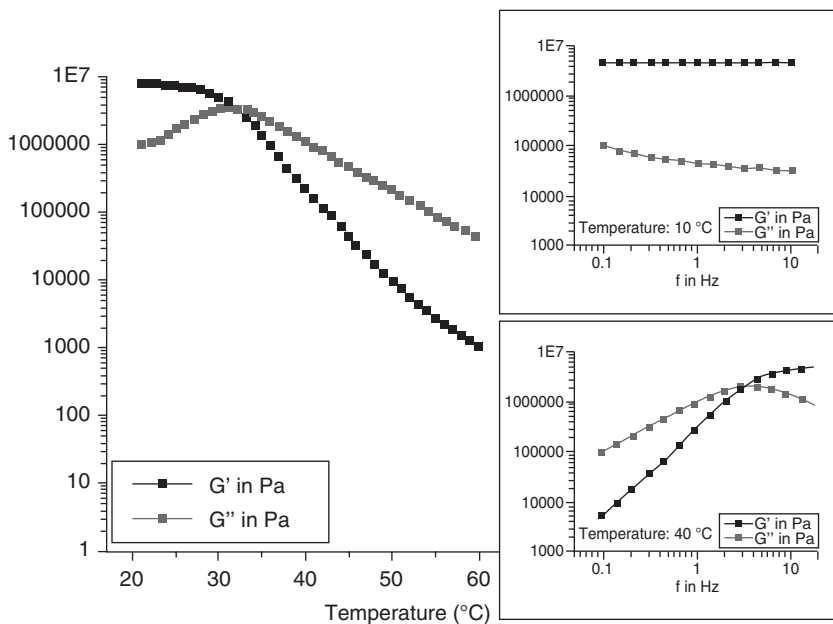


Figure 13.11 Evolution of the dynamic modulus with increasing temperature at a constant frequency of 1 Hz for a supramolecular ionic polymer formed by a stoichiometric mixture of citric acid and N,N,N',N'-tetramethyl-1-3-propanediamine.

The figures in the insets show both the moduli as a function of frequency, below and above the gel–liquid transition, respectively. Reproduced with permission from [56]. Copyright 2012, Wiley-VCH, Weinheim.

a hydrogel that is maintained by the electrostatic interactions between positively charged dendritic macromolecules on the one hand, and negatively charged clay nano-sheets [57]. The opposite charges lead to a multivalent interaction between the components, even in an aqueous environment. This non-covalent “bricks-and-mortar approach” is shown to be reversible in the interaction behavior, making it a promising principle for self-healing gels.

An actually vivid development with respect to self-healing polymer concepts is observed for polymers based on metal-ion binding motifs that can be employed as reversible crosslinks [57–59]. These materials are closely related to ionomers, with the boundaries between the two not always clear-cut. The coordination polymers usually involve charged coordinating species and/or elements of high dielectric constant, and as a consequence, show many similarities with ionomers, including microphase separation and cluster formation, making them interesting as a novel class of self-healing polymers. For example, Burnworth *et al.* have developed metallocsupramolecular polymers comprising an amorphous poly(ethylene-co-butylene) core decorated with 2,6-bis(1'-methylbenzimidazolyl)pyridine ligand end groups that complex metal salts under chain extension [60]. When exposed to UV light, the amorphous metal complexes are excited, followed by energy absorption and conversion into heat. This causes a distinct temperature increase, and a significant viscosity drop is observed, partly induced by reversible metal decomplexation. Collective M–L-bond cleavage in the light-exposed area allows M–L-bond exchange and rebonding, resulting in an extrinsically healed material. The effective self-healing process was evidenced in tensile tests of virgin, damaged, and UV-light-cured films.

Holten-Andersen *et al.* modeled their metal–ligand interaction-based self-healing polymer system after a natural product [61]. They presented a material inspired by mussel tissue containing a catechol-iron complex (Figure 13.12). While under normal conditions, the mechanical properties are close to those of covalent elastomers, and a self-healing efficiency of near 100% was reported. A major drawback for practical applications is that it only works under basic conditions.

Further support for the potential of metal–ligand-based polymers in self-healing materials is obtained by several works investigating the dynamic bond dissociation of metal complex-based supramolecular systems by mechanical exposure [62–64]. Kean *et al.* reported on metallo-supramolecular gels that are based on a family of van Koten-type pincer complexes [65]. The unique dynamic-mechanical response of the polymers could be related back to the kinetics of ligand exchange in the isolated pincer complexes. Under certain circumstances, force accelerates the dissociation in the macroscopic system [66, 67], indicating that an important attribute of self-healing materials is provided intrinsically in many metal–ligand-based polymers, namely that the transient dynamic bonds are considerably more labile than the covalent bonds involved.

In future trends, it is envisaged that ionomer- and metal–ligand-based self-healing systems will be of great potential for the development of novel real-world self-healing material applications. This class has the prospect for the discovery of a self-healing mechanism for elastomer-like polymer materials based on

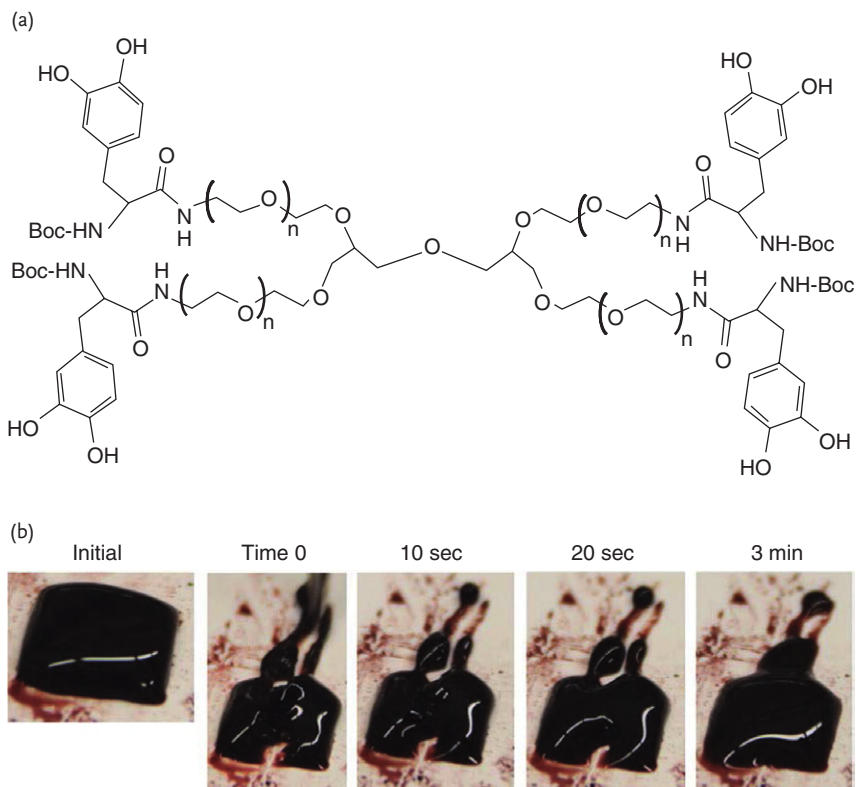


Figure 13.12 Self-healing gel based on PEG-dopa4/Fe³⁺ dynamic bonds. (a) dopa-modified polyethylene glycol (PEG-dopa4); (b) images showing the recovery of

cohesiveness and stiffness of the PEG-dopa4/Fe³⁺ gel over 3 min. Reproduced with permission from [61]. Copyright 2011, National Academy of Science USA.

commercial systems. Elastomers obtain their unique mechanical properties, combining almost ideal elasticity and toughness, from chemical or topological entanglements that serve as anchors for the elastic response [65]. Molecular defects or irregularities are, therefore, responsible for the mechanisms of failure, such as the chain scission or slipping, accompanied by irreversible changes in the molecular structure, eventually translating to the macroscopic level. Thus, dynamic bonds based on ionomers are interesting features of stress-bearing sub-chains for a nanoscale force management under acute or chronic loading settings.

When compared to other strategies for polymer self-healing developed recently, including capsule- or fiber-based systems, where the encapsulating component is filled with crosslinking agent or monomer [68, 69] and reversible covalent bonds that can heal upon irradiation or heat, dynamic bond-based self-healing strategies based on hydrogen bonds, metal–ligand interactions or ionomers show several common characteristics. The capsule or fiber approach is generally limited to duromers, as the capsules often do not withstand the harsh processing conditions.

In addition, this healing mechanism is not reversible, and cannot be repeated at a formerly already healed site. The latter point is also the case for most healing mechanisms based on covalent bonds. In contrast, the dynamic bond-based approach is reversible in nature and can be repeated many times. Some of the dynamic bond-based approaches, such as the hydrogen bonding-based approach proposed by Leibler [53], require a specifically composed material of unconventional building blocks – still too expensive for a commercial application. However, many commercial polymers can be functionalized to an ionomer with only small preparative attempt, thus providing the potential for many applications that might be covered in the future. The ability to adjust such materials by varying the ionic content or the counter-ions allows a wide range for the optimization of the materials properties with respect to a special application in a cost-effective way. A prerequisite is that the materials provide enough mobility on the scale of polymer chains to enable effective interdiffusion. In fact, to date most of the dynamic bond-based healing mechanisms can only be applied to a particular polymer that requires, for example, a low matrix glass transition, or a thermoplastic matrix [70]. Thus, regardless of the huge progress achieved recently, it is still necessary to further improve the performance of supramolecular materials in order to expand the application potential for this type of intrinsically healable materials [71].

Possible areas of application include automotive and aerospace, as well as medical devices and materials. They can be employed for parts that are inaccessible or challenging to reach for repair, for example, in buildings, shipping, underground parts, or big machinery, or for applications where an undamaged surface is important, for example, in corrosion protection [70]. Materials based on dynamic bonds based on an external trigger are particularly suited for protective coatings naturally exposed to light or heat [70]. As such, self-healing polymers will not only enhance the life-time of the polymeric component, but also the life-time of complete devices.

In all application cases, ionomers are envisaged as good members for the design of self-healing materials without the need to change the overall materials performance in a cost-effective way. Self-healing ionomeric rubbers for dampers or sealings might be part of everyday life in the future. Therefore, the research and development concerning this issue can substantially contribute to sustainable development.

References

- 1 D'Auzac, J., Prevot, J.C., and Jacob, J.L. (1995) What's new about lutoids? A vacuolar system model from hevea latex. *Plant Physiol. Biochem.*, **33**, 765–777.
- 2 Bauer, G., Nellesen, A., Sengespeick, A., and Speck, T. (2009) Fast Self-repair Mechanisms in Plants: Biological Latices as Role Models for the Development of Biomimetic Self-healing, Mechanically Loaded Polymers. *Proceedings of the 6th Plant Biomechanical Conference*, 367–373.
- 3 Eisenberg, A., and Rinaudo, M. (1990) Polyelectrolytes and Ionomers. *Polym. Bull.*, **24**, 671.
- 4 Helfand, E., and Wasserman, Z.R. (1976) Block copolymer theory. 4. Narrow

- interphase approximation. *Macromolecules*, **9**, 879–888.
- 5 Helfand, E., and Wasserman, Z.R. (1978) Block copolymer theory. 5. Spherical domains. *Macromolecules*, **11**, 960–966.
 - 6 Duvdevani, I., Agarwal, P.K., Lundberg, R.D. (1982) Blends of EPDM and sulfonated ethylene-propylene-diene (EPDM) rubber with polypropylene: structure, physical, and rheological properties. *Polym. Eng.*, **1**, 499–506.
 - 7 Leibler, L. (1980) Theory of microphase separation in block copolymers. *Macromolecules*, **13**, 1602–1617.
 - 8 Marx, C.L., Koutsky, J.A., and Cooper, S.L. (1971) Morphology of butadiene-methacrylic acid copolymers. *J. Polym. Sci. B*, **9**, 167–171.
 - 9 Holliday, L. (1975) *Ionic Polymers*, Applied Science Publishers Ltd., p. 1.
 - 10 MacKnight, W.J., and Earnest, T.R. (1981) The structure and properties of ionomers. *J. Polym. Sci. Macromol. Rev.*, **16**, 41–122.
 - 11 MacKnight, W.J., Taggart, W.P., and Stein, R.S. (2007) A model for the structure of ionomers. *J. Polym. Sci. Polym. Symp.*, **45**, 113–128.
 - 12 Wilson, F.C., Longworth, R., and Vaughan, D.J. (1968) The physical structure of ionomers. III. X-ray diffraction studies. *Polym. Prepr. Am. Chem. Soc. Div. Polym. Chem.*, **9**, 505–514.
 - 13 Longworth, R., and Vaughan, D.J. (1968) Physical structures of ionomers. *Nature*, **218**, 85–87.
 - 14 Eisenberg, A. (1970) Clustering of ions in organic polymers. A theoretical approach. *Macromolecules*, **3**, 147–154.
 - 15 Eisenberg, A., Hird, B., and Moore, R.B. (1990) A new multiplet-cluster model for the morphology of random ionomers. *Macromolecules*, **23**, 4098–4107.
 - 16 Marx, C., Caulfield, D., and Cooper, S. (1973) Morphology of ionomers. *Macromolecules*, **525**, 344–353.
 - 17 Yarusso, D.J., and Cooper, S.L. (1983) Microstructure of ionomers: interpretation of small-angle X-ray scattering data. *Macromolecules*, **16**, 1871–1880.
 - 18 Tadano, K., Hirasawa, E., Yamamoto, H., and Yano, S. (1989) Order-disorder transition of ionic clusters in ionomers. *Macromolecules*, **22**, 226–233.
 - 19 Williams, C.E. (1989) *Multiphase Macromolecular Systems*, vol. 6 (ed. B.M. Culbertson), Plenum Press, New York.
 - 20 Goodman, I. (1982) *Developments in Block Copolymers*, vols. 1 and 2, Applied Science Publishers, New York.
 - 21 Hird, B., and Eisenberg, A. (1992) Sizes and stabilities of multiplets and clusters in carboxylated and sulfonated styrene ionomers. *Macromolecules*, **25**, 6466–6474.
 - 22 Matsuura, H., and Eisenberg, A. (1976) Glass transitions of ethyl acrylate-based ionomers. *J. Polym. Sci. Polym. Phys. Ed.*, **14**, 1201–1209.
 - 23 Bailly, C.H., Leung, L.M., O’Gara, J., Williams, D.J., Karasz, F.E., and Macknight, W.J. (1987) *Structure and Properties of Ionomers*, NATO ASI S (eds M. Pineri and A. Eisenberg), D. Reidel Publishing, Dordrecht, p. 511.
 - 24 Moore, R.B., Bittencourt, D., Gauthier, M., Williams, C.E., Eisenberg, A., Ha, C., and Laboratoire, L. (1991) Small-Angle X-Ray Scattering Investigations of Ionomers with Variable-Length Side Chains. *Macromolecules*, **24**, 1376–1382.
 - 25 Kim, J.J., Nah, Y.H., Jarng, S.S.S., Hwa, Y., Jarng, S.S.S., and Nah, Y.H. (2001) Comparison of clustering in various acrylate ionomers. *Polymer*, **42**, 5567–5571.
 - 26 Otocka, E.P.P., and Eirich, F.R. (1968) Ionic bonding in butadiene copolymers. *J. Polym. Sci. [A-2]*, **6**, 921–932.
 - 27 Broze, G., Jerome, R., Teyssie, P., and Marco, C. (1983) Halato-telechelic polymers. 6. Viscoelastic properties. *Macromolecules*, **16**, 996–1000.
 - 28 Groot, R.D., and Agterof, W.G.M. (1994) Monte carlo study of associative polymer networks. II. Rheologic aspects. *J. Chem. Phys.*, **100**, 1657–1664.
 - 29 Weiss, R.A., Fitzgerald, J.J., Frank, H.A., and Chadwick, B.W. (1986) Electron spin resonance evidence of specific solvation effects in ionomer solutions. *Macromolecules*, **19**, 2085–2087.
 - 30 Utracki, L.A. (1995) History of commercial polymer alloys and blends (from a perspective of the patent literature). *Polym. Eng. Sci.*, **35**, 2–17.
 - 31 Sullivan, M.J., Melvin, T., and Nesbitt, R.D. (1990) Golf Ball Cover of

- Neutralized Poly(ethylene acrylic acid) Copolymer. U.S. Patent 4911451.
- 32 Molitor, R.P. (1974) Golf Ball Cover Compositions Comprising a Mixture of Ionomer Resins, U.S. Patent 3819768.
 - 33 Statz, R.J. (1988) Polymer preprint. Abstracts of Papers of *J. Am. Chem. Soc.*, **196**, 216.
 - 34 Smith, N.W. (1986) Ionomer Resin Films, U.S. Patent 196216.
 - 35 Fall, R. (2001) Puncture Reversal of Ethylene Ionomers – Mechanistic Studies, Master of Science, Virginia Polytechnic Institute and State University, Virginia, USA.
 - 36 Kalista, S.J. (2003) Self-Healing of Thermoplastic Poly (Ethylene-co-Methacrylic Acid) Copolymers Following Projectile Puncture, Master of Science, Virginia Polytechnic Institute and State University, Virginia, USA.
 - 37 Kalista, S., and Ward, T. (2007) Thermal characteristics of the self-healing response in poly (ethylene-co-methacrylic acid) copolymers. *J. R. Soc. Interface*, **4**, 405–411.
 - 38 Kalista, S., Ward, T., and Oyetunji, Z. (2007) Self-healing of poly (ethylene-co-methacrylic acid) copolymers following projectile puncture. *Mech. Adv. Mater. Struct.*, **14**, 391–397.
 - 39 Varley, R.J., and van der Zwaag, S. (2008) Towards an Understanding of thermally activated self-healing of an ionomer system during ballistic penetration. *Acta Mater.*, **56**, 5737–5750.
 - 40 Varley, R.J., Shen, S., and van der Zwaag, S. (2010) The effect of cluster plasticisation on the self-healing behaviour of ionomers. *Polymer*, **51**, 679–686.
 - 41 Varley, J.R., and van der Zwaag, S. (2008) Development of a quasi-static test method to investigate the origin of self-healing in ionomers under ballistic conditions. *Polym. Test.*, **27**, 11–19.
 - 42 Ghosh, S.K. (2009) *Self-healing Materials – Fundamentals, Design Strategies, and Applications* (ed. S.K. Ghosh), Wiley-VCH Verlag GmbH, pp. 73–100.
 - 43 Wu, D.-Y., Meure, S., and Solomon, D. (2008) Self-healing polymeric materials: a review of recent developments. *Prog. Polym. Sci.*, **33**, 479–522.
 - 44 Bergman, S.-D., and Wudl, F. (2007) Re-mendable polymers, in *Self-Healing Materials: An Alternative Approach to 20 Centuries of Material Science* (ed. S. van der Zwaag), Springer, pp. 45–66.
 - 45 Schüssele, A. (2012) Neue Additive Und Thermoreversible Conetzwurkssysteme Für Selbstheilende NBR-Elastomere, PhD thesis, University of Freiburg.
 - 46 Tapavicza, M., von Nellesen, A., Bertlin, J., and Schmidt, A. (2011) Self-Healing Elastomers – Healing Functionalization by Polymer Analogous Side-group Modification. *3rd International Conference on Self-Healing Materials, Bath*; Bath, UK.
 - 47 Reynolds, P.J. (2011) A Surlyn® Ionomer as a Self-Healing and Self-Sensing Composite, thesis, University of Birmingham.
 - 48 Rhaman, M.A., Penco, M., Spagnoli, G., Grande, A.M., and Landro, L. (2011) Di self-healing behavior of blends based on ionomers with ethylene/vinyl alcohol copolymer or epoxidized natural rubber. *Macromol. Mater. Eng.*, **296**, 1119–1127.
 - 49 Eisenberg, A., and Kim, J.-S. (1998) *Introduction to Ionomers*, John Wiley & Sons, Inc., New York.
 - 50 Rees, R.-W. (1987) Ionomeric thermoplastic elastomers: early research – surlyn® and related polymers, in *Thermoplastic Elastomers – A Comprehensive Review* (eds N.R. Legge, G. Holden and H.F. Schroeder), Carl Hanser Verlag, pp. 231–243.
 - 51 Wojtecki, R.J., Meador, M.A., and Rowan, S.J. (2011) Using the dynamic bond to access macroscopically responsive structurally dynamic polymers. *Nat. Mater.*, **10**, 14–27.
 - 52 Sadownik, J.W., and Ulijn, R.V. (2010) Locking an oxidation-sensitive dynamic peptide system in the gel state. *Chem. Commun. (Camb.)*, **46**, 3481–3483.
 - 53 Cordier, P., Tournilhac, F., Soulié-Ziakovic, C., and Leibler, L. (2008) Self-healing and thermoreversible rubber from supramolecular assembly. *Nature*, **451**, 977–980.
 - 54 Zhang, M.Q., and Rong, M.Z. (2012) Theoretical consideration and modeling of self-healing polymers. *J. Polym. Sci. B*, **50**, 229–241.

- 55 Gemert, G.M.L., van Peeters, J.W., Söntjens, S.H.M., Janssen, H.M., and Bosman, A.W. (2012) Self-healing supramolecular polymers in action. *Macromol. Chem. Phys.*, **213**, 234–242.
- 56 Aboudzadeh, M.A., Muñoz, M.E., Santamaría, A., Marcilla, R., and Mecerreyes, D. (2012) Facile synthesis of supramolecular ionic polymers that combine unique rheological, ionic conductivity, and self-healing properties. *Macromol. Rapid Commun.*, **33**, 314–318.
- 57 Wang, Q., Mynar, J.L., Yoshida, M., Lee, E., Lee, M., Okuro, K., Kinbara, K., and Aida, T. (2010) High-water-content mouldable hydrogels by mixing clay and a dendritic molecular binder. *Nature*, **463**, 339–343.
- 58 Sivakova, S., Bohnsack, D.A., Mackay, M.E., Suwanmala, P., and Rowan, S.J. (2005) Utilization of a combination of weak hydrogen-bonding interactions and phase segregation to yield highly thermosensitive supramolecular polymers. *J. Am. Chem. Soc.*, **127**, 18202–18211.
- 59 Kersey, F.R., Loveless, D.M., and Craig, S.L. (2007) A hybrid polymer gel with controlled rates of cross-link rupture and self-repair. *J. R. Soc. Interface*, **4**, 373–380.
- 60 Burnworth, M., Tang, L., Kumpfer, J.R., Duncan, A.J., Beyer, F.L., Fiore, G.L., Rowan, S.J., and Weder, C. (2011) Optically healable supramolecular polymers. *Nature*, **472**, 334–337.
- 61 Holten-Andersen, N., Harrington, M.J., Birkedal, H., Lee, B.P., Messersmith, P.B., Lee, K.Y.C., and Waite, J.H. (2011) pH-induced metal-ligand cross-links inspired by mussel yield self-healing polymer networks with near-covalent elastic moduli. *Proc. Natl Acad. Sci. U. S. A.*, **108**, 2651–2655.
- 62 Caruso, M.M., Davis, D.A., Shen, Q., Odom, S.A., Sottos, N.R., White, S.R., and Moore, J.S. (2009) Mechanically-induced Chemical changes in polymeric materials. *Chem. Rev.*, **109**, 5755–5798.
- 63 Paulusse, J.M.J., Huijbers, J.P.J., and Sijbesma, R.P. (2006) Quantification of ultrasound-induced chain scission in pdii-phosphine coordination polymers. *Chem.-Eur. J.*, **12**, 4928–4934.
- 64 Piermattei, A., Karthikeyan, S., and Sijbesma, R.P. (2009) Activating catalysts with mechanical force. *Nat. Chem.*, **1**, 133–137.
- 65 Kean, Z.S., and Craig, S.L. (2012) Mechanochemical remodeling of synthetic polymers. *Polymer*, **53**, 1035–1048.
- 66 Rodríguez, G., Albrecht, M., Schoenmaker, J., Ford, A., Lutz, M., Spek, A.L., and van Koten, G. (2002) Bifunctional pincer-type organometallics as substrates for organic transformations and as novel building blocks for polymetallic materials. *J. Am. Chem. Soc.*, **124**, 5127–5138.
- 67 Yount, W.C., Loveless, D.M., and Craig, S.L. (2005) Strong means slow: dynamic contributions to the bulk mechanical properties of supramolecular networks. *Angew. Chem. Int. Ed Engl.*, **44**, 2746–2748.
- 68 White, S.R., Sottos, N.R., Geubelle, P.H., Moore, J.S., Kessler, M.R., Sriram, S.R., Brown, E.N., and Viswanathan, S. (2001) Autonomic healing of polymer composites. *Nature*, **409**, 794–797.
- 69 Pang, J.W.C., and Bond, I.P.A. (2005) Hollow fibre reinforced polymer composite encompassing self-healing and enhanced damage visibility. *Compos. Sci. Technol.*, **65**, 1791–1799.
- 70 Guimard, N.K., Oehlenschlaeger, K.K., Zhou, J., Hilf, S., Schmidt, F.G., and Barner-Kowollik, C. (2012) Current trends in the field of self-healing materials. *Macromol. Chem. Phys.*, **213**, 131–143.
- 71 Urban, M.W. (2012) Dynamic materials: the chemistry of self-healing. *Nat. Chem.*, **4**, 80–82.

Part Four
Analysis and Friction Detection in Self-Healing Polymers:
Macroscopic, Microscopic and Nanoscopic Techniques

14

Methods to Monitor and Quantify (Self-) Healing in Polymers and Polymer Systems

Ranjita K. Bose, Ugo Lafont, Jesús M. Vega, Santiago J. Garcia, and Sybrand van der Zwaag

14.1

Introduction

As described in the earlier chapters of this book, the creation of self-healing materials can be regarded as a major paradigm shift in the development of new and improved materials. While in classical materials the design of new materials was driven by the wish to avoid the formation of damage in the material by external loading conditions (the “damage prevention” paradigm), in self-healing materials it is accepted that the materials will be damaged at some stage, and the challenge is to provide the new class of materials with an autonomous or stimulated healing capability (“the damage management” paradigm) in order to obtain the desired extension of the life-time (or performance time) of the material and the product made thereof. It may be relevant to define “damage” in the context of this chapter as the presence of local regions in the material with a lower performance level than that of the surrounding material. Of course, thermal, photonic or electrochemical degradation of a material as a result of, for instance, reduction of the average molecular weight or induced crosslinking, can also be regarded as the occurrence of damage, but this form of general non-localized damage is excluded in the present work as it is generally not an issue being addressed in current self-healing materials research, which focuses on materials capable of healing discrete local damage. With the shift in material design philosophy, the tools to be used in the development and characterization of material performance may also have to change. In classical material science the focus of the physical and chemical characterization techniques is primarily on the proper and preferentially quantitative description of the initial, undamaged, microstructure. The extensive suite of characterization techniques is complemented by techniques to visualize the damage upon over-exposure of the material, as well as techniques to monitor the drop in initial properties upon the occurrence of this damage. The focus on the effect of local damage on the final material and product performance has led not only to the development of many material characterization techniques, but also to fields such as damage mechanics, in which the nature and extent of the

damage is equally, if not more, important for the product performance as the intrinsic properties of the material surrounding the local damage.

In the present early stage of the development of self-healing materials we may have to look again at the range of experimental methods available to characterize not only the initial damage, but also its reduction during the healing process, in as quantitative a manner as possible.

The aim of the present chapter is to list and discuss the most important techniques for the characterization of damage in polymeric materials, and the possibility they offer to quantify the healing process. The ability to objectively describe and quantify the degree of healing of the performance level of the material is a prerequisite for the industrial development of self-healing materials, as this will enable companies to rank the performance of their materials against that of competitors, and to create a business case. As such, the need to quantify healing behavior is not very different from the need to determine properties such as strength, stiffness, or conductivity during the early days of intentional development of classical, non-self-healing materials.

In the subsequent sections we describe several methods to describe, either qualitatively or quantitatively, the initial and healed damage, and list the advantages and limitations of the pertinent techniques to describe and quantify the damage. In most subsections we also refer to examples of the application of the technique to monitor damage level reduction for a self-healing polymer system. The final section of this chapter deals with the healing of corrosion protection of metals via self-healing polymeric coatings. While the corrosion process itself is a process related to the metallic substrate, the healing is provided by the polymeric coating and, hence, deserves to be included in this chapter. As the actual mechanisms of healing in polymers and polymeric systems as such are described in detail in the other chapters of the book, they will not be discussed here.

14.2

Visualization Techniques

14.2.1

Optical Microscopy

Optical microscopy, probably the oldest and most versatile scientific technique in material characterization, is an important tool also for self-healing materials. There is a whole range of optical techniques, ranging from conventional reflection and transmission optical microscopes to fluorescence microscopy, to high resolution near-field scanning optical microscopy with resolution levels well below the diffraction limit. Increasingly, optical microscopes are equipped with high resolution digital cameras, which means that the optical image is available for automated and quantitative image analysis. As optical microscopy is a well-known technique there is no need to go into the working principle but just to focus on features and limitations relevant to self-healing. The main advantage of conventional optical

microscopy is the wide range of magnifications and the relative ease of operation, both for *ex situ* and *in situ* monitoring of damage located at the surface of the sample. In the case of transparent materials even subsurface damage (such as delamination) can be detected. A relevant limitation of optical microscopy is the resolution. For a standard optical system the spatial resolution d of detectable features is given by the diffraction limit

$$d = \lambda/2 \cdot \text{NA} \quad (14.1)$$

where λ is the wavelength and NA the numerical aperture of the system. For a regular microscope and using monochromatic green light this means a resolution of 0.2 to 0.4 μm , yet advanced lenses allow the resolution to be improved to below 0.1 μm . Although this is a rather low value, it means that the healing of cracks with small (remaining) crack openings, hair-line cracks, will be difficult to measure with some accuracy. Use of fluorescent dyes penetrating into the cracks may increase the resolution and visibility but their presence may affect the healing process and is not recommended for *in situ* healing. The use of fluorescent dyes is compulsory for “black” polymer systems such as bitumen.

While microscopy techniques are very valuable to record the damage and its recovery, the information captured is generally qualitative and not immediately suitable to yield a quantitative description of the healing process. The problem can be indicated below for two initial crack configurations.

In the situation as sketched in Figure 14.1a the initial crack is sharp and planar. While the crack width is varying with position from the crack tip, the partial healing of the crack (Figure 14.1b) can be described in a rather undisputed manner. However, for many polymer systems the crack is far from planar (a rough fracture surface is often the desirable outcome for materials developed along the classical lines), and a quantitative description of both the initial crack state and that of a partially healed crack (via the formation of bridging ligaments growing from contacting asperities) is not simple. A recent approach to link the non-smooth crack

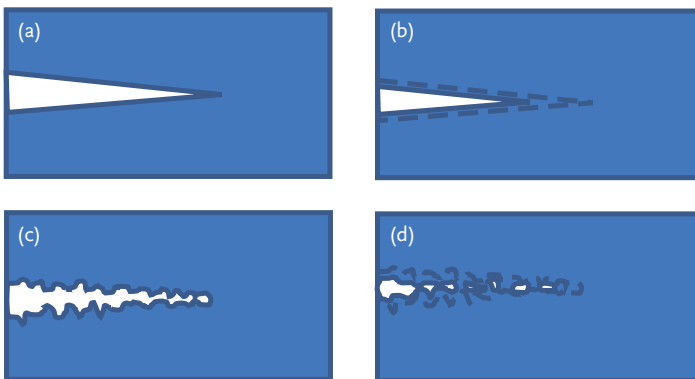


Figure 14.1 Examples of initial and healed crack configuration: (a,b) sharp planar cracks; (c,d) rough cracks.

morphology of aluminum alloys to their fracture toughness [1] may be of some use to develop methods to describe the healing kinetics of cracks in polymers in a semi-quantitative manner.

Optical techniques may also be useful to characterize healing of in-plane surface defects. Scanning laser confocal microscopy (SLCM) returns topological information about surfaces, typically with a vertical resolution of about 40 nm and a lateral resolution of about 100 nm. As the microscope operates using a (monochromatic) laser, the image quality is surprisingly high, in particular when the 3D mode is used to capture the topology of slightly rough surfaces and to convert it into a 2D image. SCLM has been used successfully to monitor the healing of polymeric surfaces, as described in Section 14.4.1.

14.2.2

Scanning (SEM) and Environmental Scanning Electron (E-SEM) Microscopy

Like the optical microscope the scanning electron microscope (SEM) is a well-known technique not requiring a further description of the operating principle. It offers a much higher resolution than optical microscopes, as well as the ability to image curved and rough surfaces. The resolution of the SEM depends on the acceleration voltage and the source. For a modern field emission gun SEM (FEG-SEM) the resolution can go down to 1 nm, so healing of very small features can be followed. Unlike optical microscopes, an SEM cannot reveal subsurface features and, hence, cannot be used to obtain information on the healing of features such as delamination. Like the optical microscope, a SEM can be fitted with a staining and heating devices in the chamber to monitor *in situ* the healing of cracks intercepting with the surface, provided the healing process does not involve any liquid or volatile substance.

The constraint of not being able to monitor healing involving liquid or volatile substances is due to the vacuum in the sample chamber required to maintain and control the electron beam. The first commercial development of the environmental SEM (ESEM) in the late 1980s allowed samples to be observed in low-pressure gaseous environments (e.g., 1–10 kPa) and high relative humidity (up to 100%). This was made possible by the development of a secondary-electron detector capable of operating in the presence of water vapor, and by the use of pressure-limiting apertures with differential pumping in the path of the electron beam to separate the vacuum region (around the gun and lenses) from the sample chamber. With an ESEM it is possible to follow *in situ* the filling and closing of cracks using the swelling reaction of a “healing” agent embedded in a polymer matrix by moist air [2]. The resolution of an ESEM is less than that of a FEG-SEM but generally more than adequate to monitor crack filling phenomena.

If even higher resolutions are required a transmission electron microscope (TEM) or cryo-TEM (keeping the sample at a low temperature to minimize heating effects) has to be used. As the samples for TEM are very thin and require very dedicated techniques to take proper samples without introducing artefacts, TEM

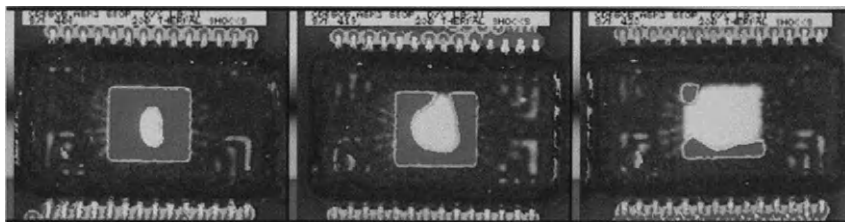


Figure 14.2 Three examples of scanning acoustical images showing delamination of the protective coating on a computer chip. The dark gray central region shows the delaminated area, the white region the intact contact zone. After Atkins *et al.* [3].

right now does not seem to be a very relevant experimental technique to study self-healing phenomena in polymers.

14.2.3

Acoustical Microscopy

A major drawback of optical and electron microscopes is their inability to visualize subsurface damage as the photons and electrons are generally absorbed by the polymer. In contrast, acoustic waves generated at 5 to 400 MHz are generally well transmitted by polymers and can be used to image subsurface damage, such as delamination in coated systems or composites. The microscope consists of a transducer emitting and recording sound waves being moved across the sample surface. Local changes in the acoustic impedance, for instance between the base polymer and air in a crack, cause ultrasonic reflections which are detected by the transducer and can be deconvoluted to yield information on the location of the defect. The technique is widely used in medical imaging (ultrasound) where the frequency of the sound waves (and hence the resulting resolution) is rather low in order not to damage the tissue. Polymers are much less vulnerable to acoustic wave damage and higher frequencies can be used. The scanning acoustical microscope has been used successfully to record subsurface damage, such as delamination in the packaging of chips in microelectronics (see Figure 14.2)

No examples of the use of acoustical imaging to monitor healing have been found in the literature yet, but the technique is even capable of monitoring *in situ* healing phenomena and hence offers great potential.

14.2.4

Computed Tomography and Micro- (Computed) Tomography

Computed (X-ray) tomography (X-ray CT) is a logical extension of the acoustical microscopy. It uses hard (penetrating) X-rays to create a large set of 2D absorption contrast images obtained at different viewing angles, and to reconstruct the internal 3D structure of the material via advanced algorithms. Conventional tomography relies on absorption contrast only, and reconstructs the internal damage and

its dimensional changes during healing with a modest precision. Analogous to optical microscopy, the resolution is determined by the wavelength of the X-rays, the difference in absorption contrast, the divergence of the X-ray beam and the quality of the algorithms used to reconstruct the 3D image. Modern CT machines for material characterization have a resolution (i.e., voxel size) of about $2\mu\text{m}^3$ and can handle polymer samples with a cross-sectional thickness of about 10 mm. As the CT image is essentially a digital image, digital image analysis techniques can be used to determine quantitatively defect dimensions in 3D, defect volume fractions, and other geometrical parameters relevant to describe the damage and its change during healing in a quantitative sense.

A substantial further reduction in resolution can be obtained when a very narrow coherent X-ray beam is used and phase contrast information is used in combination with absorption contrast information. The first demonstration of the use of micro-tomography for the characterization of self-healing reactions was by Mookhoek *et al.* [4] who imaged the internal structure of a cracked polystyrene sample containing dichlorobenzene (DCB)-filled capsules. In this work a converted SEM with a Ta foil to generate a point source for the generation of hard coherent X-rays was used. Due to the high sensitivity of the technique a clear distinction between the matrix, capsules still containing the DCB, and empty capsules having released their content into the crack could be made. The resulting image of the sample is shown in Figure 14.3, clearly providing direct visualization of the autonomous self-healing reaction in a polymer containing encapsulated liquid self-healing agents, as invented by Dr Caroline Dry for concrete matrices but made more widely known by White *et al.* [5] for polymeric matrices.

In later work, Mookhoek *et al.* used the same technique while applying hard synchrotron X-rays to monitor the healing behavior in a MMA/PS matrix containing an encapsulated solvent with a solvent (bromobenzene) strongly absorbing

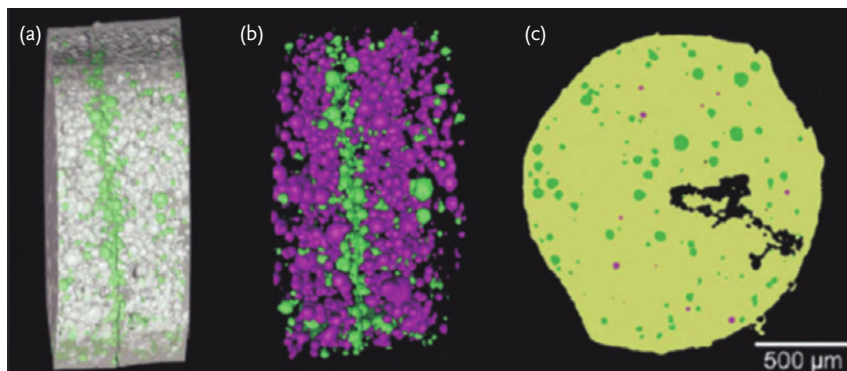


Figure 14.3 Computed tomographic images of a solvent-based self-healing thermoplastic material after fracture. (a) Side view of the cracked sample; (b) CT image showing empty capsules (green) around a crack

surface, purple capsules are still liquid filled; (c) computed top view of the healed crack surface showing a small region of imperfect healing (black region). After [4].

X-rays. For such a carefully optimized sample and experimental set-up the local solute release from single capsules after rupture could be followed *in situ* and in real time. At present the micro-tomography technique can be regarded as the most powerful visualization tool to monitor microscopic damage and healing events.

14.3

Healing of Mechanical Properties

14.3.1

Healing after Static Damage

Static damage may happen in structural polymers in the form of cracks, which may form anywhere in the polymer 3D structure and, depending on the application and source of damage, can occur over the span of multiple length scales [6]. Coatings and microelectronic packaging components have cracks that initiate on smaller scales, and once cracks have formed within polymeric materials, the integrity of the structure is significantly compromised [5]. Universal testing machines, as the name appropriately implies, have been used extensively to measure mechanical properties to estimate the extent of healing.

Tensile testing with rectangular or dog-bone geometries has been used extensively for measuring stress–strain relations of polymers. For self-healing studies, tensile experiments can be performed on the fractured and healed samples. However, healed samples face the challenges of improper alignment of the original fracture surfaces and surface roughness effects, which can lead to residual porosity in the healed fracture zone (as shown in Figure 14.1d). These disadvantages can be marginally mitigated by using samples with smaller cross-sectional area, but they in turn suffer from bending effects on bringing fractures' surfaces together. Tensile testing can still be considered suitable for systems above a threshold rigidity while at the same time using low cross-sectional area and smaller gage lengths. Several properties have been measured to quantify the extent of self-healing, and various definitions of self-healing efficiency exist, the most common being the ratio of critical loads at fracture [7–9]. The ratio of fracture toughness recovery [10–13], and the recovery of internal work or strain energy to account for non-linearity in load curve due to the new surface created by the crack, [14] are cited as self-healing efficiency. Further reports have used elongation at break [15], yield point stress [16], and force–displacement curves [17] to quantify and understand self-healing. However, due to the aforementioned challenges, these definitions of healing efficiency do not fully reflect the quality of healing.

The *lap shear* test can be used to measure tensile adhesion for self-healing systems [18]. For this set-up healing efficiency can be defined either as the ratio of ultimate shear strengths or the maximum elongation at break for the healed compared to the virgin sample. A major advantage of the lap shear test is that the fractured surfaces can be brought into contact in a controlled manner [19, 20]. The alignment and clamping conditions can also be reproduced between different

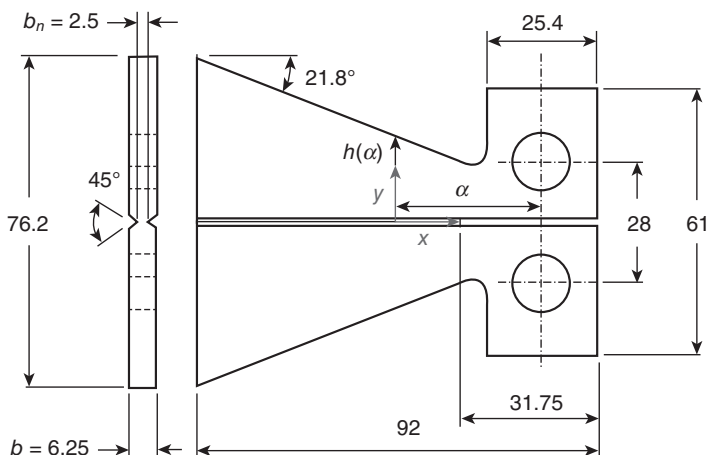


Figure 14.4 TDCB geometry to measure multiple healing cycles where fracture toughness is independent of crack length [23].

users and are less sensitive to topological defects. For self-healing systems with reversible chemistries, the lap shear experiment can be designed to accommodate experimental parameters of controlled force, curing temperatures, and times. Additionally, the test can be extended to study multiple healing cycles in sequential order for the same sample [21]. Care should be taken to distinguish between adhesive and cohesive failure for the lap shear test.

Torsion or *bending* geometries can also offer insights into the self-healing of multilayer films. For a sample that is self-healing under torsion, a threshold normal force can be applied to distinguish between the point of interfacial contact and the beginning of self-healing [22].

The *tapered double cantilever beam* (TDCB) geometry shown in Figure 14.4 offers an interesting way to quantify healing efficiency, as fracture toughness is independent of crack length [23], which is not the case for tension, compression, or bending type geometries. Therefore, the error in healing efficiency for the TDCB geometry is independent of actual healed crack length. Thus, in self-healing systems, when the crack length after a different number of healing cycles may not be constant, this set-up reflects the real healing efficiency if defined as the ratio of the fracture toughness for the healed and virgin samples. Furthermore, for samples where partial fracture happens, this geometry can be realigned relatively easily. The kinetics of the healing process can also be monitored.

Rheology can be used as a complementary technique to study chain mobility and its effect on the kinetics of self-healing in viscoelastic polymer systems above T_g [24]. *Dynamic mechanical analysis* can give further information about healing in polymer films in the context of viscoelastic properties of rubbery polymers. *Spectroscopic analysis*, such as FTIR, NMR or Raman spectroscopies, can be used to monitor the progress of healing at a molecular level where certain bonds appear or disappear in the course of self-healing [25, 26]. Electrochemical impedance spectroscopy used in Surlin ionomers has revealed interesting effects of lower

chain mobility resulting from the use of different metal ions (J.M. Vega *et al.*, unpublished data).

14.3.2

Healing after Fatigue Damage

Mechanical fatigue damage is the result of multiple loading cycles at stress levels well below the stress level leading to failure in a single loading event, that is, the static failure. As in static damage, the fatigue damage in polymers and composites generally consists of one major crack, often with some satellite cracks in the region close to the fatigue fracture plane. The fracture plane generally shows different regions: the crack initiation region, the fatigue crack propagation region, and the overload region. Generally the fracture surfaces of fatigue-failed samples are a little smoother than those for static loading. As the type of damage in fatigue failure is roughly the same as in static failure, the same sets of characterization/quantification methods may be used to describe the initial damage and its reduction during healing (see Section 14.3.1). However, there are some important differences between both failure modes which are worth addressing. In healing of static failure generally complete separation of the two parts of the sample or product is considered, while in fatigue crack studies it is very easy to stop the testing of the sample while the crack is still a partial crack, that is, the crack tip is still contained in the sample. This is an extremely important difference as far as quantification of healing efficiency is concerned:

- When the healing efficiency after (complete) static failure is to be determined, the testing requires the repositioning of the two fracture surfaces. A very small shift while repositioning the two sample halves can lead to a significant difference in registry of the two fracture surfaces, and hence to significant changes in material flow at the reassembled fracture surfaces to induce healing. As a result, the healing efficiencies of completely separated fracture surfaces will show a large amount of scatter for nominally identical testing conditions. In contrast, in (partial) fatigue failure, the two fracture surfaces will return in a much more reproducible manner to their relative position. In a rather brittle polymer, the amount of plastic deformation at the crack tip is small, and the fracture surfaces will come together rather closely and in pretty good registry upon simple unloading. Hence, for a given healing mechanism, the mechanical and physical healing efficiencies are likely to be high. In the case of more ductile polymers, the separation distances of the two fracture surfaces remain higher and healing efficiencies will be lower, yet more reproducible than for complete (static) failure.
- In the case of complete static failure quantification of the healing is best done by comparing the fracture load after healing to the original strength for a well-chosen sample geometry. In the case of partial fatigue failure the healing can be quantified via the recovery of the stiffness, or via the recovery of the residual strength. Experiments on the healing of asphalt (which can be regarded as a rather unspecified aromatic oligomer/polymer) showed that the stiffness

recovery is a more discriminating parameter than the residual strength recovery [27]. Experiments on self-healing thermal interface materials (TIM) (U. Lafont *et al.*, unpublished data) showed that the healing efficiency for the shear strength can be rather different from the healing efficiency as defined via shear displacement.

In conclusion, for the quantification of healing efficiency, studies on incompletely fractured samples seem most relevant. The techniques to be used are the same as those used for healing after (complete) static failure, but the interpretation of healing after fatigue damage may offer more insight into the effective healing potential of particular polymeric (and non-polymeric) self-healing systems.

14.3.3

Healing of Impact Damage

In contrast to static and fatigue damage, impact damage and the testing thereof is very hard to describe and to quantify, as the impact damage is a dynamic response of both the material and the impacting object (not only its velocity and kinetic energy, but also its shape), and the support or clamping of the sample during impact. However, there is a good reason to pay some attention to the healing after impact as the conditions, a very short damage formation time, followed by a long healing time at much lower stress level, are potentially very attractive for self-healing. There are two well-known cases of self-healing after impact: the healing of fiber-reinforced composites after perpendicular impact [28], and the healing of ionomers after ballistic impact [29, 30].

14.3.3.1 Impact Damage of Composites

In the case of larger scale impact damage of composites there is extensive internal crack formation due to splicing at ply level and at fiber-matrix level, and the resulting damage is geometrically very complex and hard to describe. As the amount of internal crack volume to be filled is very large, Bond *et al.* [28] correctly focussed on healing via a liquid healing agent and long distance supply thereof as the most appropriate and rather successful route to obtain self-healing. As the impact damage is highly dependent on the total system, it is impossible to design scientific tests for self-healing, yet well described technical protocols for impacting, healing and post-healing property determination (e.g., residual strength, residual stiffness) will be adequate to quantify healing and to compare different approaches. As such, the test methods are not different from those for quantification of self-healing after static and fatigue loading. In the case of small scale impact damage, the effect of the impact on the macroscopic mechanical properties will be harder to monitor and damage healing is best followed by (subsurface) visualization techniques, such as tomography and acoustical microscopy.

14.3.3.2 Healing of Ballistic Damage in Ionomers

A well-known example of healing from the early days of the field of SHM is the spontaneous hole closure of ionomer plates after ballistic impact [29]. The healing

is due to the high elasticity of the melt, the driving force for cluster reformation, and the autonomous heating of the sample in the direct vicinity of the impact site. As in impact damage on composites, the impact damage depends highly on the test conditions and mutual interactions of occurring processes, it is hard to quantify the damage and to separate the physical processes taking place. To get some further insight into the processes Varley *et al.* developed a quasi-static test in which a preheated stub is pulled through a pre-cut sample and the penetration forces and deflections are recorded as a function of speed and stub temperature, and linked to the hole closure measured optically [30]. In later work, Varley *et al.* [31] presented a simple flow device to measure the hole closure in a more quantitative manner.

14.4

Healing of Functional Integrity

14.4.1

Healing of Esthetic Damage

Scratches or surface damage, beside being esthetically undesirable, may also lead to corrosion and structural defects. Self-healing coatings, therefore, have been sought after for aerospace and automotive coatings applications. Surface healing of damage can lead to enhanced appearance and reduced corrosion, thus extending the life of the product and reducing costs. Apart from self-healing capabilities, increased scratch resistance is also of great importance in the automotive industry. Automotive clear coats were introduced to the market in the 1980s and have evolved along the way, however, the common feature retained has been the ability to resist and heal scratches. The surface gloss properties of a coating are mainly affected by scratches ranging from macroscopic to microscopic length scales. Pits and defects on the surface morphology, as well as increase in roughness, also reduce surface gloss [32]. Nissan pioneered the commercial application of self-healing protective automotive paint coatings based on reflow of polymers [33].

Gap or scratch depth, thickness and volume may be quantified using scratch testing and confocal microscopy, as described in Section 14.3.1. Optical monitoring of gap closure can also be performed by various microscopic techniques. Some specialized techniques have been reported to monitor and quantify recovery in surface gloss as follows. Localized micro-attenuated total reflectance Fourier transform infrared (ATR-FTIR) spectroscopy and internal reflection IR imaging (IRIRI) have been used in self-healing substituted chitosan polyurethane networks for small scale scratches which might affect surface gloss [34]. Typically, a crockmeter is used to measure reduction in surface gloss, or conversely recovery of surface gloss. The crockmeter test measures reflected light intensity after being subjected to a traversing tangential load of known particle size abrasive [35]. Scratch testing and confocal microscopy has been used in combination with each other to quantify healing of larger cracks which might affect surface gloss (J.M. Vega *et al.*, unpublished data). Progressive and constant load forces have been applied, as shown in

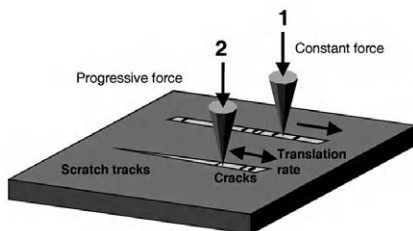


Figure 14.5 Principle of scratch testing [36].

Figure 14.5, to study the effect on scratch resistance, followed by subsequent optical tools to quantify the scratch depth and volume [36]. Quantitative measurement of the fraction of elastic, viscoelastic creep, and fracture response of a coating can be performed using an indenter tip, such as in a scanning probe microscope or a micro-indenter.

14.4.2

Healing of Thermal and Electrical Conduction

The implementation of a self-healing concept has also been achieved for material with an electrical or thermal conducting functionality. Such materials are able to recover conduction paths at different scales, depending on the used concept. The monitoring and quantification of the healing can be addressed in different ways, depending on the scale of damage and the healing concept.

14.4.2.1 Electrical Conduction Recovery

Simple current–voltage (I – V) measurements are easily applied in order to monitor a change in electronic conduction related to the healing of a conductive path. *Ex situ* types of measurements are the simplest to perform, and the following protocol is to be applied: the I – V response is recorded on a pristine sample, after damage, and finally after healing. The recovery of the conduction properties as a function of the damage size after rupture of an encapsulated solution of carbon nanotubes or charge transfer salts has been demonstrated using this technique [37, 38].

In an *in situ* type of measurement, the I – V response is monitored with time during the damaging and the healing period. For example, during quasi-static fracture tests (3–4 point bending, double-cantilever beam) the I – V profile can be monitored to investigate both the condition that leads to the decrease and rupture of the conductivity and the recovery. The limitation in performing *in situ* measurements depends mainly on practical considerations related to the material and the techniques. For example, measurement frequency needs to be adapted to the healing and damaging timescale and constant electrical connection needs to be possible during the damaging and healing cycles. If possible, *in situ* measurements will always be preferred as they can provide quantification of the healing kinetics. Using current density–voltage (J – V) measurements, extra information related to the recovery of the conduction section can be obtained. This technique will be

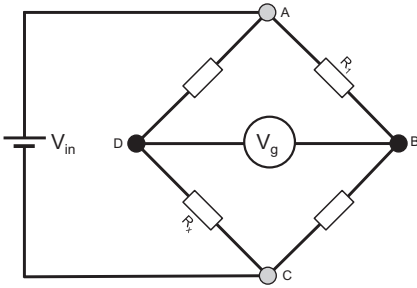


Figure 14.6 Wheatstone bridge circuit.

suitable for material with intrinsic self-healing ability, and cases where the conduction path shape is finite and confined.

If a very small change in resistivity needs to be monitored a Wheatstone bridge type of set-up will be preferred. This technique uses an electrical circuit to measure an unknown resistance. The set-up requires an electrical source with a known voltage, three resistors with a known value, and a galvanometer (Figure 14.6). In this respect this method is already widely applied when any environmental factors, such as temperature, humidity, strain, stress, or displacement, are susceptible to influence the change in the value of a resistance. Materials with self-healing ability implying a restoration of the electronic conductivity are thus eligible for this type of measurement. As described previously for the I - V measurement type, the Wheatstone bridge technique will allow monitoring of both the creation and the healing of damages. As a function of the applied stress, when the damages occur, the system resistivity will increase. Upon healing the conducting path the resistivity will decrease. Depending on the quality of the instrument used, this technique allows accurate *in situ* measurement. The damage event, the complete healing event, and also the time that is necessary after the fracture to recover the initial electrical conductivity are easily accessible within a μs timescale [39]. Commonly, an unbalanced constant voltage Wheatstone bridge circuit allows recording of the change in voltage during the restoration of the electrical conductivity.

A typical Wheatstone bridge set-up is shown in Figure 14.6 where the sample to be monitored is placed between the C and D nodes (R_x). The test procedure starts with the determination of the voltage for a broken sample (V_∞), which correspond to an infinite value of R_x , as a function of the input voltage (V_{in}). Subsequently healing can be monitored as a function of time using Eq. (14.1).

$$V_g = V_{in} \cdot \left(\frac{R_1}{R_1 + R_2} - \frac{R_4}{R_x + R_4} \right) \quad (14.2)$$

The healing process is quantified and assessed in term of V_{norm} , being a function of the original bridge voltage (V_0) corresponding to the voltage of a pristine sample (before disruption of the conduction path), V_∞ and the monitored voltage during healing V_h .

$$V_{\text{norm}} = \frac{V_h - V_{\infty}}{V_0 - V_{\infty}} = \frac{R_0 + R_4}{R_h + R_4} \quad (14.3)$$

Finally, if the healing involves changes in surface conduction, AFM can be used as a nanoprobe to map at the nanoscale the electrical conducting path and correlate it with the sample topology if necessary. This technique is potentially very powerful when investigating dimensional restoration of electrical conduction for self-healing composites.

14.4.2.2 Thermal Conduction Recovery

Microscopic and macroscopic damage in a material (crack, delamination) generally affects the thermal conduction. The thermal conductivity of a material will drop as more defects are present. During healing the sample will show a recovery of its initial thermal conductivity. *Ex or in situ* measurement can be used, depending on the damage and healing step. The recovery of a thermal path as a function of the time and heat flux can be obtained using an infrared camera. A time-dependent heat-flux mapping of one sample side will give a good insight on the recovery with the thermal path when a continuous heat source is used as probe on the opposite side. Thus the technique will be even more suitable when the healing mechanism is thermally triggered.

Time domain thermoreflectance (TDTR) is also a very efficient technique to monitor temperature decay. Because TDTR uses a mode-locked laser with picosecond pulse widths, nanoscale depth resolution can be achieved. Working at the picosecond level gives this technique the possibility to investigate intrinsic self-healing systems that relate to dynamic bonding ability involving fast molecular reaction. Information on interfacial thermal transport and bond strengths can also be achieved [40]. The TDTR data are expressed as the ratio of the in-phase and out-of-phase signal $V_{\text{in}}/V_{\text{out}}$ as a function of time. A thermal diffusion model is then used to fit the obtained data to obtain the thermal conductance. For quantitative measurements the thickness, heat capacity, and thermal conductivity of the component of the system should be known accurately.

14.4.3

Healing of Hydrophobicity and Surface Friction

14.4.3.1 Healing of Hydrophobicity

Recovery of surface hydrophobicity can be investigated in several simple ways. After damaging the surface using a blade, sand paper, or plasma etching, a drop of an appropriate liquid is placed on the surface. The surface is then tilted to a certain angle and the time for the drop to roll out is monitored. This simple technique is very efficient for macroscopic damage. However, in order to quantify and better characterize the healing related to the recovery of surface functionality, contact angle measurements are more appropriate. After damage the evolution of the contact angle is monitored as a function of time, temperature, and/or other parameters affecting the healing kinetics. Depending on the self-healing concept

used (bleeding of functional agent or self-replenishing surface) the way to induce damage is to be adapted. O₂ plasma etching is often used to mimic surface damage [41, 42]. However, if the in-depth surface property recovery is to be probed [43], one can choose ultra-microtomy to peel off the surface in a very controlled way (from 20 to 500 nm slices). The use of atomic force microscopy (AFM) to monitor force displacement is also an elegant way to investigate the surface functionality recovery. The adhesion force between the tip of the cantilever and the coating can be locally monitored. Depending on the self-healing process and its intrinsic kinetics it is thus possible to perform *in situ* measurement at the nanoscale.

14.4.3.2 Friction Recovery

Tribological experiments have been used to quantify friction recovery for liquid and solid lubricant healing systems [44, 45]. The evolution of the friction coefficient as a function of the healing process gives a good indication of the friction recovery property. In the same way, the wear rate can be used as an indicator. Fixing the load, velocity, wear track radius, and sliding distance, the monitoring of the mass difference and/or the volume difference (by interference microscopy) to the calculated value is used to calculate the wear rate. The use of AFM to investigate friction recovery will give a more localized vision of the phenomena involved during healing. In this respect the AFM tip can be used both to damage and to probe the surface. This technique is very useful when the healing involves material displacement at the molecular scale [46]. As a function of the specification of the AFM cantilever (spring constant, type of tip) a force–displacement curve can be used to get insight into the surface property recovery.

14.4.4

Healing of Protection Against Corrosion

The lowest energy state of most metals in the most common environments is their oxidized form, which means that metals tend to corrode, leading to loss of mechanical and esthetic properties. The most common and cheap way to protect metals from undesired corrosion is to apply protective layers (i.e., coatings) that offer active or/and passive protection. Coatings provide the functionality of corrosion protection to the system. The failure of the protective system leads thus to corrosion of the underlying metal. The restoration of this protective functionality is a desired concept that has been described as a self-healing mechanism and approached by different concepts.

In order to explore if a system shows self-healing functionalities (e.g., release of corrosion inhibitors, damage closure, surface coverage) the creation of an artificial defect in the coating system, and evaluation of the ability of the system to suppress or decrease corrosion to tolerable levels and restore the protective functionality has been broadly used. As corrosion processes in aqueous solution are fundamentally electrochemical processes, electrochemistry has been used as a versatile and polyvalent field to explore the self-healing capabilities.

14.4.4.1 Potentiostatic Measurements

This direct current (DC) technique has been used to study the healing capabilities of an epoxy-amine coating on steel doped with organic fillers containing inorganic corrosion inhibitors [47]. The test consists in monitoring the current density values at fixed potential ($-0.85 \text{ V}_{\text{Ag}/\text{AgCl}}$ and $-1.1 \text{ V}_{\text{Ag}/\text{AgCl}}$) with time. In this study, healing was detected by a decrease in the current density in a scratched doped-system, while the non-doped one showed an increase. A similar study was carried out using microencapsulation of liquid healing agents on coated steel plates [48]. In this case, upon polarization at 3 V, it was found that the current density of the self-healing system was two orders of magnitude lower than the reference one. This decrease suggests the formation of a barrier layer at the scribe (gap filling of the damage). Despite the first approach that this test offers, it should be noted that polarization could lead to accelerated degradation of the system, or promotion of deposition/reaction of healing agents. Therefore, measurements that do not dramatically alter the equilibrium state of the system are preferred: tests at open circuit potential (OCP) or under low polarization are more commonly used to study healing recovery of corrosion protection. As a conclusion, this technique could be used as a first approach to record healing phenomena, although complementary tests are recommended to measure the healing efficiency more quantitatively.

14.4.4.2 Electrochemical Impedance Spectroscopy

Electrochemical impedance spectroscopy (EIS) is one of the most used techniques in corrosion science to monitor local damage, and is based on the analysis of the impedance (Z) of a sample with time, where impedance represents the ability of a circuit to resist the flow of an alternating current (AC) when immersed in an electrolyte. This non-destructive technique applies a low polarization (usually $\pm 10 \text{ mV}$ over OCP) voltage difference upon which a sinusoidal current with a phase shift is obtained. The evaluation of healing properties has been made by following the total impedance on damaged systems. Sol-gel films containing nanocontainers loaded with corrosion inhibitors have shown an increase after damage [49]. Similar results were observed for microencapsulated single reactive healing agents (e.g., silyl esters) in an epoxy matrix [50] or in a complete coating system (primer + topcoat) [51]. Healing (see Figure 14.7a) has been mainly achieved by restoration of the barrier protection [51], deactivation of cathodic or anodic sites [49], or surface coverage combined with barrier protection [50]. Odd random phase multisine electrochemical impedance spectroscopy (ORP-EIS) has also been used to explore self-healing coatings using shape memory polymers [53], and shows a huge potential to monitor small scale damage in coatings and thin layers in general. Summarizing, EIS can provide useful and quantitative information about the electrochemical state of the coating and the coating/substrate interface that can be useful to monitor its (self) healing behavior.

14.4.4.3 Scanning Vibrating Electrode Technique

The scanning vibrating electrode technique (SVET) allows *in situ* monitoring of the distribution of anodic and cathodic areas at the surface. Healing can be evalu-

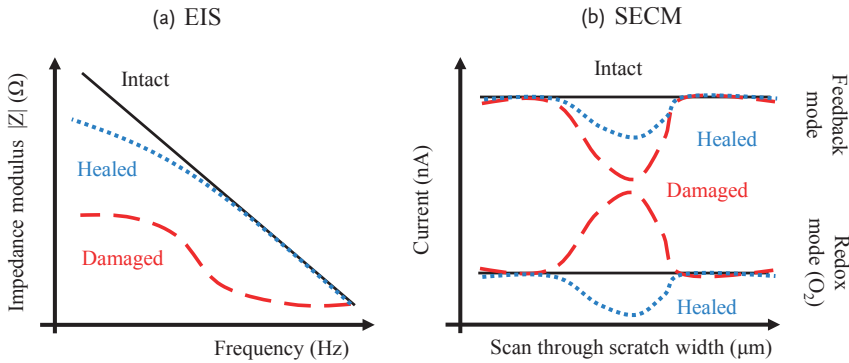


Figure 14.7 Examples of trends in SH anticorrosive coatings. (a) A typical Bode plot of an EIS experiment [50]. A drop in impedance in all frequency ranges can be seen for the damaged system, while the healed sample shows an increase in all the frequency ranges. (b) A feedback mode and redox mode trend obtained by SECM [52]. In

feedback mode after a drop in the current at the scratch the healed sample shows an increase. In redox mode the healed sample shows a change in trend showing the same curve as in feedback mode, while the damaged (or not healed) system shows higher O₂ consumption at the scratch.

ated due to the suppression or reduction of the redox activity. SVET has been widely used for self-healing coatings using corrosion inhibitors [54, 55], and more recently proven to be equally effective when analyzing the healing capabilities of microencapsulated liquid healing agents [50]. This technique is useful to obtain maps of corrosion activity at the local scale, and also provides valuable information in terms of corrosion kinetics that can be extrapolated to healing kinetics.

14.4.4.4 Scanning Electrochemical Microscopy

Scanning electrochemical microscopy (SECM) is based on reactions occurring in a mobile polarized ultramicroelectrode (UME) immersed in the bulk electrolyte. Information about the redox activity (redox mode) and topography (feedback mode) of a solid surface can be obtained. The redox competition mode has been recently employed to monitor *in situ* the evolution of the cathodic activity in two healing coatings on aluminum alloy AA2024-T3: a shape memory intrinsic healing coating [56], and an extrinsic self-healing coating using silyl ester as encapsulated single reactive healing agent [52]. Moreover, the combination of SECM modes (redox and feedback) has been recently proven to be very useful to explore self-healing properties, demonstrating the long term healing of an encapsulated silyl ester [52]. Scan-lines across the coating defect were performed to study the changes in oxygen (redox competition mode) and scratch topology (feedback mode), following thus the healing agent spreading and reaction, and the protection offered as a function of immersion time. Healing was detected due to the lack of consumption of oxygen in the system with healing agent (suggesting a barrier), and the change in trend in the redox mode to a feedback mode, where the oxygen acts as mediator (thus showing only topography) [52] as shown in Figure 14.7b. In

Table 14.1 Overview of the most relevant techniques to monitor initial damage and its reduction via self-healing, grouped by property recovery to be measured.

Recovery of property	Technique	Damage Type	Scale, location	Comments	Section	References
Visualization of damage	Optical and confocal microscopy	Scratch, scars, defects	Microscopic (minimum resolution 100 nm), surface or cross-sectional imaging	Important and versatile techniques to probe extent of damage	14.2.1	[1]
	Scanning electron microscopy		Nanoscale (minimum resolution 1 nm), surface or cross-sectional imaging	Can be used for studying smaller scale damage	14.2.2	[2]
	Acoustical microscopy	Scratches in the subsurface	Microscopic, possible to probe subsurface damage	Non-destructive test, useful for subsurface damage	14.2.3	[3]
	Computer tomography	Cracks, pits	Visualize 3D damage in entire body	Non-destructive test, possible to quantify extent of damage as well as healing using 3D image processing	14.2.4	[4, 57]
Stress, yield stress Strain, strain at break, Shear strength, Fracture toughness	Universal testing machine	Cracks, impact damage	Macroscopic to microscopic, surface or bulk	Offers a wide range of testing geometries	14.3	[5, 6, 10, 17, 21, 23]
	Rheometer and dynamic mechanical analyzer	Change in polymer network structure	Microscopic to molecular scale	Powerful techniques to study change in viscoelastic behavior of polymers, provides insights into their structure–property relationships	14.3.1	[24–26]
Surface roughness, change in surface topography	Atomic force microscopy (AFM)	Surface scratch or dislocation	Nano- to atomic scale, surface	Specialized technique to be used when changes in surface morphology need to be probed at an atomic scale	14.4.3	[46]
Scratch depth and width	Scratch testing	Scratch	Microscopic, surface	Complemented by optical or confocal microscopy	14.4.1	(J.M. Vega <i>et al.</i> , unpublished data)

Reflectance testing	Crockmeter	Scratch	Microscopic, surface	Useful for automotive clearcoats and other coating where surface gloss recovery is critical	14.4.1	[35]
Resistivity	$I-V$ or $J-V$ measurements on a Wheatstone bridge	Electrical conduction	Nano to microscopic, surface or bulk	Efficient for monitoring small changes in resistivity	14.4.2	[39]
Heat flux	Thermal conduction measurement	Thermal conduction	Micro to macroscopic, bulk	Use of picosecond pulse width in TDTR allows investigation of intrinsic self-healing systems at the molecular scale	14.4.2	[40]
Thermal conduction	Time domain thermo reflectance (TDTR)					
Contact angle	Goniometer	Loss in surface functionality	Scale is defined by droplet size, surface	Contact angle measurements provide insight regarding the surface hydrophobicity, but should be complemented by other spectroscopic techniques for probing recovery of functionality	14.4.3	[41–43]
Surface energy						
Current density	Potentiostatic	Barrier layer degradation, corrosion	Macroscopic, surface or bulk	Semi-quantitative approach to explore healing. The use of complementary techniques is generally required	14.4.4	[47, 48]
Barrier and/or active protection	Electrochemical impedance spectroscopy(EIS)		Macroscopic, surface or bulk	Most common technique to explore healing with time	14.4.4	[49, 50]
	Scanning vibrating electrode technique (SVET)		Microscopic, surface or bulk	Localized technique to detect anodic and cathodic areas on the metal surface	14.4.4	[50, 54, 55]
	Scanning electrochemical microscopy (SECM)		Microscopic, surface or bulk	Localized technique to quantify redox activity and topography on the surface	14.4.4	[52, 56]

conclusion, SECM is a polyvalent technique that can combine different parameters (modes and redox reactions) to study localized healing under immersion.

14.5

Summary

As shown in this chapter, many techniques are available to monitor damage in polymer materials in a qualitative, and sometimes even quantitative, manner. In the self-explanatory Table 14.1 the various techniques are grouped together, enabling a more rapid selection of the most appropriate technique. As in the characterization of undamaged material, the use of just one single technique will not yield a proper description of the phenomena taking place, and several techniques will have to be combined to yield a more or less quantitative description of the healing process. To allow a proper comparison of healing of comparable systems in independent investigations there is an urgent need for more standardized test configurations and data handling procedures, such as defined in ASTM or European standards for testing of undamaged materials. At the current stage of development of the field no such standards are yet in place. However, it will be clear that, given the rapidly growing commercial interest in developing self-healing materials, such standards are to be formulated in the near future.

References

- 1 Wu, X., Schlagen, E., and Van Der Zwaag, S. (2012) Linking crack tip morphology to tear toughness of hot rolled AA7050 alloys using X-ray computed tomography. *Adv. Eng. Mater.*, **14** (7), 449–456.
- 2 Micciché, F., Fischer, H., Varley, R., and van der Zwaag, S. (2008) Moisture induced crack filling in barrier coatings containing montmorillonite as an expandable phase. *Surf. Coat. Technol.*, **202** (14), 3346–3353.
- 3 Atkins, S., Teems, L., Rowe, W., Selby, P., and Vaughters, R. (1998) Use of C-SAM acoustical microscopy in package evaluations and failure analysis. *Microelectron. Reliabil.*, **38** (5), 773–785.
- 4 Mookhoek, S.D., Mayo, S.C., Hughes, A.E., Furman, S.A., Fischer, H.R., and Zwaag, S.V.D. (2010) Applying SEM-based X-ray microtomography to observe self-healing in solvent encapsulated thermoplastic materials. *Adv. Eng. Mater.*, **12** (3), 228–234.
- 5 Blaiszik, B.J., Kramer, S.L.B., Olugebefola, S.C., Moore, J.S., Sottos, N.R., and White, S.R. (2010) Self-healing polymers and composites. *Annu. Rev. Mater. Res.*, **40** (1), 179–211.
- 6 Andersson, H.M., Keller, M.W., Moore, J.S., Sottos, N.R., and White, S.R. (2007) Self healing polymers and composites, in *Self Healing Materials. An Alternative Approach to 20 Centuries of Materials Science* (ed. S. van der Zwaag), Springer, Dordrecht, pp. 19–44.
- 7 Chen, X., Dam, M.A., Ono, K., Mal, A., Shen, H., Nutt, S.R., Sheran, K., and Wudl, F. (2002) A thermally re-mendable cross-linked polymeric material. *Science*, **295** (5560), 1698–1702.
- 8 Toohey, K.S., Hansen, C.J., Lewis, J.A., White, S.R., and Sottos, N.R. (2009) Delivery of two-part self-healing chemistry via microvascular networks. *Adv. Funct. Mater.*, **19** (9), 1399–1405.
- 9 Peterson, A.M., Jensen, R.E., and Palmese, G.R. (2010) Room-temperature

- healing of a thermosetting polymer using the diels-alder reaction. *ACS Appl. Mater. Interfaces*, **2** (4), 1141–1149.
- 10 Brown, E., Sottos, N., and White, S. (2002) Fracture testing of a self-healing polymer composite. *Exp. Mech.*, **42** (4), 372–379.
 - 11 Brown, E.N., White, S.R., and Sottos, N.R. (2004) Microcapsule induced toughening in a self-healing polymer composite. *J. Mater. Sci.*, **39** (5), 1703–1710.
 - 12 Kessler, M.R., Sottos, N.R., and White, S.R. (2003) Self-healing structural composite materials. *Compos. A Appl. Sci. Manuf.*, **34** (8), 743–753.
 - 13 White, S.R., Sottos, N.R., Geubelle, P.H., Moore, J.S., Kessler, M.R., Sriram, S.R., Brown, E.N., and Viswanathan, S. (2001) Autonomic healing of polymer composites. *Nature*, **409** (6822), 794–797.
 - 14 Rule, J.D., Brown, E.N., Sottos, N.R., White, S.R., and Moore, J.S. (2005) Wax-protected catalyst microspheres for efficient self-healing materials. *Adv. Mater.*, **17** (2), 205–208.
 - 15 Tuncaboylu, D.C., Sahin, M., Argun, A., Oppermann, W., and Okay, O. (2012) Dynamics and large strain behavior of self-healing hydrogels with and without surfactants. *Macromolecules*, **45** (4), 1991–2000.
 - 16 Murphy, E.B. (2011) The return of photoelastic stress measurements: utilizing birefringence to monitor damage and repair in healable materials. *J. Mater. Chem.*, **21** (5), 1438–1446.
 - 17 Maes, F., Montarnal, D., Cantournet, S., Tournilhac, F., Corte, L., and Leibler, L. (2012) Activation and deactivation of self-healing in supramolecular rubbers. *Soft Matter*, **8** (5), 1681–1687.
 - 18 Yuan, Y.C., Rong, M.Z., Zhang, M.Q., and Yang, G.C. (2009) Study of factors related to performance improvement of self-healing epoxy based on dual encapsulated healant. *Polymer*, **50** (24), 5771–5781.
 - 19 Kavitha, A.A., and Singha, N.K. (2009) Click chemistry” in tailor-made polymethacrylates bearing reactive furfuryl functionality: a new class of self-healing polymeric material. *ACS Appl. Mater. Interfaces*, **1** (7), 1427–1436.
 - 20 Aubert, J.H. (2003) Note: thermally removable epoxy adhesives incorporating thermally reversible diels-alder adducts. *J. Adhes.*, **79** (6), 609–616.
 - 21 Lafont, U., van Zeijl, H., and van der Zwaag, S. (2012) Influence of cross-linkers on the cohesive and adhesive self-healing ability of polysulfide-based thermosets. *ACS Appl. Mater. Interfaces*, doi: 10.1021/am301879z
 - 22 Qiu, J., van de Ven, M.F.C., Wu, S.P., Yu, J.Y., and Molenaar, A.A.A. (2011) Investigating self healing behaviour of pure bitumen using Dynamic Shear Rheometer. *Fuel*, **90** (8), 2710–2720.
 - 23 Brown, E.N. (2011) Use of the tapered double-cantilever beam geometry for fracture toughness measurements and its application to the quantification of self-healing. *J. Strain Anal. Eng. Des.*, **46** (3), 167–186.
 - 24 Mauldin, T.C., Leonard, J., Earl, K., Lee, J.K., and Kessler, M.R. (2012) Modified rheokinetic technique to enhance the understanding of microcapsule-based self-healing polymers. *ACS Appl. Mater. Interfaces*, **4** (3), 1831–1837.
 - 25 Döhler, D., Michael, P., and Binder, W.H. (2012) Autocatalysis in the room temperature copper(I)-catalyzed alkyne–azide “click” cycloaddition of multivalent poly(acrylate)s and poly(isobutylene)s. *Macromolecules*, **45** (8), 3335–3345.
 - 26 Peterson, A.M., Jensen, R.E., and Palmese, G.R. (2009) Reversibly cross-linked polymer gels as healing agents for epoxy–amine thermosets. *ACS Appl. Mater. Interfaces*, **1** (5), 992–995.
 - 27 Liu, Q. (2012). Induction healing of porous asphalt concrete (Delft, Delft University of Technology).
 - 28 Trask, R.S., and Bond, I.P. (2006) Biomimetic self-healing of advanced composite structures using hollow glass fibres. *Smart Mater. Struct.*, **15** (3), 704–710.
 - 29 Kalista, S.J., Jr., Ward, T.C., and Oyetunji, Z. (2007) Self-healing of poly(ethylene-co-methacrylic acid) copolymers following projectile puncture. *Mech. Adv. Mater. Struct.*, **14** (5), 391–397.
 - 30 Varley, R.J., and Van der Zwaag, S. (2008) Development of a quasi-static test method to investigate the origin of

- self-healing in ionomers under ballistic conditions. *Polym. Test.*, **27** (1), 11–19.
- 31 Varley, R.J., and van der Zwaag, S. (2010) Autonomous damage initiated healing in a thermo-responsive ionomer. *Polym. Int.*, **59** (8), 1031–1038.
- 32 Edwards, S.A., and Roy Choudhury, N. (2004) Variations in surface gloss on rubber-modified thermoplastics: relation to morphological and rheological behavior. *Polym. Eng. Sci.*, **44** (1), 96–112.
- 33 Zheludkevich, M. (2009) Self-healing anticorrosion coatings, in *Self-Healing Materials* (ed. S.K. Ghosh), Wiley-VCH Verlag GmbH, p. 101.
- 34 Ghosh, B., and Urban, M.W. (2009) Self-repairing oxetane-substituted chitosan polyurethane networks. *Science*, **323** (5920), 1458–1460.
- 35 Ryntz, R., Abell, B., Pollano, G., Nguyen, L., and Shen, W. (2000) Scratch resistance behavior of model coating systems. *J. Coat. Technol.*, **72** (904), 47–53.
- 36 Osterhold, M., and Wagner, G. (2002) Methods for characterizing the mar resistance. *Prog. Org. Coat.*, **45** (4), 365–371.
- 37 Odom, S.A., Caruso, M.M., Finke, A.D., Prokup, A.M., Ritchey, J.A., Leonard, J.H., White, S.R., Sottos, N.R., and Moore, J.S. (2010) Restoration of conductivity with TTF-TCNQ charge-transfer salts. *Adv. Funct. Mater.*, **20** (11), 1721–1727.
- 38 Caruso, M.M., Schelkopf, S.R., Jackson, A.C., Landry, A.M., Braun, P.V., and Moore, J.S. (2009) Microcapsules containing suspensions of carbon nanotubes. *J. Mater. Chem.*, **19** (34), 6093–6096.
- 39 Blaiszik, B.J., Kramer, S.L.B., Grady, M.E., McIlroy, D.A., Moore, J.S., Sottos, N.R., and White, S.R. (2012) Autonomic restoration of electrical conductivity. *Adv. Mater.*, **24** (3), 398–401.
- 40 Losego, M.D., Grady, M.E., Sottos, N.R., Cahill, D.G., and Braun, P.V. (2012) Effects of chemical bonding on heat transport across interfaces. *Nat. Mater.*, **11** (6), 502–506.
- 41 Liu, Q., Wang, X., Yu, B., Zhou, F., and Xue, Q. (2012) Self-healing surface hydrophobicity by consecutive release of hydrophobic molecules from mesoporous silica. *Langmuir*, **28** (13), 5845–5849.
- 42 Wang, X., Liu, X., Zhou, F., and Liu, W. (2011) Self-healing superamphiphobicity. *Chem. Commun.*, **47** (8), 2324–2326.
- 43 Dikić, T., Ming, W., van Benthem, R.A.T.M., Esteves, A.C.C., and de With, G. (2012) Self-replenishing surfaces. *Adv. Mater.*, **24** (27), 3701–3704.
- 44 Hsiao, E., Barthel, A.J., and Kim, S.H. (2011) Effects of nanoscale surface texturing on self-healing of boundary lubricant film via lateral flow. *Tribol. Lett.*, **44** (2), 287–292.
- 45 Valefi, M., de Rooij, M., Schipper, D.J., and Winnubst, L. (2012) Effect of temperature on friction and wear behaviour of CuO-zirconia composites. *J. Eur. Ceram. Soc.*, **32** (10), 2235–2242.
- 46 Hsiao, E., Kim, D., and Kim, S.H. (2009) Effects of Ionic side groups attached to polydimethylsiloxanes on lubrication of silicon oxide surfaces. *Langmuir*, **25** (17), 9814–9823.
- 47 Sauvant-Moynot, V., Gonzalez, S., and Kittel, J. (2008) Self-healing coatings: an alternative route for anticorrosion protection. *Prog. Org. Coat.*, **63** (3), 307–315.
- 48 Cho, S.H., White, S.R., and Braun, P.V. (2009) Self-healing polymer coatings. *Adv. Mater.*, **21** (6), 645–649.
- 49 Shchukin, D.G., Zheludkevich, M., Yasakawa, K., Lamaka, S., Ferreira, M.G.S., and Mohwald, H. (2006) Layer-by-layer assembled nanocontainers for self-healing corrosion protection. *Adv. Mater.*, **18** (13), 1672–1678.
- 50 Garcia, S.J., Fischer, H.R., White, P.A., Mardel, J., Gonzalez-Garcia, Y., Mol, J.M.C., and Hughes, A.E. (2011) Self-healing anticorrosive organic coating based on an encapsulated water reactive silyl ester: synthesis and proof of concept. *Prog. Org. Coat.*, **70** (2–3), 142–149.
- 51 Mehta, N.K., and Bogere, M.N. (2009) Environmental studies of smart/self-healing coating system for steel. *Prog. Org. Coat.*, **64** (4), 419–428.
- 52 González-García, Y., García, S.J., Hughes, A.E., and Mol, J.M.C. (2011) A combined

- redox-competition and negative-feedback SECM study of self-healing anticorrosive coatings. *Electrochem. Commun.*, **13** (10), 1094–1097.
- 53 Jorcin, J.B., Scheltjens, G., Van Ingelgem, Y., Tourwé, E., Van Assche, G., De Graeve, I., Van Mele, B., Terryn, H., and Hubin, A. (2010) Investigation of the self-healing properties of shape memory polyurethane coatings with the “odd random phase multisine” electrochemical impedance spectroscopy. *Electrochim. Acta*, **55** (21), 6195–6203.
- 54 Lamaka, S.V., Zheludkevich, M.L., Yasakau, K.A., Montemor, M.F., Cecílio, P., and Ferreira, M.G.S. (2006) TiO_x self-assembled networks prepared by templating approach as nanostructured reservoirs for self-healing anticorrosion pre-treatments. *Electrochem. Commun.*, **8** (3), 421–428.
- 55 Lamaka, S.V., Zheludkevich, M.L., Yasakau, K.A., Montemor, M.F., and Ferreira, M.G.S. (2007) High effective organic corrosion inhibitors for 2024 aluminium alloy. *Electrochim. Acta*, **52** (25), 7231–7247.
- 56 Gonzalez-Garcia, Y., Mol, J.M.C., Muselle, T., De Graeve, I., Van Assche, G., Scheltjens, G., Van Mele, B., and Terryn, H. (2011) SECM study of defect repair in self-healing polymer coatings on metals. *Electrochem. Commun.*, **13** (2), 169–173.
- 57 White, S.R., and Geubelle, P.H. (2010) Self-healing materials: get ready for repair-and-go. *Nat. Nanotechnol.*, **5** (4), 247–248.

15

Self-Healing Epoxies and Their Composites

Henghua Jin, Kevin R. Hart, Anthony M. Coppola, Ryan C. Gergely, Jeffrey S. Moore, Nancy R. Sottos, and Scott R. White

15.1

Introduction

Epoxies are particularly popular as the matrix material for fiber-reinforced polymeric composites and structural epoxy adhesives, as they exhibit superior chemical and corrosion resistance, good mechanical and thermal properties, outstanding adhesion to various substrates, low shrinkage upon cure, and good electrical insulating properties. However, epoxies are brittle in nature and flaw sensitive; susceptible to damage induced by mechanical, chemical, thermal, UV-radiation, or a combination of these factors. Conventional approaches to managing damage in the epoxy matrix materials (e.g., damage detection, and manual repair [1]) are limited as they generally require a certain degree of manual intervention, which could be complicated, expensive, and time consuming [2].

Inspired by living systems, self-healing polymers are designed to autonomically repair damage, thus providing a means to significantly extend the service life and reliability of polymeric structural composites. Three primary conceptual approaches to self-healing have been explored in the past decade [3] (Figure 15.1). In the first, microcapsules containing reactive chemical species are incorporated into the native polymer matrix and, upon crack damage, release their contents and undergo a healing reaction. In the second, an embedded vascular network serves as a reservoir for sequestration and distribution of healing agent(s). As damage interrupts channel continuity, liquid agents infiltrate into damaged regions, facilitating healing. The third approach utilizes inherently reversible bonding in the matrix polymer to affect healing via thermally reversible reactions or re-formation of hydrogen bonds.

In this chapter, an overview of the state-of-the-art in epoxy-based systems is presented. We primarily focus on the progress toward self-healing epoxies and their composites via the above three approaches. Then we conclude with current challenges and future research directions of this emerging area.

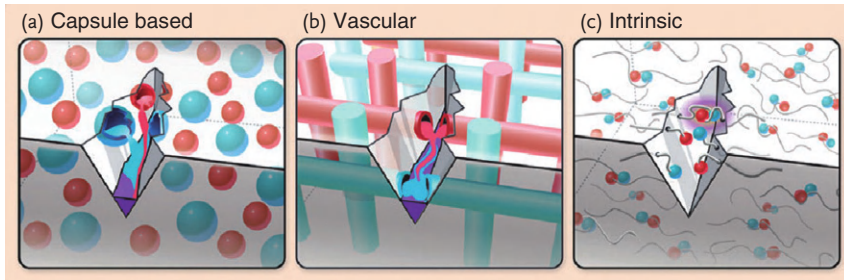


Figure 15.1 Schematics of three self-healing approaches [3]. (a) Capsule-based healing system, with the healing agent sequestered in capsules until they are ruptured by damage. (b) Vascular healing materials containing the healing agent(s) in hollow

channels or hollow fibers until damage ruptures the vasculature and releases the healing agent(s). (c) Intrinsic materials contain a latent functionality that triggers self-healing of damage via thermally reversible reactions, hydrogen bonding.

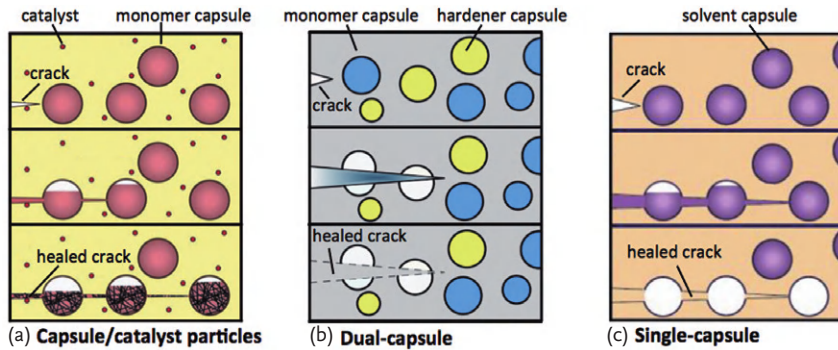


Figure 15.2 Microcapsule-based self-healing schemes. (a) Capsule/catalyst particles [4]. (b) Dual-capsule system in which both the monomer and cross-linking agent are

encapsulated. (c) Single capsule system using latent functionality of the matrix or an environmental stimulus to achieve healing [5].

15.2 Capsule-Based Healing System

Three schemes for capsule-based self-healing epoxies have been explored over the past decade. Each scheme sequesters a healing agent in discrete capsules until damage triggers release. The first method utilizes capsule/catalyst as the healing phases (Figure 15.2a). The healing agent is an encapsulated liquid monomer, while the polymerizer is a solid phase catalyst dispersed in the matrix. In the second scheme, both the monomer and polymerizer are sequestered in two distinct capsules (Figure 15.2b). The third healing system contains a single microcapsule dispersed in the epoxy matrix that relies on residual reactive functionality in the matrix or an environmental stimulus (e.g., oxidation) (Figure 15.2c).

15.2.1

Self-Healing Epoxies**15.2.1.1 Capsule/Catalyst Healing System**

Self-healing epoxy was initially achieved by incorporating a microencapsulated low molecular weight monomer (dicyclopentadiene, DCPD) and a solid phase chemical catalyst, bis(tricyclohexylphosphine)benzylidene ruthenium (IV) dichloride (Grubbs' first generation catalyst), within an epoxy matrix, as shown in Figure 15.2a [4]. Fracture of the epoxy matrix ruptured the microcapsules, releasing the DCPD monomer into the crack plane. Upon contact with the catalyst, polymerization of the monomer occurred, rebonding the crack faces and restoring mechanical integrity. Epoxy containing an optimized concentration and size of DCPD microcapsules and Grubbs' catalyst yielded up to 90% recovery of virgin fracture toughness in mode I fracture testing using a tapered-double-cantilever-beam (TDCB) specimen. In subsequent studies, Brown *et al.* showed significant life-extension for self-healing epoxy subject to fatigue loading [6, 7]. Jin *et al.* extended this healing system to a thin epoxy adhesive film, demonstrating 56% recovery of virgin fracture toughness in quasi-static mode I fracture and crack arrest in fatigue (Figure 15.3a) [8]. Kirkby *et al.* improved the healing performance with the use of shape memory alloy (SMA) wires. Improved healing resulted from a reduction in crack volume by reducing crack face separation. Heat produced by the activation of SMA wires also provided a more complete polymerization of the healing agent [11, 12]. Recently, Wilson and coworkers improved the healing efficiency by using

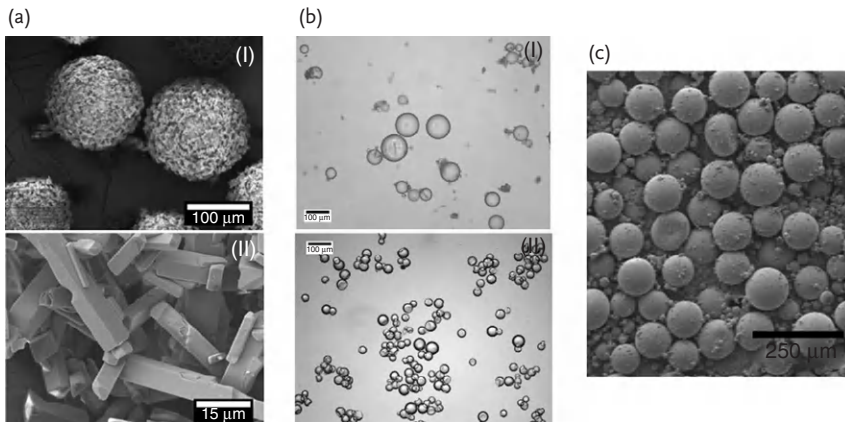


Figure 15.3 Examples of three self-healing approaches in epoxies. (a) SEM images of (I) DCPD microcapsules and (II) as-received Grubbs' first generation catalyst particles [8]. (b) Optical images of (I) PDMS microcap-

sules and (II) organotin microcapsules [9]. (c) SEM image of epoxy resin microcapsules. (Image reprinted from [10], with permission from Elsevier).

a mixture of DCPD and a monovalent adhesion promoter, dimethylnorbornene ester (DNE) [13]. The combination of DCPD and the co-healing agent DNE was successfully encapsulated, and the resulting microcapsules were used in self-healing experiments that demonstrated superior self-healing performance relative to DCPD alone.

However, the curing agent used in the epoxy, diethylenetriamine (DETA), destructively deactivates Grubbs' catalyst as the epoxy initially cures, and this destruction reduces the amount of catalyst available for healing [14]. Thus, several modifications of the healing system or methods of protecting Grubbs' catalyst were investigated, including incorporation into wax microspheres and polymer encapsulation [15–17], and catalyst morphology modifications [18]. Rule *et al.* showed circa 100% healing efficiency with Grubbs' catalyst embedded into wax microspheres [15]. Jones *et al.* examined the role of the crystal morphology and dissolution kinetics of Grubbs' catalyst on self-healing capability [18]. By balancing the competing effects of protection during sample fabrication and fast dissolution in the DCPD monomer, self-healing epoxy with optimal healing capabilities was established. The use of an alternative metathesis catalyst or healing chemistry has also been extensively explored. Second generation Grubbs' catalyst [19], Hoveyda-Grubbs' catalyst [19, 20], and tungsten hexachloride (WCl_6) catalyst [21, 22] have all shown moderate levels of healing in Mode I fracture testing. More recently, Coope *et al.* demonstrated healing using encapsulated epoxy resin and scandium (III) triflate catalyst particles [23]. Heating at 80 °C for 48 h yielded 80% recovery of virgin fracture toughness using TDCB specimens.

15.2.1.2 Dual-Capsule Healing System

Self-healing using a dual-microcapsule system, illustrated in Figure 15.2b, incorporates monomer and polymerizer which are separately encapsulated or phase separated in the matrix. PDMS/dimethyldineodecanoate tin (DMDNT) catalyst healing chemistry was used to achieve a self-healing epoxy-based coating [24]. The authors achieved successful autonomic corrosion protection of metal substrates by self-healing under ambient conditions. Recently, Mangun *et al.* extended this work to a bulk epoxy cured at 100 °C, demonstrating 52% recovery of virgin fracture toughness with the aid of an adhesion promoter (Figure 15.3b) [9]. Importantly, 28% healing efficiency was also reported for samples exposed to a high post-cure temperature of 177 °C marking the first demonstration of autonomic healing for an epoxy cured at elevated temperature.

Encapsulation of liquid epoxy monomer and its hardeners has been of particular interest since it provides a repair system that is chemically and mechanically compatible with the host epoxy matrix. Yuan *et al.* developed a dual-capsule healing system based on an epoxy/mercaptan chemistry, and demonstrated full recovery of fracture toughness [25]. Later a more thermally stable healing system was developed by adopting an alternative hardener, 2,4,6-tris(dimethylaminomethyl)phenol, in which healing efficiencies ranging from 76 to 82% were achieved for epoxies cured at temperatures up to 250 °C [26]. Xiao and coworkers introduced an encapsulated epoxy monomer and boron trifluoride diethyl etherate ($(C_2H_5)_2O \cdot BF_3$)

hardener healing system into epoxy cured at 45 °C, achieving circa 90% healing efficiency [27, 28]. Recently, a self-healing thermoset using encapsulated epoxy/amine healing chemistry was proposed by Jin *et al.* [29] in which 89% recovery of virgin fracture toughness was achieved in epoxy cured at 35 °C. However, post-cure for 1 h at 121 °C significantly decreased the healing efficiency as a result of amine diffusion from the capsule core.

15.2.1.3 Single Capsule Healing System

Self-healing via a single microcapsule healing system utilizing latent functionality has attracted increasing research interest [5, 30–33]. In these systems, a microencapsulated healing agent interacts with residual reactive functionality in the host epoxy matrix. For example, Caruso *et al.* demonstrated full recovery of Mode-I fracture toughness using a solvent promoted self-healing system [5, 30]. The epoxy matrix is swollen by solvent delivered from ruptured microcapsules, which frees residual functional groups to initiate further cross-linking. However, this healing mechanism requires a very small crack face separation to facilitate chain entanglement and cross-linking across the crack. Shape memory alloy (SMA) wires were recently introduced to reduce the crack separation after fracture to enhance the healing performance of this solvent-based healing system [34]. The requirements of chain mobility and unreacted functional groups in under-cured epoxy limit the broader applications of this type of healing system. Xiao and coworkers proposed a different method to incorporate latent functionality using $(C_2H_5)_2O \cdot BF_3$ catalyst absorbed by short sisal fibers and protected by a polystyrene coating [33]. When these fibers were incorporated into an epoxy, the catalyst evenly diffused into the matrix to provide latent functionality. A 76% recovery of impact strength was observed for samples containing epoxy microcapsules and $(C_2H_5)_2O \cdot BF_3$ catalyst-loaded fibers fully cured at 50 °C for 48 h. Liu *et al.* recently reported a self-healing epoxy coating using only epoxy capsules (Figure 15.3c). Upon damage, the released epoxy monomer reacted with the residual polyamide hardener in the matrix and polymerized under alkaline conditions [10].

Single capsule healing systems based on atmospheric oxidation of encapsulated healing agents do not require a separate catalyst or hardener. Samadzadeh and coworkers reported a self-healing epoxy coating with Tung oil as the encapsulated healing agent [35]. The core material, a type of drying oil, dries to form a tough, glossy, waterproof polymer upon exposure to oxygen. Linseed oil, another type of drying oil, was also considered as a healing agent in the development of self-healing epoxy coatings [36, 37].

15.2.2

Self-Healing Fiber-Reinforced Epoxies

Damage modes in composites are far more complex than those of pure polymer systems. With the inclusion of fiber reinforcement, researchers must demonstrate healing not only of the matrix material, but also of the interface between the reinforcement and matrix, should it occur. Capsule-based healing

in composites is particularly difficult since the inclusion of fibers in the polymer matrix limits the volume available for capsules, and ultimately, availability of healing agents.

15.2.2.1 Recovery of Mode I Fracture Toughness

Self-healing in fiber-reinforced composites using a microcapsule-based approach was initially demonstrated using quasi-static mode I fracture experiments. Kessler *et al.* utilized the DCPD/Grubbs' catalyst healing chemistry in woven E-glass/epoxy double cantilever beam (DCB) composite specimens [38]. Self-activated, room-temperature healing results demonstrated up to 80% recovery of critical strain energy release rate. In subsequent work these authors adopted a width-tapered double cantilever beam (WTDCB) geometry using woven carbon-fiber composites containing an embedded dispersion of DCPD capsules and Grubbs' catalyst particles [39]. In this full *in situ* system, 40% healing efficiency was observed at room temperature healing conditions, with up to 80% healing observed under elevated temperature (80 °C) healing conditions. Yin *et al.* studied self-healing of interlaminar fracture using E-glass/epoxy DCBs containing a microencapsulated epoxy resin and a latent hardener in the matrix ($\text{CuBr}_2(2\text{-methylimidazole})_4$) [40, 41], as shown in Figure 15.4a. Heating the samples for 1 h at 130 °C yielded an average recovery of critical strain energy release rates ranging from 28 to 51%. In all studies using DCB or modified DCB testing, authors attribute the lack of full self-healing, in part, to unrepairable fiber bridging which occurs in virgin test samples.

15.2.2.2 Recovery from Impact Damage

Self-healing of impact damage in fiber-reinforced composites is regarded as one of the most difficult areas of ongoing research because of the large damage volume and multiple failure modes. Yin and coworkers used the latent $\text{CuBr}_2(2\text{-methylimidazole})_4$ chemistry for self-healing of impact damage in woven glass/epoxy laminates [45]. Compression after impact (CAI) was used to evaluate self-healing in impacted laminates. Samples healed under elevated pressures and temperatures demonstrated 95% healing at the lowest impact energy level, but at the highest impact energy healing efficiencies dropped to 15%. Patel and coworkers investigated self-healing of impact damage in S2-glass/epoxy composites with embedded DCPD/Grubbs' healing chemistry [42]. Healing efficiencies at room temperature using CAI tests were as high as 100%, but dropped off at higher impact energies. Optical micrographs from this study at higher impact energies show only partial healing of delamination damage, which the author attributes to incomplete filling of damage volume (Figure 15.4b). Yuan *et al.* used a dual-capsule system based on epoxy/mercaptan healing chemistry to study CAI, as well as rate of damage area reduction in thin glass/epoxy laminates [46]. Backface damage areas were healed up to 96% and CAI recovery was nearly 87% for room temperature healing in samples impacted at the lowest energy level, but as with other studies, healing efficiency dropped off dramatically with increased impact energy.

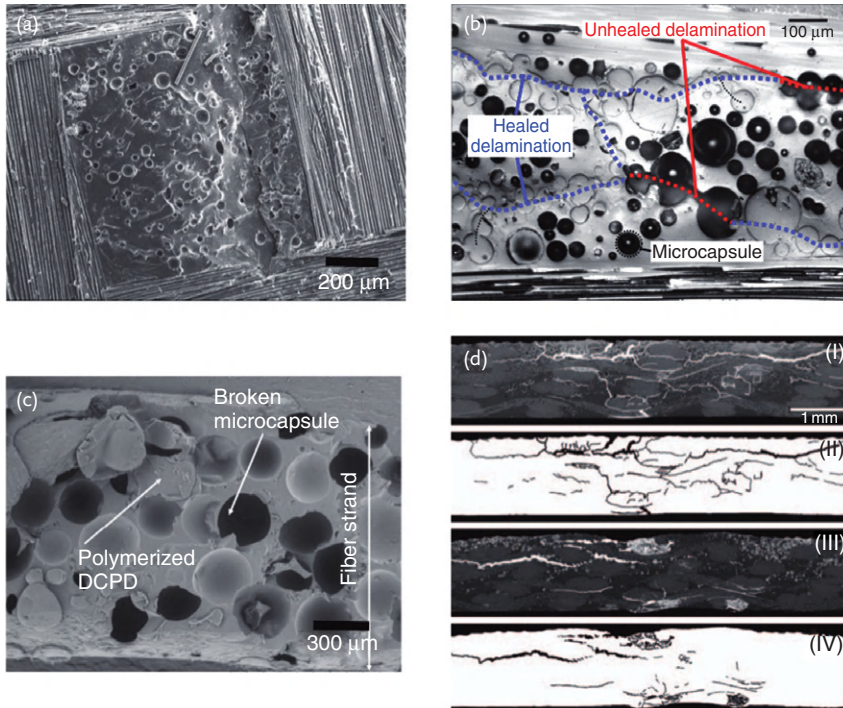


Figure 15.4 Examples of healing in composites. (a) SEM micrographs of fracture surfaces in a glass fiber-reinforced composite containing epoxy and CuBr_2 capsules following a mode-I DCB fracture test. (Image reprinted from [41], with permission from IOP Publishing). (b) An optical micrograph of a partially healed section of delamination in a glass fiber-reinforced composite containing DCPD microcapsules and wax-protected Grubbs' catalyst microspheres [42]. (c) An SEM micrograph of a healed surface in a carbon fiber-reinforced composite containing DCPD capsules and Grubbs'

catalyst particles [43]. (d) Comparison of crack damage in control and self-sealing fiber-reinforced composites following indentation damage [44]. (I) Tiled SEM images of a damaged region in a control specimen containing DCPD capsules and wax microspheres. (II) Highlighted crack damage in the damaged regions of image (I). (III) Tiled SEM images of a damaged region in a self-sealing specimen containing DCPD capsules and wax protected Grubbs' catalyst microspheres. (IV) Highlighted crack damage in the damaged regions of image (III).

15.2.2.3 Recovery of Macroscale Properties and Interfacial Bond Strength

Recovery of macroscale composite properties (stiffness and ultimate strength) is often difficult, since most self-healing chemistries target healing of matrix damage alone. Barbero *et al.* used the DCPD/Grubbs' healing chemistry to recover axial-transverse shear modulus in unidirectional laminates [47]. After applying shear stress over multiple cycles, 100% modulus recovery was observed over the first two cycles, with still noticeable recovery after eight cycles. Sanada *et al.* investigated self-healing of transverse cracks in unidirectional graphite/epoxy tensile specimens in which the fibers were coated in an epoxy/catalyst/capsule mixture before

solidification (Figure 15.4c) [48]. Here, the self-healing metric was ultimate tensile strength. Only 14% healing efficiency was achieved in the best case with capsule loading as high as 40 wt% with significantly reduced virgin properties. Sanada *et al.* also extended this work to include a computational study on self-healing of interfacial debonding [43]. Self-healing of interfacial damage and recovery of interfacial shear strength was demonstrated by Blaiszik *et al.* [49]. In this work a model composite consisting of a Grubbs' catalyst-coated glass fiber functionalized with sub-micron DCPD capsules was manufactured for single fiber pull-out testing. Up to 44% recovery of interfacial shear strength was observed following 24 h healing at room temperature.

15.2.2.4 Recovery of Barrier Properties

Fiber-reinforced epoxy composites are also often used for their barrier properties to prevent diffusion of fluids or gas through the material thickness. When cracks percolate or holes penetrate through the thickness of the material, barrier properties are degraded. Moll *et al.* demonstrated a self-sealing epoxy composite (plain weave E-glass) containing an embedded DCPD/Grubbs' healing chemistry (Figure 15.4d) [44]. Composites were damaged using a micro-indentation technique and sealing was assessed through the use of a pressurized flow cell. The percentage of samples sealed varied with capsule concentration and capsule size, but in the best case, 67% of samples sealed using this technique.

15.3

Vascular-Based Healing Systems

Vascular-based healing systems have the ability to replenish healing agents after a damage event, allowing multiple healing cycles. The method chosen for a particular application depends on the type of damage, the dimensional connectivity and architecture of the required network, and the presence of reinforcing fibers. The first channels fabricated in an epoxy material for the purpose of self-healing were made from glass pipettes. Dry embedded millimeter scale pipettes into a glass bead reinforced epoxy matrix and demonstrated the ability to release liquids from these pipettes after impact damage [50]. Motuku *et al.* compared several mediums for releasing healing agent in response to impact in glass-epoxy panels, including glass pipettes, aluminum tubes, and copper tubes. Only the channels manufactured using glass pipettes were found to rupture and release healing agent [51].

While glass pipettes can store and release liquid healing agents they are non-structural components and improved performance is achieved with hollow glass fibers (HGF) ranging from 15–60 μm . HGFs can be incorporated both as the primary reinforcing fiber [52–54], or as isolated channels surrounded by solid reinforcing fibers (Figure 15.5a) [57–59]. Other methods that have been utilized to create similar channel geometries include removal of a solid polymer or metal cord by manual extraction [60, 61], and melting of solder wire [62]. The primary

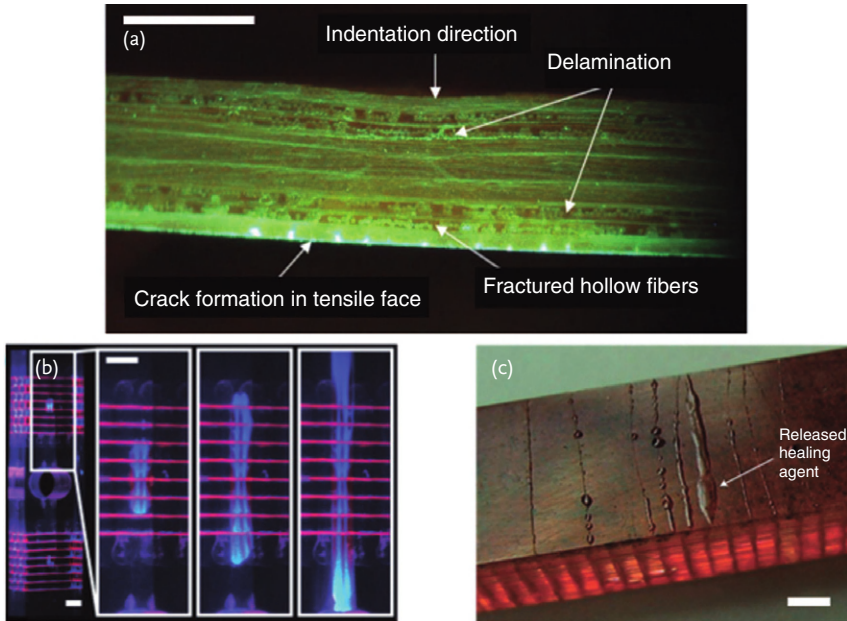


Figure 15.5 Demonstrations of vascular healing. (a) Fluorescently-dyed healing agent being released from HGFs in a composite following impact (Image reprinted from [52], with permission from Elsevier). (b) A

two-part healing agent mixing inside a crack in epoxy [55]. (c) A 3D vascular network delivering healing agent to surface cracks in a barrier coating. All scale bars represent 2 mm [56].

disadvantage of these methods is their restriction to discrete, isolated channels with one-dimensional, straight architecture. The primary method used for fabricating higher order channel architectures is direct writing of a fugitive ink scaffold [55, 56, 63–66]. In this method, the ink scaffold is printed in the shape of the desired network, surrounded with an epoxy matrix, and removed via melting. This method is restricted to low viscosity matrices because of the fragility of the ink scaffold during infiltration. Other methods for manufacturing higher order networks include catalyst-treated poly(lactic acid) “sacrificial fibers” [67], electrostatic discharge [68], and melt-spun sugar scaffolds [69]. However, none of these approaches has been used in healing systems to date.

15.3.1

Recovery of Fracture Damage

Hamilton *et al.* used a double cantilever drilled compression (DCDC) test to study healing of fracture events in a neat epoxy (Figure 15.5b) [55, 60]. Initially, micro-channels were manufactured using the direct-write method to create a series of 2D channel networks containing a two-part epoxy healing system. Specimens were tested for multiple healing cycles, attaining 86% healing efficiency after the first

healing cycle, decreasing steadily to approximately 40% healing efficiency after 13 cycles [58]. In the second study, the authors replaced the 2D passive capillary healing network with dual 1D pressurized networks containing a two-part epoxy healing system. Using a variety of dynamic pumping profiles, up to 15 cycles of 100% healing efficiency were achieved [62].

15.3.2

Recovery of Impact Damage

Out-of-plane impact damage in fiber-reinforced composites can result in extensive damage, including delamination and transverse cracking at low energies, and fiber breakage and puncture at high energies. Bleay *et al.* examined the healing of composite panels composed of 15 μm diameter HGFs filled with a two-part epoxy resin to restore the compressive strength of a panel after impact. Following an 80 J impact event, the healing agent was released into the damaged region and cured under various conditions, including elevated temperature and vacuum pressure, but only minimal healing (<10%) was observed in CAI testing [53]. Pang *et al.* used a similar approach, but included solid glass fibers in addition to HGFs as reinforcement. Self-healing specimens were shown to retain 93% of the flexural strength after impact (~0.6 J) compared to non-impacted specimens, compared to 75% retained strength for non-healed specimens [52, 54].

In a series of related works, Trask and coworkers embedded discrete HGFs with fixed spacing into glass fiber and carbon fiber reinforced laminates. The HGFs were filled with either a pre-mixed or an isolated two-part epoxy system using vacuum infiltration. Samples were subjected to low energy, quasi-static impact events and subsequently tested in four-point bending. Recovery of flexural strength was achieved in both glass and carbon fiber-reinforced composites after an elevated temperature exposure [57–59]. Norris *et al.* fabricated channels in a carbon/epoxy composite using solder wire embedded prior to composite curing and subsequently melted to form the channel. The channels were then filled with a pre-mixed epoxy healing agent and impacted (10 J). CAI testing showed that, on average, 97% of the original strength was recovered [62].

15.3.3

Healing of Coatings

Healing damage external to the vascular network isolates damage to regions that are not vascularized, improving long term performance. Toohey *et al.* introduced a sample geometry in which a brittle coating was applied to a more flexible substrate containing a vascular network fabricated by direct-write of a fugitive ink (Figure 15.5c) [56, 63]. Samples subjected to four-point bending developed cracks in the coating which were subsequently healed by capillary flow of healing agents from the underlying vascular network. Toohey *et al.* demonstrated up to 60% recovery of fracture toughness for 7 consecutive cycles for a healing system consisting of DCPD monomer sequestered in the vascular network and Grubbs' cata-

lyst embedded in the coating. In a subsequent study, Toohey *et al.* demonstrated up to 16 intermittent healing cycles using a two-part, epoxy-based healing system in which the reactive components were isolated in separate vascular networks [64]. Hansen *et al.* extended this work by creating interpenetrating vascular networks [65] and showed over 30 healing cycles with an average of approximately 50% healing efficiency. In a later study, Hansen *et al.* reduced the healing time from two days to a matter of hours by heating the sample with a third vascular network used solely for thermal regulation [66].

15.3.4

Self-Sensing, Self-Healing Vascularized Composites

In addition to self-repair, materials capable of self-sensing of internal damage provide additional safeguards against structural failures. Wu *et al.* evaluated the sensing and recovery from damage in a braided glass fiber composite loaded in tension using a dispersed network of electrically conductive carbon nanotubes (CNT) [61]. Hong *et al.* used glass microtubes containing healing agent filled with carbon powder and metal microwires to sense damage and recovery using changes in electrical resistance across the network [70].

15.4

Intrinsic Healing Systems

Intrinsic healing systems utilize bonding latent (inherent) material functionality to achieve healing. Recovery is typically accessed through a thermal treatment of the damaged material. Methods to incorporate intrinsic healing include resin design (Figure 15.6a) [71, 75–79], dissolution of healing agents that either remain miscible (Figure 15.6b) [72, 80, 81] or phase separate on cure (Figure 15.6c) [73, 82], and solid phase incorporation (Figure 15.6d) [74, 83–94].

15.4.1

Resin Design for Reversibility

An early report of crack healing in pure epoxy resin is presented by Outwater and Gerry [75]. After heating to 149°C (above its T_g), full recovery of fracture energy was observed using a double torsion specimen. Miller and Gaur investigated adhesion between fiber and resin, observing a 62% recovery in interfacial shear strength in specimens which were damaged and then re-cured [76]. Recovery was shown for four re-cure cycles, and was attributed to mechanical bonding caused by flow of the softened epoxy. Rahmathullah and Palmese used compact tension (CT) specimens thermally healed at 185°C to further investigate this phenomenon, considering the effects of stoichiometric ratio and clamping pressure [71]. Two distinct mechanisms were identified. First, at stoichiometric conditions, healing was attributed to mechanical interlocking of nodular features on the fracture

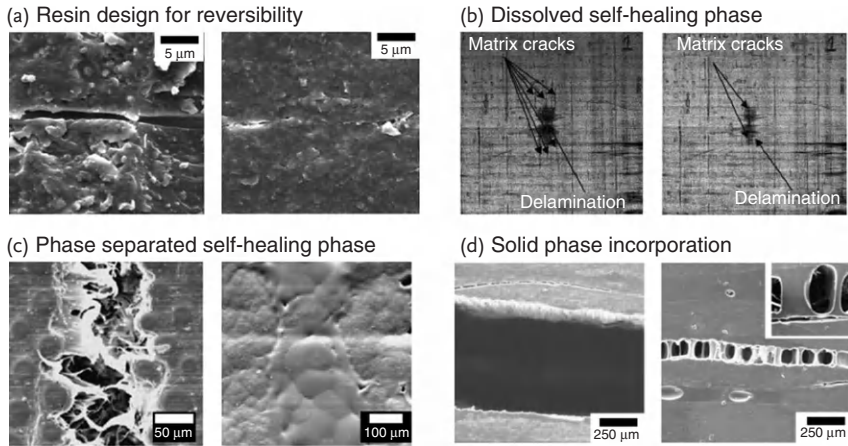


Figure 15.6 Examples of intrinsic self-healing systems before and after damage. (a) Crack interface of pure epoxy resin (Images reprinted from [71], with permission from John Wiley and Sons). (b) Healing of impact damage in epoxy/glass fiber composite panel with dissolved poly(bisphenol-A-co-epichlorohydrin) (Images reprinted from [72], with permissions Elsevier). (c) Fracture of epoxy

with phase-separated poly(ϵ -caprolactone) (Images reprinted from [73], with permission from American Chemical Society). (d) Delamination of an epoxy/carbon fiber composite with bridging of solid phase polyethylene-co-methacrylic acid when healed (Images reprinted from [74], with permission from Elsevier).

surfaces when heated above T_g , which are subsequently set when cooled. In this regime, healing efficiencies around 50% were observed. Secondly, with an excess of un-reacted epoxy groups, polymerization and covalent bonding enhanced the healing efficiency to greater than 100%.

Another approach to enhance the healing of epoxy resins is to chemically modify the resin itself. Tian *et al.* synthesized an epoxy resin which incorporates both irreversible epoxide–anhydride linkages, as well as thermally reversible Diels–Alder (DA) bonds: furfurylglycidyl ether (FGE) [77]. Healing was assessed using DCDC specimens with a thermal healing cycle of 110°C for 20 min to disconnect DA bonds, and 80°C for 72 h to reconnect bonds. The recovery of fracture toughness was greater than 95%. Peterson *et al.* investigated healing using a resin mixture consisting of FGE and diglycidyl ether of bisphenol-A (DGEBA) [78, 79]. In the first work, a bismaleimide solution was injected into the damage region [78]. Both neat and glass fiber-reinforced specimens were tested. Recovery of maximum load was an average of 70% for neat CT specimens. Although not explicitly stated, using the recovery of maximum load assumes specimens have the same crack length, due to the crack length dependence of fracture in CT specimens. Importantly, in some specimens, healing occurred at room temperature. Authors then demonstrated healing of glass fiber/polymer interfaces by functionalizing the single glass fibers using maleimide [79]. An average of 41%

recovery in interfacial shear strength was reported after accounting for frictional effects.

15.4.2

Dissolved Healing Agents

Hayes *et al.* developed a system in which a linear thermoplastic healing agent, poly(bisphenol-A-co-epichlorohydrin), was dissolved in an epoxy thermoset [72, 80, 81]. By matching the solubility parameters of the two phases, the healing agent remains fully dissolved in the matrix. The resulting domain size of healing agent is on the molecular scale. When damage occurred, samples were exposed to a thermal healing cycle between 100 and 160 °C which induced diffusion of the thermoplastic across hairline cracks, thereby healing them. Neat epoxy CT specimens containing 20 wt% healing agent showed a 64% recovery in fracture toughness when healed at 140 °C, while Charpy impact specimens containing an optimum of 7.5 wt% healing agent showed a 50% recovery of impact strength when healed at 160 °C [72, 81]. In the same work, this system was extended to glass fiber-reinforced composites, where healing was observed optically by a 30% reduction in damage area.

15.4.3

Phase Separated Healing Agents

Phase separation of a miscible blend of healing agent and resin can occur upon polymerization of the resin. Luo *et al.* demonstrated an epoxy and thermoplastic poly(ϵ -caprolactone) (PCL) interpenetrating network in which the PCL phase served as a healing agent upon exposure to 190 °C for 8 min [73]. The resulting healing agent domains are micron-scale and interconnected. Importantly, the network still remained an elastic solid above the T_g of PCL, owing to the interconnectedness of the epoxy phase, though the modulus was reduced. Recovery of peak load in single edge notched bending (SENB) specimens was greater than 100% by applying 18.7 MPa compressive stress for healing. Healing was partially attributed to the differential expansion between epoxy and PCL, which induced flow of healing agent into the damage region.

Phase separated interpenetrating networks can also be created by independent polymerization of the two phases. This offers improved processability, owing to the lower viscosity of the constituents over the resulting polymerized phases. Peterson *et al.* demonstrated such a system using a DGEBA epoxy and methacrylated phenyl glycidyl ether (MPGE) resin [82]. In this work, the authors demonstrated healing efficiency as high as 53% for the first healing cycle and 39% for the fourth cycle, with various amounts of MPGE.

15.4.4

Solid-Phase Healing Agents

Larger healing agent domain sizes can be achieved by incorporating an immiscible healing phase into the epoxy resin. Zako demonstrated this concept by incorporating

50 μm diameter epoxy particles at 40 vol% into an epoxy resin in a cross-ply glass fiber-reinforced composite [83]. To repair the damage, the specimen was heated to 120 $^{\circ}\text{C}$ for 10 min, inducing melting of the particle inclusions. Full recovery of stiffness was reported using a three-point bending specimen. In addition, fatigue testing of single edge notched tension (SENT) specimens revealed that healing resulted in nearly full recovery of rigidity, as well as an extension in fatigue life.

Preceding the work done with FGE resins, Peterson *et al.* incorporated 660 μm diameter DA cross-linked gel particles into an epoxy [84]. The reversibility of DA chemistry affords multiple healing cycles. However, an average of only 21% load recovery was observed using the CT specimen with 10 wt% healing agent. Healing was attributed solely to the healing ability of the DA healing agents, not to the inherent healing of the epoxy thermoset.

Meure *et al.* first introduced the use of thermoplastic polyethylene-co-methacrylic acid (EMAA) as a solid-phase healing agent [85]. In contrast to other thermoplastic particles, EMAA can react with the resin during the thermal healing cycle of 150 $^{\circ}\text{C}$ for 30 min. Recovery of fracture toughness was 85% using TDCB specimens. Importantly, when specimens were heated during healing, volatile gases within the healing agent expanded, forcing melted healing agent into the damage region.

A subsequent series of publications have explored the incorporation of solid-phase EMAA into carbon fiber-reinforced epoxy composites, for healing in DCB specimens. Meure *et al.* incorporated both particles and fibers, showing over 100% recovery of critical energy release rate for some specimens [88]. Varley *et al.* extended the applicability of EMAA to higher temperature cured epoxies ($T_g = 160^{\circ}\text{C}$), by applying a polyetherimide coating to a fiber mesh [89]. Recovery of peak load was up to 100%. In another study, Varley examined the applicability of a nonwoven EMAA mesh as a healing agent, achieving greater than 200% recovery in critical energy release rate [90]. Wang *et al.* used poly(ethylene-co methyl acrylate) (EMA) or EMAA films [91]. Recovery of critical energy release rates of 46 and 88% were reported for EMA and EMAA, respectively. Yang *et al.* incorporated EMAA fiber stitches perpendicular the direction of crack propagation [92]. The virgin energy release rate of specimens with EMAA stitches was 120% that of specimens without stitches, and healing efficiency was greater than 150%. Pingkerawat *et al.* compared the effect of EMAA spheres to multiple fiber mesh configurations [74]. Recovery of critical energy release rate was approximately 300% for some specimen types. The significant increase in fracture toughness after healing was attributed to the bridging of EMAA along the delamination. In a companion study, Pingkerawat *et al.* subjected the same type of specimens to fatigue loading, observing similar crack growth rates for virgin and healed specimens [93]. Hargou *et al.* applied ultrasonic welding in place of thermal healing, and were able to achieve 130% recovery in critical energy release rate while reducing the healing time from 30 min to 30 s [94].

15.5 Conclusions

Over the past decade, significant strides have been made in the field of self-healing epoxy and epoxy composites; however, there are still many areas of research that remain unexplored. In capsule-based systems the majority of prior work has focused on matrices that are cured at relatively low temperatures (ca. $<45^{\circ}\text{C}$). However, achieving successful self-healing in structural composites involves elevated temperature curing (ca. 200°C), which places significant demands on thermal and chemical stability. Additionally, capsule size is generally of the order of $100\mu\text{m}$, significantly larger than damage or defects that initiate failure, and orders of magnitude larger than the available volume in structural fiber-reinforced composites. Compounding the size scale problem the maximum damage volume that can be filled scales with capsule diameter; small capsules can only fill (and heal) small damage volume. A possible solution is to pursue healing chemistries that undergo volume expansion upon polymerization, thereby reducing the volumetric constraints on capsule size.

For vascular-based healing systems, most current research has concentrated on relatively large-scale damage caused by impact, or carefully directed damage propagation in which the vasculature can be tailored and designed for optimal performance. In general, the vascular architecture has been relatively simple, from isolated 1D or 2D channels to 3D interconnected channels of a single size scale. Healing is predominantly based on a two-part healing chemistry (e.g., epoxy) either premixed or isolated and mixed *in situ* upon damage triggering. The primary challenge for vascular-based healing systems moving forward is the manufacturing of complex vascular networks, with multi-scale, three-dimensional channel architectures for improved delivery and mixing of healing agent(s). These advances will increase performance by promoting better mixing, increasing the volumetric penetration of the network, and perhaps most importantly, providing redundancy in the network (through branched architectures) in order to prevent network failure due to blockages.

Intrinsic systems can be effective at healing small damage, in which there is intimate contact of fracture surfaces. However, to extend its applicability, mechanisms for regaining intimate contact of fracture surfaces could be incorporated, such as shape memory alloys or polymers [11, 12, 95]. Also, a mechanism to improve the transport of healing agents could be incorporated. Work by Meure suggests a passive mechanism to induce pressure gradients which transport healing agent to the damage region; however, this approach requires heat to activate [85].

No matter which self-healing approach is pursued, environmental stability and long-term performance are still unanswered and largely unexplored issues. Developing new polymer chemistries for use as healing agents, optimized for long-term storage, low viscosity, and triggerable polymerization under varying environmental conditions would be beneficial in this regard. Developing new sequestration

methods (e.g., metallic or ceramic capsules) that protect the latent (healing) chemistry is essential for the future development of the field.

References

- Hollaway, L. (1993) *Polymer Composites for Civil and Structural Engineering*, Blackie Academic and Professional, London.
- Baker, A.A., Jones, R., and Callinan, R.J. (1985) Damage tolerance of graphite epoxy composites. *Compos. Struct.*, **4**, 15–44.
- Blaiszik, B.J., Kramer, S.L.B., Olugebefola, S.C., Moore, J.S., Sottos, N.R., and White, S.R. (2010) Self-healing polymers and composites. *Annu. Rev. Mater. Res.*, **40**, 179–211.
- White, S.R., Sottos, N.R., Moore, J.S., Geubelle, P.H., Kessler, M.R., et al. (2001) Autonomic healing of polymer composites. *Nature*, **409**, 794–797.
- Caruso, M.M., Blaiszik, B.J., White, S.R., Sottos, N.R., and Moore, J.S. (2008) Full recovery of fracture toughness using a non-toxic solvent-based self-healing system. *Adv. Funct. Mater.*, **18**, 1898–1904.
- Brown, E.N., White, S.R., and Sottos, N.R. (2005) Retardation and repair of fatigue cracks in a microcapsule toughened epoxy composite – part 2: in situ self-healing. *Compos. Sci. Technol.*, **65**, 2474–2480.
- Brown, E.N., White, S.R., and Sottos, N.R. (2005) Retardation and repair of fatigue cracks in a microcapsule toughened epoxy composite – part 1: manual infiltration. *Compos. Sci. Technol.*, **65**, 2466–2473.
- Jin, H., Miller, G.M., Sottos, N.R., and White, S.R. (2011) Fracture and fatigue response of a self-healing epoxy adhesive. *Polymer*, **52**, 1628–1634.
- Mangun, C.L., Mader, A.C., Sottos, N.R., and White, S.R. (2010) Self-healing of a high temperature cured epoxy using poly(dimethylsiloxane) chemistry. *Polymer*, **51**, 4063–4068.
- Liu, X., Zhang, H., Wang, J., Wang, Z., and Wang, S. (2012) Preparation of epoxy microcapsule based self-healing coatings and their behavior. *Surf. Coat. Technol.*, **206**, 4976–4980.
- Kirkby, E.L., Michaud, V.J., Månson, J.A.E., Sottos, N.R., and White, S.R. (2009) Performance of self-healing epoxy with microencapsulated healing agent and shape memory alloy wires. *Polymer*, **50**, 5533–5538.
- Kirkby, E.L., Rule, J.D., Michaud, V.J., Sottos, N.R., White, S.R., and Månson, J.A.E. (2008) Embedded shape-memory alloy wires for improved performance of self-healing polymers. *Adv. Funct. Mater.*, **18**, 2253–2260.
- Wilson, G.O., Caruso, M.M., Schelkopf, S.R., Sottos, N.R., White, S.R., and Moore, J.S. (2011) Adhesion promotion via noncovalent interactions in self-healing polymers. *ACS Appl. Mater. Inter.*, **3**, 3072–3077.
- Brown, E.N., Sottos, N.R., and White, S.R. (2002) Fracture testing of a self-healing polymer composite. *Exp. Mech.*, **42**, 372–379.
- Rule, J.D., Brown, E.N., Sottos, N.R., White, S.R., and Moore, J.S. (2005) Wax-protected catalyst microcapsules for efficient self-healing materials. *Adv. Mater.*, **17**, 205–208.
- Patel, A.J. 2011, Autonomic Healing of Low-velocity Impact Damage in Woven Fiber-Reinforced Composites. PhD Thesis. Dissertation. University of Illinois at Urbana-Champaign.
- Jackson, A.C., Bartelet, J.A., Marczewski, K., Sottos, N.R., and Braun, P.V. (2011) Silica-protected micron and sub-micron capsules and particles for self-healing at the microscale. *Macromol. Rapid Commun.*, **32**, 82–87.
- Jones, A.S., Rule, J.D., Moore, J.S., White, S.R., and Sottos, N.R. (2006) Catalyst morphology and dissolution kinetics for self-healing polymers'. *Chem. Mater.*, **18**, 1312–1317.
- Wilson, G.O., Caruso, M.M., Reimer, N.T., White, S.R., Sottos, N.R., and

- Moore, J.S. (2008) Evaluation of ruthenium catalysts for ring-opening metathesis polymerization-based self-healing applications. *Chem. Mater.*, **20**, 3288–3297.
- 20 Guadagno, L., Longo, P., Raimondo, M., Naddeo, C., Mariconda, A., *et al.* (2011) Use of hoveyda–grubbs' second generation catalyst in self-healing epoxy mixtures. *Compos. B*, **42**, 296–301.
- 21 Kamphaus, J.M., Rule, J.D., Moore, J.S., Sottos, N.R., and White, S.R. (2008) A new self-healing epoxy with tungsten (VI) chloride catalyst. *J. R. Soc. Interface*, **5**, 95–103.
- 22 Li, H., Wang, R., and Liu, W. (2012) Preparation and self-healing performance of epoxy composites with microcapsules and tungsten (VI) chloride catalyst. *J. Reinf. Plast. Compos.*, **31**, 924–932.
- 23 Coope, T.S., Mayer, U.F.J., Wass, D.F., Trask, R.S., and Bond, I.P. (2011) Self-healing of an epoxy resin using scandium(III) triflate as a catalytic curing agent. *Adv. Funct. Mater.*, **21**, 4624–4631.
- 24 Cho, S.H., White, S.R., and Braun, P.V. (2009) Self-healing polymer coatings. *Adv. Mater.*, **21**, 645–649.
- 25 Yuan, Y.C., Rong, M.Z., Zhang, M.Q., Chen, B., Yang, G.C., and Li, X.M. (2008) Self-healing polymeric materials using epoxy/mercaptan as the healant. *Macromolecules*, **41**, 5197–5202.
- 26 Yuan, Y.C., Ye, X.J., Rong, M.Z., Zhang, M.Q., Yang, G.C., and Zhao, J.Q. (2011) Self-healing epoxy composite with heat-resistant healant. *ACS Appl. Mater. Interfaces*, **3**, 4487–4495.
- 27 Xiao, D.S., Yuan, Y.C., Rong, M.Z., and Zhang, M.Q. (2009) Self-healing epoxy based on cationic chain polymerization. *Polymer*, **50**, 2967–2975.
- 28 Xiao, D.S., Yuan, Y.C., Rong, M.Z., and Zhang, M.Q. (2008) Hollow polymeric microcapsules: preparation, characterization and application in holding boron trifluoride diethyl etherate. *Polymer*, **50**, 560–568.
- 29 Jin, H., Mangun, C.L., Stradley, D.S., Moore, J.S., Sottos, N.R., and White, S.R. (2012) Self-healing thermoset using encapsulated epoxy-amine healing chemistry. *Polymer*, **53**, 581–587.
- 30 Caruso, M.M., Delafuente, D.A., Ho, V., Sottos, N.R., Moore, J.S., and White, S.R. (2007) Solvent-promoted self-healing epoxy materials. *Macromolecules*, **4**, 8830–8832.
- 31 Sauvant-Moynot, V., Gonzalez, S., and Kittel, J. (2008) Self-healing coatings: an alternative route for anticorrosion protection. *Prog. Org. Coat.*, **63**, 307–315.
- 32 Grigoriev, D.O., Kohler, K., Skorb, E., Shchukin, D.G., and Mohwald, H. (2009) Polyelectrolyte complexes as a “smart” depot for self-healing anticorrosion coatings. *Soft Matter*, **5**, 1426–1432.
- 33 Xiao, D.S., Yuan, Y.C., Rong, M.Z., and Zhang, M.Q. (2009) A facile strategy for preparing self-healing polymer composites by incorporation of cationic catalyst-loaded vegetable fibers. *Adv. Funct. Mater.*, **19**, 2289–2296.
- 34 Neuser, S., Michaud, S., and White, S.R. (2012) Improving solvent-based self-healing materials through shape memory alloys. *Polymer*, **53**, 370–378.
- 35 Samadzadeh, M., Boura, S.H., Peikari, M., Ashrafi, A., and Kasiriha, M. (2011) Tung oil: an autonomous repairing agent for self-healing epoxy coatings. *Prog. Org. Coat.*, **70**, 383–387.
- 36 Jadhav, R.S., Hundiwale, D.G., and Mahulikar, P.P. (2010) Synthesis and characterization of phenol-formaldehyde microcapsules containing linseed oil and its use in epoxy for self-healing and anticorrosive coating. *J. Appl. Polym. Sci.*, **119**, 2911–2916.
- 37 Suryanarayana, C., Rao, K.C., and Kumar, D. (2008) Preparation and characterization of microcapsules containing linseed oil and its use in self-healing coatings. *Prog. Org. Coat.*, **63**, 72–78.
- 38 Kessler, M.R., and White, S.R. (2001) Self-activated healing of delamination damage in woven composites. *Compos. A Appl. Sci. Manuf.*, **32**, 683–699.
- 39 Kessler, M.R., Sottos, N.R., and White, S.R. (2003) Self-healing structural composite materials. *Compos. A Appl. Sci. Manuf.*, **34**, 743–753.
- 40 Yin, T., Rong, M.Z., Zhang, M.Q., and Zhao, J.Q. (2009) Durability of self-healing woven glass fabric/epoxy composites. *Smart Mater. Struct.*, **18**, 074001.

- 41 Yin, T., Zhou, L., Rong, M.Z., and Zhang, M.Q. (2008) Self-healing woven glass fabric/epoxy composites with the healant consisting of micro-encapsulated epoxy and latent curing agent. *Smart Mater. Struct.*, **17**, 015019.
- 42 Patel, A.J., Sottos, N.R., Wetzels, E.D., and White, S.R. (2010) Autonomic healing of low-velocity impact damage in fiber-reinforced composites. *Compos. A Appl. Sci. Manuf.*, **41**, 360–368.
- 43 Sanada, K., Itaya, N., and Shindo, Y. (2008) Self-healing of interfacial debonding in fiber-reinforced polymers and effect of microstructure on strength recovery. *Open Mech. Eng. J.*, **2**, 97–103.
- 44 Moll, J.L., White, S.R., and Sottos, N.R. (2010) A self-sealing fiber-reinforced composite. *J. Compos. Mater.*, **44**, 2573–2585.
- 45 Yin, T., Rong, M.Z., Wu, J., Chen, H., and Zhang, M.Q. (2008) Healing of impact damage in woven glass fabric reinforced epoxy composites. *Compos. A Appl. Sci. Manuf.*, **39**, 1479–1487.
- 46 Yuan, Y.C., Ye, Y., Rong, M.Z., Chen, H., Zhang, M.Q., *et al.* (2011) Self-healing of low-velocity impact damage in glass fabric/epoxy composites using an epoxy-mercaptop healing agent. *Smart Mater. Struct.*, **20**, 015024.
- 47 Barbero, E.J., and Ford, K.J. (2007) Characterization of self-healing fiber-reinforced polymer-matrix composite with distributed damage. *J. Adv. Mater.*, **39**, 20–27.
- 48 Sanada, K., Yasuda, I., and Shindo, Y. (2006) Transverse tensile strength of unidirectional fibre-reinforced polymers and self-healing of interfacial debonding. *Plast. Rubber Compos.*, **35**, 67–72.
- 49 Blaiszik, B.J., Baginska, M., White, S.R., and Sottos, N.R. (2010) Autonomic recovery of fiber/matrix interfacial bond strength in a model composite. *Adv. Funct. Mater.*, **20**, 3547–3554.
- 50 Dry, C. (1996) Procedures developed for self-repair of polymer matrix composite materials. *Compos. Struct.*, **35**, 263–269.
- 51 Motuku, M., Vaidya, U.K., and Janowski, G.M. (1999) Parametric studies on self-repairing approaches for resin infused composites subjected to low velocity impact. *Smart Mater. Struct.*, **8**, 623–638.
- 52 Pang, J.W.C., and Bond, I.P. (2005) “Bleeding composites” – damage detection and self-repair using a biomimetic approach. *Compos. A Appl. Sci. Manuf.*, **36**, 183–188.
- 53 Bleay, S.M., Loader, C.B., Hawyes, V.J., Humberstone, L., and Curtis, P.T. (2001) A smart repair system for polymer matrix composites. *Compos. A Appl. Sci. Manuf.*, **32**, 1767–1776.
- 54 Pang, J.W.C., and Bond, I.P. (2005) A hollow fibre reinforced polymer composite encompassing self-healing and enhanced damage visibility. *Compos. Sci. Technol.*, **65**, 1791–1799.
- 55 Hamilton, A.R., Sottos, N.R., and White, S.R. (2010) Self-healing of internal damage in synthetic vascular materials. *Adv. Mater.*, **22**, 5159–5163.
- 56 Toohey, K.S., Sottos, N.R., Lewis, J.A., Moore, J.S., and White, S.R. (2007) Self-healing materials with microvascular networks. *Nat. Mater.*, **6**, 581–585.
- 57 Trask, R.S., and Bond, I.P. (2006) Biomimetic self-healing of advanced composite structures using hollow glass fibres. *Smart Mater. Struct.*, **15**, 704–710.
- 58 Trask, R.S., Williams, G.J., and Bond, I.P. (2007) Bioinspired self-healing of advanced composite structures using hollow glass fibres. *J. R. Soc. Interface*, **4**, 363–371.
- 59 Williams, G., Trask, R., and Bond, I. (2007) A self-healing carbon fibre reinforced polymer for aerospace applications. *Compos. A Appl. Sci. Manuf.*, **38**, 1525–1532.
- 60 Hamilton, A.R., Sottos, N.R., and White, S.R. (2012) Pressurized vascular systems for self-healing materials. *J. R. Soc. Interface*, **9**, 1020–1028.
- 61 Wu, A.S., Coppola, A.M., Sinnott, M.J., Chou, T.-W., Thostenson, E.T., *et al.* (2012) Sensing of damage and healing in three-dimensional braided composites with vascular channels. *Compos. Sci. Technol.*, **72**, 1618–1626.
- 62 Norris, C.J., Meadway, G.J., O’Sullivan, M.J., Bond, I.P., and Trask, R.S. (2011) Self-healing fibre reinforced composites via a bioinspired vasculature. *Adv. Funct. Mater.*, **21**, 3624–3633.

- 63 Toohey, K.S., Sottos, N.R., and White, S.R. (2009) Characterization of microvascular-based self-healing coatings. *Exp. Mech.*, **49**, 707–717.
- 64 Toohey, K.S., Hansen, C.J., Lewis, J.A., White, S.R., and Sottos, N.R. (2009) Delivery of two-part self-healing chemistry via microvascular networks. *Adv. Funct. Mater.*, **19**, 1399–1405.
- 65 Hansen, C.J., Wu, W., Toohey, K.S., Sottos, N.R., White, S.R., and Lewis, J.A. (2009) Self-healing materials with interpenetrating microvascular networks. *Adv. Mater.*, **21**, 4143–4147.
- 66 Hansen, C.J., White, S.R., Sottos, N.R., and Lewis, J.A. (2011) Accelerated self-healing via ternary interpenetrating microvascular networks. *Adv. Funct. Mater.*, **21**, 4320–4326.
- 67 Esser-Kahn, A.P., Thakre, P.R., Dong, H.F., Patrick, J.F., Vlasko-Vlasov, V.K., et al. (2011) Three-dimensional microvascular fiber-reinforced composites. *Adv. Mater.*, **23**, 3654–3658.
- 68 Huang, J.H., Kim, J., Agrawal, N., Sudarson, A.P., Maxim, J.E., et al. (2009) Rapid fabrication of bio-inspired 3D microfluidic vascular networks. *Adv. Mater.*, **21**, 3567–3571.
- 69 Bellan, L.M., Singh, S.P., Henderson, P.W., Porri, T.J., Craighead, H.G., and Spector, J.A. (2009) Fabrication of an artificial 3-dimensional vascular network using sacrificial sugar structures. *Soft Matter*, **5**, 1354–1357.
- 70 Hong, Y., and Su, M. (2012) Multifunctional self-healing and self-reporting polymer composite with integrated conductive microwire networks. *ACS Appl. Mater. Interfaces*, **4**, 3759–3764.
- 71 Rahmathullah, M.A.M., and Palmese, G.R. (2009) Crack-healing behavior of epoxy-amine thermosets. *J. Appl. Polym. Sci.*, **113**, 2191–2201.
- 72 Hayes, S.A., Jones, F.R., Marshiya, K., and Zhang, W. (2007) A self-healing thermosetting composite material. *Compos. A Appl. Sci. Manuf.*, **38**, 1116–1120.
- 73 Luo, X.F., Ou, R.Q., Eberly, D.E., Singhal, A., Viratyporn, W., and Mather, P.T. (2009) A thermoplastic/thermoset blend exhibiting thermal mending and reversible adhesion. *ACS Appl. Mater. Interfaces*, **1**, 612–620.
- 74 Pingkarawat, K., Wang, C.H., Varley, R.J., and Mouritz, A.P. (2012) Self-healing of delamination cracks in mendable epoxy matrix laminates using poly[ethylene-co-(methacrylic acid)] thermoplastic. *Compos. A Appl. Sci. Manuf.*, **43**, 1301–1307.
- 75 Outwater, J.O., and Gerry, D.J. (1969) On the fracture energy, rehealing velocity and refracture energy of cast epoxy resin. *J. Adhes.*, **1**, 290–298.
- 76 Miller, B., and Gaur, U. (1989) Regeneration of adhesive bonding in fiber resin systems. *J. Adhes.*, **29**, 103–110.
- 77 Tian, Q.A., Rong, M.Z., Zhang, M.Q., and Yuan, Y.C. (2010) Synthesis and characterization of epoxy with improved thermal remendability based on Diels-Alder reaction. *Polym. Int.*, **59**, 1339–1345.
- 78 Peterson, A.M., Jensen, R.E., and Palmese, G.R. (2010) Room-temperature healing of a thermosetting polymer using the Diels-Alder reaction. *ACS Appl. Mater. Interfaces*, **2**, 1141–1149.
- 79 Peterson, A.M., Jensen, R.E., and Palmese, G.R. (2011) Thermoreversible and remendable glass-polymer interface for fiber-reinforced composites. *Compos. Sci. Technol.*, **71**, 586–592.
- 80 Jones, F.R., Zhang, W., and Hayes, S.A. (2007) Thermally induced self healing of thermosetting resins and matrices in smart composites. in *Self Healing Materials*, ed. S. van der Zwaag, Springer Series in Materials Science, vol. 100, pp. 69–93.
- 81 Hayes, S.A., Zhang, W., Branthwaite, M., and Jones, F.R. (2007) Self-healing of damage in fibre-reinforced polymer-matrix composites. *J. R. Soc. Interface*, **4**, 381–387.
- 82 Peterson, A.M., Kotthapalli, H., Rahmathullah, M.A.M., and Palmese, G.R. (2012) Investigation of interpenetrating polymer networks for self-healing applications. *Compos. Sci. Technol.*, **72**, 330–336.
- 83 Zako, M., and Takano, N. (1999) Intelligent material systems using epoxy particles to repair microcracks and

- delamination damage in GFRP. *J. Intel. Mater. Syst. Struct.*, **10**, 836–841.
- 84 Peterson, A.M., Jensen, R.E., and Palmese, G.R. (2009) Reversibly cross-linked polymer gels as healing agents for epoxy-amine thermosets. *ACS Appl. Mater. Interfaces*, **1**, 992–995.
- 85 Meure, S., Wu, D.Y., and Furman, S. (2009) Polyethylene-co-methacrylic acid healing agents for mendable epoxy resins. *Acta Mater.*, **57**, 4312–4320.
- 86 Meure, S., Varley, R.J., Wu, D.Y., Mayo, S., Nairn, K., and Furman, S. (2012) Confirmation of the healing mechanism in a mendable EMAA-epoxy resin. *Eur. Polym. J.*, **48**, 524–531.
- 87 Meure, S., Wu, D.Y., and Furman, S.A. (2010) FTIR study of bonding between a thermoplastic healing agent and a mendable epoxy resin. *Vib. Spectrosc.*, **52**, 10–15.
- 88 Meure, S., Furman, S., and Khor, S. (2010) Poly[ethylene-co-(methacrylic acid)] healing agents for mendable carbon fiber laminates. *Macromol. Mater. Eng.*, **295**, 420–424.
- 89 Varley, R.J., and Charve, F. (2012) EMAA as a healing agent for mendable high temperature epoxy amine thermosets. *Compos. A Appl. Sci. Manuf.*, **43**, 1073–1080.
- 90 Varley, R.J., and Parn, G.P. (2012) Thermally activated healing in a mendable resin using a non woven EMAA fabric. *Compos. Sci. Technol.*, **72**, 453–460.
- 91 Wang, C.H., Sidhu, K., Yang, T., Zhang, J., and Shanks, R. (2012) Interlayer self-healing and toughening of carbon fibre/epoxy composites using copolymer films. *Compos. A Appl. Sci. Manuf.*, **43**, 512–518.
- 92 Yang, T., Wang, C.H., Zhang, J., He, S., and Mouritz, A.P. (2012) Toughening and self-healing of epoxy matrix laminates using mendable polymer stitching. *Compos. Sci. Technol.*, **72**, 1396–1401.
- 93 Pingkarawat, K., Wang, C.H., Varley, R.J., and Mouritz, A.P. (2012) Self-healing of delamination fatigue cracks in carbon fibre-epoxy laminate using mendable thermoplastic. *J. Mater. Sci.*, **47**, 4449–4456.
- 94 Hargou, K., Pingkarawat, K., Mouritz, A.P., and Wang, C.H. (2012) Ultrasonic activation of mendable polymer for self-healing carbon-epoxy laminates. *J. Mater. Sci.*, **47**, 4449–4456.
- 95 Rodriguez, E.D., Luo, X.F., and Mather, P.T. (2011) Linear/network poly(epsilon-caprolactone) blends exhibiting shape memory assisted self-healing (SMASH). *ACS Appl. Mater. Inter.*, **3**, 152–161.

16

Self-Healing Coatings

Dmitry G. Shchukin, Dimitriya Borisova, and Helmuth Möhwald

16.1

Introduction into Self-Healing Coatings

Self-healing activity of materials generally gives information about the gap between the reference and actual level of a system parameter, and translates this information into action to alter the gap in some way [1]. Feedback is often a part of naturally occurring or constructed systems. In a feedback system cause-and-effect relations between system variables form a closed-loop wherein the output affects the input [2]. In this way, a feedback system can respond to its environment (like local pH-changes during corrosion processes). The input can also be an external signal applied to the system (like light or mechanical force) and represents the desired or reference value of a variable to be controlled. The output is the feedback action such as, for a self-healing material restoring its functionality or the functionality of the coating (in the case of self-healing coatings).

Blood clotting is an example of a useful positive feedback system in our body [3]. Upon rupture of a blood vessel wall, activated blood platelets release chemicals to attract even more platelets and form a sticky clot at the damaged site. The process continues until the hole in the blood vessel is sealed and the bleeding stopped. In fact, every useful feedback cycle is part of a response to the negative impact to the material.

Mimicking the concept of feedback-active systems in the field of synthetic coatings opens up a number of opportunities for the development of “smart” coatings with stimuli-responsive behavior. Self-healing coatings undergo a change in response to a stimulus (trigger) in order to enhance the system performance. These coatings are of great scientific and technological importance, as they can be applied in various fields, such as medicine, biotechnology, or material science. Their main, passive function as coatings is to protect the underlying substrate from contact with the environment. In addition to their barrier properties, they also possess active properties due to their environmentally responsive function.

Self-healing materials can be classified into three groups according to the general healing mechanism: vascular, intrinsic and capsule-based [4]. Each approach differs by the mechanism used to provide the healing and the triggering

mechanism. The type of group influences the damage volume that can be healed, the repeatability of healing, and the recovery rate of the self-healing material. Vascular self-healing materials contain the healing agent in a tubular network, which can be one-, two-, or three-dimensional. After the vasculature is damaged and the first delivery of healing agent occurs, the network may be refilled by an external source or from an undamaged but connected region of the vasculature. This refilling action allows multiple local healing events. Intrinsic self-healing materials do not have any healing agent but possess a latent self-healing functionality, due to their structure or chemical properties, that is triggered by an external stimulus (e.g., melting). The healing mechanism relies on chain mobility and entanglement, reversible polymerization, melting of thermoplastic phases, hydrogen bonding, or ionic interactions. The capsule-based approach involves the encapsulation of the healing agent into micro- and nanocapsules followed by their incorporation into the material matrix. This approach will be described in more details in the next sections.

16.2

Concept of Micro- and Nanocontainer-Based Self-Healing Coatings

A successful approach to impart feedback functionality to a coating is by the incorporation of encapsulated active material in the coating matrix (Figure 16.1) [5–7]. The great versatility of encapsulation technologies, active agents, and coating matrixes offers a large number of coating design strategies. Self-healing coatings can be generally classified according to the external stimulus to which they

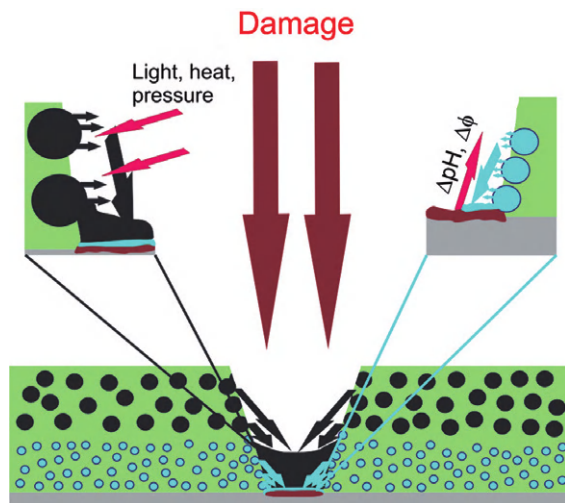


Figure 16.1 Schematic representation of nanocapsule-based self-healing coatings. Reprinted with permission from Ref [5]. Copyright 2007, The Royal Society of Chemistry.

respond. Various external stimuli of physical or chemical nature can cause a change in the coating followed by the self-recovery of an initial coating property.

Mechanical impact is an important external stimulus, which affects coating barrier properties in a negative way by causing microcracks or other microdamage in the coating. Adopting mechanical stress as a trigger to recover the mechanical stability by autonomic crack healing was demonstrated for the first time for microcapsule-based systems in 2001 by the group of S. R. White [8]. They encapsulated healing agent (a monomer) in polymer microcapsules embedded in an epoxy matrix containing a catalyst. Upon crack formation the embedded microcapsules are ruptured and the healing agent is released in the crack due to capillary forces, and comes into contact with the embedded catalyst. The resulting polymerization of the healing agent leads to crack healing and recovery of the barrier properties of the coating.

Since this breakthrough in autonomic self-healing polymer materials, most of the efforts in designing active coatings have been concentrated on encapsulation of active materials within polymer microcapsules [9–11] or microvascular networks [12, 13] that rupture upon mechanical impact. Simultaneous incorporation of two types of capsules containing different active agents [14], or micrometer-size capsules filled with reactive epoxy resin or oil [15, 16] were also reported to lead to successful crack healing. Encapsulation of highly air-sensitive and moisture-reactive materials, such as metal oxide precursors [17], organosiloxanes [18] or linseed oil [19], in polymer microcapsules is an interesting approach to the design of self-healing coatings, which respond to combined external stimuli, for example, mechanical and chemical stimuli. In such coatings, the active material is first released due to crack propagation and forms an impermeable layer only after oxidation or hydrolysis by atmospheric oxygen or humidity. Sometimes preserving the initial liquid state of the released active material can be advantageous. In self-lubricating coatings friction causes simultaneously fatigue and self-repair of the coating due to lubricant release triggered by crack propagation [20].

The encapsulation of a corrosion inhibitor in polymer capsules that can be mechanically opened was also recently reported [21]. This was realized using emulsion polymerization to synthesize polyurea microcapsules containing the liquid corrosion inhibitor 2-methylbenzothiazole. These microcapsules were dispersed in water-borne organic primer to obtain anticorrosive coatings with enhanced active corrosion resistance on aluminum substrate.

Successful self-healing in response to mechanical stress depends on the properties of the embedded microcapsules and active agent. The microcapsule size should be large enough (50–200 μm) to enable easy rupture and sufficient amount of active agent. However, the integration of big microcapsules into thin coatings is limited. Microcapsule shells should be rigid to preserve the capsule integrity during embedding in the coating matrix, and brittle to facilitate capsule rupture upon crack formation. The active agent should be of low viscosity. Ideally, the active agents should be of low cost and environmental footprint in order to make their application in industrial coatings possible.

Electromagnetic irradiation (e.g., UV light) belongs to the physical stimuli which affect coating durability the most. Various kinds of polymeric microcapsules with light responsive properties are known and suitable for application in self-healing coatings [22]. Direct incorporation of photocatalytic TiO₂ particles in polymer coatings is difficult because it would lead to oxidation of the organic components of the coating matrix. However, recent developments reported the successful encapsulation and application of TiO₂ particles and Ag nanoparticles sensitive to the IR light as a triggering component of microcapsules in nanocontainer-based self-healing coatings. The possibility of release of corrosion inhibitor and fluorescent dye from the titania-based polyelectrolyte containers under UV-irradiation was shown [23]. A polyelectrolyte shell, which modifies the outer surface of TiO₂-based containers, prevents the spontaneous leakage of the loaded material. Moreover, nanocontainers with a titania core reveal UV-stimulated release of benzotriazole (corrosion inhibitor) under UV-irradiation at least twice faster than with pH-stimulated release of the corrosion inhibitor from the same container interior. Thus, it should be noted that, for the coatings where very fast and regulated release of the inhibitor at a damaged corrosive area is necessary, the use of UV-irradiation as an external trigger is strongly preferable. A similar effect was found for nanocontainers coated with a polyelectrolyte shell containing IR-sensitive Ag nanoparticles [24]. One could terminate the corrosion process, in this case, by very intensive healing after an appearance of corrosion centers, using local IR laser irradiation. The healing ability under laser irradiation was shown by the scanning vibration electrode technique. Laser-mediated remote release of incorporated corrosion inhibitor (benzotriazole), from nanoengineered mesoporous containers with silver nanoparticles in the container shell, is observed in real time on single and multi-container levels. It was also noted that, by applying a polyelectrolyte shell with noble metal particles over the mesoporous titania via layer-by-layer assembly, it is possible to fabricate micro- and nanoscaled reservoirs sensitive to both UV and IR irradiation.

External stimuli or changes in the local environment of a coating can also be of a chemical nature (e.g., electrochemical potential, pH, ionic strength, or humidity). Self-healing coatings containing hydrogels or microcapsules with a layer-by-layer assembled polyelectrolyte shell are especially responsive to chemical stimuli. Changes in pH, ionic strength, electrochemical potential, or dielectric permeability of the solvent can trigger swelling/shrinkage of the capsules or permeability change of the capsule shells [25–27]. This property enables the release of encapsulated active material in response to external chemical stimuli, and the subsequent recovery of a coating function. For example, a self-healing coating based on polyelectrolyte microcapsules incorporated in a conducting polymer film was reported to demonstrate electrochemically reversible permeability in response to electrochemical potential change [28].

Utilizing pH shift as stimulus for corrosion inhibitor release is the natural and the most promising way to design anticorrosive coatings with sufficient corrosion resistance. That is because the corrosion process leads to local pH decrease in anodic areas and local pH increase in cathodic ones. Therefore, in order to sense

and eliminate the negative impact of corrosion, the pH response needs to be imparted to the functionalities of anticorrosive coatings.

An attractive approach to achieve this is by integrating pH-sensitive inhibitor capsules in the coating. One way to form such capsules is by the layer-by-layer (LbL) assembly of oppositely charged species (e.g., polyelectrolytes) on templating colloidal nanoparticles. The template can be either removed to form a hollow structure, or kept to provide better mechanical stability [29–31]. The advantages of this method are the variety of the charged species suitable for shell construction, the adjustable layer thickness, and flexibility. The most useful feature of LbL polyelectrolyte systems is their sensitivity to pH change, which causes switching of the capsule shell between “closed” and “open” states. Thus, local changes in pH near anodic and cathodic areas can cause the opening of the capsule shell and release of the encapsulated inhibitor. For example, silica nanocontainers with a 1H-benzotriazole (BTA) loaded LbL shell were dispersed in sol–gel coatings and demonstrated good corrosion resistance [32, 33]. However, such nanocontainers cannot prevent spontaneous leakage of the inhibitor from inside the LbL shell to the surrounding environment. This undesired inhibitor loss is very unfavorable because LbL nanocontainers with a dense silica core have already low inhibitor loading capacity.

A promising approach to increase the amount of inhibitor in LbL nanocontainers is to incorporate the inhibitor in a porous core protected by a LbL shell. This was demonstrated by inserting organic inhibitors into porous metal oxide nanoparticles (TiO_2 and SiO_2) and then coating them with polyelectrolyte multilayers. These pH-sensitive nanocontainers were dispersed in $\text{SiO}_x/\text{ZrO}_x$ sol–gel coatings and improved the coating’s corrosion inhibition properties [34]. However, the complexity of such nanocontainers restricts their up-scaling and industrial application.

In contrast, the industrially mined, viable and inexpensive halloysite nanotubes have high potential as inhibitor nanocontainers. Halloysites are two-layered aluminosilicates with hollow tubular structure. Their size varies from 1 to 15 μm in length and 10–150 nm in lumen inner diameter. Halloysite nanotubes were loaded with the inhibitor, 2-mercaptobenzothiazole, and covered by a LbL polyelectrolyte shell to improve the control over the inhibitor release [35–37]. Sol–gel coatings doped with halloysites demonstrated very good corrosion inhibition in long-term corrosion tests. These results are due to the favorable halloysite structure, which provides good inhibitor storage in the lumen and limits spontaneous inhibitor leakage due to the small-diameter (20–50 nm) ends covered by the polyelectrolyte shell. Another promising approach to keep the inhibitor inside the lumen and release it in response to a pH change is by designing pH-sensitive stoppers at the halloysite ends. Successful formation of stoppers for halloysites was demonstrated by exposing halloysites loaded with 1H-benzotriazole to a Cu(II)-containing solution to form insoluble metal–benzotriazole complexes at the halloysite ends [38]. The release time was tuned by controlling the thickness of the stopper complexes. The prolonged inhibitor release time improved the long-term corrosion resistance of sol–gel coatings.

Sufficiently active corrosion inhibition was also achieved by simpler design strategies. For example, BTA or 8-HQ-loaded halloysites without a protective shell or stoppers successfully imparted self-healing properties to sol-gel coatings [39]. The direct introduction of inhibitor-loaded TiO_2 and SiO_2 nanoparticles without protective polyelectrolyte shell in organic coatings was reported to prevent spontaneous inhibitor leakage and to increase the corrosion inhibition efficiency [40, 41]. However, the biggest drawback of the approaches described above is the low amount of inhibitor content (~5 wt%) which limits the long-term anticorrosion performance.

This disadvantage could be overcome for nanoparticle-stabilized polymer nanocontainers based on Pickering emulsions [42]. The container uptake for liquid inhibitor was 45 wt% and for solid inhibitor 20 wt%. Here, the container loading efficiency is limited by the inhibitor solubility in the emulsion oil phase forming the container core and cannot be increased by further loading cycles.

An attractive alternative to the inhibitor containers described above is mesoporous inorganic materials. For example, mesoporous silica particles with large pore volume (~1 mLg⁻¹) and surface area (~1000 m²g⁻¹), were used as nanocontainers for organic inhibitors, and demonstrated two times greater inhibitor uptake than previously reported [43–45]. The incorporation of such a high amount of inhibitor entrapped in mesoporous nanocontainers into sol-gel coatings improved significantly the coating corrosion resistance. This improvement was reported to be due to the enhanced passive and active functionalities of the anticorrosive coatings. On the one hand, the coating barrier properties were improved by reinforcement of the coating matrix due to introduction of mechanically stable, robust silica nanoparticles. This is particularly important for silica-based microcapsules while the incorporation of polymer-based microcapsules usually makes the material more brittle. On the other hand, the large amount of encapsulated inhibitor and its controlled, local release on demand upon corrosion attack provided superior active corrosion inhibition. Embedding mesoporous silica nanoparticles reinforces the coating matrix, not only due to the particle robustness but also to their monodispersity, which limits particle agglomeration and favors homogeneous distribution in the coating.

16.3

Types of Nanocontainers

Perspective nanocontainers can be divided into two families regarding their mechanical properties and compatibility to the passive matrix of the coating: (i) organic core-shell nanocontainers for organic-based coatings (pigments, finishes), and (ii) inorganic or composite nanocontainers for mostly water-based coatings.

Several approaches have been developed so far to fabricate loaded micro- and nanocontainers with an organic shell. One approach is based on the self-assembly of lipid molecules or amphiphilic block copolymers into spherically closed bilayer structures (vesicles) [46]. A second approach is to use dendrimers or hyperbranched

polymers as nanocontainers [47]. A third method comprises LbL assembly of oppositely charged species using polyelectrolytes, conductive polymers, biopolymers, and nanoparticles as constituents of the nanocontainer shell (see above) [48]. A fourth approach involves the use of ultrasonic waves to fabricate organic and composite hollow nanospheres [49].

Interfacial polymerization is conventionally used for encapsulation in polymeric shells [21, 50]. The reaction of polymerization happens on the boundary between two immiscible (usually) liquid phases. One reactive monomer is dissolved in one phase, another reactive monomer in another. When monomers meet on the interface, the polymerization reaction takes place. The whole process is divided into two steps. In the first step an emulsion is formed. The first reactive monomer is dissolved in the dispersed phase, while the continuous phase usually contains emulsion stabilizer. In the second step the second reactive monomer is added to the continuous phase, leading to the polymeric shell formation on the surface of the emulsion droplets. The liquid content of the dispersed phase becomes entrapped inside the polymer after the polymerization reaction is finished. Different kinds of emulsions can be used for interfacial polymerization. The most common way is to use conventional oil-in-water emulsions, while inverse water-in-oil and oil-in-oil emulsions have also been used. Both linear and crosslinked polymers can be used as a shell material. In practice, the choice of linear or crosslinked polymer is usually determined by the beneficial properties of the resulting polymer: mechanical strength, elasticity, chemical inertness, permeability, and so on. The processes leading to the formation of capsules are considered by experimentalists to be principally the same for both types of polymers.

Several classes of polymers – polyurethane, polyurea, methacrylates, melamine formaldehyde and polyamide were chosen as the shell for polymer microcontainers [21]. The choice of polymers was determined by practical interest: their outstanding mechanical properties and chemical resistivity were of high interest for the further application as carriers for corrosion inhibitors.

The morphology of the different types of polymer capsules was analyzed on the basis of SEM images (Figure 16.2). Different capsule shapes were observed, depending on the polymer–solvent combination: spherical, elongated, spheroidal with concavities and/or folds, and collapsed.

The appearance of small concavities is attributed to collision of capsules in the first steps of the polymerization reaction when the capsule walls are still soft. Folding, and even collapse, of capsules can happen due to the high vacuum used in SEM leading to the evaporation of the solvent, or partial extraction of the capsule liquid content during the washing procedure. Another reason for irregular shape formation can be compression or shrinkage of the polymer due to crosslinking. Capsules are considered as “collapsed” when there is no or a very small amount of liquid material left inside the capsule.

The strategy of a preparation of inorganic nanocontainers based on a mesoporous oxide core was presented in several papers [24, 43, 51]. The fabrication of a polyelectrolyte shell around the container can be achieved by LbL assembly of oppositely charged species and allows one to prevent the spontaneous release of

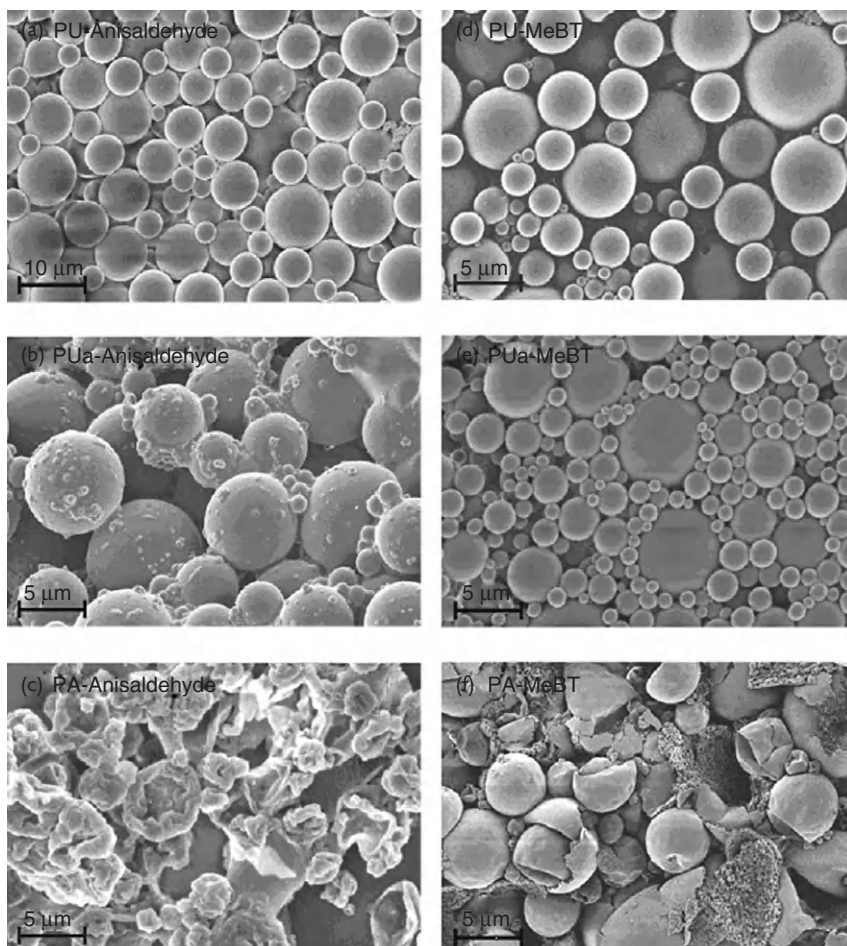


Figure 16.2 SEM images of capsules made of polyurethane (a,d), polyurea(b,e) and polyamide (c,f) with anisaldehyde (a–c) and 2-methyl benzothiazole (d–e) encapsulated. Reprinted after modification from Ref [21]. Copyright 2012, The Royal Society of Chemistry.

loaded corrosion inhibitor. The precision of one adsorbed layer thickness is about 2 nm, hence polyelectrolyte nanocontainers completely repeat the shape of the templating colloids. The SEM and TEM images (Figure 16.3) reveal a well-developed pore structure with a diameter of 70 to 90 nm. In all particles, the pores are open, not ordered and oriented from the center to the outer surface, building a complex, worm-like pore system.

A loading capacity of 409 mg(benzotriazole)/1 g(SiO₂) was found. Assuming that only the pores are filled with the benzotriazole molecules with a molar volume 87.6 mL mol⁻¹, the maximum theoretical loading capacity is 1.53 g(benzotriazole)/1 g(SiO₂). The achieved experimental loading is around one third of the maximum and could be further optimized.

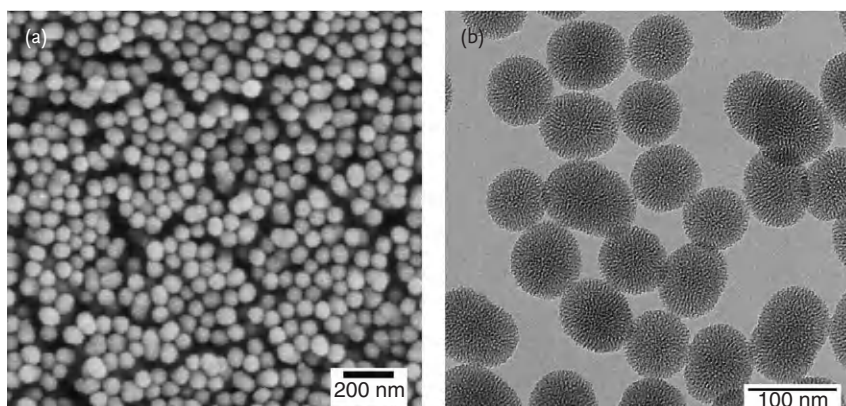


Figure 16.3 (a) SEM and (b) TEM micrographs of mesoporous silica nanoparticles. Reprinted with permission from Ref [43]. Copyright 2011, The American Chemical Society.

Tailored mesoporous silica nanoparticles are quickly becoming the delivery agent of choice for various applications in non-aqueous media [52]. Therefore, mesoporous silica nanoparticles were synthesized and functionalized with octyl groups on their outer surfaces for better dispersibility in the oil-based coating matrix [51]. These NPs were filled with benzotriazole. In order to assess their ability to disperse in media of intermediate polarity, dynamic light scattering data were obtained for kinetically stable solutions of the particles in several different solvents (ethanol, butyl glycol, 1,2-propylene carbonate: see Figure 16.4).

An average intensity-weighted hydrodynamic diameter of ~ 200 nm was obtained in all three solvent–nanoparticle mixtures, with a similar distribution. The nanoparticles were observed to remain well-dispersed for more than 1 month. The addition of a non-polar solvent (xylene) to one with intermediate polarity (butyl glycol [BG]) results in slightly more extensive flocculation, as shown by the shift in average diameter to approximately 350 nm, although the system remains generally stable.

16.4

Characterization of Nanocontainer-Based Self-Healing Coatings

As demonstrated in the previous sections, the nanocontainers can be divided into two main groups: core–shell containers with an organic shell and porous nanocontainers with an inorganic scaffold. Both groups of nanocontainers demonstrate effective self-healing properties while being incorporated into the coating matrix. However, their performance depends greatly on their compatibility with the components of the coating formulation, and the ability to prevent self-aggregation during addition of the nanocontainers into the coating.

Relatively recent research has dealt with the development of new inhibitor compounds, designed according to the principles of green chemistry [53]. This research

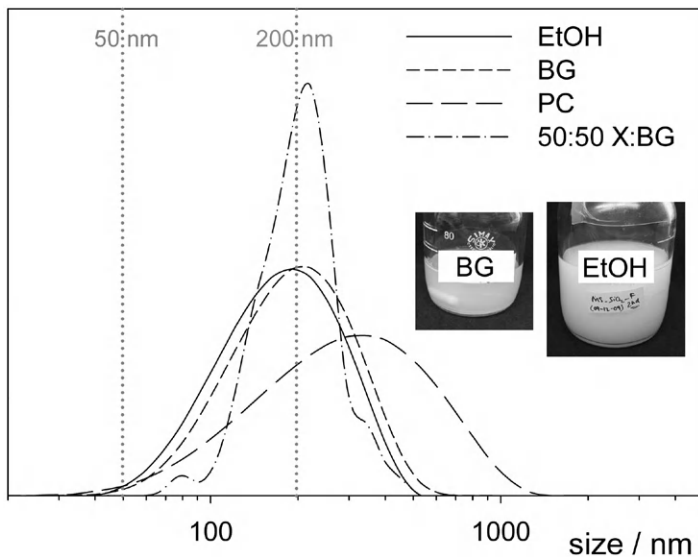


Figure 16.4 DLS profiles, and (inset) visual appearance of the NPs in different solvents of intermediate polarity. Key: EtOH = ethanol, BG = butyl glycol, PC = 1,2 propylene carbonate, X = xylene. Adapted with permission from Ref [51]. Copyright 2011, Wiley-VCH.

was focused on the use of rare-earth metal compounds as an alternative to chromates. Cerium salts were shown to provide protection for magnesium and aluminum alloys against corrosion [54–58]. Ho and coworkers tested cerium dibutyl phosphate ($\text{Ce}(\text{DBuPh})_3$) as a hybrid inhibitor with mixed inhibition functions and a low critical inhibitor concentration for protection of aluminum alloys [59].

Another Ce-organic inhibitor, Ce diethylhexyl phosphate, was encapsulated into polyamide containers from an organic phase consisting of 200 mg cerium DEtHePh, 200 mg TPhCl and 1 mL of DBuPh and polyamide core [54]. The corrosion behavior of the Ce diethylhexyl phosphate-loaded polyamide containers incorporated into an epoxy-based coating was estimated by the salt-spray chamber test (Figure 16.5). The performance of the coating directly doped with the cerium salt cannot be classified as acceptable. Multiple pitting covering almost 50% of the sample area can be seen. These results show that direct doping of the coating with the cerium salt causes serious destruction of the coating integrity and total deterioration of the coating's barrier properties. The performance of the coating modified with the Ce diethylhexyl phosphate loaded polyamide containers is better, which shows that encapsulation can sufficiently improve the final coating properties. The colloidal stability of the fabricated Ce diethylhexyl phosphate-loaded polyamide containers, however, has to be further improved, since the samples covered with capsule-modified coating reveal a substantial amount of pits.

Gel particles of micron size (microgel) were suggested as a new type of material that could be used as an “active” part of a self-healing coating system. Application of microgels is very advantageous, since they combine the attractive properties of

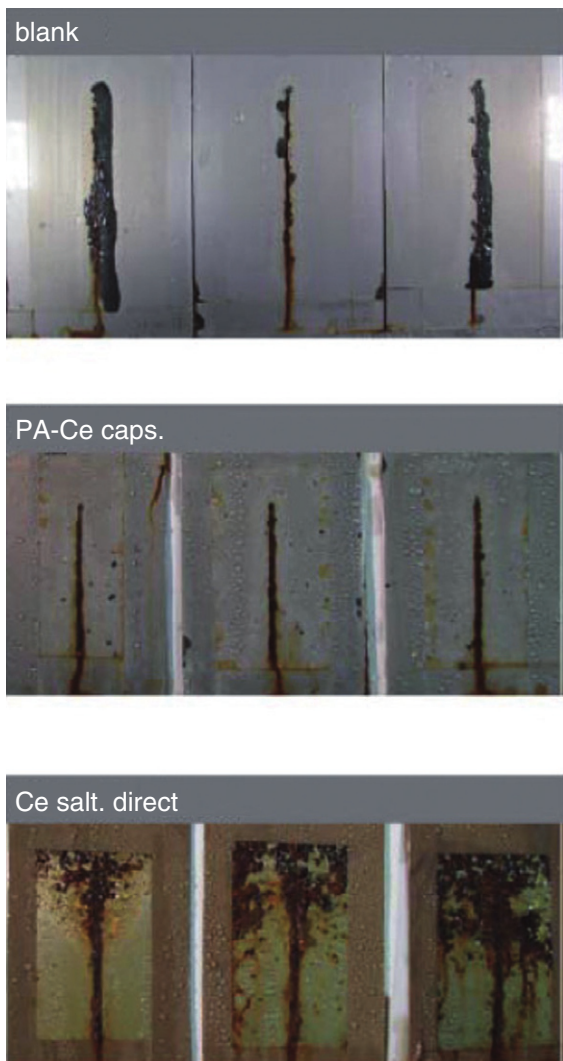


Figure 16.5 The result of a 300h long salt-spray chamber test for steel plates covered with unmodified epoxy-based coating (blank), epoxy-based coating modified with 5 wt% of cerium diethylhexyl phosphate-

loaded polyamide capsules and epoxy-based coating directly doped with 3 wt% of cerium salt. The 3 images for nominally identical conditions indicate the experimental variance.

both solid and liquid. The solid state of the particles provided by the cross-linked polymer network ensures good mechanical stability of the resulting coating system. The liquid corrosion inhibitor, being entrapped in the solid matrix, retains its mobility, providing the coating system with the self-healing capabilities [60, 61]. An attempt to consider the mentioned factors was made in Ref [21]. Polymer gel particles of micron size, containing 70wt% of the liquid corrosion inhibitor 2-methylbenzothiazole (MeBT), homogeneously distributed in the polymer matrix, are used as the “active” part of the self-healing system. The polymeric part of the gel is responsible for the mechanical properties of the particles, while MeBT, being entrapped in the solid matrix, retains its mobility, providing the coating system with the self-healing capabilities. Due to the high affinity of MeBT to the polymer matrix of the carriers, and the low solubility of MeBT in water, this type of carrier can be used in combination with any water-borne coating system. Carriers with mean diameter of $5\mu\text{m}$ were introduced into the conventional two-component water-borne epoxy primer of $30\mu\text{m}$ thickness.

The resulting microgel particles containing MeBT were introduced into the coating in the form of paste to give 5 wt% of particles. The anticorrosion performance of the modified and unmodified coatings was compared by means of SVET (scanning vibrating electrode technique). SVET measurements (Figure 16.6) allow detection of very small local electric currents in the damaged area. Appearance of

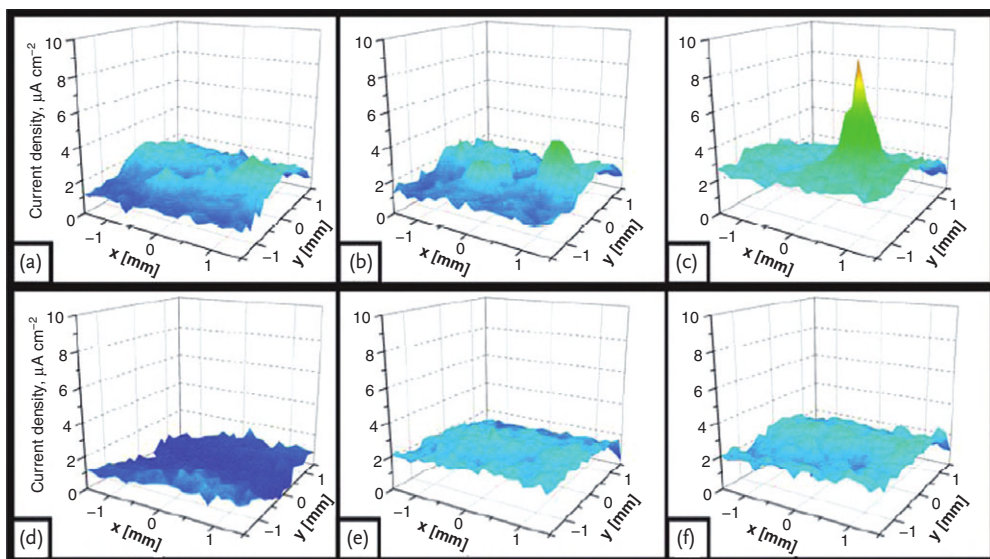


Figure 16.6 Graphical representation of the current density distribution above scratched aluminum substrates covered with (a–c) unmodified model coating and (d–f) model coating modified with 5 wt% of microgel particles containing MeBT. (a, d) correspond

to 0, (b, e) to 6, and (c, f) to 12 h of immersion in 0.1 M NaCl solution. The current density was measured $300\mu\text{m}$ above the sample surface. Reprinted with permission from Ref [21]. Copyright 2012, The Royal Society of Chemistry.

the electric current close to the surface of the metal substrate is attributed to the appearance of corrosion. The development of the corrosion process with time can be visualized by measuring the current density distribution in the area of the damaged coating. For the unmodified coating, the increase in the maximum of the current density during 12 h after immersion in the salt solution is evidence of the corrosion process development. At the same time, the modified sample shows no signs of the corrosion process. The latter means that continuous release of MeBT from the carriers, damaged by the razor blade, provides sufficient concentration of MeBT in the vicinity of the metal substrate (even considering wet conditions in the SVET experiment, i.e., partial diffusion of the inhibitor to the bulk solution).

One of the examples of the successive application of the nanocontainers based on the mesoporous inorganic scaffold is the use of mesoporous silica loaded with different inhibitors. This was realized by dispersing mesoporous silica nanocontainers loaded with the non-toxic corrosion inhibitor 2-mercaptobenzothiazole (MBT) in a hybrid sol-gel ($\text{SiO}_x/\text{ZrO}_x$) layer [44]. The concentration of embedded nanocontainers was varied from 0.04 to 1.7 wt% in order to find the optimum conditions for best anti-corrosion efficiency. The active corrosion inhibition was evaluated during a simulated corrosion process by SVET in 0.1 M NaCl. The following concentrations of MBT@SiO₂ dispersed homogeneously everywhere in the final cured coatings were studied: 0.04, 0.1, 0.2, 0.5, 0.7, 0.8, and 1.7 wt%

The coating samples were scratched in a controlled way in order to accelerate the corrosion process and assess their active anti-corrosive properties. In the SVET 3D maps this process is expressed as a single positive peak with a constant position over the course of measurement, indicating one defined pitting site being the anode (Figure 16.7).

In contrast, the cathodic current was not that well pronounced and no localized cathode was formed (not shown). The cathodic reaction generates hydroxyls, which increase the local pH. These conditions are favorable for the dissolution of the inhibitor molecules adsorbed at the NCs dispersed in the passive sol-gel coating. Thus, at the onset of corrosion the inhibitor molecules are released and diffuse to the metal surface to form a protective layer, preventing the direct contact of chloride anions with aluminum and its oxidation to Al³⁺. Therefore, an increase in the anodic current density with time can be assessed as a failure of the coating sample to inhibit corrosion evolution. In contrast, suppression of anodic activity below that of the control sample containing no active property (bare sol-gel film with 0 wt% MBT@SiO₂) is defined as self-healing. Thus, coatings with these characteristics are evaluated as successful, active corrosion-preventing coating systems.

The maximum anodic currents detected as a function of time are represented in Figure 16.8. A distinct corrosion propagation expressed by the high values of current density ($>5 \mu\text{A cm}^{-2}$) can be seen for samples with too high (0.8–1.7 wt%) and too low (0.04–0.2 wt%) MBT@SiO₂ concentration. These samples reach current densities above that of the passive control system, suggesting an unsatisfactory active corrosion protection due to an insufficient inhibitor quantity in the coating systems with low MBT@SiO₂ concentrations. In the case of too high

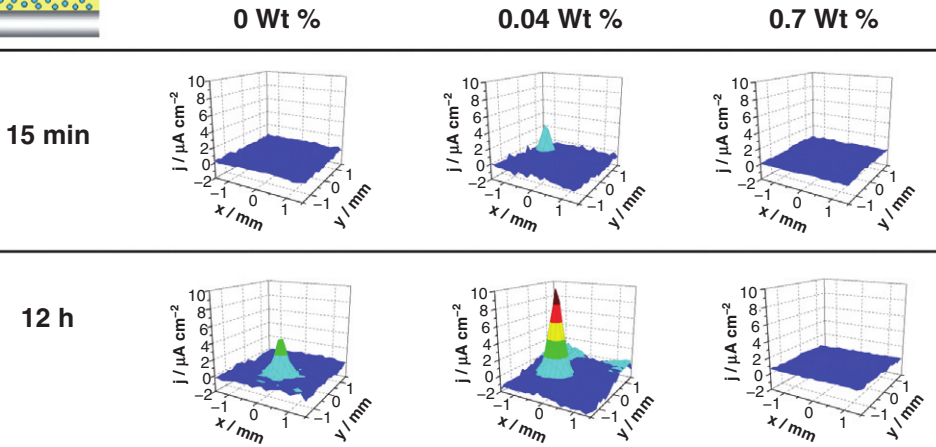
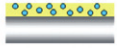


Figure 16.7 SVET 3D current density maps of aluminum (AA2024-T3) substrates coated with a sol-gel film containing different MBT@SiO₂ concentrations (0, 0.04 and 0.7 wt%). Shown systems are examples for detected high (0.04 wt%) and low (0.7 wt%)

anodic current densities in comparison to the control coating without MBT@SiO₂ after 15 min and 12 h immersion in 0.1 M NaCl. Reprinted with permission from Ref [44]. Copyright 2012, The American Chemical Society.

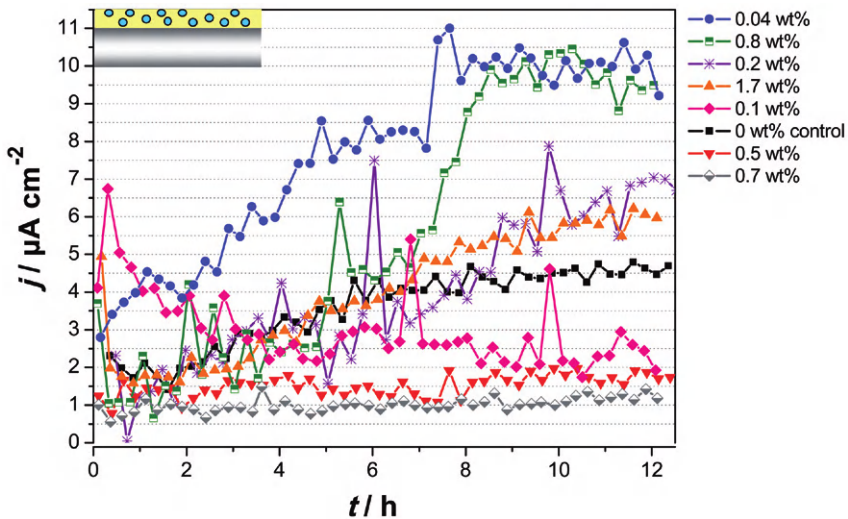


Figure 16.8 Maximum anodic current densities detected with SVET over the scanned scratched area during 12 h immersion in 0.1 M NaCl. Results for coating

samples containing different MBT@SiO₂ concentrations are shown. Reprinted with permission from Ref [44]. Copyright 2012, The American Chemical Society.

MBT@SiO₂ concentrations the poor anti-corrosive properties of the coatings could be explained by deterioration of the passive layer due to microdefects introduced by the embedded nanocontainers. Thus, according to the SVET study, a concentration window in which the corrosion process was inhibited successfully was defined to be between 0.5 and 0.7 wt% MBT@SiO₂ incorporated in a single sol-gel layer in direct contact with the metal surface.

The SVET results are also supported by the SEM micrographs depicting the scratched area after completing the SVET test. The high anodic activity detected by SVET for the control sample originates from an extensive corrosion attack. This is revealed by the formation and accumulation of large amounts of corrosion products covering the scratch in the sol-gel coating. In addition, a degradation of the integrity of the coating surrounding the scratch can be observed. This is probably due to the diffusion of the aggressive electrolyte species from the coating to the metal substrate, accounting for a bad coating-metal adhesion. In contrast, the coating exhibiting best active corrosion protection (0.7 wt% MBT@SiO₂) preserves its integrity and inhibits corrosion sufficiently.

Summarizing, the high amount of non-toxic inhibitor (20 wt%) stored by the nanocontainers was released upon corrosion attack to provide active corrosion inhibition on demand. The incorporation of MBT@SiO₂ is not always favorable for the coating anti-corrosion performance. Embedding of MBT@SiO₂ at very low concentrations (0.04 wt%) leads to good coating barrier properties but no satisfactory active corrosion resistance, due to insufficient amount of available inhibitor. In comparison, too high MBT@SiO₂ concentrations (0.8 wt%–1.7 wt%) deteriorate the coating integrity by introducing diffusion paths for the aggressive electrolyte species, which results in loss of anti-corrosion efficiency.

16.5 Conclusions and Current Trends

There is an innumerable amount of publications on responsive systems demonstrated during the last two decades describing the development of active feedback systems where the response couples back to the external or internal stimulus. There are many examples in nature and in the materials world where these systems are needed to maintain a desired function, and in the presented short review we have concentrated on one classical function of self-healing coatings – corrosion protection. This topic is of high importance since it is a modern trend to save raw material, and in most cases the corrosion processes are well understood for standard metal substrates.

We showed in our review a number of promising approaches in the specific case of anticorrosion coatings, but one has to be aware that there are also other parameters that finally decide if self-healing coatings can be marketed. There are first of all technical issues if, for example, mechanical properties, adhesion, optical appearance are not affected by a coating, and there are criteria like low cost and environmental friendliness that have to be considered. Therefore, even this rather

conventional case requires a multidisciplinary and multitechnological approach in order to achieve a specific application. On the other hand, the progress in the last years has become so fast and encouraging that one can be confident to find solutions for many different types of self-healing coatings and uses.

Additional knowledge is required in the future on the level of understanding the interplay of structural hierarchies in self-healing coatings. This is also a challenge demanding more sophisticated preparative and analytical methods covering different length scales. This typically results in studies of biomimetic systems, which is just at the beginning.

From another point of view, much of what has been learnt with repairing one functionality can be transferred to others, and we mentioned initially friction and antifungi. However, one does not need much fantasy to enlarge the catalog of possibilities in materials science and biosciences for feedback-active (most of all self-healing) coatings. Therefore, one can expect a drastic expansion of the field, including also medical applications. Many of the ideas will remain fantasy once it comes to practical applications, but we expect that even a small fraction of demonstrated approaches will make this a prospering field in future.

References

- Ramaprasad, A. (1983) On the definition of feedback. *Behav. Sci.*, **28** (1), 4–13.
- DiStefano, J.J., Stubberud, A.R., and Williams, I.J. (1995) *Schaum's Outline of Theory and Problems of Feedback and Control Systems: Continuous (Analog) and Discrete (Digital)*, McGraw-Hill, New York. [etc.].
- Pelis, K. (1997) Blood clots: the nineteenth-century debate over the substance and means of transfusion in Britain. *Ann. Sci.*, **54** (4), 331–360.
- Blaiszik, B.J., Kramer, S.L.B., Olugebefola, S.C., Moore, J.S., Sottos, N.R., and White, S.R. (2010) Self-healing polymers and composites. *Annu. Rev. Mater. Res.*, **40**, 179–211.
- Shchukin, D.G., and Möhwald, H. (2007) Self-repairing coatings containing active nanoreservoirs. *Small*, **3** (6), 926–943.
- Shchukin, D.G., Grigoriev, D.O., and Möhwald, H. (2010) Application of smart organic nanocontainers in feedback active coatings. *Soft Matter*, **6** (4), 720–725.
- Shchukin, D.G., and Möhwald, H. (2011) Smart nanocontainers as depot media for feedback active coatings. *Chem. Commun.*, **47** (31), 8730–8739.
- White, S.R., Sottos, N.R., Geubelle, P.H., Moore, J.S., Kessler, M.R., Sriram, S.R., Brown, E.N., and Viswanathan, S. (2001) Autonomic healing of polymer composites. *Nature*, **409** (6822), 794–797.
- Feng, W., Patel, S.H., Young, M.Y., Zunino, J.L., and Xanthos, M. (2007) Smart polymeric coatings – recent advances. *Adv. Polym. Technol.*, **26** (1), 1–13.
- Kessler, M.R., Sottos, N.R., and White, S.R. (2003) Self-healing structural composite materials. *Compos. A Appl. Sci. Manuf.*, **34** (8), 743–753.
- Brown, E.N., White, S.R., and Sottos, N.R. (2004) Microcapsule induced toughening in a self-healing polymer composite. *J. Mater. Sci.*, **39** (5), 1703–1710.
- Sanada, K., Yasuda, I., and Shindo, Y. (2006) Transverse tensile strength of unidirectional fibre-reinforced polymers and self-healing of interfacial debonding. *Plast. Rubber Compos.*, **35** (2), 67–72.
- Therriault, D., White, S.R., and Lewis, J.A. (2003) Chaotic mixing in three-dimensional microvascular networks fabricated by direct-write assembly. *Nat. Mater.*, **2** (4), 265–271.

- 14 Keller, M.W., White, S.R., and Sottos, N.R. (2007) A self-healing poly(dimethyl siloxane) elastomer. *Adv. Funct. Mater.*, **17** (14), 2399–2404.
- 15 Caruso, M.M., Blaiszik, B.J., White, S.R., Sottos, N.R., and Moore, J.S. (2008) Full recovery of fracture toughness using a nontoxic solvent-based self-healing system. *Adv. Funct. Mater.*, **18** (13), 1898–1904.
- 16 He, X., and Shi, X. (2009) Self-repairing coating for corrosion protection of aluminum alloys. *Prog. Org. Coat.*, **65** (1), 37–43.
- 17 Liu Harvey, A., Gnade Bruce, E., and Balkus Kenneth, J. (2010) Preparation of a delivery system for smart coatings by electrostatic deposition, in *Smart Coatings III* (eds J. Baghdachi and T. Provder), American Chemical Society, pp. 31–44.
- 18 Latnikova, A., Grigoriev, D.O., Hartmann, J., Möhwald, H., and Shchukin, D.G. (2011) Polyfunctional active coatings with damage-triggered water-repelling effect. *Soft Matter*, **7** (2), 369–372.
- 19 Suryanarayana, C., Rao, K.C., and Kumar, D. (2008) Preparation and characterization of microcapsules containing linseed oil and its use in self-healing coatings. *Prog. Org. Coat.*, **63** (1), 72–78.
- 20 Alexandridou, S., Kiparissides, C., Fransær, J., and Celis, J.P. (1995) On the synthesis of oil-containing microcapsules and their electrolytic codeposition. *Surf. Coat. Technol.*, **71** (3), 267–276.
- 21 Latnikova, A., Grigoriev, D.O., Schenderlein, M., Möhwald, H., and Shchukin, D.G. (2012) A New approach towards “active” self-healing coatings: exploitation of microgels. *Soft Matter*, **8**, 10837–10844.
- 22 Bédard, M.F., De Geest, B.G., Skirtach, A.G., Möhwald, H., and Sukhorukov, G.B. (2010) Polymeric microcapsules with light responsive properties for encapsulation and release. *Colloid Interface Sci.*, **158** (1–2), 2–14.
- 23 Skorb, E.V., Sviridov, D.V., Möhwald, H., and Shchukin, D.G. (2009) Light responsive protective coatings. *Chem. Commun.*, **40**, 6041–6043.
- 24 Skorb, E.V., Skirtach, A.G., Sviridov, D.V., Shchukin, D.G., and Möhwald, H. (2009) Laser-controllable coatings for corrosion protection. *ACS Nano*, **3** (7), 1753–1760.
- 25 Shchukin, D.G., and Sukhorukov, G.B. (2004) Nanoparticle synthesis in engineered organic nanoscale reactors. *Adv. Mater.*, **16** (8), 671–682.
- 26 Mehta, S., Kaur, G., and Bhasin, K. (2008) Incorporation of antitubercular drug isoniazid in pharmaceutically accepted microemulsion: effect on microstructure and physical parameters. *Pharm. Res.*, **25** (1), 227–236.
- 27 Köhler, K., Shchukin, D.G., Möhwald, H., and Sukhorukov, G.B. (2005) Thermal behavior of polyelectrolyte multilayer microcapsules. 1. The effect of odd and even layer number. *J. Phys. Chem. B*, **109** (39), 18250–18259.
- 28 Shchukin, D.G., Köhler, K., and Möhwald, H. (2006) Microcontainers with electrochemically reversible permeability. *J. Am. Chem. Soc.*, **128** (14), 4560–4561.
- 29 Sukhorukov, G.B., Rogach, A.L., Zebli, B., Liedl, T., Skirtach, A.G., Kohler, K., Antipov, A.A., Gaponik, N., Susha, A.S., Winterhalter, M., and Parak, W.J. (2005) Nanoengineered polymer capsules: tools for detection, controlled delivery, and site-specific manipulation. *Small*, **1** (2), 194–200.
- 30 Neu, B., Voigt, A., Mitlohner, R., Leporatti, S., Gao, C.Y., Donath, E., Kiesewetter, H., Möhwald, H., Meiselman, H.J., and Baumber, H. (2001) Biological cells as templates for hollow microcapsules. *J. Microencapsul.*, **18** (3), 385–395.
- 31 Shchukin, D.G., Sukhorukov, G.B., and Möhwald, H. (2003) Smart inorganic/organic nanocomposite hollow microcapsules. *Angew. Chem. Int. Ed. Engl.*, **42** (37), 4472–4475.
- 32 Zheludkevich, M.L., Shchukin, D.G., Yasakau, K.A., Möhwald, H., and Ferreira, M.G.S. (2007) Anticorrosion coatings with self-healing effect based on nanocontainers impregnated with corrosion inhibitor. *Chem. Mater.*, **19** (3), 402–411.
- 33 Shchukin, D.G., Zheludkevich, M., Yasakau, K., Lamaka, S., Ferreira, M.G.S., and Möhwald, H. (2006) Layer-by-layer

- assembled nanocontainers for self-healing corrosion protection. *Adv. Mater.*, **18** (13), 1672–1678.
- 34 Skorb, E.V., Fix, D., Andreeva, D.V., Möhwald, H., and Shchukin, D.G. (2009) Surface-modified mesoporous SiO₂ containers for corrosion protection. *Adv. Funct. Mater.*, **19** (15), 2373–2379.
- 35 Lvov, Y.M., Shchukin, D.G., Möhwald, H., and Price, R.R. (2008) Halloysite clay nanotubes for controlled release of protective agents. *ACS Nano*, **2** (5), 814–820.
- 36 Shchukin, D.G., and Möhwald, H. (2007) Surface-engineered nanocontainers for entrapment of corrosion inhibitors. *Adv. Funct. Mater.*, **17** (9), 1451–1458.
- 37 Shchukin, D.G., Lamaka, S.V., Yasakau, K.A., Zheludkevich, M.L., Ferreira, M.G.S., and Möhwald, H. (2008) Active anticorrosion coatings with halloysite nanocontainers. *J. Phy. Chem. C*, **112** (4), 958–964.
- 38 Abdullayev, E., Price, R., Shchukin, D., and Lvov, Y. (2009) Halloysite tubes as nanocontainers for anticorrosion coating with benzotriazole. *ACS Appl. Mater. Interfaces*, **1** (7), 1437–1443.
- 39 Fix, D., Andreeva, D.V., Lvov, Y.M., Shchukin, D.G., and Möhwald, H. (2009) Application of inhibitor-loaded halloysite nanotubes in active anti-corrosive coatings. *Adv. Funct. Mater.*, **19** (11), 1720–1727.
- 40 Balaskas, A.C., Kartsonakis, I.A., Tziveleka, L.A., and Kordas, G.C. (2012) Improvement of anti-corrosive properties of epoxy-coated AA 2024-T3 with TiO₂ nanocontainers loaded with 8-hydroxyquinoline. *Prog. Org. Coat.*, **74** (3), 418–426.
- 41 Maia, F., Tedim, J., Lisenkov, A.D., Salak, A.N., Zheludkevich, M.L., and Ferreira, M.G.S. (2012) Silica nanocontainers for active corrosion protection. *Nanoscale*, **4** (4), 1287–1298.
- 42 Haase, M.F., Grigoriev, D.O., Möhwald, H., and Shchukin, D.G. (2012) Development of nanoparticle stabilized polymer nanocontainers with high content of the encapsulated active agent and their application in water-borne anticorrosive coatings. *Adv. Mater.*, **24** (18), 2429–2435.
- 43 Borisova, D., Möhwald, H., and Shchukin, D.G. (2011) Mesoporous silica nanoparticles for active corrosion protection. *ACS Nano*, **5** (3), 1939–1946.
- 44 Borisova, D., Möhwald, H., and Shchukin, D.G. (2012) Influence of embedded nanocontainers on the efficiency of active anticorrosive coatings for aluminum alloys part I: influence of nanocontainer concentration. *ACS Appl. Mater. Interfaces*, **4** (6), 2931–2939.
- 45 Hollamby, M.J., Borisova, D., Möhwald, H., and Shchukin, D. (2012) Porous “Ouzo-effect” silica-ceria composite colloids and their application to aluminium corrosion protection. *Chem. Commun.*, **48** (1), 115–117.
- 46 Förster, S., and Plantenberg, T. (2002) From self-organizing polymers to nanohybrid and biomaterials. *Angew. Chem. Int. Ed. Engl.*, **41** (5), 689–714.
- 47 Manna, A., Imae, T., Aoi, K., Okada, M., and Yogo, T. (2001) Synthesis of dendrimer-passivated noble metal nanoparticles in a polar medium: comparison of size between silver and gold particles. *Chem. Mater.*, **13** (5), 1674–1681.
- 48 Schneider, G., and Decher, G. (2004) From functional core/shell nanoparticles prepared via layer-by-layer deposition to empty nanospheres. *Nano Lett.*, **4** (10), 1833–1839.
- 49 Shchukin, D.G., and Möhwald, H. (2006) Sonochemical nanosynthesis at the engineered interface of a cavitation microbubble. *Phys. Chem. Chem. Phys.*, **8** (30), 3496–3506.
- 50 Latnikova, A., Grigoriev, D.O., Hartmann, J., Möhwald, H., and Shchukin, D.G. (2011) Polyfunctional active coatings with damage-triggered water-repelling effect. *Soft Matter*, **7** (2), 369–372.
- 51 Hollamby, M.J., Fix, D., Dönch, I., Borisova, D., Möhwald, H., and Shchukin, D. (2011) Hybrid polyester coating incorporating functionalized mesoporous carriers for the holistic protection of steel surfaces. *Adv. Mater.*, **23** (11), 1361–1365.
- 52 Jie, L., Liong, M., Zink, J.I., and Tamanoi, F. (2007) Mesoporous silica nanoparticles as a delivery system for

- hydrophobic anticancer drugs. *Small*, **3** (8), 1341–1346.
- 53 Bethencourt, M., Botana, F.J., Calvino, J.J., Marcos, M., and Rodríguez-Chacón, M.A. (1998) Lanthanide compounds as environmentally-friendly corrosion inhibitors of aluminium alloys: a review. *Corros. Sci.*, **40** (11), 1803–1819.
- 54 Arenas, M.A., Bethencourt, M., Botana, F.J., de Damborenea, J., and Marcos, M. (2001) Inhibition of 5083 aluminium alloy and galvanised steel by lanthanide salts. *Corros. Sci.*, **43** (1), 157–170.
- 55 Dabala, M., Armelao, L., Buchberger, A., and Calliari, I. (2001) Cerium-based conversion layers on aluminum alloys. *Appl. Surf. Sci.*, **172** (3–4), 312–322.
- 56 Brunelli, K., Dabala, M., Calliari, I., and Magrini, M. (2005) Effect of HCl pre-treatment on corrosion resistance of cerium-based conversion coatings on magnesium and magnesium alloys. *Corros. Sci.*, **47** (4), 989–1000.
- 57 Fahrenholtz, W.G., O’Keefe, M.J., Zhou, H.F., and Grant, J.T. (2002) Characterization of cerium-based conversion coatings for corrosion protection of aluminum alloys. *Surf. Coat. Technol.*, **155** (2–3), 208–213.
- 58 Rudd, A.L., Breslin, C.B., and Mansfeld, F. (2000) The corrosion protection afforded by rare earth conversion coatings applied to magnesium. *Corros. Sci.*, **42** (2), 275–288.
- 59 Ho, D., Brack, N., Scully, J., Markley, T., Forsyth, M., and Hinton, B. (2006) Cerium dibutylphosphate as a corrosion inhibitor for AA2024-T3 aluminum alloys. *J. Electrochem. Soc.*, **153** (9), B392–B401.
- 60 Liu, X.X., Zhang, H.R., Wang, J.X., Wang, Z., and Wang, S.C. (2012) Preparation of epoxy microcapsule based self-healing coatings and their behavior. *Surf. Coat. Technol.*, **206** (23), 4976–4980.
- 61 Cho, S.H., White, S.R., and Brown, P.V. (2009) Self-healing polymer coatings. *Adv. Mater.*, **21** (6), 645–649.

17

Application of Self-Healing Materials in Aerospace Engineering

Liberata Guadagno, Marialuigia Raimondo, Carlo Naddeo, and Pasquale Longo

17.1

General Considerations

One of the biggest challenge facing materials scientists is the idea to put in action self-healing composites in aeronautic or in general aerospace applications. Epoxy resins are fast gaining ground as the preferred polymer to be used as carbon fiber-reinforced materials to manufacture large components able to sustain aerodynamic loads. The introduction of these resins to the aeronautic industry was mainly driven by performance gains (better design flexibility, no corrosion, easy production process, etc.) and most of all by weight reduction. This last aspect is of relevance when considering issues related to the energy resources and supply, costs in service and air pollution measures. This major advantage of the composites, the lightness, is also obtained by saving and/or increasing the material strength in such a way as to make traveling on aeroplanes more comfortable for the crew and passengers in virtue of the possibility to slightly increase cabin pressures without increasing the structure weight.

Unfortunately, composites also possess some properties which reduce their advantage with respect to traditional metal alloys. One inherent shortcoming is the poor impact damage resistance. Impact damage can be due to several factors, such as unfavorable weather conditions, stones or rocks on the keel during landing, incidental contact during maintenance, and bird strike. It may significantly affect the integrity of the composite structure of aircraft in service [1]. This process starts at the microscopic level with the formation of microvoids which then expand to generate deep microcracks within the structure [2].

Impact damage may lead to substantial matrix microcracking and delamination within the bulk of the composite, reducing the structural capability and leading to premature failure, if it is not detected and repaired. Damage can also provide a route for the ingress of contaminants into the structure [1]. The internal damage is difficult to detect and even more difficult to repair and, once it has developed, the integrity of the structure is greatly compromised. Restoration of the physico-mechanical properties of such a material, once fractured, requires either new covalent chemistry to generate additional crosslinks, or long periods of annealing

to enable thermal diffusion of unbroken, linear polymer chains into the damage-zone [3]. Several non-destructive damage detection techniques have been developed, including ultrasonics, infrared thermography, X-ray tomography, and computerized vibro-thermography. This technology can help with damage detection, but generally the repair entails strong increases in the aircraft operating costs and, in addition, sometimes the damage is not visible from outside. Furthermore, in a composite, the weave is characterized by different directions in different parts, so repairing structural parts is very difficult. Many times the current technology related to the repair methods, such as welding or patching, can be applied at the macroscopic level to either rejoin or reinforce damaged areas. However, these solutions are not always useful, either as a result of inaccessibility to the damaged area, or because they lead to changes in the strength of the material, producing inter-phase surfaces that can act as weak regions of lower mechanical performance. It has been shown, in fact, that the location of the weld remains the weakest point in the material, and thus the site for future damage to occur.

An aircraft with inherent self-healing and or protective abilities could help to significantly extend the inspection intervals, thereby increasing aircraft availability. Alternatively, existing inspection intervals could be maintained with significantly thinner structures, thereby saving airframe weight and hence reducing fuel burn, in-service cost, and the environmental impact. Recent studies have highlighted the potential of self-healing polymer composites to be used as single structural materials, and/or for sandwich structures. The main difficulty in the development of these smart materials is due to the nature of the composite used as structural materials. In fact, the self-repair activity has to be highly efficient in a relatively rigid structure (with reduced mobility of the molecular segments). In addition, most of the functionalities responsible for triggering self-repair actions have to be active after the drastic conditions of curing cycles used in the field of aeronautic materials. In fact, the high temperatures required in the curing process deactivate many of the already available self-repairing reactions.

Currently, according to the ways of healing, polymer composites can be classified into two categories: (i) intrinsic ones that are able to heal cracks by the polymers themselves, and (ii) extrinsic in which a healing agent has to be pre-embedded. A recent paper provides a compendium of many papers existing in the literature related to the self-healing materials [4]. In particular, it shows a very useful table to quickly classify the category of materials to be repaired, and related healing mechanisms.

The intrinsic self-healing composites possess a latent self-healing functionality based on specific performance of the polymers and polymeric matrices that enables crack healing under certain stimulation (mostly heating) [4]; the predominant molecular mechanisms involved in the healing processes can be due to physical interactions, and/or chemical interactions (for instance thermally reversible reactions, hydrogen bonding, ionic coupling, a dispersed meltable thermoplastic phase, molecular diffusion, etc.). A detailed description of these mechanisms is given in a recent review [5].

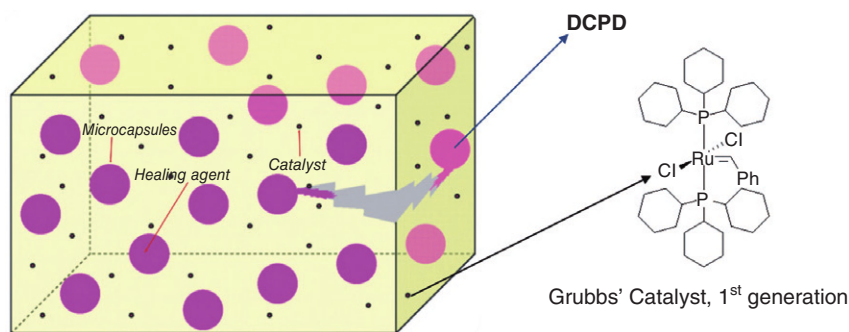
In the case of extrinsic self-healing composites, the polymeric matrix does not possess autorepair ability. A healing agent has to be stored in vessels and embedded into the polymeric matrix in advance during the manufacture of the material. As the cracks destroy the fragile vessels in which the healing agent is stored, this would be released into the crack planes, due to capillary forces, and heal the cracks. In accordance with the types of containers these materials can be classified into different groups, among which are: self-healing in terms of healant-loaded pipelines [4], self-healing in terms of healant-loaded microcapsules [4, 6], and self-healing in terms of vascular materials in which the healing agent is sequestered in a network in the form of capillaries or hollow channels [5].

For structural applications such as aeronautic materials, the extrinsic self-healing systems are of great interest because they would overcome the difficulties connected with damage diagnosis, and allow the following appropriate interventions to be reduced.

The first capsule-based self-healing system for thermosetting materials was proposed by the team from the University of Illinois [6]. The concept was based on the introduction of a microencapsulated healing agent and a suspended catalyst phase in an epoxy matrix. Since that time, advances have been made in the field following this conceptual approach and, although alternative concepts have emerged in the scientific literature, for many systems a similar healing mechanism based on the ring-opening metathesis polymerization (ROMP) of the healing agent was proposed [5, 7–19].

Among the systems relying on capsule-based concepts, the initial self-healing epoxy system involves the incorporation of a microencapsulated healing agent, dicyclopentadiene (DCPD) and a dispersed solid catalyst, bis(tricyclohexylphosphine) benzylidene ruthenium (IV) dichloride (called Grubbs' catalyst) in an epoxy-amine network [6] (see Scheme 17.1)

In these systems, an approaching crack ruptures embedded microcapsules, releasing the healing agent into the crack plane through capillary action. The reaction that allows repair of a mechanically induced damage is based on the polymerization of the healing agent that is triggered by contact with the embedded



Scheme 17.1 Design of the first self-healing system relying on capsule-based concepts.

catalyst, bonding the crack faces within the polymeric matrix. The efficiency of the self-repair function, in terms of trigger, speed and yield, is related to ROMP of the healing agent by appropriate catalysts. The healing agent is a microencapsulated liquid monomer that must have a long shelf life, prompt deliverability, high reactivity, and low volume shrinkage upon polymerization [7]. The monomer most often used as the healing agent for the manufacture of these first ingenious systems is DCPD [5, 7]. Very recently, however, blends of DCPD/5-ethylidene-2-norbornene (DCPD/ENB) or DCPD/5-norbornene-2-carboxylic acid have also been proposed [20]. Thermosetting auto-repair polymers, which have been proposed so far, include Grubbs' first-generation catalyst (G1) [5, 21–24]; and currently, the possibility of applying other ruthenium catalysts, such as second-generation Grubbs' catalyst (G2) and Hoveyda–Grubbs' second generation catalyst (HG2), is under evaluation [25–27]. This system is a challenge for epoxy structural composites: however, some drawbacks are under re-evaluation in order to be fully applied to advanced applications. These are mainly in regard to the thermal stability of the ruthenium catalysts inside the epoxy resin during the curing cycle [25, 27], and the impossibility of utilizing primary amines as hardeners, since they can poison the catalyst. At the high temperatures of the curing cycles scheduled for epoxy formulations, thermolytic decomposition can limit the usefulness of these ruthenium systems in self-healing composites based on epoxy resins. This is a crucial aspect for self-healing systems in aeronautic applications because, even if linked to the cost reduction from a process aspect, resins have been developed with low temperature manufacturing (under 100 °C), yet the problem of the material treatment at high temperature is currently under investigation.

Generally, for the mechanical targets fixed for the materials used in the aeronautic field, a glass transition temperature after wet aging of 110 °C minimum is required, and a curing temperature equal to or less than 100 °C is not enough. To achieve this goal it is necessary to make a post cure with a temperature that could be as high as 180 °C.

For aeronautic applications, it is also critical that the self-healing activity functions at low working temperatures, which can reach values as low as –50 °C. This issue is even harder to solve for space vehicles or satellites where extreme fluctuations of temperature between –150 and 150 °C are also possible. Indeed, a very efficient aeronautic or aerospace self-healing material needs to satisfy these two fundamental requirements: (i) chemical stability and high thermal stability of the self-healing components (catalysts and vessels filled with healing agents), (ii) high healing efficiency at low temperature. Some of these issues have been taken into account in recent papers.

17.1.1

Stability and Reactivity of Catalysts for Self-Healing Formulations

Wilson and coworkers have evaluated the reactivities of G1, G2 and HG2 catalysts with various monomeric healing agents with a view toward improving the self-healing performances in a variety of epoxy matrices [27]. In the same paper they

have also evaluated the thermal stability of these three catalysts embedded into the epoxy matrices with the aim of studying their stability to processing conditions during manufacturing conditions. To evaluate the thermal stability of the catalysts under simulated high-temperature processing conditions, the authors prepared fracture specimens with a tapered double-cantilever beam (TDCB) geometry. They performed different types of fracture tests, among which were self-activated tests in which the catalyst was embedded in the epoxy matrix, and the healing agent alone was injected into the crack plane, at this point the samples were left to heal for 24 h. Self-activated M_1 samples (epoxy matrix EPON 828 cured with DETA) containing 1.5 wt% of as-received catalyst were prepared and subjected to customary curing cycles [5, 8, 11, 14, 16] followed by an additional postcuring at 125 °C for 4 h before fracture testing. Samples were then fractured, and DCPD (10 μ L) was injected into the crack plane. The samples were then left to heal at either RT (room temperature) or 125 °C for 24 h. Samples healed at RT showed a retention of healing performance of 77%, 84%, and 18% for G1, G2, and HG2 catalysts, respectively. Samples healed at 125 °C showed significant improvements over those healed at RT, in fact for G1, G2 and HG2 catalysts, the retention of healing performance was 109%, 216% and 57% respectively. The lower retention of healing performance observed for HG2 catalyst was an unexpected result since HG2 is a catalyst with impressive chemical stability and recyclability [27–29], and usually Ruthenium-based catalysts are reported as exhibiting great functional group tolerance, as well as greatly enhanced air and water stability [30]. Guadagno and coworkers have dealt with the same issue from different angles, trying to understand the reason for the low retention of healing performance obtained using HG2 catalyst. In a recent paper [25] they have shown critical issues in the use of epoxy precursors in conjunction with HG2 metathesis catalyst. However, an appropriate curing cycle of the self-healing mixture allows one to overcome this critical point and, therefore, carry out the curing process at high temperatures without deactivating the self-repair activity. In particular, the authors analyzed the thermolytic stability of the HG2 catalyst in powder form, both in air atmosphere and in the epoxy matrix.

The catalyst was kept at different temperatures directly from the solid state (the same form in which it was dispersed into the epoxy mixture to manufacture epoxy systems) and, after the thermal treatment, was dissolved in a deuterated solvent (deuterated chloroform, $CDCl_3$) immediately before recording the 1H NMR spectrum. The HG2 catalyst showed exceptional stability, even after a thermal treatment at 180 °C in air atmosphere.

The stability of the catalyst was subsequently analyzed for the catalyst powder embedded inside the epoxy matrix (after the curing process at high temperatures).

In particular, using FTIR spectroscopy to monitor the reactivity of the epoxy groups [31], the authors demonstrated the reactivity, at temperatures higher than 80 °C, of the HG2 catalyst with the oxirane rings of the epoxy precursors and found compromised effectiveness in the activation of the ROMP. The same authors found a solution to preserve the catalytic activity of HG2 catalyst inside the epoxy

matrix. The addition of a step in the curing cycle, at a temperature at which the HG2 catalyst does not react in competition with the hardener (below 80 °C) allows the opening of all the oxirane rings, preserving its catalytic activity in successive curing steps at higher temperatures. In this way, the catalyst remains intact, and hence it is capable of subsequently performing its catalytic activity in the ROMP of healing agents.

This stratagem allowed the obtaining of samples cured at temperatures up to 160 °C without deactivating the self-repair activity of the formulated systems.

Curing cycles currently used in the aeronautic field for primary structures may reach temperatures up to 180 °C. Concerning this last requirement, recent works have shown very promising results when the self-healing formulation contains Hoveyda-Grubbs' 1st generation catalyst rather than G1, G2 or HG2 catalysts [32–35].

The thermal stability of each of the catalysts G1, G2, and HG1 was evaluated under conditions of actual use for applications in self-healing structural systems. The catalyst was dispersed in the epoxy matrix in its solid state and both the epoxy precursor and the composite were cured by two-stage curing cycle; after which, the catalysts were extracted with chloroform from the epoxy matrix (after the curing process at high temperatures) and analyzed by ¹H-NMR spectroscopy. Infrared spectroscopy was also used to evaluate the catalytic activity directly inside the epoxy resin after the cure processing. These results are shown in Table 17.1.

It is observable that Grubbs' 1st generation and 2nd generation catalysts are stable if the temperature of the second stage of the curing cycle is up to 150 °C for 2 h; it is not possible to formulate self-healing systems related to ROMP of the healing agents when a curing temperature of 180 °C is scheduled.

Epoxy self-healing systems containing HG1 can be processed even with a temperature of the second stage up to 180 °C.

FTIR investigation provided evidence that the catalyst HG1 embedded in epoxy formulation cured up to 180 °C activates the polymerization of ENB at room tem-

Table 17.1 Summary of the results on the thermolytic stability of Grubbs and Hoveyda-Grubbs' catalysts extracted from the formulated epoxy matrices.

Sample	Curing cycle, Temperature (time)	Catalyst state (after treatment)
EHA ^a -G1 (150)	125 °C (2 h) + 150 °C (2 h)	Not-decomposed
EHA-G1 (180)	125 °C (2 h) + 180 °C (2 h)	Decomposed
EHA-G2 (150)	125 °C (2 h) + 150 °C (2 h)	Not-decomposed
EHA-G2 (180)	125 °C (2 h) + 180 °C (2 h)	Decomposed
EHA-HG1 (150)	125 °C (2 h) + 150 °C (2 h)	Not-decomposed
EHA-HG1 (180)	125 °C (2 h) + 180 °C (2 h)	Not-decomposed

a) The EHA matrix was prepared by mixing an epoxy resin (E) (trade name EPON 828) with 37wt% of an epoxy flexibilizer (H) (trade name HELOXY 71) to improve the toughness of the material and consequently growth stability. This formulation for the epoxy matrix was used for the self-healing system already described in the literature [1, 6].

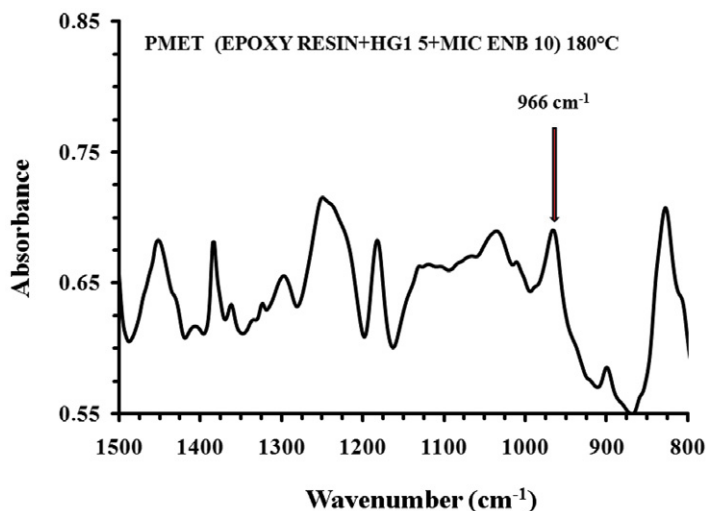


Figure 17.1 FTIR spectrum of epoxy resin containing HG1 treated with ENB.

perature. Figure 17.1 shows the spectrum of an epoxy resin containing HG1 (cured up to 180°C) treated with ENB.

In conjunction with different signals of the epoxy blend, the spectrum shows the strong band at 966 cm^{-1} due to the carbon–hydrogen bending vibration of a trans carbon double bond and, therefore, characteristic of the metathesis product (PMET). FTIR spectra obtained under the same experimental conditions for G1 and G2 catalysts embedded in the matrix cured up to 180°, did not show the signal at 966 cm^{-1} , indicating the deactivation of the catalytic functionality.

Another issue related to the stability of self-healing components is the instability of the catalysts embedded in epoxy formulations to primary amines, which represent an important class of curing agents for epoxy formulations. In order to formulate a self-healing aeronautic resin, we need to take into account that the final material must have suitable mechanical properties which depend not only on the curing cycles, but also on the chemical nature of the epoxy formulations. In the choice of epoxy mixture, it is necessary to consider that the structure of the resin strongly governs its chemical and some of its physical properties. The number of reactive sites in the epoxy precursors controls the functionality directly acting on the cross-linking density. This, combined with the nature of hardener agent, the functionality, the stoichiometry, and the curing cycle determines the final properties of the cured resin, especially in terms of mechanical and thermal properties.

Generally, hardeners (curing agents) based on the primary amines give the best mechanical performance. Unfortunately, these amines can poison many of the catalysts active in ROMP of monomers used as healing agents. The instability of ruthenium catalysts to primary amines can be a significant drawback in the design of self-healing polymers; for this reason it is fundamental to evaluate the activity of the catalysts embedded inside the specific epoxy formulation [5, 8, 36].

Table 17.2 Reaction rate and yield of ROMP reaction of DCPD and ENB with G1, G2 and HG1 catalysts.

Test	Catalyst/monomer ratio	Temperature (°C)	Time (min)	Yield (%)
1	1:1000 G1/DCPD	25	15	34
2	1:1000 G1/DCPD	0	5	0
3	1:1000 G1/DCPD	10	30	0
1	1:1000 G1/ENB	25	0.5	100
2	1:1000 G1/ENB	0	13	100
3	1:1000 G1/ENB	-10	60	17
4	1:1000 G1/ENB	-20	1440	79
5	1:1000 G1/ENB	-30	1440	74
6	1:1000 G1/ENB	-40	1440	52
1	1:1000 G2/ENB	25	1	99
2	1:1000 G2/ENB	0	50	100
3	1:1000 G2/ENB	-20	60	79
4	1:1000 G2/ENB	-30	1440	74
5	1:1000 G2/ENB	-40	1440	43
1	1:1000 HG1/ENB	25	0.5	96
2	1:1000 HG1/ENB	-20	1440	93
3	1:1000 HG1/ENB	-40	1440	99
4	1:1000 HG1/ENB	-40	240	98
5	1:1000 HG1/ENB	-50	450	99

17.1.2

Healing Efficiency at Low Temperatures

In aircraft, the operating range may vary roughly from -50 to 60°C , therefore the healing agent must be able to heal the material also at very low temperatures. Merle and coworkers in a recent patent proposed the use of 5-ethylidene-2-norbornene as a healing agent active at low temperature [37]. Guadagno *et al.* analyzed the ROMP of this healing agent using G1, G2 and HG1 catalysts. The obtained results were compared with those obtained using the most common healing agent (DCPD monomer) [32, 33, 38].

Table 17.2 summarizes data from all the performed experiments.

The self-healing functionality based on the metathesis reaction of DCPD activated by the G1 catalyst deactivates if the damage occurs at a temperature equal to or lower than 10°C . On the other hand, the metathesis reaction activated by G1 and G2 catalysts with ENB is active even at -40°C . A comparison with DCPD data highlights the advantages of ENB as healing agent: the metathesis reaction is active at very low temperatures with high value of yield and the ROMP of ENB is an extremely fast reaction. The yield reaches a value of 100% after a reaction time of 30 s at 25°C , compared to DCPD where the reaction yield is about 34% after a reaction time of 15 min.

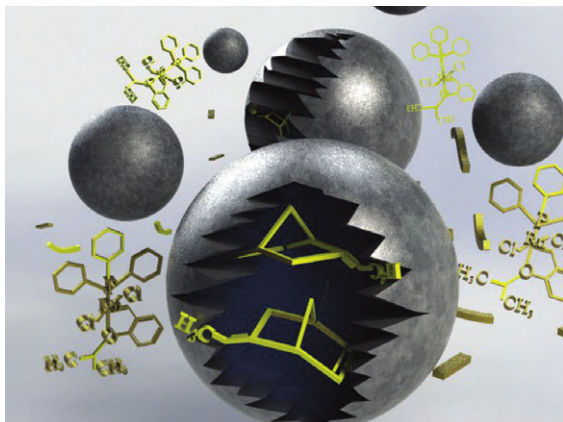


Figure 17.2 Scheme of self-healing formulation which includes: (a) capsules containing a polymerizer agent (ENB); (b) a catalyst for the polymerizer (HG1).

In the case where HG1 is used as catalyst and ENB as healing agent, the metathesis reaction is significantly active also at -50°C , whereas with G1 and G2 activity is reduced already at -40°C .

In this review two basic aspects for the application of ruthenium catalysts to aeronautic applications, and specifically for the design of self-healing structures, have been analyzed. They are: (i) the chemical stability and high thermal stability of the self-healing components, and (ii) the healing efficiency at low temperature. Results from the literature obtained for several systems comprising combinations of G1, G2, HG1 and HG2 catalysts and two different healing agents, DCPD and ENB, have been described and evaluated. The systems based on ENB as healing agent and HG1 as catalyst offer the most promising results. In fact, HG1 showed a higher thermal stability and optimal reactivity for ROMP at low temperatures. Self-healing systems with HG1 catalyst obtained by dispersing ENB-filled microcapsules at a concentration of 10 wt% into the epoxy matrix cured at up to 180°C have been also analyzed and reported in the literature. A simplified scheme of this self-healing formulation is shown in Figure 17.2.

The catalyst embedded into the epoxy matrix was reduced in the form of thin particles before formulating the self-healing system. This step is useful to provide the suitable crystal structure and morphology for an efficient autorepair function; works previously reported in literature [12] for the system DCPD/Grubbs' catalyst demonstrated the role of crystal structure/morphology; smaller particles of catalyst dissolve more quickly, leading to a more efficient healing system. For the formulation of the self-healing system corresponding to the scheme of Figure 17.2, HG1 catalyst particles were placed in a vial and pulverized by a small rotating magnet for 25 min. Figure 17.3 shows the effect of this pulverization procedure on the morphology of HG1 particles.

These catalyst particles were embedded in the solid form into the mixture of epoxy precursors.

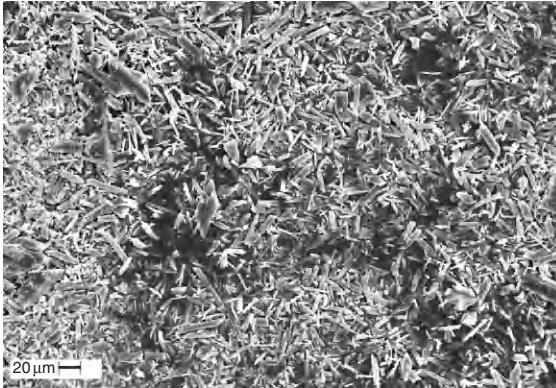


Figure 17.3 SEM image of the HG1 catalyst after pulverization treatment.

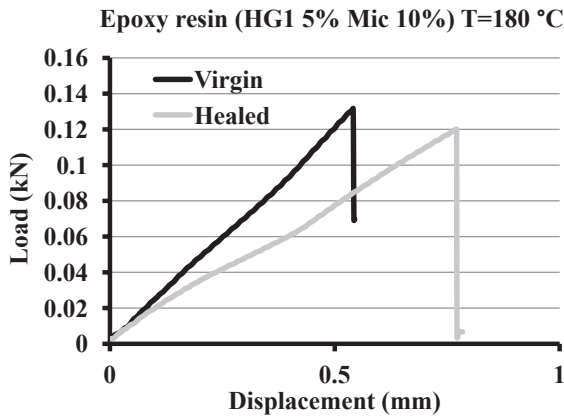


Figure 17.4 Load–displacement curves for virgin and healed epoxy sample (HG1 5% Mic 10%) cured up to 180°C.

The healing efficiency η (calculated as the ratio between the critical fracture loads of the healed and virgin samples) was obtained from load–displacement curves using an already established procedure [39, 40]. The results are shown in Figure 17.4. The healing efficiency was found to be about 91%.

17.2 Conclusions

In this chapter some of the main issues related to self-healing materials for aerospace applications have been analyzed. In particular, the attention has been focused on the development of self-healing materials to reduce the effect of the impact damage (mechanical stress, etc.) on the structural integrity of the material.

For aeronautic applications, self-healing is not an alternative to the usual repair maintenance, but rather it is for repairing at the early stage of matrix microcracking and/or in the initial stage of delamination. In case of a sudden catastrophic damage involving large zones of the materials (larger than 1000 microns) the proposed systems may not be efficient because the fracture planes could be positioned in such a way as to prevent the restoration of the chemical bonds in the damaged zone (between crack faces). Therefore, the self-healing function is a way to prevent further critical damage development. Materials for aeronautic application are processed in very drastic conditions of temperatures. Processing temperatures can reach values up to 180 °C and this can be a very critical factor for the stability of the self-healing components.

Furthermore, the operating temperature of the final materials ranges between -50 and 60 °C. Therefore the self-healing functionality must be assured at temperatures over this wide range.

Aspects related to these requirements have been analyzed and discussed in this chapter. The attention was focused on self-healing materials inspired by White's design. From the analyzed data, the self-repair function based on the metathesis polymerization of ENB activated by HG1 catalyst, with its thermolytic stability at high temperature and high activity even at very low temperature, offers the best solution among the analyzed systems. These recent results can constitute the base for improving self-healing function in aeronautic materials.

The interesting results obtained from the analysis of the ROMP inside the epoxy resin using HG1 catalyst are of general validity. These can be applied also for other proposed designs [41, 42] which deliver the healing agent into the cracks using a three-dimensional microvascular network.

References

- 1 Guadagno, L., Longo, P., Raimondo, M., Naddeo, C., Mariconda, A., Sorrentino, A., Vittoria, V., Iannuzzo, G., and Russo, S. (2010) *J. Polym. Sci. B Polym. Phys.*, **48**, 2413–2423.
- 2 Dry, C., and McMillan, W. (1997) *Smart Mater. Struct.*, **6**, 35–39.
- 3 Burattini, S., Greenland, B.W., Chappell, D., Colquhoun, H.M., and Hayes, W. (2010) *Chem. Soc. Rev.*, **39**, 1973–1985.
- 4 Yuan, Y.C., Yin, T., Rong, M.Z., and Zhang, M.Q. (2008) *Express Polym. Lett.*, **2**, 238–250.
- 5 Blaiszik, B.J., Kramer, S.L.B., Olugebefola, S.C., Moore, J.S., Sottos, N.R., and White, S.R. (2010) *Annu. Rev. Mater. Res.*, **40**, 179–211.
- 6 White, S.R., Sottos, N.R., Geubelle, P.H., Moore, J.S., Kessler, M.R., Sriram, S.R., Brown, E.N., and Viswanathan, S. (2001) *Nature*, **409**, 794–797.
- 7 Toohey, K.S., Sottos, N.R., Lewis, J.A., Moore, J.S., and White, S.R. (2007) *Nat. Mater.*, **6**, 581–585.
- 8 Brown, E.N., Sottos, N.R., and White, S.R. (2002) *Exp. Mech.*, **42**, 372–379.
- 9 Brown, E.N., White, S.R., and Sottos, N.R. (2004) *J. Mater. Sci.*, **39**, 1703–1710.
- 10 Rule, J.D., Sottos, N.R., White, S.R., and Moore, J.S. (2005) The chemistry of self-healing polymers. *Educ. Chem.*, **42**, 130–132.
- 11 Rule, J., Brown, E.N., Sottos, N.R., White, S.R., and Moore, J.S. (2005) *Adv. Mater.*, **17**, 205–208.
- 12 Jones, A.S., Rule, J.D., Moore, J.S., White, S.R., and Sottos, N.R. (2006) *Chem. Mater.*, **18**, 1312–1317.

- 13 Kessler, M.R., and White, S.R. (2001) *Compos. A Appl. Sci. Manuf.*, **32**, 683–699.
- 14 Kessler, M.K., Sottos, N.R., and White, S.R. (2003) *Compos. A Appl. Sci. Manuf.*, **34**, 743–753.
- 15 Brown, E.N., White, S.R., and Sottos, N.R. (2005) *Compos. Sci. Technol.*, **65**, 2466–2473.
- 16 Brown, E.N., White, S.R., and Sottos, N.R. (2005) *Compos. Sci. Technol.*, **65**, 2474–2480.
- 17 Jones, A.S., Rule, J.D., Moore, J.S., Sottos, N.R., and White, S.R. (2007) *J. R. Soc. Interface*, **4**, 395–403.
- 18 Wilson, G.O., Moore, J.S., White, S.R., Sottos, N.R., and Andersson, H.M. (2008) *Adv. Funct. Mater.*, **18**, 44–52.
- 19 Rule, J.D., Sottos, N.R., and White, S.R. (2007) *Polymer*, **48**, 3520–3529.
- 20 Wilson, G.O., Caruso, M.M., Reimer, N.T., White, S.R., Sottos, N.R., and Moore, J.S. (2008) *Chem. Mater.*, **20**, 3288–3297.
- 21 van der Zwaag, S. (ed.) (2007) *Self Healing Materials: An Alternative Approach to 20 Centuries of Materials Science*, Springer Series in Materials, Springer.
- 22 Dry, C. (2007) Multiple function, self-repairing composites with special adhesives. Int Patent WO/2007/005657.
- 23 Motuku, M., Vaidya, U.K., and Janowski, G.M. (1999) *Smart Mater. Struct.*, **8**, 623–638.
- 24 Brown, E.N., Kessler, M.R., Sottos, N.R., and White, S.R. (2003) *J. Microencapsul.*, **20**, 719–730.
- 25 Guadagno, L., Longo, P., Raimondo, M., Naddeo, C., Mariconda, A., Vittoria, V., Iannuzzo, G., and Russo, S. (2011) *Compos. B*, **42**, 296–301.
- 26 Raimondo, M., Corvino, R., Guadagno, L., Longo, P., Naddeo, C., and Mariconda, A. (2011) European Polymer Congress 2011 (XII Congress of the Specialized Group of Polymers (GEP) (eds J. San Juan and L. Garcia-Fernandez), 26th June–1st July 2011, Granada, Spain. (Book of abstracts: 749, ISBN 978-84-694-3124-5).
- 27 Wilson, G.O., Caruso, M.M., Reimer, N.T., White, S.R., Sottos, N.R., and Moore, J.S. (2008) *Chem. Mater.*, **20** (10), 3288–3297 (supporting information).
- 28 Garber, S.B., Kingsbury, J.S., Gray, B.L., and Hoveyda, A.H. (2000) *J. Am. Chem. Soc.*, **122** (34), 8168–8179.
- 29 Wakamatsu, H., and Blechert, S.A. (2002) *Angew. Chem. Int. Ed.*, **41** (5), 794–796.
- 30 Grubbs, R.H. (ed.) (2003) *Handbook of Metathesis*, Wiley-VCH Verlag GmbH, Weinheim, Germany.
- 31 Guadagno, L., Vertuccio, L., Sorrentino, A., Raimondo, M., Naddeo, C., Vittoria, V., et al. (2009) *Carbon*, **47** (10), 2419–2430.
- 32 Guadagno, L., Raimondo, M., Naddeo, C., Mariconda, A., Corvino, R., Longo, P., Vittoria, V., Russo, S., and Iannuzzo, G. (2011) Process for preparing self-healing composite materials of high efficiency for structural applications. Patent Publication number: US 2011118385 (A1).
- 33 Guadagno, L., Longo, P., Raimondo, M., Mariconda, A., Naddeo, C., Sorrentino, A., Vittoria, V., Iannuzzo, G., Russo, S., and Calvi, E. (2010) A composite material which is self-repairing even at low temperature. Patent N° EP2257422.
- 34 Guadagno, L., and Raimondo, M. (2012) *Infrared Spectroscopy – Materials Science, Engineering and Technology* (ed. T. Theophanides), InTech, pp. 285–300, ISBN 978-953-51-0537-4.
- 35 Raimondo, M., and Guadagno, L. (2012) *AIP Conf. Proc.*, **1459**, 223–225. doi: 10.1063/1.4738450; ISBN 978-0-7354-1061-9.
- 36 Wilson, G.O., Porter, K.A., Weissman, H., White, S.R., Sottos, N.R., and Moore, J.S. (2009) *Adv. Synth. Catal.*, **351**, 1817–1825.
- 37 Merle, P., Guntzburger, Y., Haddad, E., Hoa, S.V., and Thatte, G. (2007) Self Healing composite material and method of manufacturing same. Patent application number: US 20070873950 20071017.
- 38 Guadagno, L., Raimondo, M., Iannuzzo, G., and Russo, S. (2010) *AIP Conf. Proc.*, **1255** (1), 267–269.
- 39 Mostovoy, S., Crosley, P.B., and Ripling, E.J. (1967) *J. Mater.*, **2**, 661–681.
- 40 Beres, W., Ashok, K.K., and Thambraj, R.A. (1997) *J. Test. Eval.*, **25**, 536–542.
- 41 Toohey, K.S., Sottos, N.R., Lewis, J.A., Moore, J.S., and White, S.R. (2007) *Nat. Mater.*, **6** (8), 581–585.
- 42 Toohey, K.S., Hansen, C.J., Lewis, J.A., White, S.R., and Sottos, N.R. (2009) *Adv. Funct. Mater.*, **19** (9), 1399–1405.

Index

a

acoustical microscopy 341, 346
 acrylates 27, 218
 acrylonitrile liquid rubber 79
 activation energy 132, 202, 209
 addition–fragmentation chain transfer 27, 189, 233
 addition polymerization 224
 aerospace applications, of self-healing composites
 – curing cycles 406
 – general considerations for 401–405
 – – healing efficiency at low temperatures 408–410
 – – stability and reactivity of catalysts 405–407
 – self-healing system, design of 404
 – structural applications 403
 amine-epoxy healing system 225–227
 amino silane 222
 amphiphilic comb copolymers 101
 amphiphilic polymers 84
 anionic polymerization 44, 206, 207
 anionic reactions 235, 236, 237
 anisotropy 199
 annealing 78, 80, 401
 anthracenes 26, 27, 45, 48, 176, 232, 233
 anticorrosive coatings 383–386
 antioxidants 235
 apolar liquid 248
Aristolochia macrophylla 62, 69–72, 75, 81
 artificial leukocytes, designing of 101–103
 – methodology for 103–105
 – “repair-and-go” scenario 108
 – steady shear flow, effect of 105–108
 – utility of applying a pulsatile flow 108–110

aspartic imide 79
 association constant 34, 35, 130, 279, 280, 283, 285
 atomic force microscopy (AFM) 201, 254, 350, 351
 atom transfer radical polymerization (ATRP) 160, 295
 attenuated total reflectance Fourier transform infrared (ATR-FTIR) spectroscopy 347
 attenuated total reflection (ATR) 65
 axial compression 166
 azide–alkyne cycloadditions 22, 225
 azide–alkyne healing system 225
 azobenzene 48, 176

b

ballistic damage in ionomers, healing of 346, 347
 ballistic impact 35, 323, 328, 346
 barbituric acid 34, 50, 51, 131, 277, 292, 294, 295
 Belousov–Zhabotinsky reaction 305
 bending tests, for multilayer films 344
 benzotriazole (BTA) 256, 260–262, 384, 385, 388, 389
 Bergman cyclization 205
 – swelling activation of 206
 binding energy 277, 279
 biochemical healing 8
 bio-inspired healing agents 67
 bio-inspired self-healing elastomers
 – ionic elastomers 78, 79
 – micro-encapsulation 77, 78
 – nitrile butadiene rubber (NBR) blends 80
 – supramolecular co-networks 79, 80

- bio-inspired self-sealing membranes,
 - concept generators
 - latex plants 63–69
 - lianas 69–72
 - succulent plants 72–75
 - biomimetics 49, 62, 72, 75–77, 85, 101, 178, 277, 396
 - bio-inspired physical transfer 82–84
 - foam coating 81
 - self-repairing elastomers 64, 68
 - biosensors 302
 - bio-synthesis 63
 - biradical transition 163
 - blow films 322
 - Boltzmann constant 94
 - bond lifetime 280–282, 288
 - boundary conditions 103, 105, 303
 - “bricks and mortar” morphology 155
 - Brownian motion 11, 104, 117
 - bulk materials 36, 176, 189, 284–297
 - butadiene 157
- C**
- callus formation 63, 73
 - Campanulaceae 63
 - Campanula glomerata* 63, 67
 - Campanula latifolia* 63, 67
 - capsule-based self-healing epoxies 362
 - self-healing epoxies
 - – capsule/catalyst healing system 363, 364
 - – dual-capsule healing system 364, 365
 - – single capsule healing system 365
 - self-healing fiber-reinforced epoxies 365, 366
 - – barrier properties, recovery of 368
 - – impact damage, recovery from 366
 - – macroscale properties and interfacial bond strength, recovery of 367, 368
 - – mode I fracture toughness, recovery of 366
 - carbene catalyst 10
 - carbon–carbon bonds 38, 95, 156, 157
 - carbon fibers 164, 218, 220, 226, 229, 366, 370, 374, 401
 - carbon nanotubes (CNTs) 227, 256, 257, 259, 348, 371, *see also* halloysite nanotubes; multi-walled carbon nanotubes (MWCNT)
 - catalytic species, activation of 204–207
 - catechol-iron complex 36, 329
 - cationic curing 20
 - cationic ring-opening polymerization 223
 - cells, *see* plant cells
 - center-of-mass diffusion 124
 - chain mobility 12, 13, 27, 188, 209, 233, 276, 281, 284, 288, 293, 294, 326, 344, 345, 365, 382
 - charge transfer 292, 348
 - chemical
 - coagulation 65
 - degradation 1, 7, 337
 - equilibrium 202, 207–210
 - healing 9, 315
 - oxidation 263
 - chiral magnets 302
 - chitosan polyurethane networks 347
 - cinnamoyl groups 45, 232
 - cis–trans* isomerisation 48
 - click chemistry 10, 16, 21, 22, 139, 251
 - click reactions 21, 22, 51, 225
 - coatings, *see also* self-healing coatings
 - acrylic 224
 - extrusion 322
 - foam 81, 82, 85
 - fracture response of 348
 - healing of 370, 371
 - organic-based 386
 - powder 160
 - self-sealing 81, 82
 - sol–gel 256, 261, 263, 393, 395
 - surface gloss properties of 347
 - coaxial electrospinning 250
 - cold-curing 227, *see also* heat-curing
 - compact tension (CT) 167, 371
 - composites
 - fiber-reinforced 346, 366, 370, 373–375
 - healing of impact damage of 346
 - self-sensing, self-healing vascularized 371
 - compression after impact (CAI) 366
 - compression molding 321
 - compression test 80, 159, 160, 200, 201, 387
 - computed (X-ray) tomography (X-ray CT) 341–343, 346
 - computerized vibro-thermography 402
 - condensation polymerization 180, 254, 304
 - conformational entropy 13, 92, 155
 - constrained geometries simulate external force (COGEF) 202
 - constraint release (CR) 127, 134
 - contour length fluctuations (CLF) 127–129, 134
 - copolymerization 159, 160, 233, 236
 - copper(I) catalyzed alkyne-azide cycloaddition (CuAAC) 21, 51, 53
 - core–sheath nanofibers 255, 264

- core-shell nanofibers 84, 85, 250, 255, 257
 - corrosion 228, 395
 - inhibitors 255, 256, 260–263, 351, 352, 383–388, 392, 393, 395
 - methods for healing of protection against 351
 - – electrochemical impedance spectroscopy 352
 - – potentiostatic measurements 352
 - – scanning electrochemical microscopy 353–356
 - – scanning vibrating electrode technique 352, 353
 - resistance 215, 361, 383–386, 395
 - coumarin 45, 47, 48, 177–188, 234
 - photodimerization of 186
 - covalent chemistry 10, 236, 401
 - covalent network formation
 - irreversible 16–22
 - reversible 22–28
 - crack formation 7, 139, 346, 383
 - crack healing 12, 13, 153, 154, 168, 186, 188, 189, 257, 383
 - in glassy polymers 13
 - light-induced 232
 - crack propagation 167, 178, 186, 345, 374, 383
 - crockmeter test 347
 - crosslinked polymers, *see* thermosets
 - crosslinking 9, 160
 - autocatalytic behavior 21
 - bonds 193
 - chemical 2, 10
 - density 36
 - photochemical 2
 - reversible 2
 - stress-induced 164
 - crystallization effects 285
 - curing agents 20, 364, 407
 - current density 352, 393
 - current density–voltage (J – V) measurements 348
 - current–voltage (I – V) measurements 348
 - cyclic dienes 157, 232
 - cyclic monomers 26, 232
 - cyclic oligomers 208, 236
 - cycloaddition reaction 21, 22, 27, 45, 139, 157, 158, 173, 209, 210, 225, 232
 - cyclooctene 44
 - cyclopentadiene dimer 157
 - cyclopentadienyl trimer 162
 - cycloreversion reaction 22, 164
- d**
- damage-healing cycles 229
 - damage-induced cracking 215
 - Debye function 120, 121
 - deformation of polymers 194–196
 - degree of crystallinity 195
 - delamination 247, 339–341, 350, 366, 370, 374, 401, 411
 - Delosperma cooperi* 62, 72–75
 - dendritic macromonomers 48, 176, 329
 - dendritic polymer 84, 233
 - density functional theory (DFT) 91
 - diblock copolymers, melt morphology of 304, 305
 - diacyldiaminopyridine 34
 - 2,7-diamido-1,8-naphthyridine 34, 277
 - 2,6-diaminotriazine (DAT) 277, 285, 287
 - dicyclopentadiene (DCPD) 16, 26, 44, 139, 218–221, 237, 251, 363
 - encapsulation of 253
 - self-healing behavior of 232
 - dicyclopentadienyl monomer 157
 - dielectric constant 316, 317, 320, 329
 - dielectric spectroscopy (DR) 116, 117, 123
 - Diels–Alder (DA) bonds 372
 - Diels–Alder (DA) reactions 10, 16, 22, 141, 156–161, 173, 204, 231, 232
 - dienophile 22, 27, 156, 157, 159, 161, 164, 189, 204
 - differential scanning calorimetry (DSC) 139, 220, 288, 317
 - temperature-modulated 165
 - diffuse neutron scattering (DNS) 134
 - diffusion 9, 11–13, 104, 117, 124, 134, 135, 148, 153, 154, 186, 229, 233, 350, 368, 393
 - dihydrodicyclopentadiene 16
 - dimerization constant 279
 - dimethylnorbornene ester (DNE) 364
 - direct current (DC) technique, for study of healing capabilities 352
 - dissolved healing agents 373
 - disulfide bridges 27, 234
 - dithioester 157
 - DNA base-pairing 34
 - double cantilever drilled compression (DCDC) test 369
 - double cleavage drilled compression (DCDC) 166, 167
 - drought layer of dead cells 62
 - dual-capsule healing system 364, 365
 - dual cross-linked nanogels, designing of 92, 93
 - methodology for 94–97

- optimization of mechanical response for 101
 - results on application of tensile deformation at
 - – constant force 97
 - – constant velocity 97–101
 - ductility 97–99, 101
 - dynamers 277
 - dynamic coordination bonds 35
 - dynamic electric permittivity 117
 - dynamic light scattering 389
 - dynamic mechanical analysis (DMA) 53, 116, 139, 165, 220, 344
- e**
- E. characias* 63
 - Eisenberg–Hird–Moore (EHM) model 317
 - elastic deformation 320, 324
 - electrical conducting functionality, healing of 348–350
 - electrochemical impedance spectroscopy (EIS) 344, 345, 352
 - electrocyclic ring-opening reaction 44, 45
 - electromagnetic irradiation 384
 - electron density 157, 319
 - electron spin resonance (ESR) spectroscopy 167, 194
 - electrospinning technique 250, 251, 257
 - electrostatic interactions 195, 301, 304, 305, 317, 329
 - elongational flow 198, 201
 - emulsification 223, 250
 - emulsion polymerization 248, 251, 383
 - E. myrsinites* 63
 - endothermic enthalpy of reaction 161
 - energy dispersive X-ray spectroscopy 257
 - energy dissipation 195, 196
 - enthalpic interactions 14, 103
 - environmental scanning electron (E-SEM) microscopy 340, 341
 - EPIKURE 3274 20
 - epiphytic growth habits in plants 61
 - EPON 815C 20
 - EPON 828 21, 22, 405
 - epoxide chemistry 10
 - epoxides 16, 20, 222, 224, 227, 372
 - epoxy-amine resin 20
 - epoxy-based healing system 227, 228, 361, 401
 - capsule-based healing 362
 - – self-healing epoxies 363–365
 - – self-healing fiber-reinforced epoxies 365–368
 - design for reversibility 371–373
 - intrinsic healing systems
 - – dissolved healing agents 373
 - – phase separated healing agents 373
 - – resin design for reversibility 371–373
 - – solid-phase healing agents 373, 374
 - vascular-based healing 368, 369
 - – fracture damage, recovery of 369, 370
 - – healing of coatings 370, 371
 - – impact damage, recovery of 370
 - – self-sensing, self-healing vascularized composites 371
 - epoxy curing 20
 - epoxy + latent hardener/catalyst healing system 222–224, *see also* epoxy-based healing system
 - epoxy resins, *see* epoxy-based healing system
 - esthetic damage, healing of 347, 348
 - 2,4-*bis* (2-ethylhexyl-ureido)toluene (e, EHUT) 277
 - 5-ethylidene-2-norbornene (ENB) 16, 220, 221, 404, 408
 - Euler scheme 104
 - Euphorbia amygdaloides* 63
 - Euphorbia* plant species 63, 65, 67, 75
 - extrinsic self-healing materials 10, 215–218, *see also* intrinsic self-healing materials
 - catalytic systems
 - – azide-alkyne healing system 225
 - – DCPD/5-ethylidene-2-norbornene (ENB) + Grubbs' catalyst healing system 220, 221
 - – dicyclopentadiene (DCPD) + Grubbs' catalyst healing system 218–220
 - – epoxy + latent hardener/catalyst healing system 222–224
 - – siloxane-based healing system 221, 222
 - – thiol-ene healing system 224, 225
 - – thiol-epoxy healing system 224
 - – thiol-maleimide healing system 225
 - non-catalytic systems
 - – amine-epoxy healing system 225–227
 - – epoxy-based healing system 227, 228
 - – isocyanates-based healing system 228
 - – molecular interdiffusion 228, 229
 - – vinyl ester healing system 228
 - novel approaches and perspectives for 264, 265
 - self-healing systems 216, 217
 - extrusion coatings 322
- f**
- fatigue crack propagation 345
 - fatigue damage 224
 - healing after 345, 346

fatigue loading 222, 346, 363, 374
 fatigue testing 374
 fiber formation 282, 285
 fiber-reinforced composites 164, 346, 366,
 370, 373–375
 Fickian diffusion 124, 126
Ficus benjamina 62, 63–69, 75
 field emission gun SEM (FEG-SEM) 340
 finite modulus of elasticity 147
 Flory–Fox equation 13
 Flory–Huggins approximation 143
 fluorescence microscopy 338
 fluorescence polarization 199
 fluoroalkenes 163, 165
 foam coating 72, 81–85
 Fourier transformation 122, 127
 Fourier transform infrared (FTIR)
 spectroscopy 344, 406
 fracture damage, recovery of 369, 370
 fracture load 345, 410
 fracture toughness 166, 167, 215, 223, 227,
 251, 343, 363, 364, 370, 374
 free energy 10, 13, 142, 277
 free energy density 143
 freely jointed chain (FJC) 117–119
 free radical polymerization 160, 161, 249,
 295
 free radicals 161, 167, 168
 friction coefficient 351
 friction recovery, for lubricant healing
 systems 351
 Friedel–Crafts alkylation 159
 functional integrity, healing of
 – electrical conduction recovery 348–350
 – esthetic damage 347, 348
 – friction recovery 351
 – hydrophobicity 350, 351
 – protection against corrosion 351
 – – electrochemical impedance spectroscopy
 352
 – – potentiostatic measurements 352
 – – scanning electrochemical microscopy
 353–356
 – – scanning vibrating electrode technique
 352, 353
 – thermal conduction recovery 350
 furan 26, 157, 159, 160, 165, 167, 232
 furan-maleimide-based polymers 22
 furfurylglycidyl ether (FGE) 372

g

Gaussian distribution 120, 198
 gelation 140
 – micro-phase order–disorder transition
 147

– phase separation and 147–149
 – states of 144
 – thermodynamics of 141–143
 gel point 140, 142–147, 281
 gel-to-sol transition 165, 176
 gel transition 143
 glass fiber-reinforced composites 219,
 372–374
 glass fibers 164, 225, 228, 256, 368, 370,
 372
 glass transition temperature 11, 13, 139,
 153, 159, 183, 184, 195, 220, 254, 263, 306
 glycidyl methacrylate (GMA) 227
 graft-polymers 279, 281
 Grubbs' catalyst 16, 17, 49, 139, 208,
 218–221, 237, 259, 363, 364, 403, 404

h

halloysite nanotubes 256, 261, 385, *see also*
 carbon nanotubes (CNTs); multi-walled
 carbon nanotubes (MWCNT)
 Hamilton Wedge 34, 50, 51, 277
 healing agents 218, 223
 – dissolved 373
 – phase separated 373
 – polyurethane-based 228
 – solid-phase 373, 374
 healing performance, efficiency and
 assessment of 165–168
 heat-curing 20, 227, *see also* cold-curing
 heat flux 350
 heteroatom–carbon bonds 157
 heterolytic bond cleavage 197
Hevea brasiliensis 63–69, 316
 Hevein dimers 64, 78
 hierarchical Bell model (HBM) 92, 95
¹H-NMR spectroscopy 406
 hollow glass fibers (HGFs) 218, 225, 226,
 228, 256, 368, 370
 homoditopic heterocomplementary
 monomers 130
 homolytic bond cleavage 196, 197
 homolytic photolysis 27, 233
 homopolymerization 159, 225
 homopolymers 131, 178, 198, 321
 Hoveyda–Grubbs' second generation catalyst
 (HG2) 219, 364, 403, 404, 406
 hybrid nanopastules 251
 hydrogels 27, 148, 149, 283, 329, 384
 hydrogen-bonded polymers 28
 hydrogen-bonding brush copolymer (HBP)
 294–296
 hydrogen bonds 28, 33, 34, 37, 76, 115,
 130, 131, 186, 195, 229, 277, 301
 – activation energy 132

- dynamics of 279, 280
- re-formation of 361
- sextuple 34
- hydrophilic monomers 251, 253
- hydrophobe 248
- hydrophobic
 - cracks 102, 103, 105
 - interactions 301
 - nanoparticles 101–103, 105
- hydrophobicity, healing of 350, 351
- hydroxy end-functionalized
 - polydimethylsiloxane (HOPDMS) 221
- hydroxyl radicals 71, 203

- i**
- impact damage, healing of
 - ballistic damage in ionomers 346, 347
 - composites 346, 370
- imprinted polymers 48
- infrared (IR) spectroscopy 65, 165, 196, 406
- infrared thermography 402
- inorganic nanocapsules 251
- inorganic–organic composite 164, 165
- in situ* polymerization 218
- in situ* scanning vibrating electrode 256
- intelligent materials 85, 173, 189
- interfacial polycondensation 251
- interfacial polymerization 218, 228, 263, 387
- interfacial shear strength 220, 368, 371, 373
- interfacial step-growth polymerizations 248
- interfacial thermal transport 350
- intermolecular forces 11
- intermolecular interactions 186
- internal reflection IR imaging (IRIRI) 347
- interpenetrating polymer networks (IPN) 154, 155
- intra-chain monomers 120
- intrinsic healing systems
 - dissolved healing agents 373
 - phase separated healing agents 373
 - resin design for reversibility 371–373
 - solid-phase healing agents 373, 374
- intrinsic self-healing materials 10
 - molecular interdiffusion of 229–231
 - other systems 236
 - reversible bond formation
 - – anionic reactions 235, 236
 - – Diels–Alder/Retro–Diels–Alder reaction 231, 232
 - – disulfide bridges 234
 - – photochemical trigger 232–234
 - – pH-responsive systems 236
 - – radical fission/recombination 234, 235
- self-healing systems 230
- ionic bond 76
- ionomeric elastomers 68, 78, 79
- ionomers 28, 35
 - applications and availability of 320–322
 - basic principles of 315–319
 - definition of 315
 - Eisenberg–Hird–Moore (EHM) model 317
 - healing of ballistic damage in 346, 347
 - methacrylate-based 317
 - order–disorder transition 317, 326
 - properties of 319, 320
 - in self-healing systems 322, 323
 - – actual developments and future trends 327–331
 - – general mechanism 323–326
 - – healing mechanism 325
 - thermally reversible crosslinked system 319
 - thermal properties of 326
 - thermoplasts 324
- isocyanate chemistry 10
- isocyanates-based healing system 228
- isotopic substitution 117

- l**
- laticifers 63, 64
- lap shear test 343, 344
- laser light scattering 194
- latex-based self-sealing 63–69
- latex coagulation 64, 65, 67, 68, 75, 78
- laticifers 63, 64
- lattice Boltzmann model (LBM) 103, 104
- lattice-gas 143
- lattice spring model (LSM) 92, 94, 103
- layered double hydroxides (LDHs) 263
- leaching 80
- leukocytes 91, 92
 - artificial leukocytes, designing of 101–110
- Lewis acid 157, 223
- lianas, self-sealing and self-healing in 69–72
- ligand–metal bond 205
- light-responsive capsules 258–260
- lignifications 63
- linear metallosupramolecular polymers 36
- lipophobe 248
- liquid crystals 176
 - phase structure of 177
 - polymers 178

- living polymerizations 51, 161, 207
- lower critical solution temperatures (LCSTs) 148, 263
- lutoids 64, 65, 68
- m**
- macromonomers 17, 20, 48, 132, 176
- maleimides 20, 22, 26, 44, 156, 157, 159, 160, 167, 225, 231
- mechanical decomposition 163, 164, *see also* thermal decomposition
- mechanical deformations, of plant organs and cells, 62
- mechanically induced self-healing 44
- nanocapsules 251–255
 - nanofibers and nanotubes 255–258
- mechanical properties, healing of
- after fatigue damage 345, 346
 - after impact damage, *see* impact damage, healing of
 - after static damage 343–345
- mechanical stress in materials 164, 208
- development of 194
 - dissipation of 194
 - effect of 193
- mechanochemical activation, of catalysts 44
- mechanochemical damage
- deformation 194–196
 - heterolytic bond cleavage 197
 - homolytic bond cleavage 196, 197
- mechanochemical network formation
- mechanochemical activation of catalysts 44
 - reactive species, generation of 38–44
- mechanochemical reactions 10, 45, 194, 198, 200–203, 205
- mechanochemistry 2, 38, 193, 194, 201, 210, 211
- mechanophore activation 200, 201
- mechanophores
- activation of
 - – compression 200, 201
 - – other methods for 201, 202
 - – tensile testing 198–200
 - – torsional shear testing 200
 - – ultrasound 198
 - concept of 194
 - mechanical force, effect of 196
 - mechanochemical damage
 - – deformation 194–196
 - – heterolytic bond cleavage 197
 - – homolytic bond cleavage 196, 197
 - mechanochemical self-healing strategies
 - – activation of catalytic species 204–207
 - – disruption of equilibrium 207–210
 - – production of reactive species 202–204
 - positioning of 194
- melt viscosity 126, 127, 320
- merocyanin (MC) 197, 199
- metal bonding 28, 50
- metallic nanoparticles 265
- metal–ligand complex 305, 311
- metal–ligand interactions 35, 36, 301–303, 307–309, 311, 327, 329, 330
- metallopolymers 301, 302, *see also* organometallic polymers
- binding constants for 303
 - boundary conditions 303
 - complexation of 304
 - gels 306
 - hydrophilic properties of 305
 - metal incorporation in 304
 - metal–ligand interactions 302, 307, 309
 - self-healing 307–309
 - stimuli-responsive 305–307
 - thermodynamic property of 302
- metallo-proteins 301
- metallo-supramolecular gels 281, 329
- metallo-supramolecular polymers 36, 176, 329
- metal–metal complexes 2, 287
- metal oxidation 305
- methyl barbiturate 79
- Michael addition reaction 22, 225
- micro-cracks 77, 80
- microencapsulation 16, 49, 77, 78, 80, 237
- of liquid healing agents 352
- microphase separation 148, 184, 282, 285, 286, 305, 316, 320, 329
- theory of 50, 131, 132
- micro- (computed) tomography 341–343
- micro-laminate 85
- micro-optic-mechanical-system 75
- mini-emulsions 248, 249, 254
- radical polymerization 251
- mixed silane 222
- molar feed ratios 180
- molecular diffusion 8, 9, 11, 50, 117, 229, 402
- across crack interface 153, 154
- molecular dynamics 34, 91, 139, 140, 197, 202, 257
- molecular interdiffusion 11, 13, 38
- of intrinsic self-healing materials 229–231
 - of thermoplastics 228, 229

- molecular orbitals 157, 163
 molecular selfassembly 10
 molecular “switching” 44, 48
 molecular toolbox 36
 mono-functional contaminants 130
 Monte Carlo simulations 91
 Morse potential 104, 196
 multiple time healing 50, 51
 multivalent metal–ligand interactions 35, 36
 multi-walled carbon nanotubes (MWCNT) 227, *see also* carbon nanotubes (CNTs); halloysite nanotubes
- n**
- nanocapsules 251–255
 – characteristics of 252
 nanocomposite materials 164
 nanocontainers, types of 386–389
 nanofibers 255–258
 – characteristics of 256
 nanoparticles 9, 11, 91
 – chemisorbtion of 104
 – diffusion of 104
 – self-healing 14
 nanoporous magnets 302
 nanotubes 255–258, *see also*, carbon nanotubes (CNTs); halloysite nanotubes; multi-walled carbon nanotubes (MWCNT)
 naphthalene-diimide 277, 291, 297
 Navier–Stokes equation 103
 near-field scanning optical microscopy 338
 neutron scattering 115, 117, 119, 123, 133–135
 neutron spin echo (NSE) spectroscopy 121, 128, 135
 Newtonian liquid-like behavior 149
 Newton’s equations of motion 103
N-heterocyclic carbene (NHC) 44
 nitrile butadiene rubber (NBR) blends 78, 80
 NO–C bonds healing mechanism 161–163
 non-covalent forces 195
 norbornene 16, 44, 221
 nuclear magnetic resonance (NMR) 117, 165, 344
 nucleation 198
 nucleobases 34, 131, 285
- o**
- odd random phase multisine electrochemical impedance spectroscopy (ORP-EIS) 352
 oil-in-water (o/w) emulsion 218, 228, 248, 387
 olefin metathesis 10
 oligomers 84, 131, 207, 208, 236, 284, 345
 open circuit potential (OCP) 352
 optically healable metallosupramolecular polymers 176
 optical microscopy 338–340, 342, 366
 organic monomers 304
 organic radicals 161
 organometallic polymers 197, 205, 303, 304
 Ostwald ripening 248, 251
 oxidative burst 62
 oxygen radicals 71
- p**
- palladated pincer complexes 36
 patching 9, 14, 402
 perfluorocyclobutanes 163, 164, 165, 209
 pericyclic reaction 48
 phase decay 147
 phase segregation 285
 phase separation 250, 306, 320
 – and gelation 147–149
 – healing agents 373
 – rate of 148
 photochemical healing 45, 173, 176, 177
 photochemical modulation 176
 photochemical trigger 232–234
 photocrosslinking 48, 183, 184
 photocycloaddition 173, 174, 177, 232
 photodegradable polymers 259
 photodimerization reactions 173, 177, 178, 180, 183, 184, 186, 188, 234
 photoinduced cyclodimerization 173
 photoinitiators 189, 224, 233
 photoirradiation 47, 209, 259
 photo-remendable polyurethane 176
 – molecular design of
 – – dihydroxy coumarin derivatives 179–182
 – – monohydroxy coumarin derivatives 178, 179
 – photo-remendability, evaluation of 185–188
 – reversible photo-crosslinking behaviors of 182–185
 photoreversible reactions 173
 pH-responsive systems 236, 260–263
 – characteristics of 261
 pH-value 44, 48
 physical crosslinking points 35
 π -dissociation energy 163
 π -electron-poor moieties 37, 291

- π -electron-rich moieties 37, 291
- π - π stacking interactions 28, 37, 276, 291, 292, 297, 301
- pincer complexes 36, 329
- plant cells
 - division 63, 71–73
 - turgor 75, 80
 - wall 62, 71, 72
- plasma etching 350, 351
- plastic deformation 71, 199–201, 310, 324, 345
- plasticization of the cell wall 62
- platinated pincer complexes 36
- plateau modulus 128, 132, 281, 288, 293
- poly(acrylate) 21, 60, 61
- poly(acrylate amide) 34
- polyaddition reaction 26, 247
- polyanions 263
- poly(butadiene)s (PBDs) 286
- polybutylacrylate (PBA) 84
- poly(*n*-butyl acrylate) (PnBA) 288
- poly(ϵ -caprolactone) (PCL) 373
- polycations 263
- polycondensation 16, 17, 27, 28, 130, 180, 221, 247, 251
- polydiethoxysiloxane (PDES) 221
- poly(dimethyl siloxane) (PDMS) 102, 222
- polyelectrolytes 249, 260–262, 315, 384–386, 388
 - fabrication of 387
- poly(ethylacrylate) (PEA) 282
- poly(ethylene glycol) (PEG) 38, 283
- polyethyleneimine (PEI) 78, 80
- polyethylene-*co*-methacrylic acid (PEMAA) 35, 228, 229
- polyglycerol 176, 233
- polyimide copolymer 291, 292, 297
- poly(isobutylene) (PIB) 21, 34, 50, 132, 225, 285, 292
- polyisoprene 63
- polymer block copolymers 131
- polymer chains
 - application to self-healing 130–133
 - diffusion of 139, 153
 - dynamics of 120–123
 - Kratky representation of 120, 121
 - log–log representation of 120, 121
 - Rouse model for 123, 124
 - structures of 117–120
 - tube model for 124–130
- polymer characterization, techniques for
 - dielectric spectroscopy (DR) 117
 - dynamic mechanical analysis (DMA) 116, 117
 - nuclear magnetic resonance (NMR) 117
- polymer fibers 256
- polymer/glass interface 164
- polymeric microcapsules 92, 105, 384
- polymer nanocapsules 251, 263
- polymer nanofibers 257
- polymethylmethacrylate (PMMA) 231
- poly(*N*-acetyleneimine)s 26
- poly(*N*-isopropyl acrylamide) (PNIPAM) 148, 149, 263
- polyol stearate 81, 84
- poly(perfluorocyclobutane) (PPFCB) 163
- poly(phenylene ether) (PPE) 38
- polysaccharides 62, 71
- poly(styrene) 34, 294, 296
- poly(styrene-maleic anhydride)-*block*-polystyrene (PSMA-*b*-PS) 251
- poly(THF) polymers 285
- poly(urea-formaldehyde) (PUF) nanocapsules 218, 251
- polyurethane 234
 - crosslinked 185, 188
 - foam system 83, 84
 - healing agents 228
 - heterogeneous network 173
 - molecular design containing
 - dihydroxy coumarin derivatives 179–182
 - monohydroxy coumarin derivatives 178, 179
 - reversible photochemical reaction 177
 - self-healing additives for 84
 - self-repairing capacity of 85
- polyvinyl chloride (PVC) 84
- poly(vinylpyrrolidone) 38
- potentiostatic measurements, for study of healing capabilities 352
- powder coating 160
- protection against corrosion, methods for healing of 351
 - electrochemical impedance spectroscopy 352
 - potentiostatic measurements 352
 - scanning electrochemical microscopy 353–356
 - scanning vibrating electrode technique 352, 353
- protein bonds 65
- proton NMR 218
- pulsed field gradient nuclear magnetic resonance (PFG-NMR) 117
- pultrusion 85
- pyrenyl endgroups 37

q

quasi-elastic dynamic scattering 121
 quasi-elastic NSE spectroscopy 128
 quasi-static fracture tests 348
 quenching 193

r

radical chain growth 161
 radical exchange reaction 27, 161
 radical fission/recombination 234, 235
 radical photoinitiator 224
 radius of gyration 91, 118
 Raman spectroscopy 344
 redox-responsive systems 263, 264
 repair efficiency 82–85
 retro-Diels–Alder (rDA) reaction 16, 22,
 156, 231, 232, 237
 reversible addition fragmentation chain
 transfer (RAFT) copolymerization 176,
 208, 233
 reversible bond 2, 27, 140, 156, 229, 231,
 281, 361
 – formation of
 – – anionic reactions 235, 236
 – – Diels–Alder/retro-Diels–Alder reaction
 231, 232
 – – disulfide bridges 234
 – – photochemical trigger 232–234
 – – pH-responsive systems 236
 – – radical fission/recombination 234, 235
 reversible photodimerizable chromophores
 233
 reversible photodimerization 234
 reversible polymerization 168, 382
 reversible terminators 161
 rheology analysis, for study of chain mobility
 344
 ring-closing metathesis (RCM) 44
 ring-opening metathesis polymerization
 (ROMP) 16, 17, 44, 139, 218–221, 237,
 251, 403, 404, 406–409, 411
 ring-opening reactions 10, 44, 45
 Rouse model, for short polymer chains
 123, 124, 126, 134, 135
 Rouse-rate 124
 Rouse-type segment diffusion 128
 rubber 39, 51, 67, 77, 79, 80, 84, 131, 132,
 184, 232, 289
 – crosslinked 27, 64
 – self-healing supramolecular 50
 – self-sealing process 64
 – supramolecular 132, 290
 – synthetic 38
 – thermal expansion 80

– thermoreversible 33, 34
 – vulcanized 202, 203
 rubber elasticity 155
 Runge–Kutta algorithm 94

s

sacrificial bonds 91, 92
 sacrificial fibers 369
 scanning acoustical microscope 341
 scanning electrochemical microscopy
 (SECM) 353–356
 scanning electron microscopy (SEM) 224,
 254, 340, 341, 387, 388
 scanning laser confocal microscopy (SLCM)
 340
 scanning vibrating electrode technique
 (SVET) 261, 352, 353, 392–395
 sclerenchyma fibers 70
 scratch resistance 347, 348
 sealing cell 71, 72
 self-consistent-field (SCF) 91
 self-healing bulk materials 284–297
 self-healing coatings
 – adhesion to metal substrate 395
 – anti-corrosion performance of 395
 – barrier properties 386, 395
 – current trends 395, 396
 – design of 383
 – healing of esthetic damage in 347, 348
 – industrial application 385
 – micro- and nanocontainer-based 382–386
 – nanocontainer-based
 – – characterization of 389–395
 – – schematic representation of 382
 – – types of 386–389
 – overview of 381, 382
 – surface gloss properties of 347
 self-healing elastomers
 – bio-inspired 63–69, 77, 78
 – development of 67
 self-healing fiber-reinforced epoxies 365,
 366
 self-healing materials
 – bio-inspired 85
 – challenges and limits for 265
 – chemical healing processes 9
 – classification of 381
 – concept for design and classification of
 8–11
 – development of 338
 – extrinsic, *see* extrinsic self-healing
 materials
 – healing efficiencies of 166
 – hydrolysis of 235

- intrinsic, *see* intrinsic self-healing materials
- mechanically induced self-healing in, *see* mechanically induced self-healing
- methods for encapsulation of
 - electrospinning 250, 251
 - emulsion droplets as templates 247–250
- pH responsive nanocontainers for 260–263
- responsiveness to environmental stimuli 36
- stimuli-responsive, *see* stimuli-responsive self-healing materials
- supramolecular bonds in 28
- self-healing mechanism
 - application of polymer chains in 130–133
 - chemical principles of 15–48
 - categories of 15
 - covalent network formation 16–28
 - mechanochemical network formation 38–44
 - supramolecular network formation 28–37
 - “switchable” network formation 44–48
 - for functional integrity, *see* functional integrity, healing of
 - irreversible covalent network formation concepts for 18, 19
 - mechanically induced, *see* mechanically induced self-healing
 - for mechanical properties, *see* mechanical properties, healing of
 - mechanochemical induced 38–44
 - multiple *versus* one-time self-healing 49–53
 - nanoparticle-based 11, 14
 - physical principles of 11–14
 - reversible covalent network formation concepts for 23–26
 - stages of 12
 - visualization techniques
 - acoustical microscopy 341
 - computed tomography and micro-(computed) tomography 341–343
 - environmental scanning electron (E-SEM) microscopy 340, 341
 - optical microscopy 338–340
 - scanning electron microscope (SEM) 340, 341
- self-healing metallopolymers 307–309
- self-heal, triggered 10, 297
- self-lubricating coatings 383
- self-repairing materials and structures, development of 75–85
 - bio-inspired self-healing elastomers
 - ionomeric elastomers 78, 79
 - micro-encapsulation 77, 78
 - nitrile butadiene rubber (NBR) blends 80
 - supramolecular co-networks 79, 80
 - self-sealing foam coatings 81, 82
 - bio-inspired chemical transfer 84, 85
 - bio-inspired physical transfer 82–84
- self-sealing and self-healing in plants
 - and infection by bacteria and fungi spores 62
 - latex plants 63–69
 - lianas 69–72
 - multiple evolution of self-repair processes 62
 - overview of 62, 63
 - phases of 62
 - succulent plants 72–75
- self-sealing foam coatings 81, 82
 - bio-inspired chemical transfer 84, 85
 - bio-inspired physical transfer 82–84
 - repair efficiency of 84
- semi-interpenetrating polymer network (SIPN) 155
- shape-memory alloy (SMA) 219, 363, 365
- shape memory assisted self-healing 155
- shape-memory polymer (SMP) matrix 116, 229
- silica (SiO₂) nanoparticles 261, 389, 393
- siloxane-based healing system 221, 222
- single capsule healing system 365
- single edge notched bending (SENB) 373
- single edge notched tension (SENT) 374
- single molecule force spectroscopy measurements (SMES) 201
- size-exclusion chromatography (SEC) 165
- small-angle neutron scattering (SANS) 119–121, 133
- small-angle X-ray scattering (SAXS) 131, 132, 286–288, 319
- soft matter 115, 116
- sol-gels 148, 393
 - anticorrosion coating 261
 - coatings 256, 263, 385, 386, 393, 395
 - transition
 - healing efficiencies 231
 - viscoelastic properties of 143–147
- solid-phase healing agents 373, 374
- solid state materials 200, 306
- solvodynamic shear 198

- sonication of polymer 196, 198, 203–205, 210
 - soxhlet extraction 154
 - spectrophotometers 194, 262
 - spectroscopic analysis, for monitoring
 - progress of healing 344
 - spiropyran (SP) 45, 197, 199
 - stable free radical polymerization (SFRP) 161
 - stacking 37, 130, 277, 282, 285, 291, 297, 301, 327
 - static damage, healing after 343–345
 - static loading 345
 - stimuli-responsive metallopolymer 305–307
 - stimuli-responsive self-healing materials
 - light-responsive capsules 258–260
 - pH-responsive systems 260–263
 - redox-responsive systems 263, 264
 - temperature-responsive systems 263
 - strain energy 139, 195, 343, 366
 - stress equilibrium 75
 - stress-induced isomerization 164
 - stress relaxation 27
 - styrene-maleic anhydride copolymer (PSMA) 251
 - SupraB* 292, 294
 - supramolecular complexes 37, 291
 - supramolecular co-networks 79, 80
 - supramolecular forces 9, 53
 - supramolecular gels 280–284, 289, 329
 - supramolecular hydrogen-bonded networks
 - bond dynamics of 279, 280
 - in bulk 276
 - elastic and viscous behavior 292
 - in gels 276
 - reversibility and dynamics of 275
 - sticky-reptation 276
 - sticky-Rouse 276
 - supramolecular hyperbranched polymer (SHP) 176
 - supramolecular interactions 9, 10, 15, 36, 37, 131, 133, 276, 277, 281, 292, 293
 - supramolecular polymers 115, 130, 210
 - binding energy 277
 - binding motifs utilizing hydrogen bonds 278
 - bondings 282, 289
 - bulk materials 284–297
 - concept of 275
 - degree of polymerization 280
 - gels 280–284
 - healing efficiency 277, 291
 - hydrogen bonds, dynamics of 279, 280
 - network formation in 28–37
 - self-healing in 277, 284
 - surface conduction, healing of 350
 - surface damage 176, 177, 339, 341, 347, 351
 - surface gloss 347
 - surface morphology 347
 - surface rearrangement 12, 13
 - surface roughness 12, 14, 343
 - suspension radical polymerization 200, 247
 - swelling 9, 11, 14, 73, 205, 263, 305, 340, 384
 - “switchable” healing 36
 - “switchable” network formation 44–48
 - “switchable” polymer systems 15
 - synthetic self-mending materials, design principles 91
- t**
- tapered double cantilever beam (TDCB) 344, 363, 364, 374, 405
 - tautomers 280
 - Taylor cone 250
 - temperature-responsive systems 263
 - tensile adhesion, for self-healing systems 343
 - tensile modulus 21, 37, 292, 297
 - tensile testing 198–200, 343
 - tetraethylorthosilicate (TEOS) 254
 - tetrafluoroethene 163
 - 2,2,6,6-tetramethyl-1-piperidinyloxy (TEMPO) 161
 - thermal conduction functionality, healing of 350
 - thermal cyclization 165
 - thermal cycloaddition reaction 163
 - thermal decomposition 163, 164, *see also*
 - mechanical decomposition
 - thermal diffusion 350, 402
 - thermal healing
 - chemical methods for 155, 156
 - – alternative mechanism 163
 - – perfluorocyclobutanes 163, 164
 - – thermoreversible mechanisms 156–163
 - cycle 372, 373, 374
 - physical methods for
 - – interpenetrating networks 154, 155
 - – molecular diffusion across crack interface 153, 154
 - – shape memory assisted self-healing 155
 - thermal interface materials (TIM) 346
 - thermally reversible crosslinked system 27, 319

- thermoplastics 139
- additives 218, 229
 - block copolymers 131
 - branched 194
 - elastomers 33, 34, 294
 - linear 154, 194, 373
 - molecular interdiffusion of 228, 229
 - self-healing of 11, 153
- thermo-reversible gels 141
- thermoreversible mechanisms, for thermal healing
- Diels–Alder reactions 156–161
 - NO–C bonds 161–163
- thermoreversible rubber 33
- thermosets 33, 34, 154, 164, 208
- self-healing in 10, 11
 - viscoelastic properties of 144
- thiocarbonyl bond 157
- thiol chemistry 10
- thiol-ene healing system 224, 225
- thiol-ene polymerization 208
- thiol-epoxy healing system 224
- thiol-maleimide healing system 225
- thiol-yne click reactions 21, 22
- thymine (Thy) 34, 131, 132, 277, 285
- time domain thermorefectance (TDTR) 350
- time flux 350
- tissue regeneration 1, 8, 63
- p*-toluene sulfonic acid 84
- torsional shear testing 200, 344
- trans–cis photoisomerization 176
- transesterification 44, 208
- transition metals 36, 303, 304, 307, 316
- transmission electron microscopy (TEM) 319, 340, 388, 389
- triethylene glycol dimethacrylate (TEGDMA) 251
- trifluorovinylethers (TFVE) 163, 164
- trithiocarbonate (TTC) 176, 233
- tube model, for short polymer chains 122, 124–130, 134
- turbulent flow 201
- u**
- ultramicroelectrode (UME) 353
- ultra-microtomy 351
- ultrasound transducer 198
- ultraviolet irradiation 177
- ultraviolet/ozone (UVO) treatment 102
- upper critical solution temperatures (UCSTs) 147, 148, 263
- UPy-polymer 284
- urazole 34, 286, 287
- 2-ureido-4[1 *H*]-pyrimidinone dimers 277
- ureido–pyrimidone bond 33
- UV-based healing system 232, 237
- UV irradiation 176–178, 180, 182, 183, 189, 224, 233, 234, 259, 260, 384
- UV–vis spectroscopy 186, 187, 196
- v**
- van der Waals forces 195
- vascular-based healing systems 368, 369, 375
- coatings, healing of 370, 371
 - principle of 49, 50
 - recovery of
 - – fracture damage 369, 370
 - – impact damage 370
 - self-sensing, self-healing vascularized composites 371
- Verein Deutscher Ingenieure (VDI) 75, 76
- vicinal fluorination 163
- Vinca* plant species 65
- vinyl ester healing system 228
- viscoelastic deformation 71
- viscoelasticity 117, 320
- of sol–gel transition 143–147
- viscoelastic polymer systems, self-healing in 344
- viscous flow 195
- w**
- waste storage system 63
- Weiner process 104
- welding 9, 11, 13, 14, 374, 402
- wetting 12, 13, 154, 186, 187, 227
- Wheatstone bridge circuit 349
- Williams–Landel–Ferry (WLF) equation 287
- wound healing 73, 91
- x**
- X-ray tomography 341, 402
- y**
- Young’s modulus 68
- z**
- zero-shear viscosity 145, 286, 293